

Advances in Oil and Gas Exploration & Production

Hamid N. Alsadi

# Seismic Hydrocarbon Exploration

2D and 3D Techniques

 Springer

---

# **Advances in Oil and Gas Exploration & Production**

*Series editor*

Rudy Swennen, Department of Earth and Environmental Sciences,  
K.U. Leuven, Heverlee, Belgium

The book series *Advances in Oil and Gas Exploration & Production* publishes scientific monographs on a broad range of topics concerning geophysical and geological research on conventional and unconventional oil and gas systems, and approaching those topics from both an exploration and a production standpoint. The series is intended to form a diverse library of reference works by describing the current state of research on selected themes, such as certain techniques used in the petroleum geoscience business or regional aspects. All books in the series are written and edited by leading experts actively engaged in the respective field.

The *Advances in Oil and Gas Exploration & Production* series includes both single and multi-authored books, as well as edited volumes. The Series Editor, Dr. Rudy Swennen (KU Leuven, Belgium), is currently accepting proposals and a proposal form can be obtained from our representative at Springer, Dr. Alexis Vizcaino (Alexis.Vizcaino@springer.com).

More information about this series at <http://www.springer.com/series/15228>

---

Hamid N. Alsadi

# Seismic Hydrocarbon Exploration

2D and 3D Techniques

 Springer

Hamid N. Alsadi  
Data Processing Section  
Ministry of Oil  
Baghdad  
Iraq

ISSN 2509-372X                      ISSN 2509-3738 (electronic)  
Advances in Oil and Gas Exploration & Production  
ISBN 978-3-319-40435-6              ISBN 978-3-319-40436-3 (eBook)  
DOI 10.1007/978-3-319-40436-3

Library of Congress Control Number: 2016942906

© Springer International Publishing Switzerland 2017

This work is subject to copyright. All rights are reserved by the Publisher, whether the whole or part of the material is concerned, specifically the rights of translation, reprinting, reuse of illustrations, recitation, broadcasting, reproduction on microfilms or in any other physical way, and transmission or information storage and retrieval, electronic adaptation, computer software, or by similar or dissimilar methodology now known or hereafter developed.

The use of general descriptive names, registered names, trademarks, service marks, etc. in this publication does not imply, even in the absence of a specific statement, that such names are exempt from the relevant protective laws and regulations and therefore free for general use.

The publisher, the authors and the editors are safe to assume that the advice and information in this book are believed to be true and accurate at the date of publication. Neither the publisher nor the authors or the editors give a warranty, express or implied, with respect to the material contained herein or for any errors or omissions that may have been made.

Printed on acid-free paper

This Springer imprint is published by Springer Nature  
The registered company is Springer International Publishing AG Switzerland

---

## Preface

The favorable reception of the first edition of this book (seismic Exploration, published by Birkhauser Verlag in 1980) stimulated my belief in the need of an updated book that includes the advances in the techniques which have taken place during the past three decades. In preparing the present updated volume, I have taken into consideration the remarks and suggestions of the users of the 1980 edition from both of the academic and industrial work domains.

Since 1980, when the first edition of this book was published, great developments in the seismic exploration technology have taken place. These developments have occurred in all of the three exploration phases: acquisition, processing, and interpretation techniques. The most prominent advances which have taken place in these years are the widespread implementations of the 3D surveying, pre-stack migration, and growing interpretation techniques in both structural and stratigraphic exploration. As it is familiar with the exploration geophysicists, this subject (seismic exploration) is fully dealt with in many original and authentic internationally known text books. In this publication, no new subjects added to those found in the other standard books which are well known in the geophysical library. In fact, these and other related scientific papers and research reports formed solid references for the present book. There are, however, differences in the design and presentation approach.

In its design, the book is intended to be a comprehensive treatise of the seismic exploration tool, addressing audiences in both of the academic and industrial establishments. It is made up of 12 chapters covering the basic aspects of the seismic reflection exploration subject, starting with the basic theory, followed by the applied data acquisition technology, and ending with the processing and interpretation. In presenting the subject matter, emphasis is made on the practical aspects of the subject, using clear and simplified presentation, avoiding excessive descriptions and unnecessary lengthy comments. Numerous illustration figures (>390 figures) have been used throughout the book to aid in clarifying the concepts and procedures involved in any standard seismic exploration survey. In this way, the book can be considered as a very useful introductory teaching manual for university students taking seismic reflection exploration as part of a postgraduate course.

The chapters of the book are sequenced in the order of the activities normally executed in a standard seismic exploration survey: field acquisition, processing, and interpretation. Chapter 1 is an introductory chapter in which a brief historical note and short review of the geophysical exploration methods are given. This is followed by four chapters covering the theoretical aspect of the subject including basic principles and definitions of seismic waves, with a special chapter assigned for the seismic wave propagation velocity. The propagation phenomena, reflection, diffraction, transmission, and refraction, are dealt with in Chaps. 4 and 5. The following two chapters are devoted to the two main tools applied in seismic exploration, namely the 2D and 3D surveying techniques.

Due to its important role in understanding of the processing steps applied in seismic data processing, a chapter (Chap. 8) is assigned solely for the seismic signal. This chapter is structured on the theme of considering the seismic reflection wavelet as a propagating signal in the same way as the electromagnetic signal is treated by the communication theory applied in electromagnetic wave propagation. Including a chapter on seismic signals, preceding the processing chapters, is a feature by which this book has deviated from other conventional publications. Data processing is presented under two headings: processing tools (Chap. 9) and the normally applied processing sequence (Chap. 10). Chapter 11 covers some specialized seismic exploration tools sometimes used in support of the conventional seismic reflection and refraction surveying. The book is concluded with Chap. 12 on interpretation.

I would like to express my gratitude to my wife Asira and my sons (Eng. Majid, Ph.D., Eng. Muhanad, M.Sc., Thurayah, B.Sc., and Eng. Mahir, B.Sc.), for their continuous support and help throughout the past three years. My work in the writing of the book has incurred an additional burden to the family especially during the abnormally difficult times, which our country has experienced in the past twelve years.



Baghdad, Iraq  
December 2015

Hamid N. Alsadi

---

# Contents

<b>1</b>	<b>Introduction</b> . . . . .	1
1.1	Historical Review . . . . .	1
1.1.1	Elasticity and Seismic Waves (Báth 1979) . . . . .	1
1.1.2	Earthquake Seismology (Richter 1958). . . . .	2
1.1.3	Exploration Seismology (Telford et al. 1990) . . . . .	2
1.1.4	Summary of Exploration Seismology History (Sheriff and Geldart 1995) . . . . .	3
1.2	The Geophysical Exploration Project . . . . .	3
1.3	Geophysical Exploration Methods . . . . .	4
1.3.1	The Seismic Method . . . . .	4
1.3.2	The Gravity Method . . . . .	4
1.3.3	The Magnetic Method . . . . .	6
1.3.4	The Electrical Method. . . . .	7
1.3.5	The Radioactivity Method . . . . .	9
1.4	Oil Well Drilling. . . . .	9
1.4.1	Drilling of the Exploration-Well . . . . .	10
1.4.2	The Oil-Well Rotary Drilling . . . . .	10
1.4.3	The Drill-Hole and Well Casing . . . . .	11
1.5	Well Geophysical Logging . . . . .	11
1.5.1	Electrical Logging . . . . .	12
1.5.2	Radioactivity Logging . . . . .	14
1.5.3	Acoustic Logging . . . . .	16
1.5.4	Log Interpretation . . . . .	19
1.6	Latest Developments in Well Logging . . . . .	19
1.6.1	Logging While Drilling Technique . . . . .	20
1.6.2	Borehole Imaging Tools. . . . .	20
1.7	Well Completion. . . . .	20
<b>2</b>	<b>Seismic Waves</b> . . . . .	23
2.1	The Fundamental Conditions . . . . .	23
2.2	Theory of Elasticity . . . . .	23
2.2.1	Stress . . . . .	24
2.2.2	Strain . . . . .	26
2.2.3	Common Types of Strain . . . . .	26
2.2.4	The Volume-Changing Strain . . . . .	27
2.2.5	The Shape-Changing Strain . . . . .	28
2.2.6	The Cubical Dilatation. . . . .	28

2.2.7	Stress-Strain Relationship . . . . .	29
2.2.8	Hooke's Law for Isotropic Media . . . . .	29
2.2.9	The Elastic Moduli . . . . .	30
2.2.10	The Elastic Moduli Interrelationships . . . . .	32
2.3	Wave Motion Equation . . . . .	32
2.3.1	One-Dimensional Scalar Wave Equation . . . . .	33
2.3.2	The Scalar and Vector 3D Wave Equations . . . . .	34
2.3.3	Plane Waves . . . . .	35
2.3.4	The P- and S-Waves . . . . .	36
2.4	Classification of Common Elastic Waves . . . . .	36
2.4.1	Body Waves . . . . .	37
2.4.2	Surface Waves . . . . .	38
2.4.3	Seismic Noise . . . . .	39
2.5	Propagation of Seismic Waves . . . . .	40
2.5.1	Elements of the Seismic Field . . . . .	41
2.5.2	Concepts of Wave-Fronts and Rays . . . . .	41
2.5.3	Huygens' Principle . . . . .	42
2.5.4	The Concept of the Interface . . . . .	42
2.5.5	Changes of Propagation Direction at Interfaces . . . . .	43
2.5.6	Wave Conversion at Interfaces . . . . .	44
2.5.7	Energy Partitioning and Zoeppritz Equations . . . . .	45
2.5.8	Amplitude Variation with Angle of Incidence . . . . .	46
2.6	Effect of the Medium on Wave Energy . . . . .	46
2.6.1	Geometrical Spreading . . . . .	47
2.6.2	Inelastic Attenuation . . . . .	48
2.6.3	Seismic Wave Energy Measurement and the DB Unit . . . . .	49
2.6.4	The Logarithmic Decrement . . . . .	49
2.6.5	Wave Dispersion . . . . .	49
<b>3</b>	<b>The Seismic Velocity . . . . .</b>	<b>53</b>
3.1	Introduction . . . . .	53
3.2	Factors Influencing Seismic Velocity . . . . .	53
3.2.1	Lithology Effect . . . . .	53
3.2.2	Elasticity and Density Effects . . . . .	54
3.2.3	Porosity and Saturation Fluid Effects . . . . .	54
3.2.4	Depth and Geological Age Effects . . . . .	56
3.2.5	Overburden Pressure Effect . . . . .	56
3.2.6	Other Velocity-Affecting Factors . . . . .	57
3.3	The Velocity Function . . . . .	58
3.4	Types of Velocity Functions . . . . .	59
3.4.1	Instantaneous Velocity . . . . .	59
3.4.2	Interval Velocity . . . . .	60
3.4.3	Average Velocity . . . . .	60
3.4.4	Root Mean Square Velocity . . . . .	61
3.4.5	Stacking Velocity . . . . .	62

3.4.6	The Apparent Velocity . . . . .	63
3.4.7	The Group and Phase Velocities . . . . .	64
3.4.8	Representations of the Velocity Functions . . . . .	64
3.5	Velocity Determination Methods . . . . .	64
3.5.1	The Well Velocity Survey . . . . .	65
3.5.2	The Up-Hole Velocity Survey . . . . .	66
3.5.3	Continuous Velocity Logging . . . . .	66
3.5.4	( $X^2 - T^2$ Method) . . . . .	67
3.5.5	( $T - \Delta T$ ) Method . . . . .	67
3.5.6	Velocity Analysis Method . . . . .	68
3.5.7	Seismic Velocity Inversion . . . . .	69
3.6	Uses of the Seismic Velocity Data . . . . .	69
<b>4</b>	<b>Seismic Wave Reflection and Diffraction . . . . .</b>	<b>71</b>
4.1	The Commonly-Recorded Seismic Events . . . . .	71
4.2	Wave Changes at Reflection Interface . . . . .	71
4.2.1	Reflection Coefficient at Inclined Incidence . . . . .	72
4.2.2	Reflection Coefficient at Normal Incidence . . . . .	73
4.2.3	Geometry of Reflection from Dipping Reflectors . . . . .	74
4.2.4	Geometry of Reflection from Horizontal Reflectors . . . . .	75
4.2.5	Reflection from Multiple Reflectors . . . . .	75
4.3	The NMO and DMO Concepts . . . . .	76
4.3.1	The Normal Move-Out (NMO) Concept . . . . .	76
4.3.2	The Dip Move-Out (DMO) Concept . . . . .	79
4.4	The CDP, CRP, and CMP Concepts . . . . .	79
4.4.1	CDP, CRP, and CMP in Case of Horizontal Reflector . . . . .	80
4.4.2	CDP, CRP, and CMP in Case of Dipping Reflector . . . . .	80
4.5	The Seismic Wave Diffraction . . . . .	81
4.5.1	The Point-Diffractor . . . . .	82
4.5.2	Diffraction from Terminating Reflectors . . . . .	83
4.5.3	Diffraction Seismic Image . . . . .	83
4.5.4	Diffraction Travel-Time Function . . . . .	84
4.5.5	The Diffraction Hyperbola . . . . .	85
4.5.6	Distortion Effects of Diffraction . . . . .	86
4.5.7	The Exploding-Reflector Model . . . . .	86
<b>5</b>	<b>Seismic Wave Transmission and Refraction . . . . .</b>	<b>89</b>
5.1	Seismic Wave Transmission . . . . .	89
5.1.1	Transmission Coefficient at Normal Incidence . . . . .	89
5.1.2	The Two-Way Transmission Coefficient . . . . .	90
5.1.3	Attenuation Due to Reflection and Transmission . . . . .	90
5.1.4	Role of Transmission in Seismic Exploration . . . . .	91

5.2	Seismic Wave Refraction . . . . .	92
5.2.1	Snell's Law of Refraction. . . . .	92
5.2.2	The Critical Refraction and Head Wave Generation . . . . .	95
5.2.3	Ray-Path Geometry and Travel-Time Curves. . . . .	96
5.2.4	Refraction Travel-Time Function. . . . .	96
5.2.5	The Delay-Time Concept . . . . .	98
5.2.6	Refraction in a Multi-layer Medium. . . . .	99
5.2.7	Refraction in a Medium of Linear Velocity Variation . . . . .	99
5.2.8	Refraction from a Faulted Refractor. . . . .	100
5.2.9	Applications of Seismic Wave Refraction. . . . .	100
<b>6</b>	<b>2D Seismic Reflection Surveying . . . . .</b>	<b>105</b>
6.1	Reflection Surveying Concepts . . . . .	105
6.1.1	The Spread Configuration . . . . .	105
6.1.2	The Seismic Trace. . . . .	106
6.1.3	The Shotpoint. . . . .	107
6.1.4	The Seismic Profiling Technique. . . . .	107
6.1.5	The Fold of Coverage . . . . .	108
6.1.6	The CDP Trace Gather . . . . .	110
6.2	Seismic Reflection Data Acquisition . . . . .	113
6.2.1	Seismic Energy Sources . . . . .	113
6.2.2	Seismic Detectors . . . . .	119
6.2.3	The Seismic Data Recording. . . . .	121
6.2.4	Data Playback and Display. . . . .	126
6.3	Seismic Noise Characterization and Attenuation . . . . .	126
6.3.1	Random Noise Attenuation. . . . .	127
6.3.2	Coherent Noise Attenuation . . . . .	127
6.4	Field Measures for Signal Enhancement. . . . .	131
6.4.1	The Noise Test . . . . .	131
6.4.2	The Experimental Shooting . . . . .	134
6.4.3	Determination of the LVL Properties. . . . .	134
6.5	The Seismic Field Crew . . . . .	136
<b>7</b>	<b>3D Seismic Reflection Surveying . . . . .</b>	<b>139</b>
7.1	Introduction . . . . .	139
7.1.1	Nature Is Three Dimensional . . . . .	139
7.1.2	1D-2D-3D Terminology. . . . .	140
7.1.3	Limitations of 2D Seismic Surveying. . . . .	141
7.1.4	Merits of the 3D Technique . . . . .	143
7.1.5	Survey Preplanning . . . . .	146
7.1.6	Cost Considerations of 3D Surveys. . . . .	146
7.2	Definitions and Basic Principles . . . . .	148
7.2.1	Definition of 3D Surveying . . . . .	148
7.2.2	The 3D Spread-Geometry. . . . .	149
7.2.3	Concept of the Trace Azimuth . . . . .	149

	7.2.4	The CDP Bin and Bin Attributes . . . . .	150
	7.2.5	The Surface and Sub-surface Coverage . . . . .	150
	7.2.6	The Seismic Data Volume . . . . .	151
7.3		3D Field Data Acquisition . . . . .	153
	7.3.1	Types of Marine 3D Spreads . . . . .	153
	7.3.2	Types of Land 3D Spreads . . . . .	155
	7.3.3	The Swath Shooting Technique . . . . .	156
	7.3.4	Types of Templates Used in Swath Shooting . . . . .	156
	7.3.5	The Loop Shooting Technique . . . . .	159
	7.3.6	The 3D Survey Design . . . . .	159
7.4		Processing of 3D Data . . . . .	164
	7.4.1	The Field Data Processing . . . . .	166
	7.4.2	The Final Data Processing . . . . .	166
	7.4.3	3D Data Displays . . . . .	166
<b>8</b>		<b>The Seismic Reflection Signal . . . . .</b>	<b>169</b>
8.1		Definition of the Seismic Signal . . . . .	169
	8.1.1	The Seismic Signal Parameters . . . . .	170
	8.1.2	The Seismic Signal Spectrum . . . . .	170
	8.1.3	Comparison with the Radar Signal . . . . .	172
	8.1.4	The Seismic Reflection-Signal Changes . . . . .	172
8.2		The Seismic Trace . . . . .	173
	8.2.1	The Convolutional Model of the Seismic Trace . . . . .	174
	8.2.2	The Synthetic Seismogram . . . . .	175
	8.2.3	The Digital Seismic Trace . . . . .	176
8.3		The Wavelet Concept . . . . .	177
	8.3.1	Definition of the Seismic Wavelet . . . . .	177
	8.3.2	Energy and Delay Properties of Wavelets . . . . .	178
8.4		Sampling and the Digital Function . . . . .	178
	8.4.1	The Digital Function . . . . .	179
	8.4.2	The Sampling Process . . . . .	179
	8.4.3	Representation Methods of the Digital Function . . . . .	180
8.5		The Sampling Theorem and Aliasing . . . . .	181
	8.5.1	The Sampling Theorem . . . . .	181
	8.5.2	The Aliasing Phenomenon . . . . .	182
	8.5.3	The Aliasing Frequency Computation . . . . .	183
	8.5.4	Effect of Sampling on Signal Spectrum . . . . .	185
	8.5.5	Aliasing in the Frequency Domain . . . . .	185
	8.5.6	The Remedy for the Aliasing Effect . . . . .	186
8.6		Signal Resolution and Resolution Power . . . . .	187
	8.6.1	Vertical Resolution of Seismic Signals . . . . .	187
	8.6.2	Horizontal Resolution of Seismic Signals . . . . .	189
	8.6.3	Fresnel Zone Formula . . . . .	189

8.7	The Common Numbering Systems . . . . .	190
8.7.1	Numbering System Concept . . . . .	191
8.7.2	Applications of the Concept . . . . .	191
8.7.3	Counting in the Different Numbering Systems . . . . .	195
<b>9</b>	<b>The Seismic Processing Tools . . . . .</b>	<b>197</b>
9.1	The Seismic Processing Tools. . . . .	197
9.1.1	The Sine Function. . . . .	197
9.1.2	The Degrees-Radians Relationship. . . . .	198
9.1.3	Parameters of the Sine Function . . . . .	198
9.1.4	The Frequency Concept . . . . .	199
9.1.5	The Phase Concept . . . . .	200
9.1.6	Temporal and Spatial Frequencies . . . . .	200
9.1.7	Propagating Sine Wave . . . . .	202
9.2	Fourier Analysis and Concept of Spectra . . . . .	203
9.2.1	Fourier Series . . . . .	203
9.2.2	Gibbs' Phenomenon . . . . .	205
9.2.3	Fourier Transform . . . . .	205
9.3	Concept of the Frequency Spectrum . . . . .	206
9.3.1	The Line Spectrum . . . . .	207
9.3.2	The Continuous Spectrum . . . . .	207
9.3.3	The Fourier Power Spectrum . . . . .	207
9.3.4	The Two-Domain Concept . . . . .	208
9.3.5	Spectrum of the Rectangular Pulse . . . . .	209
9.3.6	Spectrum of the Spike Pulse. . . . .	210
9.3.7	The Dirac-Delta Function . . . . .	210
9.3.8	Frequency Limits of Fourier Spectra . . . . .	211
9.4	The Phase Spectrum . . . . .	212
9.4.1	The Zero-Phase Spectrum. . . . .	212
9.4.2	The Linear-Phase Spectrum . . . . .	213
9.4.3	The Constant-Phase Spectrum . . . . .	213
9.5	Spectra of Observational Data. . . . .	214
9.5.1	Truncation Effect and Windowing. . . . .	215
9.5.2	The Rectangular Window (Box-Car) . . . . .	216
9.5.3	Triangular Window (Bartlett) . . . . .	217
9.6	Correlation Functions. . . . .	218
9.6.1	Cross Correlation Function, $C_{12}(\tau)$ . . . . .	218
9.6.2	Autocorrelation Function $C_{11}(\tau)$ . . . . .	218
9.6.3	Properties and Applications of Correlation Functions . . . . .	219
9.6.4	Correlation Functions in the Frequency Domain . . . . .	219
9.7	Convolution . . . . .	220
9.8	Deconvolution . . . . .	221
9.8.1	Deconvolution Main Objectives . . . . .	222
9.8.2	Spiking (Whitening) Deconvolution. . . . .	223
9.8.3	Gapped Deconvolution. . . . .	224
9.8.4	Noise Behaviour Under Deconvolution . . . . .	225

9.9	Frequency Filtering . . . . .	226
9.9.1	Definition of the Filtering Process . . . . .	226
9.9.2	Role and Objectives of Filtering in Seismic Exploration . . . . .	227
9.9.3	Concept of the Linear System . . . . .	228
9.9.4	The Filter Impulse Response . . . . .	229
9.9.5	Mechanism of the Filtering Process . . . . .	230
9.9.6	Filtering in the Two Domains . . . . .	230
9.9.7	Types of Filters . . . . .	231
9.9.8	Application of the Band-Pass Filter . . . . .	231
9.9.9	Filter Shape (Side-Lobes Problem) . . . . .	232
9.9.10	Effect of the Filter Length . . . . .	233
9.9.11	Effect of the Filter Spectrum Shape . . . . .	233
9.9.12	Minimization of the Truncation Effect . . . . .	235
9.9.13	Filter Normalization . . . . .	235
9.9.14	Time-Variant Filtering . . . . .	236
9.9.15	The Filter Tests . . . . .	237
9.9.16	Phase Removing Filtering . . . . .	238
9.10	Frequency-Wave Number (FK) Filtering . . . . .	238
9.10.1	The t-x and F-K Domains . . . . .	238
9.10.2	Application of the F-K Filtering . . . . .	239
9.11	Seismic Trace Equalization . . . . .	240
9.11.1	The Need for Trace Equalization . . . . .	240
9.11.2	Time-Invariant Equalization . . . . .	242
9.11.3	Time-Variant Equalization . . . . .	242
9.12	Trace-Samples Manipulations . . . . .	243
<b>10</b>	<b>Processing of Seismic Reflection Data . . . . .</b>	<b>245</b>
10.1	General Overview . . . . .	245
10.1.1	Main Processing Objectives . . . . .	246
10.1.2	Role of Processing in Seismic Exploration . . . . .	247
10.1.3	Main Processing Activities . . . . .	247
10.1.4	The Processing Sequence . . . . .	248
10.2	Data Re-organization . . . . .	250
10.2.1	Seismic Data Copying, Reformatting, and Loading . . . . .	250
10.2.2	Data De-multiplexing . . . . .	250
10.2.3	Sweep Removal . . . . .	251
10.2.4	Vertical Stacking . . . . .	252
10.2.5	Geometry Data and Field Statics Loading . . . . .	252
10.2.6	Trace Header Assignment . . . . .	253
10.2.7	Data Re-sampling . . . . .	253
10.3	Pre-stack Processing . . . . .	253
10.3.1	Trace Editing . . . . .	253
10.3.2	Noise Attenuation . . . . .	254
10.3.3	True Amplitude Recovery . . . . .	254
10.3.4	Field Static Correction . . . . .	256
10.3.5	Application of Deconvolution . . . . .	259
10.3.6	Trace Equalization . . . . .	262
10.3.7	CMP-Sorting . . . . .	263

	10.3.8	NMO Correction . . . . .	264
	10.3.9	Trace Muting . . . . .	267
10.4		Stack and Post-stack Processing . . . . .	268
	10.4.1	CMP Stacking of Seismic Traces . . . . .	269
	10.4.2	CMP Stacking . . . . .	269
	10.4.3	Vertical Stacking . . . . .	270
	10.4.4	Horizontal Stacking . . . . .	270
	10.4.5	Diversity Stacking . . . . .	271
	10.4.6	The Stack Section . . . . .	271
10.5		Seismic Migration . . . . .	272
	10.5.1	Distortions in the Stack Section . . . . .	272
	10.5.2	Problem Statement . . . . .	273
	10.5.3	Geometry of the Distortions . . . . .	275
	10.5.4	Relationship of Post-migration Dip to Pre-migration Dip . . . . .	275
	10.5.5	Types of Migration Techniques . . . . .	276
	10.5.6	Time Versus Depth Migration . . . . .	281
	10.5.7	Migration Parameters . . . . .	282
	10.5.8	Migration Techniques in Future . . . . .	284
10.6		Application of Filtering and Equalization . . . . .	285
	10.6.1	Frequency Filtering . . . . .	285
	10.6.2	Equalization . . . . .	285
	10.6.3	Data Storage and Display . . . . .	286
10.7		Parameter Optimization . . . . .	286
	10.7.1	Velocity Analysis . . . . .	286
	10.7.2	Residual-Static Analysis . . . . .	287
	10.7.3	Deconvolution Analysis . . . . .	289
	10.7.4	Filter Analysis . . . . .	289
	10.7.5	Equalization Analysis . . . . .	290
	10.7.6	Mute Analysis . . . . .	290
<b>11</b>		<b>Extra Exploration Tools . . . . .</b>	<b>291</b>
11.1		Seismic Exploration with S-waves . . . . .	291
	11.1.1	Shear-Waves Generation . . . . .	291
	11.1.2	Role of the Shear-Wave Velocity in Interpretation . . . . .	292
11.2		Vertical Seismic Profiling (VSP) . . . . .	292
	11.2.1	Field Set-up and Types of VSP . . . . .	292
	11.2.2	The VSP Field Operation . . . . .	293
	11.2.3	The VSP Seismic Record . . . . .	293
	11.2.4	The VSP Data Processing . . . . .	294
11.3		Seismic Tomography . . . . .	295
	11.3.1	The Forward and Inverse Modeling Concepts . . . . .	295
	11.3.2	Types of Seismic Tomography . . . . .	296
	11.3.3	Interpretation of Tomography Data . . . . .	296
11.4		4D (Time-Lapse) Surveying . . . . .	297
11.5		Multi-component (3C and 4C) Recording . . . . .	297
11.6		Passive Seismic Surveying . . . . .	298
11.7		Tau-P Transform . . . . .	298

---

11.8	Amplitude Variation with Offset (AVO) . . . . .	299
11.9	Seismic Attributes . . . . .	299
<b>12</b>	<b>Interpretation of Seismic Reflection Data . . . . .</b>	<b>301</b>
12.1	Scope and Objectives . . . . .	301
12.2	The Seismic Interpretation Tools . . . . .	301
12.3	The Seismic Structural Interpretation . . . . .	302
12.3.1	Structural Interpretation Sequence . . . . .	302
12.3.2	The Seismic Structural Features . . . . .	304
12.4	The Seismic Stratigraphic Interpretation . . . . .	306
12.4.1	Role of the Seismic Wavelet in Stratigraphic Interpretation . . . . .	306
12.4.2	Basic Stratigraphic Concepts . . . . .	307
12.4.3	Reflection Configuration Patterns . . . . .	308
12.4.4	Seismo-Stratigraphic Features . . . . .	310
12.4.5	Stratigraphic Interpretation Sequence . . . . .	315
12.5	Direct Hydrocarbon Detection and Seismic Attributes . . . . .	316
12.5.1	Hydrocarbon Indicators . . . . .	316
12.5.2	Seismic Attributes . . . . .	317
	<b>References . . . . .</b>	<b>321</b>
	<b>Index . . . . .</b>	<b>325</b>

## 1.1 Historical Review

The science of Seismic Exploration is in essence based on the elastic-wave phenomenon and its applications in exploring subsurface geological structures with what they contain from minerals, water, and hydrocarbon deposits. This phenomenon depends largely on the elastic properties of the medium within which the wave field prevails. The earliest discoveries were, in fact, made in the field of elasticity property and its role in generation and propagation of the elastic waves. Following to these activities, intensive studies were conducted on the elastic waves generated by earthquakes which are considered to be natural energy sources causing seismic waves. In the last phase of the research development, the seismic phenomenon created by natural earthquakes was simulated using artificial seismic energy sources directed towards geological exploration. For economic benefits, the seismic exploration technology was further developed as a specialized method used in mineral and petroleum exploration.

In view of this piece of information, it is possible to review the development of the seismic exploration under the three historical phases:

- Historical Development of Elasticity and Seismic Waves
- Historical Development of Earthquake Seismology
- Historical Development of Exploration Seismology

### 1.1.1 Elasticity and Seismic Waves (Båth 1979)

The first scientist who investigated the elastic behavior of bodies is Galileo (1564–1642), who, in 1638 investigated the elastic behavior of a loaded beam attached at one end to a wall. In 1660, Hook's law was established. This law forms the basis for the mathematical theory of Elasticity.

In 1828, the French scientist, S. D. Poisson found that two types of waves (the longitudinal and transverse elastic waves) can travel through an elastic medium with propagation velocities,  $V_P$  and  $V_S$  where the ratio ( $V_P/V_S$ ) is equal to square root of 3. This result was later confirmed by Stokes in England in 1849, who labeled the two wave-types by P for the longitudinal and S for the transverse waves. Stokes also showed that the applied stress onto a body can be analyzed into normal component causing compression (or tension) and tangential component causing shear deformation. The two moduli which Stokes defined to express these effects (body resistances to stresses) are what is now known as the moduli of compressibility and rigidity of materials.

In 1887, Lord Rayleigh, in England, discovered a type of elastic waves which can propagate over the surface of a medium with velocity ( $V_R$ ) which is lower than  $V_S$  in the same medium. This was followed by another similar discovery, in 1911, of another type of surface waves: the Love

waves, named after its discoverer, the Englishman A. E. H. Love.

### 1.1.2 Earthquake Seismology (Richter 1958)

Very large number of earthquakes is continuously occurring on various parts of the Earth. If small shocks are counted, 100 000 shocks a year is considered to be a conservative estimate (Richter 1958, p. 8). These events have furnished most of the fundamental information concerning seismic waves and other aspects of the earthquake seismology. Pre-historic earthquakes were reported in terms of their destruction effects and loss of lives. In Gutenberg's handbook of Geophysics (*Handbuch der Geophysik*, volumes 1–4, Berlin 1929), valuable information on earthquake occurrence in pre historic times were indorsed. In particular, he mentioned in volume-4 (pp. 803–804), that pre-historic destructive earthquakes were reported to have occurred at different places of Mesopotamia. In this region four destructive earthquakes have occurred within the period (1260–550) BC.

In the year (132 AD), the Chinese philosopher Chang Heng devised a detection instrument to detect the arriving earthquake impulse marking the first step in instrumental seismology (Bullen 1965). However, the proper documentation and scientific investigations of earthquakes started with the introduction of the detection instrument (the seismograph) at the end of the 19th century. In 1880, Grey, Milne, and Ewing (working in Japan) developed the first scientific seismograph-based analyses of earthquake-generated seismic waves. The main large-magnitude historic earthquakes which are scientifically described (based on seismograph data) are the following:

Lisbon-Portugal in 1755,  
Cutch- India in 1819,  
Naples-Italy in 1819,  
Mino Owari-Japan in 1891,  
San Francisco-USA in 1906,  
Kwanto-Japan in 1923.

In recent times, we may add Agadir-Morocco in 1960, Kobe-Japan in 1995, Fukushima-Japan in 2011, and Katimando-Nipal in 2015.

### 1.1.3 Exploration Seismology (Telford et al. 1990)

The normal mineral and oil exploration seismology is, in principle, the same as earthquake seismology. The main difference is in the energy source used to generate the seismic waves. The natural energy source used in earthquake seismology is replaced by the artificial mechanically-generated seismic energy. Broadly speaking, earthquake seismology was developed during the first half of the nineteenth century, whereas the oil-prospecting seismic-techniques were developed during the first half of the twentieth century, using the refraction and reflection techniques.

The tragic incident of the Titanic ship that was hit and sunk by an iceberg in 1912, has motivated R. Fessenden (Canadian) to use the phenomenon of reflection of acoustic waves in detecting icebergs. He also worked on using the principle in detecting submarines during the First World War (1914–1918). At about the same time, L. Minntrop (German) devised a seismograph with which he succeeded to detect salt domes in Germany. With his newly founded company (Seismos), the first refraction shooting was conducted. This refraction-based survey resulted in 1924 in the discovery of the Orchard Dome southwest of Houston, Texas, USA. Refraction exploration was then extensively applied until 1930 when the method gave way to the more effective method of reflection shooting.

Based on Fessenden work in 1913 and Karcher application efforts in Oklahoma, USA, in the early 1920s, reflection seismology was developed into an efficient exploration tool. After 1930, reflection exploration was used on wide commercial scale. A new era in the method development was the introduction in the early 1950s of the analogue data recording and playback data processing. In 1953, the analogue magnetic tape recording and

processing was introduced. About 10 years later the digital systems were introduced and began to replace the analogue systems rather rapidly. One of the important features of the magnetic tape recording was the ability of data storage, playback, and processing for the purpose of the signal enhancement of the reflection seismic event.

#### 1.1.4 Summary of Exploration Seismology History (Sheriff and Geldart 1995)

The main historical developments, the seismic exploration method has witnessed can be summarized as follows:

Year	Nature of development
1913	Invention of instruments (by R. Fessenden) to record acoustic waves in water to detect icebergs. His patent (issued in 1917) was the first in USA, on application of seismic waves for exploration
1914	Invention of portable seismographs (by L. Minntrop) to record seismic waves generated by artificial explosions. These detectors were used to locate enemy artillery during World War-1. He was awarded a US patent for this technique in 1923
1923	Use of first seismic refraction shooting. Conducted in the Gulf Coast area, resulted in 1924 in the discovery of the Orchard Dome, Texas, USA
1926	Use of seismic reflection shooting in the state of Oklahoma, USA
1927	Use of first well velocity survey
1933	Use of multiple geophone per seismic channel (the geophone group)
1936	First reproducible photographic recording developed by F. Rieber
1944	Introduction of large-scale marine surveying
1952	Introduction of the analogue magnetic recording and play-back recording
1953	Introduction of the Vibroseis and Weight-dropping as energy generators

(continued)

Year	Nature of development
1954	Introduction of the continuous velocity logging
1963	Introduction of the digital seismic data-recording
1965	Introduction of the Air-gun as seismic energy source
1972	Bright spot and direct hydrocarbon detection techniques
1975	Introduction of Seismic Stratigraphy
1976	3D seismic reflection surveying, became in common use
1985	Introduction of the interpretation workstation
1990	Application of the satellite global positioning system (GPS)

A full coverage and detailed account on the historical development of the exploration seismology is given by Sheriff and Geldart (1995, pp. 3–32).

## 1.2 The Geophysical Exploration Project

A geophysical exploration-project normally follows a sequence of activities starting with field work and ending up with production of the subsurface geological model of the project area. An exploration project passes through a sequence of three phases, normally executed in sequence.

The starting phase of a survey is collecting the field raw data through standard field procedures by which the geophysical measured values are recorded, usually on magnetic tapes. After completing the acquisition work, the recorded data are passed on to a processing centre where it is subjected to certain processing steps for purpose of certain corrections and enhancing of the geophysical signal. The third and last phase of the project is to interpret the final processed data to extract the subsurface geological model of the area under exploration. The three phases of exploration work is summarized in Fig. 1.1.

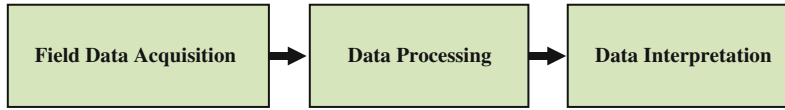


**Fig. 1.1** The three phases of the seismic exploration project

### 1.3 Geophysical Exploration Methods

The main exploration methods employing geophysical principles are:

- (i) Seismic
- (ii) Gravity
- (iii) Magnetic
- (iv) Electrical
- (v) Radioactivity
- (vi) Electromagnetic

Seismic method is by far the most widely applied method in the exploration of oil and gas deposits. Gravity, magnetic, electrical, and radioactivity methods provide support data in the oil exploration and also applied as the main tools for other mineral exploration. Geophysical techniques which are using the Earth geophysical potential fields (as gravity and magnetic fields) are often called (Potential Methods).

These methods are briefly defined as follows:

#### 1.3.1 The Seismic Method

This method is based on generating seismic waves by a mechanical energy source at a point on, or just below, the ground surface and recording the arrival at another surface point of the reflected (or refracted) waves. From the travel-time measurements of these waves and wave motion-velocity, the structural variation of subsurface geological layers are mapped. Under favorable conditions, study of the seismic wavelet can provide information on the stratigraphic nature and hydrocarbon contents of the traversed rocks. The raw seismic data (normally recorded on magnetic tapes), are passed through a sequence of processing steps followed by a set of certain interpretation procedures in order to obtain the final result, which is a model of the subsurface geological structure.

Detailing of this technique is the subject of this monograph.

There are two main techniques involved by the seismic method; the reflection and the refraction methods (Fig. 1.2).

In a seismic experiment, there are generally four types of wave arrivals that can be detected by a receiver placed at an offset-distance from the seismic source. These are:

- Reflection Arrivals
- Refraction Arrivals
- Diffraction Arrivals
- Direct (Transmission) Arrivals

These four types of seismic wave arrivals can be considered to be the main seismic exploration-tools involved in any seismic exploration project.

#### 1.3.2 The Gravity Method

In this method the acceleration due to the Earth gravitational force is measured at a grid of points distributed over the survey area. The observed gravity values are reduced to what they would be, had they been measured at a fixed datum level (normally fixed at the sea level). The so-corrected gravity values are contoured to show the variation of the gravity values (in acceleration units) throughout the area.

It is known that gravity changes depend on changes in density as well as on the depth of the causing geological anomaly. Thus, as the density increases (relative to the host medium), the gravity attraction (or acceleration value) of a rock mass at a given depth increases. If, however, a constant-density rock mass exists at different depths, the corresponding gravity values are different. Gravity values of deeper rocks are less than those for shallower rocks. A typical example for this case is the gravity changes normally exhibited over an anticline, where the gravity

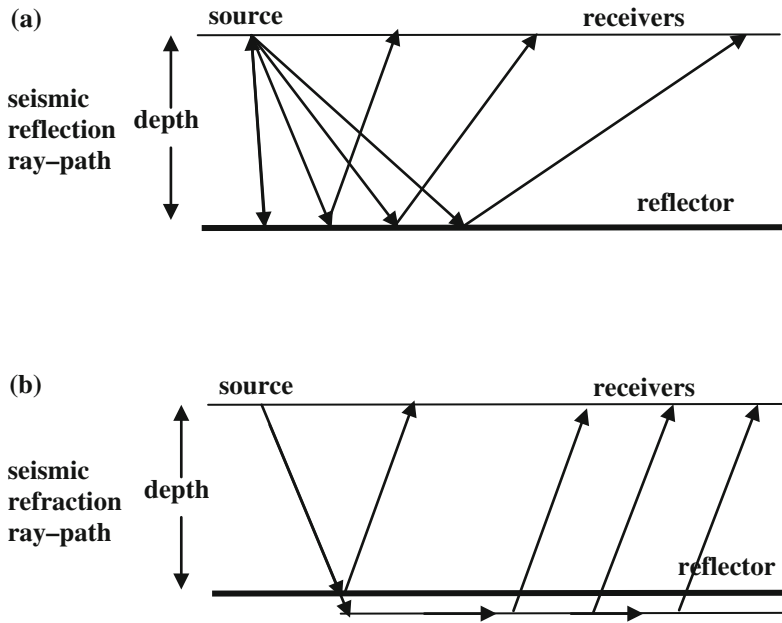


**Fig. 1.2** Essence of the two seismic techniques; reflection (a) and refraction (b)

change (called the gravity anomaly) is greater over the anticline axis falling to lower values over the flanks. A structural feature showing relative density-deficiency (such as a salt dome), gives an inverted bell-shaped anomaly normally referred to as (negative anomaly) which is of opposite shape-changes to that exhibited by the relatively denser-rock geological anomaly (positive anomaly). The principle is shown in Fig. 1.3.

The measuring instruments, normally used in gravity surveying, are called the gravity meters (or gravimeters). These are designed to measure gravity variations rather than absolute gravity values. These instruments are capable to measure gravity changes to less than a tenth of a milligal. The gravity unit (the gal) is defined to be equal to  $1 \text{ cm/s}^2$ . Thus the gravimeter is capable of measuring gravity variations to within about

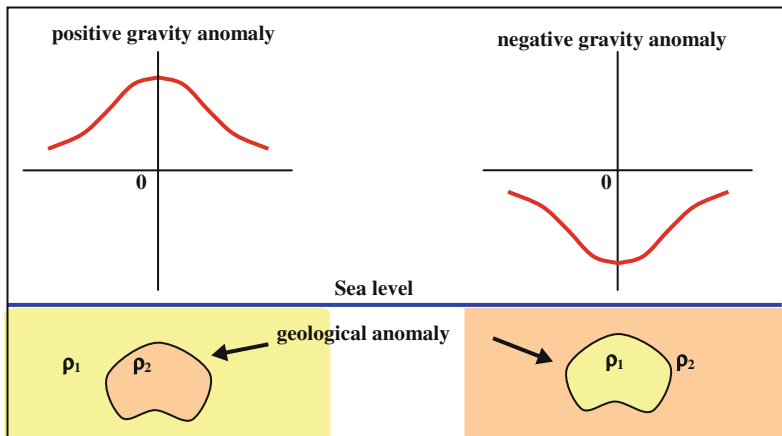


**Fig. 1.3** Dependence of the algebraic sign of gravity-anomaly on whether the contrast is surplus or deficiency. Positive sign is given to case of density

surplus where body density ( $\rho_2$ ) is greater than that of the host medium (density,  $\rho_1$ ), and vice versa, given ( $\rho_2 > \rho_1$ )

ten-millionth of the Earth's total gravity field which is about 9.8 k gal.

Gravity surveying is ideally suited to map subsurface rock layers or mineral deposits that show depth-variations such as folded strata, or density-changes as in cases of salt domes, heavy mineral deposits, and subsurface cavities. Because of the two factors affecting the measured gravity change (density and depth), interpretation of the gravity data suffers from ambiguity in the determination of the real geological anomaly responsible of creating the gravity anomaly. For this reason an additional tool or information is needed to determine the true causal geological anomaly.

Details of this method can be found in many standard geophysical publications. A simplified monograph on the subject that can be referred to is Alsadi and Baban 2014.

### 1.3.3 The Magnetic Method

As often stated in the geophysical literature, the magnetic method is considered to be the oldest method applied in geophysical exploration. The Magnetic Phenomenon is force of attraction or repulsion due to electron arrangement in certain substances having magnetic properties. The magnetic body (magnet) is considered to be made up of small parts called (magnetic domains) which are lined up in the same direction. Unlike the case of gravity, the magnetic body has always two poles (dipole-body); one has attraction effect and the other has repulsion effect. An end-point of a long bar magnet can be considered as an isolated magnetic pole for certain computational purposes. The concept of line-force representing the magnetic field and the convention used in force direction relative to the magnetic poles are shown in Fig. 1.4.

Magnetic surveying, basically depends on the variation in the body-ability of being magnetized when exposed to a magnetic field. This property (called the magnetic susceptibility), differs with different materials. Sedimentary rocks are generally of small susceptibility values compared with metamorphic or igneous rocks. For this

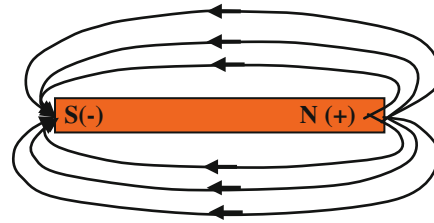


**Fig. 1.4** Magnetic poles of a magnetic body, are two points near magnet ends to which force lines are pointing; the North (+N) and South (-S) poles. Arrows indicate the conventional movement-direction of a unit positive pole placed in the magnetic field

reason, magnetic surveying is normally carried out to explore magnetized materials, such as iron-ore deposits, igneous intrusions, and surfaces of basement rocks. Rocks which have high-susceptibility mineral contents, acquire magnetic intensity by magnetic induction process. This leads to creating of a new magnetic field which is added to the already existing Earth ambient magnetic field. The field magnetic survey aims at recording of the measured magnetic field which is then subjected to processing and isolating the magnetic anomalies making them ready for interpretation. The value of the magnetic anomaly is proportional to the intensity of magnetization caused by the geological anomaly. After certain processing measures these anomalies are interpreted to reveal the causal geological structure.

The unit of magnetic-field measurement is the Oersted, where one Oersted is equal to one dyne per unit magnetic pole. In practice, another smaller unit ( $\gamma = 10^{-5}$  Oersted) is used. More recently an SI unit called nanotesla where 1 nanotesla is equal to 1 gamma. The SI (Système International) uses MKS measurement units. The total magnetic field of the Earth is about half an Oersted.

In petroleum exploration, aeromagnetic surveying are usually conducted to delineate major structural changes of areas such as sedimentary basins, and regional geological changes including mapping of sedimentary basins and major rift zones. On smaller scales, magnetic surveying can be used to detect magnetic minerals such as magnetite and other iron ore deposits. The

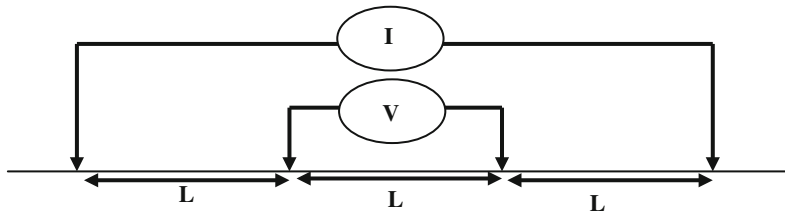


**Fig. 1.5** Principle of the Wenner configuration used in electrical resistivity surveying.  $I$  and  $V$  denote electric current and voltage respectively.  $L$  is the distance between electrodes

method is used to explore near-surface geological changes (such as dykes and sills). Another typical field of application of the magnetic surveying is exploration of buried archaeological objects.

As it is the case with all of the other exploration potential methods, the magnetic method suffers from the ambiguity problem in the interpretation process. The degree of uncertainty due to this problem is reduced by using additional independent geological information.

### 1.3.4 The Electrical Method

This method is based on the relationship between the electrical conductivity (or electrical resistivity) property and electrical current (or electrical voltage). Some electrical surveys are based on artificially-generated electrical currents while others are using the Earth naturally-generated electrical currents. These are summarized in the following table:

By artificial electrical field methods	By natural electrical field methods
(i) Electrical Resistivity	(i) Self Potential (SP)
(ii) Induced Polarization (IP)	(ii) Telluric Currents
(iii) Equipotential & Electromagnetic (EM)	(iii) Magneto telluric Currents

Electrical methods are mainly used for exploration of ore-bodies, minerals, ground water resources and for relatively shallow geological anomalies. Because of lack of deep penetration, its use for oil exploration is limited. Most of the methods are effective only for shallow depths which are not exceeding few hundred meters.

### Artificial-Source Electrical Methods

#### (i) Electrical Resistivity Surveying:

In the electrical resistivity method, a direct electric current (DC) electric, or very low frequency current (AC), is introduced into the ground. From the voltage drop measured over a defined distance, the effective (apparent) resistivity is mapped and then interpreted in terms of geological changes. The simplest field technique, called Wenner configuration, consists of two current electrodes and two voltage measuring electrodes as shown in Fig. 1.5.

The two approaches (forward and inverse) modeling processes are applied in interpreting resistivity data. The more widely used method is done by applying a trial-and-error method (model-analysis method). By comparing of the observed data with curves computed for defined geological models, a subsurface geological model is determined.

Resistivity surveying is particularly effective in exploring discontinuities as in determination of layering, faults, sills and dykes, especially when these are not too deep features. The method is usually applied in engineering geophysical studies, as in determination of the water table and other ground-water investigations.

#### (ii) Induced Polarization Surveying

The Induced Polarization method (IP method) uses the decay time of an electric potential, induced after an electric current fed to the ground, is switched off. The phenomenon is associated with electrochemical reactions activated by the electric current which disturbs the ion distribution in the affected ground material. The voltage level, attained due to the applied electric current, gets

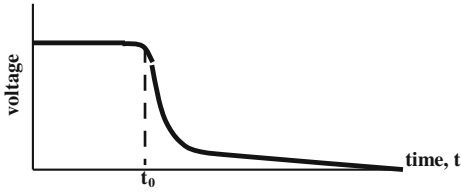


**Fig. 1.6** The procedure used in the IP method. Voltage drop after the applied electric current is switched off at time ( $t_0$ )

back to normal state after the applied electric current is suddenly stopped at a certain instant. The process is sketched in Fig. 1.6.

The method is used mainly for purposes of metallic minerals and ground water exploration. For the field surveying, the same electrode set up for resistivity is also used. Thus using four electrodes (called dipole-dipole array) is used in IP surveying. The polar dipole system is preferred where the voltage electrode spacing is decreased to minimize the effect of wire-currents.

### (iii) Equipotential and Electromagnetic (EM) Surveying

Equipotential surveying uses the electric potential generated by a fixed electric-current electrode while the electric potential is mapped by a moving electrode. Instead of using direct current (DC) electrodes, another method, the Electromagnetic (EM) method, uses an electric alternating current (AC) of few hundred-to-few kilohertz, induced into the ground by a source-coil and received by another coil, the receiver-coil. The transmitter coil induces an alternating (primary) magnetic field, while the receiver coil senses the ground-generated alternating (secondary) magnetic field combined with the primary. The combined magnetic fields induce AC in the secondary coil. This current is then measured and converted into the combined magnetic field at the location of the receiver. From comparison of the combined magnetic field with the primary magnetic field (which is known), the contribution of the anomalous body is determined and then interpreted into geological information.

In addition to ground surveying, there is the airborne EM surveying where the transmitter coil is fixed to the aircraft and receiver is mounted in

a “bird” trailed behind. The EM method is used for exploring base-metals and ground water accumulations.

### Natural-Source Electrical Methods

There is another less commonly applied electrical group of methods which are dependent on measurements of the earth natural electric field. Self Potential (SP), Telluric Current and Magneto-Telluric methods are typical examples of such techniques. These methods are used to determine large-scale crustal structural variations as sedimentary basins and regional-scale geological variations.

#### (i) Self Potential (SP) Surveying

Mineralized zones found in the upper part of the Earth crust and some ore bodies found at shallow depths, develop their own natural electric fields. In particular, a metallic sulfide body which has part of it above the water table and the rest of it, is below it. With this condition, such a phenomenon is created. The body acts as a natural battery where ions, due to differential oxidation, move from one part of the body to the other. The electrical currents are formed as a result of chemical reaction that takes place with the aid of the electrolytes present in the host medium.

The potential difference measured on the surface will map the potential anomaly caused by the body. The behavior of the electric potential due to presence of a sulfide body is shown in Fig. 1.7.

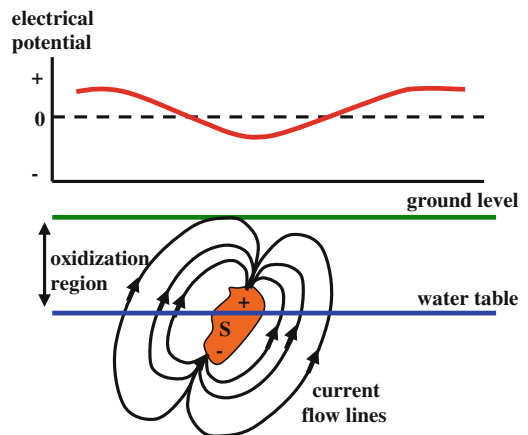


**Fig. 1.7** Sulfide body (S) acting as a natural battery, causing abnormality in the generated electrical potential

The SP method is typically used to map the electrochemical potential variations, generated by buried sulfide bodies.

#### (ii) Telluric Currents Surveying

The term (telluric currents) is used for the natural electric currents that flow horizontally in the upper part of the Earth crust. Variation of the current-density, over the earth surface is governed by the rock-resistivity changes. Thus, if a salt dome, for example, is found imbedded within relatively high conductivity-formations, the lines of currents flow will by-pass the salt body causing distortions in the potential gradient in the overlying surface cover. From the detected anomalous potential gradient, the geological changes causing the changes in the potential gradient, can be determined.

#### (iii) Magneto-Telluric Currents Surveying

Another related method, the so-called (magneto-telluric method), involves simultaneous measurements of both voltage created by the telluric currents and the magnetic field induced by these currents. Plots of the alternating voltage and that of the associated magnetic field (as function of frequency) can give information on the resistivity as function of depth.

#### (iv) Audio-Frequency Magnetic Surveying

There is still another closely related method which uses the audio-frequency variations in the Earth electric field, to study the earth resistivity variations. This method is called Audio-Frequency Magnetic method, termed (AFMAG) method.

### 1.3.5 The Radioactivity Method

Some naturally occurring substances, such as Uranium and Thorium, emit particles and radiation energy, as a result of atomic disintegration. These chemical elements are called (radioactive elements), and the phenomenon of the radiation, emitted in the form of particles and rays, is called (radioactivity). Three types of radiation (Alpha-, Beta-, and Gamma-radiation) are released in a radioactivity process. Radiation and energy characteristics of these types of radiation are

summarized in the following table (Maton et al. 1995, p. 269).

Radiation type	Radiation characteristics	Energy characteristics
Alpha particles	Positively-charged protons	Can be stopped by a sheet of paper
Beta particles	Negatively-charged electrons	Can pass through as much as 3 mm of Aluminum
Gamma rays	High-frequency electromagnetic waves	Can pass through several centimeters of Lead

All of the three types of radiation have the ionizing ability when colliding with atoms. This effect is the basis of radioactivity detection.

A detection instrument (the Geiger counter) was designed by Hans Geiger in 1928. It consists of a tube filled with an inert gas (helium or argon) at a reduced pressure. When radiation enters the tube, it removes electrons from the atoms of the gas, making them positively charged ions. The electrons move to wire in the tube, setting up an electric current which is amplified and fed into the recording device. The current produces clicking sound that pulsates at a rate which is depending on the radiation strength. A counting unit (counter), attached to the wire, measures the created current and gives a proportional radioactivity-reading.

## 1.4 Oil Well Drilling

Drilling of the oil exploration well is considered to be the last phase of any oil exploration project. This type of work provides the direct information as regards geological and geophysical properties of the subsurface rock medium. The obtained drilling data give direct recognition of the rock formations and their mineral and fluid contents (hydrocarbons and water). Associated with the drilling process, are certain activities which help in getting these useful data. Most important of these are laboratory analyses of the rock cuttings



**Fig. 1.8** A typical rotary drilling rig, set up for oil-well drilling operation

and from well cores. Also, drilling parameters and the well geophysical logging give valuable geological and geophysical information.

The common way followed in drilling is what is known the rotary drilling which is done by use of the drilling rig, especially designed to carry out this operation. A photo of typical oil-well rig is shown in Fig. 1.8.

#### 1.4.1 Drilling of the Exploration-Well

Since the first 69-ft oil-well (drilled by Drake in Pennsylvania, USA in 1859), drilling technology has witnessed great advances in the capability of drilling deep wells and in the control on the direction of the drilled well. Inclined wells and even horizontal drilling are now in common application.

Drilling of the first oil well after completing the geophysical exploration activities is called (Exploration drilling) or (Wildcat drilling). There are other types of drilling labeled according to the purpose of the drilled well. For instance, it is called Production drilling when the well is designed for normal oil production, and observation drilling for monitoring the behavior of the oil reservoir. Wells for water or gas injection are

especially drilled for injecting water or gas to enhance the reservoir pressure.

An exploration well provides the following useful information:

- Drilling parameters (like drilling rate) give indications on the physical nature of rocks penetrated by the drilling process.
- Rock cuttings and cores provide direct information on the rock lithology and thicknesses of the penetrated rock formations.
- Circulating drilling mud, cores, and cuttings provide indications of presence of hydrocarbons.
- Well logs (as electrical logs, radioactivity logs, and sonic logs) furnish valuable information on geological changes and on hydrocarbon contents.

#### 1.4.2 The Oil-Well Rotary Drilling

The common technique applied in drilling oil wells is what is called (Rotary Drilling). The drilling process is done by rotating a column of steel pipes, with a drilling head (called the Bit) attached to its end. The rotating bit carves a hole through the rocks and in this way a drill-hole is made. Drilling mud is pumped through the pipe, returning to surface via the space between the drill pipe and well wall. Mud circulation will carry rock cuttings to surface and provide cooling and lubrication to the drilling process.

Drilling operation is done by the drilling rig, which is a mechanical steel structure designed in the form of a tower of height of (120–150 ft). A schematically representation of a typical oil-well drilling rig, with its principal parts, are shown in Fig. 1.9.

The drilling rig, shown in Fig. 1.9, is made up of the drill tower (called derrick), drill pipes, drilling floor (Kelly Bush), and other facilities to provide energy for rotating the pipe column and to circulate the drilling mud. The grinding process is executed by the rotating bit attached to the end of the drill pipe. The more common types of bits are the grinding bits which produce rock cuttings that are removed by the circulating mud, and the coring tubular bits producing rock-cores.

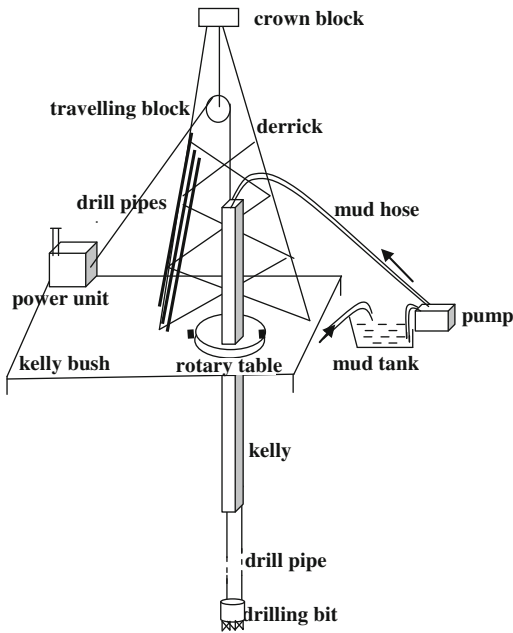


**Fig. 1.9** A simplified sketch showing the main parts of a rotary drilling rig

### 1.4.3 The Drill-Hole and Well Casing

During the drilling process, drilling mud is circulating carrying with it the produced rock cuttings. According to the extent of penetration into the well wall of drill-fluid, three types of zones are recognized. These are Fig. 1.10:

#### Mud-Cake Zone (MZ)

This is a thin coating of well-wall which is of few tenths of an inch.

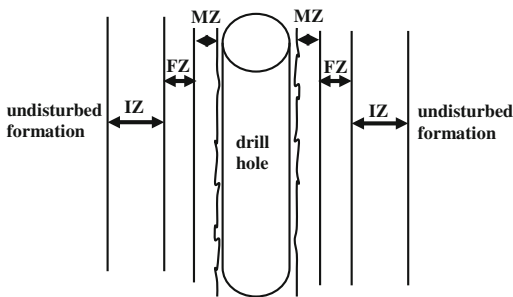


**Fig. 1.10** Mud invasion-zones into the well wall, labeled: mud-cake zone (MZ), flushed zone (FZ), and invasion zone (IZ)

#### Flushed Zone (FZ)

Natural fluid is completely replaced by the drilling fluid (several inches).

#### Invasion Zone (IZ)

Drilling fluid infiltrated into region surrounding the well (few inches as in shale to several feet as in porous sandstone).

After removing of the drill pipes, a pipe column is lowered into well, then cement is pumped in, to hold it tight in place. Casing prevents caving and fluid seeping. However, to allow oil and water to flow into well, the casing is later-on perforated at the appropriate places.

Electric logs cannot usually be run with casing and sonic logging is severely disturbed. In general all logging processes are carried out in uncased (open-hole) wells.

## 1.5 Well Geophysical Logging

After completion of the drilling operations of a well, a group of technical activities (well logging) are done to extract direct information on the rock formations penetrated by the drilling process. Study of the penetrated rock formations (commonly referred to as formation evaluation) includes examination of its contents of rock cuttings, detection of hydrocarbon matter, and documentation of lithological and palaeontological changes. The greater bulk of activities done at this stage is the geophysical logging of the drilled well which is always done as a concluding stage of the drilling operation of drilled exploration wells. Well logging gives direct determination of petrophysical properties of the penetrated rock formations. These are essential practices needed in the rock-formation evaluation and reservoir characterization processes.

The well log (or wireline log, as it is often referred to) is recorded by a special well logging tool (called the sonde), carrying sensors which are lowered into the hole by a cable. The standard procedure is to start the measurements at the bottom of the hole and moved upwards through the borehole. Measurement of a certain geophysical parameter is done either continuously or at discrete

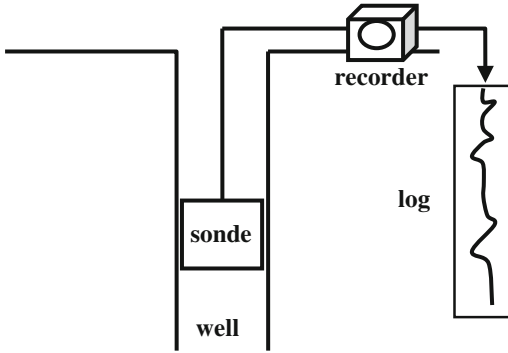


**Fig. 1.11** Principles of well logging

points. The output is recorded and normally produced as charts showing the value of the measured parameter as function of well-depth (Fig. 1.11).

The well logging process results in measurements-data normally plotted as charts called (well logs). Since it was introduced (by Schlumberger in 1928), the geophysical well logging technique has vastly developed into an indispensable formation-evaluation tool for the rocks penetrated by drill-holes. Logging methods can be divided into the three principal methods: electrical-, radioactivity-, and acoustic-logging.

### 1.5.1 Electrical Logging

Basically, electrical logging involves measurements of the variations of electrical resistivity and natural potential of rocks down the drilled well. Depending on the applied electrode configuration, the following techniques are in common use.

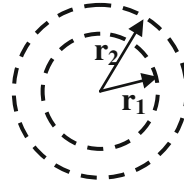
#### (i) Electrical Resistivity Logging

This type of electrical logging is based on a configuration whereby a DC (or low frequency AC) source electrode is lowered down the drill-hole and measuring the potential drop across a set of potential electrodes. The output is a continuous record of the variation of the electrical potential (or the corresponding apparent resistivity), with depth. This method must be applied in uncased wells.

Assuming spherical radiation of electric current is emitted from the point-source electrode,

the potential drop ( $\Delta V$ ) is related to the resistivity ( $\rho$ ) as follows:

From Ohm's Law we have, the potential ( $V$ ) across the radius ( $r$ ) of a sphere is expressed as ( $V = I R = I \rho r / 4\pi r^2 = I \rho / 4\pi r$ ),  $R$  is the electrical resistance.



Thus, over the separation distance ( $r_1 - r_2$ ), we get:

$$\Delta V = (I\rho/4\pi)(1/r_1 - 1/r_2) = I\rho/4\pi r_1 \quad (\text{for } r_2 \gg r_1).$$

Hence, resistivity ( $\rho$ ) is given by:

$$\rho = 4\pi r_1 \Delta V / I$$

There are two types of configurations, the normal-sonde and the lateral-sonde logging (Fig. 1.12).

The resistivity log expresses measurements of the electrical resistivity in the usual (ohm units) for the rock medium surrounding the drill-hole. Penetration distance of the electric field in the penetrated rocks depends on the electrode spacing-distance. The larger the electrode spacing, the greater is the penetration distance (Fig. 1.13).

The normal sonde electrode-configuration includes two electrodes: one source and one receiver spaced few feet apart. The instrument reading which is given in apparent resistivity units reflects the properties of the region near the source-electrode. The other type (the lateral-sonde configuration) is equipped with three electrodes; one source and two receivers. A variation was made on the lateral sonde whereby the current rays spread out horizontally (focused rays) rather than radially (unfocussed) spreading. This modified procedure is called (laterologging) and the produced resistivity chart is called (laterolog). The lateral logs give more accurate

**Fig. 1.12** The two types of electrode configurations used in resistivity well logging: normal sonde and lateral sonde configurations

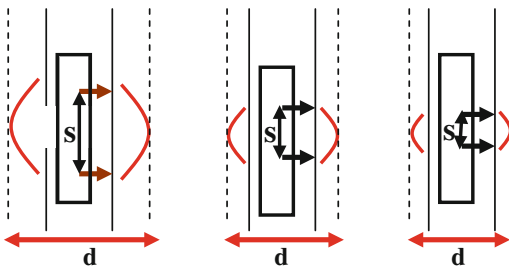
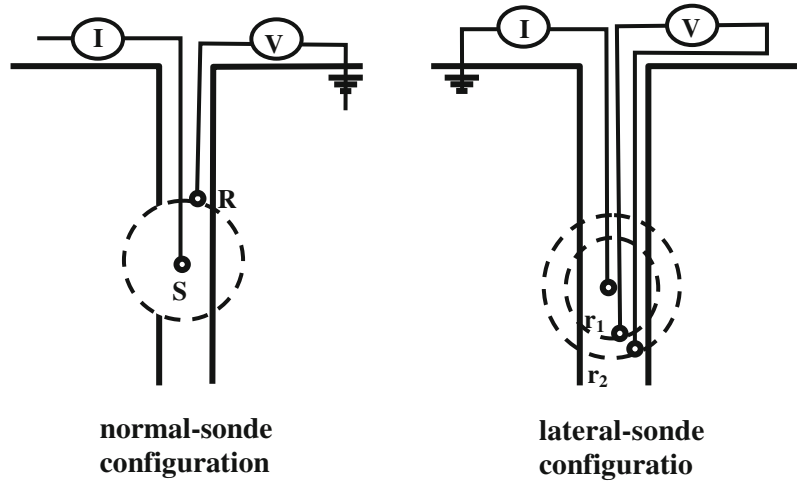


**Fig. 1.13** Lateral distance ( $d$ ) penetrated in resistivity logging is proportional to electrode spacing ( $s$ )

and sharper boundary detection, in addition to reduction of effects of the mud and hole-diameter variations.

Resistivity logs help in the diagnosis of types and boundaries of formations. For example, low resistivity indicates higher porosity and permeability of water saturated formations, whereas increase of resistivity can reflect existence of oil and gas. In general, low-porosity rocks (as shale) and porous rocks saturated with salty water exhibit low resistivity. On the other hand, porous rocks saturated with low-salt fresh water, or saturated with oil will exhibit high resistivity. On this basis, resistivity logs serve as important and effective indicators for presence of oil.

**(ii) Electrical Induction Logging**

The logging sonde uses coils instead of normal metal-piece electrodes. A primary coil carrying an AC current creates an alternating magnetic

field which induces electric currents into the rock formations. These currents, in turn, create secondary magnetic field which induces, in the receiving secondary coil, an AC which varies with the resistivity of the formations. The coil-sondes configuration is shown in Fig. 1.14.

Like lateral logging, there is a variation made on induction logging to give focused current radiation, for getting sharper boundary indication. Induction logging is used in wells filled with conducting, or non-conducting, drilling-mud.

**(iii) Spontaneous Potential (SP) Logging**

This logging method depends on measurements of the natural electric potential (in millivolt units) of the rock medium surrounding the surveyed well. It is normally referred to as self-potential or spontaneous potential (SP) logging. It is used

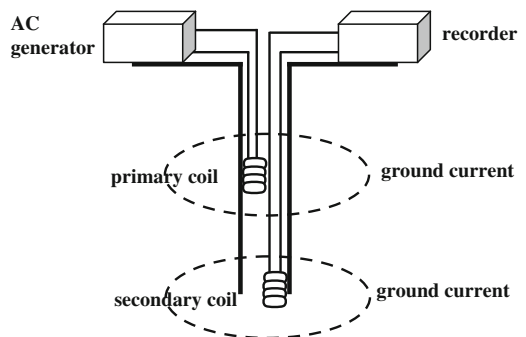
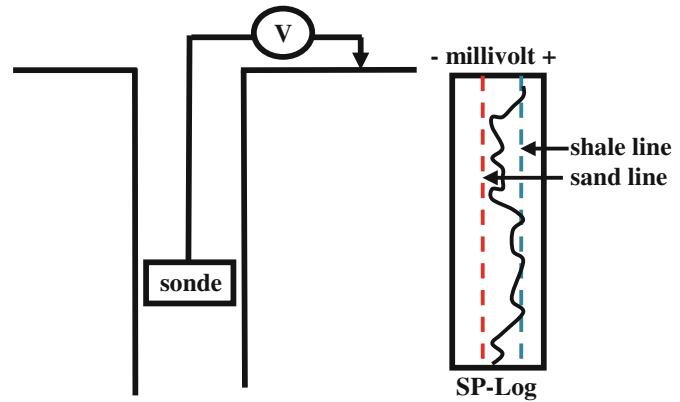


**Fig. 1.14** Coil-sondes configuration used in induction logging

**Fig. 1.15** Configuration used in spontaneous potential logging with schematic representation of the SP log



only in an uncased holes filled with conductive mud. The measuring sonde is of simple configuration. It consists of only two electrodes: one is lowered into the well by an insulated cable and the other is fixed at the ground surface (Fig. 1.15).

This method, which needs no artificial current, can detect natural potential differences which develop at formation boundaries. Compared with resistivity logs, the SP logs give more sharp changes and hence more accurate formation-boundaries. Like lateral logging mentioned above, there is a variation made on induction logging to give focused current radiation for getting sharper boundary indication.

Interpretation of the SP logs depends on the manner of the electrical potential variation. As a general rule, changing of the log values towards positive potentials is considered as an indicative of impermeable rocks as shale or tight limestone or tight sandstones. When the change is towards negative potential, it is interpreted as being due to porous sandstones or porous limestone. In this way, the SP logs give useful indications on lithology, water salinity and help in determination of formation boundaries. In particular, it shows the boundaries of formations in sand-shale sequences. These are determined with the help of drawing lines (sand and shale base-lines) in the produced SP log (shown in Fig. 1.15). It is commonly observed that shale beds give the same level of SP-readings allowing for drawing a straight line indicating shale SP-value. This is called (the shale line). Similarly a (sand line) can

be drawn for sandstone SP-value. The inflection points in the SP-log indicate formation boundaries.

### 1.5.2 Radioactivity Logging

Radioactivity is the phenomenon of emission of particles and photons of electromagnetic energy from an atom. This radiation process occurs either naturally from unstable nuclii or induced by bombarding of stable nuclii by photons or atom particles. Examples of such radioactive elements are Uranium, Thorium Rubidium and Potassium 40 which is most commonly found in shale and clay and less in sandstone and limestone.

There are three types of radiation: Alfa particles formed of charged helium nuclii, Beta particles formed of high speed electrons, and Gamma rays of electromagnetic wave-energy. Out of these, only gamma ray is used in well radioactivity logging. The detection instrument is a Geiger or more usually is the scintillation counter which consists of a special crystal (like sodium iodide), which emits flashes of light as they absorb gamma-ray photons, hence the name (scintillation counter). A photoelectric tube converts these flashes into electric currents which are displayed in the form of a continuous chart (the radioactivity log).

Radioactivity logs provide important information on rock lithological types, especially on those containing certain concentrations of

radioactive minerals. Thus, these methods are ideal indicators of shale and clays which, by nature, contain radioactive minerals in their makeup.

Three methods of gamma radioactivity logging are in common use. These are: Natural Gamma-ray, Gamma-ray rock-density, and neutron Gamma-ray Logging methods.

### (i) Natural Gamma-Ray Logging

This method uses a detector mounted on a sonde to measure the naturally emitted gamma rays from the radioactive minerals existing in the rock formations. Unlike electrical logging, gamma-ray logging can be run in cased wells, as well as in uncased wells, with detection penetration of few feet from the well walls. The resolution power of formation-boundaries is affected by the counting time of the instrument and sonde logging speed. Reasonable results are obtained with a counting time of 2 s and sonde speed of 15 cm/s. Measurements can be made in cased wells, but the intensity of radiation is reduced by about 30 % in this case (Kearey and Brook 2002, p. 244).

In general, log values are interpreted as increase of the shale percentage, while the fall in the log-values is interpreted as indication for sandstones and limestone rocks. To aid interpretation, it is possible to draw shale-lines and sand-lines on the log chart. An advantage of the gamma log is its capability of differentiating between shale and sandstones independent of the porosity and permeability characteristics of the rocks.

### (ii) Gamma-Ray Rock-Density Logging

The sonde contains a gamma-ray source and a scintillation counter to detect the gamma-ray which is back-scattered from the formations and received by a detector fixed at a certain distance from the source. It is also called (gamma-gamma logging) method.

The gamma-ray photons collide with the electrons of the elements in the formation resulting in loss of photon energy and back scattering of gamma-ray which has a wavelength different from that of natural gamma-rays. This is called (Compton Scattering Effect). The collision

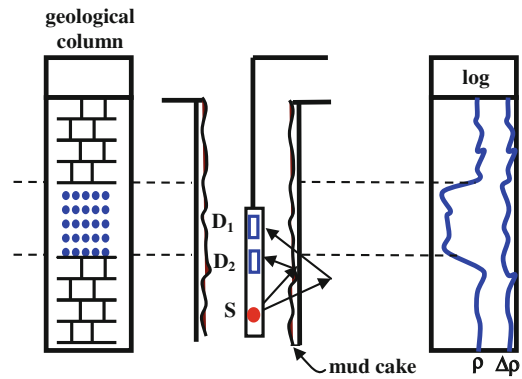


**Fig. 1.16** Principle of gamma-gamma log recording. Detectors, ( $D_1$ ) and ( $D_2$ ) record secondary and mud-cake radiations respectively and the symbol ( $S$ ) represents the source. Logs ( $\rho$ ) and ( $\Delta\rho$ ) represent bulk density and mud-cake correction respectively

rate and the back-scattered (secondary radiation) are proportional to electron density which is, in turn, proportional to rock-formation density. The principle of the gamma-gamma logging is shown in Fig. 1.16.

In practice, the gamma-ray detector is shielded to record only the secondary radiation, and the sonde is firmly pressed to well-wall and moved slowly (less than 30 ft/min) in order to maintain good contact. The produced chart (gamma-gamma log) expresses the formation-density log.

A variation to the method is introduced to provide corrections for mud-cake effect. As shown in the figure, above, a secondary detector  $D_2$  is included in the sonde which is responding to mud-cake and small wall irregularities. The resulting log (called Compensated Density Log) shows both of the bulk density ( $\rho$ ) and the density-correction log ( $\Delta\rho$ ).

Interpretation of the density log is based on the direct proportionality existing between the recorded scattered gamma ray intensity and the number of electrons found in the scattering rocks. The number of the scattered electrons is, in turn, proportional to rock bulk density.

This type of log can be used in computing porosity ( $\phi$ ) by using the following relationship:

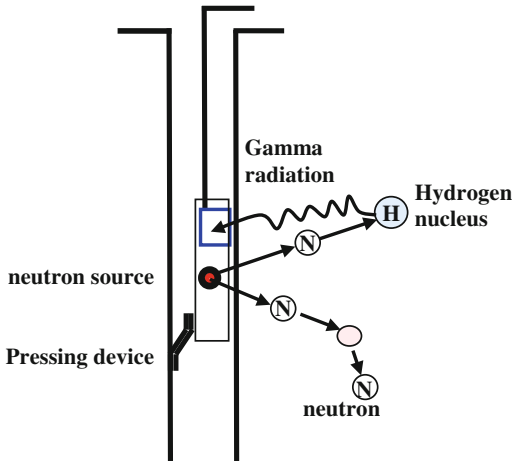


**Fig. 1.17** Principle of Neutron Gamma-Ray logging

$$\phi = (\rho_m - \rho_f) / (\rho_m - \rho_f)$$

where,  $(\rho_m)$ ,  $(\rho_f)$ , and  $(\rho_f)$  represent matrix density, log read-density, and pore fluid density respectively.

### (iii) Neutron Gamma-Ray Logging

The sonde consists of a neutron source and detecting scintillation counter placed at a fixed distance apart. The source is a small radioactive body (such as Plutonium-Beryllium) which emits neutrons during the process of radioactive decay.

When the source-generated neutron collides with a hydrogen nucleus (which is of a matching mass) its kinetic energy is reduced to an extent that it can be captured by a large nucleus (as the hydrogen nucleus) causing emission of a secondary gamma radiation (capture gamma radiation). The principle of the logging is sketched in Fig. 1.17.

In the logging process, the sonde is moved at a speed of 30 ft/min with 2 s for the counting time. A skid (pressing device) is provided to keep the sonde in close contact to the wall. The gamma radiation, generated by the capturing-phenomenon, comes from the material surrounding the drill-hole. The produced log (which can be run in a cased or non cased well) is

displayed in the appropriate measuring units or in porosity percentages directly.

The intensity level of measured radiation is proportional to concentration of hydrogen, which exist in water, in hydrocarbon, and in hydrous minerals such as silicate-clays, micas, amphiboles, and gypsum. Thus in carbonates and sandstones, hydrogen source is water and hydrocarbon found in the pores of the rock. In shale, however, mica and clay minerals contribute to hydrogen content as well as from pore water. In this case other types of logs (e.g. gamma-ray logs) are needed to distinguish shale from water-saturated porous sandstones or limestones. In general neutron logs are best in following up the porosity variation of porous rocks using the direct proportionality between porosity and gamma-ray intensity-level.

In short, Neutron logs, depend on the gamma-ray generated from neutron bombardments of hydrogen atoms. The generated gamma ray, which is proportional to concentration of the hydrogen element in the penetrated rocks, is dependent on the water and hydrocarbon fluids in the rocks. This also means that high log values indicate high porosity. It is useful to note that in case of presence of hydrocarbon gas in high porosity formations, density logs (gamma-ray rock density logs) is expected to give low log values compared with the neutron log vales at the same zone, where the neutron readings expected to be relatively high. This means that both of the logs (density and neutron logs) are necessary in order to detect hydrocarbons (oil or gas).

## 1.5.3 Acoustic Logging

The purpose of this type of logging is basically for getting information on velocity of propagating acoustic (seismic) waves. Sonic logging, well velocity surveying (well shooting) and VSP surveying are included in this type of well-logging.

### (i) Sonic Logging

The logging sonde, in its standard form, consists of two receivers about 1 ft apart and a source at

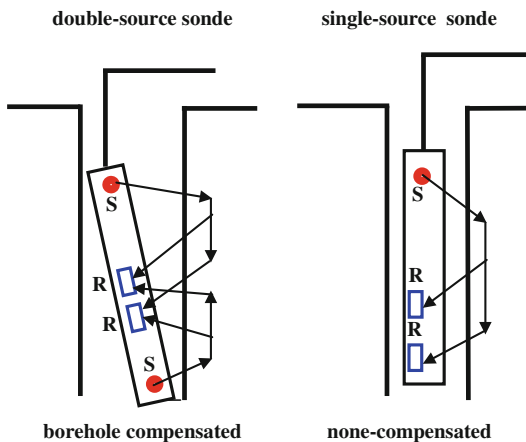


**Fig. 1.18** Configuration of source (S) and receiver (R) of the sonde employed in sonic logging

about 3 ft from the nearest receiver. To correct for tilting and hole-irregularities effects, a dual source sonde is used, making what is called a borehole-compensated sonde (Fig. 1.18).

The electronic structure of the sonde is designed in such a way, that the output is made to be the difference in the travel-times to the two receivers. The time difference, measured in time-units per 1-ft, called (interval transit time), is plotted (normally in micro seconds) against depth to give the continuous wiggly curve known as the (sonic log). In the compensated sonic logging, seismic pulses are emitted alternately from the two sources and the transit times from the two oppositely traveling refracted P-waves are averaged electronically. The output (transit time) is plotted against depth, giving the borehole-compensated (BHC) sonic log (Fig. 1.19).

The borehole compensated sonde (BHC) gives an average interval transit time which is plotted on a paper strip. The produced log in this case is normally referred to as BHC sonic log which is used to identify lithologies, determine formation boundaries, and in computing synthetic seismograms. The interval transit time can be integrated down the well to give the total travel time. This type of logging can only be run in an open (uncased) hole.

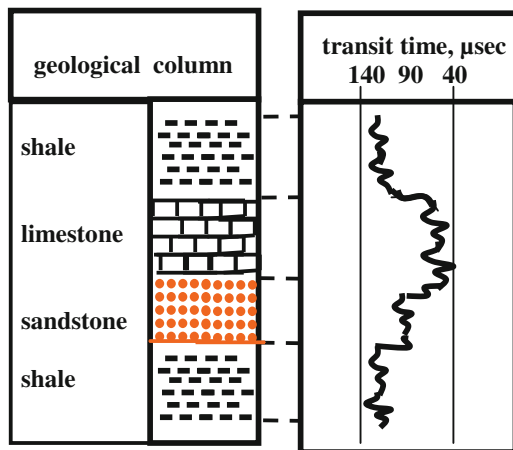


**Fig. 1.19** Sketch sonic log of a hypothetical geological column

Sonic logs provide the interval transit time which represent travel-time (usually in microsecond units) of the P-wave in covering a distance (usually 1 ft). This parameter (the interval transit time) is useful in computing the porosity ( $\phi$ ) by using the following relationship:

$$\phi = (\Delta t_f - \Delta t_m) / (\Delta t_f - \Delta t_l)$$

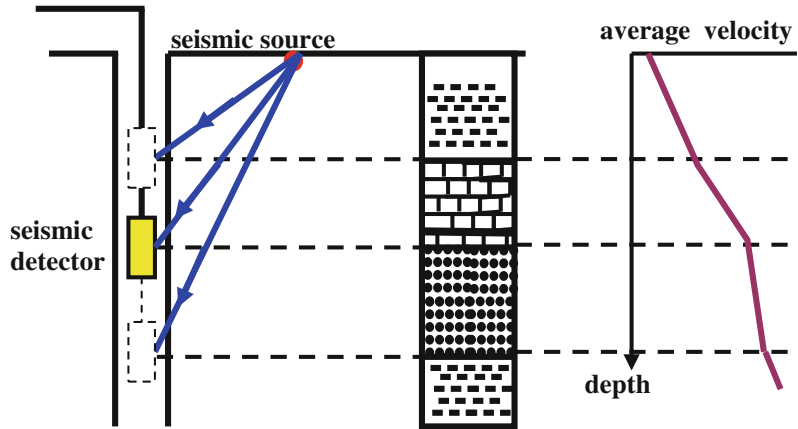
where,  $(\Delta t_m)$ ,  $(\Delta t_f)$ , and  $(\Delta t_l)$ , represent transit times of matrix material, of pore fluid, and log read-transit time respectively.

(ii) **Well Velocity Surveying**

A hydrophone-type detector is lowered down the well which is filled with the drilling fluid. The travel time of the seismic wave generated by a surface-placed shot and received by a detector placed at a formation boundary is recorded. The full log is obtained by repeating the recording at each boundary traversed by the well. From the measured travel time of direct arrivals, the average velocity and interval velocity are plotted as function of well-depth. The velocity survey is also called (check-shot survey). Principle of the velocity survey setup and velocity-depth plot is shown in Fig. 1.20.

The obtained velocity information is used to calibrate the sonic log and check the sonic-log

**Fig. 1.20** Principle of the well velocity surveying and a typical velocity-depth plot obtained from the survey



integrated time (hence the name, check-shot surveying).

**(iii) Vertical Seismic Profiling (VSP)**

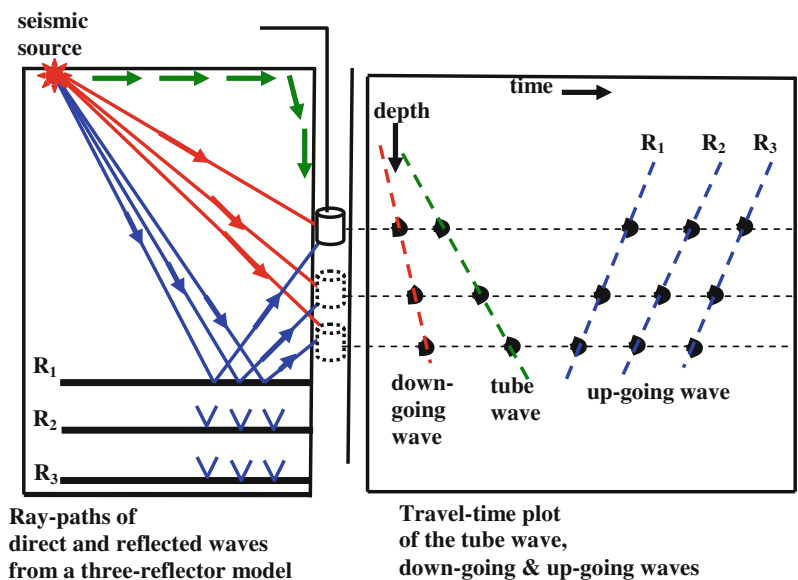
Basically the measurement set-up is the same as the check-shot recording system. The difference is in the recording duration time which is here extended to allow recording reflected waves as well as the direct arrivals. At each detector stop-location (normally at 25 m spacing), the recorded seismic trace is allowed to include events from up going reflected waves in addition to the first arrival (direct wave) event. The terms (down-going wave) and (up-going wave) are

normally applied to refer to the direct and reflected waves respectively. The ray paths of the VSP shooting and the corresponding travel-time plot of the recorded waves are schematically shown in Fig. 1.21.

A seismic pulse is generated on the surface from dynamite explosion or from an air gun submerged in a water filled hole. This is repeated at all of the hydrophone positions, normally positioned at 25 m-spacing down the well.

With an appropriate processing sequence, the final corrected VSP section is produced. Processing includes, data editing, correction to vertical time and velocity filtering for separating unwanted

**Fig. 1.21** Ray-path diagram and the corresponding travel time plot of a VSP survey of a geological model made up of three reflectors



events. It is evident from the VSP section that downward events (primary and multiples) increase in time with depth, and the upward events (primary and multiples) decrease in time with increasing depth. By arranging the produced seismic traces (25 m spaced down the hole) a seismic VSP section is obtained. Each seismic trace of a VSP section contains events from down-going waves (direct and multiples arrival) and from up-going waves (reflections and multiples).

The main application of VSP is providing seismic section of reflectors which have not been reached by the drilling. In fact the VSP data are equivalent to both the check-shot data and the sonic-derived synthetic seismogram.

#### (iv) Other Logging Techniques

Some logs are used to give geometrical information on the deviation from the vertical (hole-drift angle) as well as the azimuth of the deviation. Other logs are made to give the bedding dip (dip-meter logs) and measurements of the well-hole diameter (caliper logs).

On more limited scale of application, other types of well logging have been used. Specially modified borehole-gravimeters, magnetometers, and thermometers are examples of such tools. Geothermal prospecting is applied to detect geological features which affect heat flow such as shallow salt domes, faults and dykes. Also ground water is investigated by this method.

### 1.5.4 Log Interpretation

The process of analysis and interpretation of well logs is sometimes called (Formation Evaluation). Normally all the logs obtained for a well and their analysis-results are presented in one combined display called the (composite log). This comprehensive log usually contains all (or most) of the following log data:

- Geological column showing lithological and palaeontological information
- Borehole compensated sonic log
- Gamma-ray and Neutron logs
- Resistivity and SP logs

Drilling information (drilling rate, mud density variation)

Caliper and dip-meter logs.

The main information which can be obtained from well logs can be summarized as in the following table

Log Type	Application	Comment
Electrical Logs <ul style="list-style-type: none"> <li>• Resistivity</li> <li>• Induction</li> <li>• Spontaneous Potential</li> </ul>	<ul style="list-style-type: none"> <li>• Fluid-type identification</li> <li>• Porosity evaluation</li> <li>• Boundary determination</li> <li>• Shale and sand lines</li> </ul>	Logging is done in uncased wells
Radioactivity Logs <ul style="list-style-type: none"> <li>• Natural gamma-ray</li> <li>• Gamma-ray density</li> <li>• Neutron gamma-ray</li> </ul>	<ul style="list-style-type: none"> <li>• Shale/sandstone</li> <li>• Formation density</li> <li>• Porosity</li> <li>• Fluid type</li> </ul>	Logging is done in cased wells
Acoustic Logs <ul style="list-style-type: none"> <li>• Sonic logs</li> <li>• Well velocity</li> <li>• VSP</li> </ul>	<ul style="list-style-type: none"> <li>• Lithology types</li> <li>• Formation Boundaries</li> <li>• Synthetic seismograms</li> <li>• Seismic-velocity functions</li> <li>• Reflection identification</li> </ul>	Logging is done in cased and in uncased wells

### 1.6 Latest Developments in Well Logging

Since the introduction of well logging by Schlumberger brothers in 1927, logging techniques passed through a series of advances which are concerning measurements approach and measurement accuracy. The new techniques, aided with the specialized computer software, have led to increased work efficiency and increased detection resolution. The two prominent developments happened to the logging techniques are the logging while drilling (LWD) procedure and borehole imaging tools.

### 1.6.1 Logging While Drilling Technique

In late 1980s a new logging procedure, logging while drilling (LWD), was introduced. This technique is similar to the conventional wireline logging except that it (the LWD) uses sensors which are incorporated in the drilling bit assembly, and thus the measurements are made during the drilling process. This measurement procedure coupled with specialized computer software provides fast geological information as lithology, porosity, fluid contents, and drill-hole direction.

### 1.6.2 Borehole Imaging Tools

Borehole imaging is a logging technique that can provide small-scale images of the borehole wall and the penetrated rock lithology. One of these methods (based on electrical micro-imaging processes) was developed by Schlumberger under the trade-name; formation micro-imaging (FMI). In 1986, Schlumberger developed a dip-meter called the formation micro-scanner (FMS). Later versions of this logging tool were called formation micro-imager (FMI) which is based on micro-resistivity measurements.

The operation of the FMI tool is based on recording changes (and not absolute values) in electrical resistivity of rock formations. It provides, with high resolution power, identification of sedimentary characteristics and fracturing picture in the penetrated rock column, in addition to measuring formation dip.

## 1.7 Well Completion

Well completion in petroleum production, is the process of making a drilled well ready for production (or fluid injection). This principally involves preparing the bottom of the hole to the required specifications, running in the central production tubing and its associated down-hole tools as well as perforating and stimulating as required. Sometimes, the process of pipes

running-in and cementing the casing is considered as integral part of the completion process.

To prevent caving in of the well walls, drilling is stopped at various depths, and a steel pipe (casing) is lowered into the well and fixed in position by pumping cement mixture in the space between the casing pipes and the well walls (cementing process). According to the planned drilling program, drilling after casing being cemented is continued with a different (usually smaller) bit-size. At this stage, the drilled hole is lined by the appropriate casing which is likewise cemented in. The drill-casing-and-cementing phases are repeated until the final planned total depth is reached. The end result of the casing operations is a set of concentric pipes each of which is ending at the earth surface. When the planned total depth is reached, all used drill pipes including the attached drilling bit, are withdrawn. The next operation is perforation of the parts of the casing facing the oil bearing formations. The so-produced holes are made to allow the oil to

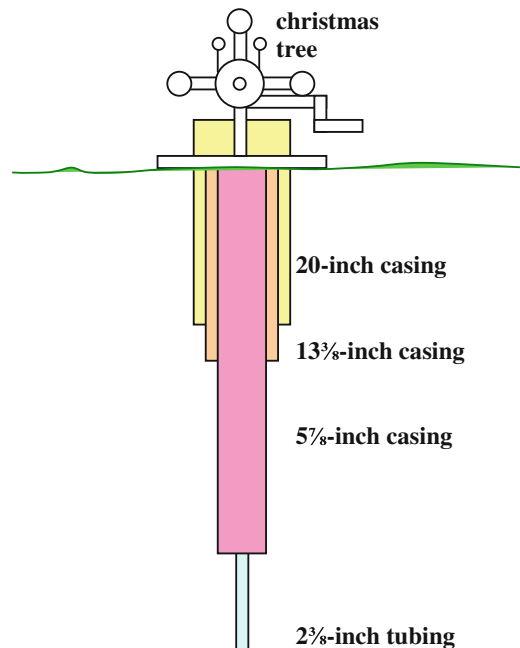


**Fig. 1.22** The final setup of the drilled well after casing and installment of the well head monitoring gauges (the Christmas tree)

seep inside the central production tubing of the well.

The last stage in preparing the well for the production process is fixing of a group of flanges which provide a sealing structure connecting together all the surface ends of the casing tubes. This part of the well which contains pressure

equipment in addition to the mechanical system that provide the blowout prevention (BOP) is called the well head which is also equipped with an assembly of valves that controls flow, and any other possible interventions. This assembly is normally referred to as the Christmas tree (Fig. 1.22).

---

## 2.1 The Fundamental Conditions

An application of an external force, on part of a medium (elastic medium), leads to creation of internal opposing forces which intend to resist the deformations caused by that external force. Typical forms of the resulting deformations are changes in volume and/or in shape which are created at the affected location. In consequence, the medium will return to its original condition after the external force is removed. This property of resisting of changes in volume and in shape and return to original conditions after removal of the external force is called (elasticity). Provided that the changes are small, rock media in nature are considered to be perfectly elastic in nature.

As a result of the elasticity property of media, the changes (volume and shape changes) oscillate about their neutral positions and, at the same time, propagate away from the energy source-location. Energy transfer in this manner (motion that leaves out no permanent distortions) is commonly referred to as (wave motion).

The fundamental condition for the creation and propagation of seismic waves (seismic field) is a source of mechanical energy of impulsive type which is initiated within an elastic medium. The energy source may be natural (as in earthquake-generated waves) or artificial (as in firing of a dynamite charge). In both cases wave

motion of elastic waves are generated and can be recorded by the appropriate detection instruments. These are normally referred to as the (seismic waves).

---

## 2.2 Theory of Elasticity

As it is stated above, the fundamental conditions for a seismic field to be created is that the medium must possess the elasticity property. Two main concepts are governing the propagation of seismic waves in an elastic medium: the (stress) and the (strain). Stress represents the external force applied to the elastic medium, and strain is the resulting changes in volume and in shape. The relation between stress and strain, for a particular medium (perfectly elastic medium), gives evaluation expressions for the elasticity property of that medium. The stress-strain proportionality constants are the elastic coefficients which serve as measures of the elasticity of a particular medium.

The principal types of changes experienced by a medium due to passage of a seismic wave are re-distribution of the internal forces (stress changes) and modification of the volume and geometrical shape (strain changes). The theory of elasticity deals with analysis of these principal effects and the related physical changes.

### 2.2.1 Stress

In the broad sense, stress is represented by a force (called traction) which is acting on a finite area occupying an arbitrary position within the medium. However, for more precise definition, the stress ( $\mathbf{T}$ ) is defined to be a limiting value of the ratio of a force ( $\mathbf{F}$ ) acting on an elementary area ( $\Delta\mathbf{A}$ ) which is diminishing to zero. That is:

$$\mathbf{T} = \lim_{\Delta\mathbf{A} \rightarrow 0} (\mathbf{F}/\Delta\mathbf{A})$$

In general, the stress ( $\mathbf{T}$ ) is a vector that can be resolved into components parallel and perpendicular to the area ( $\Delta\mathbf{A}$ ). The normal component ( $\mathbf{T}_z$ ) is called the normal stress or dilatational or pressure stress as it is sometimes called. The other two components ( $\mathbf{T}_x$  and  $\mathbf{T}_y$ ) which are in the plane of the elementary area, are called tangential or shearing stresses (Fig. 2.1).

The stress system within a body is completely defined if, at each point in that body, the normal stress and the two shearing stresses are all determined for three mutually perpendicular plane areas.

It follows, therefore, that nine stress components are needed to completely define the stress at a given point. This nine-component set constitutes what is known as the (stress tensor) at that point. Once the nine components are defined at a certain point (with respect to a given area-set) it is possible, through suitable mathematical transformation, to determine the stress with respect to any other area-set defined for that point.

The three mutually perpendicular elementary areas, called an (area set), and the nine components of the stress tensor is shown in Fig. 2.2.

A stress component may be represented by ( $T_{ab}$ ) where a (=x, y, z) stands for the area-set and b (=x, y, z) for the direction of the component. Using this convention, the nine components of the stress tensor (shown in Fig. 2.2) may be written as in Table 2.1.

For a stressed body which is in equilibrium (i.e. experiencing no rotation), it can be shown (see Bullen 1965, p. 10) that, due to the symmetry of a stress tensor acting on a body in a state of equilibrium, we have  $T_{ab} = T_{ba}$ . Applying this property to this stress system, we get reduction in the number of the components to a total of six components which are independent of each other. That is Table 2.2:

These six components are sufficient to define the stress system at a point within a stressed body. Further simplification is possible if the three areas of an area-set are chosen such that the normals to these areas are coincident with the directions of the normal stresses. With this kind of set-up the shearing components will all reduce to zero leaving only the components ( $\mathbf{T}_{xx}$ ,  $\mathbf{T}_{yy}$ ,  $\mathbf{T}_{zz}$ ) for the definition of the stress system. In such a case, when the shear components become all equal to zero, the components ( $\mathbf{T}_{xx}$ ,  $\mathbf{T}_{yy}$ ,  $\mathbf{T}_{zz}$ ) are referred to as the principal stresses.

For the simple one-dimensional case, when a force ( $\mathbf{F}$ ) is acting uniformly at the cross-sectional area ( $\mathbf{A}$ ) of a bar or a metal wire, stress is defined as the force per unit area of the cross sectional area, ( $F/A$ ). This stress is called tensile stress when the force is a pull-force and it is called compressive stress when it is a push-force.

Units of stress is the same as those used in measuring pressure (force per unit area), and in the SI unit system the unit is Newton per square

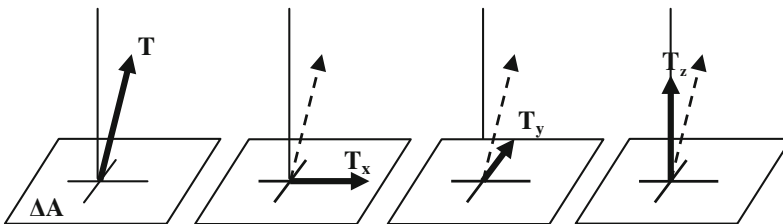
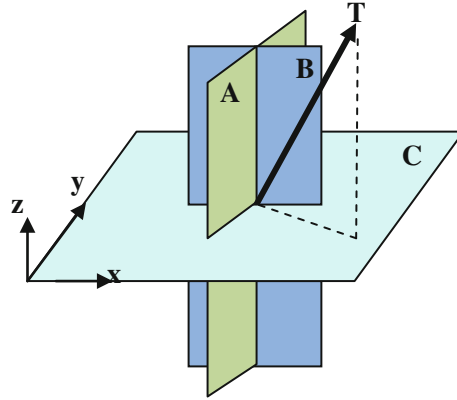


**Fig. 2.1** Stress ( $T$ ) and its components ( $T_x, T_y, T_z$ ) acting on the elementary area ( $\Delta A$ )

**The three mutually perpendicular areas (A, B, C)**



**The three stress components ( $T_x$ ,  $T_y$ ,  $T_z$ ) per each of the three areas (A, B, C)**

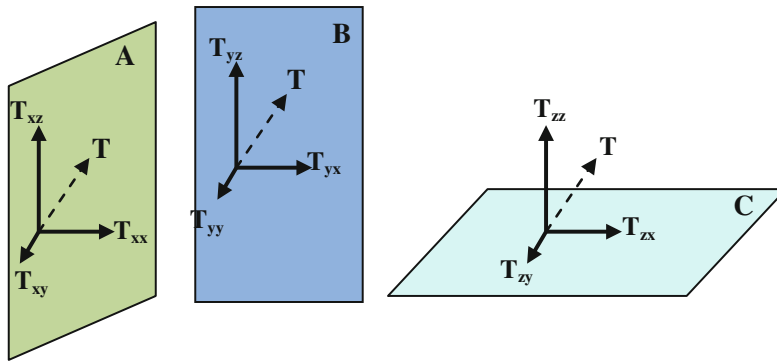


**Fig. 2.2** The stress components. The mutually perpendicular planes (A, B, C) making up the area-set and the nine components of the involved stress tensor

**Table 2.1** The complete nine components of the stress tensor

Stress component along the:	Area (a) perpendicular to: x-axis	Area (b) perpendicular to: y-axis	Area (c) perpendicular to: z-axis
(a) x-axis	$T_{xx}$	$T_{yx}$	$T_{zx}$
(b) y-axis	$T_{xy}$	$T_{yy}$	$T_{zy}$
(c) z-axis	$T_{xz}$	$T_{yz}$	$T_{zz}$

**Table 2.2** The six independent components of the stress tensor

Stress component along the:	Area (a) perpendicular to: x-axis	Area (b) perpendicular to: y-axis	Area (c) perpendicular to: z-axis
(a) x-axis	$T_{xx}$		
(b) y-axis	$T_{xy}$	$T_{yy}$	
(c) z-axis	$T_{xz}$	$T_{yz}$	$T_{zz}$

meter (N/m<sup>2</sup>) which is called Pascal, where one Pascal is equal to 1 N/m<sup>2</sup>.

### 2.2.2 Strain

In reference to Fig. 2.3, let us consider the two points (P<sub>1</sub> and P<sub>2</sub>) located within an unstressed body, where the first point, P<sub>1</sub> is located at (x, y, z) and the second point (P<sub>2</sub>) at (x + dx, y + dy, z + dz). Now, we let this body to deform as a result of a stress system created within it. If the two points (P<sub>1</sub> and P<sub>2</sub>) were displaced from their original positions by equal displacements (D, say), then it is considered that there is no strain taking place. Strain occurs only when there is variation of displacement of any point, within that medium, with respect to the others. In the language of mathematics, we say that strain depends on the derivatives of the displacement-components with respect to the chosen coordinates (x, y, z). The concept is clarified in Fig. 2.3.

In general, when a body is subjected to elastic stress, both of its size and shape will change. As it is mentioned above, the resulting changes represent elastic strains when each point of the stressed body experiences a displacement of its own which is different from the displacements experienced by the other points of the body. This implies that there are two types of strains, namely the “volume strain” and the “shape strain” (Fig. 2.4).

### 2.2.3 Common Types of Strain

Mathematical analyses of strain show that the total strain of a three dimensional body, depends on only six different derivatives of displacements. These strain components (e<sub>ab</sub>), can be written down as follows (Richter 1958, p. 236):

$$\begin{aligned}
 e_{xx} &= \partial D_x / \partial x \\
 e_{yy} &= \partial D_y / \partial y \\
 e_{zz} &= \partial D_z / \partial z \\
 e_{xy} &= (\partial D_x / \partial y + \partial D_y / \partial x) / 2 \\
 e_{xz} &= (\partial D_x / \partial z + \partial D_z / \partial x) / 2 \\
 e_{yz} &= (\partial D_y / \partial z + \partial D_z / \partial y) / 2
 \end{aligned}$$

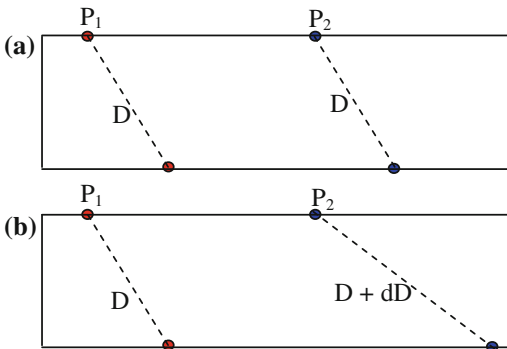


**Fig. 2.3** Displacement of two adjacent points in a medium under stress. **a** Case of equal point-displacements giving no-strain state. **b** Case of different point-displacements giving the strain state

These equations represent two groups of strain components of a strained elastic body. The first group (e<sub>xx</sub>, e<sub>yy</sub>, e<sub>zz</sub>) involve purely translational displacement resulting in compressional or dilatational strain. The second group (e<sub>xy</sub>, e<sub>xz</sub>, e<sub>yz</sub>) involve purely rotational deformation resulting in shear strain. As it is stated in our discussion of stress, the compressional (or dilatational) strains are called (principal strains) when the shearing strains are all of zero values. Common types of strains are cases of compression, bulk contraction, tension, and shear strains.

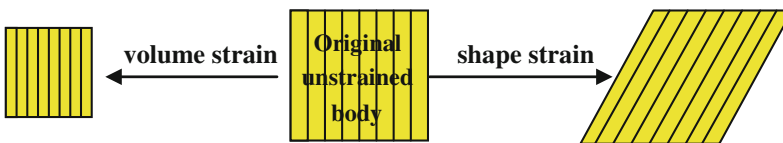
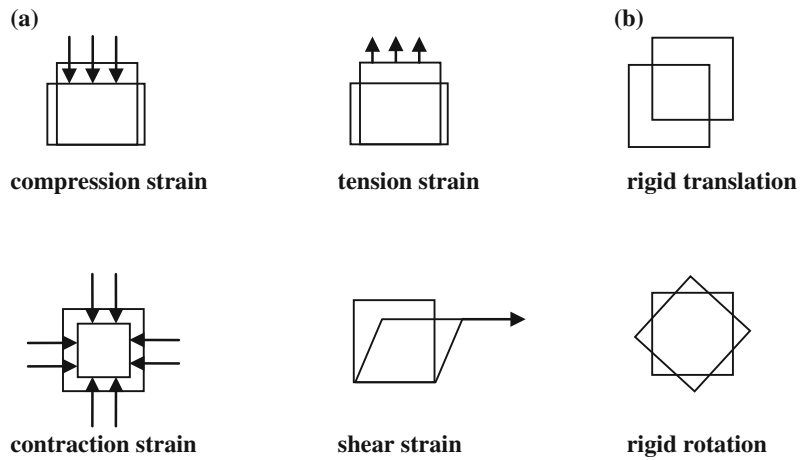


**Fig. 2.4** The two types of strain; “volume” and “shape” strains

**Fig. 2.5** Types of simple strains (a) and no-strain changes (b)



Rigid body-translation and rotation represent cases of no strain, since no volume and no shape deformation are involved. In Fig. 2.5, an elementary cube (shown here in plan) is used to show simple types of elastic deformation (strain) and no-strain changes.

In general, an elastic body under stress can experience two types of distortions; changes in volume and changes of shape. These changes, which occur as result of stress, are expressions of the physical properties of the stressed body. In its simple form, elastic strain can be divided into two main types. These are: the volume-changing strain (leading to body compression or dilatation) and the shape-changing strain (leading to body shape distortion).

**2.2.4 The Volume-Changing Strain**

The familiar example on this type of strain is the longitudinal strain of a body under an extensional

(or compressional) stress. The longitudinal strain (e) is defined to be the change in length in a certain dimension, of a body under stress relative to its original length. For a rectangular lamina of dimensions ( $\Delta x$  by  $\Delta y$ ), the longitudinal strains ( $e_x$  and  $e_y$ ) in the  $x$  and  $y$  directions are defined as (Fig. 2.6):

The longitudinal strains can be extensional (tensile strain) or compressional (contraction strain). Longitudinal strains ( $e_x$  and  $e_y$ ) are defined as:

$$e_x = D_x / \Delta x$$

$$e_y = -D_y / \Delta y$$

where ( $D_x$  and  $D_y$ ) are the changes in length in  $x$  and  $y$  directions respectively.

The minus sign that appeared in the  $e_y$  expression is entered to denote that the change ( $D_y$ ) is compression which is in opposite direction to the dilatation change ( $D_x$ ), in the  $x$ -direction.

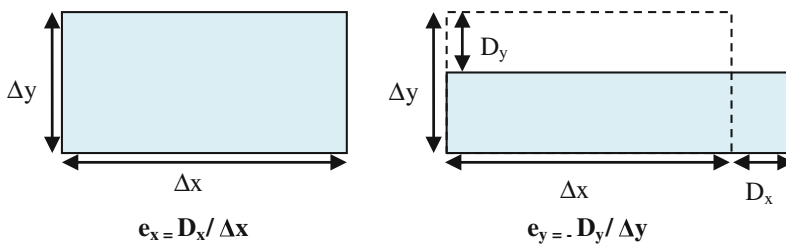


**Fig. 2.6** Definition of the longitudinal strain as applied for a rectangular lamina of dimensions ( $\Delta x$  by  $\Delta y$ )

**Fig. 2.7** Concept of shear or angular strain,  $e_{xy}$  where:  
 $(e_{xy} = (\alpha + \beta)/2$   
 $= (D_x/\Delta y + D_y/\Delta x)/2$

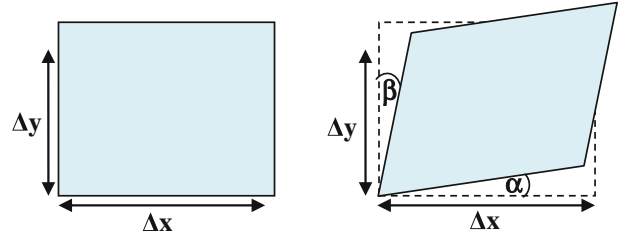
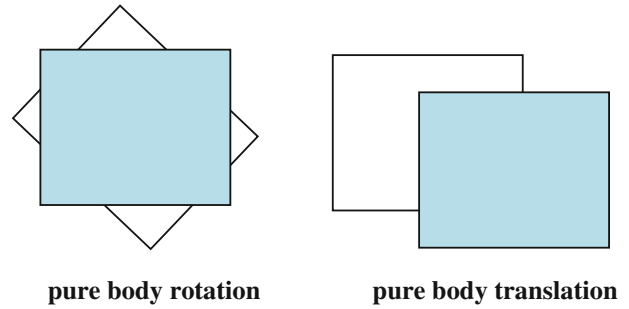


**Fig. 2.8** Pure rotation and pure translation changes of a body, are not considered to be elastic strains



**2.2.5 The Shape-Changing Strain**

As longitudinal strain gives expression for the volume changes resulting from stress application, the shear strain gives the corresponding measure for the shape deformation. Using the example above ( $\Delta x$  by  $\Delta y$  rectangular lamina). The shear strain (also called angular strain) is considered to be the average of the two angles by which two neighboring sides rotate as a result of the shearing stress. Thus, the shear strain ( $e_{xy}$ ) is defined as:

$$e_{xy} = (\alpha + \beta)/2$$

where ( $\alpha$  and  $\beta$ ) represent the angles of rotation of the two sides ( $\Delta x$  and  $\Delta y$ ) brought about by the shear stress (Fig. 2.7).

Since these two angles are very small (usually so, in seismic-field conditions), they can be represented by their corresponding tangents, giving

$$e_{xy} = (\alpha + \beta)/2 = (D_x/\Delta y + D_y/\Delta x)/2$$

where the angles ( $\alpha$  &  $\beta$ ) are in radians.

It should be emphasized that strain occurs only if the body particles experience unequal

displacements. When the displacements are equal a body may experience pure translation (rigid body-translation) or pure rotation (rigid body-rotation), as shown in Fig. 2.8.

Rigid-body changes which do not involve volume or shape changes, such as these, are not considered to be elastic strains.

**2.2.6 The Cubical Dilatation**

A parameter, closely related to longitudinal strain and of special importance in the theory of elasticity is the Cubical Dilatation ( $\theta$ ). At a certain point within a strained medium, this is defined as the fractional change in a unit volume surrounding that point. Thus, for a three dimensional body with longitudinal strains ( $e_{xx}$ ,  $e_{yy}$ ,  $e_{zz}$ ), the cubical dilatation can be computed as follows:

$$\theta = (1 + e_{xx})(1 + e_{yy})(1 + e_{zz}) - 1$$

For small strains  $e_{xx}$ ,  $e_{yy}$ ,  $e_{zz}$  (which is the case in seismic-field conditions), the products of these terms may be neglected giving the result:

$$\theta = \epsilon_{xx} + \epsilon_{yy} + \epsilon_{zz} = D_x/\Delta x + D_y/\Delta y + D_z/\Delta z$$

The sign convention of  $(\theta)$  is negative for compression and positive for expansion strains.

### 2.2.7 Stress-Strain Relationship

It is a common experience that a body under stress undergoes deformation of a form and value depending on the applied load and on the physical properties of that body. Bodies of the type which, under stress, exhibit a proportional strain are called elastic bodies. When the proportionality is linear, these are called perfectly elastic bodies.

Normally, bodies, under increasing stress, exhibit linear stress-strain behavior up to a certain stress-limit, beyond which the material may still be elastic but with no more linear relationship. Usually there is a point (the elastic limit) after which the deformation becomes irrecoverable and in this case the body behavior is described to be plastic. An increase of stress beyond the elastic limit produces large increase in strain, and it does so even with decreasing stress. With further increase of an extensional stress (tensile loading) for example, a point is reached where the body can no longer sustain the applied stress. At this point (called the rupture point) the body breaks up. Behavior of a ductile solid-body under an increasing extensional stress is shown in Fig. 2.9.

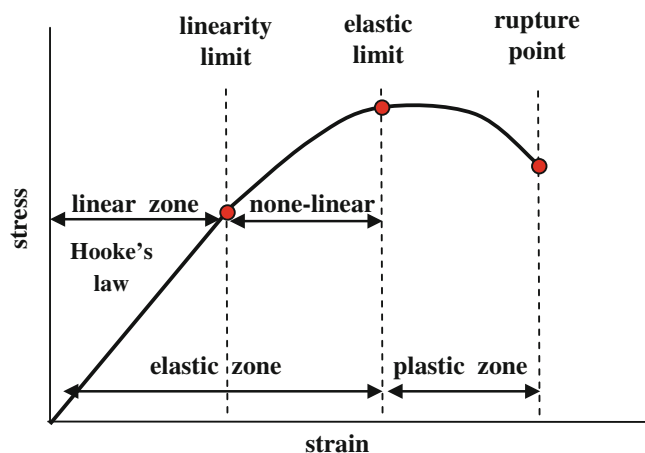
For an isotropic body (physical properties are independent of direction) and for an elastic body, under small strain, strain varies linearly with the applied stress. This linear stress-strain relationship is governed by a well-known mathematical equation. It is the Hooke's law.

### 2.2.8 Hooke's Law for Isotropic Media

In its simple form, Hooke's law states that the strain-stress relationship is linear. It is applicable to the behavior of stressed bodies when stresses are sufficiently small. If several stresses are acting on a body, the net strain produced is the sum of the individual strains. This is one of the important outcomes of the linearity property of the stress-strain relationship of isotropic media under small strains. A medium under stress condition, in which Hooke's law holds, is called Hookean medium.

When the stressed bodies are isotropic (their physical properties do not change with direction) the linear stress-strain relationship becomes relatively simple linear function (Sheriff and Geldart 1995, p. 37). The linear equation that connects stress to strain of isotropic media is commonly found in the geophysical literature, as in Bullen (1965, p. 20), McQuillin et al. (1984, p. 11), Sheriff and Gildart (1995, p. 37).

**Fig. 2.9** Elastic and plastic zones shown by a solid ductile body under an increasing tensile stress



The linearity property governed by Hooke's law means that there is a proportionality-constant for the linear stress-strain relation for any particular body under stress. Mathematical studies showed that, for an isotropic body, two elastic coefficients are sufficient (Richter 1958, p. 238). These are the Lamé's coefficients ( $\lambda$  &  $\mu$ ), which are sufficient in characterizing the elastic properties of a medium.

By use of Lamé's coefficients ( $\lambda$  &  $\mu$ ), Hooke's law can be presented in the following compact form:

$$\mathbf{T}_{ij} = \lambda \theta \delta_{ij} + 2\mu \mathbf{e}_{ij}$$

where the symbols ( $i$  &  $j$ ) take the values  $x$ ,  $y$ , and  $z$ , and the term  $\delta_{ij} = 1$  when ( $i = j$ ), and  $\delta_{ij} = 0$  when ( $i \neq j$ ).  $\mathbf{T}$  and  $\mathbf{e}$  are the stress and strain respectively.

This compact form of the Hooke's law can be presented in the following explicit equations:

$$\begin{aligned} \mathbf{T}_{xx} &= \lambda \theta + 2\mu \mathbf{e}_{xx} \\ \mathbf{T}_{yy} &= \lambda \theta + 2\mu \mathbf{e}_{yy} \\ \mathbf{T}_{zz} &= \lambda \theta + 2\mu \mathbf{e}_{zz} \end{aligned}$$

For pure shear strain (that is with no change in volume, for  $\theta = 0$ ), the Law expresses the relations for purely shearing strain, that is:

$$\begin{aligned} \mathbf{T}_{xx} &= 2\mu \mathbf{e}_{xx} \\ \mathbf{T}_{yy} &= 2\mu \mathbf{e}_{yy} \\ \mathbf{T}_{zz} &= 2\mu \mathbf{e}_{zz} \end{aligned}$$

From this equation, it is evident that, the stress is consisting of the sum of two parts; the first part ( $\lambda \theta$ ), involving the elastic coefficient ( $\lambda$ ) multiplied by the volume change (the dilatation,  $\theta$ ) and the second part ( $2\mu \mathbf{e}_{ij}$ ) which is involving the second elastic coefficient ( $\mu$ ) multiplied by the longitudinal strain ( $\mathbf{e}_{ij}$ ). The coefficients ( $\lambda$  and  $\mu$ ) are called Lamé's constants. These two constants (and other related constants) which are representing proportionality constant between stress and strain, are normally referred to as the elastic coefficients, or elastic moduli.

## 2.2.9 The Elastic Moduli

The elastic modulus of a body is the proportionality constant of the stress-strain linear relationship. It expresses an important physical property which is the extent of resistance of that body to the applied stresses. Moduli of important practical applications are Young's Modulus, bulk modulus, and shear modulus. These are defined in the following discussions.

### (i) Young's Modulus and Poisson's Ratio

Let a simple tensile stress ( $\mathbf{T}_x$ ) be applied to an isotropic bar placed along the  $x$ -axis. This will cause the bar to experience a longitudinal extension ( $\mathbf{e}_x$ ) in the  $x$ -direction and, at the same time, it experiences lateral contractions along  $y$ - and  $z$ -directions. Being an isotropic body, the contractions in the  $y$ - and  $z$ -directions ( $\mathbf{e}_y$ , &  $\mathbf{e}_z$ ) are equal. These changes (expressed by the strains  $\mathbf{e}_x$ ,  $\mathbf{e}_y$ , &  $\mathbf{e}_z$ ) are governed by the elastic coefficients of the stressed body. The coefficients which govern the stress-strain relation, in the presence of the tensile stress ( $\mathbf{T}_x$ ), are Young's modulus ( $\mathbf{Y}$ ) and Poisson's ratio ( $\sigma$ ).

For a one-dimensional stress acting on a body obeying Hooke's law, Young's modulus ( $\mathbf{Y}$ ) is the proportionality constant in the linear relation that connects stress ( $\mathbf{T}_x$ ) with strain ( $\mathbf{e}_x$ ). The relationship is:

$$\mathbf{T}_x = \mathbf{Y} \mathbf{e}_x$$

In the case of a rectangular rod of length ( $\mathbf{L}$ ), cross-sectional area ( $\Delta\mathbf{A}$ ) stretched by ( $\Delta\mathbf{L}$ ) due to force ( $\mathbf{F}$ ), Young's modulus ( $\mathbf{Y}$ ) is given by Fig. 2.10:

$$\mathbf{Y} = \mathbf{T}_x / \mathbf{e}_x = (\mathbf{F} / \Delta\mathbf{A}) / (\Delta\mathbf{L} / \mathbf{L})$$

Young's modulus is measured by pressure units (as psi, dyne/cm<sup>2</sup> or N/m<sup>2</sup>).

The Poisson's ratio ( $\sigma$ ), on the other hand, is defined as the ratio of transverse strain ( $\mathbf{e}_y$  or  $\mathbf{e}_z$ ) to longitudinal strain ( $\mathbf{e}_x$ ). For an isotropic body, this is given by:

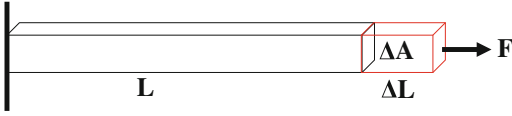


**Fig. 2.10** An elastic rectangular rod under extension force

$$\sigma = -e_y/e_x = -e_z/e_x$$

The minus sign is used to indicate that ( $e_y$ ) and ( $e_z$ ) are contractions for elongation ( $e_x$ ).

(ii) **The Bulk Modulus**

The Bulk modulus ( $\mathbf{B}$ ) is defined to be the ratio of change in hydrostatic pressure ( $\Delta P$ ), acting on a solid body of volume ( $V$ ), to the relative decrease in its volume ( $\Delta V/V$ ). For a cube of volume ( $V$ ) under hydrostatic pressure-change ( $\Delta P$ ), the bulk modulus ( $\mathbf{B}$ ) is given by (Fig. 2.11):

$$\mathbf{B} = -\Delta P/(\Delta V/V) = -V \cdot (\Delta P/\Delta V) = -\Delta P/\theta$$

The minus sign is entered to denote volume decrease for increase in compression and ( $\theta$ ) is the cubical dilatation:

The Bulk Modulus ( $\mathbf{B}$ ) is a measure for the body resistance to uniform compression. An equivalent expression for the bulk modulus can be given in terms of density change ( $\Delta \rho$ ) instead of the volume change. Thus, the definition becomes:

$$\mathbf{B} = +\rho(\Delta P/\Delta \rho)$$

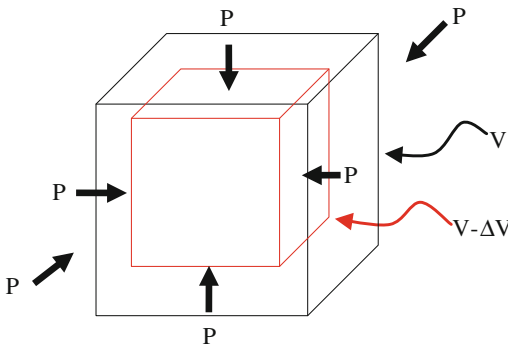


**Fig. 2.11** An elastic cube under hydrostatic compression forces

The plus sign is entered to denote density increase for increase in compression.

It is sometimes called (Incompressibility) and its inverse ( $1/\mathbf{B}$ ) is called (Compressibility). Its SI unit is the pressure measuring unit (the pascal).

(iii) **The Shear Modulus**

The shear modulus, ( $\mu$ ), which expresses the relationship between shearing stress and shearing strain, is defined as the ratio of the shear stress ( $T_{xy}$ ) and the shearing strain ( $e_{xy}$ ) represented by the resulting angular change. For tangential force ( $F$ ) acting on the face of a rectangular block of area ( $\Delta A$ ), the shear modulus ( $\mu$ ) is defined as follows (Fig. 2.12):

$$\mu = T_{xy}/e_{xy} = (F/\Delta A)/(\Delta x/h)$$

The strain ( $e_{xy}$ ) in this case is tangent of the angle of shear ( $\theta$ ), or the angle in radians for small value of the angle ( $\theta$ ). That is,

$$\mu = T_{xy}/\theta$$

The angle ( $\theta$ ) is normally called angle of shear and the coefficient ( $\mu$ ) is the shear modulus or rigidity modulus as it is sometimes called. Measurement unit of the shear modulus is pressure units as in the case of Young's modulus.

It is to be noted here that ( $\mu$ ) serves as measure for the resistance of an elastic solid body to shearing deformation (i.e. to shape changes) and that is why it is called rigidity modulus. For this reason, it is equal to zero for a fluid medium as it has zero-resistance to shape-changes.

(iv) **Lame's Elastic Coefficients**

Lame's coefficients (also called Lame's parameters) are two parameters ( $\lambda$  &  $\mu$ ) which are used

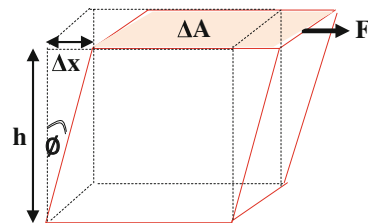


**Fig. 2.12** An elastic rectangular block under shearing force ( $F$ ) acting on area ( $\Delta A$ )

**Table 2.3** The mathematical interrelationships of elastic moduli, for an elastic isotropic body (Sheriff 1973, pp. 69–70)

Modulus	Relation-1	Relation-2
Young's modulus ( $Y$ )	$Y = \mu(3\lambda + 2\mu)/(\lambda + \mu)$	$Y = 9B\mu/(3B + \mu)$
Bulk modulus ( $B$ )	$B = (3\lambda + 2\mu)/3$	$B = Y/3(1 - 2\sigma)$
Shear modulus ( $\mu$ )	$\mu = 3(B - \lambda)/2$	$\mu = Y/2(1 + \sigma)$
Lame's modulus ( $\lambda$ )	$\lambda = (3B - 2\mu)/3$	$\lambda = \sigma Y/(1 + \sigma)(1 - 2\sigma)$
Poisson's modulus ( $\sigma$ )	$\sigma = \lambda/2(\lambda + \mu)$	$\sigma = (3B - 2\mu)/(6B + 2\mu)$

in characterizing the elastic properties of an isotropic medium. These two coefficients give complete elastic characterization of homogenous and isotropic media. They serve as the proportionality constants in the stress-strain linear relationship which is mathematically expressed by Hooke's law.

To understand the physical implication of the first coefficient ( $\lambda$ ), let us assume a solid cube being stretched by a tensile stress ( $\mathbf{T}_{zz}$ ) resulting in a corresponding tensile strain ( $\mathbf{e}_{zz}$ ). The lateral tensile stress ( $\mathbf{T}_{xx}$ ) needed to prevent lateral contraction is, according to (Sheriff 1969), given by ( $\mathbf{T}_{xx} = \lambda \mathbf{e}_{zz}$ ). This relation furnishes the formal definition of the Lamé's coefficient ( $\lambda$ ). The second coefficient ( $\mu$ ) is the shear (or rigidity) modulus.

Both of Lamé's coefficients ( $\lambda$  &  $\mu$ ) are functions of other elastic constants. For instance, they are functions of Young's modulus ( $Y$ ) and Poisson's ratio ( $\sigma$ ). The relations are:

$$\lambda = \sigma Y / (1 - 2\sigma) \cdot (1 + \sigma)$$

$$\mu = Y / 2(1 + \sigma)$$

Other relations are presented in Table 2.3.

### 2.2.10 The Elastic Moduli Interrelationships

For a homogeneous and isotropic medium under stress, the stress-strain relationship is linear within the elastic (Hookean) state. The proportionality constants are the elastic moduli or

elastic constants, as we mentioned above. In addition to the two Lamé's coefficients ( $\lambda$  &  $\mu$ ), the other moduli: Young's modulus ( $Y$ ), Bulk modulus ( $B$ ), and Poisson's ratio ( $\sigma$ ) can be used in characterizing the elastic properties of an isotropic body. Any of these moduli can be expressed in terms of two other moduli as it is summarized in Table 2.3:

It is evident from this table that any one of the five constants can be expressed in terms of any two of the remaining constants. This implies that any two of these three constants can be used to define the elastic properties of a homogeneous and isotropic medium.

For most rocks, values of the moduli ( $Y$ ,  $B$ , &  $\mu$ ) lie in the range ( $2 \times 10^{10} - 12 \times 10^{10}$ ) N/m<sup>2</sup>, with ( $Y$ ) being the largest and ( $\mu$ ) the smallest of these three (Sheriff and Geldart 1995, p. 38). Table of values of elastic moduli of rocks have been published by Birch (1966).

## 2.3 Wave Motion Equation

If two neighboring points in a stressed medium experience the same stress, no motion of one of them will occur with respect to the other. However, relative motion will take place when there is a stress difference. In other words, motion occurs when there is a stress gradient. This reminds us of an analogous case we met in the creation of strain (see Sect. 2.2). The two cases may be expressed as follows: Displacement gradient is required to create strain and stress gradient is required to cause motion.

### 2.3.1 One-Dimensional Scalar Wave Equation

In this section, we shall deal with the wave motion equation which expresses the motion of a disturbance in one dimension. The disturbance in this particular case is the scalar quantity, the cubical dilatation ( $\theta$ ).

Let us consider an elementary parallelepiped (of dimensions:  $\delta x$ ,  $\delta y$ ,  $\Delta z$ ) located inside an elastic isotropic medium (Fig. 2.13).

At each face of this elementary body, when it is under elastic stress, there exist three stress components: one is normal and two are tangential to the particular face. The three stress-components ( $T_{xx}$ ,  $T_{yx}$ , and  $T_{zx}$ ) are acting on the face perpendicular to the  $x$ -axis. Under elastic stress-strain conditions, each of these components will have a gradient in the  $x$ -direction ( $\partial T_{xx}/\partial x$ ,  $\partial T_{xy}/\partial x$ , and  $\partial T_{xz}/\partial x$ ). For a complete three dimensional state, additional similar gradients occur in the other two directions (y-direction and z-direction).

In order to simplify the mathematical derivation of the equation of seismic wave motion, let a plane compressional seismic wave to be advancing in the  $x$ -direction. In this case the three stress-components are reduced to only one component ( $T_{xx}$ ) creating the corresponding strain ( $e_{xx}$ ). When a seismic plane wave propagates in the  $x$ -direction, the two faces (perpendicular to the  $x$ -axis) of the parallelepiped will be unequally displaced, and hence, it is subjected to an elastic strain ( $e_{xx}$ ) which is, by definition, given by the displacement gradient ( $\partial D_x/\partial x$ ).

This strain ( $e_{xx} = \partial D_x/\partial x$ ) is produced by the corresponding stress gradient ( $\partial T_{xx}/\partial x$ ).

By making use of the fact that the net force acting on any face is given by the stress acting on that face times the face area, we get the resultant force ( $F_x$ ) in the  $x$ -direction due to the stress change ( $\partial T_{xx}/\partial x$ )  $\cdot \delta x$  that occurred across the distance ( $\delta x$ ). This is computed as follows:

$$F_x = (\partial T_{xx}/\partial x) \cdot \delta x \cdot \delta y \cdot \delta z$$

By applying Newton's second law of motion we can express ( $F_x$ ) in terms of mass of the parallelepiped ( $\delta x \cdot \delta y \cdot \delta z$  times density  $\rho$ ) multiplied by acceleration ( $\partial^2 D_x/\partial t^2$ ) in the  $x$ -direction giving:

$$\delta x \cdot \delta y \cdot \delta z \cdot \rho (\partial^2 D_x/\partial t^2) = (\partial T_{xx}/\partial x) \cdot \delta x \cdot \delta y \cdot \delta z$$

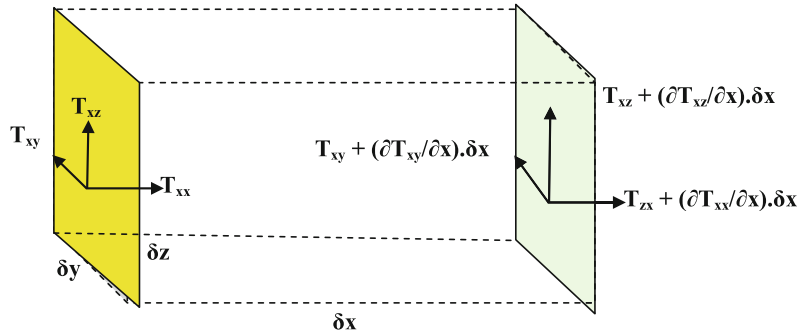
or:

$$\rho (\partial^2 D_x/\partial t^2) = (\partial T_{xx}/\partial x)$$

This is the one-dimensional (dimension,  $x$  in this example) wave motion equation which describes particle motion (displacement,  $D_x$ ) in terms of the applied stress ( $T_{xx}$ ). However, the motion can be expressed in terms of displacement only. This is done by using the stress-strain linear relationship expressed by Hooke's law equation for isotropic media ( $T_{xx} = \lambda \theta + 2\mu e_{xx}$ ). Substituting for ( $T_{xx}$ ), the previously-derived wave equation becomes:

$$\rho (\partial^2 D_x/\partial t^2) = \lambda (\partial \theta/\partial x) + 2\mu (\partial e_{xx}/\partial x)$$

**Fig. 2.13** A small parallelepiped element of volume under elastic stress



Since, by definition,  $(\theta = \mathbf{e}_{xx} + \mathbf{e}_{yy} + \mathbf{e}_{zz})$  and  $(\mathbf{e}_{yy} = \mathbf{e}_{zz} = \mathbf{0})$  in this case (case of restricting the disturbance to be displacement in the x-direction, with no lateral contraction), we can readily write:

$$\rho(\partial^2 \mathbf{D}_x / \partial t^2) = (\lambda + 2\mu)(\partial \mathbf{e}_{xx} / \partial \mathbf{x})$$

or,

$$(\partial^2 \mathbf{D}_x / \partial t^2) = [(\lambda + 2\mu) / \rho] (\partial^2 \mathbf{D}_x / \partial x^2)$$

This is a partial differential equation of the form  $(\partial^2 \mathbf{y} / \partial t^2 = v^2 \partial^2 \mathbf{y} / \partial x^2)$ , which has the general solution,  $\mathbf{y}(\mathbf{x}, \mathbf{t}) = \mathbf{f}(\mathbf{x} - \mathbf{vt}) + \mathbf{g}(\mathbf{x} + \mathbf{vt})$ . In analogy to this standard form of partial differential equation, we can write the solution of the one-dimensional wave equation as:

$$\mathbf{D}_x(\mathbf{x}, \mathbf{t}) = \mathbf{f}(\mathbf{x} - \mathbf{vt}) + \mathbf{g}(\mathbf{x} + \mathbf{vt}),$$

where,  $\mathbf{v} = [(\lambda + 2\mu) / \rho]^{1/2}$ .

This solution represents one dimensional wave equation, which is a disturbance (particle displacement,  $\mathbf{D}_x$ ) moving with speed of  $(\mathbf{v})$  in the positive x-direction as expressed by the first term,  $\mathbf{f}(\mathbf{x} - \mathbf{vt})$ . The second term,  $\mathbf{g}(\mathbf{x} + \mathbf{vt})$  represents a wave moving in the negative x-direction.

### 2.3.2 The Scalar and Vector 3D Wave Equations

Solution of the one-dimensional wave equation,  $\mathbf{q}(\mathbf{x}, \mathbf{t})$  expresses the variation of the disturbance ( $\mathbf{q}$ ) along the travel distance ( $\mathbf{x}$ ) at any time ( $\mathbf{t}$ ). In the three-dimensional case, we have the dependant variable;  $\mathbf{q}(\mathbf{x}, \mathbf{y}, \mathbf{z}, \mathbf{t})$  which possesses, at any time ( $\mathbf{t}$ ), a defined value at any point in the surrounding space  $(\mathbf{x}, \mathbf{y}, \mathbf{z})$ .

The standard wave equation describes the strain-changes as function of space and time as it propagates (with constant velocity) through a perfectly elastic medium. It can be shown (see for example Richter 1958, pp. 657–658; Sheriff and Geldart 1995, pp. 39–40) that the standard

three-dimensional wave-motion equation is a linear second order partial differential equation. The general wave equation of a disturbance,  $\mathbf{q}(\mathbf{x}, \mathbf{y}, \mathbf{z}, \mathbf{t})$  moving in space with velocity  $(\mathbf{v})$ , is given by:

$$\partial^2 \mathbf{q} / \partial t^2 = v^2 [\partial^2 \mathbf{q} / \partial x^2 + \partial^2 \mathbf{q} / \partial y^2 + \partial^2 \mathbf{q} / \partial z^2].$$

or (using Laplacian operator  $(\nabla^2 \mathbf{q} = \partial^2 \mathbf{q} / \partial x^2 + \partial^2 \mathbf{q} / \partial y^2 + \partial^2 \mathbf{q} / \partial z^2)$ , this can be written as:

$$\partial^2 \mathbf{q} / \partial t^2 = v^2 \nabla^2 \mathbf{q}$$

In seismic waves there are two types of disturbance ( $\mathbf{q}$ ) which propagate through the Earth materials. These are the two forms of elastic strains which represent the scalar “volume” changes (expressed by the cubic dilatation,  $\theta$ ) and the vector “shape” changes (expressed by the shear strain,  $\psi$ ).

#### (i) The Scalar quantity ( $\theta$ )

This is the scalar cubic dilatation ( $\theta$ ). It represents disturbance (volume-changes) that moves in space with velocity  $(\mathbf{v})$ , where  $\mathbf{v} = [(\lambda + 2\mu) / \rho]^{1/2}$ . According to the wave motion equation (see for example, Richter 1958, p. 658):

$$\rho \partial^2 \theta / \partial t^2 = (\lambda + 2\mu) \nabla^2 \theta$$

By definition, the cubic dilatation ( $\theta$ ) is related to displacement  $\mathbf{D}$  (vector quantity of components  $\mathbf{D}_x, \mathbf{D}_y, \mathbf{D}_z$ ) by the formula  $(\theta = \partial \mathbf{D}_x / \partial \mathbf{x} + \partial \mathbf{D}_y / \partial \mathbf{y} + \partial \mathbf{D}_z / \partial \mathbf{z})$ . Using vector notation, the scalar quantity ( $\theta$ ) is, therefore, the divergence of the vector ( $\mathbf{D}$ ). That is:

$$\theta = \text{div } \mathbf{D} = \nabla \cdot \mathbf{D}$$

#### (ii) The Vector quantity ( $\psi$ )

The second type of moving disturbance is the vector quantity (shear strain,  $\psi$ ). It represents (shape-changes) which moves with velocity,  $\mathbf{v} = [(\mu / \rho)]^{1/2}$ . The three components of the vector ( $\psi$ ) are  $(\psi_x, \psi_y, \psi_z)$ , defined by (Richter 1958, p. 658):

$$\begin{aligned}\psi_x &= (\partial D_z / \partial y - \partial D_y / \partial z) \\ \psi_y &= (\partial D_x / \partial z - \partial D_z / \partial x) \\ \psi_z &= (\partial D_y / \partial x - \partial D_x / \partial y)\end{aligned}$$

Each of these three components moves with velocity ( $\mathbf{v}$ ) in accordance to the following wave-motion equations.

$$\begin{aligned}\rho \partial^2 \psi_x / \partial t^2 &= \mu \nabla^2 \psi_x \\ \rho \partial^2 \psi_y / \partial t^2 &= \mu \nabla^2 \psi_y \\ \rho \partial^2 \psi_z / \partial t^2 &= \mu \nabla^2 \psi_z\end{aligned}$$

It is clear from the definitions of the components of the vector quantity ( $\psi$ ) that each of the components ( $\psi_x, \psi_y, \psi_z$ ) is the **curl** of the corresponding displacement-components ( $D_x, D_y, D_z$ ) as expressed above. That is:

$$\psi_x = \text{curl}_x D = \nabla \times D$$

Similarly, for the other two components ( $\psi_y, \psi_z$ ).

### 2.3.3 Plane Waves

A plane wave is defined as that wave for which the moving disturbance is constant at all points of any plane perpendicular to the propagation direction (Fig. 2.14).

For the seismic plane waves, the elastic disturbances,  $\theta(\mathbf{x}, t)$ , or  $\psi(\mathbf{x}, t)$  are functions of the travelled distance ( $\mathbf{x}$ ) only. In either of these two types of disturbances, therefore, the wave front is

represented by a plane normal to the  $x$ -axis. Further, when the moving disturbance  $\mathbf{f}(\mathbf{x} - \mathbf{vt})$  is in the form of sinusoidal function the moving disturbance is referred to as (plane harmonic wave). Such a function is:

$$\mathbf{f}(\mathbf{x}, t) = \mathbf{a} \cos \mathbf{k}(\mathbf{x} - \mathbf{vt}),$$

where ( $\mathbf{a}$  &  $\mathbf{k}$ ) are constants.

According to Fourier Theorem, a moving pulse of an arbitrary shape can be transformed into its harmonic components by superposing many sinusoidal functions, each of which is of the form:

$$\mathbf{f}(\mathbf{x}, t) = \mathbf{a} \cos \mathbf{k}(\mathbf{x} - \mathbf{vt}),$$

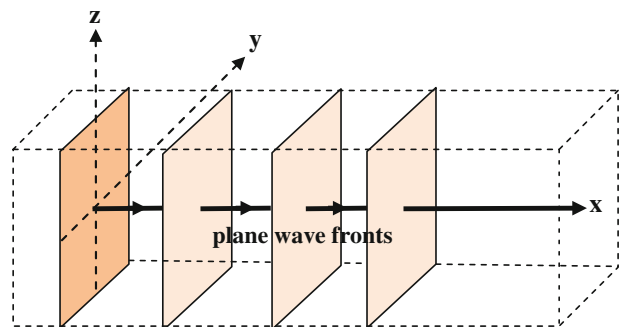
or,

$$\mathbf{f}(\mathbf{x}, t) = \mathbf{a} \cos 2\pi(\mathbf{x}/\lambda - t/\tau)$$

This equation is showing that  $\mathbf{f}(\mathbf{x}, t)$  is a periodic function of ( $\mathbf{x}$  &  $t$ ) which is oscillating with wavelength ( $\lambda$ ) and period ( $\tau$ ) in respect to distance and time respectively, where  $\mathbf{k}$  ( $=2\pi/\lambda$ ) is called the wave number. The factor ( $\mathbf{a}$ ) represents the amplitude of the particular harmonic component. The two forms of these two equations are equivalent since  $\mathbf{v} = \lambda/\tau$ .

Periodicity of the harmonic plane wave is expressed by two parameters. These are the spatial frequency in cycle per meter ( $f_x$ ) and the temporal frequency in cycle per second ( $f_t$ ). These are related to the wavelength ( $\lambda$ ) and to the wave period ( $\tau$ ) by the relations ( $f_x = 1/\lambda$ ) and ( $f_t = 1/\tau$ ) respectively.

**Fig. 2.14** Wave fronts of a plane wave advancing in  $x$ -direction



### 2.3.4 The P- and S-Waves

As it is presented above, there are two types of disturbance that can move in accordance with the standard wave motion equation. These are the scalar cubic dilatation ( $\theta$ ) and the vector shear strain ( $\psi$ ).

From the wave equation it can be shown that the disturbance ( $\theta$ ) moves faster than the other disturbance ( $\psi$ ). Thus, when the two disturbances are generated by a certain source, the ( $\theta$ -wave) arrives earlier than the ( $\psi$ -wave). For this reason the two waves are called Primary (**P-wave**) and Secondary (**S-wave**) respectively.

It is to be noted that the ratio of the P-wave velocity ( $v_p = [(\lambda + 2\mu)/\rho]^{1/2}$ ) to the S-wave velocity ( $v_s = [\mu/\rho]^{1/2}$ ) is equal to  $[(\lambda + 2\mu)/\mu]^{1/2}$ . Using the relationship connecting ( $\lambda$ ) and ( $\mu$ ) in which  $\lambda/\mu = 2\sigma/(1 - 2\sigma)$ , we can write:

$$v_p/v_s = [(2 - 2\sigma)/(1 - 2\sigma)]^{1/2}$$

This formula clearly shows that the ratio of the P-wave velocity ( $v_p$ ) to the S-wave velocity ( $v_s$ ) is function of Poisson's ratio ( $\sigma$ ) only.

According to (Dobrin 1960, p. 18), Poisson's ratio ( $\sigma$ ) generally ranges from 0.05 to 0.40, averaging about 0.25 for hard rocks. With this value ( $\sigma = 1/4$ ), the velocity ratio ( $v_p/v_s$ ) becomes  $3^{1/2}$  ( $=1.732$ ). This means that P-wave moves with velocity which is about 1.7 times as fast as the S-wave moving in the same medium. It is useful to note that P-wave velocity is

330 m/s in air, 1450 m/s in water, and (2000–6000) m/s in rocks.

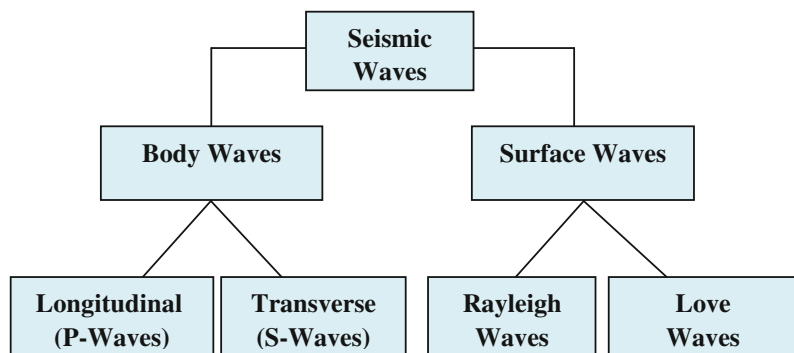
A solid medium having its Poisson's ratio equal to (1/4) is called Poisson's solid (Sheriff 2002, p. 266).

### 2.4 Classification of Common Elastic Waves

From analyses of stress and strain, we have seen that strain is, in general, made up of two types of elastic disturbance; the cubic dilatation and the shear strain. Solution of the equation of motion showed that each of these types of deformation travels through the medium with its own velocity. The first type of disturbance represents the moving "volume" strain and the second type involves the "shape" strain. The first type is called Longitudinal, Compressional, or Primary wave (or just P-wave) which travels faster than the second type which is called Transverse, Shear, or Secondary wave (or just S-wave).

These two types of waves (P- and S-waves) belong to a class of waves (called body waves) because they can propagate through the interior of the earth body. This group of waves is called so to differentiate them from another class of waves which move on and near the free surface of the medium, called (surface waves) which include Rayleigh- and Love-waves. Classification of the common elastic (seismic) waves is shown in Fig. 2.15.

**Fig. 2.15** Classification of the common seismic waves



### 2.4.1 Body Waves

Body waves are waves that can travel through an elastic materialistic medium in any direction. As they move, the waves may experience changes in their energy level and in their travel-path geometry subject to the physical properties of the medium. There are two sub-types of these waves; the longitudinal and the transverse waves (Fig. 2.16).

#### (i) Longitudinal Waves

This type of waves is also known as compressional, Primary, or just P-wave. The travelling disturbance in this case is “volume” deformation expressed by the cubical dilatation ( $\theta$ ) as defined above.

The particles of the medium, traversed by a plane P-wave, vibrate about their neutral positions in the direction of the wave propagation. The travel path consists of a sequence of alternating zones of compressions and rarefactions (Fig. 2.16a). This is the type of waves which is commonly employed in seismic reflection and refraction exploration work.

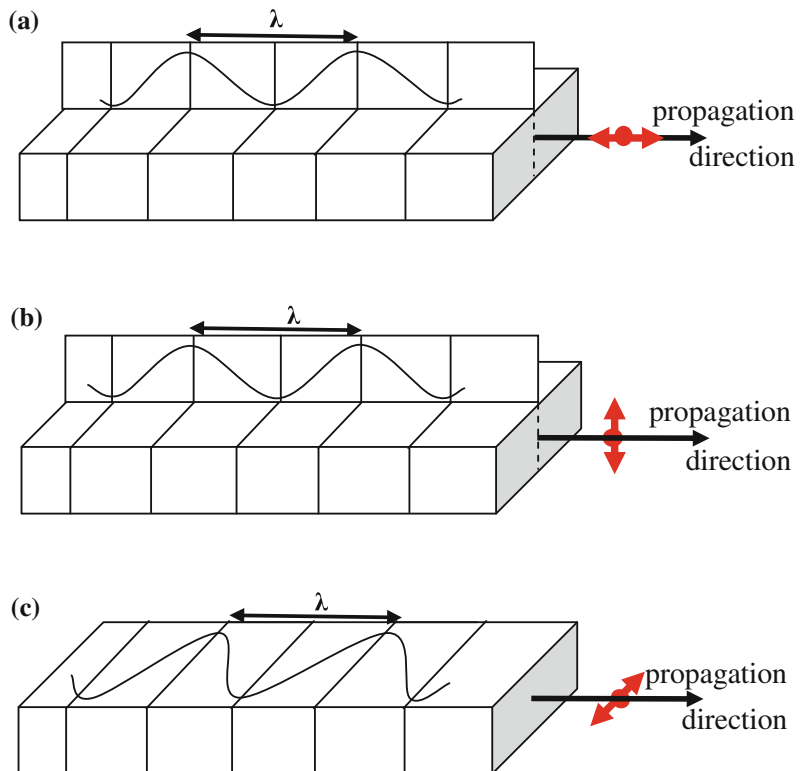
P-wave is the fastest wave for a given medium and, therefore, its arrival at a certain observation point is the earliest among the seismic wave-types. This is a common observation of seismologists working on analysis of earthquake seismograms. Propagation velocity ( $v_p$ ) of P-wave depends on the medium density ( $\rho$ ) and elastic properties ( $\lambda$  &  $\mu$ ) and it is given by the expression  $v_p = [(\lambda + 2\mu)/\rho]^{1/2}$ .

#### (ii) Transverse Waves

The travelling disturbance in this case is the shear strain or “shape” deformation. The medium which is traversed by this type of waves experiences no volume changes. A consequence of the shear strain (rotation of part of the medium) is the transverse displacement of the path particles relative to the propagation direction. They are also called (shear waves) or (Secondary, or just S-waves).

A horizontally moving S-wave, which is so polarized that the particle motion is confined to vertical plane, is known as SV-wave (Fig. 2.16 b). When the polarization plane is horizontal, it is

**Fig. 2.16** Particle displacement-mode of a medium traversed by plane body-waves,  $\lambda$  is wavelength. **a** P-wave, **b** SV-wave, **c** SH-wave



called SH-wave (Fig. 2.16c). The velocity of S-waves,  $v_s$  is given by  $v_s = [\mu/\rho]^{1/2}$ . In liquid-media, where ( $\mu = 0$ ), S-waves do not propagate.

### 2.4.2 Surface Waves

As it is implied by its name, surface waves are waves that move on the free surface of the earth. The main features common among all surface waves, observed on earthquake seismograms, are their relatively large amplitudes (high energy content) and low frequencies when compared with the body waves. In addition to that, they move with velocity which is generally slower than body waves moving in the same medium. It is a common observation that the dispersion phenomena are more prominent in surface waves due to dependence of the velocity on the frequency of individual harmonic component.

The main sub-types of surface waves are Rayleigh waves and Love waves (Fig. 2.17).

#### (i) Rayleigh Waves

Rayleigh waves, which were discovered by an English scientist, Lord Rayleigh in 1885, are usually developing at the free surface of a semi-infinite solid medium. Its wave amplitude decays rapidly with increasing depth. The travelling disturbance in this case is a sort of combination of particle-motions of both P- and SV-waves. The particle motion, which has a retrograde elliptical orbit, takes place in a vertical plane parallel to propagation direction (Fig. 2.17a). The minor axis of the elliptical orbit is parallel to wave motion direction and it is equal to two-thirds of its major axis. Rayleigh waves travel on the surface of a solid medium with velocity of 0.92 of the velocity of S-waves moving in that medium (Bullen 1965, p. 90). In a sense, Rayleigh waves are similar to the familiar water waves, with a fundamental difference, and

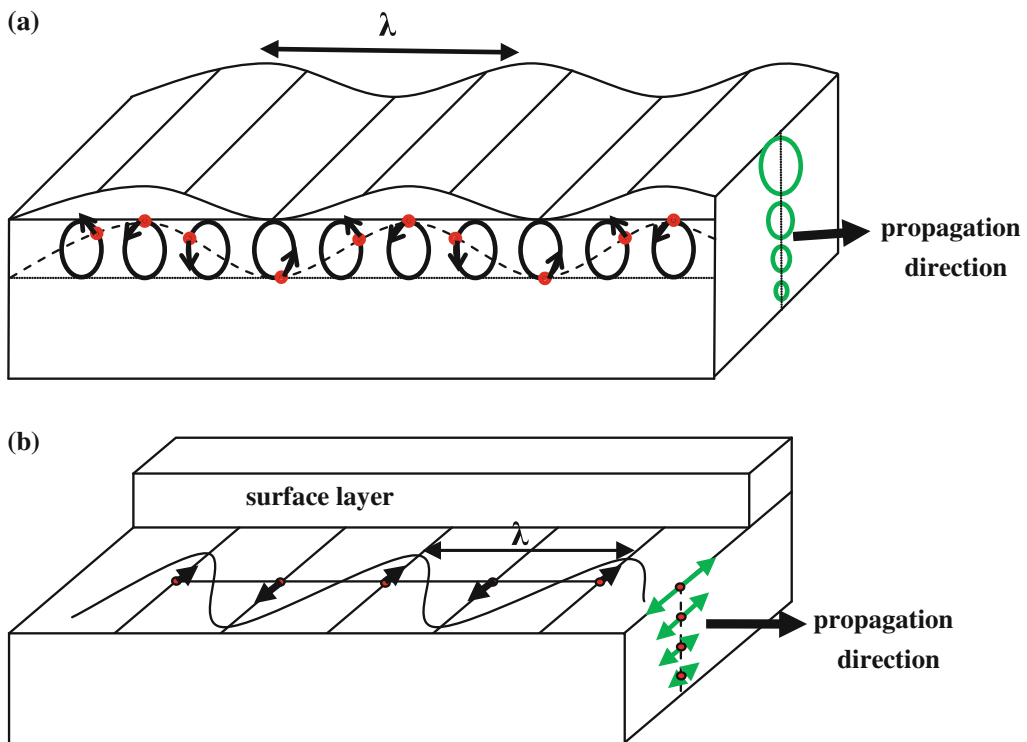


**Fig. 2.17** Particle displacement-mode of a medium traversed by plane surface-waves, ( $\lambda$ ) is wavelength. **a** Rayleigh Wave, **b** Love Wave

that is the particle motion in case of Rayleigh waves describe an elliptical path whereas the particle-motion path in case of water waves are circular in shape.

In the case where the semi-infinite medium is overlain by a low-velocity surface layer, Rayleigh waves exhibit a phenomenon known as (dispersion). Harmonic components of longer periods (lower frequencies) travel faster. Consequently, the Rayleigh wave seismograms would, in general, show decrease in period along the wave-train. Components of too-long wavelengths (too long compared with the thickness of the surface layer) penetrate deeper and travel with velocity of about 0.9 times the S-wave velocity in the subsurface material. The short wavelengths travel mainly in the surface layer with velocity of about 0.9 times the S-wave velocity in the surface layer.

Surface waves, normally seen on shot records, obtained in seismic reflection surveys, are commonly called (ground roll) and these are identified to be of Rayleigh-wave type. Sometimes, these are called pseudo-Rayleigh waves (Sheriff 2002). Ground-roll waves are considered to be unwelcome noise and efforts are usually made to get rid of them or at least minimize their masking effect caused to the seismic reflection signal.

#### (ii) Love Waves

This is the second sub-type of surface waves which was discovered, in 1911, by another English geophysicist named A.E.H. Love (1863–1940). It develops only in cases where a solid elastic semi-infinite medium is overlain by a horizontal low-velocity layer. Like SH-wave vibration mode, the particle movement is transverse and is confined to the horizontal plane (Fig. 2.17b). Love waves travel by multiple reflections between the top and bottom boundary-planes of the surface layer. The propagation velocity approaches S-wave velocity in the subsurface medium for very long wavelengths and to that of the surface layer for short wavelengths (Dobrin 1960, p. 23). Love waves always exhibit dispersion. As in the case of Rayleigh waves, Love waves propagation-velocity increases with the period of the harmonic component. Again, the vibration amplitude decays exponentially with depth in the lower medium.

Since they possess no vertical component, Love waves are not detected by the geophone or by any such-like vertical-component sensing instrument.

### 2.4.3 Seismic Noise

Broadly speaking, the term (noise) used in seismology, is applied to all types of disturbance which may interfere with (and impose masking effects to) the seismic signal of interest. In this way, the concept of seismic noise bears a relative implication. Thus, when the interest is focused on reflected body waves, surface waves and other non-reflection waves (as direct and refraction arrivals) are considered to be the unwanted troublesome noise. If the interest is in the refraction arrivals, reflection arrivals become the unwanted noise. In the strict sense, however, the ambient seismic disturbances (usually of random energy distribution which form the background of a distinct travelling signal) are considered to be the seismic noise.

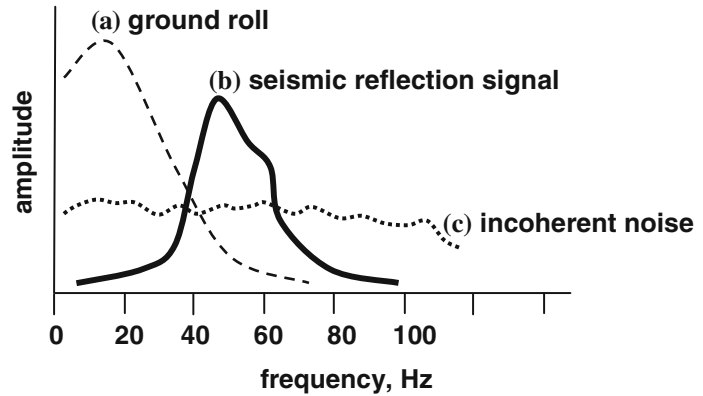
Seismic noise has destructive effects on the seismic signals of interest. A signal recorded amid a background of noise is distorted and weakened because of the interfering noise. Signal resolution is badly affected with noise development. A measure for the signal resolution, called the signal-to-noise ratio (S/N ratio) is usually applied. It is defined to be the ratio between signal amplitude detectable amid a background seismic noise.

In exploration seismology seismic noise is divided into two main types; coherent and incoherent noise (Fig. 2.18).

#### (i) Coherent Noise

Coherent noise is a seismic event characterized by a distinct apparent velocity and well-defined onset. In reflection seismology, coherent noise which appear on shot records, are source-generated seismic events. They are made up mainly of surface waves (ground roll) and air-waves which are of fairly narrow bandwidth with low frequency range. Frequency content of this type of noise is typically below 20 Hz (Fig. 2.18).

**Fig. 2.18** Sketch showing amplitude spectra of common coherent noise, ground roll (a), and incoherent noise, random noise (c), in relation to that of the reflection signal (b)



### (ii) Incoherent Noise

Unlike coherent noise, the incoherent noise consists of seismic events with unpredictable amplitude and onset. This type of noise, which is basically of random nature, forms the seismic-energy background of any seismic shot-record. In earthquake seismology it is commonly known as (microseisms), and in prospecting seismology it is called (incoherent background noise), or (ambient noise) as it is sometimes referred to. In addition to the randomness nature, the incoherent noise is characterized by a broad amplitude spectrum that covers a wide range of frequencies compared with the nearly limited bandwidth of reflection signals or coherent noises (Fig. 2.18). In the geophysical literature we sometimes meet terms like (white noise) indicating wide-band noise, and (red noise) for low-frequency random noise.

Intensive research work has been undertaken, directed towards a greater understanding of the source and characteristics of the incoherent noise. It is now generally accepted that it is generated as a result of external energy sources like wind movements, sea-waves collisions with sea coasts, in addition to other various natural and artificial man-made activities.

Because of seismic noise which are unavoidable seismic events which get recorded alongside the objective signal, the signal-to-noise-ratio (S/N) becomes an important parameter in signal detection studies. The S/N ratio is used as measure for the signal quality-level. Signal clarity (S/N enhancement) is a central objective, aimed

at, in seismic data acquisition. Several ways and means are followed in the field-acquisition stage or in the following data-processing stage to get enhanced S/N ratio. Suitable measures are applied to the parameters of the seismic source and detectors as well as those measures applied in processing work, in order to attenuate these noises and enhance the S/N ratio.

## 2.5 Propagation of Seismic Waves

Seismic waves are generated from a sudden change in the internal strain occurring inside an elastic medium. The generating source may be natural as in the case of earthquakes or artificial, like exploding a charge of dynamite, as normally done in seismic exploration. All parameters of an advancing seismic wave (waveform, speed, and travel-path geometry) may change during the wave propagation. Form and magnitude of these changes depend on the physical properties of the host medium. Whether the source is natural or artificial, a seismic field is created when a sudden pressure pulse is initiated. The generated seismic energy moves away from the source zone in a form of a wave motion propagation. Under these conditions (seismic energy source within an elastic medium), the seismic wave spreads out from the source zone in every possible direction. A travel ray-path, in a particular medium, is defined once the locations of both of the source-point and detector-point are defined.

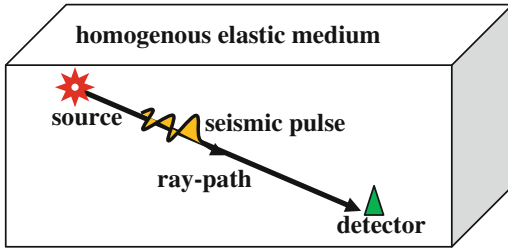


**Fig. 2.19** Elements of the seismic field, shown for an idealized homogenous and elastic medium

### 2.5.1 Elements of the Seismic Field

In case of an idealized simple medium (one which is homogeneous, isotropic, and perfectly elastic medium) the wave-motion propagation is expected to be along straight ray-paths, with constant velocity. A seismic field is created when a mechanical energy within an elastic medium generates a seismic pulse that propagates through that medium. The fundamental elements of a seismic field are, thus, a source of mechanical energy, elastic medium, and detector.

Except for the geometrical spreading effect, the wave moves through such an idealized medium, with no changes taking place on ray-path direction or on the waveform of the travelling seismic pulse (Fig. 2.19).

### 2.5.2 Concepts of Wave-Fronts and Rays

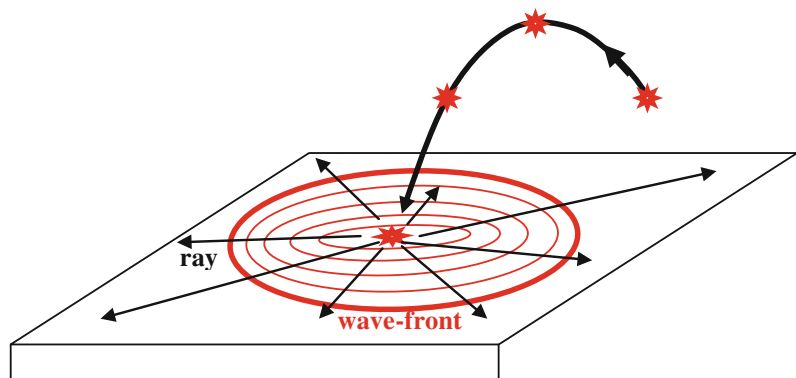
From a mechanical energy-source, (such as a mechanical pressure pulse), a seismic wave

spreads out into the three dimensional space of the host medium. If the medium is homogeneous, the seismic energy would advance in every possible direction with constant velocity. This means that after any given travel-time the energy would have reached points of equal distances from the source. These points fall on a spherical surface which is marking the (**wave-front**). For a harmonic seismic wave, the wave front is defined to be the locus of points having the same phase of particle vibration.

At any point in the wave-field, the line which is perpendicular to the wave front at a certain instant represents a (**ray**). The ray is an imaginary line normal to the wave front at a certain point which indicates the motion-direction of the advancing wave at that point. Near the source point, the wave fronts of seismic waves travelling through a homogeneous medium are of spherical shapes and thus the rays are straight lines radiating in all directions from the source point. At very large distances, the wave fronts are approximating to planes and the rays, in this case, become parallel straight lines perpendicular to the plane wave-fronts.

The familiar example is the wave which develops on the surface of water when a small solid object (a pebble, say) is dropped vertically into it. The crests and troughs of the generated wave spread out from the source-point in the form of concentric circles. In fact these circles are depicting the surface expression of the spherical wave-fronts which are advancing through the three-dimensional space of the water medium. By definition, the ray at any point on

**Fig. 2.20** Concepts of the wave fronts and rays as seen when a water wave is created from dropping a pebble into a still pond



the wave front is a line drawn normal to the spherical wave-front (circles on the surface plane) at that point. Concepts of the wave-front and rays are shown in (Fig. 2.20) for a case of dropping a pebble into a still pond.

### 2.5.3 Huygens' Principle

Huygens' Principle states that each point on a wave-front acts as a source of a new wave which, in a homogeneous medium, generates a secondary spherical wave-front, the envelope of which defines the position of a wave generated at some later time.

Huygens' model of wave propagation requires that the secondary wave-fronts are active only at the points where the envelope touches their surfaces. The wave energy is spreading out from the primary source-points in all directions, but their mutual interactions make the resultant disturbance zero everywhere except at the points where they touch the common envelope. Applying the principle on plane-wave propagation in a homogeneous, and in an inhomogeneous medium, is shown in Fig. 2.21.

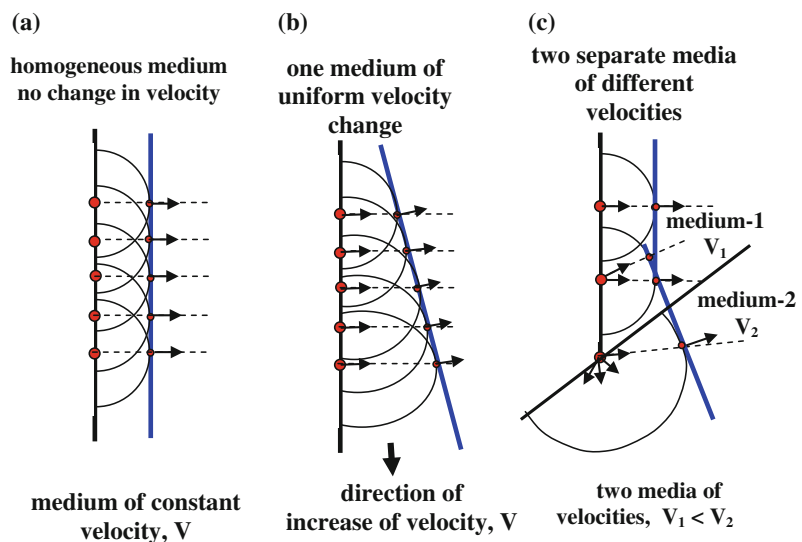
### 2.5.4 The Concept of the Interface

The Interface is that boundary-surface separating two different media. As far as the changes (changes in spectral structure and propagation direction) of seismic waves are concerned, two media are considered to be different if both of the wave propagation velocity and the medium bulk density are different. Since velocity is function of elastic coefficients, it can be said that density and elastic properties are the factors which control the specific characters of the media. The parameter which expresses the combined effect of velocity and density is called (acoustic impedance) which is defined to be the product of velocity by the density.

To clarify the concept of the interface and the roll of the acoustic impedance waves hitting an interface let us consider a two-layer model which consists of two adjacent media ( $M_1$  &  $M_2$ ) of velocities and densities ( $v_1$  &  $\rho_1$ ) for medium ( $M_1$ ) & ( $v_2$  &  $\rho_2$ ) for medium ( $M_2$ ). The acoustic impedances ( $z_1$  &  $z_2$ ) for the two layers are ( $z_1 = \rho_1 v_1$ ) and ( $z_2 = \rho_2 v_2$ ) as shown in Fig. 2.22.

In analogy to the role of electrical impedance in the flow of electrical current, the acoustic impedance expresses the extent of resistance the

**Fig. 2.21** Plane-wave propagation according to Huygens' Principle. **a** Through a homogeneous medium where velocity is constant. **b** Inhomogeneous medium of velocity which is uniformly changing across the propagation direction. **c** Two media of different velocities



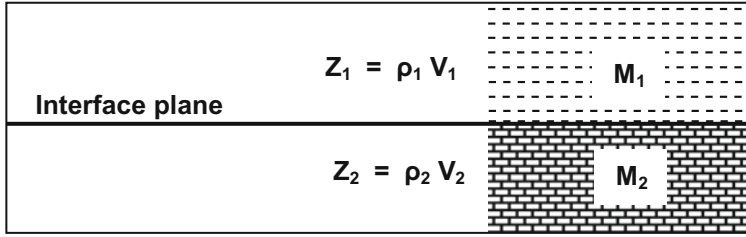


**Fig. 2.22** Concept of the Interface and definition of the Acoustic Impedance,  $z (=ρv)$

seismic energy meets when traversing a medium. The higher the acoustic impedance, the lower the particle vibration-velocity will be, and vice versa. Acoustic impedance is measured by  $(kg s^{-1} m^2)$  or by the equivalent  $(Ns m^3)$  units.

At an interface, an incident seismic wave (normally a P-wave in seismic exploration work) would, under certain geometrical conditions, give rise to wave conversion in addition to reflection, refraction, and diffraction. These cases shall be dealt with in some details in the following discussions.

**2.5.5 Changes of Propagation Direction at Interfaces**

In an idealized homogenous and elastic medium, a seismic wave propagates with no changes taking

place on ray-path direction or on the waveform of the travelling seismic pulse. In nature, however, the medium is far from this idealized form. In the solid crust of the Earth, it is commonly made up of rock layers of varying physical properties and varying geometrical forms and sizes.

In such inhomogeneous environments a moving seismic wave would suffer from a number of changes whenever it meets an interface across which there is change in the properties of the medium. In particular, changes in energy content, waveform (spectral structure), propagation velocity, direction of motion, and new wave generation. These changes, are generated at the interface planes defining the layer bounding surfaces (Fig. 2.23).

The common changes in ray-path direction, which are of significance to exploration seismology, are: reflection, refracted transmission

**Fig. 2.23** **a** Infinite, elastic homogeneous medium showing straight ray-path. **b** Inhomogeneous (layered) medium showing changes in ray-path direction

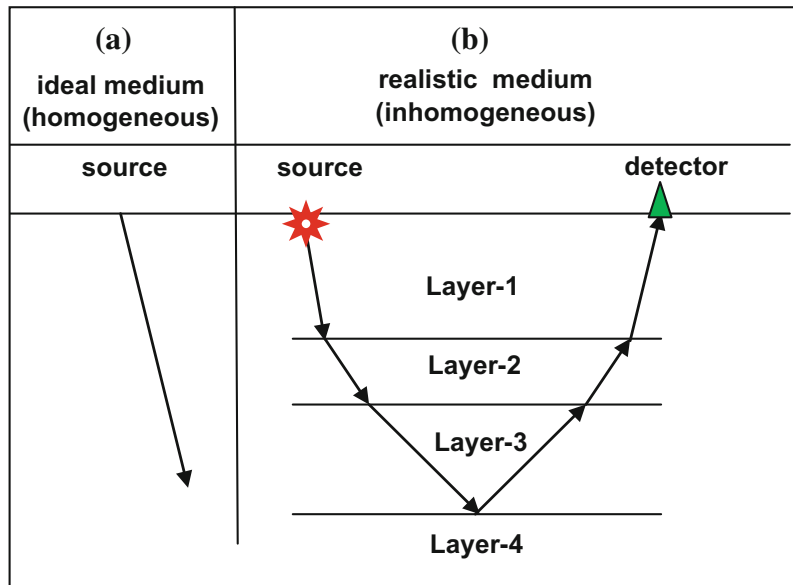
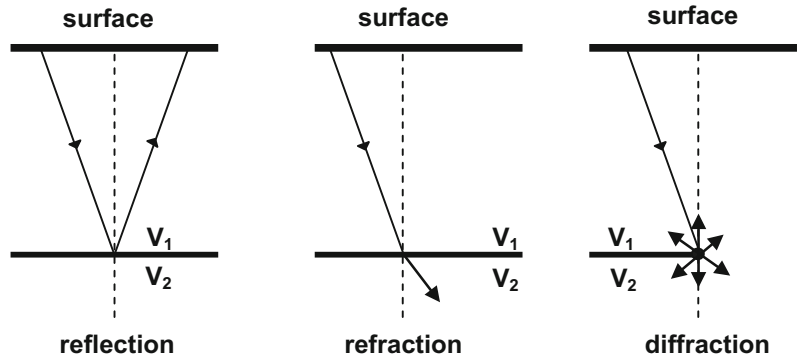


**Fig. 2.24** Ray-path geometry of the three most common wave propagation ray-paths: reflection, refraction, and diffraction



(refraction), and diffraction. These shapes of the moving wave ray-path occur at the boundaries of media having different seismic propagation velocities (Fig. 2.24).

**2.5.6 Wave Conversion at Interfaces**

When a seismic wave impinges on an interface separating two media, which differ in acoustic impedances, the incident seismic energy is partly reflected and partly transmitted with certain waveform changes. When the ray-path of an incident seismic wave is oblique, that is inclined with respect to an interface, new waves are generated. If, for example, the incident wave is P-wave (or SV-wave) separating two solid media

of different density and elastic properties (different acoustic impedances), four new wave phases are generated; reflected and refracted P- and SV-waves. If, however the incident is SH-wave, the generated waves are only reflected and refracted SH-wave. The SV-waves, generated from an incident P-wave, (or P-waves generated from an incident SV-wave) are called (converted waves) (Fig. 2.25).

An incident seismic wave onto an interface will be partly reflected and partly transmitted across the interface. In general, the interface will bring about wave conversion, reflection, transmission, and diffraction. It should be noted here that refraction is a special case of transmission. Refraction (ray-path bending) occurs only in the case of inclined incidence.

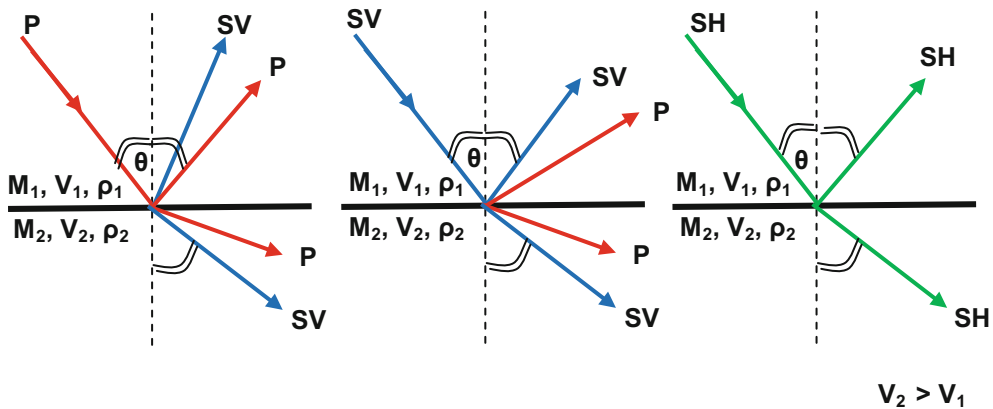


**Fig. 2.25** Wave conversion at an interface for three types of incident waves (*P*, *SV*, and *SH* waves). The symbol ( $\theta$ ) denotes angle of incidence

### 2.5.7 Energy Partitioning and Zoeppritz Equations

The mathematical expressions describing the energy partitioning of an obliquely incident wave among the created converted waves, were derived first by Knot (1899) and later on by Zoeppritz (1907), but not published until (1919). Using an approach (based on displacement computations), Zoeppritz has derived the equations (commonly known as Zoeppritz equations) which express the relative energy partitioning as function of angle of incidence and acoustic impedances of the media separated by the involved interface.

In the geophysical literature, these equations are presented in the form of curves for certain two-layer models with defined density and elasticity properties (see for example, Grant and West 1965, p. 54, Telford et al. 1990, p. 157, Sheriff 2002, p. 401). A complete coverage of various types of incident waves, with different types of media, is found in (Ewing et al. 1957).

Because of the numerous possible parameter-values required to define the behavior of energy-distribution as function of incidence angle, many curves are required for the various cases. These cases represent selected types of

incident waves (P, SV, SH) and impedances elements (velocity and density) for each of these wave-types. A typical set of Zoeppritz curves for the case of an obliquely incident P-wave is shown in Fig. 2.26.

Referring to Fig. 2.26, it can be seen that, for normal incidence (angle of incidence = 0), no S-wave is generated and thus all the energy is shared by the reflected and transmitted (refracted) P-wave. At a small angle of incidence, the converted S-waves are of small energy level. As this angle increases the generated S-waves grow stronger at the expense of reflected and refracted P-waves. At the critical angle of the incident P-wave, the transmitted P-wave energy falls to zero, and at the same time, both of reflected P-wave and reflected S-wave grow large. Build-up of energy of reflected P-wave, as the critical angle is approached, is referred to as (wide-angle reflection). This phenomenon (increase of reflection coefficient near the critical angle) is sometimes made use of in seismic reflection exploration (Sheriff 1973, p. 241).

Further, as the angle of incidence approaches grazing incidence (angle of incidence = 90), energy of the reflected P-wave increases and, at grazing incidence (where there is no vertical component for the incident P-wave), the S-waves disappear and no transmission process occurs

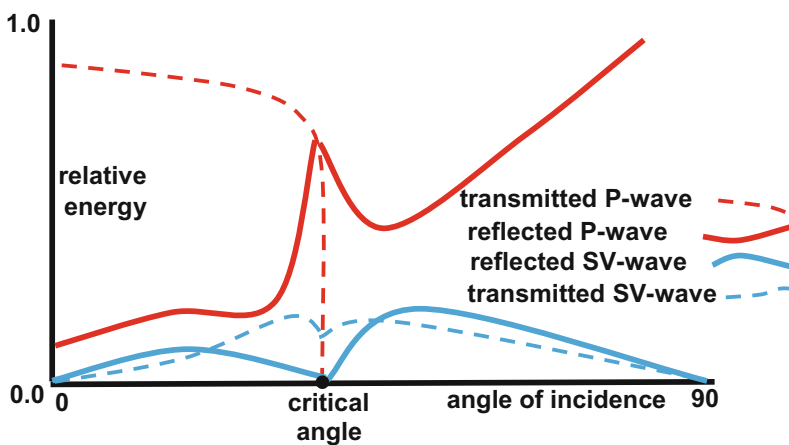


**Fig. 2.26** Typical Zoeppritz curves of energy partitioning as function of angle of incidence. The curves are for the converted waves created by an oblique incident

P-wave at an interface separating two media of specified properties (sketched, based on Dobrin and Savit 1988, p. 43)

and consequently all the incident energy is confined to the reflected P-wave.

### 2.5.8 Amplitude Variation with Angle of Incidence

For non-normal incidence, an incident P-wave leads to wave conversion in which both reflected and transmitted P- and S-waves are obtained. The obliquely-incident wave energy is distributed among all the converted waves in such a way depending on the properties of the involved media on both sides of the interface. According to Zoeppritz equations, the reflection coefficient is function of rock properties (density and elastic properties) in addition to the angle of incidence. For a given reflector, the amplitude variation with angle of incidence (AVA) of a reflected seismic wave is found to be dependent on Poisson's ratio as well as on impedance contrast across the reflection interface. In this way, the parameter (AVA) possesses the same information contained in a combined P- and S-waves data.

It is important to note that Zoeppritz equations give direct relation of amplitude variation with angle of incidence (AVA) and not amplitude variation with offset (AVO). However, offset is proportional to angle of incidence, in

case of reflections from a given horizontal reflector. There are, however, situations where the angle of incidence does not vary with the offset. Thus, in a multi-reflector case, the angle of incidence (which is equal to angle of reflection for the same wave-type), varies with reflector depth for a fixed offset. Also, in certain cases, it is possible to get different offsets for a fixed value of reflection angle. These two cases which occur in multi-reflector situation are shown in Fig. 2.27.

As expressed by Zoeppritz equations, the reflection coefficient shows variation with increasing angle of incidence (or with increasing offset). Depending on the distribution of the acoustic impedance on both sides of the interface, the reflection coefficient can vary from large-negative to large-positive values. This behavior (variation of reflection coefficient with angle of incidence) can therefore be used as an indicator to predict lithological changes or type of fluid deposits.

### 2.6 Effect of the Medium on Wave Energy

Due to the earth filtering effect and other causes, the wavelet generated by the source energy, is changed from its initial high-energy, impulsive

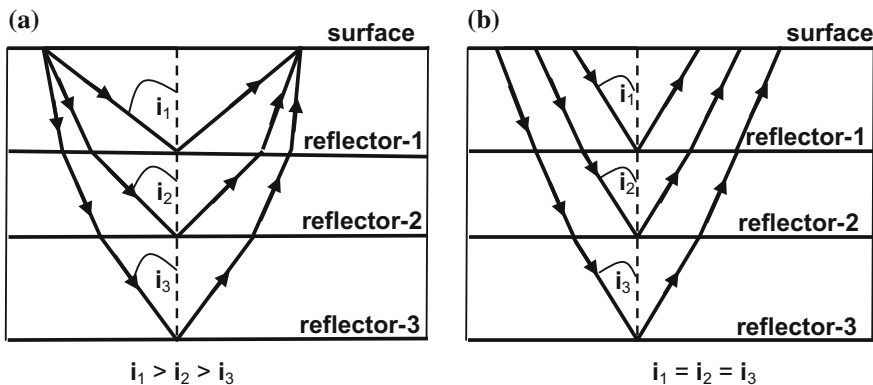


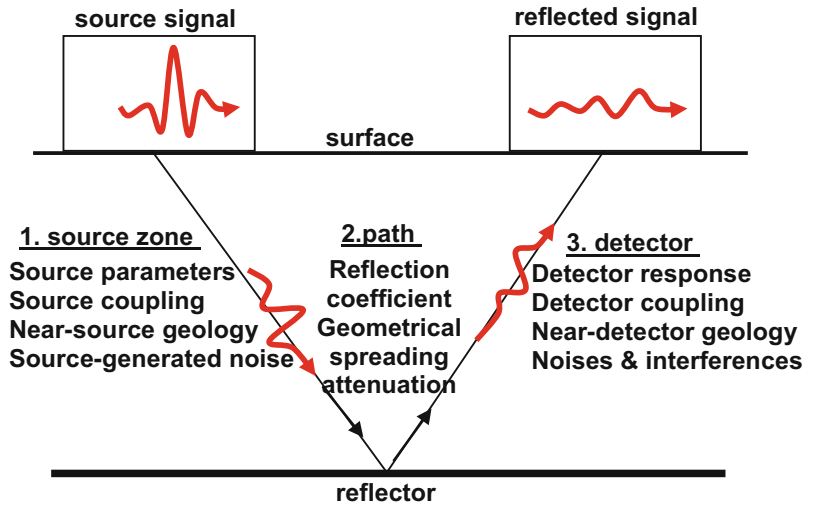
**Fig. 2.27** Variation of reflection angle with reflector depth for a fixed offset and variation of receiver offset for a fixed reflection angle. **a** Angle of incidence ( $i$ ) decreases

with increase of reflector depth for fixed offset, and **b** angle of incidence is constant for varying offset

**Table 2.4** Factors contributing to energy changes of a travelling seismic signal

1. In the source zone	2. In the path zone	3. In the detector zone
Energy-Source parameters	Reflection coefficient	Detector response
Source coupling	Geometrical spreading	Detector coupling
Near-source geology	Inelastic attenuation	Near-detector geology
Source-generated noise	Wave conversion	Surface noises
Noises and interferences	Noises and interferences	Noises and interferences

**Fig. 2.28** Reflection–signal playground. The source impulse getting weaker and broader as it progresses along its reflection travel-path. Factors affecting the signal prevailing in the three zones: source-, path-, and detector-zone



form into a lower energy and stretched-form wavelet when observed at the end of its travel-path. Taking the case of reflection of a seismic signal, the complete signal play-ground and the main factors, contributing to the signal energy changes, are summarized in Table 2.4 and Fig. 2.28.

We have already discussed the energy changes (expressed by the reflection and transmission coefficients) due to incidence of a seismic wave onto an interface. Two other important types of energy changes due to the medium through which the wave is propagating are to be discussed. These are the geometrical spreading and the inelastic attenuation effects.

### 2.6.1 Geometrical Spreading

In case of a homogeneous medium, seismic energy generated at the source, spreads out as spherical wave fronts concentric at the source point. Due to expansion of the advancing wave-front, wave energy is distributed over increasing wave-front surfaces. Mechanism of reduction of the wave energy level with travel-distance can be presented with the aid of (Fig. 2.29).

Referring to Fig. 2.29, let a source energy ( $E$ ) be generated at the source point, then, after travelling distances ( $r_1$ ) and ( $r_2$ ) the corresponding energy-density of the spherical wave fronts will be ( $e_1$ ) and ( $e_2$ ) respectively. The same

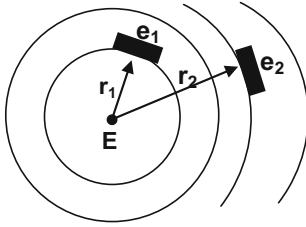


**Fig. 2.29** Wave-fronts generated by a point source are spreading out as spherical wave-fronts in a homogenous medium

energy quantity ( $E$ ) is distributed over the wave-fronts of radii ( $r_1$  and  $r_2$ ), hence:

$$E = 4\pi(r_1)^2 \cdot e_1 = 4\pi(r_2)^2 \cdot e_2$$

giving,

$$e_1/e_2 = (r_2)^2/(r_1)^2$$

or, (since energy is function of the square of amplitude,  $a$ ),

$$a_1/a_2 = r_2/r_1$$

This result has shown that amplitude attenuation due to spreading of the wave-fronts (called geometrical spreading) is proportional to the travelled distance. In isotropic media, the energy spreads out in the form of advancing spherical surfaces. For this reason the phenomenon is sometimes called (spherical divergence).

The amplitude value is related to the travelled distance ( $r$ ) according to inverse relation. Thus, ( $a$ ) is proportional to ( $1/r$ ), or to ( $1/v(t) \cdot t$ ), where  $v(t)$  is the velocity expressed as function of travel-time ( $t$ ). For a medium made up of parallel layers, it was shown by Newman (1973) that geometrical spreading depends on ( $1/v^2(t) \cdot t$ ) and not on ( $1/v(t) \cdot t$ ), that was derived for homogeneous media.

It is important to be aware that geometrical spreading is independent of frequency.

## 2.6.2 Inelastic Attenuation

Due to friction between the vibrating particles of a medium traversed by a propagating seismic wave, some of the vibration energy is lost as a result of being converted into heat. The amount of loss increases with the increase of distance ( $r$ ) from source point. Experimentally, this is found to take an exponential function of the form:

$$a(r) = a_0 e^{-\alpha r},$$

or,

$$a(t) = a_0 e^{-\alpha \cdot v(t) \cdot t}$$

where,  $a(r)$  is the amplitude at distance ( $r$ ), ( $a_0$ ) is the initial amplitude, ( $\alpha$ ) is the attenuation coefficient (expressing amplitude reduction due to absorption), ( $v$ ) propagation velocity, ( $t$ ) travel-time, and ( $e$ ) is base of natural logarithm ( $=2.71828$ ).

Earthquake seismologists often express the attenuation function in a different form (see for example Båth 1974, p. 275),

$$a(t) = e^{-\omega t/2Q},$$

Comparing this form with the form involving the absorption coefficient ( $\alpha$ ), the  $\alpha$ - $Q$  relationship is obtained. That is:

$$\alpha = \pi f/Qv$$

This means that the absorption coefficient ( $\alpha$ ) is linearly dependant on frequency, implying that higher frequencies are attenuated faster with increasing distance (or with time). This is supported by experimental evidences, which are proving that the earth is acting as a high-cut (or low-pass) filter to travelling seismic waves. That is why frequencies decrease with depth, as it is commonly observed on raw reflection-records.

The parameter ( $Q$ ), called the quality factor, expresses the absorption-capability of the

medium. It is dimensionless quantity and independent of frequency. The quality factor is inversely proportional to the attenuation factor ( $\alpha$ ). The term  $1/Q$  is called the specific dissipation.

### 2.6.3 Seismic Wave Energy Measurement and the DB Unit

We are all familiar with the units with which physical quantities are measured. Common examples are: gram for measuring mass, meter for lengths, and seconds for time. Ratios, on the other hand, have no units as such. The decibel unit (or db), which is one-tenth of the bell unit, is introduced for measuring values of ratios in just the same way as in measuring masses, lengths, and other physical quantities. The db unit seems to have been developed in connection with measuring energy- or power-ratios of sound-wave intensity expressed by its wave energy or by its wave amplitude. Likewise, the db-unit is usually used in measuring seismic wave energy.

The decibel is defined to be the unit of measuring a power (energy) ratio ( $E$ ), expressed in logarithmic domain to the base 10, hence,

$$[E]_{db} = 10 \log_{10} E = 20 \log_{10} A$$

where the power quantity ( $E$ ) is related to the square of amplitude ( $A$ ).

From this definition, it is apparent that the ratio expressed in decibels is positive when  $E > 1$ , and negative for  $E < 1$ , and it is zero when  $E = 1$ . Another useful note is that ratios (in the db-domain) are added or subtracted corresponding to multiplication or division of the original ratios. For example the ratio of (2/1) in db units, is  $20\log(2)$  which is equal to (6 db), and that of the ratio (1/2), it is (-6 db).

### 2.6.4 The Logarithmic Decrement

There is an attenuation parameter, called the logarithmic decrement ( $\delta$ ), closely associated with the inelastic attenuation coefficient ( $\alpha$ ). This

parameter is defined to be the natural logarithm of the ratio of two neighboring amplitudes of a gradually fading wave-train. This is customarily measured by the ratio of two amplitudes separated by one wavelength (Fig. 2.30).

By definition, the logarithmic decrement ( $\delta$ ) is given by:

$$\delta = \ln(a_1/a_2) = \ln e^{-\alpha r} / e^{-\alpha(r+\lambda)} = \ln e^{\alpha\lambda}$$

hence,

$$\delta = \alpha\lambda$$

From this result the mathematical relations connecting ( $\alpha$ ,  $Q$ , and  $\delta$ ) can be readily obtained. Thus,

$$\alpha = \delta/\lambda = \pi f/Qv,$$

Due to these natural attenuation effects, the reflection arrivals from deep reflectors are much weaker than those coming from shallow reflectors. If a raw seismic trace is displayed, the reflection-events from deep reflectors are so weak that they can be barely noticeable. However, when the attenuation due to spherical divergence (geometrical spreading) and due to absorption, is compensated, all events (shallow and deep events) can all be clearly seen (Fig. 2.31).

### 2.6.5 Wave Dispersion

Wave dispersion is a phenomenon that occurs to the propagating wave for which velocity is

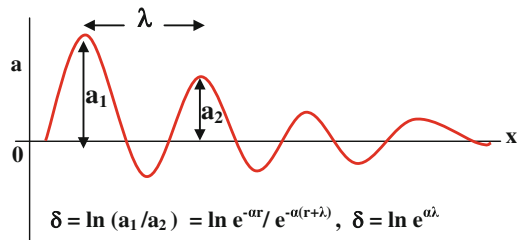
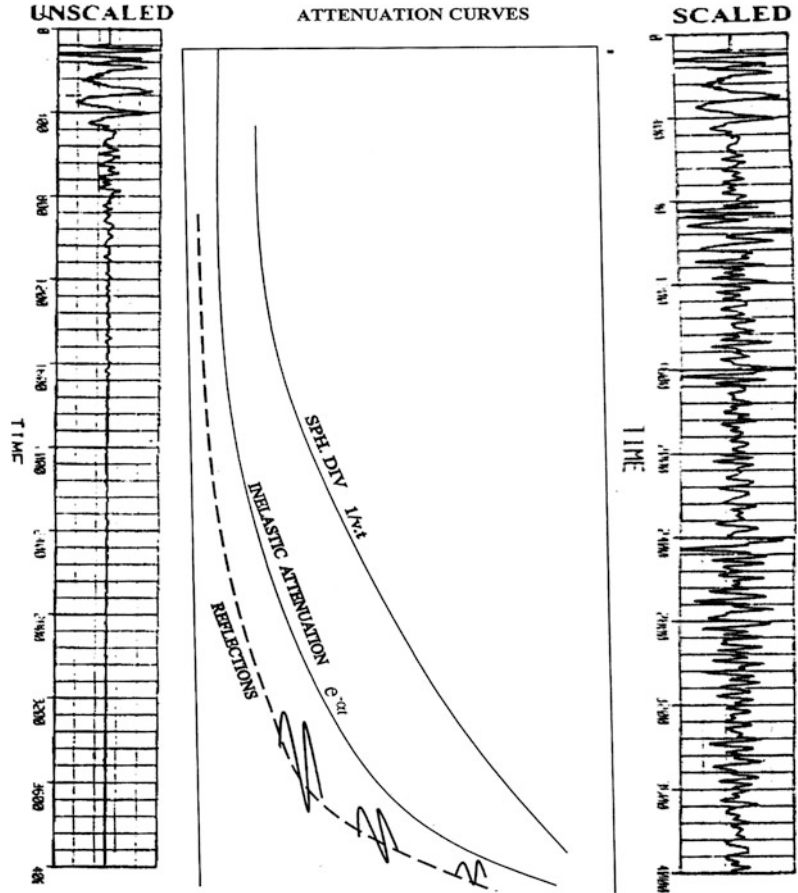


Fig. 2.30 Definition of the logarithmic decrement ( $\delta$ )

**Fig. 2.31** Seismic trace before application (unscaled) and after application (scaled) of the spherical divergence and inelastic attenuation corrections



function of the frequency component of the travelling wave. Dependence of velocity on frequency means that each frequency component of a seismic signal moves with its own velocity. Thus a wave, composed of several frequency-components will experience component-separation, and hence, change-of-form that occurs during travel. Distortion of the wave-form due to dependence of the velocity on individual frequency-components is called (wave-dispersion).

The dispersion phenomenon leads to changing of the shape of the wave train with travelled distance. Each frequency component (that is, each wave-phase) moves with its own individual velocity (the phase velocity,  $V$ ). This is the velocity with which a given point, marked on the

travelling wave, is moving. The wave-train or the energy package (expressed by the envelope of the wave train) is travelling with different velocity called (group velocity,  $U$ ) as shown in Fig. 2.32.

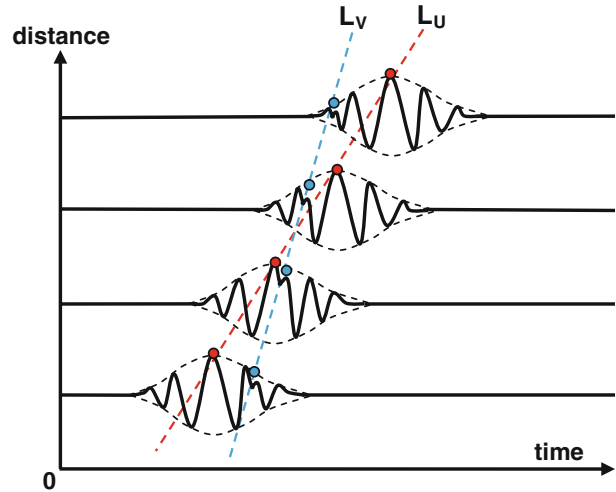
The group velocity ( $U$ ) is mathematically related to the phase velocity ( $V$ ) and wavelength ( $\lambda$ ) of the frequency component, by:

$$U = V - \lambda(dV/d\lambda)$$

where,  $V$ ,  $\lambda$ , and  $dV/d\lambda$  are average values for the range of frequencies making up the principal part of the pulse (Telford et al. 1990, p. 154).

When the phase velocity ( $V$ ) increases with increase of the component period, it is termed as (normal dispersion), and in this case the group

**Fig. 2.32** A wave train showing normal dispersion as it is propagating. The group velocity ( $U$ ) and phase velocity ( $v$ ) are given by the slopes of the lines  $L_U$  and  $L_V$  respectively



velocity is less than the phase velocity ( $U < V$ ). For the opposite case (inverse dispersion), it is when phase velocity decreases with period we get ( $U > V$ ). In the absence of dispersion, the two velocities are equal ( $U = V$ ) and no distortion to the wav-form occurs.

Dispersion phenomenon occurs in a dispersive medium, as when surface waves are travelling through a semi-infinite medium which is overlain by a low velocity surface layer. Dispersion of seismic body waves (P- and S-waves) are too small to be detected in practice.

---

### 3.1 Introduction

The wave-propagation velocity plays a fundamental role in the theory and application of seismic waves. It enters in the wave-motion equation as well as in the wave changes occurring at interfaces. Seismic-energy partitioning at interfaces (reflection and transmission coefficients) is governed by variations of the acoustic impedance which is, in turn, dependent on the wave velocity. For a given seismic wave-type, velocity of any type of seismic waves is function of density and elastic constants of the medium in which the wave is moving. Further, we have for a given medium; each wave type has its own propagation velocity. Thus, for example, P-waves move faster than S-waves which, in turn, move faster than Rayleigh waves. In the common earth material where Poisson's ratio is about  $(1/4)$ , P-wave is nearly  $(1.7)$  times as fast as S-wave and  $(1.9)$  times as fast as Rayleigh wave in the same medium. That is why we see in a typical earthquake seismogram, that P-waves arrive first, followed by S-waves and then followed by Rayleigh waves (Fig. 3.1).

---

### 3.2 Factors Influencing Seismic Velocity

Since velocity of a seismic wave is basically a function of the physical properties (density and elasticity) of the traversed medium, it is naturally

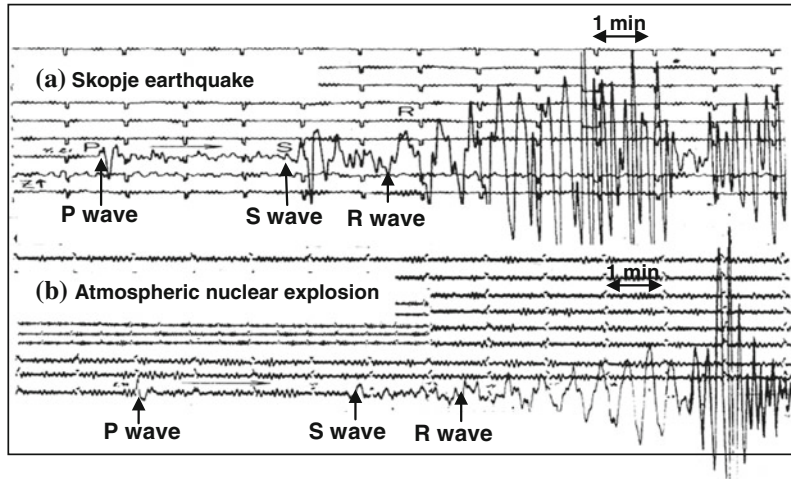
affected by these properties. The main factors affecting the propagation velocity of seismic waves are: rock lithology, elastic coefficients, bulk density, and fluid contents. These factors are here-below briefly presented.

#### 3.2.1 Lithology Effect

In nature, rocks differ widely in their chemical and physical properties. These properties (density, porosity, fluid saturation, crystallization, mineral content, rock texture) make up the lithological type of rocks. This means that the seismic velocity, which is a function of the overall physical properties, depends on the lithological nature of the medium. Igneous rocks, for example, are normally characterized by their high seismic velocity compared with the sedimentary rocks.

It is very common that a rock type is characterized by a wide range of velocities rather than by one single value. This is because of variation of properties found within the one defined rock-type. A sandstone rock, for example, may have a velocity value anywhere in the range of approximately  $(2-6)$  km/s. The corresponding range for limestone is  $(3-7)$  km/s. Usually, there are overlaps in the velocity ranges for the different lithologies. For this reason it is difficult to identify the type of lithology on basis of velocity criterion alone. The following Table 3.1 contains ranges of values of P-wave velocity, bulk density, and

**Fig. 3.1** Long period vertical-component seismograms recorded at Uppsala (Sweden). **a** Skopje earthquake, July 26, 1963, mag. 6.0. **b** An atmospheric nuclear explosion, mag. 5.4. Arrivals of *P*, *S*, and Rayleigh (*R*) waves are as shown (Båth 1973)



acoustic impedance for the most commonly known rock-types (Al-Sadi 1980, p. 70).

### 3.2.2 Elasticity and Density Effects

The wave motion equation of seismic waves includes the velocity factor present in its mathematical expressions. For a solid homogeneous medium, the propagation velocity for P- and S-waves ( $v_p$  and  $v_s$ ) are functions of elastic constants of the medium (Lame’s elastic constants,  $\lambda$  and  $\mu$ ) as well as its bulk density ( $\rho$ ). These functions are:

$$v_p = [(\lambda + 2\mu)/\rho]^{1/2}$$

and,

$$v_s = [\mu/\rho]^{1/2}$$

Although the mathematical expressions of the velocity-density relations show that velocity is inversely proportional to the square root of density, it is a common observation that velocity appears to be increasing as density increases (Nafe and Drake 1963; Gardner et al. 1974). The explanation for this discrepancy, is that as the material becomes more compact (that is as density increases) its elastic

coefficients increase in such a way that it offsets the effect introduced by the density increase. An empirical relationship between P-wave velocity ( $v$ ) and bulk density ( $\rho$ ) for the common sedimentary rocks (sandstone, shale, limestone, anhydrite ...) is given as follows (Gardner et al. 1974):

$$\rho(v) = kv^{1/4}$$

where ( $k$ ) is equal to 0.31 when ( $v$ ) is in m/s and equal to 0.23 when ( $v$ ) is in ft/s.

Density values for common rock types are found in Table 3.1 presented above.

### 3.2.3 Porosity and Saturation Fluid Effects

Porosity (defined as the pore volume per unit volume) has an effective role in seismic velocities because of its direct relation to the bulk density. In a porous rock, velocity is affected by porosity as well as on the type of interstitial fluid. In general there is an inverse relationship between porosity ( $\emptyset$ ) and velocity ( $v$ ) of rocks. Velocity of a fluid-saturated rock is given by the following empirical formula which is normally called the time-average equation (Wyllie et al. 1958):

**Table 3.1** Propagation velocities of compressional waves, densities, and acoustic impedances for selected media

Medium	Density, $\rho$ (gm/cm <sup>3</sup> )	Velocity, $V_p$ (m/s)	Acoustic impedance, $Z$ (gm/s cm <sup>2</sup> ) $\times 10^{-4}$
Air	0.0013	330	0.004
Aluminium (P)	2.70	6300–7100	170–192
Anhydrite (P)	2.82–2.93	3500–5500	99–161
Basalt (S)	2.70–3.30	5500–6300	149–208
Chalk (P)	1.94–2.23	2100–4200	41–94
Clays (P)	1.5–2.5	1100–2500	17–63
Copper (P)	8.96	4820–5960	432–534
Diabase (P)	2.80–3.11	5800–6600	162–205
Dolomite (P)	2.75–2.85	3500–6900	96–197
Dunite (S)	3.20–3.31	7500–8100	240–268
Gabbro (P)	2.85–2.92	6450–6700	184–196
Gneiss (P)	2.66–2.73	3500–7500	93–205
Granite (P)	2.52–2.82	4750–6000	120–169
Granodiorite (P)	2.67–2.78	4600–4880	123–136
Gypsum (P)	2.31–2.33	2000–3500	46–81
Ice (G)	0.97–1.07	3100–4200	30–45
Limestones (P)	2.58–2.80	3400–7000	88–196
Marble (P)	2.75	3750–6940	103–191
Marl (G)	2.25–2.86	2000–3500	45–100
Moraine (P)	1.5–2.0	1000–2700	15–54
Oil (P)	0.6–0.9	1275 (23 °C)	8–11
Peridotite (S)	3.15–3.28	7800–8400	246–276
Rock salt (G)	2.14–2.18	4200–5500	90–120
Sand (P)	1.60–1.90	600–1850	10–35
Sandstones (P)	2.15–2.70	2100–4500	45–122
Shale (G)	2.41–2.81	2700–4800	65–135
Water (G)	0.98–1.01	1430–1590	14–16

Symbols (P, G, and S) indicate references:  
(P) Parasnis (1971) (G) Gurvich (1972) (S) Sharma (1976)

$$1/v = \phi/v_f + (1 - \phi)/v_m$$

or, in terms of interval transit time,  $T (= 1/v)$ ,

$$T = \phi T_f + (1 - \phi)T_m$$

where, ( $v_f$ ) and ( $v_m$ ) are the velocities of the fluid content and rock matrix respectively, and ( $T_f$ ) and ( $T_m$ ) are the corresponding transit times

Another velocity-porosity relationship was developed (Pickett 1969) which does not explicitly

involve the effects of the rock and fluid contents individually. It has the form:

$$1/v = C_1 + C_2\phi$$

where  $C_1$  and  $C_2$  are constants, depending on lithology and depth of burial.

Velocity-change with porosity depends on the type of fluid (gas, oil, water) and the pressure it is subjected to. Velocity decreases with increase of gas saturation. Gas has more effect than liquid (such as oil or water) in lowering velocity. It is

noted that only a small amount of gas, present in pores, produces sharp decrease in velocity, but further increase in gas saturation produces only a minor effect. This phenomenon was applied as a tool for detection of hydrocarbon accumulation in oil traps. Being more compressible than oil or water, gas has the effect of lowering the velocity much more than the presence of oil or water as interstitial fluids. Due to its effect on the elastic properties of rocks, even a small quantity of gas present in the pores, would result in large reduction in velocity (Sheriff and Geldart 1995, p. 109). Clearly, this property has an important application in hydrocarbon exploration.

### 3.2.4 Depth and Geological Age Effects

With depth of burial and with geological age, in general, rock material becomes more compact. This would result in increase in elastic constants as well as in the density and, consequently, increase in velocity. Dependence of velocity ( $v$ ), of a particular geological bed, on geological age ( $g$ ), existing at depth ( $h$ ), is expressed by the following empirical formula (Faust 1951):

$$v(g, h) = k(g \cdot h)^n$$

where ( $k$ ) is constant (equal to 125.3 when depth in feet, velocity is in ft/s, and geological age in years). The index ( $n$ ) is found in this study to be equal to (1/6). In a later study (Gregory 1977) made on sand- and shale-formations data, the index ( $n$ ) is found to be equal to (1/4).

Variation of velocity with the depth of burial was investigated by a number of geophysicists (e.g. West 1950; Kaufman 1953; Acheson 1963), confirming the general trend of velocity increase with depth.

As the function,  $v(h, g)$  is showing, geological age bears a relationship with velocity similar to that of the depth factor. It shows that velocity is in general increasing with depth and geological age. The explanation is that, grain compaction increases with increase of depth and geological age. In consequence, elastic constants are increased

resulting in a velocity increase with both depth and geological age.

Faust formula (Faust 1951), for a given geological interval, can be presented in terms of the interval transit time,  $T (=1/v)$ . This form is presented as follows (Pennebaker 1968):

$$T(h) = Ch^{-n}$$

or,

$$\log T(h) = -n \cdot \log h + \log C$$

where ( $C$ ) is constant related to the rock lithology, pore pressure, and geological age.

For sand-shale sequence, Pennebaker (1968) found that the index ( $n$ ) has a value of about (1/4). This is considered to be representing a geological section existing under normal compaction-pressure. As it is seen above, the ( $T-h$ ) relation is linear when it is expressed in the log-domain. Thus, when a linear ( $\log T - \log h$ ) relation is obtained in a certain study, the geological section is considered to be under normal compaction pressure conditions. Deviation from the linear relation (straight-line relation) is normally considered as indicative of abnormal pressure situation. This is another useful and effective tool that can be used to investigate subsurface pressure conditions and as an indicator for other stratigraphic features.

### 3.2.5 Overburden Pressure Effect

A theoretical relationship developed by Gassman (1951) showed that velocity of a rock-bed model made up of spherical tightly-packed grains varies as ( $P^{1/6}$ ), where  $P$  is the applied compaction pressure. The similarity of this result to Faust's empirical formula (Faust 1951) suggests that increase in velocity (i.e. decrease in the interval transit time) is due to increasing pressure imposed by the overburden rocks.

Compaction of a saturated porous layer is function of the weight of the overlying material (i.e. due to the overburden pressure,  $P_o$ ) and the pressure of the saturation fluid (the pore pressure,  $P_p$ ). Since

the effect of ( $P_p$ ) in compressing the porous rocks is in opposite direction to that created by ( $P_o$ ), the compaction net effect (compaction pressure,  $P_c$ ) is proportional to the pressure difference ( $P_o - P_p$ ). That is:

$$P_c = P_o - P_p$$

As rock compaction process brings about a corresponding change in the physical properties, it is expected that seismic velocity (or interval transit time) would vary with the applied compaction pressure. Velocity increases with increasing compaction pressure and decreases with increase of interstitial pore pressure. This velocity-pressure relationship forms the basis used in predicting subsurface pressure conditions from seismic velocity data. Use of seismic velocity as an indicator of pressure conditions was used by several workers like Pennebaker (1968), Reynolds (1970), Louden et al. (1971), and Aud (1974). Departure of the measured velocity of a given geological section from the normal-compaction trend serves as indicator of abnormal-pressure zone.

### 3.2.6 Other Velocity-Affecting Factors

In addition to the above mentioned factors, there are other less important factors which can cause small effects on seismic velocity. Examples of such factors are pore shape, anisotropy, temperature, and wave-frequency. It is found that velocity decreases slightly with increase of temperature. It is found that, for an increase of 100 °C, velocity decreases by about 5 % and that the velocity drop-rate is considerably more when the rocks are saturated with heavy crude oil or tar. Velocity in water saturated rocks experiences sudden increase as temperature is lowered to the freezing point (Sheriff and Geldart 1995, pp. 120–121).

Velocity is practically unchanged over a broad frequency range. Small change is observed in case of body-wave dispersion (velocity variation with frequency). Low-frequency components are “faster” because of frequency-dependant absorption

phenomenon. In case of anisotropic medium, velocity varies with changes in propagation direction. The main factors affecting velocity can be summarized as follows:

#### (i) Lithology

In general, igneous and metamorphic rocks have larger velocity values than sedimentary rocks. Sub-types of rock lithologies are characterized by wide ranges of velocities which are overlapping with each other. For example, the velocity-range for sandstone (2–5) km/s is overlapping with that of shale (1.5–4.5) km/s, and so on.

#### (ii) Elasticity and Density

Theoretically, velocity is directly proportional to elastic constants and inversely with density. However, because of the greater effect of elasticity, it is observed that velocity has an apparent direct proportionality with density changes.

#### (iii) Porosity and Saturation Fluid

Velocity is inversely proportional to porosity, and the change in velocity depends on the type of pore fluid. Velocity is lowered when the pores are filled with water or oil, and more lowered when the pores are filled with gas.

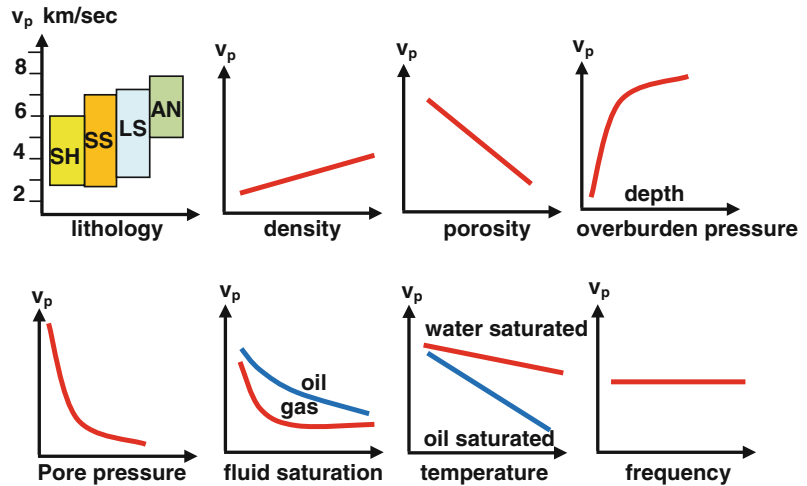
#### (iv) Depth and Geological Age

In general, velocity increases as both of the overburden depth and geological age increase. A power-law relationship is connecting the velocity with the depth and geological age. The power index for sand-shale sequence is found to be around the value of (1/6–1/4).

#### (v) Overburden Pressure

Due to compaction caused by the overburden weight, elastic constants as well as density get increased. There is a direct relation between velocity and the net compaction pressure which is equal to the difference between pore pressure and overburden pressure (geostatic pressure as it is sometimes called). Velocity increases with increasing compaction pressure and decreases with increase of interstitial pore pressure.

**Fig. 3.2** Main factors affecting seismic P-wave velocity ( $v_p$ ). The symbols *SH*, *SS*, *LS*, and *AN* denote shale, sandstone, limestone, and anhydrite respectively



(vi) Other Minor Factors

Pore shape: Velocity decreases when pores are elongate.

Anisotropy: Velocity varies with changes in propagation direction.

Temperature: Velocity slightly decreases with increase of temperature.

Frequency: Velocity practically unchanged with frequency. With normal dispersion, low-frequency components are “faster” because of frequency-dependant absorption phenomenon.

Main factors affecting velocity are shown in Fig. 3.2.

### 3.3 The Velocity Function

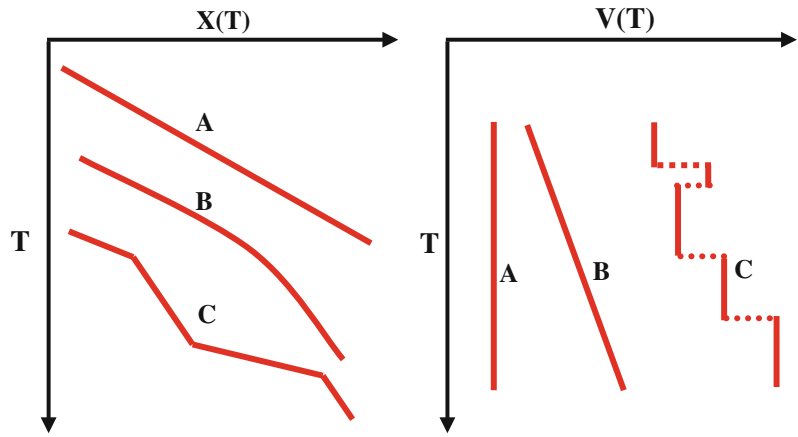
Seismic propagation velocity, as we have seen from the previous discussion, depends on a number of variables, like type of lithology, geological age, density, porosity, pressure, and depth. In seismic reflection exploration work, velocity is usually presented as mathematical functions. The velocity function is taken to describe its variation with reflection travel-distance (or, more often, with travel-time).

Since the real earth is not homogeneous (typically layered medium), seismic waves move with different velocities in different parts of its travel-path. In this case, it becomes very useful to

express the propagation velocity ( $V$ ) as a mathematical function of the travel-distance,  $V(x)$  or function of travel-time,  $V(t)$ . For practical applications, velocity is, more often, expressed as function of vertical reflection time, that is, as function of the two-way (reflection) vertical time  $V(T)$ . In a homogeneous, uniformly changing, or layered medium, the distance-versus-time functions can be linear, curved, or segmented respectively. The corresponding  $V(T)$  functions can be plotted as curved or straight lines. Typical velocity functions are shown in Fig. 3.3.

Due to the geological complexity of the earth, it is not, in practice, possible to express seismic velocity-variation in the form of an explicit mathematical function. However, under certain conditions, a geological medium is approximated by a defined set of specifications that can allow derivation of a mathematical function describing the variation of velocity along the travel-path. One of these models is one in which the instantaneous velocity ( $V$ ) increases linearly with depth ( $h$ ). This model is expressed by the linear function;  $V(h) = V_0 + kh$ , where ( $V_0$ ) is the velocity value at the surface ( $h = 0$ ) and ( $k$ ) is the velocity-depth gradient. The significance of this relation is that it gives a close approximation to the actual velocity variation observed in many sedimentary-basin areas (Dobrin 1960, p. 77). Derivation of the ray-path geometry (which turns out to be of circular form) and travel-time functions, are given by several authors (see for

**Fig. 3.3** Sketches of velocity functions for three cases: **a** homogeneous medium,  $V(T)$  is line of zero slope, **b** uniformly changing velocity,  $V(T)$  is line of constant slope, **c** layered medium, curve is made up of zero-slope linear segments



example, Nettleton 1940, pp. 257–261 or Sheriff and Geldart 1995, pp. 93–94).

### 3.4 Types of Velocity Functions

Unlike electromagnetic waves which are all of one type (e.g. wave of visible light which is of S-wave type), seismic waves are of many types, each of which has its own velocity-value which is dependent upon the density and elastic constants, as mentioned above. Because of the inhomogeneous nature of the crustal part of the Earth (which is typically made up of layered rock media), several types of velocity functions are needed to express velocity variation as function of travelled distance. Five velocity-types are in common use in seismic exploration. These are:

- (i) Instantaneous Velocity ( $V$ )
- (ii) Interval Velocity (IV)
- (iii) Average Velocity (AV)
- (iv) Root Mean Square (RMS) Velocity (RV)
- (v) Stacking Velocity (SV)

#### 3.4.1 Instantaneous Velocity

In cases where the subsurface geology is of variable nature, the seismic velocity which is governed by the physical properties of the medium will accordingly be changing with changes

of the location in the travel-path of the moving wave front. This means that at any point of the travel-path, the velocity can be measured or computed at that point. This is the (instantaneous velocity) which can be defined to be the velocity of wave motion at a given point in a medium traversed by an advancing seismic wave.

Mathematically, the instantaneous velocity ( $v$ ) at a point is given by the slope of the tangent to the distance-versus-time curve at that point (Fig. 3.4).

The instantaneous velocity, ( $v$ ) of a wave moving along a distance ( $x$ ) is defined as:

$$v = dx/dt$$

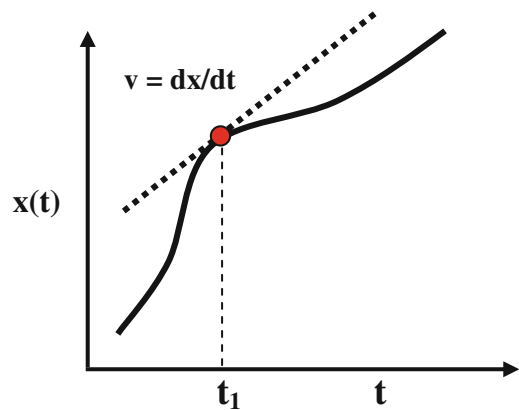


**Fig. 3.4** Definition of the instantaneous velocity ( $v$ ), given by the slope of the tangent to the  $x-t$  curve,  $v = dx/dt$  at  $t = t_1$

The closest example to the instantaneous velocity is the velocity function in which the interval transit time (which is equal to the reciprocal of velocity) is measured across each depth-interval of one meter down a drill hole. The resulting record (the sonic log) gives detailed velocity-information at points spaced by 1 m interval. This is a practical approximation of the instantaneous velocity-variation with depth.

### 3.4.2 Interval Velocity

The interval velocity (**IV**) is defined to be the average velocity over an interval of the travel-path. It is usually measured or computed for individual geological layers. Thus, the interval velocity, of a geological formation of thicknesses ( $\Delta h$ ) and interval transit time ( $\Delta t$ ), is given by  $IV = \Delta h / \Delta t$ . For a multi-layer geological section, the interval-velocity function is

covering that distance. In seismic exploration work, the average velocity is computed for a set of layers, usually starting from the datum plane down to the required reflector level.

For a vertical travel-path, the average velocity of a geological section made up of (**n**) layers will be given by dividing the total thickness  $h_n (= \Delta h_1 + \Delta h_2 + \Delta h_3 + \dots + \Delta h_n)$  by the travel-time  $t_n (= \Delta t_1 + \Delta t_2 + \Delta t_3 + \dots + \Delta t_n)$ , that is:

$$AV_n = h_n / t_n$$

or,

$$AV_n = \frac{(\Delta h_1 + \Delta h_2 + \Delta h_3 + \dots + \Delta h_n)}{(\Delta t_1 + \Delta t_2 + \Delta t_3 + \dots + \Delta t_n)}$$

An example of computation is shown in Fig. 3.6.

The average velocity (**AV**) can be calculated for a multi-layer section, given the interval velocities (**IV**) for each of the section layers. This can be done by the following formula:

$$AV_n = (\sum IV_n \cdot \Delta t_n) / \sum \Delta t_n$$

constructed by computing the interval velocity for each layer of that section (Fig. 3.5).

### 3.4.3 Average Velocity

As the name implies, the average velocity (**AV**) is obtained from dividing the total distance travelled by the wave by the time spent in

It is also possible to derive the interval velocity of a certain layer in a pack of layers, given the average velocity data. Thus, in order to compute the interval velocity (**IV<sub>n</sub>**) of the **n**th layer, we need to know the two average velocities, (**AV<sub>n</sub>**) and (**VA<sub>n-1</sub>**) for the section from the datum level down to the base and down to the top

**Fig. 3.5** Interval velocity function of a three-layer geological section.  $IV_1$  at depth  $\Delta h_1$ ,  $IV_2$  at depth  $\Delta h_1 + \Delta h_2$ , and  $IV_3$  at depth  $\Delta h_1 + \Delta h_2 + \Delta h_3$

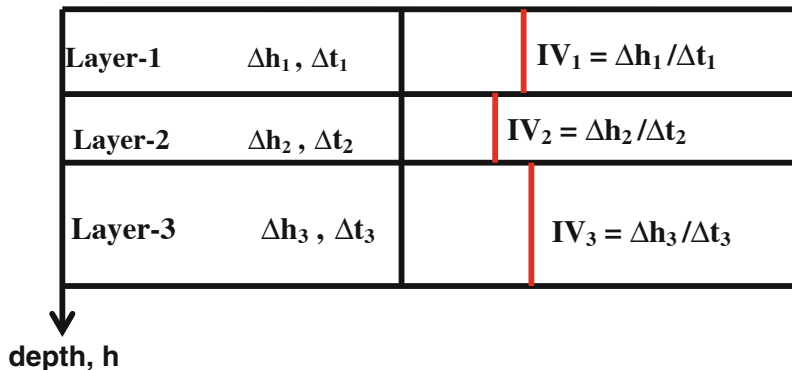
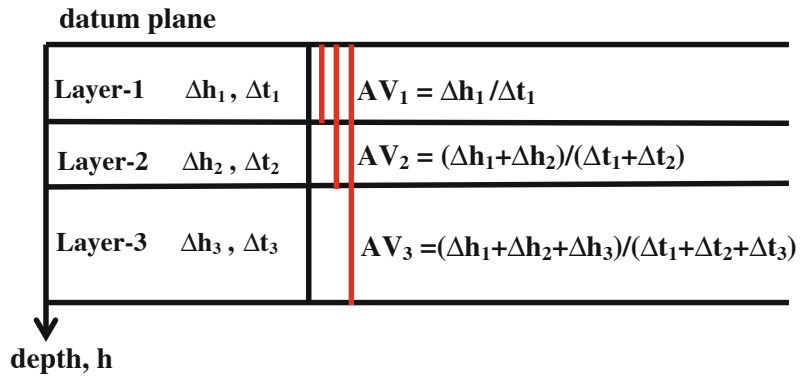


**Fig. 3.6** Average velocity ( $AV_1, AV_2, AV_3$ ) function of one, two, and three-layers of thicknesses ( $\Delta h_1, \Delta h_2, \Delta h_3$ ). The corresponding interval travel times are ( $\Delta t_1, \Delta t_2, \Delta t_3$ )



of that layer respectively. Using the corresponding travel times, ( $T_n$ ) and ( $T_{n-1}$ ), the required formula is:

medium (medium made up of horizontal layers of different interval velocities). A three-layer model is shown in the following Fig. 3.7.

$$IV_n = (AV_n \cdot T_n - AV_{n-1} \cdot T_{n-1}) / (T_n - T_{n-1})$$

### 3.4.4 Root Mean Square Velocity

Root mean square (RMS) velocity ( $RV$ ) is defined as the square root of the average of the squares of the

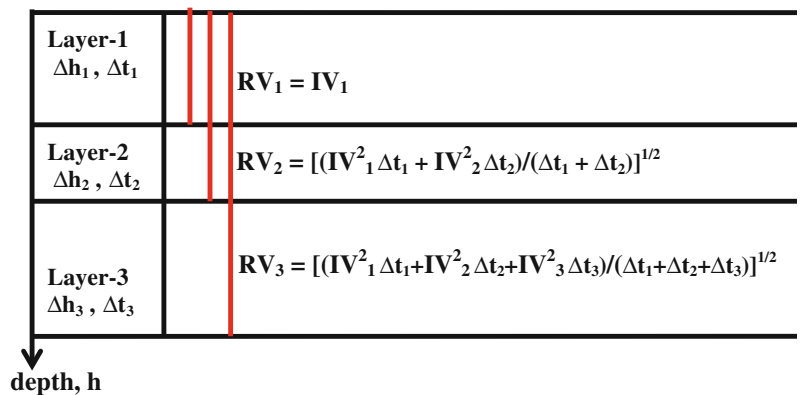
The root mean square velocity ( $RV$ ) can be calculated from the interval velocity data ( $IV$ ), down to the  $n$ th layer, by use of the following formula:

$$RV_n = [(\sum IV_n^2 \cdot \Delta t_n) / \sum \Delta t_n]^{1/2}$$

weighted interval-velocities, where the weighting factors are the layer thicknesses or the interval transit times. In seismic exploration, the RMS velocity, like other types of velocities, is usually computed for vertical ray paths of waves traversing a multi-layer

From the RMS velocity ( $RV$ ), it is possible to derive the interval velocity ( $IV$ ), given the two RMS velocities for the section, from the datum level down to the base ( $RV_n$ ) and down to the top ( $RV_{n-1}$ ) of that layer. Using the

**Fig. 3.7** Root mean square (RMS) velocity ( $RV_1, RV_2, RV_3$ ) function of one, two, and three-layers of thicknesses ( $\Delta h_1, \Delta h_2, \Delta h_3$ ). The corresponding interval travel times are ( $\Delta t_1, \Delta t_2, \Delta t_3$ )



corresponding travel times, ( $T_n$ ) and ( $T_{n-1}$ ), the required formula is (Dix 1955):

$$IV_n^2 = [(RV_n^2 \cdot T_n - RV_{n-1}^2 \cdot T_{n-1}) / (T_n - T_{n-1})]$$

For a given geological section, the RMS velocity is typically a few percents larger than the corresponding average velocity (Sheriff 1973, p. 228).

### 3.4.5 Stacking Velocity

Stacking velocity is the main velocity variable that enters in the NMO-correction formula (explained in Sect. 4.3). It is applied to remove the time-contribution of the receiver-to-source distance (called, offset) from the total reflection travel-time. This is clarified in the following (Fig. 3.8).

Stacking velocity is determined by velocity analysis technique whereby the time contribution of offset is removed before stacking of the CMP

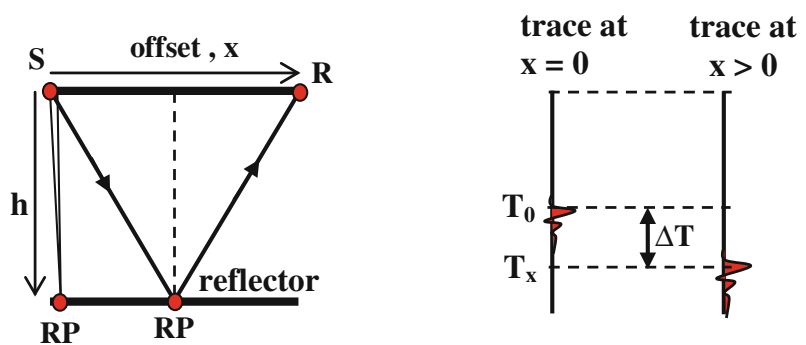
gather-traces. This is one of the fundamental processing steps (called NMO correction) which

bring about coherency of the reflection arrivals which, on stacking, give enhanced reflection event. It is called stacking velocity because of its role in enhancing the stacked reflection signal. Since its direct role is in the NMO correction, the term (NMO velocity) will be more appropriate than the commonly applied term (stacking velocity). The CMP concept is explained in Sect. 4.4.

Role of the stacking velocity in enhancing the reflection signal is schematically shown in Fig. 3.9.

In dipping parallel reflectors (dip angle,  $\theta$ ), with parallel velocity layering, the stacking velocity (call it  $V_S$ ) is equal to RMS velocity ( $V_{RMS}$ ) divided by cosine of the dip angle ( $\theta$ ) that is (Sheriff and Geldart 1995, p. 134):

**Fig. 3.8** Definition of the stacking velocity. It enters in the NMO correction formula ( $\Delta T = T_x - T_0$ ), where  $T_0$  and  $T_x$  are the reflection travel-times for zero-offset and  $x$ -offset respectively



$$T_0 = 2h/V$$

$$T_x = (4h^2 + x^2)^{1/2} / V$$

$$\Delta T = T_x - T_0 = [(x/V)^2 + (T_0)^2]^{1/2} - T_0$$

**V is the stacking velocity**

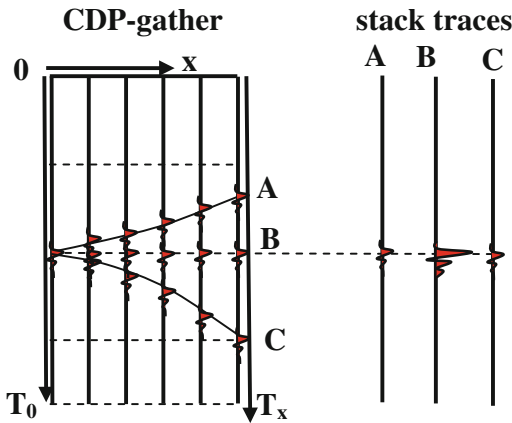


**Fig. 3.9** Role of the stacking velocity in the *NMO*-correction of a *CDP* trace gather. In this model, three stacking velocities were applied (cases: A, B, and C). The optimum velocity (case, B) gave the highest stacked signal

$$V_s = V_{RMS} / \cos \theta$$

This relation between the stacking velocity and RMS velocity can be applied by interpreters in their interpretation work of seismic reflection data and in velocity-changes studies.

Stacking velocity is sometimes called RMS velocity, because stacking velocity is the nearest in value to RMS velocity in a multi-layer medium. Like RMS velocity, stacking velocity is slightly greater than the average velocity.

### 3.4.6 The Apparent Velocity

The Apparent Velocity ( $V_a$ ) is defined as the propagation velocity measured in the direction

other than the true propagation direction. In seismic exploration, the apparent velocity is often dealt with in connection with the movement of plane wave-front advancing along a path inclined with respect to the ground surface. A plane wave approaching a ground surface with true velocity ( $V$ ), along a ray-path making an angle ( $\theta$ ) with the normal to the surface will have an apparent velocity ( $V_a$ ) of its motion along the surface (Fig. 3.10).

During a time interval ( $\Delta t$ ), the wave front moves a distance of ( $V\Delta t$ ) with the true velocity ( $V$ ), while, at the same time, the moved distance at the surface ( $\Delta x$ ) is covered by the apparent velocity ( $V_a$ ), that is:

$$V_a = \Delta x / \Delta t$$

hence,

$$V_a = V / \sin \theta$$

This relation shows that the apparent velocity is always greater than the true velocity by a factor depending on the angle of approach ( $\theta$ , in this example). The apparent velocity approaches infinity when ( $\theta = 0$ ), that is when the wave path direction is perpendicular to the surface plane. In any case the apparent velocity is always greater than the true velocity with which the wave is approaching the horizontal surface plane.

Another point of interest which is related to this subject is the apparent wavelength. Suppose that the measurements were taken for time of one period ( $\Delta t = \tau$ ), distance measured over the surface corresponding to time of one period will be

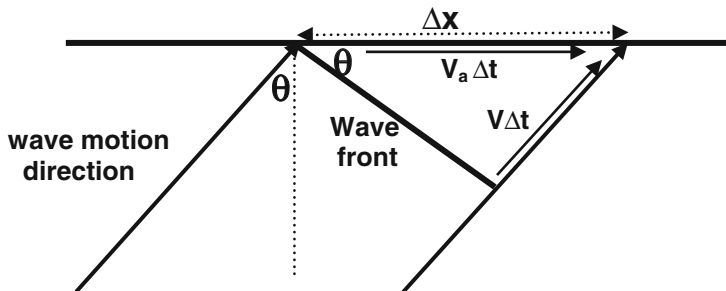


**Fig. 3.10** Ray path geometry of a plane wave approaching the surface plane at an approach angle ( $\theta$ ). Velocity in the ray-path direction ( $V$ ), and velocity of wave front measured on the horizontal plane surface is the apparent velocity ( $V_a$ )

one apparent wavelength ( $\Delta x = \lambda_a$ ), hence (using the relationship;  $\lambda = V\tau$ ):

$$\lambda_a = \lambda / \sin \theta = 2\pi / k_a$$

where ( $k_a$ ) is the corresponding apparent wave number.

### 3.4.7 The Group and Phase Velocities

The group velocity and phase velocity are distinguished in cases of dispersive waves. This phenomenon has practically no applications in the field of seismic-exploration, since the body waves, which are used in seismic exploration show no significant dispersion. Wave dispersion is common with surface waves under certain conditions. Wave dispersion occurs as result of variation of velocity with frequency, and in this case, two velocities are distinguished; the group velocity and phase velocity.

The group velocity is defined to be the velocity with which the seismic energy-packet (represented by the wave-train envelope) travels. The phase velocity, on the other hand, is the velocity of a certain frequency component of the moving wave. As usual, the two velocities differ in value and consequently, a wave-peak, or a wave-trough appears to move within the wave-train. Detailed account on this subject is found in the geophysical literature as in Richter (1958, pp. 243–244), Telford et al. (1990, pp. 153–154), and Sheriff and Geldart (1995, pp. 60–62).

### 3.4.8 Representations of the Velocity Functions

The velocity types that play important roles in seismic exploration are: interval velocity, average velocity, RMS velocity, and stacking velocity. In reflection seismology these velocities are usually plotted as functions of reflection travel time, as shown in Fig. 3.11.

As far as velocity types are concerned, there are other types of velocities of less importance to the seismic exploration applications. Most important of these are the apparent velocity, group velocity, phase velocity.

## 3.5 Velocity Determination Methods

Seismic velocity plays an important role in all activities involved in seismic exploration surveying. Its importance stems from the fact that the end product of any seismic survey is a time-image (and not depth image) of the subsurface geology. Thus, to convert the time-image data into depth domain, velocity must be made available. In seismic reflection surveying, velocity computations, aim at finding the seismic velocity (average- or interval-velocity) expressed as function of depth. There are several ways to compute the seismic velocity-function. Velocity computations are made either by methods based on borehole data or by methods based on analysis of seismic data. The two groups of velocity determination methods are:

**Fig. 3.11** Representation of the main types of velocity functions used in seismic reflection exploration

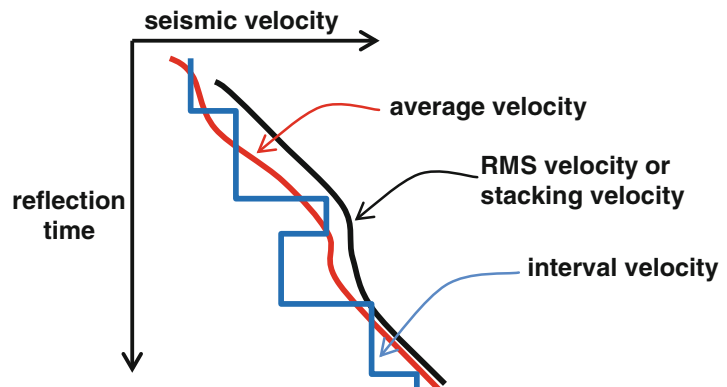
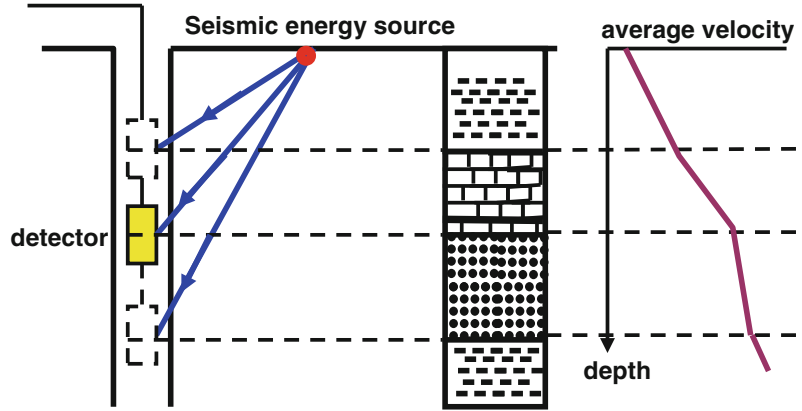


**Fig. 3.12** Method of well velocity surveying. The detector is placed at a geological-formation boundary. The curve is representing the computed average velocity as function of depth



Borehole-Based Methods

- (i) Well Velocity Surveying
- (ii) Up-hole Velocity Survey
- (iii) Continuous Velocity Survey

Seismic Data Analysis Methods

- (iv)  $(X^2 - T^2)$  Method
- (v)  $(T - \Delta T)$  Method
- (vi) Velocity Analysis
- (vii) Seismic Inversion

**3.5.1 The Well Velocity Survey**

The normal well velocity surveying proceeds by generating seismic waves from a seismic energy source located on the surface near the well head. The directly arriving wave is recorded by a detector placed at a certain depth inside the well (usually at a boundary of a geological formation). The shooting and recording process is repeated at all of the geological-boundaries penetrated by the drill-hole. For more detailed surveying, recordings are made at additional intermediate detector-positions of smaller spacing. From the source-to-detector travel time, corrected to the vertical path, the average velocities are calculated and plotted against depth (Fig. 3.12).

The source is either dynamite charge fired in a shallow drill-hole or air-gun operated in a mud pit. The detector is normally a specially-designed geophone provided with a lever that makes the geophone to be well-pressed against the borehole

wall. It may be a hydrophone-type detector suspended inside the well which is filled with the drilling fluid.

The average velocity ( $V_{av}$ ) is computed from the slant travel time ( $T$ ) of the direct wave recorded by the detector placed at depth ( $h$ ) using the formula (Fig. 3.13):

$$V_{av} = h / T_s \cos \theta$$

The interval velocity of a certain geological formation is derived by dividing the formation thickness by the interval transit time of that formation. Another way of computing of the interval velocity is calculated by the mathematical relationship connecting the interval velocity with the average velocity.

The computed velocity function is very important for the interpretation process. It is used for calibrating the sonic log and check the integrated time of the sonic log, hence the name (check-shot surveying) which is sometimes used as another name for the well shooting method.

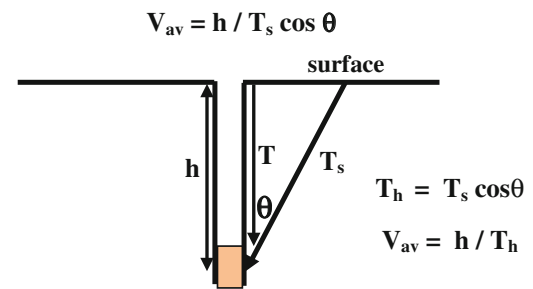


**Fig. 3.13** Computation principle of the average velocity

### 3.5.2 The Up-Hole Velocity Survey

This method is applied to determine velocity changes in relatively shallow depths, in the range 50–100 m. Its typical application is velocity-determination of the near-surface weathered zone. The same principles used in well-velocity surveying are applied in this method, but with the source-detector configuration reversed. In the up-hole case, the sources (small dynamite charges) are placed inside the borehole at few-meter spacing and sequentially fired. The detection system is placed on the surface at a location near the well-head. Velocity computation follows the same equations quoted above (Fig. 3.13).

### 3.5.3 Continuous Velocity Logging

This method uses a recording system consisting of a borehole-logging tool, called the (sonde). In its standard form, it contains a seismic-pulse source and two receivers, one foot apart, and source placed three feet from the nearest receiver. Sound pulses, emitted from the source at uniform time intervals, are detected by the two receivers. Due to the fact that P-wave velocity in the drilling fluid is lower than that of the rock-medium surrounding the well, the transmitted P-wave gets refracted at the wall-side, moving into the rock medium and then recorded by the receivers.

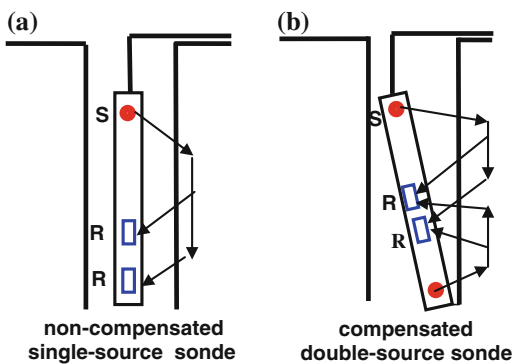


**Fig. 3.14** Schematic representation of the source-receiver configuration used in the logging sonde. **a** None-compensated, single-source sonde. **b** Compensated, dual-source sonde

The electronic structure of the sonde is designed in such a way that the output is made to be the difference in the travel-times to the two receivers. The time difference, measured in time-units per one-foot, called (interval transit time), is plotted (normally in micro-second units) against depth to give the continuous wiggly curve known as the (sonic log). Sonde basic structure is shown in (Fig. 3.14a).

To avoid tilting and hole-irregularities effects, two seismic-pulse sources are used instead of one, making what is called a (borehole-compensated sonde) as shown in (Fig. 3.14b). Seismic pulses are emitted alternately from the two sources and the transit times from the two oppositely traveling refracted P-waves are averaged electronically. The borehole compensated sonde (BHC) gives an average interval transit time which is plotted on a paper strip. The produced log in this case is normally referred to as BHC sonic log.

The BHC-log is used in computing synthetic seismograms, in identifying lithologies, and in determining formation boundaries (Fig. 3.15). The interval transit time can be integrated down the well to give the total travel time of the part of the well for which continuous velocity logging was conducted.

### Seismic Data Analysis Methods

Reflection travel-time function, in a homogeneous and isotropic medium, is of a hyperbolic

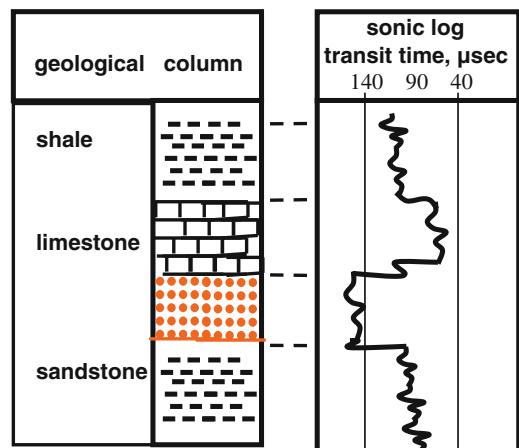


**Fig. 3.15** Use of BHC sonic-log in determination of formation boundaries and in recognizing lithologies

form. The reflection time ( $\mathbf{T}_x$ ) is function of reflector depth ( $\mathbf{h}$ ), receiver-offset ( $\mathbf{x}$ ), and propagation velocity ( $\mathbf{V}$ ). The well-known travel-time function for horizontal reflector is:

$$\mathbf{T}_x = \left[ (\mathbf{x}/\mathbf{V})^2 + (\mathbf{T}_0)^2 \right]^{1/2},$$

where,  $\mathbf{T}_0 = 2\mathbf{h}/\mathbf{V}$ .

Dependence of the reflection travel-time on velocity can be used as basis for analytical determination of seismic velocities. Two main approaches for velocity determination belong to the analytical methods. These are the reflection travel-time computations and velocity processing analysis.

### 3.5.4 ( $\mathbf{X}^2 - \mathbf{T}^2$ Method)

Since the early years of seismic reflection exploration, methods based on travel-time analysis were applied to determine velocity. In 1938, Green (1938) published a simple method of velocity calculation based on travel-times of reflection arrivals using the reflection travel-time equation,  $(\mathbf{T}_x)^2 = (\mathbf{x}/\mathbf{V})^2 + (2\mathbf{h}/\mathbf{V})^2$  or  $(\mathbf{T}_x)^2 = (\mathbf{x}/\mathbf{V})^2 + \mathbf{T}_0^2$ , and computing the velocity from the slope given by  $(1/\mathbf{V})^2$  of the  $(\mathbf{T}_x)^2 - (\mathbf{x})^2$  straight-line plot. The symbol ( $\mathbf{T}_0$ ) represents the two-way vertical reflection time from a reflector at depth ( $\mathbf{h}$ ). Furthermore, the depth ( $\mathbf{h}$ ) of the reflector, can be calculated from the intercept  $(\mathbf{T}_0)^2$ .

Another way of using the reflection travel-time equation is by recording reflection arrivals at two different-offset receivers. Thus, for such two reflection experiments, the times ( $\mathbf{T}_1$ ) and ( $\mathbf{T}_2$ ) corresponding to offsets ( $\mathbf{x}_1$ ) and ( $\mathbf{x}_2$ ) are given by:

$$(\mathbf{T}_1)^2 = \left[ (\mathbf{x}_1/\mathbf{V})^2 + (\mathbf{T}_0)^2 \right]$$

$$(\mathbf{T}_2)^2 = \left[ (\mathbf{x}_2/\mathbf{V})^2 + (\mathbf{T}_0)^2 \right]$$

hence, the velocity ( $\mathbf{V}$ ) can be calculated from:

$$\mathbf{V}^2 = \left[ (\mathbf{x}_1)^2 - (\mathbf{x}_2)^2 \right] / \left[ (\mathbf{T}_1)^2 - (\mathbf{T}_2)^2 \right]$$

To get more accurate results, the computation is repeated for larger number of offsets.

### 3.5.5 ( $\mathbf{T} - \Delta\mathbf{T}$ Method)

Another approach, based on the travel-time function is the ( $\mathbf{T} - \Delta\mathbf{T}$ ) method. By definition, ( $\Delta\mathbf{T}$ ) stands for the difference between reflection travel-time ( $\mathbf{T}_x$ ) of a seismic wave received by an x-offset detector and the corresponding zero-offset time ( $\mathbf{T}_0$ ). It is expressed by:

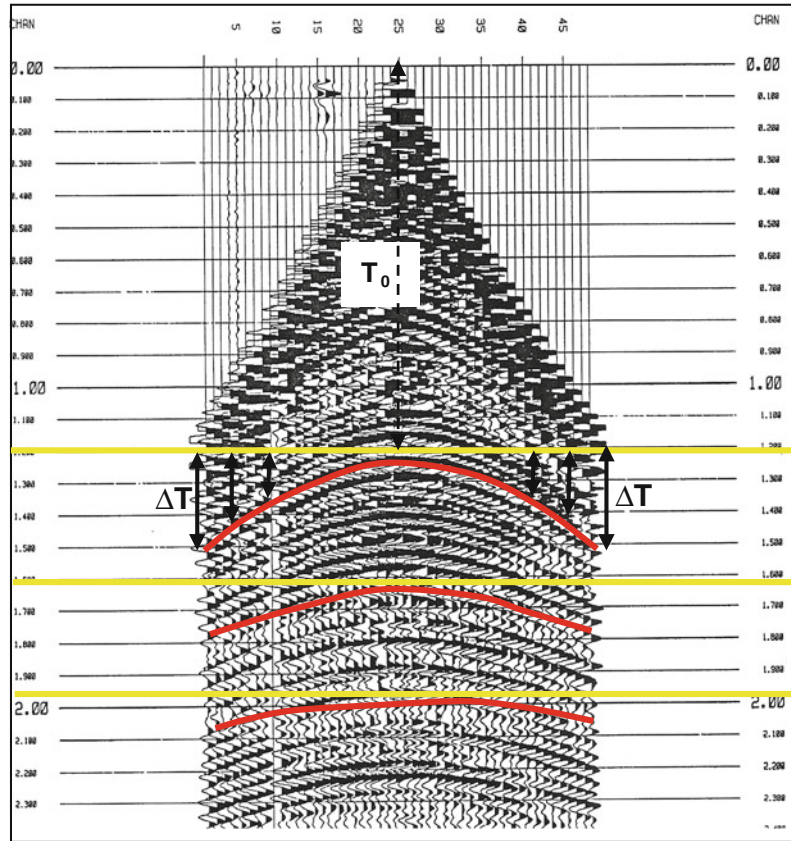
$$\Delta\mathbf{T} = \left[ (\mathbf{x}/\mathbf{V})^2 + \mathbf{T}_0^2 \right]^{1/2} - \mathbf{T}_0, \text{ (exact form)}$$

$$\Delta\mathbf{T} = \mathbf{x}^2/2\mathbf{T}_0\mathbf{V}^2, \text{ (approximate form)}$$

These equations show that ( $\Delta\mathbf{T}$ ) is function of the three variables ( $\mathbf{x}$ ,  $\mathbf{T}_0$ , and  $\mathbf{V}$ ), implying that it is possible to calculate the velocity ( $\mathbf{V}$ ), given ( $\Delta\mathbf{T}$ ,  $\mathbf{x}$ , and  $\mathbf{T}_0$ ). The parameter ( $\Delta\mathbf{T}$ ) can be readily measured from the reflection record with reasonable accuracy. Since the other variables ( $\mathbf{x}$  and  $\mathbf{T}_0$ ) are known quantities (i.e. they can be determined from a shot record), the velocity ( $\mathbf{V}$ ) can be computed. To increase the accuracy, many shot records should be used in the computations. One must remember that these equations are all based on the assumption that the reflectors are horizontal planes. If, however, the reflectors are dipping, the error can be minimized by using a centre-spread and using the average value of ( $\Delta\mathbf{T}$ ) by measuring it from traces having the same offset and located on either side of the source (Fig. 3.16).

It should be noted here that both of these two methods ( $\mathbf{X}^2 - \mathbf{T}^2$  and  $\mathbf{T} - \Delta\mathbf{T}$  methods) are now obsolete and they are replaced mainly by the velocity analysis techniques.

**Fig. 3.16** Shot record showing three reflection-events. The parameters ( $T_0$  and  $\Delta T$ ) are shown for the first reflector



### 3.5.6 Velocity Analysis Method

This method is closely related to the ( $T - \Delta T$ ) method described above. Both methods depend on computing ( $\Delta T$ ) as accurately as possible. The process of velocity analysis normally follows a trial-and-error approach. A set of trial velocity functions are applied in NMO-correcting the traces of a CMP-gather. The criterion used in recognizing the correct velocity is the S/N ratio of the stacked NMO-corrected reflection signal. The end- result of the analysis is a stacking velocity for each reflection event, plotted as function of reflection two-way vertical time.

The stack trace is obtained from summing (stacking) the CMP-gather traces after being

NMO-corrected. The correct stacking velocity is the velocity which, on NMO correction, makes all reflection events in the gather in phase, and when these are stacked, a strong reflection signal is obtained. Application of too-low velocity in the correction formula results in NMO-overcorrection, and application of too-high velocity will result in NMO-under-correction. Deviation of the applied velocity from the optimum value (that is the velocity is not too low and not too high), shall lead to fall of the amplitude of the stacked reflection signal. This phenomenon is shown schematically in Fig. 3.9.

Velocity analysis is one of the mandatory steps normally executed in processing of the seismic reflection data. The procedure followed

in the analysis is explained in more details in Sect. 10.7.1.

### 3.5.7 Seismic Velocity Inversion

The amplitude of a reflection signal ( $\mathbf{A}$ ) is dependent on the reflection coefficient ( $\mathbf{R}$ ) which is, in turn, depending on the acoustic impedance ( $\mathbf{Z}$ ) which is equal to density ( $\rho$ ) multiplied by velocity ( $\mathbf{V}$ ). This relationship ( $\mathbf{Z} = \rho\mathbf{V}$ ) shows that velocity can be determined from amplitude measurements, given the seismic impedance and density data. The basic principle, upon which the seismic inversion is based, will be presented in a simplified way, as follows:

For a plane seismic wave perpendicularly incident at an interface separating two layers of acoustic impedances ( $\mathbf{Z}_1$  and  $\mathbf{Z}_2$ ), the reflection coefficient ( $\mathbf{R}$ ) is given by:

$$\begin{aligned}\mathbf{R} &= (\mathbf{Z}_2 - \mathbf{Z}_1) / (\mathbf{Z}_2 + \mathbf{Z}_1) \\ &= (\rho_2 \mathbf{V}_2 - \rho_1 \mathbf{V}_1) / (\rho_2 \mathbf{V}_2 + \rho_1 \mathbf{V}_1)\end{aligned}$$

Assuming the amplitude of the incident wave is unity (1), and the reflected amplitude is ( $\mathbf{A}$ ), the reflection coefficient ( $\mathbf{R}$ ), by definition, becomes equal to ( $\mathbf{A}$ ) and hence, we can use the following equivalent form:

$$\begin{aligned}\mathbf{A} &= (\mathbf{Z}_2 - \mathbf{Z}_1) / (\mathbf{Z}_2 + \mathbf{Z}_1) \\ &= (\rho_2 \mathbf{V}_2 - \rho_1 \mathbf{V}_1) / (\rho_2 \mathbf{V}_2 + \rho_1 \mathbf{V}_1)\end{aligned}$$

giving:

$$\mathbf{Z}_2 = [(\mathbf{1} + \mathbf{A}) / (\mathbf{1} - \mathbf{A})] \cdot \mathbf{Z}_1$$

Since density variation is very small, compared with velocity variation, that is putting ( $\rho_1 = \rho_2$ ), the direct ( $\mathbf{A}-\mathbf{V}$ ) relationship can be obtained which is:

$$\mathbf{V}_2 = [(\mathbf{1} + \mathbf{A}) / (\mathbf{1} - \mathbf{A})] \cdot \mathbf{V}_1$$

This is an inverse problem in which the acoustic impedance (expressed by velocity) can be obtained from amplitude data. If the velocity ( $\mathbf{V}_1$ ) of the surface layer of a layered medium is known then using the inversion formula,  $\mathbf{V}_2 = [(\mathbf{1} + \mathbf{A}) / (\mathbf{1} - \mathbf{A})] \cdot \mathbf{V}_1$ , the velocity ( $\mathbf{V}_3$ ) of the neighboring deeper layer is computed. By repeating the computation, velocities of the rest of layers are sequentially determined.

Normally this approach is applied in transforming a seismic stack section into acoustic impedance section, or into what is called pseudo-impedance when density is ignored. The computations are normally carried out by software especially designed for this purpose.

## 3.6 Uses of the Seismic Velocity Data

All types of the seismic velocity have important role in the seismic exploration activities (data acquisition, processing, and interpretation). Velocity enters in the travel-time functions of all body and surface waves (direct, reflected, refracted, and diffracted waves). To start with, velocity governs reflection and transmission coefficients. In processing of seismic data, velocity forms an important factor in travel-time corrections like

**Table 3.2** Fields of application and precision assessment of various types of velocity (after Al-Chalabi 1979)

Velocity	Main uses	Precision requirements
Stacking velocity	Stacking of seismic sections Migration processing Estimation of RMS velocity	Modest to low Modest to low Dependant on situation
RMS velocity	Migration-velocity estimation Interval-velocity estimation Average-velocity estimation	Generally modest Dependant on situation Dependant on situation
Interval velocity	Lithologic and stratigraphic studies Interpretation works Abnormal pressure detection Ray tracing computations Migration processing Average-velocity estimation	High to modest Modest to low High to modest Dependant on situation Generally modest Dependant on situation
Average velocity	Depth conversion Interpretation works	Generally modest Modest to low

Precision requirements: high = 0.1–1.0 %, modest = 1–5 %, low >5 %

static and dynamic (NMO) corrections. Amplitude compensations (as in geometrical spreading and inelastic absorption) and seismic migration depend on velocity. In interpretation activities, velocity has a fundamental role in time-to-depth

conversion and in mapping structural and stratigraphic features.

Summary of fields of application and precision assessment of the various velocity-types are given in the following Table 3.2.

In the real Earth Crust, a seismic wave may meet a variety of geological changes. Typically, the media traversed by seismic waves are made up of layered rock formations of different physical properties and different geometrical shapes. In such environments, some of the seismic wave energy gets reflected from interfaces or diffracted from structural obstacles. The rest of the incident wave is transmitted through the interfaces with their ray-paths being bent (refracted) in case of inclined incidence and with no bending when ray-path is perpendicular to an interface.

In this chapter, discussion shall deal with the reflection and diffraction of seismic waves since they are physically more closely related to each other. Transmission with its special case, the refracted transmission (refraction) shall be dealt with separately in the following chapter.

---

## 4.1 The Commonly-Recorded Seismic Events

A seismic event on a shot record may be created as result of certain type of wave arrival (direct, refracted, reflected, or diffracted) depending on the nature of the involved interface and on the detector position. All of these four types of seismic events play important roles in seismic exploration activities. In normal seismic reflection records, these events are diagnosed by their recorded wave-arrivals as shown in Fig. 4.1.

A diffraction event bears a marked relation with reflection events since both are types of seismic energy generated from an intervening reflector. A plane surface (surface-reflector) causes reflection and point obstacle (point-reflector) causes diffraction.

---

## 4.2 Wave Changes at Reflection Interface

The reflection process involves two main types of changes. These are: change in the propagation direction and change in the energy content (Fig. 4.2).

The two types of changes occurring in the reflection phenomenon involve the wave energy content and its travel-path geometry. These are:

(i) Change in Energy content:

In the process of reflection, the energy content of the incident wave is shared among all of the reflected and transmitted waves. Consequently, the amplitude of any of the reflected waves is always less than that of the incident wave. Distribution of the incident seismic energy is governed by a measurement parameter, the reflection coefficient.

(ii) Change in Propagation Direction:

At the interface, part of the incident seismic energy is reflected following a travel path defined by the law of reflection which states

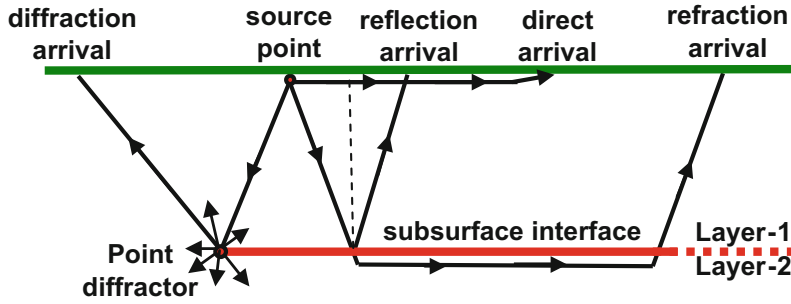


**Fig. 4.1** The four principal types of wave arrivals (direct, reflection, refraction, and diffraction) representing the commonly recorded seismic events

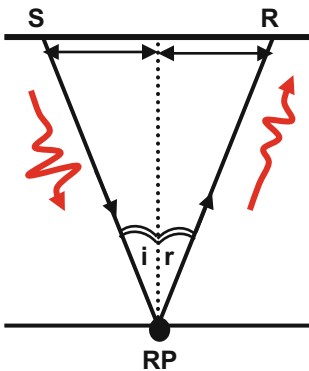


**Fig. 4.2** Reflection of a seismic wave from an interface. Travel path from the source point (*S*) to receiver (*R*) via the reflection point (*RP*). Change in travel-path direction and reduction in energy content

that angles of incidence and reflection are equal provided that these are of the same wave types. The geometry of the reflection travel-paths are normally expressed by certain adequate mathematical functions.

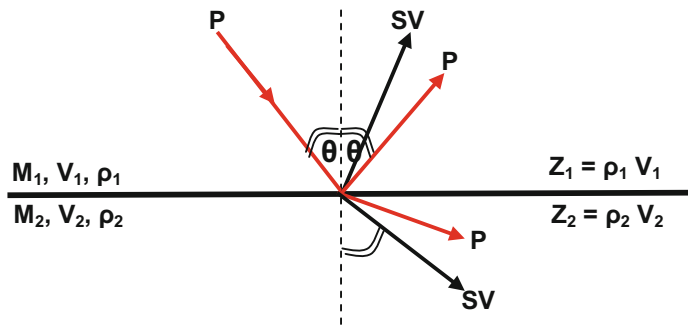
These two types of changes are dealt with in some details in the following discussions.

### 4.2.1 Reflection Coefficient at Inclined Incidence

A P-wave hitting an interface at an angle of more than zero degrees with the normal (inclined incidence) will lead to two reflected waves (P and SV) and two transmitted waves (P and SV). The law of wave reflection at interfaces (angle of incidence and that of reflection are equal) is applicable only for alike wave-phases. Thus, when the incident wave is a P-wave, the reflected P-wave follows the normal law of reflection (Fig. 4.3).

Since the energy of the incident wave is shared by the four generated waves (reflected P and SV and transmitted P and SV), any of the generated waves will be of less energy level (less

**Fig. 4.3** Inclined incidence of P-wave at an interface. Two reflected and two transmitted (*P* and *SV*) waves



incidence angle = reflection angle =  $\theta$

amplitude) compared with the incident wave. The ratio of the reflected amplitude to that of the incident represents the reflection coefficient.

Zoeppritz equations provide the mathematical expressions for the reflection and transmission coefficients of all of the produced waves (two P-waves and two SV-waves in this example). The important feature here is that the reflection and transmission coefficients are functions of both of the angle of incidence and the contrast in acoustic impedance existing across the interface.

The fundamental theoretical principles upon which solution of Zoeppritz equations is based on, is the fulfillment of the conditions which require that all normal and tangential stresses and displacements at the interface are continuous. For displacement continuity, the sum of normal and tangential displacement-components (at the interface) in the first medium must be equal to the corresponding sum in the second medium. Concerning stress, it is required that, the sum of normal and tangential stress-components are similarly equal. Another important note in this contest is that Zoeppritz equations are based on the assumption that all the involved waves are pure sine waves of same frequency which drops out of the equations (Richter 1958, p. 670). This means that no frequency change taking place in reflection and transmission processes.

#### 4.2.2 Reflection Coefficient at Normal Incidence

The mathematical derivation of Zoeppritz equations for the case of inclined incidence is of complicated nature. However, computations become less complicated in the case of normal incidence. A P-wave, for example, hitting an interface in the direction of the normal to the plane of the interface (angle of incidence equals zero) will give rise to only reflected and transmitted P-waves. No wave conversion and no refraction shall take place in this case (Fig. 4.4).

The efficiency of an interface in reflecting seismic energy is expressed by the reflection coefficient which is defined by the ratio of reflected amplitude ( $A_r$ ) to the incident amplitude ( $A_i$ ).

Sometimes, the reflection coefficient is defined in terms of energy ratios instead of amplitude ratios. With this approach, the coefficients are expressed by squares of the amplitudes.

By applying the stress and strain continuity-conditions at the interface level ( $z = 0$ ), it is possible to derive expressions for the reflection and transmission coefficients in terms of the contrast in acoustic impedance (see Sheriff and Geldart 1995, p. 76). The reflection coefficient ( $R = A_r/A_i$ ) and transmission coefficient ( $T = A_t/A_i$ ) for the case of normal incidence, are given in terms of the contrast in the acoustic impedance ( $Z$ ) of the two media on either side of the interface. Thus, by definition, the reflection and transmission coefficients ( $R$  and  $T$ ) are:

$$R = A_r/A_i = (\rho_2 v_2 - \rho_1 v_1)/(\rho_2 v_2 + \rho_1 v_1) \\ = (Z_2 - Z_1)/(Z_2 + Z_1)$$

$$T = 1 - R = A_t/A_i = C/A = 2\rho_1 v_1/(\rho_2 v_2 + \rho_1 v_1) \\ = 2Z_1/(Z_2 + Z_1)$$

If ( $R$ ) is positive, compression displacement is reflected as compression because, by reflection in this case, both of the wave-motion direction and particle displacement are reversed. If, however, ( $R$ ) is negative, a compression is reflected as dilatation, meaning that we get ( $180^\circ$ ) phase change in this case.

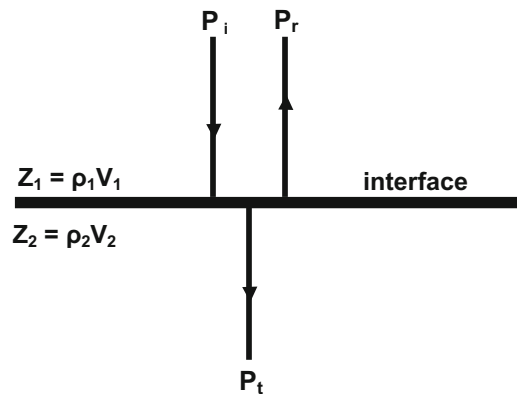


**Fig. 4.4** Reflection in case of normal incidence of P-wave at an interface. The incident, reflected, and transmitted waves are  $P_i$ ,  $P_r$  and  $P_t$  respectively

It is evident from these equations (case of normal incidence) that the reflection coefficient depends only on the contrast in the acoustic impedance ( $Z_2 - Z_1$ ). The greater the contrast, the larger reflection coefficient will be. This implies that no reflection occurs from an interface across which the acoustic impedance assumes the same value, even if either velocity or density varies individually across the interface.

The reflection coefficient ranges in value from  $(-1)$  to  $(+1)$  depending on the acoustic impedances ( $Z_1$  and  $Z_2$ ). When the acoustic impedance ( $Z_2$ ) in the second medium (medium in which transmission occurs) is greater than that in the first medium (medium of incident wave,  $Z_1$ ) a compression displacement is reflected as compression, and the reflection coefficient is positive. In the opposite case, that is when ( $Z_1 > Z_2$ ), a compression is reflected as rarefaction (phase change =  $\pi$ ) and the reflection coefficient becomes negative. Reflection coefficient is zero when the two acoustic impedances ( $Z_1$  and  $Z_2$ ) are equal, which means that there is no interface existing in the way of the incident wave.

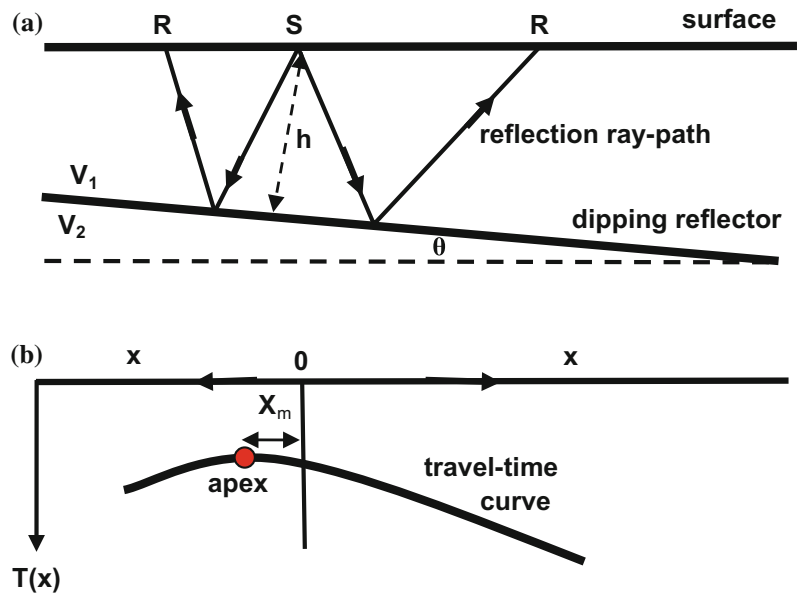
Another useful feature which may be deduced from the reflection coefficient expression, is the

case where the acoustic impedance in one of the two adjacent media is approaching zero or infinity. Thus, when ( $Z_1$ ) is very small compared with ( $Z_2$ ), that is when ( $Z_1$ ) approaches zero, ( $R$ ) approaches unity ( $R = 1$ ). In this case, the interface is considered to be ideal reflector since this means that all of the incident energy is reflected and no part of it is transmitted through. A good approximation of this kind of situation is the earth free-surface which is an interface between the upper air-medium and the lower rock-medium. Because of the vast difference between the acoustic impedances of these two media, the reflection coefficient approaches the value of  $(+1)$  for a source located in the air and  $(-1)$  for a source located inside the rock-medium. The interface in both cases is equally efficient in the reflecting process, but in the second case there occurs a polarity reversal, or phase change of ( $\pi$ ) for an incident sine wave.

### 4.2.3 Geometry of Reflection from Dipping Reflectors

The general case of reflection geometry is the case of inclined (dipping) reflector (Fig. 4.5).

**Fig. 4.5** Ray-path (a) and travel-time curve (b) of a seismic wave generated at the source point ( $S$ ), reflected from a dipping interface, and received by receivers ( $R$ ). Interface is separating media of velocities  $V_1$  and  $V_2$



The travel-time function of a seismic wave reflected from an interface which is dipping by angle ( $\theta$ ) in the source-to-receiver direction is given by:

$$T_x = (x^2/V^2 + 4z^2/V^2 + 4xz \sin \theta/V^2)^{1/2}$$

or,

$$T_x = (x^2/V^2 + T_0^2 + 2x T_0 \sin \theta/V)^{1/2}$$

where ( $T_0 = 2z/V$ ), represents the two-way reflection travel-time for the case of zero-offset receiver (receiver placed at  $x = 0$ ), and ( $z$ ) is the length of the travel-path which is perpendicular to the dipping reflector.

This equation can be expressed in an approximate form, using the binomial expansion (with truncation of the resulting series after the first term) which gives:

$$T_x \approx x^2/2T_0V^2 + T_0 + x \sin \theta/V$$

where ( $T_x$ ) is the travel-time, ( $V$ ) the wave velocity, ( $x$ ) source-receiver distance. The dip angle ( $\theta$ ) is given a minus sign when the dip is in the receiver-to-source direction.

This is a hyperbola having its apex located at the point ( $x_m, T_m$ ) where:

$$x_m = -2z \sin \theta, T_m = 2z \cos \theta/V$$

This means that the apex of the reflection hyperbola is shifted by ( $2z \sin \theta$ ) in the up-dip direction for a dipping reflector with angle of dip ( $\theta$ ). It should be noted here that ( $\theta$ ) denotes the apparent dipping in the source-receiver direction. Determination of the true dip (i.e. maximum dip) can be achieved using two apparent dips measured in two different directions (see for example Nettleton 1940).

#### 4.2.4 Geometry of Reflection from Horizontal Reflectors

For a horizontal reflector the travel-time function is obtained by putting ( $\theta = 0$ ) in the function for the dipping reflector, giving:

$$T_x = (x^2/V^2 + 4z^2/V^2)^{1/2}$$

This is also a hyperbola having its apex located at the point ( $0, 2z/V$ ) which is symmetrical about the time-axis. Using ( $z = VT_0/2$ ), this becomes:

$$T_x = (x^2/V^2 + T_0^2)^{1/2}$$

As in the previous case, this equation can be expressed in an approximate form by using the binomial expansion. The reflection function in this case becomes:

$$T_x \approx x^2/2T_0V^2 + T_0$$

Ray path and the corresponding travel-time curve of reflection from a horizontal interface, is shown in the following Fig. 4.6.

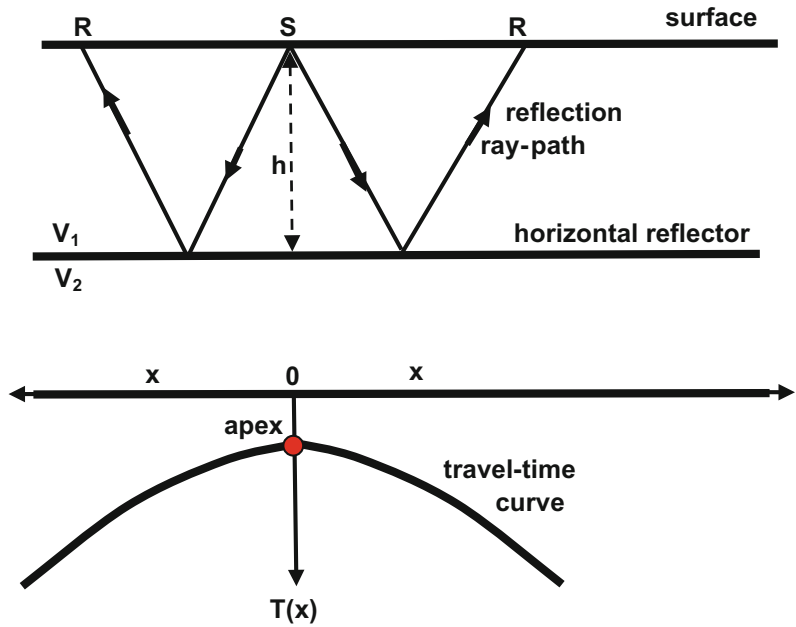
#### 4.2.5 Reflection from Multiple Reflectors

It is possible that a seismic wave arrives at a point on the surface after being reflected several times from a number of interfaces. The first arrival (called the primary reflection) is the strongest, followed by other reflection arrivals (the multiple reflections) which are of less energy.

A well known type of multiple is the (ghost reflection) which occurs when a wave travels upwards from a source-point located at a certain depth and is reflected by the free earth surface or by the base of a low-velocity surface layer (the weathering zone). Because of the short extra travel path, the multiple arrives at a short time-interval after the primary reflection. On the seismic section it appears as a weak reflection event which is closely following the stronger primary reflection, and for this appearance it was named ghost reflection.

Several other types of multiples may occur depending on the structural form of the medium. Multiple reflections include also reflected refraction or refracted reflection. Identification of these wave arrivals is very important, since

**Fig. 4.6** Ray-path and travel-time curve of a seismic wave reflected from a horizontal interface. *S* and *R* are source and receiver points respectively



mistaking a multiple for a primary reflection introduces a serious error in the interpretation results. Some of the commonly known types of multiples are shown in Fig. 4.7.

### 4.3 The NMO and DMO Concepts

The reflection travel-time function plays a fundamental role in seismic exploration. With velocity data, the travel time function can give valuable information of the subsurface geological structure. Closely associated with the reflection travel time function are other similar functions which have equally important applications in the seismic reflection exploration. These are the Normal Move-Out (NMO) and the Dip Move-Out (DMO).

#### 4.3.1 The Normal Move-Out (NMO) Concept

The Normal Move-Out (NMO) is defined as the difference ( $\Delta T$ ) between reflection travel-time ( $T_x$ ) and the two-way vertical travel-time ( $T_0$ ). For a single horizontal reflector found at the base of a homogenous layer (of constant velocity), the NMO parameter ( $\Delta T$ ) is given by Fig. 4.8.

$$\Delta T = T_x - T_0$$

We shall now consider the cases which are involved in NMO computation for a single horizontal reflector and multiple horizontal reflectors:

#### (i) NMO in Case of Horizontal Reflector

For a horizontal reflector, the NMO equation takes the following form:

$$\Delta T = T_x - T_0 = \left[ (x/V)^2 + T_0^2 \right]^{1/2} - T_0$$

This equation can be expressed in another form, using the binomial expansion (with truncation of the resulting series after the first term). This form gives:

$$\Delta T = x^2 / 2T_0 V^2$$

This is considered as an accepted approximation since  $(x/VT_0 \ll 1)$ , which is usually the case in seismic reflection exploration. In this mathematical process, the exact form of ( $\Delta T$ ) is transformed from its hyperbolic function to the approximate form which is a parabolic function.

Both forms of these two equations show that ( $\Delta T$ ) is function of three variables; the receiver

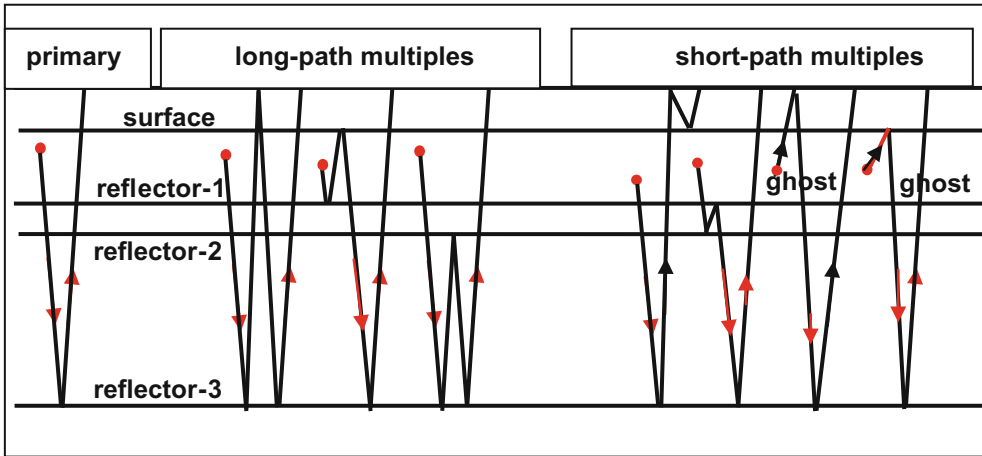


Fig. 4.7 Types of multiple reflections

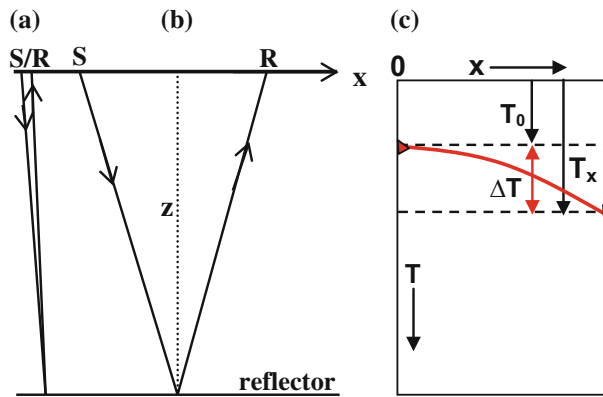


Fig. 4.8 The NMO concept. **a** Two-way vertical ray-path. **b** Two-way slant ray-path. **c** Reflection arrival times corresponding to the ray-paths of **a** and **b**. The NMO ( $\Delta T$ ) is shown as the difference, ( $T_x - T_0$ )

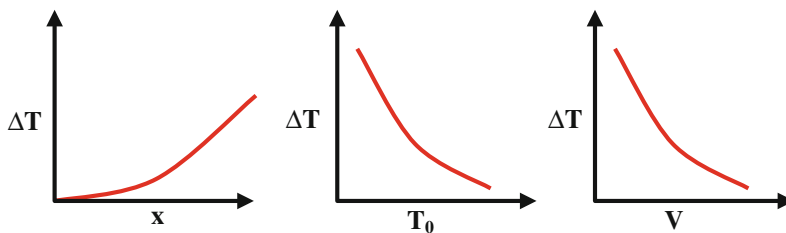


Fig. 4.9 NMO ( $\Delta T$ -function) direct variation with ( $x$ ) and inverse variation with both  $T_0$  and  $V$

offset ( $x$ ), velocity ( $V$ ), and the two-way vertical time ( $T_0$ ). The proportionality is direct with ( $x^2$ ) and inverse with both ( $V$ ) and ( $T_0$ ). These changes are shown as follows Fig. 4.9.

For a given offset ( $x$ ), the time ( $T_x$ ) can be readily measured for a certain reflection event appearing on the seismic trace recorded at that offset. From these data, the NMO ( $\Delta T$ ) can be

accurately calculated (from the given NMO equations) provided that the velocity ( $V$ ) is known.

Application of the NMO concept is centered on velocity determination which is normally determined by a special processing step, the velocity analysis process (Sect. 10.7.1).

**(ii) NMO in Case of Multiple Horizontal Reflectors**

In an n-layer medium, the ray reflected from the base of the nth layer will arrive at the receiver placed on the surface, after it has been refracted at each interface met with during the total reflection travel-path (Fig. 4.10).

The difference between this case and the single layer case is that here we have more than one velocity with which the reflection wave has travelled. The NMO-velocity, in this case (multi-layer case) must be a sort of average or effective velocity depending on the individual velocities of the multi-layer medium. According to (Dix 1955), the root mean square velocity should be used in this case as its value is the closest to the effective velocity for the multi-layer medium. The RMS velocity can be derived from the interval velocities of the layers which are making up the geological section existing above the nth reflector in this case. Thus, the functions for the reflection travel-time ( $T_x$ ) and NMO ( $\Delta T$ ) for multi-reflector case will be in the form:

$$T_x = \left[ (x/V_r)^2 + T_0^2 \right]^{1/2}$$

$$\Delta T = x^2 / 2T_0 V_r^2$$

where ( $V_r$ ) is the root mean square velocity for the whole traversed multi-layer medium. The velocity ( $V_r$ ) can be computed from the interval velocities of individual layers using the formula given in Chap. 3, Sect. (3.4.4).

**(iii) NMO in Case of a Dipping Reflector**

The travel-time of a wave reflected from a given horizontal reflector is least in the case where the source and receiver occupy a common position, that is in the zero-offset ( $x = 0$ ) situation. Thus, as the offset increases the travel time increase. In other words, the NMO increases with the offset relative to the vertical reflection time. When the reflector is dipping the increase in travel-time becomes function of both the offset ( $x$ ) and dip ( $\theta$ ). This is expressed by the dipping-reflector travel-time equation. Thus:

$$T_x = (x^2/V^2 + T_0^2 + 2x T_0 \sin \theta / V)^{1/2}, \text{ exact form}$$

or,

$$T_x \approx x^2 / 2T_0 V^2 + T_0 + x \sin \theta / V, \text{ approximate form}$$

**Fig. 4.10** Ray-path geometry of reflected waves, in a three-reflector model. Within each layer the ray-path is straight line because velocity is assumed to be constant for the layer

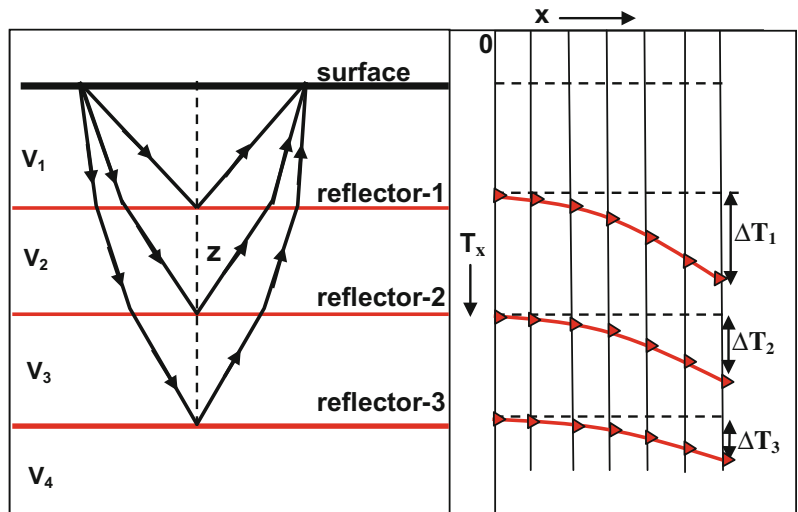
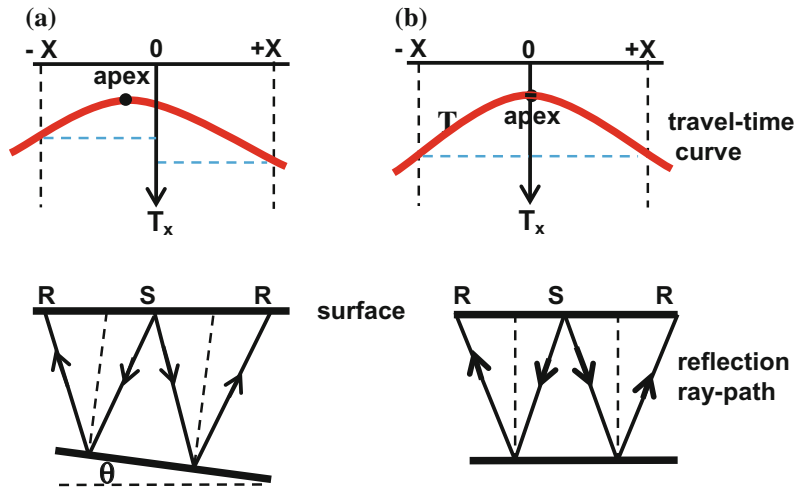


**Fig. 4.11** Reflection ray-paths and travel-time curves for two cases; **a** dipping reflector and **b** horizontal reflector. *S* and *R* are source and receiver points respectively



In the case of a horizontal reflector, reflection travel-times received at two receivers of equal offsets are equal, whereas, in the case of a dipping reflector, the travel-times of rays received at two receivers of equal offsets are not equal. In this case (case of two receivers of equal offsets), and because of dip, the ray-path in the down-dip direction is longer than that in the up-dip direction (Fig. 4.11).

$$\Delta T_d = 2x \sin \theta / V$$

Or, for small  $\theta$  (in radians) we can write,

$$\Delta T_d = 2x \theta / V$$

This can be used in calculating the dip angle ( $\theta$ ), where ( $\theta = V\Delta T_d/2x$ ).

### 4.3.2 The Dip Move-Out (DMO) Concept

Dip move-out ( $\Delta T_d$ ) is defined as the difference in travel-time ( $T_{+x}$ ) and ( $T_{-x}$ ) of rays reflected from a dipping reflector to receivers of equal and opposite offsets; ( $+x$  and  $-x$ ) (Kearey and Brooks 2002, p. 46). That is:

$$\Delta T_d = T_{+x} - T_{-x}$$

Using the reflection travel-time equation (the approximate form), we get:

### 4.4 The CDP, CRP, and CMP Concepts

According to the simple laws of reflection, the reflection point is located vertically below the source-receiver mid-point. This point is given more than one name, depending on its identity criteria. It is called reflection point (RP) because it is the point where reflection occurs, and depth point (DP) or mid-point (MP) because its position is at a subsurface interface or because its position is vertically below the source-to-receiver mid-point. All these three points coincide when reflector is horizontal (Fig. 4.12).

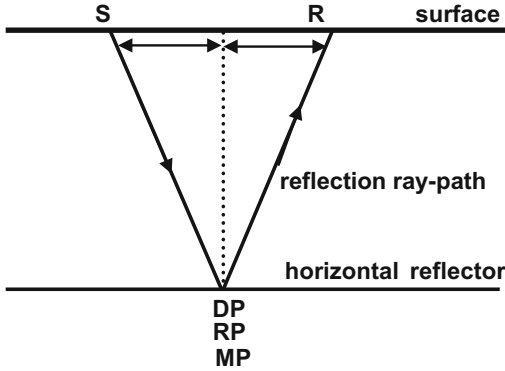


**Fig. 4.12** Definition of the depth point (*DP*), located vertically below the mid-point of the source-receiver distance. It is the reflection point (*RP*), or mid-point (*MP*)

These points are described as common points (*CDP*, *CRP*, *CMP*) in cases where multi-reflections occur for the particular point. In other words, a point is described as common when it becomes common to more than one reflection.

#### 4.4.1 CDP, CRP, and CMP in Case of Horizontal Reflector

By use of certain source-receiver layout, it is possible to shoot a number of shots such that the reflection points resulting from this number of shots coincide on each other, that is one point-location will serve as common point to all of the implemented shots. In this type of repeated shooting-spread, the reflection point becomes known as common depth point (*CDP*), common reflection point (*CRP*), or common mid-point (*CMP*). These points are shown in Fig. 4.13.

The four reflection ray-paths, shown in Fig. 4.13, have one common depth point (the *CDP*), will each produce a seismic trace. These traces belong to the same depth point (*CDP*) and thus they form a group of traces called the (*CDP-Gather*). In this case (case of horizontal reflector) the *CDP* and the other points (*CRP* and *CMP*) will coincide on each other.

Ever since the *CDP* concept was introduced by Mayne (1962, 1967) it has been applied on a routine basis in execution of seismic reflection

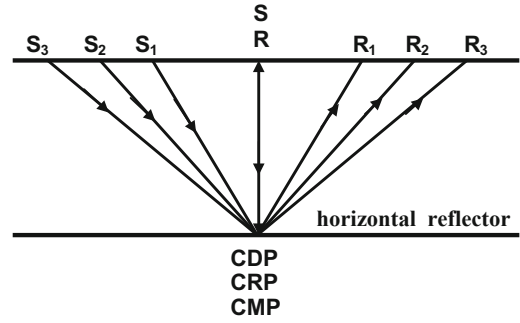


**Fig. 4.13** Definition of the common points (*CDP*), (*CRP*), and (*CMP*), which coincide on each other in case of horizontal reflector

surveying. Application of the concept usually results in great enhancement of the reflection signal by summing together (stacking) the *CDP-Gather* traces.

#### 4.4.2 CDP, CRP, and CMP in Case of Dipping Reflector

For a horizontal plane reflector, the points (*DP*, *RP* and *MP*) coincide at a point which is located vertically below source-to-receiver midpoint. In the case of dipping reflector, however, the reflection point gets shifted up-dip by a distance depending on the offset as well as on the dip angle of the reflector. The up-dip shift is given by:

$$\Delta L = x^2 \cos \theta \sin \theta / D$$

where ( $\Delta L$ ) is the up-dip shift of the reflection point (*RP*), ( $x$ ) is half the source-receiver offset, ( $\theta$ ) is reflector dip-angle, and ( $D$ ) is the length of reflection ray-path which is normal to the reflector (Deregowski 1986). The ray-path geometry and location of the reflection point (*RP*) are shown in Fig. 4.14.

In case of repeated shooting (as it is done in the usual seismic reflection profiling surveying), the reflection points (*RP*s) get dispersed along the dipping reflector-plane. For a given reflector, the amount of up-dip shift ( $\Delta L$ ) increases with the square of the receiver-offset

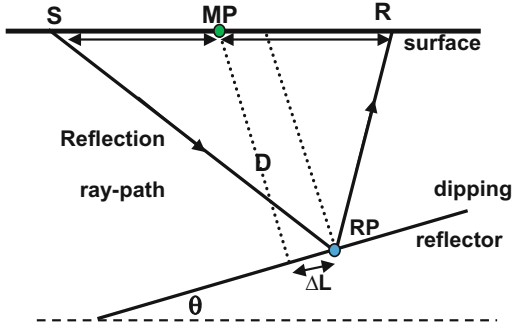


**Fig. 4.14** Up-dip shifting of reflection point (RP) in case of dipping reflector. *S* and *R* are source and receiver points respectively and  $\Delta L$  is the up-dip shift of the *RP*

and inversely proportional to the normal midpoint-reflection distance (**D**). Spreading out of the reflection points in the up-dip direction is shown in Fig. 4.15.

Referring to Fig. 4.15, the four reflection ray-paths, having one common point (the CMP), will each produce a seismic trace. These traces are reflected from dispersed reflection points ( $RP_1, RP_2, RP_3,$  and *RP*) and not from one point as in the case of a horizontal reflector. For this type of source-receiver set-up, there is one point that is common to all of these ray-paths, which is the source-receiver midpoint (the CMP). Thus, the group of traces which belongs to common point is the group of traces belonging to the common mid-point (the CMP-Gather).

An important note is worth mentioning here, it is that, with this type of source-receiver layout, we cannot have a common reflection point (CRP). However, in processing (as in DMO, and

in pre-stack migration), reflection arrivals of a CMP-gather traces, from a dipping reflector, are corrected such that the end result will be corresponding to rays being reflected from a common reflection point (CRP) located at the CMP of that gather. In other words, the dispersal of the RPs of non-zero offset ray-paths is removed (Fig. 4.16).

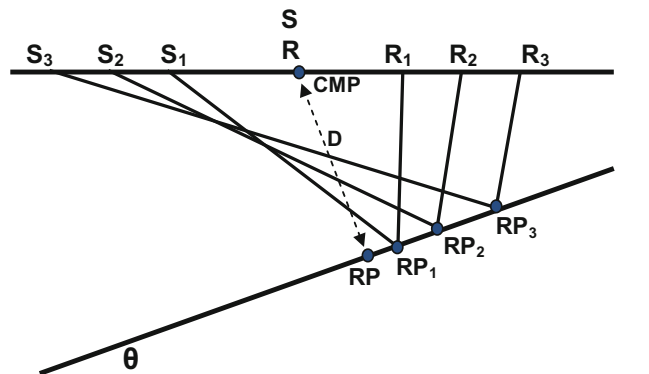
The CMP concept is fundamental issue of the seismic reflection profiling technique. This is because it covers the general case of the geometry of the reflection interfaces, regardless of their dips.

An important step carried out in seismic data processing is stacking (summing up) of the CMP seismic traces (normally called the CMP-gather). In case of dip, the CDP and CRP are no longer applicable, whereas, the CMP principle is applicable to all dipping and horizontal reflectors as well. The role of the CMP concept shall be more clarified in the coming chapters.

### 4.5 The Seismic Wave Diffraction

A part of a seismic wave-energy is reflected when the wave hits a continuous plane interface surface. However, when the interface is not a continuous plane but of curvature which is large in comparison with the curvature of the incident wave-front, the change in propagation direction does not follow the known laws of reflection. If the intervening obstacle, to an advancing seismic wave, is of size approaching to a “point-reflector”, the wave radiates from that obstacle,

**Fig. 4.15** Definition of the common midpoint (CMP) obtained from multi-reflection experiment, in case of a dipping reflector



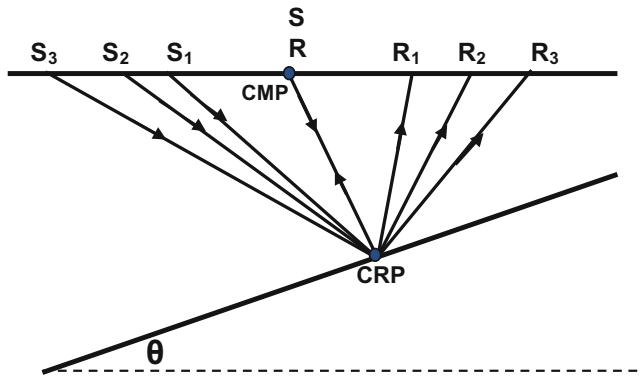
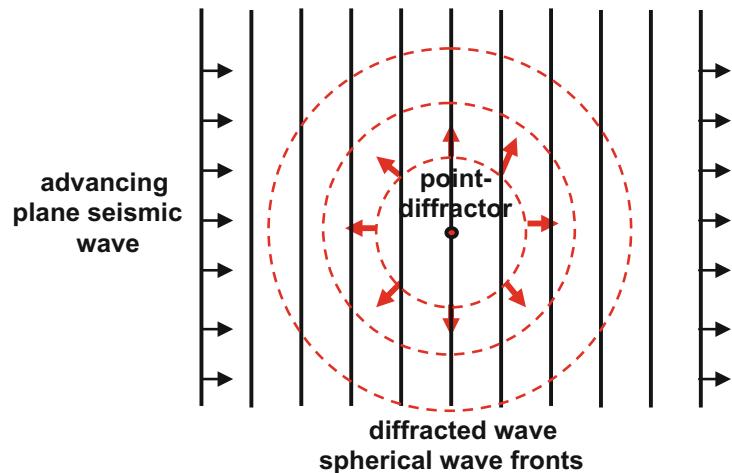


**Fig. 4.16** Definition of the common reflection point (*CRP*) obtained from multi-reflection experiment. For dipping reflector, the (*CRP*) is located at one reflection point which is coincident with the end point of the normal from the *CMP*

**Fig. 4.17** Generation of a diffracted wave with spherical wave fronts as an advancing plane seismic wave hits a small obstacle (point-diffractor)



in every possible direction giving a phenomenon called (diffraction) and the wave which leaves the obstacle after incidence is called (diffracted wave).

A closely related term is (wave scattering) which is used to describe diffracted wave-field caused by small structural irregularities, as for example found with seismic energy reflected from rugged basement surfaces.

#### 4.5.1 The Point-Diffractor

A structural obstacle, having radius of curvature which is shorter than that of the incident wavelength, acts as a diffraction-generating point (or diffraction point). An obstacle of

this type is normally referred to as a point-diffractor.

The diffraction phenomenon can be explained by considering the diffraction point as a point-source which, upon being hit by an incident wave, becomes an activated source that radiates waves in all directions. According to Huygens' principle, an obstacle hit by an incident wave becomes an energy-source from which seismic waves are generated and transmitted in all possible directions. If a plane seismic wave, for instance hits a point-diffractor embedded in a homogeneous medium, a diffracted wave with spherical wave fronts will be generated. The diffracted wave will move away from that source-point causing interference with the incident wave-train and all other waves that may be coexisting at the time (Fig. 4.17).

### 4.5.2 Diffraction from Terminating Reflectors

One of the most common examples of diffraction which are met with in seismic exploration, are those created from discontinuous reflectors as they occur when formations are faulted. Thus, when a plane seismic wave is normally incident on the surface of a faulted geological bed, it will be reflected from that surface and diffracted from the reflector termination-end which is acting as a diffraction source or diffraction-generating point (Fig. 4.18).

Reflector termination, as in the case of a fault or a pinchout, for example, acts like a point diffractor, whose response, on a zero-offset traces (such as a stack section), is a diffraction hyperbola, which is also called the curve of maximum convexity.

### 4.5.3 Diffraction Seismic Image

The amplitude of diffraction wave attains its maximum value at the detector located vertically above the termination point of the reflector, and it decreases with increasing offset-distance from this point. The rate of attenuation of a diffracted wave with increasing detector-offset is greater than that of normal reflection wave in the same medium. We may also note that the polarity of the diffraction arrival in the forward branch of the

diffraction hyperbola is opposite to that in the backward branch. As regards the waveform (wave spectrum structure) of the diffracted wave, there is a general decrease in high-frequency content which, like amplitude behavior, gets more severely attenuated as the travel distance increases (McQuillin et al. 1984, p. 24).

In case of diffraction from the termination edge of a reflector, the polarity of the diffracted wave is reversed ( $180^\circ$  phase change) in the forward branch of the diffraction hyperbola compared to that in the backward branch. The terms, forward and backward, branches of the hyperbola are used to specify the two branches of the diffraction hyperbola. The forward branch is the branch which tends to carry the reflection forward, and the backward branch is the branch that lies underneath the reflection image (Telford et al. 1990, p. 178).

Diffraction ray-path from a terminating diffracting edge and the corresponding seismic image (diffraction hyperbola) is schematically illustrated in Fig. 4.19.

Discrimination of diffraction events on seismic records (diffraction seismic image), based on waveform characteristics, is practically not possible. However, identification of diffraction is possible by its characteristic travel-time curve. Diffraction travel-time curve is different from those of the other types of waves as it will be explained in the following discussion concerning the travel-path geometry of the propagating diffraction waves.

**Fig. 4.18** Occurrence of diffracted wave due to a normal-incident plane wave onto a terminating reflector. Wave fronts and rays of these waves are drawn

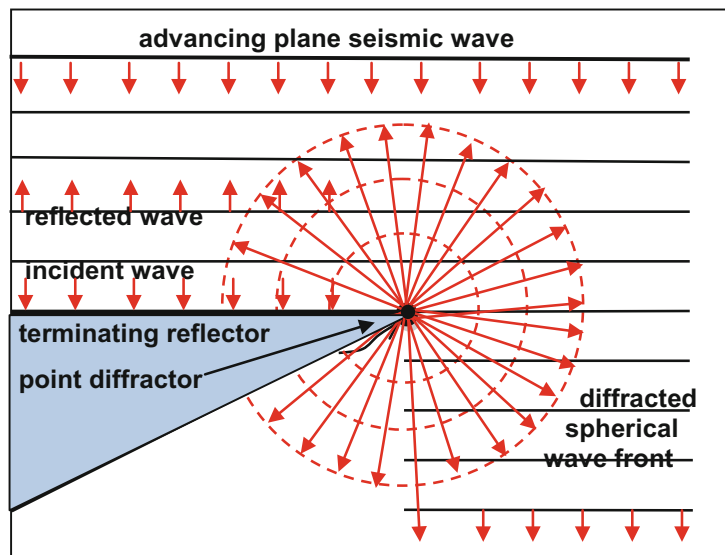


**Fig. 4.19** Sketch showing, **a** terminating reflector model with vertical incidence and diffraction ray-paths and **b** its seismic image for both reflection and diffraction arrivals

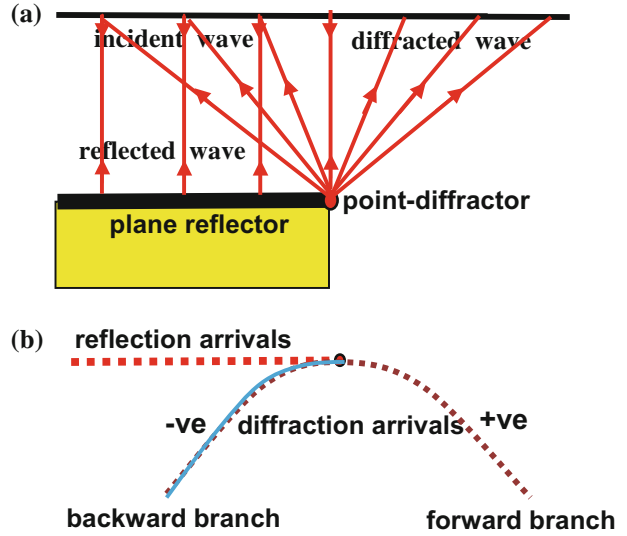
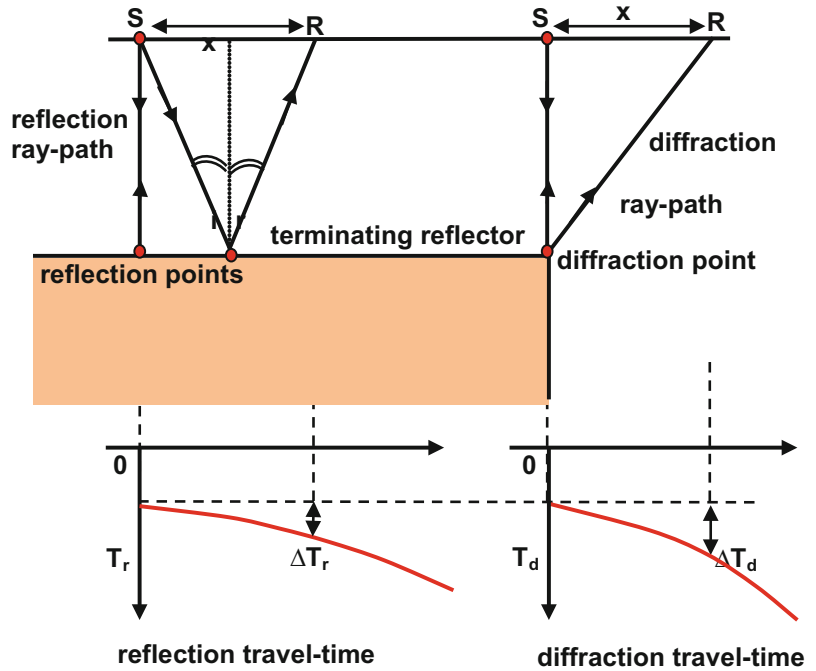


**Fig. 4.20** Reflection and diffraction ray-paths, with their respective travel-time curves. The diffraction normal move-out ( $\Delta T_d$ ) is greater than the reflection normal move-out ( $\Delta T_r$ ) for the same offset ( $x$ )



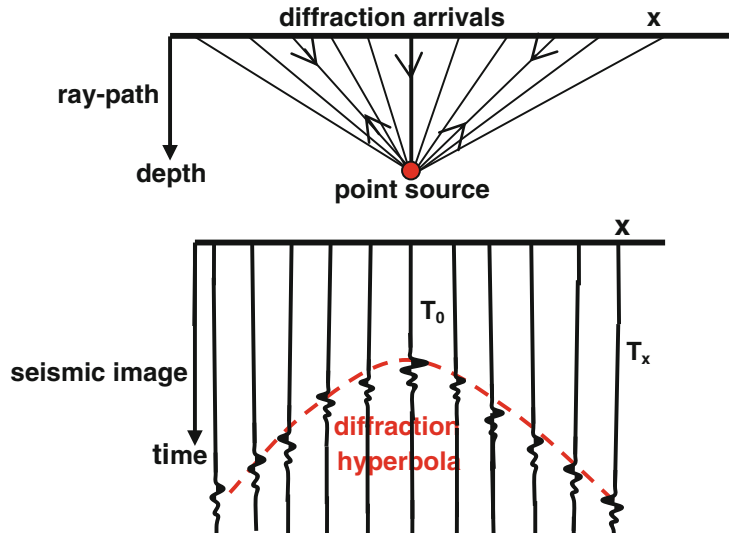
**4.5.4 Diffraction Travel-Time Function**

Identification of diffraction is possible by use of its travel-time curve, which, like reflection travel-time, is of hyperbolic form, but with larger

normal move-out. To compare diffraction hyperbola with the reflection hyperbola for a given interface, consider the terminating reflector shown in Fig. 4.20.

From the geometry of the reflection ray-path and for diffraction ray-path from its termination

**Fig. 4.21** Point-source diffraction ray-path and its seismic image, which is a hyperbolic curve centered at the point diffractor



edge, we have for the same offset ( $x$ ), the travel time function ( $TD_x$ ) for diffraction, and ( $TR_x$ ) for the reflection, are given by:

$$TD_x = \left[ \left( \frac{x}{v} \right)^2 + \left( \frac{T_0}{2} \right)^2 \right]^{1/2}$$

$$TR_x = \left[ \left( \frac{x}{v} \right)^2 + T_0^2 \right]^{1/2}$$

and,

$$\Delta T_d = TD_x - T_0 = \left[ \left( \frac{x}{v} \right)^2 + \left( \frac{T_0}{2} \right)^2 \right]^{1/2} - T_0/2$$

$$\Delta T_r = TR_x - T_0 = \left[ \left( \frac{x}{v} \right)^2 + T_0^2 \right]^{1/2} - T_0$$

where, ( $\Delta T_r$ ) and ( $\Delta T_d$ ) are the normal move-out for the reflection and diffraction respectively, and ( $v$ ) is the propagation velocity. For small offset-to-depth ratio, that is for ( $x/vT_0 < 1$ ), these equations can be approximated by:

$$\Delta T_r \approx x^2 / 2T_0v^2$$

and,

$$\Delta T_d \approx x^2 / T_0v^2$$

giving,

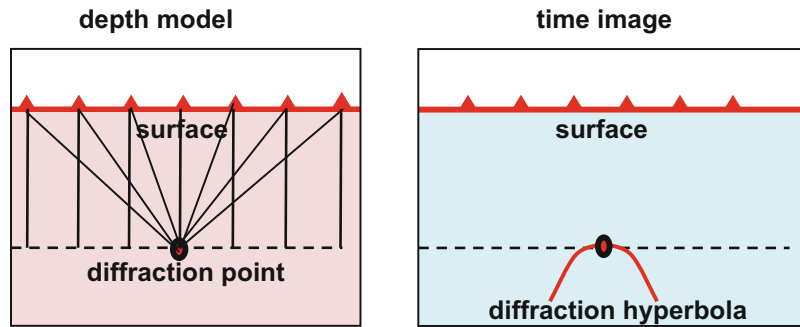
$$\Delta T_d \approx 2\Delta T_r$$

This shows that the normal move-out of a wave diffracted from a terminating reflector is approximately equal to double that of a wave reflected from the same interface at the same offset. This important feature is used in discriminating diffraction from reflection events.

### 4.5.5 The Diffraction Hyperbola

The seismic image of the diffraction arrivals is (for constant velocity) a hyperbolic curve centered about the diffraction source-point. A diffraction event such as this is expected to appear on a seismic section made up of zero-offset traces. The

**Fig. 4.22** The seismic response of a diffraction point is a hyperbolic curve, the diffraction hyperbola



seismic stack section is effectively a section of zero-offset traces (Fig. 4.21).

Diffraction hyperbolae are often observed on seismic stack sections, indicating point-source diffractions, as those generated by faults and pinchouts. A seismic diffraction event (diffraction hyperbola) appearing on seismic stack section can be considered as the seismic response of a depth section of a homogeneous medium containing a point-source diffractor (Fig. 4.22).

#### 4.5.6 Distortion Effects of Diffraction

In nature interfaces are not always plane and continuous surfaces. There are cases where these surfaces are irregular as the surfaces of reef bodies or discontinuous as the faulted beds or pinchouts as found with angular unconformities. When a seismic wave is incident on such subsurface features, diffracted waves are generated and transmitted through the medium, interfering with, and distorting other co-existing waves such as reflection events, the main objective in normal seismic exploration.

On a seismic stack section, which is effectively made up of zero-offset traces, the diffraction arrivals (diffraction event) appear as a hyperbolic curve whose apex is coincident with the causing diffraction point. Faulting is one of the principal sources of diffraction waves seen in stack sections. A reflector termination caused by faulting, generates diffraction arrivals. Because

of their interferences, these arrivals are distorting or masking the reflection events and causing smearing effects at the fault-zone leading to decrease in fault-resolution. Example of the interferences introduced as a result of fault-generated diffraction hyperbolae are shown in Fig. 4.23.

Although diffraction events (diffraction hyperbolae) are introducing masking effects to the primarily targeted reflection events, they (diffraction events) can help interpreters in identifying faults and other diffraction-sources. In general, diffraction events on stack sections are considered to be unwanted distortive events which must be removed or at least attenuated as much as possible. The common way to remove the diffraction events (diffraction hyperbolae) is by application of the seismic migration which is one of the principal steps applied in processing of seismic reflection data.

#### 4.5.7 The Exploding-Reflector Model

In accordance to Huygens' principle, the exploding reflector model is a model in which a reflection interface is considered to be formed of infinite number of closely packed diffraction points and that these points explode at a given start-time, generating seismic waves. The exploding reflector modeling process requires that each point of the reflector is sending seismic rays, in every direction (exploding) at a

**Fig. 4.23** Distortions due to diffraction hyperbolae, created by a faulted reflector, from two diffraction points. The forward and backward branches show polarity reversal

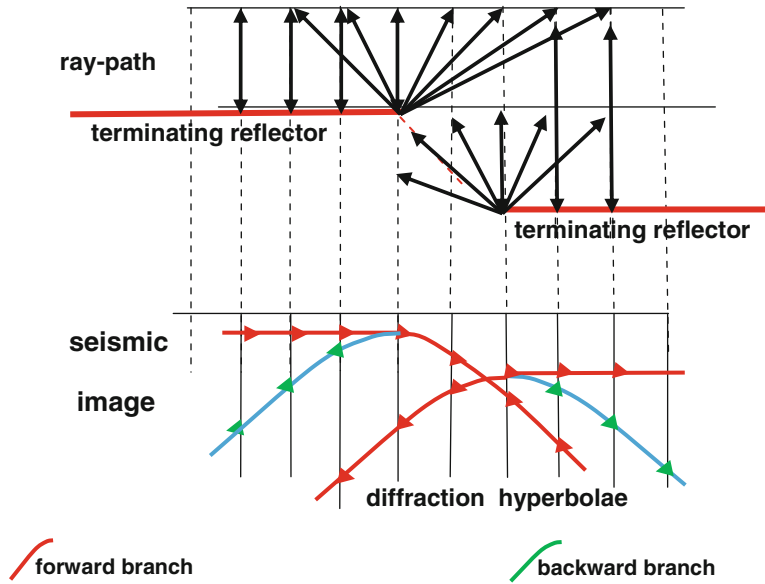
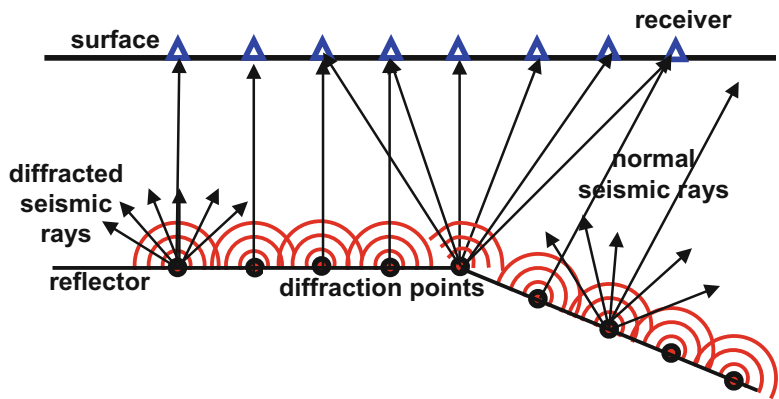


**Fig. 4.24** The exploding reflector model. Seismic energy transmitted from the diffraction points simultaneously and recorded by receivers placed on the surface



common start time. The moving seismic amplitude is considered to be of magnitude proportional to the normal-incidence reflection coefficient.

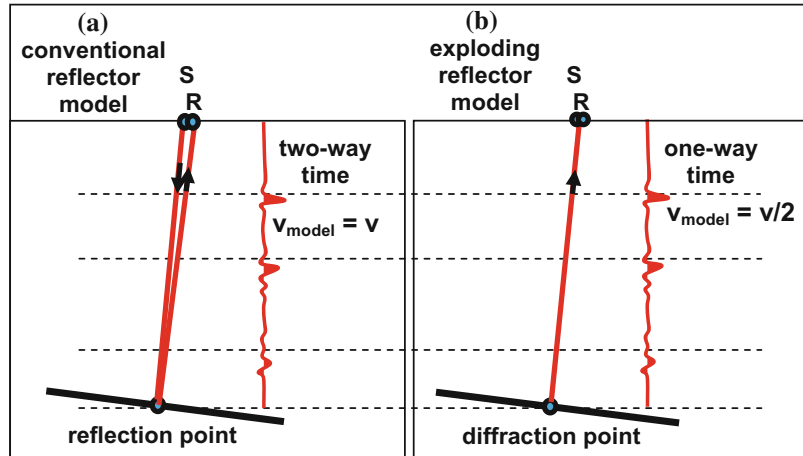
The generated waves are made to propagate to the surface with velocity half that of the actual velocity. With this velocity-value the one-way travel-time to the surface becomes equal to the two-way reflection travel-time for zero-offset receivers placed on the surface (Sheriff 2002, p. 127). Consideration of the reflection process as being formed from the interactions of seismic

wave fronts of waves diffracted from closely packed diffraction points (making up the reflection surface), is called exploding reflector model.

The resulting wave field generated according to the exploding-reflector model shall propagate along the normal-incidence ray-paths. The concept is schematically shown in Fig. 4.24.

Compared with the conventional record section, the section produced from the exploding reflector model, is the same as the conventional section having propagation velocity equal to half of the true velocity (Fig. 4.25).

**Fig. 4.25** Sketch showing two cases of zero-offset trace and its corresponding raypath. **a** Conventional two-way travel-time, **b** exploding reflector model, one-way travel-time with model velocity equal to half that of the true velocity



Application of the exploding reflector concept in computing the seismic reflection section is a direct-modeling (forward-modeling) process. Algorithms have been developed for computations

of migration (both of the pre- and post-stack migration processing) using the exploding-reflector concept. This approach proved to result in great reduction of the migration computational cost.

The term (transmission) is customarily used to indicate the general case of wave propagation where the moving seismic wave crosses an interface whether the incidence is normal or inclined. When an obliquely incident wave is transmitted across an interface, it is bent at the interface towards, or away from, the normal at the point of incidence. This is the well known phenomenon of (refraction). A refracted wave is, therefore a transmitted wave resulting from an inclined incidence. No refraction occurs when the wave is incident perpendicularly at an interface. Thus, it can be said that the refraction phenomenon is a special case of transmission. It (refraction) occurs only with normal incidence.

## 5.1 Seismic Wave Transmission

When a seismic wave hits an interface, part of the wave energy is reflected and the rest is transmitted across that interface. The amount of energy which is reflected from an interface is determined by the reflection coefficient and what is left from the incident energy is transmitted across the interface into the second medium. At the interface the ray-path is bent if the incidence is oblique and continues with unchanged direction when the incidence is normal to the interface.

In the real layered Earth crust, the initiated seismic energy, the source function  $s(\mathbf{t})$ , is recorded as  $\mathbf{r}(\mathbf{t})$  after it penetrates all the rock

layers down to a reflector and up to the surface. Among other factors, reflection and transmission coefficients cause attenuation to the wave energy as it is experienced by the recorded function  $\mathbf{r}(\mathbf{t})$ . It should be remembered that there is a reflection and transmission processes taking place at each interface existing in the traversed geological section (Fig. 5.1).

### 5.1.1 Transmission Coefficient at Normal Incidence

The transmission coefficient (or transmittance, as it is sometimes called) is defined to be the ratio of the amplitude of the transmitted wave to that of the incident wave. Sometimes this is expressed in terms of energy instead of amplitude. At normal incidence, the transmission coefficient ( $\mathbf{T}$ ), expressed as a ratio of the transmitted amplitude ( $\mathbf{A}_t$ ) to the incident amplitude ( $\mathbf{A}_i$ ), thus:

$$\mathbf{T} = \mathbf{A}_t / \mathbf{A}_i$$

As it is with the reflection coefficient, the transmission coefficient is function of the acoustic impedances of the two media separated by the involved interface. For an interface separating two media of acoustic impedances ( $\mathbf{Z}_1$  and  $\mathbf{Z}_2$ ), the transmission coefficient ( $\mathbf{T}$ ), is related to the impedances by:

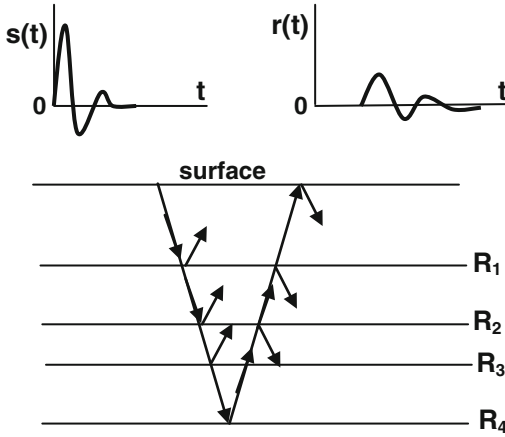


**Fig. 5.1** Wave-attenuation due to reflection and transmission processes which are normally occurring in a real layered rock medium.  $s(t)$  and  $r(t)$  are source receiver time-functions respectively

$$T = 2Z_1 / (Z_2 + Z_1)$$

It is apparent from this formula that as the contrast in the acoustic impedances is smaller the transmission coefficient becomes greater, and in the limit when they are equal ( $Z_1 = Z_2$ ), transmission coefficient ( $T$ ) becomes unity and all of the seismic energy shall pass through and no reflected energy will take place.

For the case of inclined incidence, the transmission coefficient, like the reflection coefficient, depends on both of the angle of incidence and on the contrast in the acoustic impedance of the adjacent media. Unlike reflection, however, there is no special situation whereby phase change occurs.

**5.1.2 The Two-Way Transmission Coefficient**

The transmission coefficient ( $T$ ) is related to the reflection coefficient ( $R$ ) by the expression (see Sect. 4.2.2):

$$T = 1 - R$$

For a given interface, the ( $T$ - $R$ ) relationship is ( $T_1 = 1 - R$ ) for a wave incident (normal incident) from the low-impedance ( $Z_1$ —medium) to the high-impedance ( $Z_2$ —medium), and ( $T_2 = 1 + R$ ) for transmission in opposite direction. On this basis the two-way transmission coefficient (call it  $T_{12}$ ) for an interface penetrated twice (one is in opposite direction to the other) is given by the product ( $T_1 \cdot T_2$ ), that is:

$$T_{12} = (1 - R) \cdot (1 + R) = 1 - R^2$$

And in terms of impedances it is given by:

$$T_{12} = 4 Z_1 Z_2 / (Z_2 + Z_1)^2$$

The two-way transmission coefficient ( $T_{12}$ ) is useful in computing the effective attenuation factor of a wave reflected from a subsurface interface after being transmitted through several layers during its total reflection travel path.

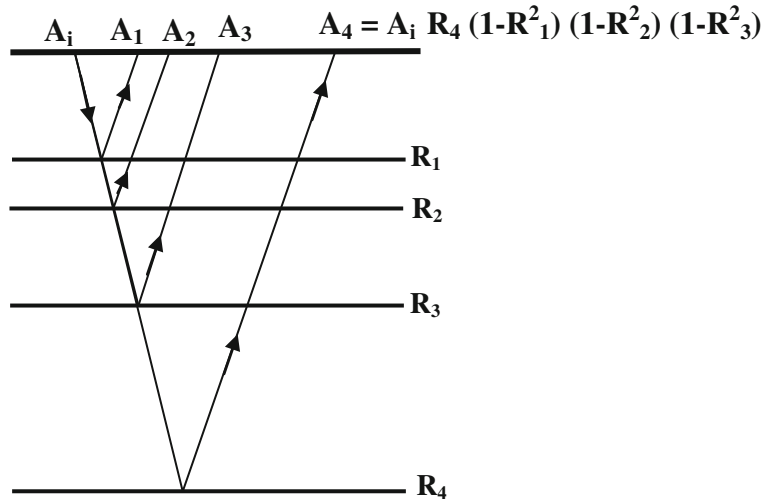
**5.1.3 Attenuation Due to Reflection and Transmission**

For an  $n$ -layer medium, the wave which is reflected from the  $n$ th interface and received at the surface would have crossed the ( $n - 1$ ) interfaces twice. Assuming normal incidence, the effective attenuation factor ( $RT_n$ ) of a wave reflected from the base of the  $n$ th subsurface interface) and transmitted through ( $n - 1$ ) interfaces will be given by:

$$RT_n = A_n / A_i$$

By use of the concept of the two-way transmission coefficient, it is possible to derive a formula that computes the net attenuation due to the combined effects of the reflection and transmission coefficients. In a multi-layer geological model

**Fig. 5.2** Reflection and transmission ray-path of a wave traversing a 4-layer medium. ( $A_4$ ) is wave-amplitude reflected from the 4th reflector (vertical incident is assumed)



( $n$  layers), the reflection-transmission process of an initial incident amplitude ( $A_i$ ) will experience attenuation due to the double crossings which occur at ( $n - 1$ ) interfaces. In a multi-layer model, the amplitude ( $A_n$ ) is received at the surface after covering the whole of the reflection travel path, from the point of the incident amplitude ( $A_i$ ) to the receiver point. Ray-path geometry of such a multi-layer model is shown in Fig. 5.2.

Applying the two-way transmission coefficient we can write:

$$\begin{aligned} A_1 &= A_i R_1 \\ A_2 &= A_i R_2 (1 - R_1^2) \\ A_3 &= A_i R_3 (1 - R_1^2) (1 - R_2^2) \\ &\vdots \\ A_n &= A_i R_n (1 - R_1^2) (1 - R_2^2) (1 - R_3^2) \dots (1 - R_{n-1}^2) \end{aligned}$$

A general recursive formula can be derived by dividing the amplitude of the  $n$ th reflector by that of the ( $n - 1$ ) reflector, giving:

$$A_n = A_{n-1} R_n (R_n / R_{n-1}) (1 - R_{n-1}^2), \quad n \geq 2$$

Repeating, this formula is valid for ( $n \geq 2$ ), and for ( $n = 1$ ), we have  $A_1 = A_i R_1$ .

In conclusion the effective attenuation factor  $RT_n (= A_n / A_i)$  due to reflection-transmission process for a wave reflected from the  $n$ th reflector of a multi-layer geological section, is

function of the reflection coefficients of the existing  $n$ -reflectors ( $R_n$ ). For vertical incidence, it is given by:

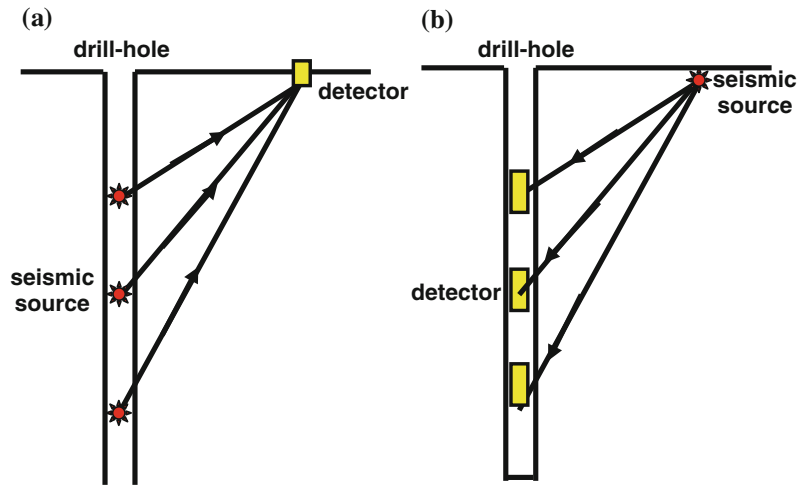
$$RT_n = R_n (1 - R_1^2) (1 - R_2^2) (1 - R_3^2) \dots (1 - R_{n-1}^2)$$

With knowledge of the number of reflectors in a section and their reflection coefficients, it is possible to compute the extent of attenuation a reflected wave experiences in covering the complete source-to-receiver reflection-travel-path.

#### 5.1.4 Role of Transmission in Seismic Exploration

Seismic wave transmission surveys make use of seismic waves which are directly propagating from sources to receivers. The normal direct wave, which is always recognized on seismic reflection and refraction-shooting records, is a typical transmission method used to calculate the velocity of the surface layer. In exploration seismology, there are several transmission-based methods which are applied for specific exploration purposes. Up-hole surveying, well velocity surveying, vertical seismic profiling (VSP) fan shooting, and seismic transmission tomography, are typical examples of exploration practices employing the seismic wave transmission phenomenon. The up-hole surveying and that of well-velocity are defined here-below (Fig. 5.3).

**Fig. 5.3** Examples of exploration activities employing seismic wave transmission. **a** An up-hole survey and **b** well velocity survey



### (i) Up-hole Surveying

In principle, the field arrangement is similar to that used in the well velocity surveying. The difference is that, in the up-hole surveying the source points are placed at different depths inside the drill-hole, while the detector is placed on the surface, close to the head of the bore-hole.

### (ii) Well Velocity Surveying

The normal survey procedure starts with placing the detector at a certain depth inside the well, while the shot is on the surface. The source-to-detector direct-arrival is recorded. From the transmission travel times, corrected to the vertical path, the average velocities are calculated and plotted against depth.

It should be noted here that the transmitted waves are, in general, experiencing refraction of various severities, since, in nature, no perfectly normal incidence to interfaces are expected to occur during the wave propagation.

amount of bending (angle of refraction) and the sense of bending (towards or away from the normal) are governed by the velocities of the two layers separated by the interface. The refracted ray is bent away from the normal in case of the velocity in the medium in which the wave is refracted) is greater than that in the medium that hosts the incident wave. The bending of the refracted wave is towards the normal when the velocity of the medium, in which refraction occurs, is of lower value (Fig. 5.4).

In essence, the phenomenon of ray bending (wave refraction) at an interface occurs only when the incidence direction is inclined to the interface. No bending occurs with perpendicular incidence.

## 5.2.1 Snell's Law of Refraction

Where there is a change in the propagation direction on crossing the interface, the transmitted wave is normally referred to as refracted wave. This takes place only when the incidence is inclined with respect to the interface plane. The degree of the ray bending (expressed by the angle of refraction) depends on the velocity contrast of the media on either side of the interface. Refraction is an expression for geometrical changes of the wave ray-path on crossing an interface and not for changes in energy content.

## 5.2 Seismic Wave Refraction

A seismic wave incident on an interface is partly reflected and partly transmitted. In the general case where the wave is obliquely incident on the interface, the transmitted wave changes direction (refracted). It will be bent either towards the normal line (normal to the interface at point of incidence) or away from that normal. The

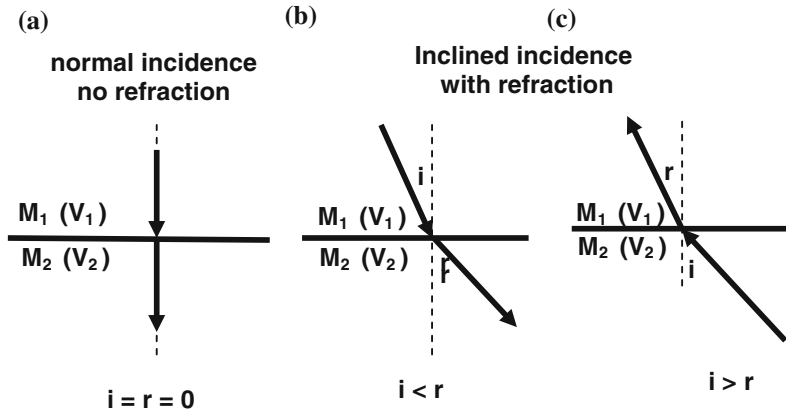
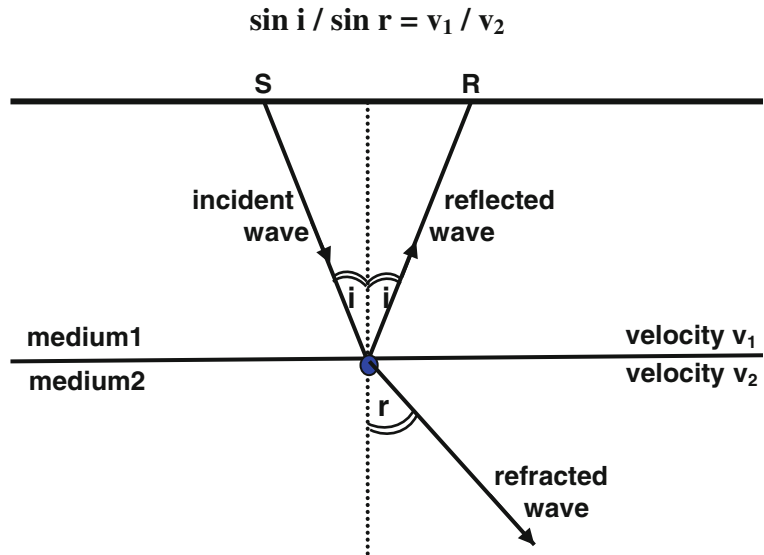


**Fig. 5.4** Occurrence of refraction in case of oblique incidence. **a** Normal incidence, no refraction, **b** oblique incidence, from medium  $M_1$  to medium  $M_2$ , **c** incidence direction reversed. The velocities of the two media are  $V_1$  and  $V_2$ , where  $V_1 < V_2$

**Fig. 5.5** Reflection and refraction of a seismic wave at an interface separating media ( $M_1$ , velocity  $v_1$ ) and ( $M_2$ , velocity  $v_2$ ) where  $v_2 > v_1$



$$\sin i / \sin r = v_1 / v_2$$

Refraction of an incident seismic wave at an interface is governed by Snell's law which states that the ratio of the sine of angle of incidence ( $i$ ) to the sine of angle of refraction ( $r$ ) is equal to the ratio of velocity in the first medium (in which the wave is incident) to that of the second medium (in which the wave is refracted). In reference to Fig. 5.5, Snell's law takes the following form:

Referring to Fig. 5.6, the wave front (AB) of a plane seismic wave is hitting an interface existing between the two media ( $M_1$  and  $M_2$ ), at an incidence angle ( $i$ ). Point (B) requires an interval of time ( $\delta t$ , say) to reach the interface after point (A) has reached it. During this interval, the wave

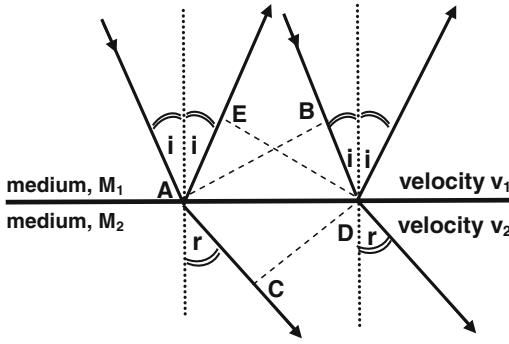


**Fig. 5.6** Refraction geometry of a seismic plane wave at an interface separating two media;  $M_1$ , velocity  $v_1$  and  $M_2$ , velocity  $v_2$

front would have travelled the distance of  $(v_1 \cdot \delta t)$  into the medium ( $M_1$ ) and  $(v_2 \cdot \delta t)$  into the second medium ( $M_2$ ). Being a plane wave, the wave front is plane surface which is represented by the line (AB) for the incident wave, (DE) for the reflected wave in medium ( $M_1$ ) and line (CD) for the refracted wave in medium ( $M_2$ ).

From the geometry of the wave path we note that the two right angle triangles (ABD) and (AED) are equal, with  $(AE = BD = v_1 \cdot \delta t)$ , giving equal reflection and incidence angles in support of the law of reflection. In the same Fig. 5.6, by examining the two right-angle

triangles (ABD and ACD), we can write  $(\sin i = BD/AD)$  and  $(\sin r = AC/AD)$ , giving the following relationship:

$$\sin i / \sin r = BD / AC = v_1 \cdot \delta t / v_2 \cdot \delta t = v_1 / v_2$$

that is,

$$\sin i / \sin r = v_1 / v_2$$

which is the well-known Snell's law that governs the direction of the refracted wave relative to that of the incident wave.

The generalized form of Snell's law expresses the relation connecting the reflection and refraction angles with that of the incidence wave, for all of the wave types resulting from an inclined incidence. Thus if a P-wave is obliquely incident on an interface separating two solid media, four wave-types are generated. These are two reflected waves (P- and SV-wave) and two, transmitted (refracted) waves (P- and SV-wave), as shown in Fig. 5.7.

In the above example, if SV is the incident wave instead of the P-wave, four similar waves are also generated: two reflected waves (SV and P) and two refracted waves (SV and P). It is not always all the four wave-types are generated at

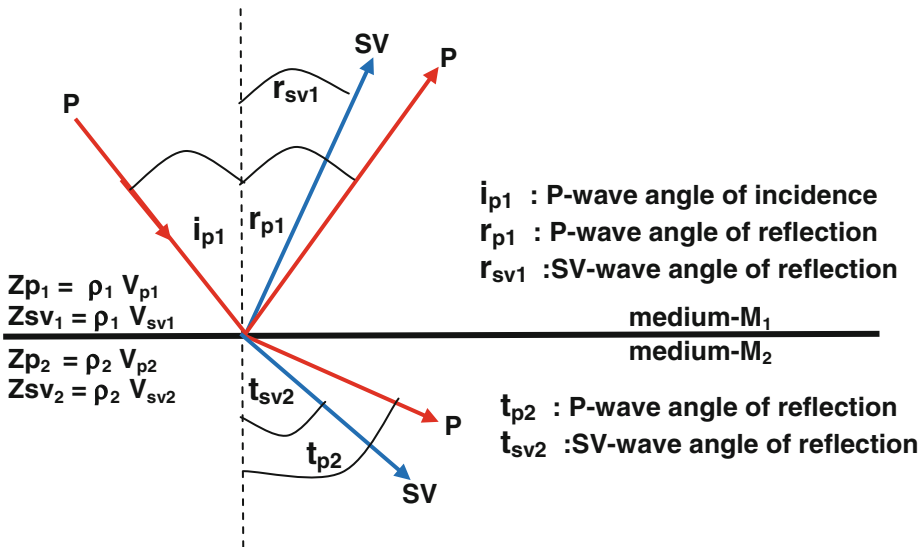


**Fig. 5.7** An obliquely incident P-wave and the generated four wave phases: reflected and refracted P- and SV-waves

an interface. If medium-2, for instance, is liquid, no transmitted SV-wave is formed.

Using the symbols shown in Fig. 5.7, the generalized Snell's law is quoted as follows (Sheriff 1973, p. 200):

$$\frac{(\sin i_{p1})/v_{p1} = (\sin r_{p1})/v_{p1} = (\sin r_{sv1})/v_{sv1} = (\sin t_{p2})/v_{p2} = (\sin t_{sv2})/v_{sv2} = k$$

← incident P
← reflected P&SV
← refracted P&SV

where  $(k)$  is constant for the given layer-set, as the two media ( $M_1$  and  $M_2$ ), adopted in this example. Velocities in ( $M_2$ ) are assumed to be higher than those in ( $M_1$ ).

We may note that angles of incidence and reflection are equal only when the reflected wave is of the same type as that of the incident. Also, no wave conversion occurs when the obliquely incident wave is SH-wave or when the wave (of any type) which is of normal incidence. With the wave conversion phenomenon in mind, one can envisage the complexity of the seismic wave-field developed in an inhomogeneous and stratified subsurface medium.

incidence angle ( $i$ ) increases, and when it reaches a value of ( $i = i_c$ ), refraction angle reaches the value ( $r = 90^\circ$ ). The angle of incidence ( $i_c$ ) for which the angle of refraction ( $r$ ) becomes ( $90^\circ$ ) is

called (the critical angle for refraction). For greater values of this angle there will be no refraction of the wave into the second medium, and in this case, the incident wave will be totally reflected.

Since  $(\sin 90^\circ)$  is equal to unity, Snell's law, at the critical angle ( $i_c$ ), becomes:

$$\sin i_c = v_1/v_2$$

Hence, the critical angle of incidence, for any specific interface, will be given by:

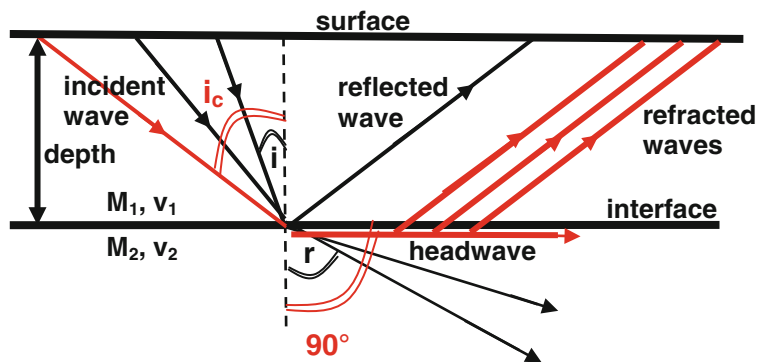
$$i_c = \sin^{-1}(v_1/v_2)$$

### 5.2.2 The Critical Refraction and Head Wave Generation

Consider a geological model made up of a medium ( $M_1$ ) of velocity ( $v_1$ ) overlying a medium ( $M_2$ ) of higher-velocity ( $v_2$ ). An obliquely-incident wave in the first medium shall refract on hitting the separating interface. In such a model, the refraction angle ( $r$ ) increases as the

In this state, where the incident angle is equal to the critical angle ( $i_c$ ), a special refracted wave (called the head wave) is generated. This critically refracted wave travels along the interface with the velocity ( $v_2$ ) of the second medium ( $M_2$ ). This wave is refracted back to the earth's surface at the same angle ( $i_c$ ) and with the propagation velocity of the upper medium ( $v_1$ ). Development of head waves is shown in Fig. 5.8.

**Fig. 5.8** Development of the head wave at critical angle of incidence,  $i_c$  for ( $r = 90^\circ$ ). Increase of the angle of refraction ( $r$ ) with increase of angle of incidence ( $i$ )



Head waves have great practical importance as they form the fundamental basis of seismic refraction exploration.

### 5.2.3 Ray-Path Geometry and Travel-Time Curves

On seismic shooting records, three main wave-arrivals are usually observed. These are the direct, refracted, and reflected waves. Their travel-time functions are linear for the direct and refracted arrivals, but hyperbolic for the reflected wave. At the critical distance ( $x_c$ ), where the incidence is at the critical angle ( $i_c = \sin^{-1}(v_1/v_2)$ ), a head wave is generated which is refracted to surface at an angle equal to the critical angle. The distance ( $0$  to  $x_c$ ), no refraction arrivals exist, hence it is a (shadow zone) for refracted waves (Fig. 5.9).

For a given interface separating two constant-velocity media, the refraction travel-time function is a straight line tangent to the reflection hyperbola at the point where both of these waves arrive at the same time. The distance at which reflection time equals the refraction time, which occurs at the critical angle, is called the critical distance.

Due to its shorter travel-path, the direct wave, at small receiver distance, arrives earlier than the refraction wave. However, after some time, the faster refraction wave catches up and surpasses

the direct wave. The source–receiver distance ( $0$  to  $x_{cr}$ ), at which the refraction wave overtakes the direct wave, in the same layering set-up, is called the (cross-over distance).

The velocities of the two involved layers ( $v_1$  and  $v_2$ ) are computable from the slopes of the travel-time lines (as seen from the figure above). The velocity is the inverse of the slope of the time–distance line.

### 5.2.4 Refraction Travel-Time Function

A travel-time function of a moving wave expresses the mathematical relation between the time covered by the moving wave and the source–receiver distance. This is also depending on the velocity values of the two involved media. Two cases are presented here; these are cases of horizontal and dipping plane interfaces.

#### (i) Case of Horizontal Refractor

Consider first a simple one-refracting horizontal interface separating two layers of velocities ( $V_1$  and  $V_2$ ) as shown in Fig. 5.10.

Referring to this figure, the refraction ray-path consists of three segments, AB, BC, and CD. The refraction travel time  $T(x)$  is given by  $AB/V_1 + BC/V_2 + CD/V_1$ . That is:

$$T(x) = 2z/V_1 \cos i_c + (x - 2z \tan i_c)/V_2$$

or, (using  $\sin i_c = V_1/V_2$  from Snell’s law and the sine-cosine relationship)

$$T(x) = [x \sin i_c + 2z \cos i_c]/V_1$$

or,

$$T(x) = x/V_2 + 2z(V_2^2 - V_1^2)^{1/2}/V_1 V_2$$

where ( $i_c$ ) is the critical angle, and ( $z$ ) is depth of the interface. The two velocities, ( $V_1$  and  $V_2$ ) are velocities of the two layers. These are equal to the reciprocals of the slopes of the direct and refracted travel-time curves respectively.

It is readily noted that refraction travel-time function is linear in ( $x$ ), and its curve is straight line of slope equal to ( $1/V_2$ ) and its intercept ( $T_0$ ) is given by:

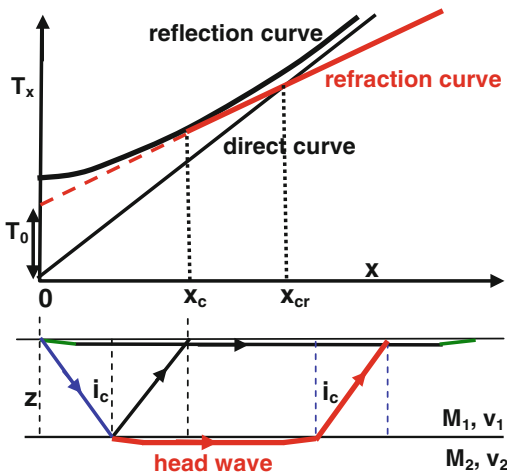


**Fig. 5.9** Ray-paths and travel-time curves of direct, critically-refracted, and reflected waves, with critical distance ( $0$  to  $x_c$ ) and cross-over distance ( $0$  to  $x_{cr}$ )

**Fig. 5.10** Ray-path geometry of a wave refracted from a horizontal interface

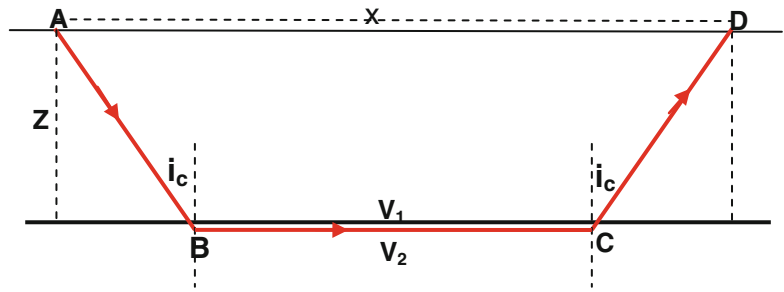
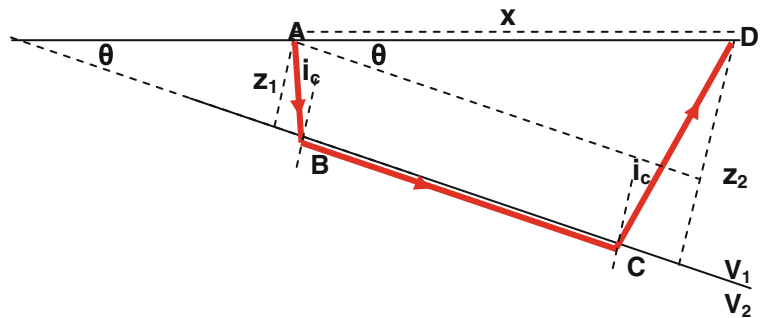


**Fig. 5.11** Ray-path geometry of a wave refracted from a dipping interface



$$T_0 = 2z(V_2^2 - V_1^2)^{1/2} / V_1 V_2.$$

$$z = 1/2 x_{cr} [(V_2 - V_1) / (V_2 + V_1)]^{1/2}$$

The depth ( $z$ ) can be calculated from this equation, where:

$$z = T_0 V_1 V_2 / 2(V_2^2 - V_1^2)^{1/2}.$$

Thus, with the velocity ( $V_1$ ) which is obtained from the travel-time of the direct wave, and ( $V_2$ ) from the refraction travel-time, the interface depth ( $z$ ) can be calculated.

An alternative way of computing the depth ( $z$ ) of the refractor is by use of the cross-over distance ( $x_{cr}$ ). By definition, the travel-time of the direct wave, at the cross-over distance, is equal to that of the refracted. Thus, by equating the two travel times at the cross-over distance ( $x_{cr}/V_1 = x_{cr}/V_2 + 2z(V_2^2 - V_1^2)^{1/2}/V_1 V_2$ ), to give:

**(ii) Case of Dipping Refractor**

As it is with the case of horizontal refractor, the ray-path in the case of dipping refractor (dip angle,  $\theta$ ) consists of three segments; AB, BC, and CD (Fig. 5.11).

The travel time  $T(x)$ , in down-dip shooting, is given by  $AB/V_1 + BC/V_2 + CD/V_1$ , where:

$$AB/V_1 = z_1/V_1 \cos i_c,$$

$$BC/V_2 = [x \cos \theta - z_1 \tan i_c - (z_1 + x \sin \theta) \tan i_c] / V_2,$$

$$CD/V_1 = (z_1 + x \sin \theta) / V_1 \cos i_c$$

( $z_1$ ) is the perpendicular distance from the source at point (A) to the interface and ( $z_2$ ) is the perpendicular distance from the receiver at point (D) to the interface.

Hence, for down-dip shooting, the refraction travel-time function is given by:

$$T(x) = [x \sin(i_c + \theta) + 2z_1 \cos i_c] / V_1$$

and for up-dip shooting, where  $(\theta)$  is given negative sign, the function becomes:

$$T(x) = [x \sin(i_c - \theta) + 2z_1 \cos i_c] / V_1$$

The angle of dip  $(\theta)$  can be computed from two refraction-experiments: one down-dip giving a straight line having slope  $(S_d)$  and the other is up-dip which gives a straight line of slope  $(S_u)$ . From the travel-time functions for the two experiments, we have:

$$S_d = [\sin(i_c + \theta)] / V_1$$

$$S_u = [\sin(i_c - \theta)] / V_1$$

Hence,

$$i_c + \theta = \sin^{-1}(V_1 S_d) \text{ and}$$

$$i_c - \theta = \sin^{-1}(V_1 S_u), \text{ giving:}$$

$$\theta = (\sin^{-1} V_1 S_d - \sin^{-1} V_1 S_u) / 2$$

In order to calculate  $(\theta)$  from this formula, the velocity  $(V_1)$  must be known. This is obtained from the slope of the direct wave which is always available in such experiment. The travel-time curve of the direct wave is straight line passing through the origin  $(T(x) = x/V_1)$  and its slope is equal to the inverse of the wave propagation velocity. We may further note that  $(\theta)$  is the

apparent angle of dip in the direction of the shooting-line (x-axis direction).

### 5.2.5 The Delay-Time Concept

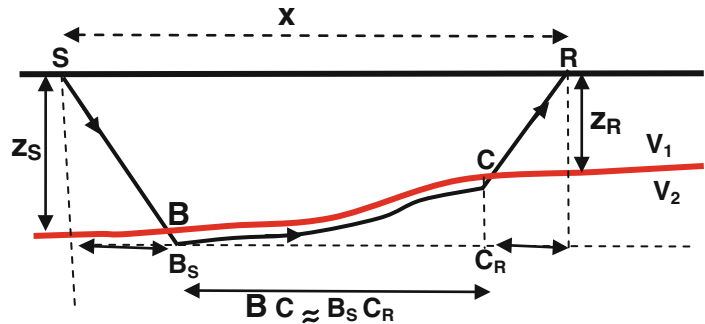
Travel-time functions that we have dealt with so far are based on the assumptions that the interfaces are regular plane surfaces. In nature, however, this is not always the case. By application of these functions on the more realistic cases, where refractors are irregular and dipping surfaces, inaccurate results may be obtained. The concept of (delay-time), introduced by Gardner (1939), serves as a tool for more accurate interpretation of refraction survey-data where the waves are refracted from irregular and dipping refractors.

The delay-time  $(\delta T_x)$  is defined to be the difference between the actual refraction travel-time  $(T_a)$ , corrected for the depth and velocity variations of the weathering zone, and travel time required to traverse the horizontal distance between the source and the receiver at the highest velocity encountered on the ray-path (Sheriff 2002). Referring to Fig. 5.12, the delay-time is represented by the difference between the time the wave takes in covering the actually travelled path (SBCR) and the distance  $(SR = x)$  with the refractor velocity  $(V_2)$ .

The delay time  $(\delta T_x)$  can be mathematically expressed as:

$$\delta T_x = T_a - x/V_2$$

**Fig. 5.12** The delay time concept, case of a wave refracted from an irregular dipping interface



In case of one horizontal refractor, the refraction travel-time function, is given by:

$$\mathbf{T}_a = \mathbf{x}/V_2 + 2\mathbf{z} \left[ (V_2)^2 - (V_1)^2 \right]^{1/2} / V_1 V_2$$

That is:

$$\mathbf{T}_a = \mathbf{x}/V_2 + \mathbf{T}_0$$

Hence,

$$\mathbf{T}_a = \mathbf{x}/V_2 + \delta\mathbf{T}_x$$

This result shows that the delay time concept is applicable to horizontal refractors. In fact the application of the concept on irregular reflectors is based on the assumption that the refractor is nearly horizontal under both of the source and receiver points. This means that more accurate results are obtained when the refractor is of mild undulations and of relatively small dip. The assumption is that the distance measured along the refractor surface is approximately equal to its projection distance onto the horizontal plane at the surface. The approximation ( $BC \approx B_S C_R$ ) is shown in Fig. 5.12.

The delay time ( $\delta\mathbf{T}_x$ ) is usually presented in two separate components: delay-time associated with the source point ( $\delta\mathbf{T}_S$ ) and delay-time associated with the receiver point ( $\delta\mathbf{T}_R$ ). Thus we have:

$$\delta\mathbf{T}_x = \delta\mathbf{T}_S + \delta\mathbf{T}_R$$

It should be noted that, when the refractor is horizontal, each of the delay-time components becomes equal to half of the intercept time that is:

$$\delta\mathbf{T}_S = \delta\mathbf{T}_R = \mathbf{T}_0/2$$

Where, ( $\mathbf{T}_0 = 2\mathbf{z}[(V_2)^2 - (V_1)^2]^{1/2}/V_1 V_2$ ) is the intercept time.

The main application of the concept is in the determination of the refractor depth. The depth of the refractor at the source point ( $\mathbf{z}_S$ ) and receiver point ( $\mathbf{z}_R$ ) can be computed if velocity information is available. According to Sheriff and Geldart (1995, p. 439), computation results are

sufficiently accurate; provided that the refractor-dip is less than about  $10^\circ$  ( $\text{dip} < 10^\circ$ ).

## 5.2.6 Refraction in a Multi-layer Medium

In case of multi-horizontal reflector, the refraction travel-time function is derived by applying the same principles used in the case of a single refractor that is Snell's law is applied to determine ray-path direction every time the wave crosses an interface. The velocities of the traversed layers must be increasing with depth in order that a head wave is created at the last refractor in the traversed layered medium.

For the general case where the medium is made up of  $\mathbf{N}$  horizontal layers of thicknesses  $\Delta\mathbf{z}_n$  ( $n = 1, 2, 3, \dots, \mathbf{N} - 1$ ) and increasing velocities  $V_n$  ( $n = 1, 2, 3, \dots, \mathbf{N}$ ), the refraction travel-time of a wave critically refracted at the base of the last layer (layer  $\mathbf{N} - 1$ ), is given by Nettleton (1940, p. 253):

$$\mathbf{T}(\mathbf{x}) = \mathbf{x}/V_N + 2 \sum_{n=1}^{\mathbf{N}-1} \Delta\mathbf{z}_n \left[ (V_N)^2 - (V_n)^2 \right]^{1/2} / V_n V_N$$

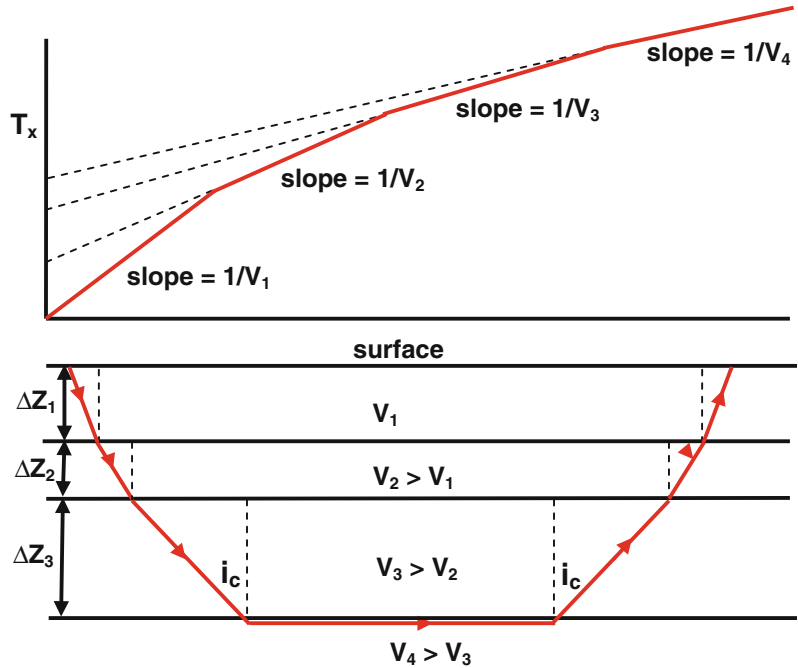
Reference to Fig. 5.13, showing a 3-layer model, the travel-time function,  $\mathbf{T}(\mathbf{x})$ , of the wave refracted from the base of the third layer, is given by:

$$\begin{aligned} \mathbf{T}(\mathbf{x}) = \mathbf{x}/V_4 &+ 2\Delta\mathbf{z}_1 \left[ (V_4)^2 - (V_1)^2 \right]^{1/2} / V_1 V_4 \\ &+ 2\Delta\mathbf{z}_2 \left[ (V_4)^2 - (V_2)^2 \right]^{1/2} / V_2 V_4 \\ &+ 2\Delta\mathbf{z}_3 \left[ (V_4)^2 - (V_3)^2 \right]^{1/2} / V_3 V_4 \end{aligned}$$

## 5.2.7 Refraction in a Medium of Linear Velocity Variation

A non-linear travel-time function arises in the case of a refracted wave travelling down a medium, the velocity of which is function of depth. For the case where the velocity is linear

**Fig. 5.13** Ray-path geometry and corresponding refraction travel-time curves for three horizontal refractors



function of depth,  $V(z) = a + bz$ , ( $a$  and  $b$  are constants), then the travel-time function is given by Nettleton (1940, pp. 257–261) and Dobrin (1960, pp. 77–78):

$$T(x) = (2/b)\sinh^{-1}(bx/2a)$$

The ray-path, in this case, is of circular shape of radius ( $r = z_m + a/b$ ), where ( $z_m$ ) is the maximum depth of penetration which is given by:

$$z_m = \left[ (x/2)^2 + (a/b)^2 \right]^{1/2} - a/b$$

Geometrical shape of ray-paths and travel-time curve are shown in Fig. 5.14.

### 5.2.8 Refraction from a Faulted Refractor

Refraction surveying can be used to detect a fault and determine its throw. Consider a two-layer system where the high-velocity layer (velocity,  $V_2$ ) is vertically faulted (fault throw,  $\Delta Z$ ) as shown in Fig. 5.15. The travel-time curve of refraction experiment across the strike of the fault plane will

consist of two parallel but displaced linear segments of slope equal to the inverse of the velocity of the faulted layer (slope =  $1/V_2$ ). These two segments correspond to the refracted arrivals from the reflector’s original surface and from the down-thrown surface respectively.

In reference to Fig. 5.15, the fault throw ( $\Delta Z$ ) is calculated from the difference in intercept times ( $\Delta T$ ), and the angle ( $i_c$ ) which is equal to  $\cos^{-1}(\Delta P/\Delta Z)$ . Since  $\Delta P = \Delta T \cdot V_1$ , and ( $\sin i_c = V_1/V_2$ ), we can write:

$$\Delta Z = \Delta T V_1 V_2 / \left[ (V_2)^2 - (V_1)^2 \right]^{1/2}$$

For more accurate determination of the throw ( $\Delta Z$ ) and fault location, another reversed refraction survey is needed to be conducted.

### 5.2.9 Applications of Seismic Wave Refraction

Refraction field work involves laying out a spread made up of sources and detector, that suite recording both of the direct and refracted wave-arrivals. Because of the relatively long

**Fig. 5.14** Sketch of ray-path geometry and travel-time curve for a medium of linearly increasing velocity with depth

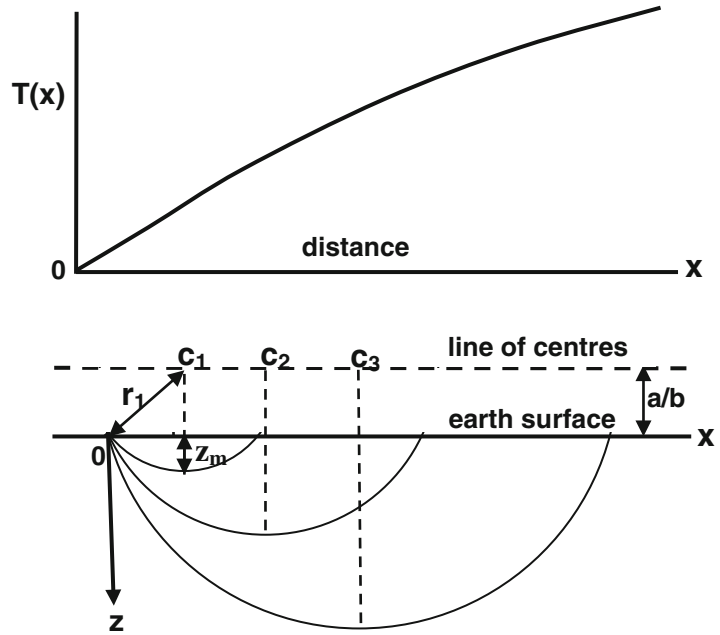
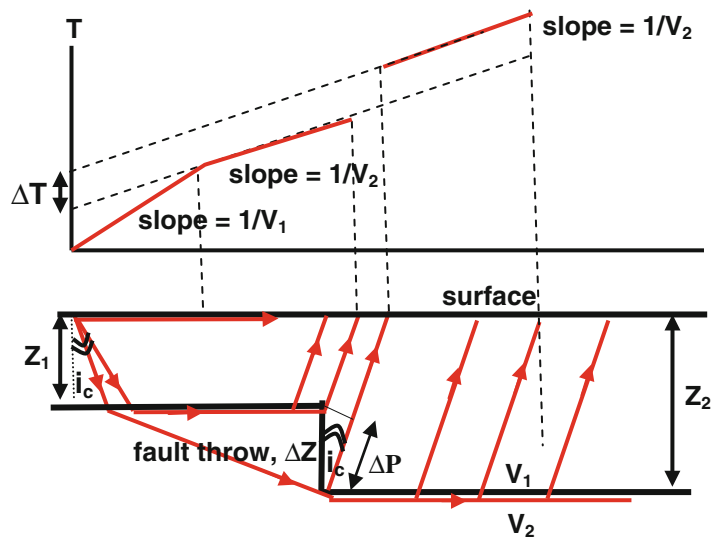


**Fig. 5.15** Ray-path geometry and corresponding refraction travel-time curves for refraction across a faulted horizontal refractor



travel-path, refraction arrivals suffer from attenuation in both of the energy and high frequency contents. To lessen these adverse effects, an adequate increase in energy source and adequate detector frequency response are used.

The main fields of application of refraction waves are:

- (i) Large-scale refraction profiling

- (ii) Small-scale refraction surveys
- (iii) Seismic fan shooting
- (iv) Seismic tomography

(i) **Large-Scale Refraction Profiling**

Large-scale refraction can be used in exploring geological rock layering of regional dimensions. Source-receiver spreads can be employed to survey lines of several kilometers to several tens

of kilometers. In this case, a profiling technique is followed where the line (of say 20–30 km length) is covered in a series of few-kilometer long segments. The source for the nearest segment may be few kilograms of dynamite-charge, which can be increased to several tens of kilograms for the large offset spreads. The technique is applied to map regional-scale geological layering of an area.

Larger refraction-spreads and greater source-energy were used, in the study of the Earth-crust. For this purpose, spreads of more than 500 km, using several tons of dynamite for the source energy have been used. Irrespective of the scale-size of the refraction-based exploration, the basic principles of the refraction method used, is the same. The final result is linear event from which the velocity and thickness information are obtained.

#### (ii) Small-Scale Refraction Surveys

Normally, a small spread (100–150 m) is employed. Depending on the shot position with respect to the detectors, there are two types of spread; one is centre-spread type and the other is end-on like arrangement. Typically, detectors in these spreads are laid down at 5–10 m spacing.

This type of surveys is usually used in geophysical engineering purposes, as in investigating local geological changes. A typical application of

small-scale refraction is in determination of the physical characteristics (thickness and seismic velocity) of the surface weathering zone. This activity is often carried out by seismic crews working in seismic reflection exploration.

#### (iii) Seismic Fan Shooting

This is one of the early techniques of using refracted waves in locating anomalous velocity bodies, such as buried salt domes. The detection points (receivers) are laid out in fan-like arrays at distances from a common source point. This is the reason for labeling the method by this name. More than one fan-spread is usually applied in the one survey. A sketch of two-fan surveys is shown in Fig. 5.16.

Those ray-paths penetrating the anomalous body will show abnormal travel-times compared with the others which are missing that body.

In case of a high-velocity body (as a salt dome), a time lead of the arrival time of the received refracted wave will be observed. Thus, by plotting the arrival times against the source-receiver distance, the abnormal values compared with a “normal curve”, delineation of the anomalous body is determined. For referencing purposes, the normal time-distance curve is obtained, in a near-by location where there are no anomalous bodies. This reference curve is obtained by plotting refraction arrival times

**Fig. 5.16** Source-receiver lay out used in seismic fan shooting

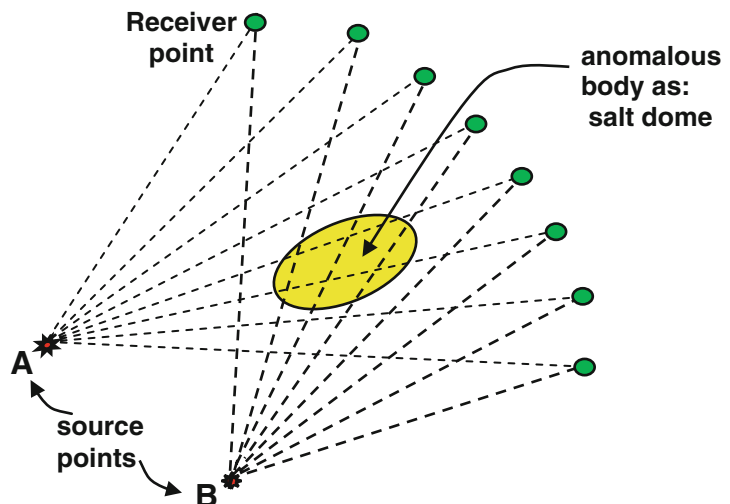
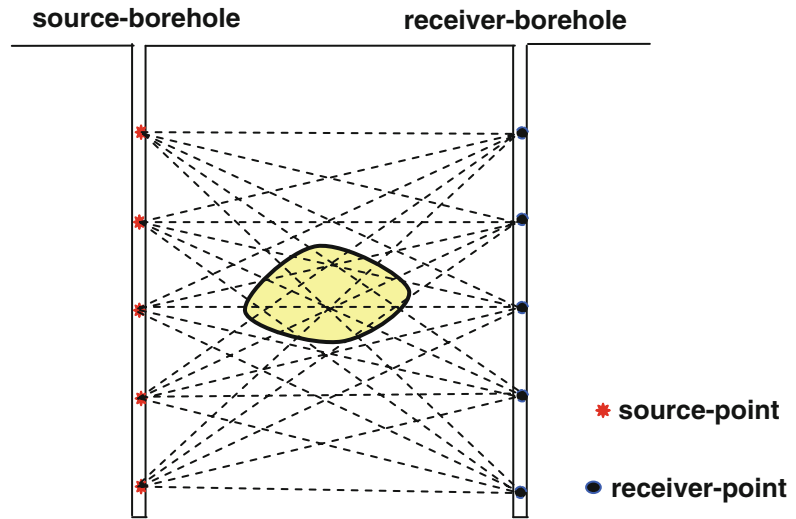


**Fig. 5.17** Seismic tomography, by borehole-to-borehole observation. All the involved ray-paths and a traversed anomalous body are shown



against source-receiver distances. For more accurate mapping of the anomalous body more than one source point is used for the same receiver array. This is similar to the scheme used by the modern tomography procedure followed in exploring anomalies by source-receiver recording systems. More detailed description of the method is presented in the geophysical literature like Nettleton (1940), Båth (1971) and Kearey et al. (2002, p. 116).

#### (iv) Seismic Tomography

The word (tomography) is of Greek-language origin, meaning (cross-section drawing). In the seismic field, tomography found its way as an effective exploration tool under the name of Seismic Tomography. This technique has been applied successfully in imaging seismic velocity variation and producing subsurface geological models. Seismic tomography is considered to be one of the modern techniques used in seismic exploration.

Seismic tomography is a type of inverse modeling (inversion process) which uses acquired seismic data to generate earth models (usually in terms of velocity and dimension information). The more applied technique in this field is the (transmission tomography) which requires putting the source points in a borehole and the receiver points at another borehole or at

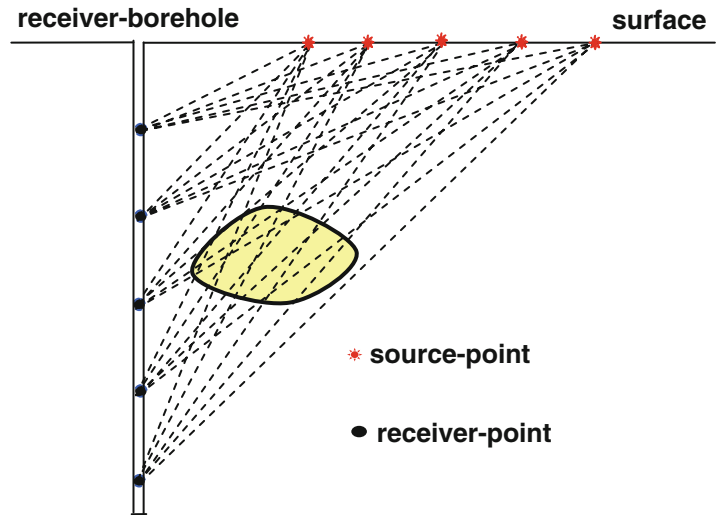
the surface. Like any other inversion process, seismic tomography aims at determination, as accurately as possible, of the earth structural model for the area under study.

Seismic transmission tomography deals with seismic transmission waves which, in general, experience refraction processes at boundaries where velocity changes. There are two types of seismic tomography, reflection and transmission. Reflection tomography deals with reflection travel-time measurements, while transmission tomography deals with source-to-receiver ray-paths along which the seismic waves are directly transmitted. The more commonly applied technique is the transmission, borehole-to-borehole (also called cross-hole) technique. In this method (cross-hole method), a set of source points are distributed down a borehole and another set of receivers are located in the other borehole, as shown in Fig. 5.17.

Another form of the seismic tomography is the surface-to-borehole technique. In this method the source points are located on the surface and the receiver points are distributed down the borehole, as shown in Fig. 5.18.

Interpretation of the data recorded from the cross-hole surveying (or from that of the surface-borehole) aims at velocity distribution in the medium between the source and receiver

**Fig. 5.18** Definition of seismic tomography, using the method of surface-to-borehole observations. All the involved ray-paths and a traversed anomalous body are shown



sets. Iterative, forward modeling is usually applied with the help of an especially-designed tomography-algorithm, starting with an assumed model of velocity distribution. The model is changed after each comparison pro-

cess, until computed travel-times become closest to the measured travel-times. The end objective of the whole process is to determine the subsurface geological model as accurately as possible.

The seismic reflection method depends on the same principle of the well-known echo phenomenon. A mechanical shock generates a seismic wave (normally, P-wave) which propagates through the earth material. On hitting a surface of a rock layer (an interface), the incident wave-energy is partly transmitted (passing through the interface), and partly reflected back to the earth free surface.

The earliest successful application of seismic reflection technique was made about 1930 (Nettleton 1940, p. 233). Since then, and due to its great efficiency in the exploration work, the method was intensively applied in exploring subsurface oil-traps. In its conventional form, the technique is based on initiating of a seismic wave and recording its reflection arrivals by detectors deployed on the earth surface along a straight line. The normally applied technique, the seismic reflection surveying, is based upon the use of a linear source-receiver spread moving along a defined seismic line. To cover a complete survey of an area, the process is repeated for all lines of a defined line-network designed for that area.

The end result of this technique is obtaining a two-dimensional seismic section for each seismic line, which is, in effect, expressing the variation of seismic-reflection amplitude as function of the two variables: distance,  $x$  and depth,  $z$ . The section lies in the vertical plane that coincides with the surface survey-line. For this reason, the method is called two-dimensional 2D surveying to differentiate it from the 3D surveying which

produces a data volume in which the seismic amplitude is function of the variables ( $x$ ,  $y$ , &  $z$ ).

Reflected waves carry useful exploration information in two forms: the travel-time and waveform changes. Both of these two types of changes are functions of the physical properties and layering geometry of the subsurface geology. In other words, the seismic information furnished by reflection surveying, can supply two main types of exploration knowledge which are: structural exploration information from travel-time measurements, and stratigraphic exploration information from wave-form measurements. These two types of changes constitute the principal seismic tools for exploring the subsurface structural and stratigraphic geology (Fig. 6.1).

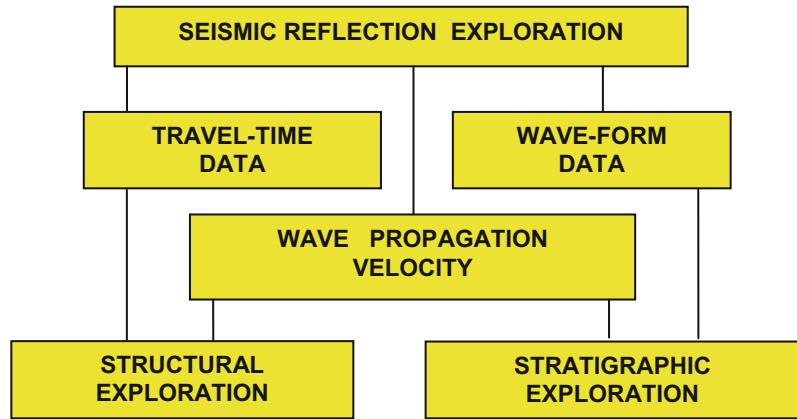
---

## 6.1 Reflection Surveying Concepts

### 6.1.1 The Spread Configuration

The shooting spread used in seismic surveying is defined as the geometrical relationship between the location of the source-point and that of the receiver-array. This shot-receiver configuration is kept unchanged during surveying of the seismic line. The main elements of a spread are the source-point (commonly known as the shot-point), and number and inter-spacing of the receiver-points. In practice shot-points and receiver-points are not points but sets of points. Thus a receiver point is usually made up of a

**Fig. 6.1** The two types of knowledge (in addition to propagation velocity) obtainable from seismic reflection surveying: travel-time for structural exploration and waveform for stratigraphic exploration



group of detectors (geophones) and the shot-point consists of a group of source-points. That is why these are commonly referred to as geophone group and shot pattern. For computation purposes, their geometrical centres are used to represent the shot-point and receiver-points locations respectively. The shape of the shooting spread and its main elements are shown in Fig. 6.2.

Based on the position of the shot-point in relation to the receiver-point, there are three types of spread configuration in common use. The shot-point may be located at one end of the receiver linear array giving a type called (end-on spread). Another type of spread is the one in which the shot-point is located within the spread it is called (split- or unbalanced-spread), and when it is located exactly at the centre of the receiver array-line, it is called (centre spread). The three common spread types are shown in Fig. 6.3.

The number of the active receiver points (or seismic channels) per spread is customarily fixed at a whole-number which is customarily taken as

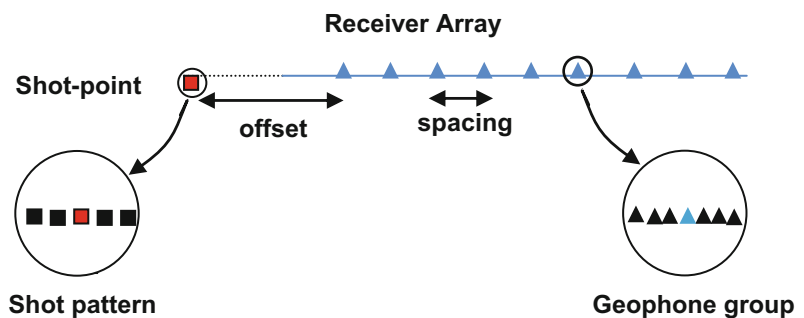
multiple of the number (12). In 2D seismic surveying the number of spread-channels used has increased from 48 in the early 1970s to 240; and 360 channels in the following forty years. In 3D surveying the number may exceed 1200.

### 6.1.2 The Seismic Trace

The seismic trace, considered to be the building brick for the whole seismic survey data, is a graph representing the recorded amplitude variation as function of reflection travel-time. The trace contains all the outputs of an active seismic channel during the recording time. It is, in fact, a record of the whole sequence of the reflection arrivals as well as other arrivals such as direct waves, refracted head waves in addition to the various types of seismic and none-seismic noises. There are three common modes of trace-display. These are:

- (i) Wiggly-trace, when the amplitude variation is represented by a wiggly line recorded.

**Fig. 6.2** Geometrical shape of the shooting spread



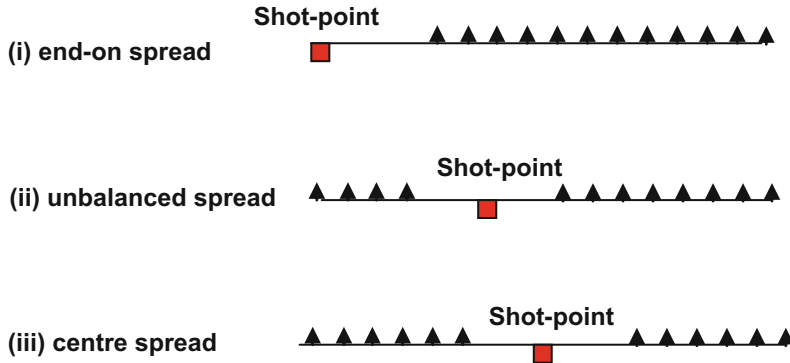


**Fig. 6.3** Types of commonly used shooting spreads

- (ii) Variable-area trace, when the peak-parts of the wiggly trace are blacked in.
- (iii) Variable-density trace, when the amplitude variation is represented by an appropriate shade-intensity.

Usually, the field shot-records are displayed in wiggly-trace mode (Fig. 6.4).

Seismic stack sections are displayed by superimposing the wiggly- and variable-area modes of display.

### 6.1.3 The Shotpoint

A seismic survey of a certain seismic line starts with deployment of the spread elements (shot and receivers) along that line. The designed spread, which consists of linear array of receiver-points which are co-linear with the shot-point, is laid down along the line to be surveyed. When activating the energy source (as firing a dynamite charge), a seismic wave-front advances through the medium in the form of spherical surfaces (spherical when the medium is homogenous and isotropic). The seismic rays are reflected from intervening interfaces, back to the surface to be detected by the geophone groups planted on the surface. The reflection arrivals are then fed into the recording system via the electrical channels which are displayed in a trace-gather (the shot-gather).

Each recorded trace (provided by an active channel of the spread) represents a series of wave arrivals of signals reflected from a subsurface

reflection point (RP) or common depth point (CDP). Referring to Fig. 6.5, a seven-channel spread (end-on type) produced a shot record containing seven traces that have been reflected from corresponding seven CDPs.

An actual record of a 48-trace shot-point obtained from a centre-spread is given here-below Fig. 6.6. It is showing fairly clearly, reflection arrivals as well as direct and refracted arrivals.

### 6.1.4 The Seismic Profiling Technique

Seismic surveying along a linear track is carried out by a technique known as (multi-channel profiling technique). The survey procedure involves the use of a fixed-shape spread that moves along a linear course at a regular move-up shift. The first shot-record is obtained from the spread which is laid out at the start-point of the line. In the following step, the second shot is recorded after shifting the spread location by a certain step-up distance. This process (shift-and-shoot process) is repeated from start point to the end point of the line. The move-up distance is normally made to be integral multiple of the receiver-point spacing. A map of all locations that have been occupied in surveying the entire line is called (surface-coverage map).

For more clarification of the profiling technique, an example is given in Fig. 6.7 which shows a seismic line of length of 39 receiver stations, surveyed by an end-on spread. The

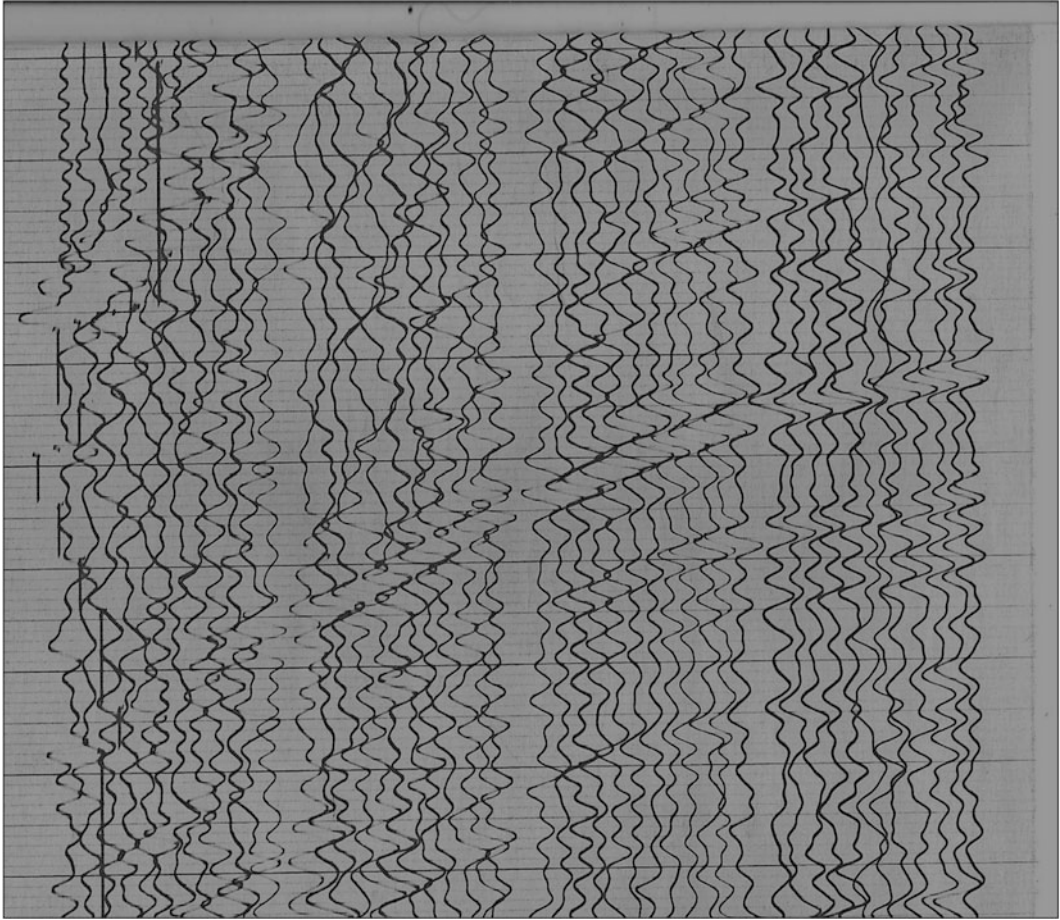


**Fig. 6.4** Part of 48-channel shot-record showing reflection arrivals and random seismic noise. Traces are displayed in wiggly-trace mode

surface coverage, shown in Fig. 6.7, consists of seven positions of the spread that advanced along the line at move-up shifts of four receiver-stations per shift.

Because this procedure gives a seismic section representing a profile of the earth along the surveyed seismic line, it is referred to as a profiling technique.

### 6.1.5 The Fold of Coverage

By definition the CDP is a subsurface point located vertically below the source-receiver

midpoint. This means that each receiver-point of a spread will receive a seismic arrival reflected from a CDP located below the source-receiver midpoint. In fact, shooting of one spread, the reflector will be sampled by a number of reflection points (CDPs) equal to the number of the spread active receivers. From the geometry of the spread ray-path, the CDP spacing will be half that of the receiver points of the spread. Thus, the subsurface coverage (CDP-line) covered from shooting one shot will be about half the spread length (Fig. 6.8).

Seismic profiling procedure is accomplished by repeating the shooting process (shot firing and

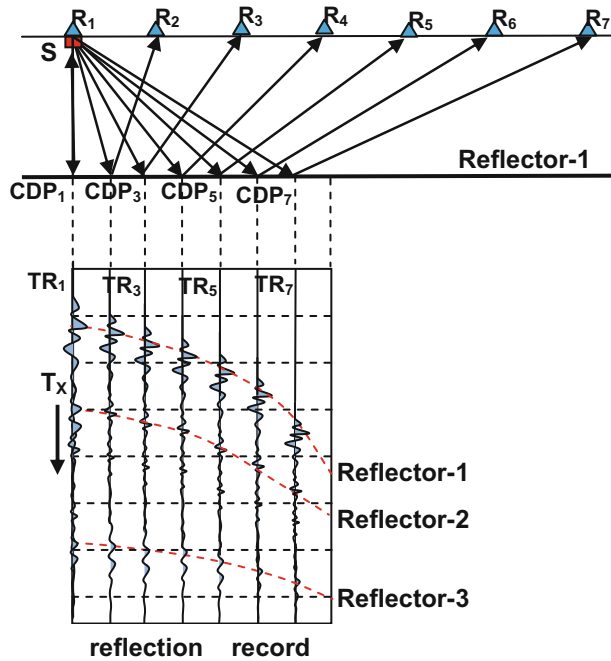


**Fig. 6.5** Shot-point ray-paths and its corresponding seismic shot record. Spread (end-on type), made up of 7 receiver-points ( $R_1, \dots, R_7$ ) producing 7 seismic traces ( $TR_1, \dots, TR_7$ ) reflected from 7 CDPs ( $CDP_1, \dots, CDP_7$ )

reflection-arrivals recording) at a series of equally spaced shot-point locations along the surface line. By making the spread move-up distance equal to half of the spread length, one reflection per one CDP will result for the entire line. The resulting seismic section in this case is commonly known as (single-fold section). For larger move-ups, gaps will result in the sampled reflector. That is, certain CDPs will not have reflections at all. On the other hand, if the move-up distance is smaller than half the spread length, then CDPs will get more than one reflection, giving the case of multi-fold profiling technique. The number of reflections realized per CDP is called the fold of coverage, (or just, fold). Of course the shorter the move-up, the greater the fold will be.

Considering an example of a seismic profiling case in which a twelve-channel spread is used. The effect of the move-up distance on the fold of coverage is clarified in Fig. 6.9. In this example,

it is shown that when the spread move-up is too large (larger than half the spread), the subsurface coverage is incomplete, with gaps in the CDP sequence where patches of the reflector are giving no-reflection information Fig. 6.9a. When the 12-channel spread is made to advance by 6-receiver station move-up rate, the reflector is completely covered with single-fold coverage (Fig. 6.9b). In the third case (Fig. 6.9c), the spread is made to move with a spread move-up distance of two receiver-stations, which resulted in threefold coverage for the whole line except for the less-than threefold zones (called fold tails) at the beginning and at the end of the line. In this example, the fold, in the tail-zone, is building up from a single fold at the first CDP to threefold over 8 CDPs. The same thing occurs at the end of the line but in reverse direction.

In a regular shooting, which is normally applied in seismic profiling, the fold of

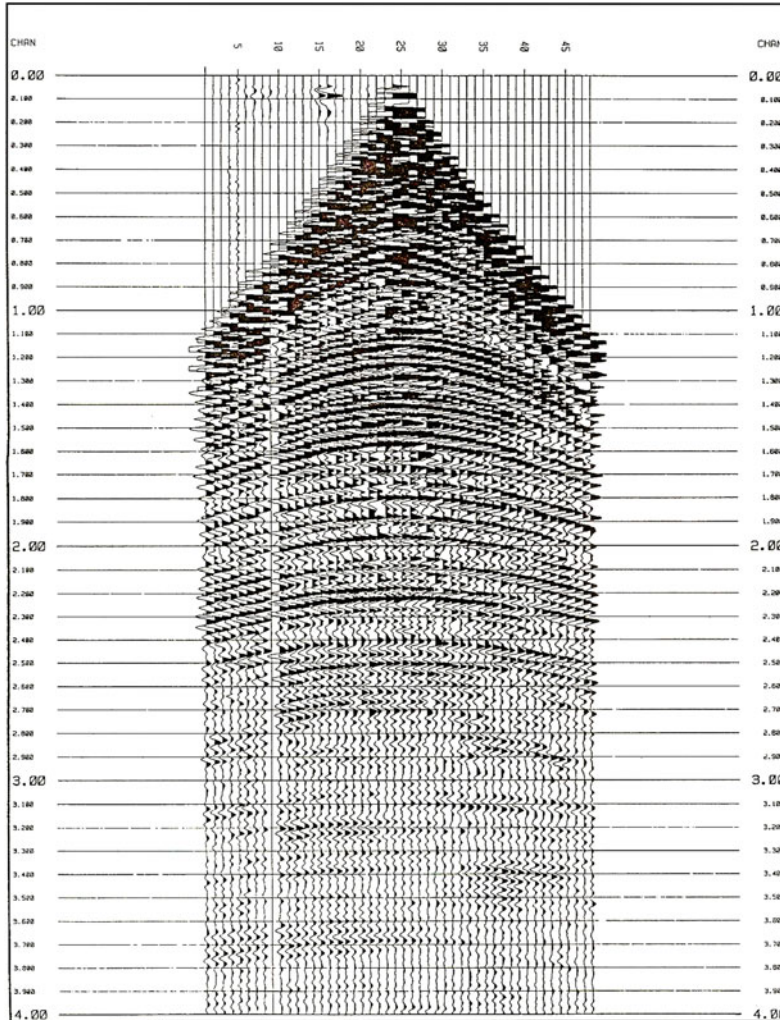


**Fig. 6.6** An actual 48-trace shot record showing clear reflection arrivals with relatively high-amplitude direct and refracted arrivals. Traces are displayed in variable-area mode of display

coverage ( $F$ ) can be calculated from the following formula:

$$F = N/2n$$

where, ( $N$ ) is the total number of the spread active receiver-channels and ( $n$ ) is the move-up distance expressed in number of receiver-station spacing covered in one move-up distance.

This equation shows that the fold is directly proportional to the number of channels and inversely proportional with the move-up distance.

The fold of coverage is a major factor in increasing the signal-to-noise ratio ( $S/N$ ). In fact

there is a direct relationship between fold and reflection signal-quality appearing in the stack trace. However the relation is not linear but follows a power law of the form ( $F^{1/2}$ ) (Robinson 1983a, p. 111). Accordingly, the rate of change in the ( $S/N$ ) enhancement diminishes with the increase of fold (Fig. 6.10).

### 6.1.6 The CDP Trace Gather

As mentioned above, a shot-gather is the group of traces recorded by the spread channels of that shot. Thus, a seven-channel shot has seven recorded

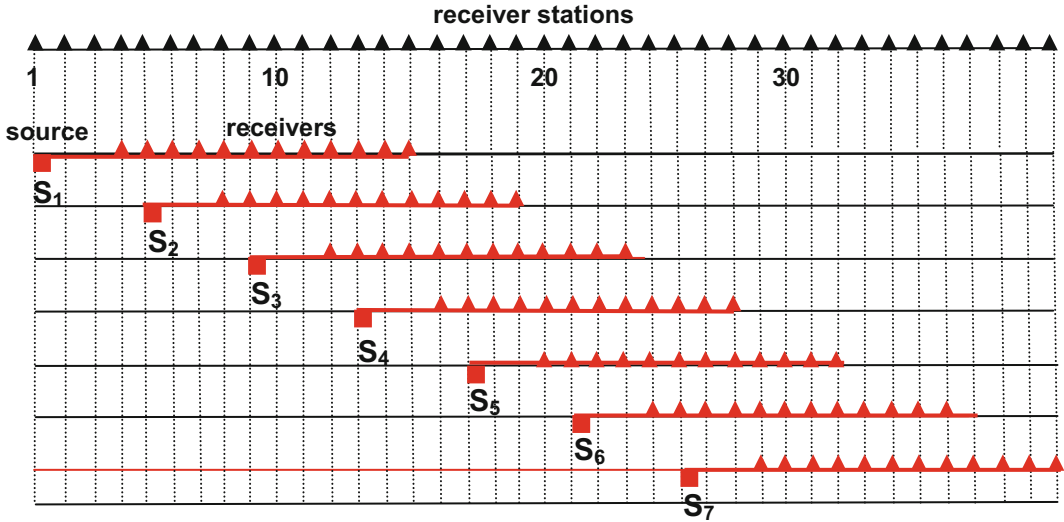


**Fig. 6.7** Surface coverage of a line made up of 7 spread move-up shifts

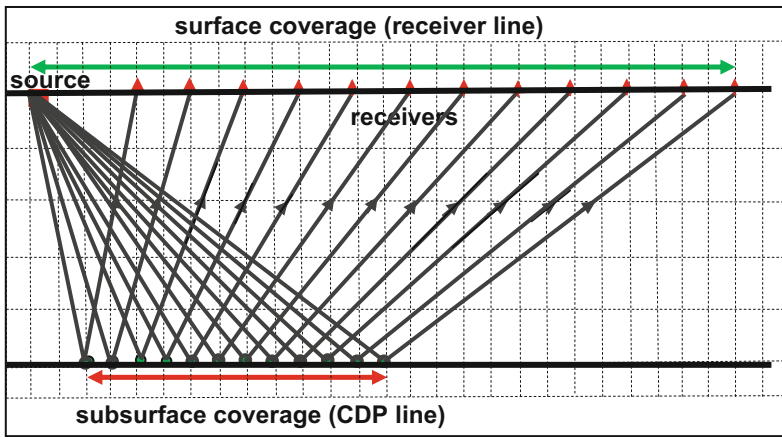


**Fig. 6.8** Shooting spread surface-coverage, reflection ray-path, and CDP subsurface coverage, as realized from one seismic shot-point

seismic traces. Likewise, the CDP-gather is a group of seismic traces which belong to one CDP. Naturally, the number of traces in a certain CDP is equal to the fold of coverage in that CDP.

In a certain seismic profiling process, the traces obtained for each shot (shot-gather), are re-grouped into CDP gathers ready for being stacked after being subjected to certain processing steps which aim at enhancing the reflection signal. To explain

this regrouping process (trace re-sorting), a simple profiling example is given here (Fig. 6.11).

In this example (shown in Fig. 6.11) we have a survey made up of five shots (A, B, C, D, and E). Shot-A of traces ( $a_1, a_2, \dots, a_6$ ) and shot-B of traces ( $b_1, b_2, \dots, b_6$ ), and so on, for the rest of shots. The complete surface coverage is occupying a total of 11 receiver-stations with one receiver-station for the spread move-up distance.

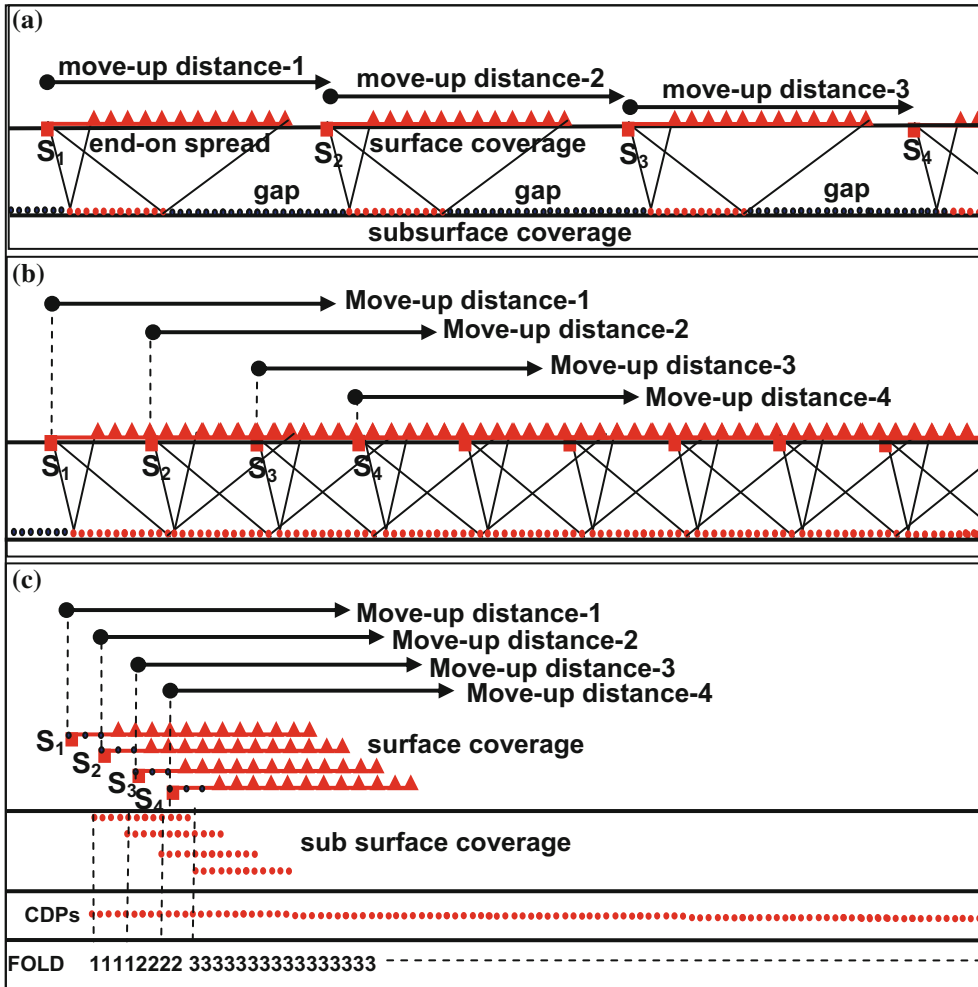


**Fig. 6.9** Surface and subsurface coverage in seismic profiling surveying using an end-on spread. Move-up distance: greater than half spread length (a), equal to half spread length (b), and more than half spread length (c).

Spread move distance is 2 receiver-stations, resulting in nominal fold of 3, with tail-fold at beginning and end of the line

Corresponding to this surface coverage, is a subsurface coverage made up of 14 live CDPs, ( $CDP_1, CDP_2, \dots, CDP_{14}$ ). The trace gather for  $CDP_1$  (CDPG-1) consists of one trace ( $a_1$ ). For the second CDP (CDPG-2) the gather has also one trace ( $a_2$ ). The CDPG-3 has two traces ( $a_3 + b_1$ ), and so on. The number of traces per CDP is representing the fold of coverage.

Identifying the trace gathers (for shots and CDPs) is much simplified by drawing what is

known the (Coverage Diagram). In Fig. 6.11, the shot-gather is indicated by the horizontal arrow, and the CDP-gather is indicated by the vertical arrow. Number of traces in each gather, represents the fold of coverage. In this example, the fold is equal to 3 for the range ( $CDP_5-CDP_{10}$ ), and tail fold for the ranges ( $CDP_1-CDP_4$ ), and for ( $CDP_{11}-CDP_{14}$ ). The re-distribution of the traces from the shot-gathers to CDP-gathers (called CDP sorting) is shown in the following figure (Fig. 6.12).

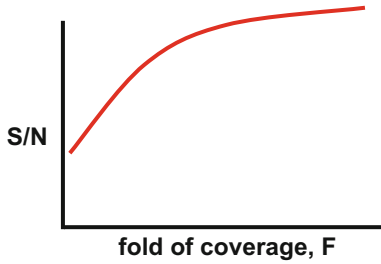


**Fig. 6.10** Curve expressing type of dependence of the S/N ratio on fold of coverage of reflection signal. The curve is of the power-law form ( $F^{1/2}$ )

## 6.2 Seismic Reflection Data Acquisition

In seismic reflection data acquisition, we are, in general, dealing with generating and detecting P-waves which are propagating from the source region and getting reflected from subsurface interfaces. The complete data acquisition process involves seismic source generation, reflected wave detection, and digitally data recording.

In order to record the reflection arrivals with minimum distortions, optimum operation parameters (called field parameters) are determined and applied in conducting the seismic survey. The

seismic field-crew usually carries out certain field activities directed towards determination of the optimum survey parameters and optimum survey procedures. Optimization of survey parameters and survey procedures are collectively referred to as (survey design) which is normally outlined in the work plan normally prepared for the seismic survey.

### 6.2.1 Seismic Energy Sources

The traditional method applied in generating seismic waves is exploding dynamite in shot-holes. There are however, other methods which have been introduced as alternative seismic energy sources. Choice of the source-type depends on the surface conditions prevailing in the given survey area. The main criteria considered in evaluating a particular source-type are the following:

- strong enough to generate strong seismic signal that can be reflected from deep interface and be detectable at the farthest receiver (receiver of maximum offset).
- the generated seismic signal is rich in high frequency components to be able to resolve closely spaced reflectors.
- the generated noise is of least energy level.

SHOTS & CDPS	receiver-stations														
	1	2	3	4	5	6	7	8	9	10	11				
SHOT-A CDP-A	S <sub>A</sub>	a <sub>1</sub>	a <sub>2</sub>	a <sub>3</sub>	a <sub>4</sub>	a <sub>5</sub>	a <sub>6</sub>	Spread move-up direction →							
SHOT-B CDP-B		S <sub>B</sub>	b <sub>1</sub>	b <sub>2</sub>	b <sub>3</sub>	b <sub>4</sub>	b <sub>5</sub>	b <sub>6</sub>							
SHOT-C CDP-C			S <sub>C</sub>	c <sub>1</sub>	c <sub>2</sub>	c <sub>3</sub>	c <sub>4</sub>	c <sub>5</sub>	c <sub>6</sub>						
SHOT-D CDP-D				S <sub>D</sub>	d <sub>1</sub>	d <sub>2</sub>	d <sub>3</sub>	d <sub>4</sub>	d <sub>5</sub>	d <sub>6</sub>					
SHOT-E CDP-E					S <sub>E</sub>	e <sub>1</sub>	e <sub>2</sub>	e <sub>3</sub>	e <sub>4</sub>	e <sub>5</sub>	e <sub>6</sub>				
CDP SEQ.		1	2	3	4	5	6	7	8	9	10	11	12	13	14
FOLD		1	1	2	2	3	3	3	3	3	2	2	1	1	

**Fig. 6.11** Example of profiling process, where a 6-channel end-on spread moving at one receiver-station move-up distance. Shot-gather is indicated by the

horizontal arrow and the CDP-gather is indicated by the vertical arrow. Nominal fold is 3 over the central 6 CDPS and the tail-fold zones are at beginning and end of line

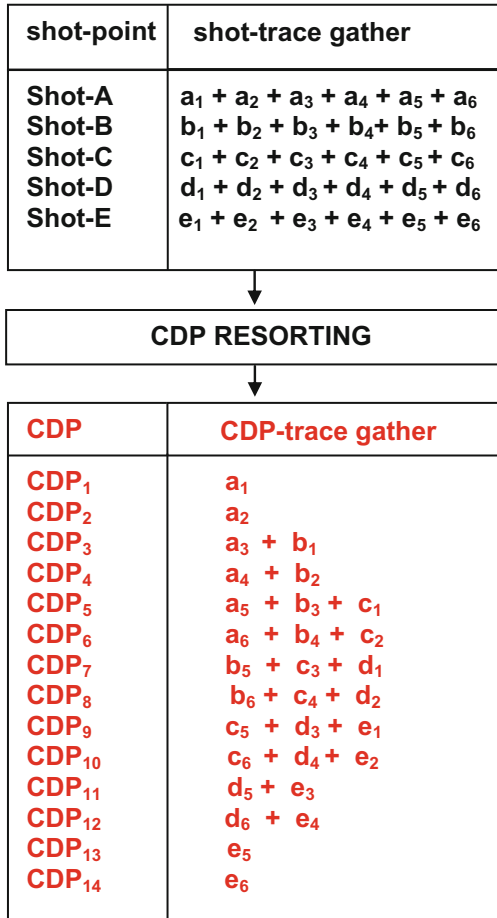


**Fig. 6.12** The CDP sorting process of the profiling case, given in the example shown in Fig. 6.11

Depending on the surface environments, the source types are classified into land- and marine-sources. Here-below are brief definitions of these seismic-energy types.

**Land Seismic Sources**

**(i) Dynamite**

This is one of the most common types of seismic source used in land seismic surveying. Normally, a certain dynamite charge is exploded inside a drilled hole at a depth ranging from few meters to several tens of meters. Typically, the drilled hole is of diameter of about 10 cm and depth of about (5–15 m). Ideally the charge depth should be placed deeper than the base of the weathered layer (low-velocity layer, LVL, as it is often

called), in order to avoid high-frequency filtering and seismic-pulse weakening caused by that layer. To increase the charge-coupling with the surrounding medium, the hole is filled with water or with mud-water mixture (Fig. 6.13).

The most common way of using this method is placing the dynamite charge at the bottom of a drilled hole. However the charge, under certain conditions, may be placed in shallow holes or even at a height above the ground. A method called Air-shooting or Poulter method (Poulter 1950), involves simultaneous firing of a number of charges placed on poles in the air. This is not an efficient method since the ground surface is of high reflection coefficient and thus a relatively small portion of the generated energy is transmitted into the earth, and most of the energy is reflected back from the surface and in generating surface waves. This method (Poulter method) is not in common use at present.

In general, the dynamite source is characterized by its high energy level, and of wide frequency band, though it involves a certain degree of danger and needs special storage conditions and strict safety measures.

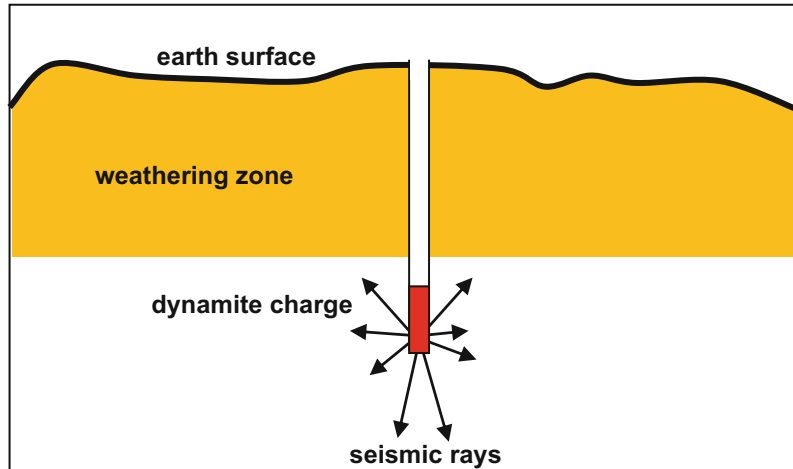
**(ii) Weight Dropping**

The Weight Dropping method (also called Geograph or Thumper) involves dropping a weight of about 3 tons from a height of about 3 m on to the ground (Fig. 6.14).

The seismic energy generated from the impact of the falling mass with the ground is considered to be weak in comparison with the dynamite explosion. In order to strengthen the generated seismic signal, the dropping shot is repeated number of times (30–60) shots done at the same location and electronically summed up to produce one shot-record. This technique of summing corresponding traces of shots of common location (called vertical stacking) is normally applied in this and in other cases of weak energy sources.

Compared with the other energy sources, weight dropping gives fairly high frequency, but less than dynamite-generated pulses. It is safe, fast, and cheap in operation. The draw-back of the method is development of strong surface waves and, because of the filtering effect of the

**Fig. 6.13** Dynamite seismic-energy source



surface (low velocity layer, LVL), the high frequency components are severely attenuated. This method is rarely applied at present.

**(iii) Gas Exploding**

This is another impulsive source (known as Dinoseis) in which the energy is created by exploding a mixture of oxygen and propane gases contained in a confined chamber, the bottom of which is a moveable plate resting on the ground surface. The so designed chamber is attached to

the bottom of a heavy vehicle to increase coupling of its plate with ground surface (Fig. 6.15).

On detonating the gas mixture, a sudden pressure impact occurs which is transmitted through the base-plate to the ground surface. By hydraulic system the plate is locked into position after the impact, to prevent repeated impacts.

Being a relatively weak-energy source, more than three units are fired simultaneously by a control signal sent from the recording system, and the shot is repeated many times, then vertical stacking is applied to get improved S/N ratio.

The general features of Dinoseis are similar to the Weight Drop method. Both are surface sources which are generating relatively weak seismic energy, developing strong surface waves, and producing low-frequency seismic pulses. The method is rarely applied these days.

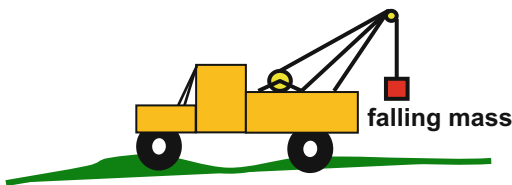
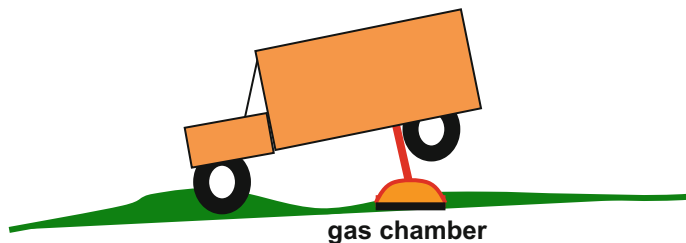


**Fig. 6.14** Weight-Dropping seismic-energy source

**Fig. 6.15** Gas exploding seismic-energy source



#### (iv) Dynamite Cords Exploding

This seismic source, well known by the name (Geoflex), consists of an explosive cord which is buried in the ground at a shallow depth (about half a meter depth). It is laid down by a hydraulically-operated plough which is especially designed for this purpose (Fig. 6.16).

Implementation of the Geoflex method starts with laying the explosive cord (about 100 m length) inside a trench of about a half-meter depth and detonated at one end. While the explosive-generated energy is travelling very fast through the cord from the detonation point, seismic waves are generated from each point of the cord at delayed times. This will cause these waves to have phase differences bringing about the filtering effect similar to that made by source-arrays. Points of the earth surface coinciding with the cord, are receiving the liberated energy not at the same time, but in sequential manner. For this reason, the down-going wave-front becomes inclined with respect to the horizontal level. Along this wave-front (shown by dotted lines in Fig. 6.16), highest energy level is obtained. In effect, there will be a filtering effect such that the near-surface horizontally travelling energy (surface waves) will be filtered out before reaching detectors.

The main advantages of the Geoflex method, is the attenuation of the surface waves, in addition to generating wide-band seismic waves. Regarding field operation the method is fast and simple

in laying the explosive cords. Since the method depends on trenches for the explosive cords, it means that it is not possible to be used in areas of too hard surface layer or in cities or villages. It is not advisable to be used in areas where the surface layer is too thick, since in such conditions the transmitted energy will be much weakened.

#### (v) Vibroseis

This is a non-impulsive seismic-energy source which was introduced in early 1950s and rapidly gained popularity as an acquisition tool. In 1982, over 40 % of worldwide seismic surveys were using it (McQuillin et al. 1984, p. 38). Unlike impulsive sources, Vibroseis method creates mechanical energy which is continuously vibrating for certain time duration. A mechanical, truck-mounted vibrator is hydraulically driven, produce electronically controlled vibration. The generated energy is conveyed to the ground by a metal pad (about 1 m<sup>2</sup>) attached beneath the truck (Fig. 6.17).

When in operation, the Vibroseis system transmits into the earth a seismic signal vibrating at frequency which is varying linearly with time. This electronically-controlled vibration function is called the Sweep. In practical application, the sweep duration (called sweep length) is normally within the range (10–20) s. Over this time-span the sweep-frequency applied is (10–50) Hz. Apart from the taper imposed at both ends of the sweep (about half a second in length), the

**Fig. 6.16** Geoflex seismic-energy source. The dotted lines represent the in-phase generated waves

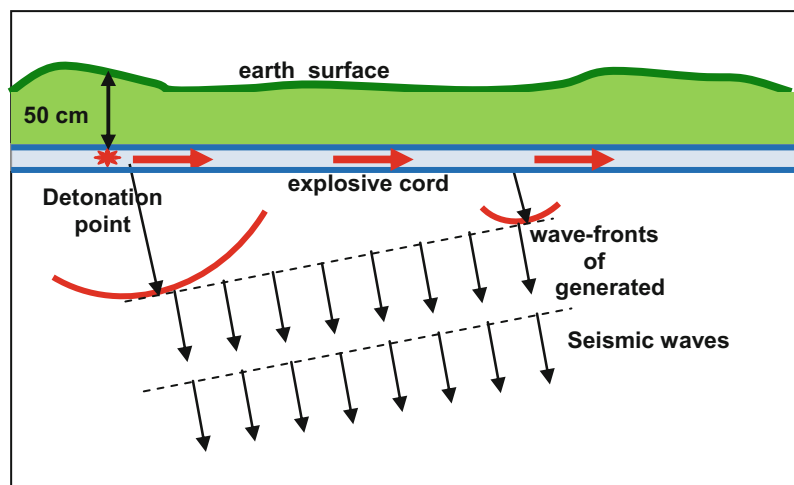
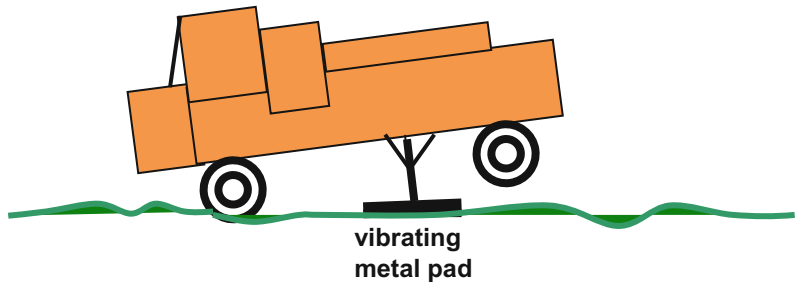


**Fig. 6.17** Vibroseis seismic energy source



amplitude is kept constant during operation time. Further, the sweep may be started at low frequency then it is linearly increased (up-sweep) or started by high frequency (down-sweep). The up-sweep vibration is the more commonly applied method. A schematic representation of the sweep is shown in Fig. 6.18.

As it is expected, the output reflection signals of Vibroseis-generated energy are not short wavelets, as normally seen with impulsive sources. The reflection signal, in case of Vibroseis sources, is as long as the sweep-length used in the survey operation. In consequence, we get overlapping of the long reflection signals, and in this case, it will be very hard to distinguish individual reflection events on Vibroseis records. Comparison between outputs of vibroseis and impulsive sources is shown in Fig. 6.19.

The time between the end of the sweep, sent by the vibrator, and the end of the recording time is referred to, as the (listening time).

**The Sweep Removal**

The seismogram,  $y(t)$ , obtained from exploration using impulsive sources, is the result of convolution of the source pulse  $s(t)$  by the reflectivity function  $h(t)$  of the subsurface reflectors in addition to noise  $n(t)$ , that is:

$$y(t) = s(t) * h(t) + n(t)$$

The recorded seismogram is near-impulsive form if the source function is of an impulsive form, as in case of dynamite source for example. In Vibroseis shooting, the source function is not an impulse, but a long time function represented by the sweep. This means that the recorded seismogram is made up of overlapping sweeps which is far from the familiar impulsive seismogram.

To convert the Vibroseis-generated seismogram into impulsive ready-to-interpret form, a signal compression process must be performed. This process (called sweep removal) is done in processing stage by the cross-correlation process.

**Fig. 6.18** Vibroseis sweep signals. **a** Up-sweep, **b** Down-sweep, **c** Up-sweep with taper applied at both ends

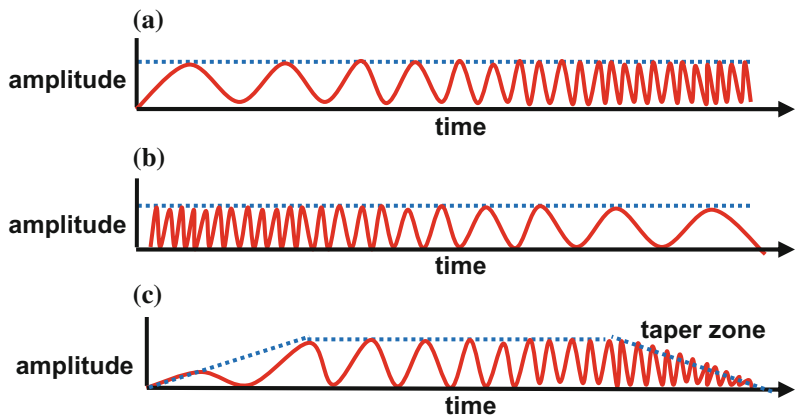
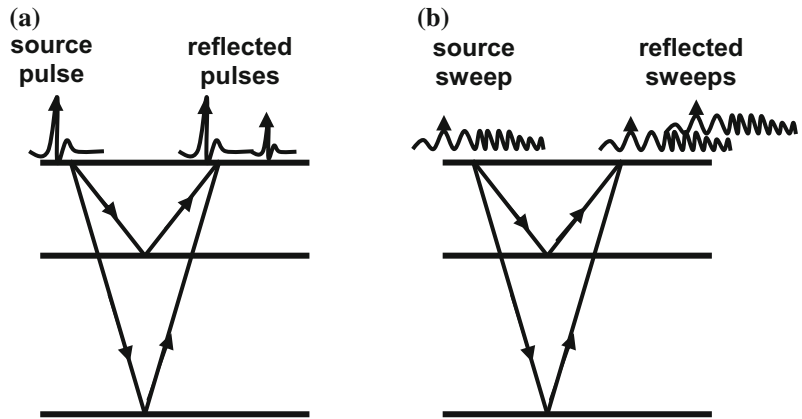


**Fig. 6.19** Ray-path geometry and reflection arrivals. **a** case of impulsive source and **b** Vibroseis source where reflected sweeps are overlapping



In order to extract the impulsive-like record of the reflections in their actual reflection-times, the recorded traces are cross-correlated with the applied sweep. This process can be done in the field within the recording unit of the Vibroseis system, or later by the processing software (see processing section).

The main advantages of the Vibroseis method are being fast, safe, and comparatively cheap to run. It can be applied along roads and even in cities since it causes no damaging effects on environments. Technically, it has the advantage of having the source-function being under control. The sweep parameters (time duration, frequency range, and taper) can be changed at will. The main problem with the method is the low source energy-level. Like other weak surface sources, vertical stacking is carried out at the same time as the recording is going on. In normal surveying work, several Vibroseis-trucks (typically 4) are operating at the same time, and about 20–60 vibrations are conducted per each shot-point location. The shot-gather traces per each shot, are obtained from vertical stacking of all of the recorded traces involved in the one shot-point.

### Marine Seismic Sources

The most common types of seismic energy sources are:

- (i) *The Air-Gun* is a widely used energy source in marine seismic surveying. It generates energy by discharging highly compressed air into the water. A variation of this method

is the (Unipulse), where the air continues flowing into the generated bubble for some time after the initial discharge. This is done to lessen the effect of the sudden bubble collapse which results in bubble oscillation.

- (ii) *The Steam-Gun* (also called Vaporchoc) utilizes hot steam instead of air. It is considered to be better than the Air-Gun, because with using hot steam, the effect of bubble oscillation is reduced.
- (iii) *The Gas-Gun* is still another similar marine source which uses explosion of a mixture of propane and oxygen contained in a steel chamber. The pressure pulse created by the explosion of the propane-oxygen mixture is passed to the water via a flexible seal which forms part of the chamber. The (Aquapulse) works on this principle.
- (iv) *Dynamite explosion* is implemented as a marine energy source. A method called (Maxipulse) uses small dynamite charges fired directly in the water body. Another similar method (Aquaseis) uses long detonating cord.
- (v) *Electrical Arc Discharge* is used to generate energy by electrical discharge in water. Examples of this method are the (Sparker) and the Wasp. This is a relatively weak energy source which is more suited for shallow-geology exploration.

Out of these methods, the Air-Gun is by far the most commonly used type of energy source in

seismic marine surveying. In certain situations, the Air Gun, is used as a land seismic source by generating a seismic pulse from an Air-Gun submerged in a water-filled pit made on the earth surface. Typical example of such an application is in providing the seismic energy for VSP surveying.

It should be noted here that the names of the energy types are trademarks given to them by their originators. The following Table 6.1 contains a summary of the types of seismic sources, with their trademark references.

### 6.2.2 Seismic Detectors

Earth movement due to the arrival of a seismic wave is generally very small. The vibration amplitude is of the order of  $10^{-8}$  of an inch (Gardner 1938). In addition to the small-amplitude feature, the seismic waves have two other criteria which the detection and recording equipments should be able to cope with. These are the wide amplitude-range and the wide frequency-range.

The seismic detection process is based on conversion of the ground vibration to an electrical signal by a special transducer which can respond to seismic amplitude and frequency full ranges and without distortions. Seismic detectors are of two main types, the geophones for use in

land and hydrophones for use in marine environments.

#### (i) The Geophone

Detection of reflection arrivals in land surveying is done by geophones (seismometers as they are sometimes called). The geophone is a seismic-detection instrument which can transform the ground vibration motion into an electrical voltage. The most commonly applied geophones in seismic reflection surveys are the electromagnetic type. It operates on the principle of voltage generation in a coil moving within a magnetic field. The generated voltage is proportional to the velocity of the motion of the coil relative to the magnet. For this reason, geophones of this type are normally referred to as (velocity geophones).

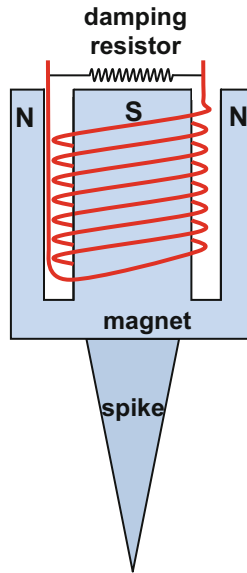
The geophone is made up of a permanent cylindrical magnet and a coil suspended by leaf-springs inside a circular slit made in the magnet. The slit is separating the magnetic south-pole (inner part of the magnet) from the north-pole (outer part). The magnet is firmly attached to a case which is fitted with a spike for easy fixing on the ground in an upright position (Fig. 6.20).

For operation, the geophone is planted vertically into the ground. In this position the magnet will vibrate in vertical direction when the ground is seismically activated, and the coil stays

**Table 6.1** Types of seismic sources, with their trademark references

	Land sources	Trademark reference
i	Geograph	Mandrel Industries & McCollum Exploration Co.I
ii	Dinoseis	Sinclair Research Inc.
iii	Geoflex	Imperial Chemical Industries Ltd.
iv	Vibroseis	Continental Oil Co.
	<i>Marine sources</i>	
i	Unipulse	Petty-ray Geophysical Inc
ii	Vaporchoc	Compagnie Generale de Geophysique
iii	Aquapulse	Western Geophysical Co.
iv	Aquaseis	Imperial Chemical Industries Ltd.
v	Maxipulse	Western Geophysical Co.
vi	Wasp	Teledyne Exploration Co.

**Fig. 6.20** Schematic representation of the electromagnetic geophone. Symbols *N* and *S* denote magnetic north pole and south pole respectively



stationary because of its inertia. The generated voltage in the coil is function of the vibration rate and the coil parameters (number of turns, radius, and field intensity of its magnet).

In order to reduce oscillation, geophones are normally provided with a damping resistor shunted across the geophone terminals. The damping device controls the frequency-response of the geophone vibration. Typical forms of the geophone response characteristic curves for different damping factors, are shown in Fig. 6.21.

Too heavy damping (over-damping) reduces detection sensitivity, while too little damping (under-damping) will lead to continued oscillation. Critical damping is defined to be the

maximum damping applied without stopping the oscillation. Damping of about 0.7 times the critical damping gives a response which increases smoothly with increase of frequency. This damping factor ( $D = 0.7$ , in Fig. 6.21) is the damping which is normally applied in seismic surveying environments.

#### (ii) The Hydrophone

This is a geophone-equivalent detector used in detecting seismic waves in marine surveying environments. The hydrophone is a pressure-sensitive detection device that uses substances that generate electrical voltage proportional to pressure changes caused by the arrival of a seismic signal. Such a substance (called piezoelectric substance) has a property of generating an electric voltage when subjected to pressure. Piezoelectric transducers are also called electrostrictive devices (Sheriff 2002, p. 263). The pressure changes, caused in a water medium, due to passage of a seismic wave, are proportional to the velocity of the water particles set into motion by the signal (Dobrin and Savit 1988, p. 63).

In marine surveying, hydrophones are housed in a special hose filled with a certain liquid of such a density that makes the net density of the hose (containing the hydrophones and liquid) approximately equal to that of water in order to facilitate controlling its depth below water surface and in reducing effects of external sudden forces affecting the streamer (cable jerking).

Marine data acquisition is conducted by towing the hose, equipped with hydrophones (called streamer) behind the survey boat (Fig. 6.22).

**Fig. 6.21** Schematic representation of the geophone frequency response curves. Three curves of three different damping factors ( $D$ )

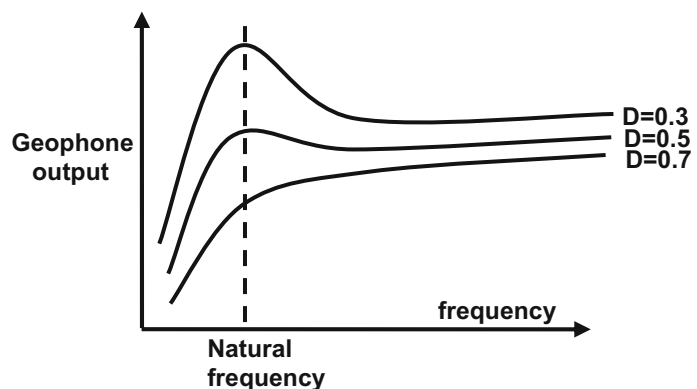
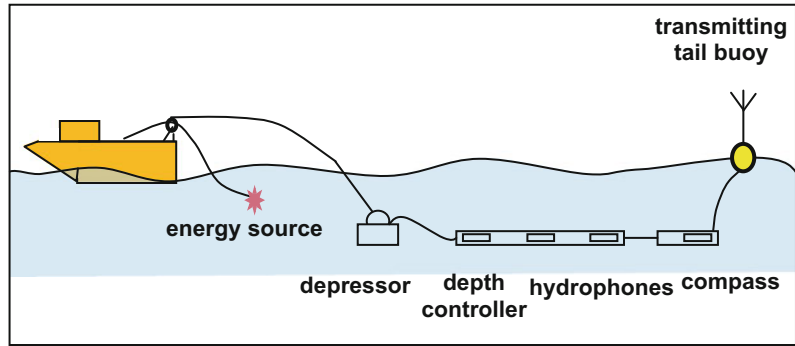


**Fig. 6.22** Elements of the marine-surveying spread (the streamer)



### 6.2.3 The Seismic Data Recording

For about 30 years after seismic exploration was introduced, seismic shot-records were directly recorded on paper as wiggly traces. In the early 1950s, however, recording of seismic data on magnetic tapes was introduced in analogue mode. After about ten years, the more superior digital recording technique was introduced. Soon after mid 1965, the analogue method was completely superseded by the digital method. Despite the fact that analogue recording is now considered to be obsolete, (that is, no more in application), a brief description of the analogue system is presented here-below. This will be useful as the digital system involves some of the components of the analogue system.

#### (i) The Analogue Recording System

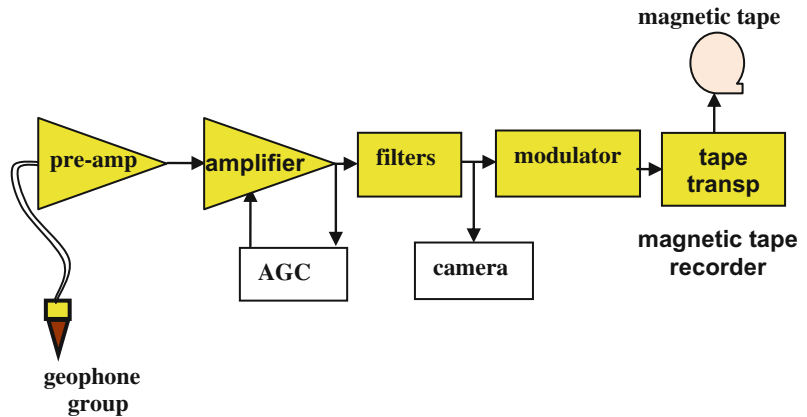
The analogue recording system carries out the recording in two stages: the amplification process followed by the recording process. In the first stage, the seismic signal, received from the geophone group, is amplified so that it will be at a level that suits the following recording stage. The seismic signal may be too small for the recorder to detect, or too large for the recording unit to handle without being saturated. In order to cope with this wide range of amplitude variation (estimated to be 80–100 db) amplification factor is made to be variable. This is done by using a special electronic unit called the automatic gain control (AGC), which makes the amplifier gain to vary with the amplitude level of the incoming

signal. With this unit the too-small amplitude is increased and the too-large amplitude is reduced. This operation results in compressing the signal amplitude-range to that value which is matching the dynamic range of the recording unit. The technique of amplitude matching with the recorder, for undistorted output, is an essential feature of all seismic recording systems. A modification of the AGC is the programmed gain control (PGC) with which the gain is not tied up to the input amplitude-variation. A PGC-coupled amplifier has its gain that varies with record time by a preset (programmed) time-dependant function. This is usually made available as an option, applied when it is required.

Next to the amplification part is the magnetic recording system which produces a permanent record of the data stored on magnetic tapes. This is accomplished either directly or after being frequency-modulated (FM). A carrier frequency (typically, 4 kHz) is modulated by the signal received from the amplification system. In this way it can produce a recorded signal of S/N ratio up to 60 db, and frequency response which is practically flat over 3–200 Hz (Evenden et al. 1971).

Through a playback of the recorded magnetic tape, or directly from the amplifier output, a visual display may be obtained. The display unit (camera unit) is usually included in the recording system. This unit uses the principle of galvanometer deflection caused by voltage variation. By certain optical arrangement, galvanometer

**Fig. 6.23** Schematic diagram showing the signal flow in an analogue recording system



deflections are recorded on photographic paper. The output is usually a wiggly trace record with timing lines superimposed on it. A simplified block diagram of the complete analogue recording system is shown in Fig. 6.23.

A complete analogue seismic recorder is normally built, in such a way that each geophone-group has its own complete recording channel that consists of a complete amplifier-to-modulator chain of units. This electronic chain which starts from the geophone connection and ending at the recording magnetic-head is called a channel. Thus, a 24-channel station is equipped with 24 channels for seismic data and few more channels for recording the (time-break), the (timing signals), and (up-hole time). These additional channels are usually referred to as the (auxiliary channels).

#### (ii) The Digital Recording System

The main feature of the digital recording instrument is that it converts the incoming analogue seismic signal to digital form. In this process the signal is converted into a series of discrete values at uniform time-intervals. This technique proved to give higher fidelity recorded signal than analogue method. In digital form, the seismic signal can be subjected to various mathematical analyses using more sophisticated digital software.

The digital recording system can be divided into two main parts: the analogue-, and the digital parts, separated by the multiplexing unit (Fig. 6.24).

#### The Analogue Part

The seismic signal outputted by the geophone group, which is in the form of an analogue electrical voltage, is transmitted through cable or by radio waves, to the recording system. The incoming signal is first amplified by the (Pre-amplifier) by applying a certain gain-factor which is fixed at a constant value for all of the active channels. After this step, the signal passes to a group of analogue filters. These filters, which are optional to apply, include (low-cut filter) for reducing low-frequency noise and (notch filter) for removing mono-frequency interfering signals, such as the 50 or 60 Hz signals picked up from high-tension power lines. Another filter which is always applied is the (anti-alias filter). This a high-cut filter applied to prevent frequency aliasing which occurs when frequency components are of higher frequency than Nyquist frequency. Like all analogue filters, the anti-alias filter has non-zero phase characteristics. This implies that each frequency component of the seismic signal will have its own time-delay. Consequently, certain wave-form distortions occur whenever an analogue filter is applied.

#### The Multiplexing Unit

The multiplexer is an electronic device that makes contacts between all of the active channels in turn, with the following digital part of the recording system. Effectively, the multiplexer reduces the many analogue-data channels to a single channel that carry the data in a sampled form (Fig. 6.25).

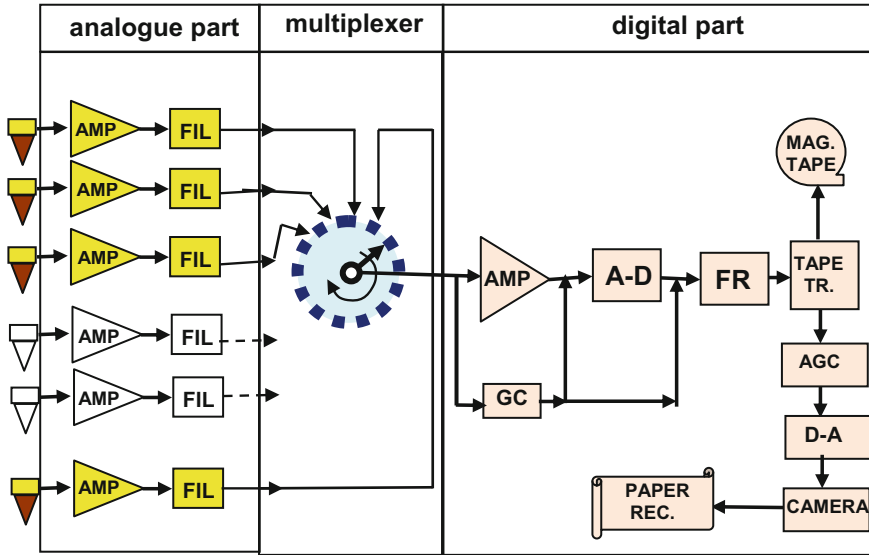


Fig. 6.24 Schematic diagram showing the signal flow in a digital recording system

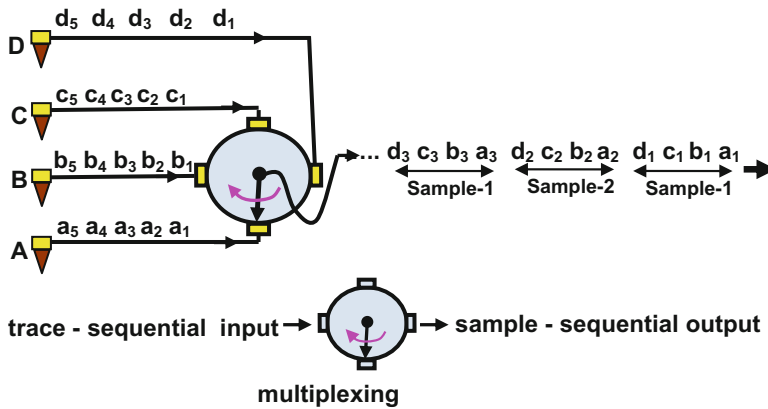


Fig. 6.25 Principle of the multiplexer operation, trace-sequential input with sample-sequential output, using 4 channels (A, B, C, D)

To conceive the multiplexing operation, let us consider a mechanical device in the form of an arm rotating with constant rotation speed where the arm head will trace a circular ring. Referring to Fig. 6.25, consider four channels, arranged equally spaced on that ring. In the first rotation cycle, the arm shall make contacts with the channels (A, B, C, and D) in that order. In this cycle, the multiplexer will output amplitudes, ( $a_1, b_1, c_1,$  and

$d_1$ ) in this sequence. In the second rotation cycle the outputted amplitude-values (samples) will be ( $a_2, b_2, c_2,$  and  $d_2$ ). With continued rotation, the output through a single channel will continue feeding the A-D conversion unit, until the end of the recording time. In this way, the seismic data has been converted from trace-sequential amplitude-values to sample-sequential mode, as it is shown in this figure (Fig. 6.25).

### The Digital Part

The first unit of the digital part of the system is the gain-controlled amplifier which keeps the discrete sample-values, received from the multiplexer, at an appropriate level, matching the dynamic range of the A-D unit. In analogue recording system, gain control is applied continuously to the input signals which may undergo gain changes as with application of automatic gain control (AGC) or programmed gain control (PGC). The main disadvantage in that case, is that the modifications done to the seismic traces, are permanent and the original signal level cannot be recovered.

This problem is solved by a special digital amplification system called, (the binary gain-ranging amplifier) or (the digital gain amplifier). This system applies the appropriate gain and at the same time stores that applied gain-values alongside the sample-time. In other words, the applied gain is recorded as a function of time which can be recovered at any time after recording is completed. With this provision, the applied gain and the original seismic traces can be recovered from the recorded data whenever needed. The gain control unit (GC) is associated with the digital amplification unit for the purpose of keeping the sample value within the dynamic range of the following A-D conversion unit.

The early recording systems, were provided with this type of amplifiers (called gain-ranging amplifiers) in which amplification values are varied in 6-db steps rather than continuously as in the case of the AGC units used in analogue recording system. In the early 1970, development occurred in digital amplification, when a more advanced technique called (Instantaneous Floating Point amplification) was introduced. These are fast (near instantaneous gain changes) and of higher dynamic range. The dynamic range is defined to be the ratio of the strongest to the weakest signals which can be recorded. The dynamic range of the analogue recording system is rated at about 40 db whereas the digital system (using binary words of 14 bits) has a dynamic range of 84 db.

Next to the amplification system, comes the analogue-to-digital unit (A-D converter), which performs two functions: measuring the sample-value and expressing the measured values into binary words. Thus, each sample is expressed in binary word, normally of 14 data bits (bit is 1 or 0) and a flag-bit denoting the algebraic sign (1 for negative and 0 for positive). The measuring procedure is done electronically in a part of the A-D unit called (sample-and-hold circuit) by successive comparison of the sample value (voltage quantity) with pre-defined standard voltage-quantity.

The output of the (A-D) unit is a sequence of sample-values expressed in binary words which flows into the next unit; the formatting unit (or formatter). Formatting process involves re-distribution of the digital bits (the ones and zeros) of the binary words into a pre-defined arrangement with which the bit-position map will be stored on the digital magnetic tape. In addition to the seismic binary words re-formatting, other related information is also made ready to pass with the seismic data to the tape transport unit. Seismic traces, auxiliary traces, tape- and trace-headers are the data which this unit is organizing to be ready for passing to the following unit. According to the bit distribution made by the formatting unit, the sample values (expressed in binary words) are recorded on the magnetic tape.

In addition to bit-location arrangement, the formatting unit generates error-checking bits, called (Parity Bit). For parity checking across the recorded magnetic tape, the formatting unit places a digit, of one or zero, in a defined track in the tape according to whether the total number of ones (to be written across the tape at the sample location) is even or odd respectively. In the play-back of the tape, if a bit is missing from the recorded tape, the parity bit will indicate this as a recording error. In case of a parity error, it is possible to exclude the erroneous binary word by a special command in a later stage.

The final stage in the flow of the signal is the tape drive (or the tape transport unit) which records the formatted data on magnetic tapes. About

twenty years ago, the tapes in common use were 21 track-one inch tapes or 9 track-half inch tapes. In that recording system the first track is usually assigned for the parity check. At present narrower tapes (e.g. 4 mm tapes) and higher recording density tapes (in forms of small cartridges) were introduced for the seismic data recording.

### (iii) Concept of the Dynamic Range

Any measuring or sensing instrument (geophone, amplifier, recording system) has a bounded capability of faithful detection. The system noise-level sets the detection lower limit, while the system technical characteristics set the detection upper limit. For a given system, dynamic range is defined to be the ratio (normally expressed in db's) of maximum measured amplitude to the minimum recoverable signal, where the minimum signal is taken to be the noise amplitude-level.

The dynamic range (**DR**) is expressed by the ratio:

$$\mathbf{DR} = [\mathbf{A}/\mathbf{a}]_{\text{db}}$$

where, (**A**) is the maximum signal amplitude which a system can measure (with tolerable distortion level) and (**a**) is the system noise-level.

The concept is often applied in evaluating the detection and measuring capabilities of recording systems. The early seismic analogue systems which were recording directly on paper have dynamic range of about 25 db. The dynamic range of analogue systems recording on magnetic tapes is about 45 db. In case of digital recording systems, the dynamic range is dependent on the number of bits used in expressing the sample value. For 14-bit recording, it is equal to 84 db.

### (iv) The Magnetic Tape Recording

The magnetic tape is a plastic strip, coated with magnetic material, is divided into tracks of cells. After being digitized, each sample-value is represented by a binary word which is recorded on the magnetic tape by magnetization status of the cells.

When the cell is magnetized it represents (1) and when it is not, then it is (0). This concept is clarified from the following example (Fig. 6.26).

An analogue signal, shown at the top of Fig. (6.26), is digitized and its sample values are measured and converted into 8-bit binary words. The eight bits of each sample (each binary word) are recorded across the tape by magnetizing the cell when the bit is (one) and demagnetizing the cell when it is (zero). The sign bit (marked as S-bit) is a flag indicating the algebraic sign of the sample value. It is assigned the value of (one) for negative sign and (zero) for positive sign. For example, a sample value of minus nineteen (-19), the binary word in this example (9-track tape) is (100010011), and for a value of (+27), say, will be (000011011), where the first digit is for the sign (the sign bit).

In the case the recorded data is in multiplexed form, the sequence followed will be in sample sequential, and if the data is in demultiplexed form, the recording will be in trace-sequential mode. Normally, the magnetic tape is divided into blocks where the first block (called the header block) carries general information like record number, sampling period, record length, and other recording parameters. The next block is the seismic data which are usually in multiplexed form. Along with each sample value, the applied gain for that sample and sign-bit flag are recorded. One track is reserved for the parity-check for checking the bit-column across the tape. The end block contains information signaling the end of that set of recorded data.

The Society of Exploration Geophysicists (SEG) has developed several seismic data recording formats since the 1960s when the digital recording system was introduced. In 1967, the formats SEG-A, SEG-B, and SEG-X, were published. Later on, other formats were published, as SEG-C in 1972, SEG-Y in 1975 and SEG-D in 1980. The formats of SEG-C and SEG-Y are recording the data in de-multiplexed mode, whereas SEG-D can record in both

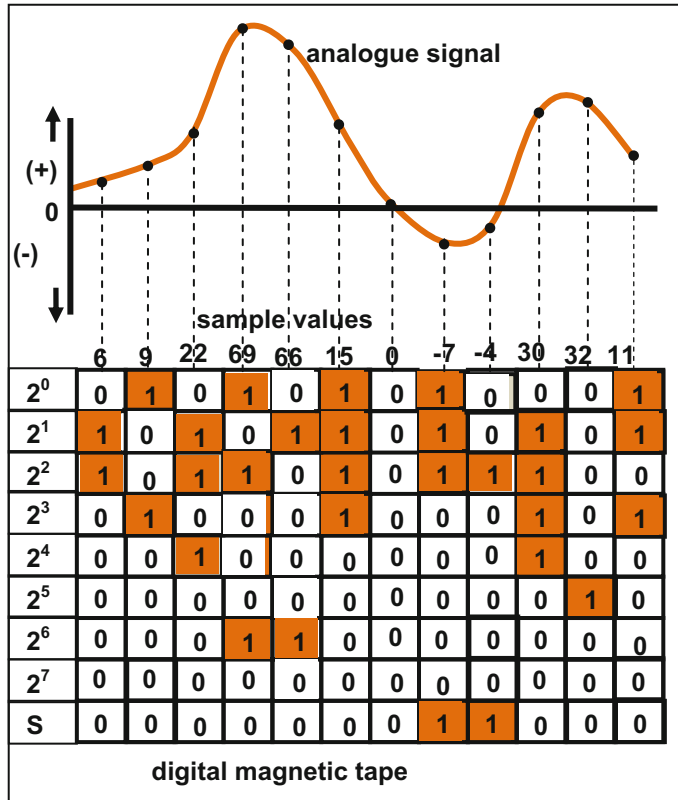


**Fig. 6.26** Simplified sketch showing the principle of 9-track tape recording format. The binary word for each sample value consists of 8 bits plus the sign bit (S)

multiplexed and de-multiplexed modes. At present, field recording is mostly done using de-multiplexed SEG-D format.

Developments in the tape-recording techniques concerned mainly the packing density and storage capacity. The density was developed from 800, 1600, then 6250 byte per inch. The tapes used nowadays are of 8 or 4 mm width, contained in cartridges or cassettes.

### 6.2.4 Data Playback and Display

For quality control (QC) purposes, the end result of the recording station (the shot trace-gather) needs to be displayed. The playback process is the reverse of the recording process. It is done through a complete playback system which consists of a digital AGC, a digital-to-analogue

(D-A) converter, demultiplexer, and the camera unit which displays the shot trace-gather (usually in wiggly-mode traces) on the computer monitor or on paper. A typical shot record is presented in Fig. 6.27.

This figure shows about one second of data of a shot record made up of 48 seismic channels plus two auxiliary channels (at the left side of the record): the time break indicating the zero-time of the shot, and up-hole-time. Traces are displayed in wiggly mode of display.

### 6.3 Seismic Noise Characterization and Attenuation

As we mentioned in a previous discussion, all non-reflection arrivals are considered noise which cause distortions and masking effects to the

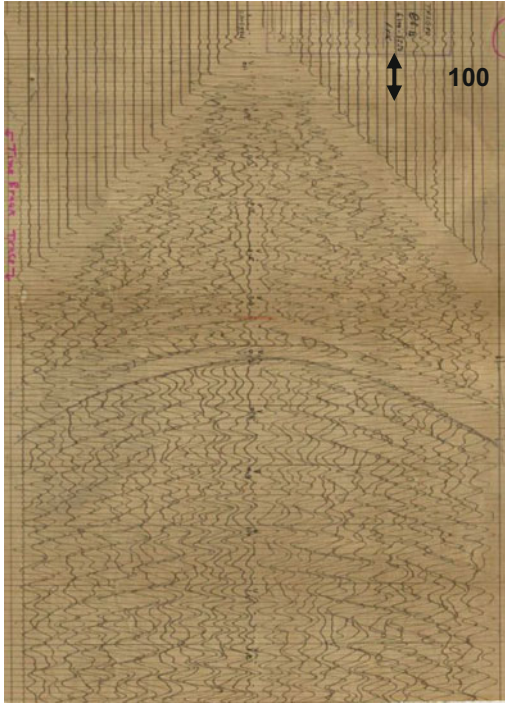


**Fig. 6.27** Seismic record playback of 48-channel shot record displayed in wiggly mode

desired reflection arrival (seismic signal). The coherent noise are non- reflection seismic events that may appear on a seismic record. Examples of these “noises” are surface-waves (ground roll), air-waves, or body waves (direct-, refracted-, and multiples). These noises and interferences are generated from the source seismic-energy. The other type (incoherent noises) is mostly of non-source origin. They are attributed to natural and artificial activities such as microseisms, wind blowing on land or on trees or from traffic or man-made jerking actions. Incoherent seismic noise, which is of random nature, forms the familiar seismic background of seismic shot-records.

### 6.3.1 Random Noise Attenuation

The multi-detector receiver has the ability to remove, or lessen the effects of, both of the coherent and the incoherent noises. With this

type of receivers, two factors are in operation in noise attenuation. These are the number of detectors in the one receiver (for attenuating random noise and enhancing the reflection signal) and lay-out geometry of the detectors to attenuate the coherent noises which are made up mainly of surface waves.

The reflection signal approaches the detection elements, deployed on the surface, simultaneously (in phase) and hence shall interfere constructively, when outputs of the detectors are summed up together. The detected noise, being random, shall interfere destructively and hence gets attenuated. This process can be achieved in the process of electronic stacking that is when the detection elements (geophones) are connected electronically to form one output channel (Fig. 6.28).

The seismic recording system is usually equipped with filtering provisions which can be applied to filter out noises based on frequency characteristics of the dominant noise. The horizontally moving surface waves (and other coherent noises), on the other hand, will be attenuated by summing wave amplitude-values of different algebraic signs. Extent of attenuation is dependent on array geometry as shall be explained in the next paragraph.

### 6.3.2 Coherent Noise Attenuation

Attenuation of coherent noise is normally carried out by special design of the receiver array configuration. The filtering action is governed by the array’s number of elements, and element spacing. This is expressed in terms of a mathematical formula for the receiver array-parameters (number of elements and element spacing) and the apparent wavelength of the targeted coherent noise. Any receiver array has its own response formula, called the array response characteristics which control filtering efficiency of the horizontally moving surface waves (the ground roll and such like waves).

#### (i) The Array Response Concept

An array is a term used for a group of detectors (geophones) connected to one output channel, or

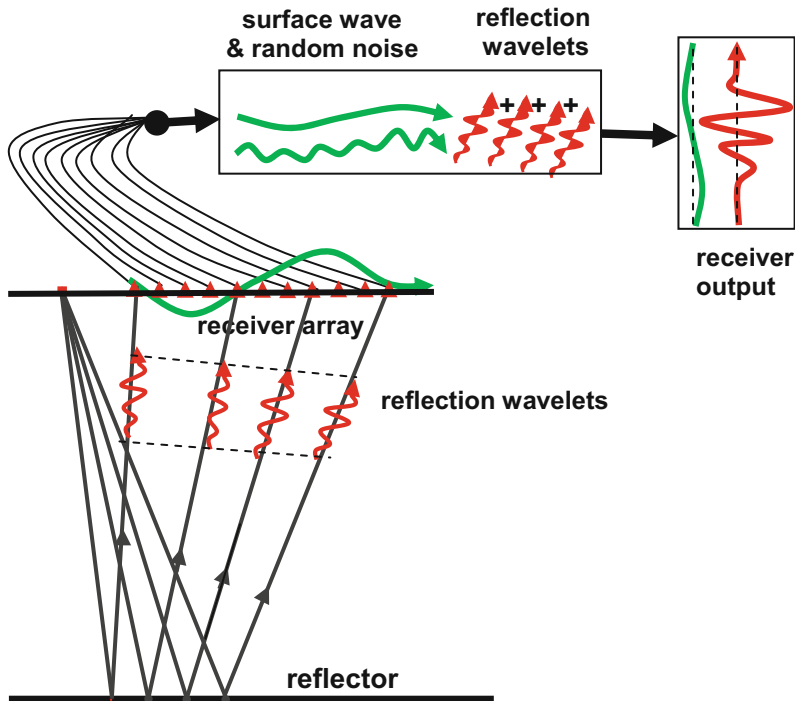


**Fig. 6.28** Role of a multi-detector receiver in attenuating random (and coherent) noises and enhancing reflection signal of a vertically arriving reflected wave

a group of shot holes of a shot-point pattern. Compared with a single-element receiver, a multi-element receiver (receiver made up of many geophones), has the capability of attenuating horizontally moving waves in addition to enhancing the signal-to-random noise ratio by a factor depending on the square root of the number of the array elements. Efficiency of the array in attenuating surface waves is expressed by a characteristic function called the array response, defined to be the ratio of the amplitude of an array-output to that of the same number of the array-elements gathered together at one location (Sheriff and Geldart 1995, p. 247). This is expressed in the form of a mathematical function called (directional response function, or just directivity function).

The theory, on which the concept is based, is the same whether it is applied to the shot hole-pattern or to the receiver geophone array. Instead of using a single source point, a source array (shot-hole pattern, in case of dynamite

source) is used. The array source-elements (shot-holes, for example) are detonated simultaneously generating body waves which reach the detector array after being reflected from subsurface interfaces. At the same time, the source-generated surface waves travel from the source to the receiver. As it is with the receiver array, the nearly vertical incident body waves are in phase and hence they interfere constructively to give enhanced reflected signal. For attenuation of the surface waves, the length of the source array should be equal to the wavelength of the generated surface waves.

The response of any given array (having given number of elements with given element spacing) can be presented in the form of a curve known as (response curve or directivity curve). The abscissa is the ratio of the wavelength of surface waves (coherent noise) to element spacing, and the ordinate is the array output expressed as the ratio of the array-output to that of the same number of elements gathered together at one

location. The array response is normally expressed in db units.

The basic principle is that waves travelling in near vertical direction are enhanced while those travelling horizontally are attenuated. This technique has been borrowed from engineering work done in radio-antenna design (Dobrin and Savit 1988, p. 99). The application of the principles in geophone- and source-arrays was published as early as mid-1950s (Lombardi 1955) and (Parr and Mayne 1955).

### (ii) The Array Response Function

Directivity curves express the array response to the different wavelengths of horizontally travelling surface waves. For a linear array consisting of  $n$  elements with  $\Delta x$  inter-spacing, the response function,  $R(\beta)$ , is given by:

$$R(\beta) = \frac{\sin n\beta}{\sin \beta}$$

where,  $\beta = \pi\Delta x/\lambda$ , and  $\lambda$  is the apparent wavelength of the surface waves travelling in the direction of the linear array.

The  $R(\beta)$  function is periodic, repeating at a period of  $(\beta = \pi)$ . The function is fully defined in the range of  $(\beta = 0$  to  $\pi)$ , that is, in the range  $(\Delta x/\lambda = 0$  to  $1)$ . The curve, within this range, is symmetrical about the point  $(\beta = \pi/2)$ , that is about  $(\Delta x/\lambda = 1/2)$ , and it crosses the  $\beta$ -axis at the points  $\beta = \pi/n, 2\pi/n, 3\pi/n, \dots, (n - 1)\pi/n$ . The curve has a total of  $(n)$  maxima, where the principal one is located at  $(\beta = 0)$ , and the peaks of the side lobes occur at the mid points between the zeros of the function.

Mathematical derivation is based on summing of spatial harmonic waves moving along a linear array made up of  $n$  elements, arranged at constant interspacing  $\Delta x$  (Sheriff and Geldart 1995, p. 247).

### (iii) The Array Response Curve

The response curve is normally plotted as relative response against  $(\Delta x/\lambda)$ , or against  $(\lambda)$ . The response value is plotted directly or in db units. As it is mentioned above, the response, by definition, is expressed by the ratio between the array output and that of the same elements gathered at one location, that is when  $(\Delta x = 0)$ . It should be

emphasized that  $(\lambda)$  is representing the apparent wavelength measured in the array direction. Typical response curves (directivity curves) of geophone linear-arrays are shown in Fig. 6.29.

The characteristics of the array response are summarized as follows:

- The response curve repeats itself at  $(\Delta x/\lambda = 1)$ , that is at  $(\Delta x = \lambda)$ , so it is completely defined in the interval  $(\Delta x/\lambda = 0-1)$ .
- The curve is symmetrical about the point  $(\Delta x = \lambda/2)$
- It has  $(n)$  lobes (maxima), where the principal main lobe centered at  $(\lambda = \infty)$  and another equal lobe (the first alias lobe) centered at  $(\lambda = \Delta x)$
- It has  $(n - 1)$  nodes (zero-response) at  $\lambda = n\Delta x, n\Delta x/2, n\Delta x/3, \dots, n\Delta x/(n - 1)$ . At these points the attenuation is infinite, that is there is no output.
- It has  $(n - 2)$  side lobes found in the range  $\lambda = n\Delta x$  to  $n\Delta x/(n - 1)$ . This zone, called the (reject zone) or the (effective array length), is the zone where the most effective noise-attenuation occurs. Sometimes the reject zone is taken to be the zone found between the 3 or 6 db points. A response curve for an 8 elements linear array is shown in Fig. 6.30.

This figure shows that, the attenuation-zone (reject zone) lies between  $(\lambda = 8\Delta x)$  and  $(\lambda = 8\Delta x/7)$ . This zone can be made wider (extended) and its response level lowered further, by increasing the number of elements  $(n)$ . However this will cause narrowing of the pass band (marked by the first lobe where  $\lambda \geq n\Delta x$ ) and increasing its cutoff slope.

The role of the directivity curves is in evaluation of array performances in attenuation of horizontally moving surface waves. Given the wavelength of the dominant coherent noise, a seismic detector array can be designed such that its response is most effective in attenuation of the noise having that wavelength. From the drawn curve, one can directly read the relative noise-cancellation effect corresponding to the wavelength of the dominant surface waves  $(\lambda)$ , or to the parameter  $(\Delta x/\lambda)$ . This means that we need

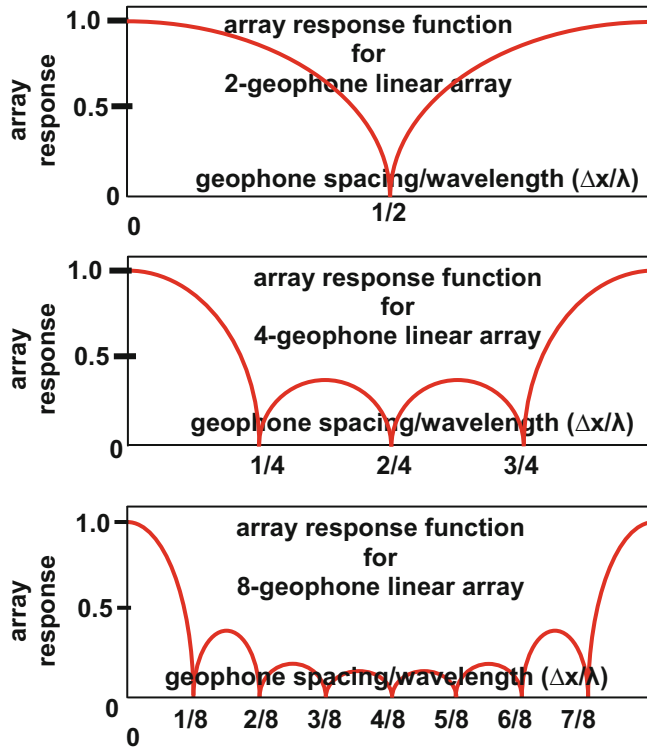


Fig. 6.29 Schematic representation of response curves for different linear arrays

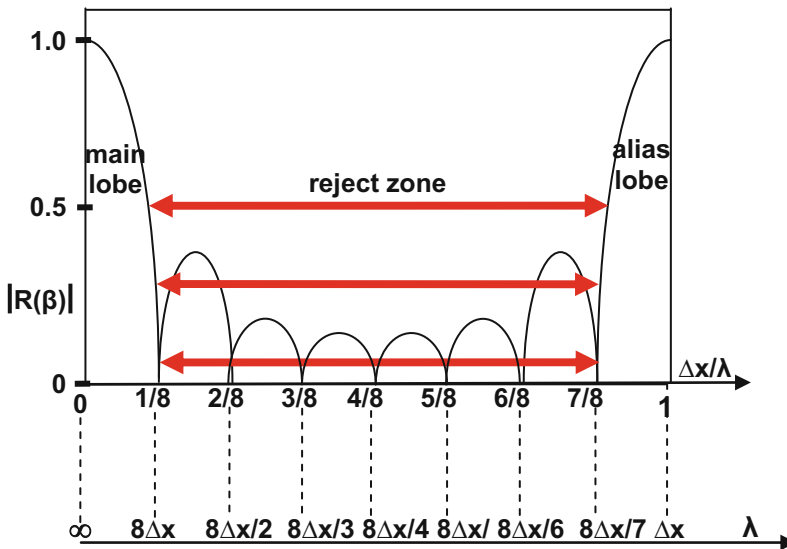


Fig. 6.30 Schematic representation of response curve for 8-element linear array, showing the main and alias lobes in addition to the array's reject zone

to know the wavelength of the surface-waves in order to design the geophone array which is appropriate for the attenuation of the surface waves. The wavelength, which is representative of this type of coherent noise, is normally determined by special seismic experiment called the (noise test).

## 6.4 Field Measures for Signal Enhancement

Before commencing a seismic reflection survey, certain field procedures are normally carried out to determine the nature of the dominant noise in the area in order to be able to design the source and receiver parameters which can output strongest reflection signal and least possible noise level. For noise analysis, a special seismic experiment is done in the field, called the noise test (called also, walk-away or micro-spread test). Analysis of the resulting seismic record will lead to determination of coherent noise parameters such as apparent wavelength, velocity, periods, and frequency, which are necessary in the design process for both of the source and receiver arrays.

### 6.4.1 The Noise Test

There are two types of field procedures that can be followed to conduct the noise test in the field. These are the fixed-spread method and the fixed-shot method (Fig. 6.31).

The fixed spread method is done by using end-on spread which is made up of geophones spaced at short distances (typically, 5-m spacing). After the first shot is fired and the shot record is produced, the shot is moved along the spread line by a distance equal to the spread length, and the second shot-record is obtained. This shift-and-record action is repeated a number of times such that the resulting combined record will have its maximum offset to be about equal to the maximum offset planned for that survey. An alternative method (called, the fixed-shot method) is conducted by fixing the shot location and move the receiver spread (along the spread line) away, hence, the term (walk-away test).

In both methods, each receiver point is occupied by a single geophone or by a group of geophones gathered in one location to give clearest noise possible (Fig. 6.32).

The more commonly applied method is the fixed-spread method because it is easier to move the shot location than moving the spread.

Noise-test operation is normally including measures for studying the broad-side noise as well as the inline coherent noise. For this purpose, another spread is laid perpendicular to the normal inline spread (Fig. 6.33).

The end result of the field operations in conducting the noise test is a noise-test record in which the 5-m-spaced traces are drawn. It is important to note that no filtering should be applied during the recording process. For interpretation purposes, the noise-record display should be produced without any type of time-variant scaling. Any amplitude distorting process should be avoided in order to be

(a) fixed spread with moving shot



(b) fixed shot with moving spread

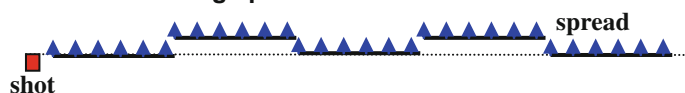
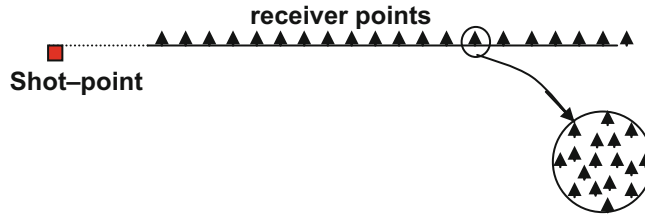
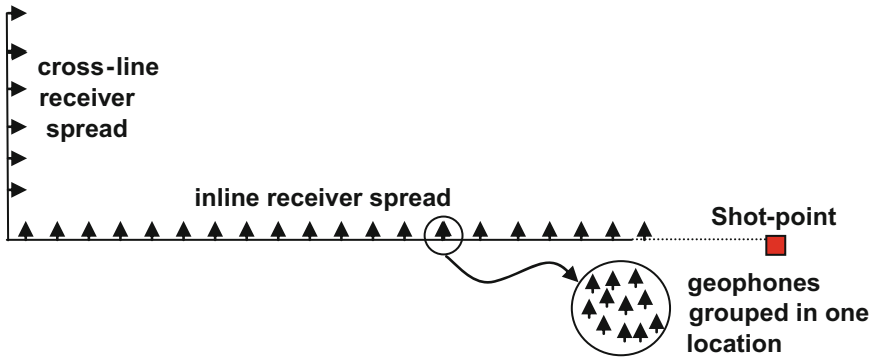


Fig. 6.31 The two alternative methods used in noise-test surveying



**Fig. 6.32** Survey spread used in noise test surveying



**Fig. 6.33** Noise test L-shaped spread to detect both of the inline and cross-line coherent noises. A receiver point may be occupied by a single geophone or by a group of geophones

able to measure relative amplitudes, and for easier event identification. However, time-invariant scaling can be applied. Principal seismic noise events (and other wave arrivals) are schematically shown in Fig. 6.34.

Interpretation of the noise-test data is normally done visually. It starts with identification of the types of noises and other types of seismic events. The main events a noise-test record contains are: direct waves, refracted waves, reflected waves, back-scattered waves, and air waves.

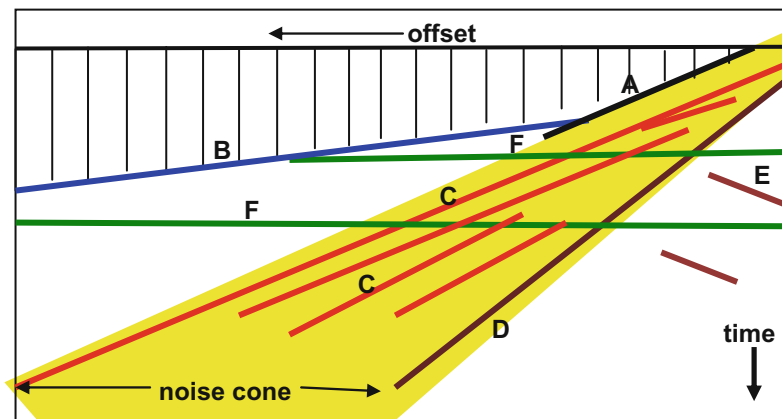


**Fig. 6.34** Schematic representations of the main events, normally found in a noise-test record. **a** Direct wave, **b** refracted wave, **c** ground roll, **d** air wave, **e** back-scattered waves, **f** reflected waves. The group of events between events (a) and (d) forms the noise cone

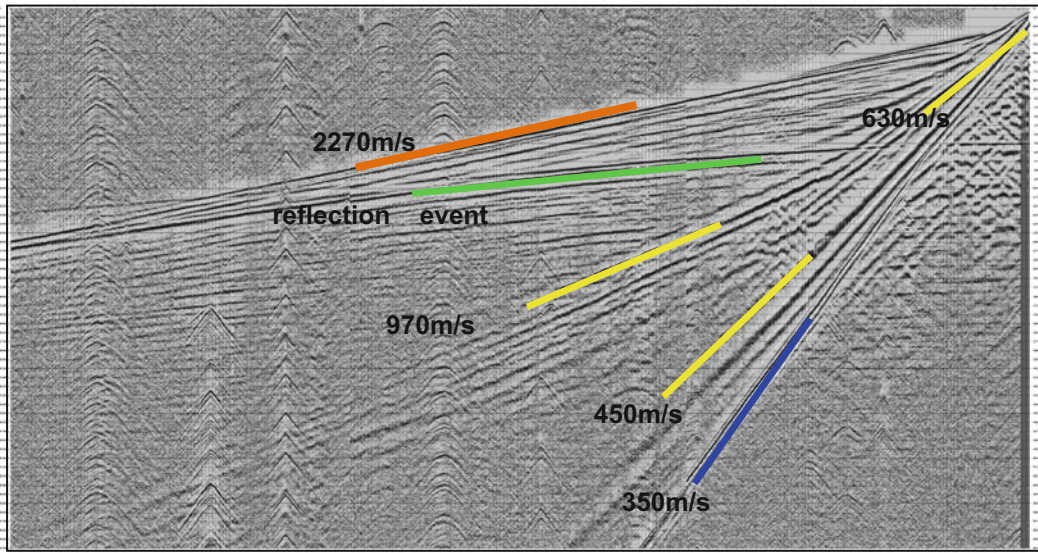


**Fig. 6.35** Actual noise-test record, showing reflection, refraction, sound, and surface waves

ground roll, air-wave (sound wave travelling through air), back-scattered waves, and wave arrivals of energy reflected from deep interfaces. The strongest events, appearing in a noise-test record, consist of surface waves, covering a range of apparent velocities and apparent wavelengths. These events make up the coherent noise forming a group of large-amplitude events known as the (noise cone). An actual record of noise test is shown in Fig. 6.35.

In interpreting the actual noise record, given in Fig. 6.35, it is found that it contains body waves (direct, refraction, and reflection events), surface waves (ground roll), and air wave (sound wave). The wave parameters: velocity ( $v$ ) and

period ( $\tau$ ) are manually measured from the paper record. From these parameters, frequency ( $f$ ), and wavelengths ( $\lambda$ ) are then calculated using the relations ( $f = 1/\tau$ ,  $\lambda = v/f$ ). Interpretation results are found to be as quoted in the following Table 6.2.

These data show that the most distortive event is the surface wave-3 (of velocity 970 m/s and wavelength 108 m). It has the largest amplitude and largest extent, covering all the record time and all of the offset range in this exemplar. On average the wavelength (100 m) can be considered as representative of the surface waves in the survey area, and can be adopted in the design of the geophone and shot-hole arrays.

**Table 6.2** Values of velocities, frequencies, and wavelengths obtained from interpretation of the noise record shown in Fig. 6.35

Wave type	V (m/s)	f (Hz)	$\lambda$ (m)
Sound wave	350	12	29
Surface wave-1	450	4	113
Surface wave-2	630	8	79
Surface wave-3	970	9	108
Refraction wave	2270	25	91

### 6.4.2 The Experimental Shooting

The source parameters depend on the type of the source used to generate the seismic energy. For the dynamite source, there are three main parameters. These are: charge depth, charge weight, and shot-hole pattern. The optimum charge depth and charge weight are determined through direct experimental shooting. For the charge depth, several trial shots are conducted such that the charge weight is fixed while varying the depth. The same approach is followed in optimizing the charge weight that is by fixing the depth and varying the weight of the charge Fig. 6.36.

As for the shot-hole pattern, the suitable number of shot-holes is determined by applying the same principles applied in the case of the receiver geophone array. However, very often and for economical reasons, this is determined by the experimental-shooting method alongside with the determination of optimum charge depth and charge weight. Conducting multi-shot sources is another approach for increasing the signal-to-noise ratio. This is normally done in case of surface-sources as in the case of vibroseis and weight dropping techniques. A typical plan for an experimental shooting for optimizing the source parameters is as shown in Table 6.3.

The shot records for these trial shots should be outputted with no filtering and with no time-variant scaling being applied to them. A comparative study of the obtained records is

done visually to determine the best parameters. Choosing the appropriate parameter is based on reflection-signal strength, frequency content, reflection-signal resolution, noise level, and extent of penetration depth.

### 6.4.3 Determination of the LVL Properties

The earth surface is characterized by its non-uniform topography (variable elevation), and the surface layer is, in general, made up of loose low-velocity material. This layer, (commonly referred to as the low-velocity layer, LVL) is made-up of one or more layers of velocity and thickness that can vary with location within the survey area. The LVL thickness and velocity are typically of ranges (10–50) m and (500–1500) m/sec respectively.

Because of the large velocity contrast normally found between the LVL material and that of the medium below it, the base of the LVL acts as a strong reflector and refractor. Multiple reflections (reverberation and ghosts) can also develop in such environments. Effect of the LVL is not restricted to the travel-time changes, but also on the reflection waveform. In particular, high-frequency components of the travelling seismic waves experience severe attenuation in the LVL due to the relatively strong absorption phenomenon.

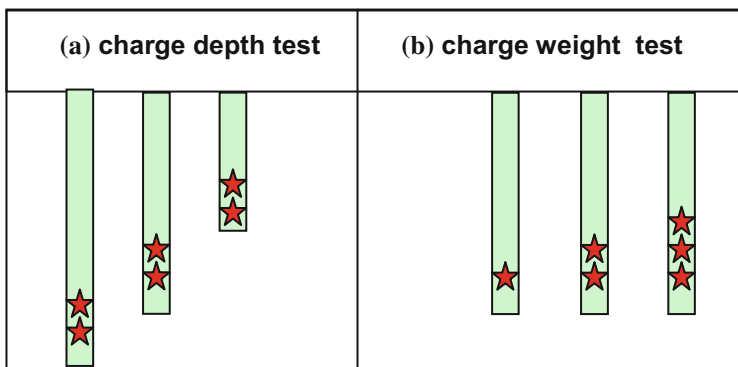


**Fig. 6.36** Experimental shooting for determination of: **a** charge depth and **b** charge weight

**Table 6.3** A typical plan for an experimental shooting for optimizing the source parameters

No.	Shot-hole depth (m)	Number of holes	Charge weight (kg)/hole	Shot-hole Spacing (m)
1	6	2	3	25.0
2	6	3	3	12.5
3	6	4	3	8.3
4	9	2	4	25.0
5	9	3	3	12.5
6	9	4	4	8.3
7	12	2	3	25.0
8	12	3	3	12.5
9	12	4	4	8.3

An integral part of the field activity in a seismic reflection survey is determination of the properties of the surface layer, the LVL. In particular, effort is made to determine the thickness and velocity which are essential information needed in correction-computations of the reflection and refraction travel times. The commonly applied methods are the up-hole surveying and specially designed refraction surveying.

**(i) LVL Characterization by Up-hole Surveying**

The up-hole survey involves drilling a borehole of depth exceeding the expected LVL thickness, normally within the range (50–100 m). Small charges (dynamite capsules) are fired at a series of

points arranged at certain depths inside the borehole Fig. 6.37.

These dynamite capsules are fired in sequence starting at the base of the hole and continuing upward till the last shot which is nearest to surface. For recording the arrivals at the surface, a group of geophones are usually planted at equal distances from the surface location of the hole.

For analysis and interpretation of the recorded data, travel times (reduced to vertical travel-path) are plotted against depth. From the slope of the resulting plot, and the depths of the points at which slopes show abrupt changes, the velocity and thickness of the LVL layer (or layers) are calculated.

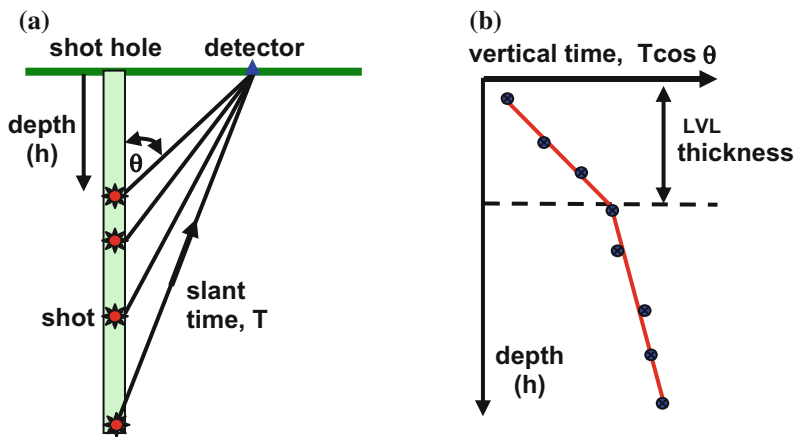


**Fig. 6.37** Up-hole survey: **a** travel-path and **b** plot of vertical travel time ( $T\cos\theta$ ) against depth ( $h$ ), where ( $T$ ) is the slant time and ( $\theta$ ) is the angle between travel-path and the borehole

### (ii) LVL Characterization by Refraction Surveying

Because the surface weathered-layer is usually of velocity lower than that of the underlying bedrock, the refraction method lends itself as a tool for determination of its thickness and velocity. For the same reason, the surface layer is normally referred to as the low-velocity layer (LVL). The refraction survey is conducted using a special short spread, typically (150–250 m) provided with 24 channels.

There are two alternative field methods to conduct the survey: fixed-spread method, and fixed-shotpoint method. In the first method, two shot-points are recorded, one on either end of the fixed-in-place spread. This is, in effect, two end-on shots are implemented for the fixed spread. In the second method two shots, fixed at the same point are fired. For the first shot, the spread is located on one side of the shot-point, and for the second shot, the spread is moved to the other side of the shot-point location. This is a spread set-up similar to centre-spread shooting. The two methods are in Fig. 6.38.

From travel-time curves, both of the velocity and thickness are computed from the slopes and time intercept of the produced curves. It is worth noting here that the travel-times of both of the direct- and refracted-arrivals are linear functions of distance. The velocity ( $v_0$ ) of the direct wave and that of the refracted wave ( $v_1$ ) are given by

the reciprocal of the corresponding slopes. Thickness ( $z$ ) can be measured from its relation to the intercept time ( $t_i$ ), where,  $t_i = 2z[(v_2)^2 - (v_1)^2]^{1/2}/v_1v_2$ . The LVL parameters (thickness and velocity) are computed from the data obtained from the two implemented shots.

## 6.5 The Seismic Field Crew

Survey work of an area is carried out by a team of workers made up of professionally prepared personnel who are technically equipped to cope with all of the activities needed to complete the seismic survey. This is the seismic crew, or seismic party as it is sometimes called.

A seismic crew consists of a number of sections each of which is specialized in one of the field survey activities. The main sections are:

### (i) Data Recording Section

This section is under the management of the Observer, who is responsible of the technical management of the recording system (recording station) and magnetic tape recording. Under this section is the group of workers for geophone planting and control of the activities taking place over the seismic line during shooting. The Observer usually submits complete daily documented reports.

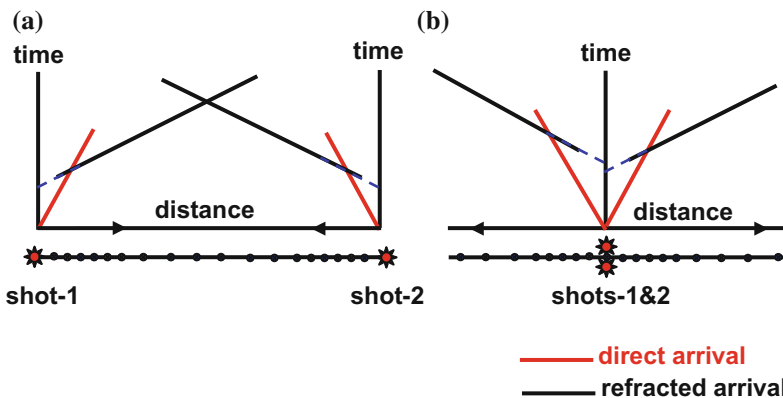


**Fig. 6.38** Two methods of refraction survey specially designed for determination of the LVL properties (thickness and velocity), **a** fixed spread, and **b** fixed shot-point method

(ii) Topographic Surveying Section

Fixing on the ground, of the survey points (shots and receivers) and measuring coordinates (x, y, & z) of each of these points. These data, in addition to data concerning geographical nature and surface environments, are documented and reported.

(iii) Drilling Section

This is concerned with drilling the shot-holes, and other holes needed by the survey, such as the deep holes needed for up-hole surveys.

(iv) Shooting Section

Workers in this section do all the necessary steps needed to prepare a shot-hole. This involves preparation of the right amount of charge and placing it at the required depth and filling the hole with water and mud mixture to secure coupling. The section is also

responsible for the dynamite storage and transport taking all the safety and security precautions.

(v) Mechanical Engineering Section

For mechanical work needed by the crew as maintenance of drilling machines, trucks, electricity generators and the Vibroseis systems.

(vi) Administration and Finance Section

This section is responsible for personnel recruitment, living requirements, transport, communications, material storage and all finance affairs.

These are the main sections of a typical crew using dynamite for the seismic energy source. All the sections are headed by the party chief who is managing the crew work through direct contacts with the crew and through the daily meetings held every night with the sections' heads.

In the years following the dramatic introduction of the analogue and digital data recording and processing, the main development-trends were in increasing recording channels and in more advanced magnetic tape technology. These developments have led, in the early 1970s, to more effective exploration techniques including the introduction of seismic three dimensional (3D) surveying. The first proper 3D exploration work was conducted using fixed cross spreads by Walton in the early 1970s (Walton 1972), and soon after the 3D seismic method entered application on commercial-production basis. At present the 3D seismic surveying became very common especially for detail exploration and development of oil fields.

---

## 7.1 Introduction

### 7.1.1 Nature Is Three Dimensional

The sub-surface geology targeted by seismic exploration is, in essence, three-dimensional in nature. The seismic field created in seismic reflection surveys is likewise, three-dimensional (3D). In an ideal homogeneous medium, the wave-front of the advancing seismic wave is of

three-dimensional shape, which is spherical, in a homogeneous medium. In reality, the geological medium is made-up of different rock layers of different physical properties and different geometrical shapes. With this realistic type of environments, the advancing wave-front, is still having the three dimensional form but no more perfectly spherical.

The created seismic rays travel in every direction in the space surrounding the source zone. In other words, the geological field, as well as the seismic field in which it is created, is 3D in nature (Fig. 7.1).

In the conventional 2D shooting, the seismic field is created as three-dimensional wave-field, but detected by two-dimensional array of detection-points. Thus, the 2D surveying is concerned with a limited portion of the reflected 3D wave-energy. The rest of the reflected energy, with all the useful information it is carrying, is left to pass undetected.

In the 3D technique the source energy is utilized more efficiently, since most of the reflected 3D wave front will be detected. It is, in fact, considered to be the more logical approach for seismic exploration than the conventional 2D, because the 3D surveying conforms to the 3D nature of the subsurface geology.

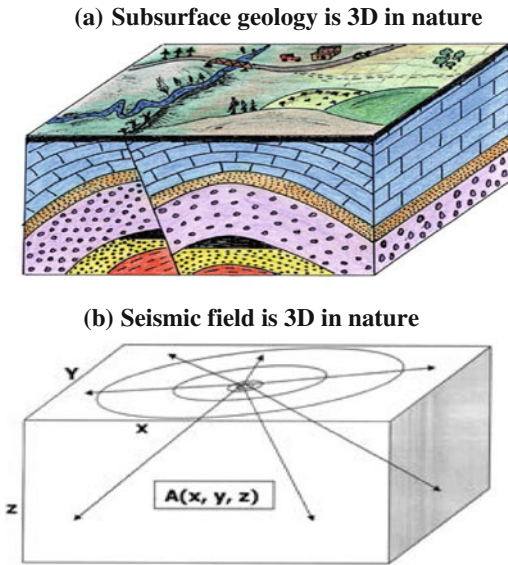


**Fig. 7.1** By nature, both of the subsurface geology (a) and the seismic field (b) created to explore it, are three dimensional

### 7.1.2 1D-2D-3D Terminology

A seismic trace can be viewed as a time function of the seismic amplitude which is normally representing variation of vibration-velocity as function of recording time. If we disregard its position information (that is neglecting the  $x$ - $y$  coordinates of its CMP location), the seismic trace is represented as a one-dimensional (1D) function of amplitude with time,  $f(t)$ , or with depth,  $f(z)$ . The synthetic seismogram is another example of the 1D seismic-function. It represents reflection-amplitude variation with the depth of the drill-hole. The sonic log expresses variation

of the transit-time with the depth of the well which is also a 1D function.

In the conventional 2D seismic surveys, where the shot-point and receiver-points are co-linear, the resulting stack section consists of a series of seismic traces each of which belongs to a CMP location. The stack traces of a stack section are uniformly spaced along the distance coordinate ( $x$ ). Thus the seismic amplitude in the produced section is function of both trace-position ( $x$ ) on the seismic line and the two-way reflection time ( $t$ ). This means that the amplitude in the produced seismic section, is represented by the two-dimensional (2D) function  $f(x, t)$ , or  $f(x, z)$  when time is scaled by the propagation velocity.

With the 3D shooting technique, the produced CMP-locations form a two-dimensional array over the surveyed reflectors. In this case, we have a seismic trace for each of these CMPs, forming a data volume in which the seismic amplitude is represented as a function of its position in space, defined by the three-dimensions ( $x, y$ , and  $t$ ) or by the dimensions ( $x, y, z$ ) when the third dimension is expressed in terms of depth,  $z$ . Thus, the amplitude is expressed as three-dimensional (3D) function,  $f(x, y, t)$  or  $f(x, y, z)$ .

In reference to (Fig. 7.2), the three terminology definitions are considering the seismic amplitude (a) as function of depth (z), function of ( $x, z$ ), or function of ( $x, y, z$ ).

The end product of the 3D seismic surveying is a seismic data volume which represents a three-dimensional function  $a(x, y, z)$  expressing the variation of seismic amplitude (a) with the

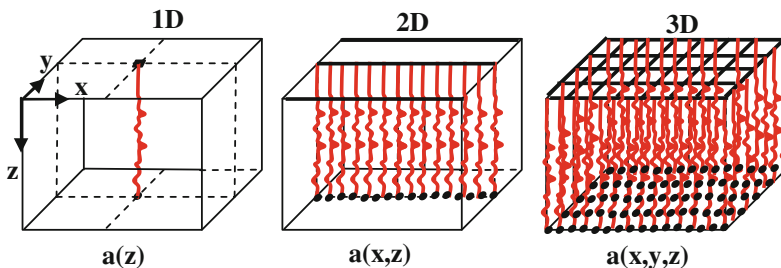


**Fig. 7.2** Seismic data represented as 1D-function (seismic trace), as 2D-function (seismic section), or as 3D-function (seismic data volume). The corresponding functions are  $a(z)$ ,  $a(x, z)$ ,  $a(x, y, z)$

three coordinates:  $x$ ,  $y$ , and  $z$ . In this way, one may consider the 2D section as a special case of the more general 3D data-volume, in which one of the dimensions ( $x$  or  $y$ ) is equal to zero. In the geophysical literature it is customary to use the terminology (data-box, or data-volume) for the whole stack-data set outputted by the 3D survey. For display purposes, 2D sections from the data volume, in both vertical and horizontal directions, can be obtained.

### 7.1.3 Limitations of 2D Seismic Surveying

Despite its outstanding success in subsurface exploration which has been achieved throughout the past years, the conventional 2D seismic method is facing certain difficulties in retaining its well-established success standard. This is due to the fact that most of the large structural traps with clear geophysical anomalies have already been discovered and what remained undiscovered are those which are characterized by being small in size, complex in structure, weak in seismic response, and may be situated in inaccessible areas. Limitations of the 2D seismic surveying may be summarized as follows:

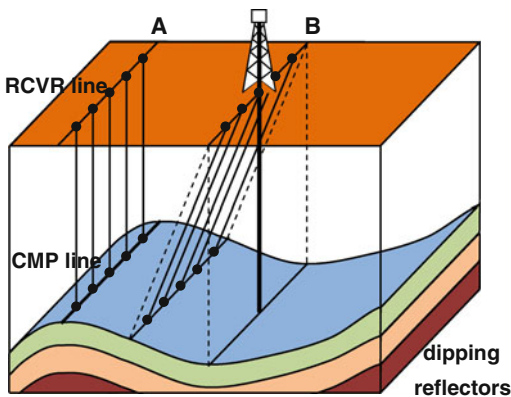


**Fig. 7.3** Reflection ray-paths for zero-offset receivers in 2D surveying. **a** Line shot along strike direction, located directly above an anticline of non-pinging axis. **b** Line shot parallel to line (a), but at horizontally-shifted position

#### (i) Erroneous Image Positioning

Geometry of the 2D seismic line, assumes that the source-receiver line, the incident seismic ray, and the reflected ray are all lying in one vertical plane (the ray-path plane). Further, the reflection point is located vertically below the source-receiver mid-point. This is, in fact true only when the reflector is a horizontal plane surface or the seismic line is shot along the non-pinging axis of an anticline for example (Fig. 7.3a). In the case of a dipping reflector, however, the reflection events may be received from points located outside the vertical plane which is, in 2D surveying, assumed to be the plane of the reflection ray-path (Fig. 7.3b).

A dry well may be obtained due to erroneous positioning of the seismic image that may appear on the 2D seismic section.

An example showing erroneous image-positioning is the case of a seismic line passing near-by a dome. The 2D line does not cross the structural dome and yet the produced seismic section shows an anticlinal image (Fig. 7.4).

Appearance of the image of a subsurface dome, which is not crossed by the vertical plane containing the seismic line, is due to reflections from the sides of the offside dome.

#### (ii) Distortion due to Dipping Reflectors

Strictly speaking, the 2D surveys give true structural pictures only when the surveyed areas are made up by horizontally layered geology. In general, there is always a certain amount of image distortion produced by 2D method whenever dipping reflectors exist. In processing of 2D data, the reflection events are assumed to have been received from reflection points which are located vertically below the surface seismic-line. When the reflectors are not horizontal, and not continuous, planes the 2D data will give erroneous subsurface images. With 2D migration, distortions due to reflectors, dipping in the source-receiver direction, can be corrected, whereas distortions due to dipping in other directions cannot be corrected. Regarding dip-effect on seismic results we can distinguish the following three cases:

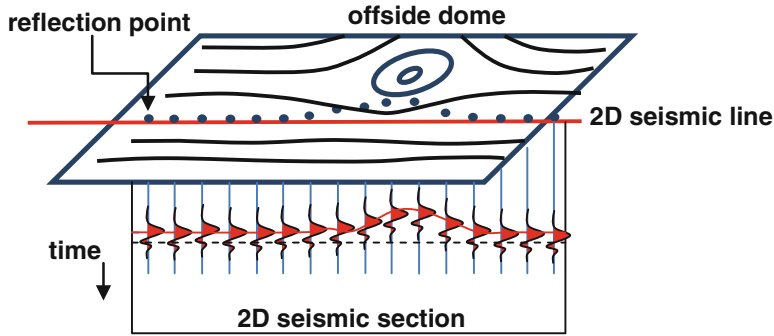


**Fig. 7.4** 2D seismic line shot and an offside dome. The produced seismic section shows a false structure due to reflections from the side of the offside dome

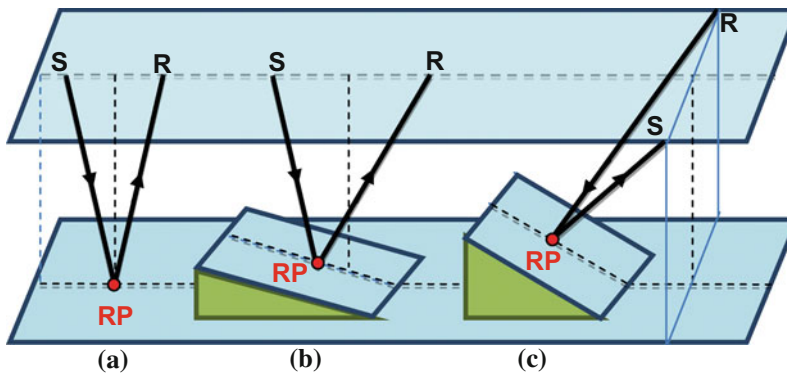


**Fig. 7.5** Distortion effect of dip direction on reflection point location. **a** Case of no dip, **b** dip in the *S-R* direction, and **c** dip is perpendicular to *S-R* direction. *S* and *R* are the source and receiver points respectively

(Case-1) Dip is of zero value (Fig. 7.5a)

In this case, where the reflectors are horizontal planes, the reflection point is located vertically below the shot-receiver midpoint, hence the reflection images, produced by 2D data, are found in their proper positions, and no distortions occur in this case.

(Case-2) Dip is in the shot-receiver direction (Fig. 7.5b)

In this case, the reflection point is shifted up-dip by an amount of shift which is dependent on the dip value. The 2D method is adequate for this type of situation provided that the resulting stack section is corrected through an appropriate 2D-migration process.

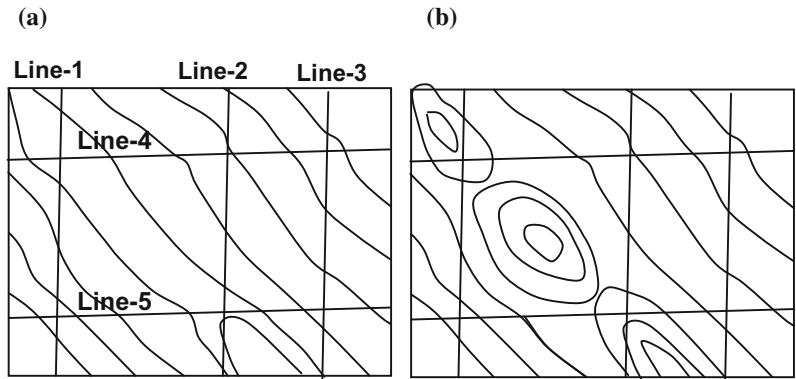
(Case-3) Dip has component perpendicular to the shot-receiver direction (Fig. 7.5c)

The reflection point, in this case, is shifted outside the shot-receiver vertical plane. In this type of situation 3D survey has to be conducted and the resulting data-volume must be subjected to 3D migration process in order to get the correct subsurface structural image.

Distortion always occurs in case of dipping reflectors and the distortion-severity depends on the dip and on dip direction. Thus, if a line in 2D survey happened to be along the dip-direction, then the reflection ray-path will be in the source-receiver vertical plane, and in this case, no out-of-plane reflection points shall



**Fig. 7.7** Sketch maps showing isochrones contour maps from: **a** 2D survey and **b** from 3D survey which is revealing more structural details than the 2D map



the 2D seismic technique. These limitations were removed or very much reduced by the application of the 3D method. The advantages of the 3D surveying may be grouped under the following three groups of application domains:

**(i) In the Geophysical Domain**

3D surveying is furnishing good control on the determination of processing parameters, such as static values, stacking velocity, and dip-vectors, and hence it allows more effective three-dimensional migration process. Increased efficiency in the use of seismic source energy, due to the large number of active detection channels normally used in 3D field acquisition. The 3D data processing provides the stack data-volume, which allows displaying vertical sections at any

direction, in addition to possibility of getting horizontal sections (time-slices) at any level within the data-volume (Fig. 7.8).

**(ii) Capability of Surveying Inaccessible Areas**

As far as seismic surveying is concerned, an area is considered to be inaccessible, when neither seismic energy-sources nor receivers are allowed to be located within the area boundary. An inaccessible area can be surveyed by deploying the receivers on the boundary of the area and shooting at source-points which are also distributed over the area boundary. The surveying is conducted by shooting the source points in sequence while the receiver spread is kept fixed throughout the shooting process. For each shot,

**Fig. 7.8** Types of sections which can be extracted from the 3D data box

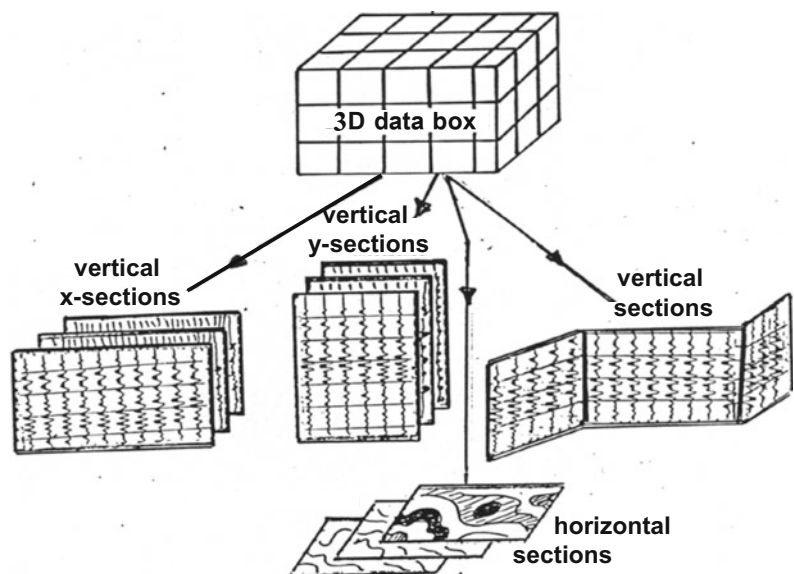
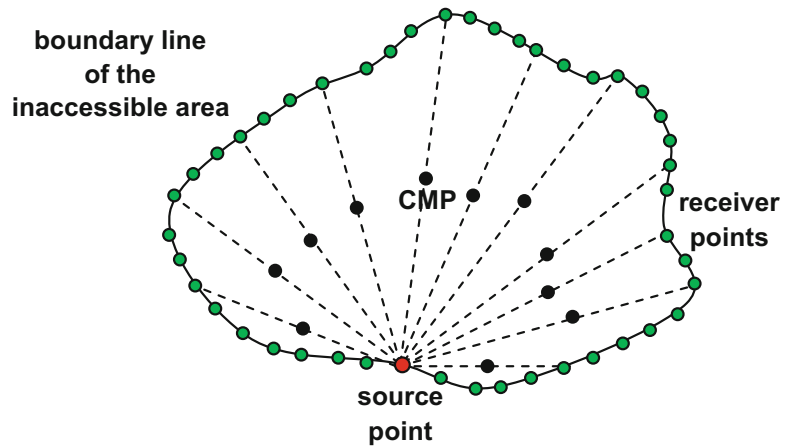


**Fig. 7.9** Concept of loop shooting applied in 3D surveying of inaccessible areas. A *CMP* is created at the middle of each source-receiver distance. Receivers are deployed around the inaccessible area



there will be a number of CMPs located at the source-to-receiver midpoints, which will be located within the surveyed area (Fig. 7.9).

By this type of shooting (called loop-shooting), the area will be covered with CMPs without having survey points (sources or receivers) existing within the area. Special software can handle the recorded data and get it processed to produce a 3D data-volume.

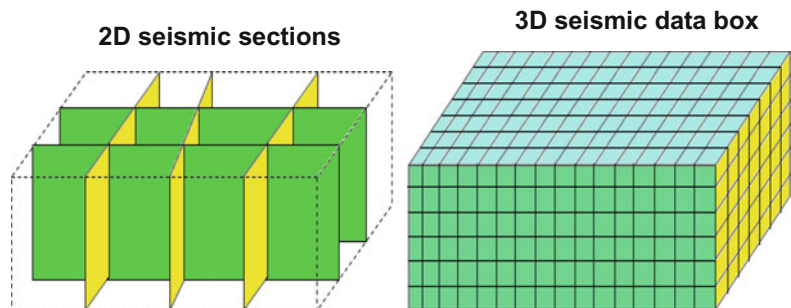
Although this technique makes seismic surveying of an isolated inaccessible area possible, it suffers from a number of weak points. The distribution of both of the recorded CMPs and the fold of coverage are not uniform. Also, it is possible to lose shallow reflections with traces recorded at large-offset receivers. These limitations become less effective, the smaller the area and the deeper the targeted reflectors. Application of the concept (loop spread surveying) was dealt with in more detail in (Alsadi 1992, 1994).

### (iii) In the Geological and Reservoir Domains

The 3D data can furnish accurate information on the subsurface geological structure of the area. Unlike 2D data, it can resolve small and complex structural and stratigraphic anomalies. It provides direct information (with no interpolation procedure) of the subsurface geology expressed in its real three-dimensional image. Due to the dense sampling points of the geological space, the 3D data becomes more readily-interpretable, leading to increased degree of accuracy and much improved resolution-power (Fig. 7.10).

In the reservoir domain, 3D data provide delineation of the 3D shape and spatial limits of oil-fields as well as giving more accurate estimation of their hydrocarbon reserves. The data can help in outlining oil/water contact which can assist in more accurate emplacement of development and production wells. Reservoir studies,

**Fig. 7.10** Sketch showing that the 3D data provides more dense sampling points of the subsurface geological space than the 2D data



based on 3D data, help in more accurate reservoir characterization in terms of facies distribution and fluid content. Such information would lead to more accurate oil-field characterization and enhanced production rates.

#### (iv) **In the Economical Domain**

Despite the overall high cost and long survey duration compared with the 2D method, the 3D method is considered to be cost-effective when the merits of its results are taken into consideration. From the economical point of view, 3D data would give increasing success-ratio (producer-to-total wells ratio) and improving well production-rates. The over-all field evaluation-cost is reduced through less development-wells, proper well emplacement and shorter development-period.

In view of its exploration efficiency, the 3D method gives an enhanced success ratio of development drilling and increase in the oil reserves. These features form the basis for the justification of conducting 3D surveys especially for oil-field appraisal and field development. In comparison with development drilling, the justification is even stronger in comparison with the 2D method. For example, a 10 km<sup>2</sup> 3D survey may cost no more than 10 % of that of drilling a well of 3000 m-depth. The overall saving achieved from a 3D survey is represented by reduced field-evaluation costs and by earlier production due to shortened development-period.

### **7.1.5 Survey Preplanning**

Although, in principle, work preplanning is essential in any seismic surveying project, it becomes more necessary prerequisite when dealing with 3D surveying. The urge for the preplanning phase stems from the complex nature of the 3D surveying work which involves large financial investments. A feasibility study should be conducted as a joint effort by a team of personnel from all parties concerned with the 3D survey project. In particular, the team should include specialists in the data acquisition, data processing and interpretation, as well as experts on legal and contractual matters. The task of this team is to carry out the preplanning

study and prepare its final report for guiding work in the plan implementation.

The preplanning phase is an important prerequisite needed in order to facilitate the work execution especially in the data-acquisition stage. Pre-knowledge of the area assist the geophysicist to be prepared, and make the necessary provisions for any problem that may crop up during the work. Examples of such problems are: skip shots, make-up shots, seismic-energy to be used, work permit, and other administration and logistical matters.

The preplanning report of a 3D seismic survey normally covers the following basic items:

- (i) Compilation and assessment of available technical data.
- (ii) Survey objectives.
- (iii) Operational constraints.
- (iv) Survey-design plan.
- (v) Scouting and preliminary tests.
- (vi) Work organization and scheduling.
- (vii) Cost analysis.
- (viii) Health, safety, and environment protection.

It should be noted here, that the item of the contract preparation is deliberately omitted from the above mentioned list. The omission of this item is made on the basis that it represents an independent piece of work to be carried out in the following stage, rather than being part of the preplanning report. This is natural procedure, since the contract items are depending on the survey parameters which need to be prepared and made ready before starting of contract drafting. Here-below we shall give brief explanatory notes for each of the items included in the preplanning report.

### **7.1.6 Cost Considerations of 3D Surveys**

3D surveying is usually quoted as being a costly process. To be more objective, however, the cost assessment must be made in relation to the turnover benefits. In fact, even 2D surveying can become very expensive when using very small line spacing, and high fold of coverage. It is

generally accepted now that the 2D and 3D methods become equivalent cost-wise when the 2D lines are spaced by about half a kilometer.

The 3D surveying is considered to be cost-effective compared with the 2D method considering the merits of the 3D data. Comparison between 2D and 3D survey-cost is more meaningful, when it is realized that 3D data provide dense spatial sampling of reflectors, enhanced structural resolution, and undistorted 3D images.

**The 3D-Survey Cost Elements**

In discussing survey costs, and 3D-to-2D cost comparison, it is of course very difficult to quote precise figures. However, it is possible to give a fair assessment of the main elements of the cost. These elements are important issues to be considered in cost analysis of any 3D surveying project.

The main cost-elements of the 3D survey can be summarized as follows:

**(i) Surface Conditions**

Difficulty in quoting precise figures is due to the wide variation between types of surveys. In particular, prevailing surface conditions, and types of the applied survey parameters differ from survey to survey. In the present world-wide seismic industry, the cost of the data-acquisition of onshore surveys (on-land surveys) is approximately in the range of (5–10) k\$/km for 2D method and (20–40) k\$/km<sup>2</sup> for 3D. The cost of processing and interpretation is estimated to be in

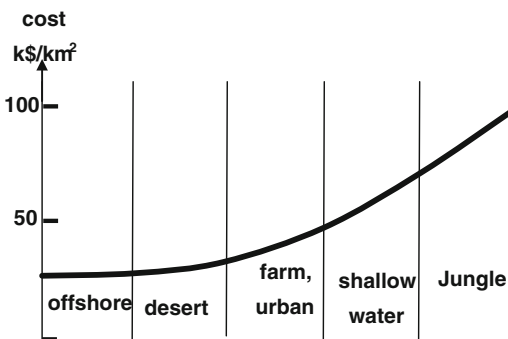


**Fig. 7.11** Sketch showing dependence of survey cost (cost of field data acquisition) on surface environment

the region of (10–15) % of the cost of the data acquisition. These figures are near-realistic when the survey-points for both methods are spaced by 50 m and the coverage folds are 1600 and 3200 % for the 3D and 2D respectively. In general, the cost of 3D surveying depends on the surface environment of the survey area (Fig. 7.11).

**(ii) Dependence of Cost on Survey Parameters**

The survey parameters which are most influential on survey cost are the spread parameters, fold of coverage, bin size, and shot density used in a given survey. These elements are interrelated in their cost contribution. Thus, fold (**F**) may be statistically estimated from the formula:c

$$F = N_{tr}/N_{bin}$$

where, **N<sub>tr</sub>** and **N<sub>bin</sub>** are the survey total number of traces and total number of bins respectively.

By substituting the product (shot density, **SHD**) x (survey Area) x (live channels per shot, **N<sub>CHN</sub>**), for **N<sub>tr</sub>**, and (survey area/**Bin Size**) for **N<sub>bin</sub>**, we get the important relation:

$$F = SHD \times N_{CHN} \times Bin\ Size$$

Hence,

$$SHD = F/(N_{CHN} \times Bin\ Size)$$

Since total survey-work depends on shot density (**SHD**), this formula is showing that the total work done in conducting a 3D survey (and hence total cost) is directly proportional to fold of coverage and inversely proportional to bin size and number of active channels used per shot.

A closely related to cost, is the (turnaround time), or the duration of the complete 3D survey. For a given survey (given area size and given survey parameters), survey duration depends on the work-production rate, which is, in turn, dependant on the applied work parameters, like survey parameters, type of energy source, surface conditions, field processing, topographic survey, permit fees, and number of “work-shifts” followed in conducting the survey.

It is found that the field data-acquisition of a land 3D survey of a 500 km<sup>2</sup>-area, say, would last for about (2–3) months. Adding to this, time needed for processing and interpretation, the total duration time to complete a 3D project of such an area is estimated to be in the order of about (6–8) months.

## 7.2 Definitions and Basic Principles

### 7.2.1 Definition of 3D Surveying

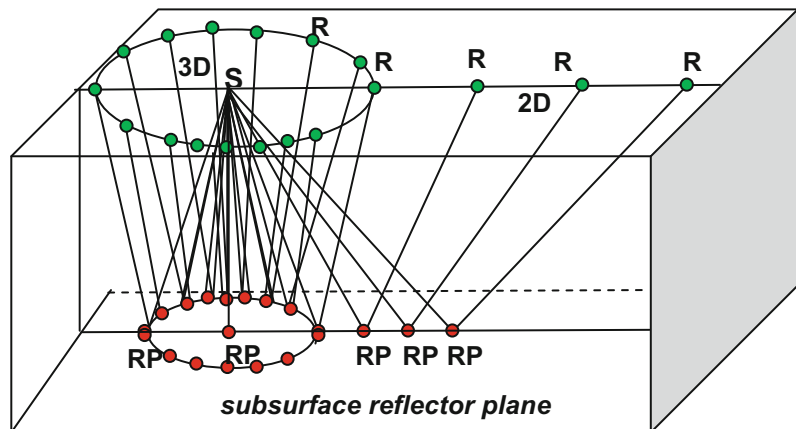
Consider a case where seismic energy, generated at a surface point, is reflected from a subsurface horizontal planer reflector. The generated seismic wave-front, which is of 3D form, spreads out through the geological medium (assumed to be homogenous) with a velocity decided by the physical properties of the medium. At the instant the wave-front hits the reflection plane, a circular zone of it (of the reflection plane) will be illuminated by the incident wave-front which is, according to reflection laws, reflected back to the surface.

Using the ray-concept, detection points distributed over a surface circle centered about the source point, will receive reflected energy from reflection points located on a corresponding subsurface circle. Based on the laws of reflection, the

subsurface circle will have a radius of half that of the surface circle, and all reflected waves received by the detectors, distributed over the surface circle, will have arrived at the same time. However, if the receiver points are laid down on a straight line passing through the source point, the reflection points from which the incident energy is reflected and detected by the co-linear receivers, will fall on a subsurface straight-line with point-spacing equal to half that of the receive points. In this case, the detected reflection information (seismic amplitude) is restricted to the 2D vertical plane containing the reflection ray-paths (Fig. 7.12).

As this figure is showing, the difference between 2D survey and 3D survey is based on the way the spread elements are distributed on the surface. In fact, what makes a survey 2D or 3D is the way the receivers are deployed on the surface. In 2D surveying, receivers are laid down in line with the source point, and the used spread is linear, made up of one-dimensional array of receivers, and in this case, the reflection points will fall on a subsurface straight line which is the projection of the receiver line onto the horizontal reflection-plane. In the case of 3D surveying, the spread consists of receivers which are distributed over an area, and the used spread consists of a two-dimensional array of receivers. The reflection points in this case will be distributed over a subsurface area of the reflector-plane.

**Fig. 7.12** 3D survey is when source and receiver points are covering an area, whereas 2D survey receivers are co-linear with the source point



### 7.2.2 The 3D Spread-Geometry

The spread in the 2D geometry consists of a receiver points co-linear with the source point, whereas the spread in 3D survey takes the geometrical form of a rectangular grid of receiver points. Typical 2D and 3D spreads are shown in the following Fig. 7.13.

Whether it is 2D or 3D survey, the reflection-points (RPs), created from firing a shot-point, are spaced by half the receiver spacing. The spread used for 3D surveying (3D spread) is normally covering a rectangular area. From geometrical consideration, it can be seen that the subsurface area covered by the reflection points is also a rectangle which is of an area equal to quarter of the area covered by the 3D spread. This can be readily observed from the Fig. 7.13.

Shot-records, obtained from 2D and 3D spreads, are shown schematically in the following Fig. 7.14

### 7.2.3 Concept of the Trace Azimuth

Considering horizontal plane reflectors, all the reflection ray-paths, of the CDP trace-gather in 2D surveying, are coincident on one common vertical plane (the ray-path vertical plane). In the 3D method, however, each reflection ray-path may fall in its own vertical plane. These ray-path planes are generally not coinciding on each other, because of the varying source-receiver directions (azimuths) of the CDP gather-traces. Thus, the receiver azimuth in 2D surveying is constant. It is in the direction of the seismic line. The corresponding azimuth, in 3D surveying, is variable because of varying receiver bearing in relation to the source point.

The ray-path planes of the reflection seismic rays (of a 3D-survey shot-point) are vertical planes but they assume different directions. This is the case because the receiver points are located at different bearings in relation to the shot location. The ray-path bearing, with respect to the

**Fig. 7.13** Type of spread decides whether the survey is 2D or 3D.

**a** One-dimensional array spread for 2D survey and **b** two-dimensional array spread for 3D survey

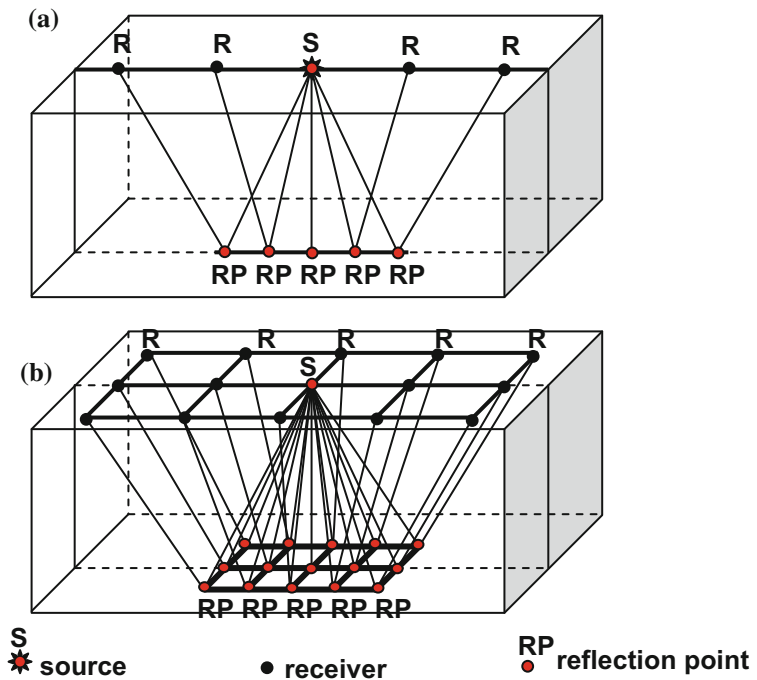
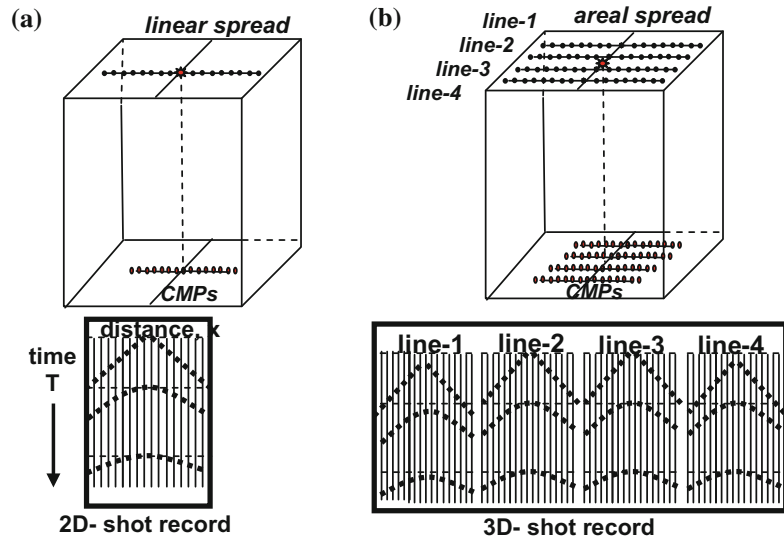


**Fig. 7.14** Sketch showing 2D and 3D shot-records. **a** 2D-survey linear surface spread, mapping line of CMPs, **b** 3D-survey of areal spread, mapping an area of CMPs



shot point, is usually referred to as the azimuth. Azimuth variation is considered as an advantage of the 3D data because with this feature the reflection seismic waves shall sample the rock medium in three-dimensional space and not restricted to one plane as the 2D data is providing. The concept is shown in Fig. 7.13.

#### 7.2.4 The CDP Bin and Bin Attributes

In normal profiling technique followed in 2D surveying, the spread moves along a uniformly spaced station-points, at equal move-up rate. In this way, the reflection points of each CDP trace-gather are all coinciding at the CDP. Sometimes, due to a shifted placement of a shot-point, one (or more than one) reflection point may fall outside the CDP location. In CDP sorting, a search distance (usually defined to be equal to half of the CDP-spacing) is set in processing. All traces found within the search distance of a CDP are included in the trace gather of that CDP.

The same principle is applied to the CDP-grid in case of 3D surveying, except that in 3D, we have a (search-area) instead of the 2D search-distance. The search area is normally having a rectangular shape (or square shape)

centered about the CDP. The width and length of this search area are equal to the CDP spacing in the two perpendicular directions of the survey station-grid. This search area is called the (bin) and the traces included within it form the bin-gather. The process of sorting of traces into the appropriate bin is called bin-gridding or binning. These concepts are shown in Fig. 7.15.

The bin is normally specified by certain properties or identification criteria. The bin can be rectangular or square in shape, having a defined dimensions and surface area commonly referred to as the (bin size). Other parameters of the bin concerns its trace gather. These parameters, called the (Bin Attributes), include the trace offset, azimuth, and fold of coverage. Normally, the bin attributes are displayed in a special diagram called the spider diagram as shown in Fig. 7.16.

#### 7.2.5 The Surface and Sub-surface Coverage

In the normal swath shooting, the surface of the survey area becomes covered by two sets of mutually perpendicular lines (the station lines). These are the receiver lines and the shot-lines. The corresponding subsurface lines are the sub-lines (inlines) and cross-lines which intersect at

**Fig. 7.15** Definitions of **a** the search distance in 2D surveying, and **b** search area (Bin) in 3D surveying

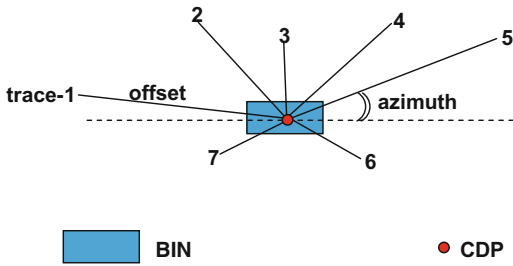
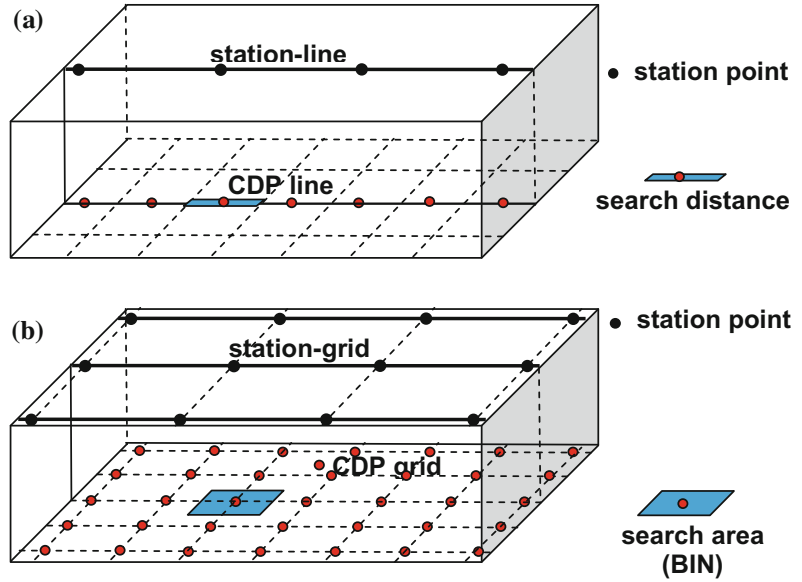


**Fig. 7.16** Spider diagram showing the bin attributes (offset, azimuth, and fold) of a bin having 7 traces in its gather (fold = 7)

bin centres. By definition, the bin is a subsurface rectangular (or square) area having dimensions which are equal to half of the corresponding surface receiver-station spacing (Fig. 7.17).

The subline and cross-line seismic sections are made up of sequence of stack traces, each of which is located at a bin centre. In this sense, subline and cross-line seismic stack sections are considered as of subsurface locations and not surface locations.

### 7.2.6 The Seismic Data Volume

The end-product of a 2D-data processing, is the 2D seismic stack section. In case of the 3D

seismic surveying, the corresponding end-product is a three-dimensional space of stacked traces called the “data volume” or the “data box” as it is sometimes called. The data volume represents a three-dimensional function in which the seismic amplitude varies with the three coordinates;  $(x, y, t)$ . The reflection-time ( $t$ ) may be replaced by the depth dimension ( $z$ ), where  $(z = tv/2)$  and  $v$  is velocity.

The data volume (in digital form) consists of discrete volume-elements, called the (resolution cells) defined as parallelepipeds of dimensions  $(\Delta x, \Delta y, \Delta t)$ , where  $(\Delta x)$  and  $(\Delta y)$  are the CMP spacing in the inlines and cross-lines respectively. The third dimension  $(\Delta t)$  is equal to the sampling period of the stack traces. This volume element is considered to be the building brick of the data box, the ultimate product of the seismic 3D survey.

The resolution cell is also called the (voxel), in analogy to the term (pixel) used for the unit of a digital picture. The data volume is a subsurface data-set, made up of voxels of dimensions  $(\Delta x, \Delta y, \Delta t)$  as illustrated in Fig. 7.18.

With the help of special processing software, it is possible to extract a variety of seismic sections from the data-volume. Normally, three types of mutually perpendicular sections can be

**Fig. 7.17** Surface lines (receiver and shot lines) and sub-surface lines (sublines *SL* and cross-lines *XL*). Bin dimensions are half the corresponding receiver spacing lines

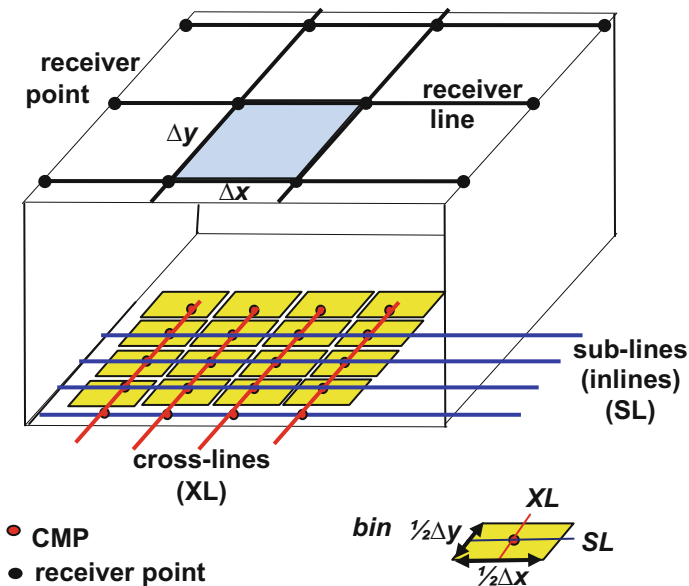
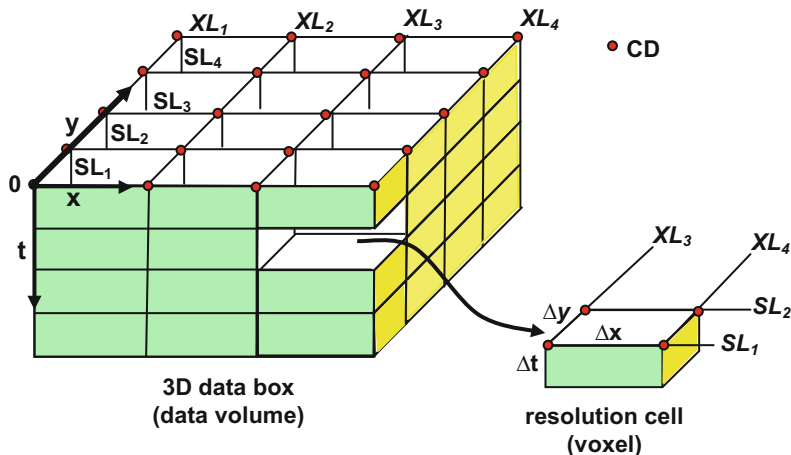


**Fig. 7.18** Definition of the resolution cell (the voxel); the building brick of the seismic data volume



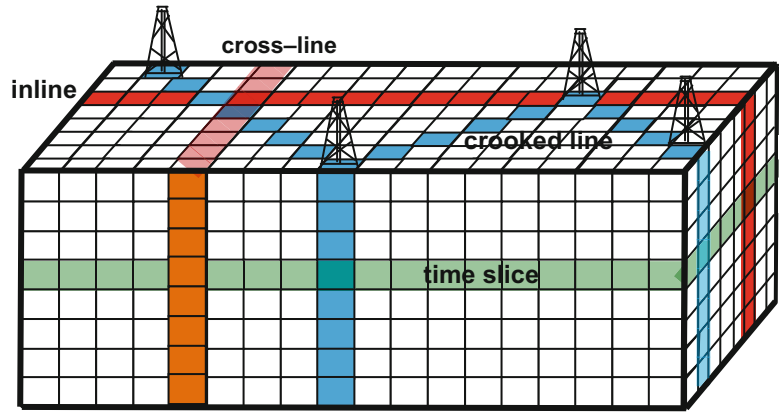
extracted. A vertical section may be obtained along any subline, or along any crossline, and a horizontal section (called a “time slice”) can be obtained at any reflection-time. It is also possible to obtain a vertical section connecting points at arbitrary locations as for example, sections along distances connecting several well locations. A section which is not a subline or a crossline is normally referred to as a crooked, oblique or diagonal section (Fig. 7.19).

The horizontal section, called seiscrop section, or more often called (time slice), is a

representation of the seismic amplitude values which fall on the same reflection-time. In fact, it is the locus of equal-time amplitudes existing in the data volume. In color displays, the time-slice plots are given in color-coded amplitude-values with clear distinctions between peak- and trough-values.

The time slice has a similar form as that presented by the time contour map. The difference between the time slice and the structural contour map is that in time slice, we display different amplitude values at constant reflection time (time

**Fig. 7.19** The 3D data volume, with the four possible sections obtainable from the data volume (*inline*, *cross-line*, *crooked line*, and *time slice*)



of the time slice). The structural contour map shows different time values of the same reflection surface. Briefly stated we say that time slice is showing different amplitudes measured at one time-slice, and in contour map, we display the same reflection event (belonging to a given reflector surface) at different time values. Several reflectors may be represented in a given time-slice, but different time-values of the same given reflector, are shown in a given contour map.

Derivation of structural contour maps from time-slice sections can, in principle, be obtained by marking the amplitudes of the same seismic reflector, on a sequence of time-slices, and projecting the picked values for that reflector on one map.

### 7.3 3D Field Data Acquisition

In 2D seismic surveying, the shooting spread consists of a shot point and receiver points which are all arranged in one straight line (linear spread). In the 3D surveying, however, these survey-points are distributed over an area (areal spread). Essentially the field work consists of a set of procedures which implement certain geophysical parameters. The field parameters are normally adopted through compromising between the ideal technical requirements and the overall acquisition cost. Certain test-recording

and data analyses are applied in the field to determine the optimum parameters applied in the data acquisition.

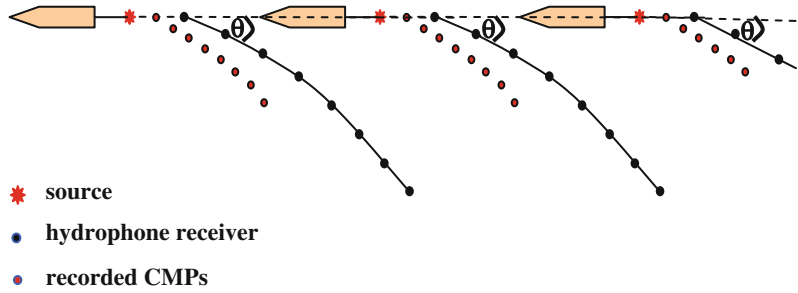
Here below, are the main aspects of the data-acquisition requirements involved in 3D seismic reflection surveying. Spread parameters and shooting procedure is most important aspect of the 3D field acquisition activities. Many types of spread are in application, which can be discussed under two main headings: marine and land 3D spreads.

#### 7.3.1 Types of Marine 3D Spreads

Conventionally, marine 3D surveying is conducted by using spreads similar to those used in land 2D seismic surveying. The boat and the towed-behind streamer is recording as it moves along straight-line courses. The technique differs from the normal 2D surveying in that the survey shooting is conducted along closely spaced parallel lines. Line spacing (typically, 100–200 m), is kept constant throughout the survey area.

With the progress that took place in the navigation techniques and in navigation data processing, certain improvements were introduced on the applied spreads. In cases of calm seas, the survey boat and its trailing streamer move along a straight line. In other cases, and because of local sea cross-currents, the streamer may drift

**Fig. 7.20** The feathering effect occurring in marine surveying. The angle ( $\theta$ ) is the feathering angle



away from the boat linear course. This is referred to as the (feathering effect), and the angle between the drifted cable and the linear boat-track is called the feathering angle (Fig. 7.20).

The shape of the drifted cable, for each shot, is determined from the readings of the special compasses fitted along the cable. Because of changes of sea conditions, the cable shape and the feathering angle change from shot to shot. Consequently, distribution of the subsurface

reflection points varies as shooting progresses. Computations of the reflection points and CMP distributions are done in the processing stage based on the gathered boat readings of the cable geometry during shooting.

To increase survey efficiency, multi-source and multi-streamers have been used in the marine surveying. Examples of marine spreads which can be configured are: single source-single streamer, dual source-single streamer, single source-dual streamer, and dual source-triple streamer (Fig. 7.21).

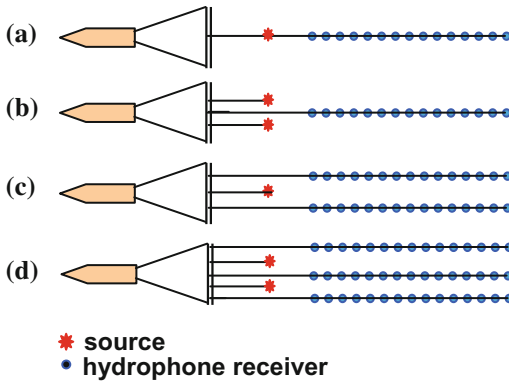


**Fig. 7.21** Types of spreads used in marine 3D surveying. **a** Single source-single streamer, **b** dual source-single streamer, **c** single source-dual streamer, **d** dual source-triple streamer

Spread movement during recording, is done normally along parallel straight lines (parallel linear paths). Because of the long streamer-line towed behind, the boat needs to turn with a relatively large steering radius in order to record the following line. A variation of this method is shooting along circular paths. The boat moves along overlapping or spiral circular paths. The advantages of the circular type of spread, is that the survey is completed with no times lost due to long-time turns of the boat needed in case of straight-line surveying. These types of spread-movements are shown in Fig. 7.22.

It should be noted here that, deviation of the streamer course-line from the linear form (caused by the circular spread or by the feathering effect),

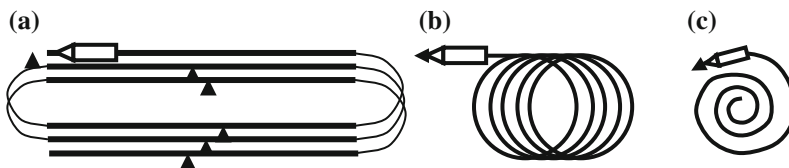
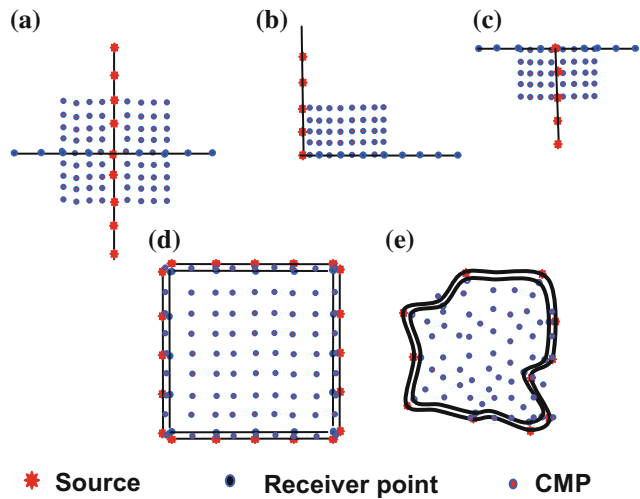


**Fig. 7.22** Types of spread movements used in marine 3D surveying. **a** Parallel linear path, **b** Overlapping circular path, **c** Spiral circular path

**Fig. 7.23** Special types of land 3D spreads.  
**a** X-Spread. **b** L-Spread.  
**c** T-Spread.  
**d** Square-Spread.  
**e** Loop-Spread



gives certain amount of azimuthal variation. This makes the marine surveying to be approaching the proper 3D surveying.

### 7.3.2 Types of Land 3D Spreads

The normal spread used in land 3D surveying consists of source-lines perpendicular to receiver lines. Examples of these special types of spread (not in common use at present) are X-spread, L-spread, T-spread, square-spread (called Seis-square), and Seis-loop (Fig. 7.23).

In order to obtain multiple reflection points and increase of fold of coverage, several parallel survey lines (source-lines and receiver-lines), are used in the X-, L-, and T-spread. In the case of the square spread, source-points and receiver-points are distributed uniformly around a square. If each survey point is occupied by a source point and receiver point, the area defined by the square becomes filled with CMP points of high fold of coverage, distributed over a uniform CMP-grid. If, however, the source points and receiver points are laid out around an arbitrary loop (loop-spread), the area enclosed by the loop becomes filled with CMPs, but in an unorganized distribution. Special software can be used in this case, to sort the created CMPs into a defined bin-grid.

### The Rectangular Spread

The most commonly applied shooting spread, used in land 3D surveying, is the rectangular-shaped spread, normally referred to as the spread template. It consists of a number of parallel receiver lines with a shot-line perpendicular (or inclined) to the shot-line. The shot-line is inclined with respect to the receiver lines, usually at an angle of 45°. The group of shots per shot-line is normally referred to as a shot-salvo. A typical form of the normally-applied rectangular spread (spread template) is shown in Fig. 7.24.

This type of spread is used in the land-surveying technique called (swath-shooting).

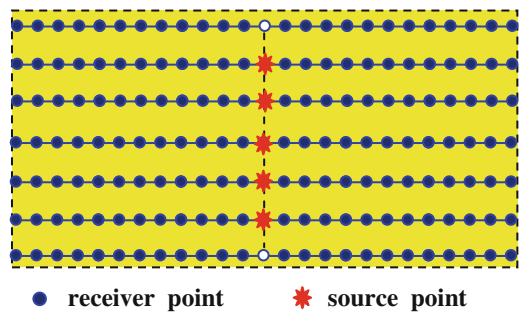


**Fig. 7.24** Spread template commonly used in Swath shooting. Source line is perpendicular to receiver lines. Spread is made up of 7 receiver lines and 5-shot salvo

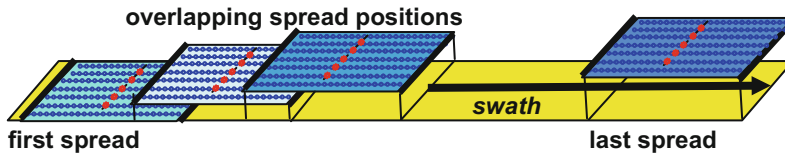


**Fig. 7.25** Spread movement (shift-and-shoot movements) over the swath, with overlapping shooting spreads

### 7.3.3 The Swath Shooting Technique

The swath is defined to be a strip of the survey area of width equal to the width of the used spread that moves along the defined strip in a roll-along movement similar to the “shift-and-shoot” technique used in conventional 2D profiling surveying (Fig. 7.25).

In practice, when the template reaches the end of the first swath, the template is re-configured at the near-by end of the adjacent swath, then carrying out the “shift-and-shoot” process from end to end. In this way all the rest of swaths are sequentially covered. In general, swaths are not laid down side by side, but laid down with overlap to obtain fold build-up (Fig. 7.26). Greater fold coverage is obtained with bigger overlap made between adjacent swaths.

Swath shooting is a common acquisition technique implemented in today’s land 3D surveys. It has the advantages of being simple to configure, and efficient to execute in the field. It

gives uniform bin fold and adequate offset and azimuth coverage. On the other hand, swath shooting requires land with fully accessible space, and type of surface conditions which allow the appropriate freedom for the survey maneuvering.

A typical example, of shooting parameters applied in swath survey, is given here-below (Table 7.1).

### 7.3.4 Types of Templates Used in Swath Shooting

There are many types of templates that can be used in swath shooting. A template may contain one, or more than one, shot-lines which are arranged to be in-centre, off-centre, or at ends of the template. The more common types are those where the shot-lines are perpendicular to the receiver lines. Another variation is to have the shot-lines inclined with respect to the receiver-lines (Fig. 7.27).

**Fig. 7.26** Template movements along the sequence of five overlapping swaths

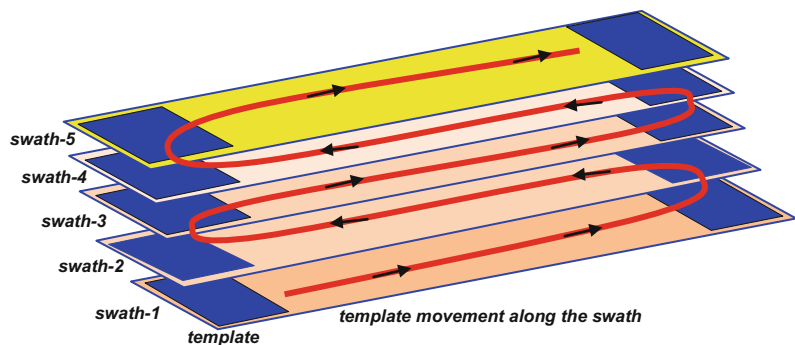
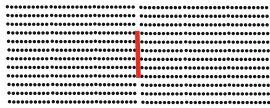


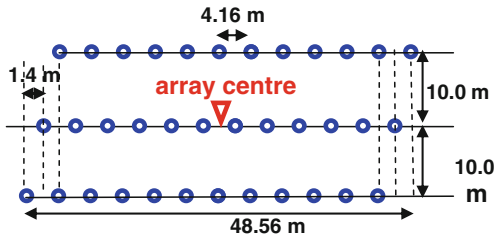
**Table 7.1** Typical values of operation parameters used in 3D swath shooting

1. Spread (template) configuration parameters



Spread shape	Symmetrical split-spread
In-line offsets	25–2975 m
Receiver-point spacing	50
Receiver-line spacing	250
Receiver lines/spread	12
Active receivers/receiver-line	120
Source-point spacing	100
Source-line spacing	150
Number of shots/salvo	8
In-line spread roll (in number of receiver-points)	5
Cross-line roll (in number of shot-lines)	3
Nominal fold	24

2. Receiver array (geophone-group) configuration parameters

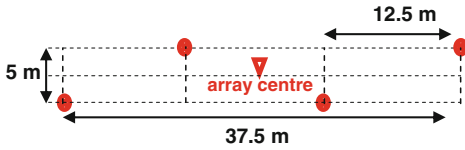


Geophone type/polarity	SM-4/SEG standard
Natural frequency	10 Hz
Critical damping	70 %
String configuration	12 geophns (2 parallel × 6 series)
Receiver array	parallelogram
Geophones/geophone-group	36
Geophone spacing	4.16 m
Number of strings	3
Stagger between strings	1.4
String separation	10 m
Array length	48.56 m
Array width	20 m

(continued)

**Table 7.1** (continued)

3. Source array configuration parameters



Source type	Vibroseis System (vibrator)
Peak force	45,000 lb
Number of vibrators	4
Sweeps per VP	1
Sweep length	16 s
Sweep frequency	8–64 Hz
Sweep taper	500 ms at both ends
Source array	Parallelogram 2 × 2
Vibrator inline stagger	12.5 m
Vibrator lateral spacing	5 m
Array length	37.5 m
Array width	5 m
4. Data recording parameters	
Recording system	I/O system-II
Channels recorded	1440 data, 4 auxiliary
Record length	6 s
Sampling period	4 ms
Tape recording format	SEGD
Recording gain	48 db
Diversity staking	Active
Stacking/correlation	Correlation after vertical stacking

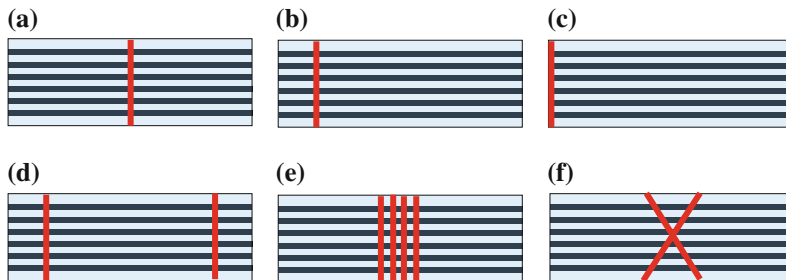


**Fig. 7.27** Types of templates used in swath shooting. **a** Centre symmetric split. **b** Asymmetric split. **c** Double off-end. **d** Double within. **e** Centre multi shot-line. **f** Centre of inclined shot-line

More elaborate spread designs are based on grouping the receiver points in blocks with the source points distributed regularly over parallel

shot-lines. One of such designs is what is called “Checkerboard” spread. An example representing this type of spread is shown in Fig. 7.28.

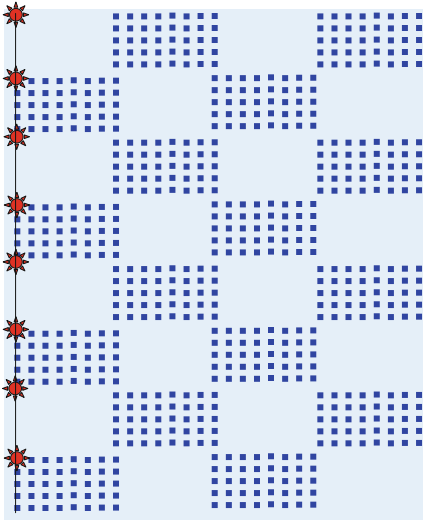


**Fig. 7.28** A checkerboard spread consisting of one 8-source shot-line with 16-receiver blocks. Each block includes 48 geophone groups (48 live seismic channels)

The template, in this checkerboard example, consists of one 8-source shot-line with 16-receiver rectangular blocks, each of which includes 48 geophone groups (48 live seismic channels per block).

### 7.3.5 The Loop Shooting Technique

There are cases where the project area is totally inaccessible (no survey equipment can enter the area) or partially accessible, where equipment can be moved along restricted routes crossing the

area. Examples of inaccessible areas are farms, built-up blocks, lakes, or isolated rugged mountains. 3D surveying of the totally inaccessible area can be carried out using a technique called “Loop Shooting”. This technique involves laying out source-points and receiver-points around the inaccessible area, forming a loop that encloses the project area (Fig. 7.29).

While sequentially shooting the source points, the receiver points, occupied by the geophone groups, are fixed in place. When the surveying process is completed, the enclosed area becomes filled with CMPs without having to move any of the survey equipments inside the area. Special processing software can be used to sort the CMPs into a defined bin-grid.

Loop shooting furnishes a solution to the problem of area inaccessibility, but not without a cost. To start with, it gives non-uniform fold and offset distribution among bin gathers. Further, shallow reflectors may be missed in case of too large survey-areas. However, with proper design of the loop-route and using the appropriate processing software, this method can give fully 3D-surveyed area, especially when the area is not too large and the target reflectors are not too shallow.

### 7.3.6 The 3D Survey Design

The principal objective of any 3D survey is to get a fully migrated seismic data volume of the target subsurface geological structure. Quality of the

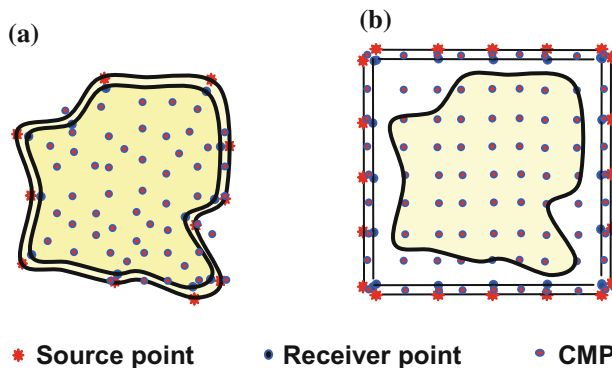


**Fig. 7.29** Loop-Spread. **a** Survey points (source and receiver points) laid down around the irregular inaccessible area. **b** Survey points laid down on the perimeter of a rectangle (or square) enclosing the survey area

final results is controlled by the procedures as well as the parameters applied in the acquisition and processing of the recorded data. In order to get clear reflection signals, optimum acquisition parameters must be applied in conducting the survey. Determination of the procedures and the acquisition parameters is involved in a special group of field activities, collectively known as the (3D survey design).

Pre-definition of depth-range of target reflectors and considering the limitations of allocated cost and time, serve as guide lines in the design process. Acquisition field parameters which need to be optimized in the survey design include the following actions:

- Source Parameters (charge size, charge depth, vibroseis parameters, shot pattern).
  - Receiver Parameters (geophone-array shape, number of geophones per group, geophone spacing, near offset, far offset).
  - Spread Template (template geometrical shape, number of active channels per receiver line, number of receiver lines per template, number of source points per shot-line, number of shot-lines per template, spread move-up distance along swath).
  - Swath Parameters (swath direction, roll-aside overlap).
  - Recording Parameters (sampling period, record length).
- Surface-area Parameters (area boundary, full-fold zone, migration-fringe width).
  - Sub-Surface Parameters (bin dimensions, offset-range, azimuth range, fold of coverage).

In order to conduct the computations and data analysis required by the survey design, a number of basic geological and geophysical parameters must be available. In particular we need to have information about the general geological nature of the area, dip variation (magnitude and azimuth), velocity-field, frequency-range, depth and extensions of target reflectors. These aspects will serve as input to the survey-design analyses which give the optimum acquisition parameters to be applied in the survey execution.

Acquisition parameters covered in a typical survey-design process can be summarized as follows:

- (i) Survey Area and Migration Fringe
- (ii) Template Parameters
- (iii) Swath Parameters
- (iv) Bin Dimensions and Bin-Attributes
- (v) Sampling Period and Record Length.

(i) **Survey Area and Migration Fringe**

A 3D seismic survey is designed in such a way that the target data-volume (areal extent and recording time-length) is obtained with full migration. An additional full-fold strip

**Fig. 7.30** Definition of the full-migration area and the migration fringe in respect to the full-fold, subsurface, and surface areas

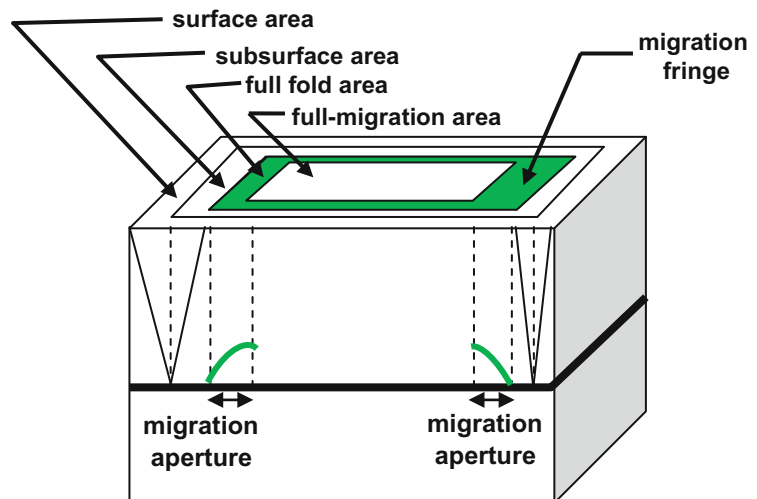
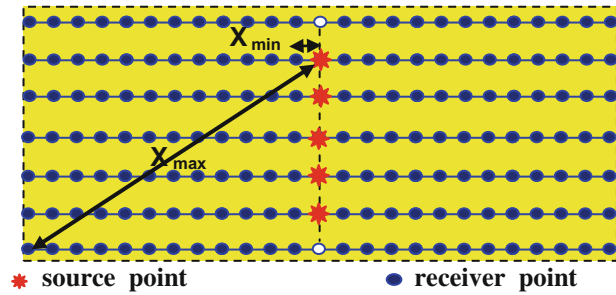


**Fig. 7.31** Computation of maximum offset ( $X_{max}$ ) and minimum offset ( $X_{min}$ ) from the geometry of the template



surrounding the target migrated area is required to insure full migration of the target area. The width of this strip (called the migration fringe) is equal to the migration aperture which is defined to be the horizontal distance a reflection event is moved by a migration process. The width of the migration fringe is function of the dip measured in the direction of the fringe width. The migration fringe is shown in Fig. 7.30.

The survey area should be large enough to include the fully migrated zone, migration fringe, “tail-fold” zone, and the required surface-coverage zone. For economic reasons, and when the S/N ratio is sufficiently high, the migration fringe may be extended in such a way as to include part of the tail zone. This step can result in reduction of the total survey area to the area which is sufficient for achieving the targeted fully-migrated data volume.

Estimation of the fringe area is considered to be an important issue in 3D surveys, since it is directly connected with the overall survey cost. The percentage cost-increase due to addition of migration fringe depends on the size of survey-area as well as on the fringe width used. Cost saving, as we mentioned above, can be effected by allowing the fringe to be extended into part of the “tail-fold” zone. According to (Sheriff and Geldart 1995, p. 452), the fringe area should be equal to the migration aperture plus the radius of the first Fresnel zone.

### (ii) Template Parameters

The template is made up of a number of receiver-lines, shot-lines, number of active channels per receiver-line, and number of source-points per shot line. A template must be so designed that it will provide a range of offsets covering a

pre-defined minimum to maximum offset values. As a rule of thumb, an offset should be roughly equal to the depth of the target reflector. Thus, by defining the depths of target reflectors, it is possible to determine a range of offsets to suit both of the targeted shallow reflectors and deep reflectors.

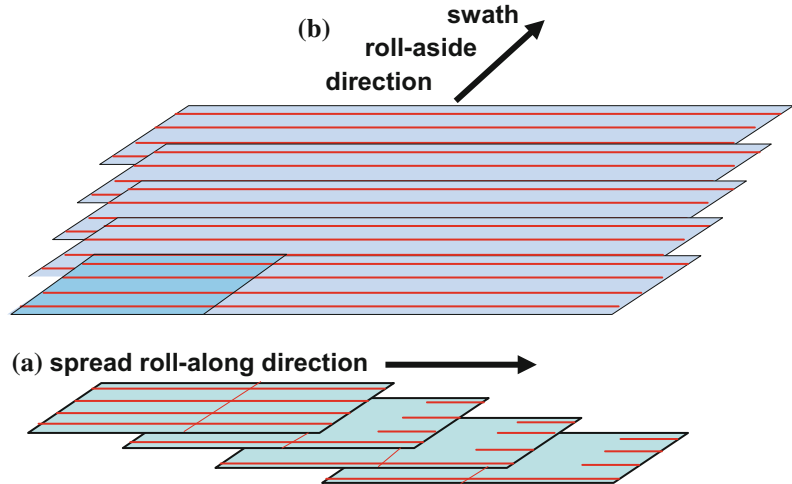
For a given bin-size, geophone group spacing becomes known, and both total active channels per receiver-line and total number of receiver-lines per template can be decided, based on the maximum offset required. Maximum offset ( $X_{max}$ ) and minimum offset ( $X_{min}$ ) can be calculated for the largest and smallest source-to-receiver points in the designed template (Fig. 7.31).

### (iii) The Swath Parameters

The main parameters of the swath are shooting direction (survey orientation) and roll-aside overlap. Swath length and swath width are controlled by the survey-area boundaries and template width respectively. Based on the fold-computation formula, the fold is function of both of the template movement-overlap and swath role-aside overlap. Hence the overlap (measured in terms of number of receiver-stations for the template movement and in terms of receiver-lines for swath movement) can be computed once the fold is defined (Fig. 7.32).

The other important parameter related to the swath is the shooting direction, or survey orientation. When there is a distinct dip-trend in the area, receiver lines are oriented in the direction of dominant dip. In practice, this constraint is relaxed for two reasons: first, dip value and dip direction are generally not constant for the same area, and second, the dip move-out effect can be taken care of, by dip move-out (DMO) correction or by pre-stack migration in the processing stage.

**Fig. 7.32** Fold build up by **a** overlapping spreads rolling-along the swath and by **b** overlapping swaths rolling-aside across the area



#### (iv) Bin Dimensions and Bin Attributes

By definition, the bin is a subsurface rectangular (or square) area having length and width dimensions. These dimensions are equal to half of the corresponding surface receiver-station spacing. In processing, seismic traces are sorted into bin gathers. This means that the bin will contain a number of traces (equal to the fold of coverage) of different offsets, and different azimuths. The centre of the bin marks the CMP at which the stack-trace of the bin-gather is located. Thus, the bin area (normally referred to as the bin size) should be small enough to achieve appropriate resolution but not too small to create empty or low-fold bins. An optimum bin size must, therefore, be determined.

The theoretical basis used for computing the optimum bin size is the same as that used for avoiding spatial aliasing in case of 2D common mid-point (CMP) spacing computations. Thus, in order to avoid spatial aliasing, at least two surface samples are required to be present for each apparent wavelength. For a given reflector dip, the apparent wavelength should be as small as possible in comparison with the CMP spacing.

From the geometry of the normal incidence reflection from a dipping reflector and using ( $\Delta x = \lambda/2$  and  $\Delta t = \tau/2$ ), a quantitative evaluation is obtained for the maximum spatial sampling interval ( $\Delta x$ ), expressed by the following

formula (Liner 2004, p. 272; Sheriff and Geldart 1995, p. 452):

$$\Delta x \leq v/4f \sin\theta$$

where ( $v = f \lambda$ ) is velocity, ( $f$ ) is the highest frequency-component, and ( $\theta$ ) is the angle of dip component in the  $x$ -direction.

Derivation of the formula can be done with the help of Fig. 7.33.

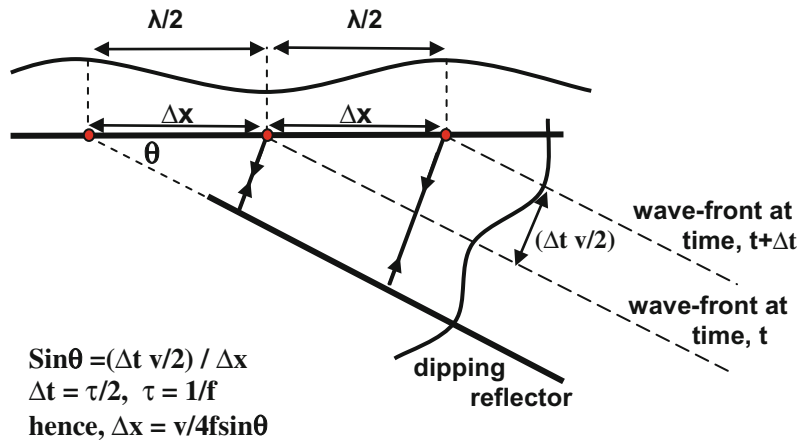
This formula expresses the relation between the CMP trace spacing ( $\Delta x$ ) and the three variables ( $v$ ,  $f$ ,  $\theta$ ). It has shown that ( $\Delta x$ ), which is representing the bin dimension in the  $x$ -direction, is directly proportional to velocity ( $v$ ) and inversely proportional to wave frequency ( $f$ ) and reflector dip ( $\theta$ ).

Typical bin dimensions used in land 3D surveys are (12.5–25) m in the inline (sub-line) direction and (25–50) m in the cross-line direction. These ranges are corresponding to (25–50) m and (50–100) m of surface sampling intervals (receiver spacing). However, when square and small enough bins are used, no spatial aliasing occurs. Small bins mean fine subsurface sampling which is necessary for increasing structural resolving power.<sup>c</sup>

#### Bin Attributes

The group of traces included in a bin gather, are traces of different offsets recorded by receivers positioned at different azimuths. The number of

**Fig. 7.33** Theoretical basis for computing the maximum spatial sampling interval ( $\Delta x$ ), which is the CMP trace interval



traces in the bin-gather represents the fold of coverage for that bin. The parameters (offset, azimuth, and fold) form the bin attributes.

In the design process, it is aimed at attribute-values that cover as wide coverage-range as possible, considering the economic constraints. Bin attributes are normally displayed in a special diagram (called spider diagram) in which offsets are drawn as straight lines radiating from the bin centre. The line length is proportional to offset value and line bearing represents the azimuth. Number of lines is equal to the fold of coverage (Fig. 7.34).

In addition to the desired large coverage-ranges of attributes, the bin should be small and square to insure equally-fine sampling in both of the sub-line (inline) and cross-line-directions.

**(v) Sampling Period and Record Length**

The sampling period normally used in the seismic recording is 2 ms. With this value, the

Nyquist frequency is 250 Hz. which is expected to be far higher than the highest frequency of recorded reflection signals. For economic reasons, the recorded data is often re-sampled to 4 ms before being inputted to processing. To make sure that no aliasing occurs, an anti-alias filter is applied in the acquisition recording stage prior to A-D conversion and it is also applied prior to any re-sampling process carried out during processing work.

The sampling period, together with the bin dimensions, set the three dimensions of the resolution cell (the voxel) which has the general form of a parallelepiped or a cube. Its volume is defined by the two horizontal dimensions ( $\Delta x$  and  $\Delta y$ ), and the vertical dimension ( $v\Delta t/2$ ), where ( $\Delta x$  and  $\Delta y$ ) are equal to the bin dimensions in the sub-line and cross-line directions, ( $\Delta t$ ) is the sampling period, and ( $v$ ) the seismic velocity (Fig. 7.35).

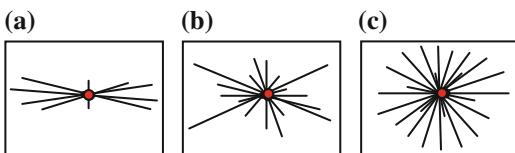


**Fig. 7.34** Bin attributes, **a** poor azimuth coverage, fold-5, **b** fair azimuth coverage, fold-9, **c** good azimuth coverage, fold-12

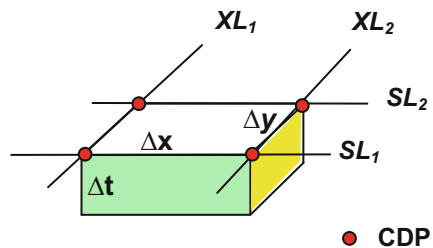


**Fig. 7.35** Definition of the resolution cell (voxel)

Size of the voxel is considered to be as measure of the 3D resolution power, where the spatial resolution is governed by the dimensions ( $\Delta x$  and  $\Delta y$ ) and the depth resolution is governed by the sampling period ( $\Delta t$ ). In a 3D data box where the bin dimensions, ( $\Delta x = 25$  m and  $\Delta y = 50$  m) and sampling period ( $\Delta t = 2$  ms), the voxel volume is  $(25 \times 50 \times 3000 \times 0.002/2) \text{ m}^3$ , assuming the velocity ( $v$ ) to be 3000 m/s. Naturally, the smaller the voxel the better is the resolution power in both horizontal and vertical directions.

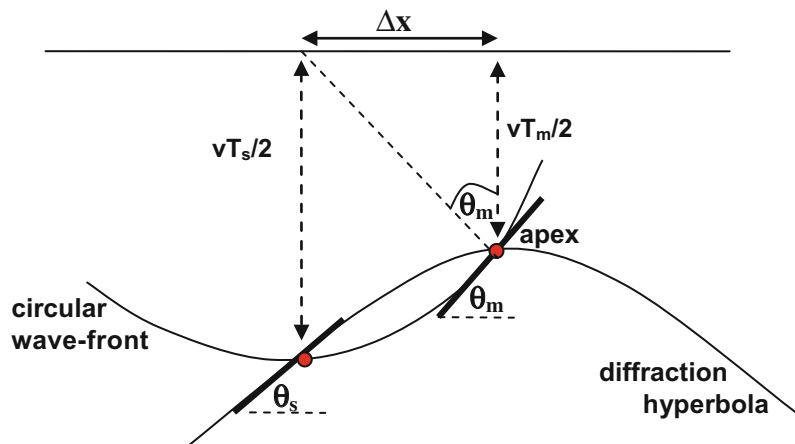
### Record Length

From our discussion of the design of the survey area, it is noted that the subsurface target area must be extended by an additional strip (the migration fringe) in order to insure complete migration. For the same reason (getting complete migration), all the seismic wave-field originating from the subsurface target volume should be included in the migration processing. This requires that a minimum recording time which is of extent that can include all diffraction energy of the deeper parts of the tails of the diffraction hyperbolae.

From the geometry of the migration of dipping reflector, the aperture radius ( $\Delta x_m$ ) is given by Fig. 7.36:

$$\Delta x_m = (vT_s/2) \sin \theta_m$$

**Fig. 7.36** Definition of the migration aperture ( $\Delta x_m$ ) and the required minimum recording time ( $T_s$ )



or,

$$\Delta x_m = (vT_m/2) \tan \theta_m$$

giving,

$$T_s = T_m \sec \theta_m$$

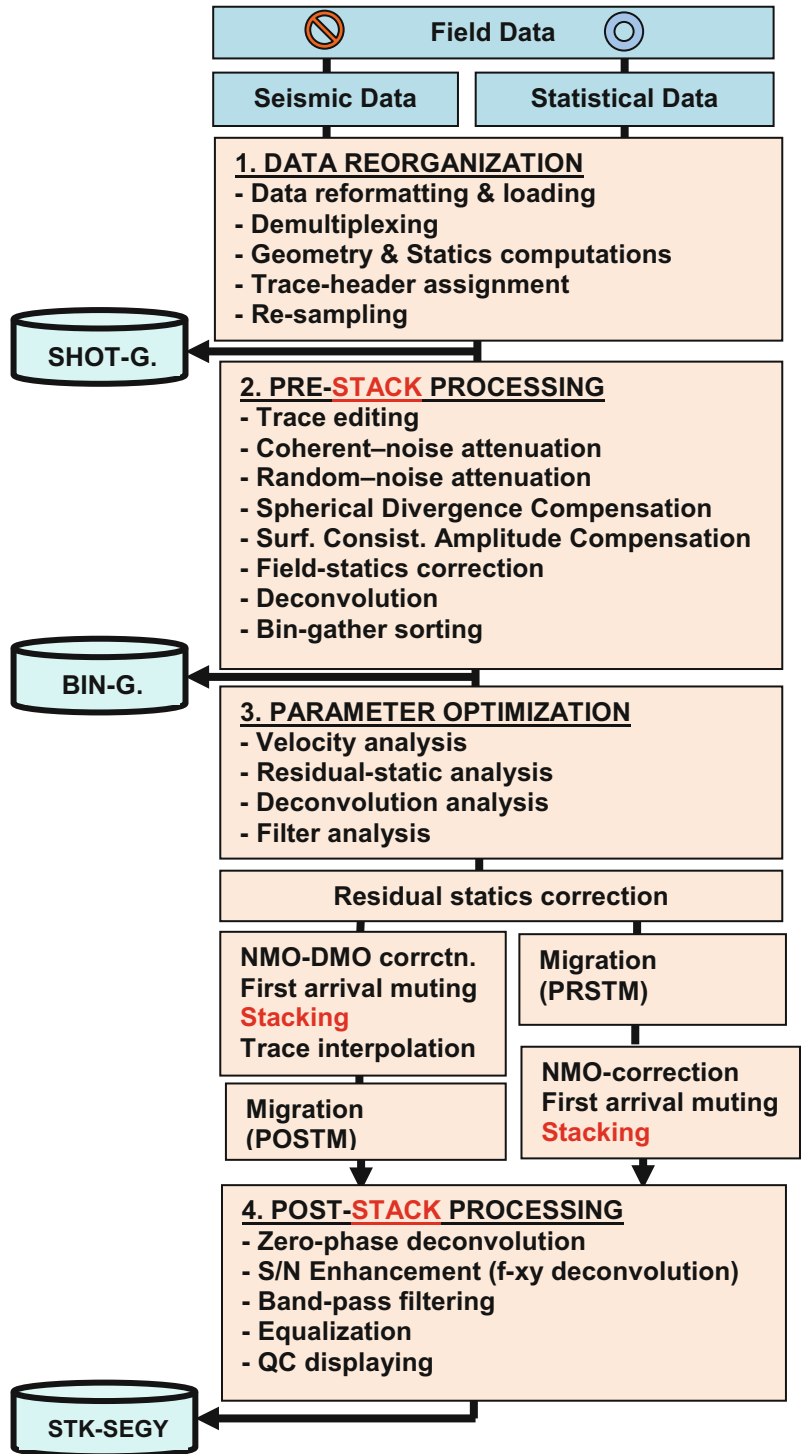
This formula shows that the migration aperture ( $\Delta x_m$ ) is directly dependant on the three factors; average velocity ( $v$ ), dip ( $\theta_m$ ), and two-way recorded reflection-time ( $T_s$ ), which is related to the true reflection time ( $T_m$ ) by the relation ( $T_s = T_m \sec \theta_m$ ).

If the dip is  $45^\circ$ , for example, migration of an event at true time ( $T_m$ ) needs to include data down to ( $T_s = T_m \sec 45^\circ = T_m \sqrt{2} = 1.4 T_m$ ). This means that an extra 40 % of the true time of the dipping segment needs to be included in the migration process in order to get complete migration. Thus recording should be down to a greater time than that of the deepest target (by extra time of about 40 %).

## 7.4 Processing of 3D Data

Seismic data processing, in all 2D and 3D surveys, aims at enhancing the reflection signal and getting accurate images of the subsurface

**Fig. 7.37** A general processing sequence for 3D data processing. SHOT-G, BIN-G, and STK-SEG Y represent optional shot-gather, bin-gather, and migrated stack data volume (in SEG-Y format) respectively



geological structure. For stratigraphic-exploration purposes, however, data-processing is directed towards preservation of the amplitude changes caused by the physical properties as well as structural changes of the subsurface rock layers. Whether it is obtained from 2D or 3D surveying, the recorded seismic reflection data is subjected to a sequence of data-analyses (data processing steps) which give the final stacked 2D seismic sections or 3D seismic data volume.

### 7.4.1 The Field Data Processing

Field crews are usually equipped with processing facilities (field processing system) used to process data for some field parameters determination and for QC purposes. Field processing is mainly done to analyze noise-test data and to determine source parameters (charge weight, charge depth, shot pattern, sweep parameters), in addition to the preliminary field processing. The field crew may shoot a short 2D test-line, which needs to be processed onsite rather than in the processing centre. In order to save time, these processing activities are usually done by the crew processing geophysicist using the crew's processing facilities, rather than sending the data to the far-away processing centre.

### 7.4.2 The Final Data Processing

Once the shooting parameters are finalized, normal production shooting is started and shot records (recorded on magnetic tapes) are shipped-out to the processing centre to be processed. As it is done with 2D data, processing of 3D data is conducted through a sequence of processing steps. The sequence of 3D

processing-steps may be grouped into four major divisions. These are:

- data re-organization,
- pre-stack processing,
- parameter optimization,
- post-stack processing.

A basic processing sequence including this four-stage processing-procedure is summarized by the flowchart shown in Fig. 7.37. This figure shows a sequence of the four groups of processing steps; data re-organization, pre-stack processing, parameter optimization and post-stack processing. The migration process is shown in two alternative positions. One option (the more common practice in nowadays processing) is the pre-stack time migration (PRSTM) and the other option is the application of post-stack time migration (POSTM). In this sense, migration is considered either part of the pre-processing stage (PRSTM) or part of the post-processing stage (POSTM).

### 7.4.3 3D Data Displays

The ultimate end-result of the processing sequence is a data-volume, which is also, called data box (Fig. 7.38).

The data volume consisting of an amplitude value at the point  $(\mathbf{x}, \mathbf{y}, t)$ , where  $(\mathbf{x})$  and  $(\mathbf{y})$ , are the bin-centre coordinates in the in-line and cross-line directions respectively. The coordinates  $(t)$  is the time value of the trace sample. Three types of displays are usually extracted from the produced data volume: an in-line, cross-line vertical-sections, and horizontal sections (time-slices). At each sample-time, a time-slice can be displayed. Examples of vertical and horizontal sections are shown in Figs. 7.39 and 7.40.

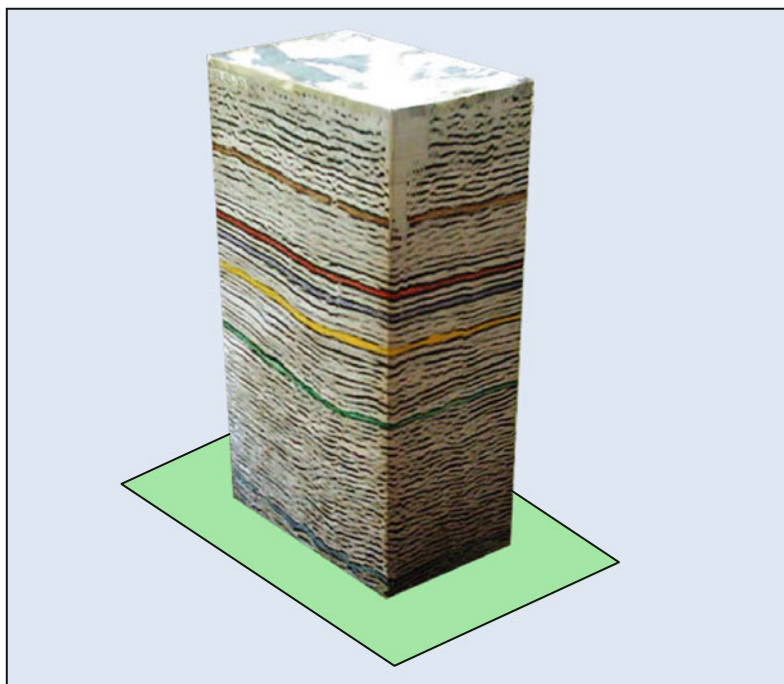


**Fig. 7.38** The 3D data volume obtained from processing of a 3D data-set of an area of (10 by 20) km<sup>2</sup>

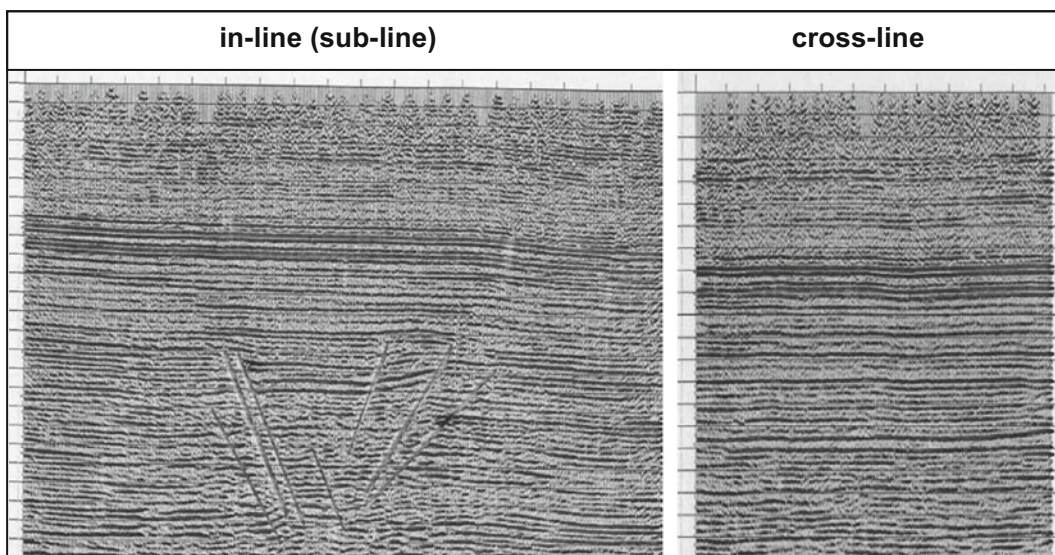


**Fig. 7.39** Vertical sections (*in-line* and *cross-line*) obtained from a 3D data volume

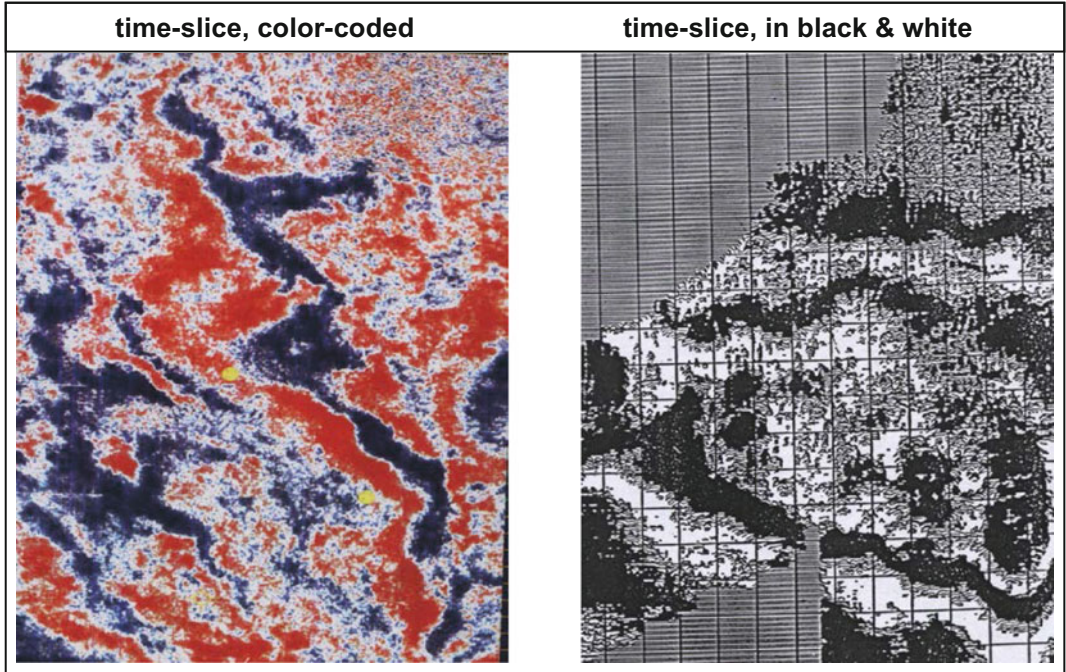


**Fig. 7.40** Time slices obtained from the 3D data volume

A seismic field is created as a result of a sudden mechanical impact that occurs at a point inside a medium. The created packet of energy (called the seismic energy pulse) spreads out from the source zone in all directions. It travels through the medium in such a way that energy moves through the particles of the medium without creating any permanent changes to the medium. Propagation of the generated seismic energy in this way is expressible in terms of a mathematical equation, the (wave-motion equation).

In a seismic reflection exploration that uses impulsive energy-sources, the generated seismic pulse is generally made up of an oscillating energy level that diminishes with time and with travel distance, forming what is normally called the (seismic wavelet). This travelling pulse (the wavelet) can be recorded by placing a seismic detector (seismometer) in, or on the surface of, the medium. The seismic wavelet detected near the source location is normally referred to as the source wavelet (or source signature), and that detected after being reflected from an interface, it is called the reflection wavelet.

In 1952, Massachusetts Institute of Technology, MIT (USA) set up and sponsored a research group, called the Geophysical Analysis Group (GAG) which was in 1953 taken over by a consortium of oil and geophysical companies. This group of scientists “had the responsibility of

finding a way to apply statistical communication theory to the seismic problem” (Enders Robinson 1983, p. 221).

The GAG research activities have resulted in furnishing a way for applying the principles of the communication theory in the analysis of seismic wavelets. In essence, the seismic wavelet is considered as a propagating signal which can be processed using principles of the communication theory in the same way as processing of the electromagnetic signal.

The GAG scientific findings in the late 1950s have set the cornerstone of modern digital processing of the seismic signal (the seismic wavelet).

---

## 8.1 Definition of the Seismic Signal

In general, the travelling seismic wavelet (detected directly, or after being reflected or refracted) is considered to be a travelling signal that bears useful information. The seismic reflection signal, normally representing the particle-vibration velocity, is a function of space and time. The value of the function at any time is defined to be the amplitude (or energy) of the signal. Usually, the seismic signal is presented as a mathematical function that expresses amplitude variation with time (Fig. 8.1).

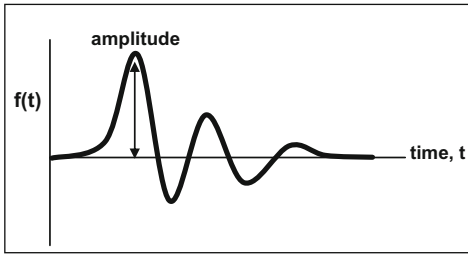


**Fig. 8.1** Seismic signal is represented by plotting the signal amplitude  $f(t)$ , as function of time,  $t$

### 8.1.1 The Seismic Signal Parameters

Treated as a mathematical function, the seismic reflection signal has a number of parameters which define its overall characteristics. These parameters, which are generally changing with travel-time, are:

- Amplitude (signal strength)
- Frequency content
- Energy content
- Propagation velocity
- Onset time
- Duration (signal length)

If the medium, traversed by the seismic signal, is perfectly elastic and homogeneous, the signal will propagate along straight ray-paths with constant velocity and with no changes in its waveform parameters, apart from the wave-spreading effect. In reality, the earth is far from being homogeneous, as it is made up of rock-layers having different physical properties and different geometrical shapes. Geological complexities in both of the structural and stratigraphic nature, incur changes on the seismic wavelet's shape, velocity, and motion direction. The changes are of two types; changes of signal-path geometry (due to interfaces effects)

and signal energy changes (due to physical properties of the medium).

Types of changes can be sorted into three groups according to the zone in the reflection travel-path from source to the receiver. The main types of changing factors are presented in Table 8.1:

It is important to note that each of the factors mentioned in this table, has its own modification-effect (imposed signature) on the travelling seismic signal and what is received, at the end of the source-to-receiver journey is the net resultant of all the effects encountered during that journey. These changes (travel-time and waveform changes) have their own individual imprints (signatures) imposed on the travelling wavelet. These effects form useful messages (information) which can be interpreted to give the subsurface structural and stratigraphic changes. The travelling seismic signal (the seismic wavelet) with the modifications it experiences during its source-to-receiver journey form the basis of its use as an oil exploration tool.

### 8.1.2 The Seismic Signal Spectrum

By using Fourier Transform, it is possible to transform the mathematical function of any signal (as the seismic signal) from its original time-domain function  $f(t)$  to the frequency domain  $F(\omega)$  with no loss of information. In this process the original time domain signal was transformed from amplitude variation with time to amplitude variation with frequency. To clarify the concept let us consider (Fig. 8.2) the two sine waves of different frequencies ( $\omega_1$  and  $\omega_2$ ), and their respective line-spectra drawn at points  $\omega_1$  and  $\omega_2$  on the frequency axis of the spectrum function,  $F(\omega)$ .

**Table 8.1** Changing factors of the seismic reflection signal during its source-to receiver travel-path

Changes in source zone	Changes in ray-path zone	Changes in receiver zone
Source type of energy source	Inelastic attenuation	Receiver detection response
Source coupling	Geometrical spreading	Detector coupling
Near-source geology	Reflection coefficient	Near-receiver geology
Source-generated noise	Wave conversion	Noises and interferences
	Noises and interferences	

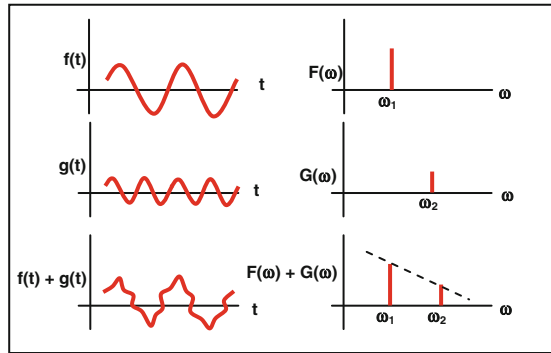


**Fig. 8.2** Concept of the frequency spectrum. The mono-frequency functions,  $f(t)$  and  $g(t)$  have one line spectrum each. Their sum,  $f(t) + g(t)$ , have two-line spectrum

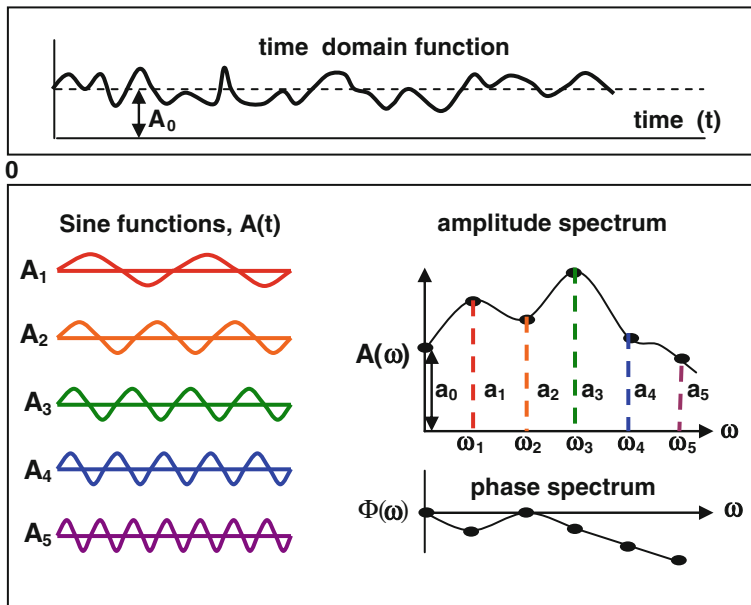


**Fig. 8.3** Pictorial representation of spectrum analysis. The signal (at top of figure) is Fourier-transformed into its frequency components shown as amplitude and phase spectra,  $A(\omega)$  and  $\Phi(\omega)$

This simplified presentation represents a synthesis process by summing two sine functions. The reverse of this process is the spectrum analysis which involves (using Fourier transform) determination of all of the frequency components of a given signal. The complete analysis is to get amplitudes and phase shifts of all frequencies

present in the analyzed signal. Two spectral parts are necessary to completely define the complete signal characteristics. These are the frequency spectrum and the phase spectrum. The two concepts are schematically shown in Fig. 8.3.

The frequency range of the seismic reflection signal is typically (20–60) Hz.

**Table 8.2** Differences between the seismic signal and the radar electromagnetic signal

Signal parameters	Seismic signal	Radar signal
Type of energy	Mechanical energy	Electromagnetic energy
Type of medium	Elastic medium	Empty space
Pulse length	10–30 s (Vibroseis)	$10^{-6}$ s
Velocity	1–5 km/s	$3 \times 10^5$ km/s
Frequency	20–60 Hz	$10^{10}$ Hz
Wavelength	20–500 m	3 cm

### 8.1.3 Comparison with the Radar Signal

Radar signal and seismic signal are similar, in that they both provide the source-to-receiver distance of a far-away object, using the wave-reflection phenomenon. The source signal used in the case of radar is typically a short pulse (of a wide frequency-band), a chirp signal (linearly-changing frequency signal), or a frequency-modulated (FM) signal. The radar function is based on two main types of measurements; the travel-time and Doppler-effect measurements. The Doppler Effect (variation of frequency with target motion) is made use of, in velocity measurement. The common feature between radar operation and seismic reflection technique is that both of them use the reflection travel-time measurement. Naturally, Doppler Effect has no application in seismic reflection operation.

The main differences between the seismic signal and the electromagnetic signal used by radar are summarized in Table 8.2.

This table shows that the parameters of the seismic signal are dispersed over a wide range of values, compared with those of the radar signal in which the parameter has only one value. This is because the radar signal is travelling through a medium which is far more homogeneous than that traversed by the seismic signal.

### 8.1.4 The Seismic Reflection-Signal Changes

The seismic reflection wavelet is, in fact, the source pulse after being modified and distorted as a result of the interactions with the travel-path

conditions. The manner and severity of these changes depend largely on:

- Geometrical shape of the traversed layers (structural changes)
- Physical properties of the layers (stratigraphic changes)
- Fluid content like water, oil, and gas (reservoir conditions)

The seismic wavelet is therefore considered as a message-bearing record of the changes which are coded in the wavelet spectrum-parameters (amplitude, frequency, and phase). In the time-domain language we say that we have waveform-deformation whereas in the frequency domain this is described as spectral-deformation.

Compared with the source function, and due to these affecting factors, the detected reflection signal becomes lower amplitude, lower frequency, extended in shape, noisy, and time-shifted with respect to its initial origin time. Mathematically, these changes can be classified into the following four types of processes: superposition, scaling, filtering, and time shifting.

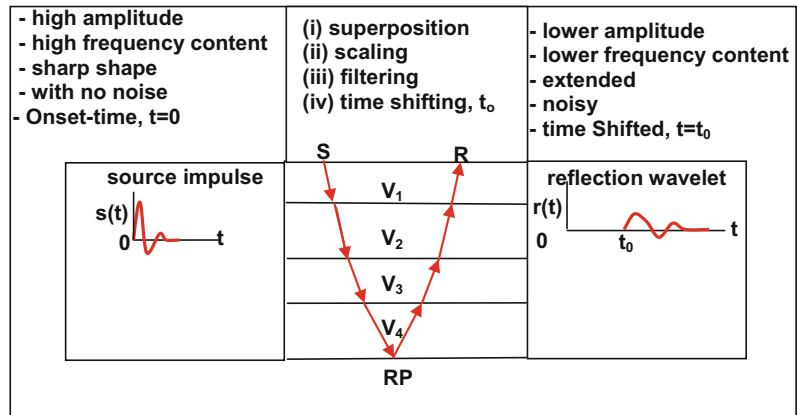
#### (i) *Superposition*

Interaction of the reflection seismic signal with noises and other interfering events (such as coherent and incoherent noise, refractions and diffractions) is a simple superposition process. The received signal is resulting from additions of all of these interferences, bringing about distortions to the wavelet geometrical shape.

#### (ii) *Scaling*

This is an arithmetic multiplication process, where the reflection wavelet is multiplied by a constant scaling factor, similar to the effect of gain-application. The effect

**Fig. 8.4** Summary of the physical changes of the reflection signal as it travels from the source point (*S*) to the detector point (*R*), via the reflection point (*RP*)



does not deform the signal but only change its size. Examples of this type of effect are the effect of the geometrical spreading and the reflection coefficient which are independent of frequency. This means that they incur no wavelet shape deformation. A scaling effect can, under certain conditions, reverse the wavelet polarity. This happens when the scalar is of negative value, as in negative reflection coefficient.

(iii) *Filtering*

Frequency filtering can be considered as a frequency selective scaling. A typical example of this type of effect is the earth high-cut filter, which is operating on the seismic wavelet attenuation throughout its travel-path. Any effect that is frequency-dependent (as the earth filtering) incurs shape-deformation to the propagating seismic wavelet. The deformation severity depends on the type of lithology and fluid-content of the geological formations traversed by the seismic signal. Being an analogue-type, the earth filtering effect introduces phase shift to the frequency components of the seismic signal.

(iv) *Time-Shifting*

The source impulse takes time to reach the detector. This is the total reflection travel-time which is depending upon the depth of the reflector as well as on the

detector offset from the source. Time-shifting becomes a deformation factor when reflectors are so close to each other that wavelet-arrivals overlap causing distortions to the wavelets and loss of the resolution of the reflection events. Phase shifts are the time shifts of the individual frequency components which, in general, take place in frequency-filtering actions. These changes are summarized in Fig. 8.4.

## 8.2 The Seismic Trace

A seismic pulse incident at an interface is partly reflected and partly transmitted into the following layer. In a multi-layer medium this is repeated at each interface present in the way of the advancing wave. A detector placed on the surface receives sequentially, the reflected wavelets, at time-intervals depending on the depths of the reflectors. The source pulse reaches the detector after being affected by the various types of modifications (as discussed above) including the process of reflection in which amplitude and polarity are governed by the reflection coefficient of the reflector. From each reflector a wavelet representing the source wavelet, scaled by the reflection coefficient, will arrive at the detection point. Thus, a series of such wavelets, each of which is shifted in time with respect to the preceding wavelet, are superimposed on each other to form a record which is the (seismic trace).

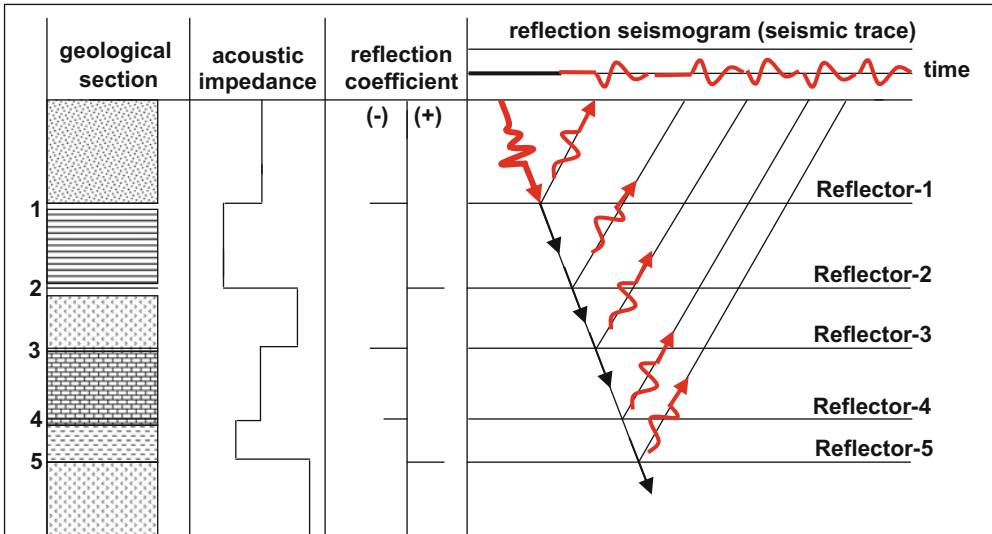


Fig. 8.5 Sketch of the convolutional model of the seismic trace (Alsadi 1980, p. 192)

### 8.2.1 The Convolutional Model of the Seismic Trace

The process, which involves multiplication of the source wavelet by the reflection coefficient, time shifting and superposition, is similar to the mathematical convolution process taking place between the source function, in this case, and the reflection-coefficient series. This is the construction mechanism model which is accepted by geophysicists for the formation of the seismic trace. This model (called the convolutional model) is applied in working out synthetic seismograms (Fig. 8.5).

The concept that the seismic signal can be represented as the convolution of the source wavelet with the earth reflectivity-series was developed by Robinson (1954). This approach (based on the communication theory) can be represented by the following mathematical form (called the seismic-trace convolutional-model equation):

where,

- f(t):** recorded seismic trace
- s(t):** seismic source wavelet
- p(t):** earth filtering effect
- r(t):** earth reflectivity function (series of the reflection coefficients)
- b(t):** detector and recording equipment response
- g(t):** geometrical spreading effect (scaling effect)
- n(t):** noises

It is to be noted here that convolution process is represented by (\*), whereas the effect of geometrical spreading, **g(t)**, is purely scaling effect, and noises, **n(t)**, has an additive effect (Fig. 8.6).

Typically, a seismic trace recorded in a seismic reflection survey, is 6-s long, digitally recorded at 2 ms sampling period (Fig. 8.7).

$$f(t) = s(t) * p(t) * r(t) * b(t) \cdot g(t) + n(t)$$

**Fig. 8.6** Elements entering in the seismic trace convolutional model

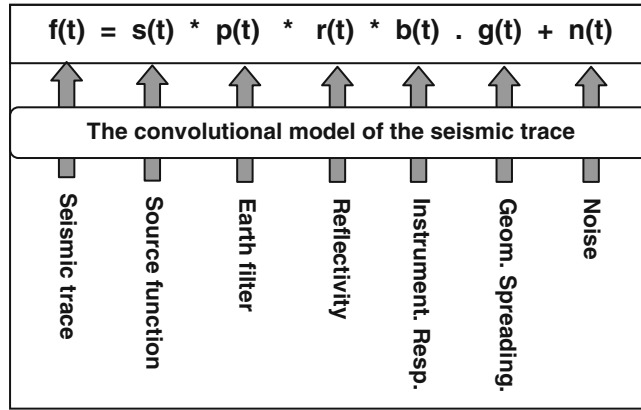
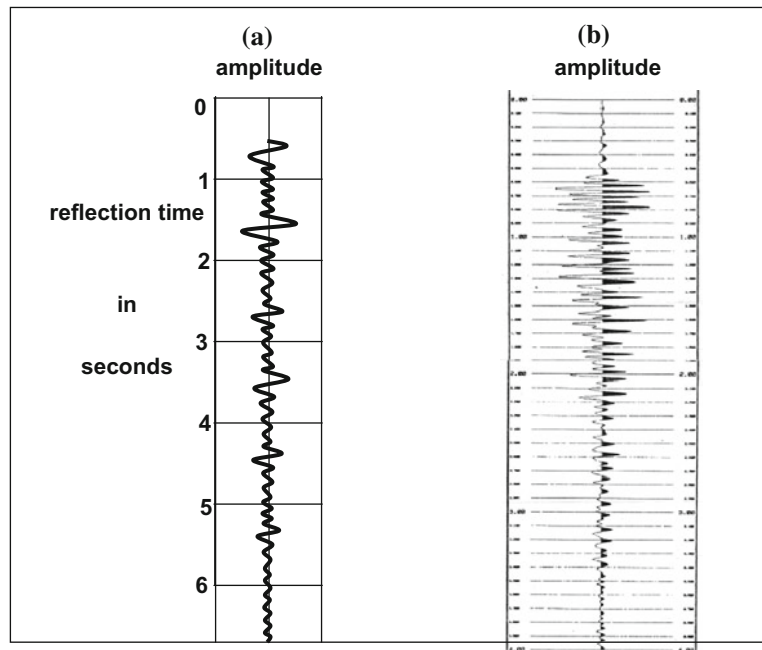


**Fig. 8.7** The seismic reflection trace. **a** Pictorial representation. **b** Actual seismic trace from a dynamite source-energy



### 8.2.2 The Synthetic Seismogram

A direct application of the concept of the convolutional model is in constructing an artificial seismic trace, commonly known as the (synthetic seismogram). The basic requirements for this process are the source wavelet and the reflectivity series, which in turn, require the distribution with depth of the layers' acoustic impedances.

The earth layering model is normally obtained from a drilled exploration-well. The well logging data furnish both of the velocity (from the sonic log) and density (from density log). From these two logs, the acoustic impedance of each layer is calculated, and hence the reflection coefficients of the layer boundaries are determined. This is the reflectivity series which will be in the form of values, ranging between (-1) and (+1),

**Fig. 8.8** Pictorial representation of the principle of computing synthetic seismograms

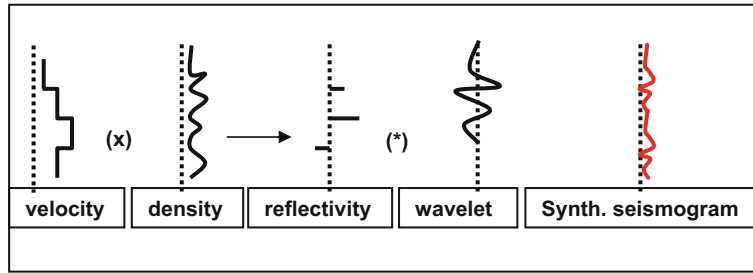
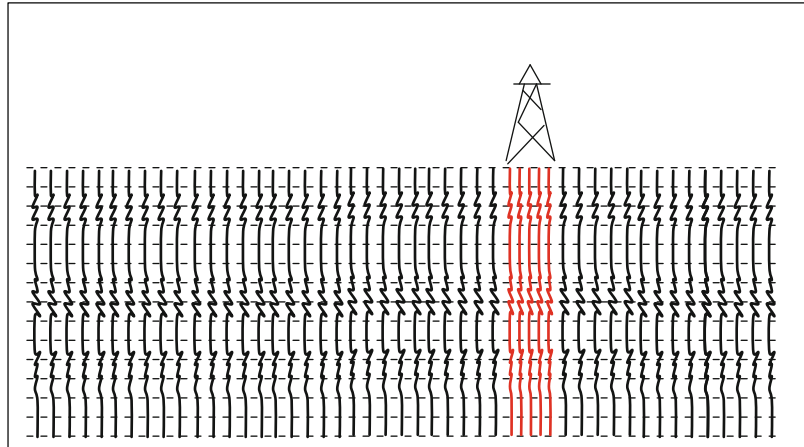


**Fig. 8.9** Application of the synthetic seismogram, which is duplicated and superimposed on the seismic stack section at the well location



representing the reflection coefficients of all of the interfaces (layer-boundaries) penetrated by the well. Convolution of the source wavelet (assumed or obtained from a near-by shot-record) with the reflectivity series, gives the synthetic seismogram. This computation method expresses the convolutional model according to which the real seismic trace is assumed to have taken place in real time seismic reflection recording.

In display of the computed synthetic seismogram, the time scale must be doubled in order to match the seismic section in which the time is a two-way vertical time. A schematic representation of the process is shown by Fig. 8.8.

Interpreters are usually provided with synthetic seismograms both with and without multiples to help in sorting out the multiple-reflections, if any.

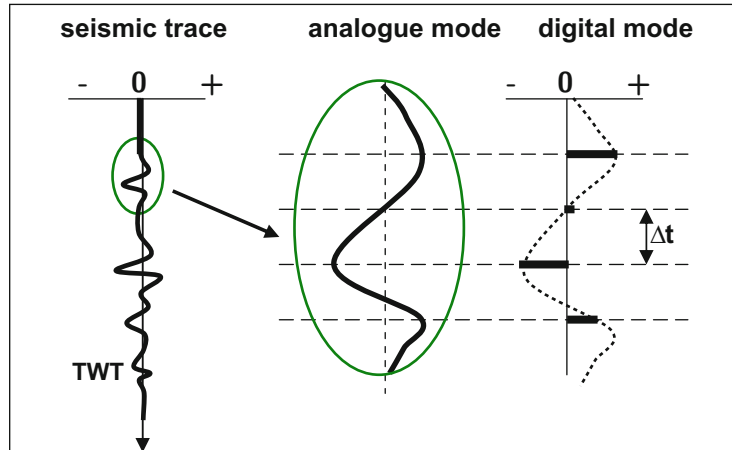
The synthetic seismogram is now considered as an indispensable tool in the hand of the interpreters to tie the seismic reflection images

with the real geological section. It is normally displayed (using several duplicated synthetic traces) superimposed on the seismic stack section at the well-location. Main purpose is to attach the stratigraphic identities for the reflection events diagnosed on the seismic stack section (Fig. 8.9).

### 8.2.3 The Digital Seismic Trace

The seismic trace received at the detection point is represented as a continuous amplitude variation with recording time. At this point it is an analogue function expressing the seismic amplitude as function of time. The recording-system transforms the amplitude-versus-time function from its analogue form to digital form, and gets it stored on the magnetic tape as a digital function (sequence of sample-values at regular time intervals,  $\Delta t$ ), where the sampling period ( $\Delta t$ ) is normally chosen to be 2 ms (Fig. 8.10).

**Fig. 8.10** The digital seismic trace, made up of a series of sample values recorded at regular time interval, which is the sampling period ( $\Delta t$ )



With the digital mode, the seismic trace storage and processing become feasible to carry out by electronic digital computation systems.

### 8.3.1 Definition of the Seismic Wavelet

A wavelet is defined as a transient signal with a definite time origin. It is characterized by two properties; it has a definite onset time and it has a finite energy (Robinson 1983, p. 128). These two characters implies that the wavelet is one-sided entity (wavelet values are zero before onset time), and it is transient with its energy diminishing after onset time. Ricker wavelet (named after Norman Ricker 1897–1980) is a special type of a theoretically-computed zero-phase wavelet commonly used in seismic modeling studies. In particular, Ricker wavelet is used in the seismogram synthesis, by convolving it with the reflectivity function, to produce the now-accepted convolutional seismic trace model (Robinson 1983, p. 224).

## 8.3 The Wavelet Concept

The seismic pulse created by a mechanical shock (seismic source) is a wavelet that is transmitted through the earth medium and detected by the receiver geophone-group and then recorded by the recording system. At the time it is recorded, the wavelet is no longer a short pulse (source impulse) as it was created at the source location, but an extended wavelet made-up of few cycles, weakened pulse having energy diminishing to zero level within a short time (tens of milliseconds) (Fig. 8.11).

**Fig. 8.11** The seismic wavelet function of travel-time,  $f(t)$ . Its value represents the particle vibration velocity in land surveys, and hydrostatic pressure in marine surveys. **a** is the source wavelet and **b** is the recorded weakened wavelet

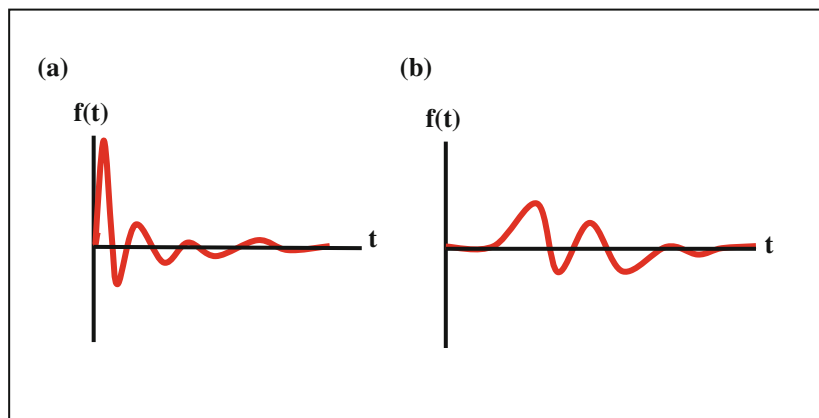
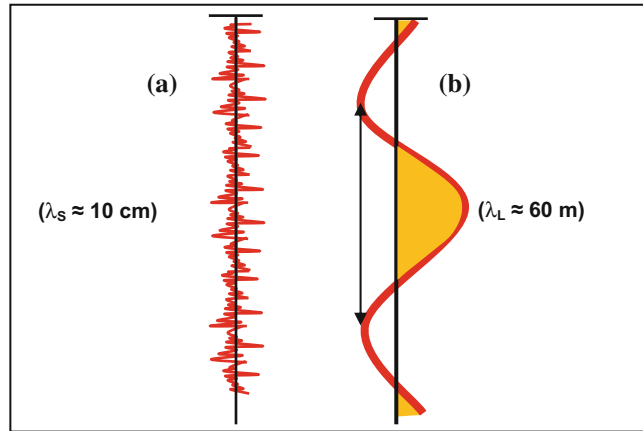


**Fig. 8.12** Different types of seismic wavelets.  
**a** high-frequency (short wavelength,  $\lambda_S$ ) as that used in sonic logging, and  
**b** low-frequency (long wavelength,  $\lambda_L$ ) wavelet as that used in the normal seismic reflection surveying



The concept may be extended to cover the Vibroseis source function which is not impulsive source, but long wavelet (about 20–50 s), reduced to the equivalent impulsive form in the processing stage. The seismic wavelet normally detected by geophones in land surveying, expresses the particle vibration velocity. It is, typically, made up of few cycles with duration of about (40–50) ms. In a medium of velocity of 2500 m/s the wavelet dominant wavelength for frequency of 40 Hz, is about 60 m. The corresponding wavelength for 20 kHz (as used in well-logging), it will be around 10 cm. Thus, one can conceive the difference between the wavelets shown by well-logs and those displayed by normal seismic traces (Fig. 8.12).

### 8.3.2 Energy and Delay Properties of Wavelets

The wavelet energy is expressed by its energy cumulative function. For a digital wavelet of sample values ( $\mathbf{a}_i$ ), its energy content is expressed as the sum of the squares of its sample-values (amplitude values). Thus, for a wavelet made up of three samples, say, ( $\mathbf{a}_0, \mathbf{a}_1, \mathbf{a}_2$ ), its total energy ( $\mathbf{E}_T$ ) is defined to be the sum of the squares of the wavelet sample values, that is:

$$\mathbf{E}_T = (\mathbf{a}_0)^2 + (\mathbf{a}_1)^2 + (\mathbf{a}_2)^2$$

The energy build-up function furnishes the means for defining the delay properties of wavelets. A wavelet that has its energy concentrated at the front of the wavelet is defined to be a minimum-delay wavelet, while a wavelet that has its energy concentrated at the end is defined to be a maximum-delay wavelet. According to this concept, the seismic source wavelet is a minimum delay wavelet. More elaborate treatment of this concept and its applications are found in (Robinson 1967).

## 8.4 Sampling and the Digital Function

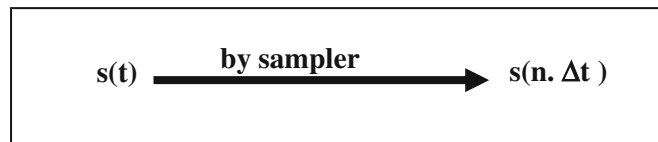
In nature, all geophysical functions are of analogue mode. These functions can be converted into digital by a process called digitization or sampling. In seismic surveying this is done by the recording system as we have explained earlier. The analogue-to-digital conversion (A-D conversion) consists of two steps; the quantization (measuring the function values at regular intervals) and then conversion into digital numbers. This process constitutes what is commonly known, the sampling process.

### 8.4.1 The Digital Function

Functions of geophysical signals can be represented either as continuous function (analogue function) in which the function is defined at all of the points along the abscissa or defined at discrete points, normally regularly spaced values (digital function). Considering time-domain functions, the analogue function is normally quoted as  $s(t)$ , and the digital function as  $s(n \cdot \Delta t)$ , where  $\Delta t$  is the sample spacing along the time-axis, normally called the sampling period. The two forms of functions are shown in Fig. 8.13.

### 8.4.2 The Sampling Process

The process of converting an analogue function into digital form (A-D conversion) is normally referred to as (digitization or sampling) process. It involves two-steps; sample definition followed by quantization and coding in which the sample value is determined and converted into digital number. The output of the sampling process is then stored on a suitable digital storage device or entered in a certain digital data processing operation. In the language of mathematics, the A-D process is represented as follows:



The main elements which define the digital function are the function values (sample values), the sample interval (sampling period), and sampling frequency which is reciprocal of the sampling period. For example, seismic traces are normally recorded at 2-ms sampling period, and processed at 4-ms sampling period. The corresponding sampling frequencies are 500 and 250 Hz respectively.

where,  $(\Delta t)$  is the sampling period and  $(n)$ , the sample order number. The sample value is given by the function value,  $s(n \cdot \Delta t)$ .

The reverse process, digital-to-analogue (D-A) conversion, can be carried out by one of the methods (staircase approximation, linear interpolation, or by curve fitting), as shown in Fig. 8.14.

Another more elaborate method based on  $(\sin x/x)$  computations can be applied for the conversion which is based on summing weighted and shifted  $(\sin c)$  functions (Báth 1974, p. 146).

**Fig. 8.13** Definition of the analogue and the digital functions

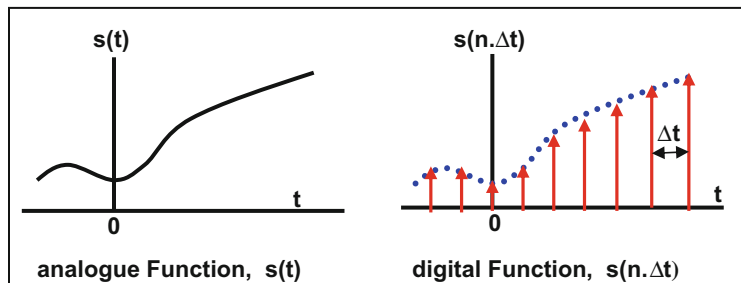
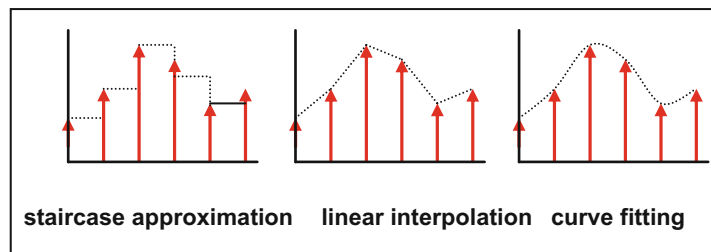


**Fig. 8.14** Means of converting a digital function to analogue mode (D-A conversion)



### 8.4.3 Representation Methods of the Digital Function

A digital function can be represented in one of the following forms:

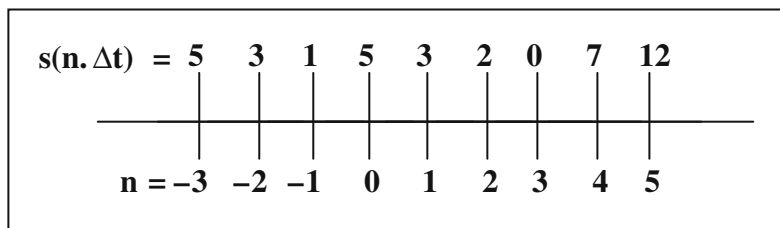
(i) **Functional Representation**

It is represented as a mathematical digital function. Example: 4-sample function:

$$\begin{aligned}
 s(n.\Delta t) &= +17 \text{ for } n = 1, 4 \\
 &= -15 \text{ for } n = 2, 3 \\
 &= 0 \text{ for } n = \text{elsewhere}
 \end{aligned}$$

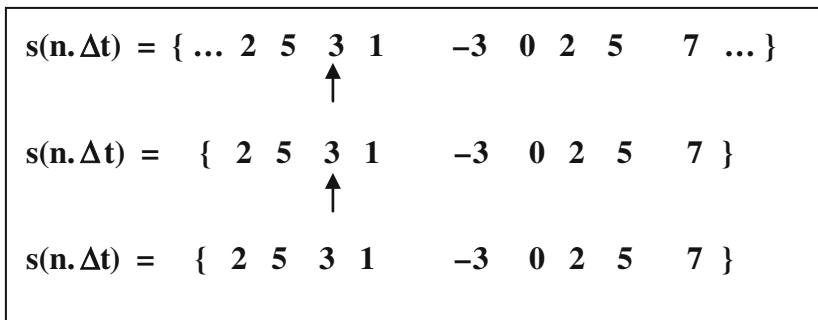
(ii) **Tabular Representation**

It is represented as a table of ordered values. Example: 9-sample function:



(iii) **Time-series Representation**

In this case, the sample at zero time is indicated by an arrow. If the arrow is not present it means that the first sample is the zero time. Putting dots (...) at the beginning and at the end of a series implies that the series is an infinite series.



(iv) **Z-transform Representation**

The z-transform is a mathematical transformation process with which a time series is expressed as a polynomial in (z). Thus, the z-transform of a digital function represented by the time series  $(a_0, a_1, a_2, \dots, a_N)$  is  $(a_0 + a_1 z + a_2 z^2 + a_3 z^3 + \dots + a_N z^N)$ , that is:



The z-transform of a digital function is a polynomial in (z) where the constant coefficients are the sample values of the digital function. The power of (z) represents the order-number (sequence number) of the sample. The z-transform polynomial  $f(z)$  of a time series ( $a_0, a_1, a_2, \dots, a_N$ ) can be written in a compact form:

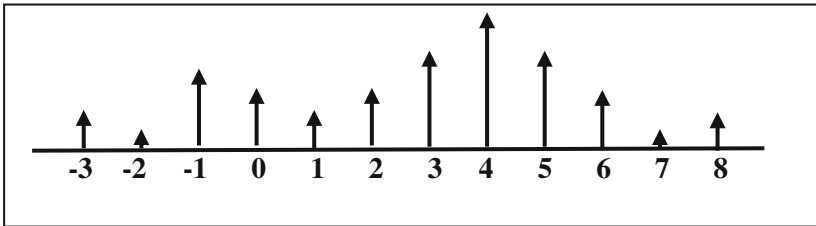
$$f(z) = \sum_{n=0}^N a_n z^n$$

where ( $n = 0, 1, 2, \dots, N$ ).

As an example, the z-transform of the digital wavelet  $a_n = \{3, 2, -1, 4, 7\}$  is given by  $f(z)$ , where:  $f(z) = 3 + 2z - z^2 + 4z^3 + 7z^4$ .

(v) **Graphical Representation**

Each sample is represented by an arrow of length proportional to the sample value.



function can be considered as a digital function sampled at zero sampling-period.

It turns out that it is possible to safely sample a signal (with no loss of information) if the digitization process is implemented with the optimum sampling period. A theorem is found which mathematically connects that optimum sampling period with the cut-off frequency of the signal. This is the Sampling Theorem.

**8.5.1 The Sampling Theorem**

This theorem (also called Shannon theorem) states that, it is possible to completely recover the original analogue function from its digital form if the sampling period ( $\Delta t$ ) is less than half of the smallest period ( $\tau$ ) present in that function. This implies that, the maximum sampling period applied, which incurs no loss in information, is

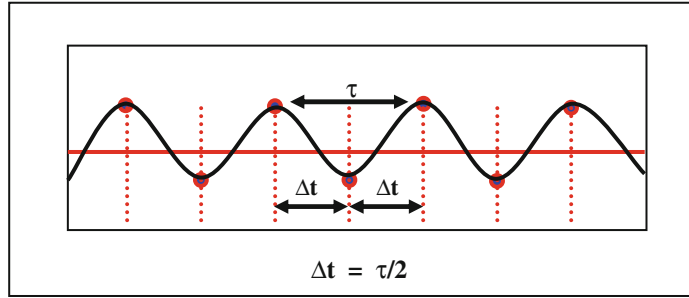
**8.5 The Sampling Theorem and Aliasing**

Digitization of a signal implies reading the signal at isolated points which means that the information of the signal in between these points is permanently lost. The amount of information lost is naturally greater as the sampling period is larger. In the sampling process, the shortest the sampling period, the better is the recovery of the details of the function. In fact, the analogue

that sampling which produces at least two samples per period of the period-component having the shortest period in that function. The concept is shown in Fig. 8.15.

In the frequency-domain language the theorem statement can be rephrased as, it is possible to completely recover the original analogue function from its digital form if the sampling frequency ( $f_s$ ) is greater than twice of the highest (maximum) frequency ( $f_m$ ) present in the original

**Fig. 8.15** The mathematical expression ( $\Delta t = \tau/2$ ), the condition required by the Sampling Theorem



analogue function. The highest frequency is also called the cut-off frequency. The complete-recovery condition can be mathematically represented by:

$$\Delta t \leq \tau/2$$

or (in terms of frequency),

$$f_s \geq 2f_m$$

There is another term which is intensively used in connection with signal's sampling, called Folding frequency or Nyquist Frequency, ( $f_N$ ), which is defined to be half the sampling frequency, that is:

$$f_N = f_s/2 = 1/2\Delta t$$

With the introduction of the Nyquist Frequency (also called folding frequency), the condition in the sampling theorem can be re-stated as (For complete recovery of the original analogue function from its digital form, the Nyquist frequency must be greater than the highest frequency present in the original signal).

The important conclusion extracted from the Sampling Theorem is that, Nyquist frequency, used in sampling of an analogue signal, must be equal or greater than the highest frequency present in that signal, that is:

$$f_N \geq f_m$$

If the sampling process is too coarse (too-large sampling periods, too-low Nyquist frequency), then the output will have certain type of distortion, normally referred to as Aliasing.

### 8.5.2 The Aliasing Phenomenon

There are three categories of sampling; fine sampling, critical sampling, and coarse sampling, depending on the magnitude of the Nyquist frequency ( $f_N$ ) relative to the cut-off frequency (maximum frequency component,  $f_m$ ) present in the original analogue signal. The categories are:

(i) **Fine Sampling ( $f_N > f_m$ )**

In this case high sampling frequency is applied where ( $f_N > f_m$ ) complying with the sampling theorem and complete recovery of the original analogue signal can be obtained, with no distortions.

(ii) **Critical Sampling ( $f_N = f_m$ )**

As in the fine-sampling case, no distortions occur in this case. It is critical, in the sense that the applied sampling frequency sets the marginal limit of the Nyquist frequency below which distortion (frequency aliasing) shall take place.

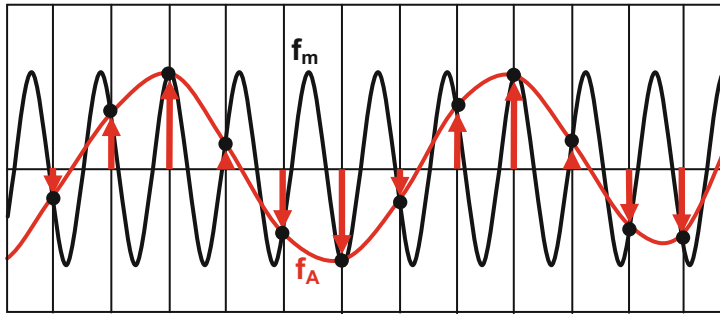


**Fig. 8.16** The aliasing phenomenon. Input frequency ( $f_{in}$ ) = 100 Hz, Sampling frequency = 120 Hz, Nyquist Frequency = 60 Hz, Aliasing frequency ( $f_A$ ) = 20 Hz

(iii) **Coarse Sampling ( $f_N < f_m$ )**

With coarse sampling (or under-sampling, as it is sometimes called), those components which are of greater frequencies than Nyquist frequency will appear as lower frequencies in the sampling output. This phenomenon, which occurs only when coarse sampling is applied, that is when ( $f_N < f_m$ ), is called (aliasing). An example of an aliasing case is shown in Fig. 8.16.

frequency ( $f_N - \Delta f$ ). This means that if the input to the sampling process is ( $f_N + \Delta f$ ), the output frequency will be ( $f_N - \Delta f$ ). The two frequencies ( $f_N + \Delta f$ ) and ( $f_N - \Delta f$ ) are called aliases of each other (Sheriff 1973, p. 4). Thus, for example, a 100-Hz signal is sampled at sampling frequency of 120 Hz ( $f_N = 60$  Hz), then the output will be:  $60 - (100 - 60) = 20$  Hz, which is the aliased frequency (Fig. 8.16).

**8.5.3 The Aliasing Frequency Computation**

In any sampling process, the frequency components in the input analogue function which are higher than Nyquist frequency will appear at the sampler output as false components (aliased components) of frequencies lower than input frequency. An input frequency component ( $f_m$ ) higher than Nyquist frequency by ( $\Delta f$ ) will appear to the sampling system, as the lower

The general rule governing any sampler input-output relationship is that any frequency component higher than the Nyquist frequency ( $f_N$ ), present in the signal prior to sampling, is outputted as alias frequency. The sampling frequency ( $f_s$ ), or the Nyquist frequency  $f_N (=f_s/2)$ , is the deciding factor for the possibility of occurrence of aliasing. Cases for the fine, critical, and coarse sampling of an input frequency of (125 Hz) are presented in Table 8.3.

In Table 8.3 one can notice that, in the first two cases (belonging to the case of fine-sampling), the Nyquist frequency is higher than the input frequency and hence no aliasing is

**Table 8.3** Cases for fine, critical, and coarse sampling of an input frequency of (125 Hz)

	Input $f_m$ (Hz)	Sampling freq. (Period)	Nyquist freq. (Hz)	Output freq. (Hz)	Output status
1	125	500 Hz (2 ms)	250	125	no aliasing
2	125	333 Hz (3 ms)	166.7	125	no aliasing
3	125	250 Hz (4 ms)	125	125	no aliasing
4	125	200 Hz (5 ms)	100	75	with aliasing
5	125	166.6 Hz (6 ms)	83.3	41.6	with aliasing
6	125	142.8 Hz (7 ms)	71.4	17.8	with aliasing
7	125	125 Hz (8 ms)	62.5	0.0	with aliasing

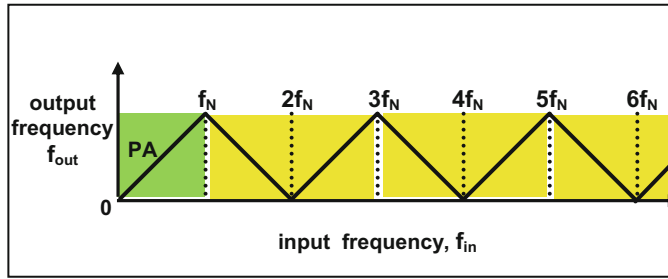


**Fig. 8.17** Input-output relationship, in a sampling process. The zone up to the Nyquist frequency ( $f_N$ ) is the principal-aliases zone (PA) in which no aliasing occurs

taking place. In the third case (the critical-sampling case), Nyquist frequency is equal to the input frequency and again no aliasing occurs. In cases (4, 5, and 6) Nyquist frequency is less than the input frequency, hence aliasing takes place. In the last case (case 7) the difference ( $\Delta f$ ) has reached its maximum value which is equal to the Nyquist value giving an output of zero-frequency.

To give a quantitative measure for the output frequency, use is made of the periodic linear relation connecting the input frequency ( $f_{in}$ ) and

applied with no aliasing effect. An input frequency, lower than the Nyquist frequency, will be outputted with no aliasing effect.

The periodic linear relation of the sampler input-output function, shown in Fig. 8.17, can be used in deriving a general formula that can be used to calculate the output aliased frequency, given the input frequency and the sampling (or Nyquist) frequency. With reference to this figure it can be shown that the output aliased frequency ( $f_{out}$ ) is related to the input frequency ( $f_{in}$ ) by the following relationship:

$$f_{out} = |f_{in} - [k + \frac{1}{2}\{1 - (-1)^k\}]f_N|$$

where,

$$k \text{ is integer} = \lfloor f_{in}/f_N \rfloor$$

output frequency ( $f_{out}$ ), as shown in Kanasewich (1973, p. 89). Because of the feature that the spectrum-part above the Nyquist frequency can be folded back about the Nyquist frequency, aliasing is sometimes called (folding) and the aliased frequency, called folding frequency. The ( $f_{in} - f_{out}$ ) relation is re-produced in Fig. 8.17.

This figure is helpful in determining the input-output relation for any sampling process, once the sampling frequency ( $f_s$ ), and hence, the Nyquist frequency ( $f_N$ ) is known. In the zone ( $0 - f_N$ ), the output frequency ( $f_{out}$ ) is the same as the input frequency. This region of the spectrum, called the principal aliases section, marks the limits of the sampling frequencies which can be

The integer ( $k$ ) is calculated from “floor truncation” of ( $f_{in}/f_N$ ), which is symbolically represented as shown above, that is,  $k = \lfloor f_{in}/f_N \rfloor$

For application, let us find the output aliased frequency for the input frequency, ( $f_{in} = 782$  Hz), sampled at 2-ms sampling period, i.e. at sampling frequency ( $f_s = 1/0.002 = 500$  Hz). The Nyquist frequency,  $f_N = 500/2 = 250$  Hz, and the integer ( $k$ ) is obtained from “truncation” of ( $f_{in}/f_N = 782/250 = 3$ ), hence,  $f_{out} = |782 - [3 + \frac{1}{2}\{1 - (-1)^3\}] \times 250| = 218$  Hz. Similarly, it is possible to calculate the aliased frequency of any other input sampled signal having frequency exceeding the Nyquist frequency. As examples

for this method of calculation, let us work out the aliased frequencies for the input frequencies ( $f_{in} = 457, 557, 957, 1957$ ) Hz, each of which is sampled at 2 ms sampling period. The output aliased frequencies for any one of these frequencies will be ( $f_{out} = 43$ ) Hz.

### 8.5.4 Effect of Sampling on Signal Spectrum

The direct effect of the sampling process on the frequency spectrum of a signal is generation of repeated spectrum-replicas of the original analogue signal. Theoretical computations have proved that Fourier transform of a digital function is itself periodic with repetition interval equal to the sampling frequency used in the sampling process (Kansewich 1973; Kulhanek 1976). Thus, after sampling of an analogue signal, its spectrum gets repeated over the frequency axis at regular spacing which is equal to the sampling frequency ( $1/\Delta t$ ), where ( $\Delta t$ ) is the sampling period.

The lower the sampling frequency the smaller the spacing becomes. With too-low sampling frequency (too large  $\Delta t$ ), the spectrum spacing gets smaller and when Nyquist frequency becomes less than the cut-off frequency of the signal ( $f_N < f_m$ ), the repeated spectra overlap and spectrum distortion occurs.

The spectrum behavior caused as a result of digitization is shown in Fig. 8.18.

### 8.5.5 Aliasing in the Frequency Domain

The analogue function can be looked upon as a digital function sampled at zero-sampling period, which will have an infinitely-long spectral repetition cycle. This is equivalent to saying that its spectrum is of non-repetitive nature in case of an analogue signal. When the analogue is converted into digital form the amplitude spectrum is repeated over the frequency axis at repetition-spacing equal to the sampling frequency ( $f_s$ ). The aliasing problem occurs when the cut-off frequency ( $f_m$ ) of the analogue signal exceeds that of the Nyquist frequency ( $f_N$ ), that is when ( $f_m > f_N$ ). In this case, the time-domain aliasing becomes spectrum overlapping in the frequency domain with the consequence of spectrum distortion due to the resulting spectrum-interference. Aliasing, in the frequency domain, is, for this reason, called spectrum contamination (Báth 1974, pp. 148–151).

The important point here is that when the input analogue signal contains frequency components higher than the Nyquist frequency ( $f_m > f_N$ ), these high frequencies will fold over and add to those frequencies existing below the Nyquist frequency. The outcome of the process in this case is spectrum distortion in the overlap zone as shown in Fig. 8.19.

**Fig. 8.18** Digitizing effect on signal spectrum: Generation of repeated spectrum-replicas at ( $1/\Delta t$ ) spacing along the frequency axis

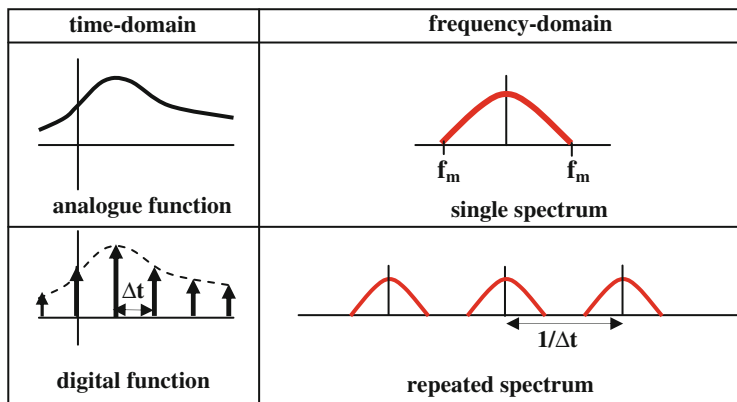
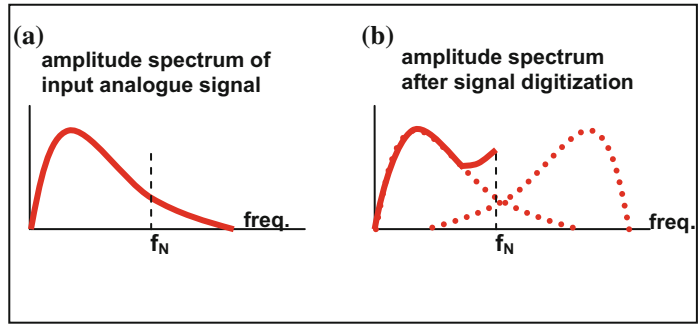


**Fig. 8.19** Spectrum distortions resulting from aliasing effect



**8.5.6 The Remedy for the Aliasing Effect**

To avoid aliasing and its distortion consequences a procedure should be taken such that the condition ( $f_N > f_m$ ) is restored. To achieve this state, one can either delete those frequencies which are greater than Nyquist frequency prior to the digitization process, or increase the sampling frequency in such a way as to get a Nyquist frequency of greater value than the cut-off frequency of the original analogue signal.

In practice this is done by application of a suitable high-cut filter (usually referred to as anti-alias filter), to the input seismic data prior to the sampling process. In effect, the application of the anti-alias filter makes the cut-off frequency of the input analogue signal, lower

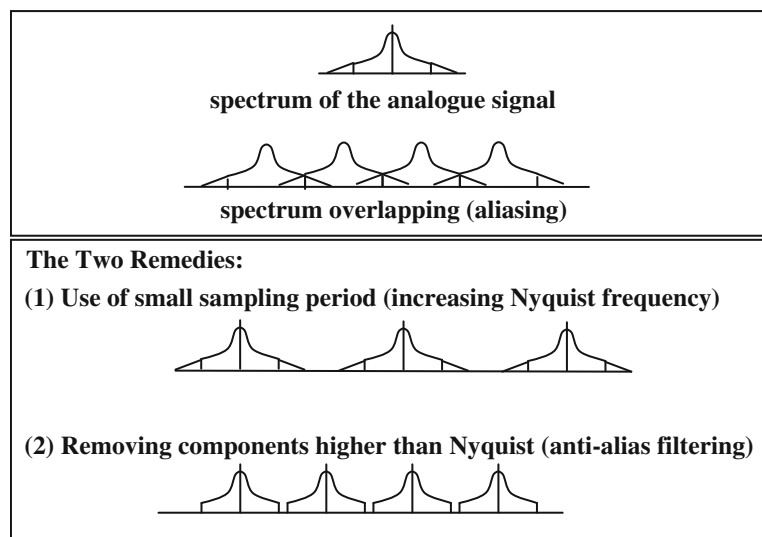
than the Nyquist value, and hence, aliasing is avoided.

In summary, in order to avoid aliasing, there are two alternative methods:

- (i) Applying higher sampling frequency (small sampling period) up to the value with which the Nyquist frequency becomes greater than the cut-off frequency of the input analogue signal.
- (ii) Applying a high cut filter (the anti-alias filter) to remove those high frequencies (from the original analogue signal) which are higher than the Nyquist frequency before starting the sampling process. The two methods are explained in (Fig. 8.20).

In seismic reflection data-recording, the sampling period is normally set at 2 ms value. This

**Fig. 8.20** The two methods used as remedies for the aliasing effect



makes the Nyquist frequency to be 250 Hz. This means that with this Nyquist value, no aliasing effect is expected since the maximum frequency (signal cut-off frequency) is expected to be far below (250 Hz). However, all recording systems are equipped with the anti-aliasing filter that can be applied when it is required. The anti-aliasing filter is normally applied whenever re-sampling of the data is carried out. Very often, in seismic data processing, the recorded digital data is re-sampled from 2 to 4 ms sampling period for economic motives.

### 8.6 Signal Resolution and Resolution Power

Resolution is defined as the ability of distinguishing individual objects gathered to gather in one group, or the details of shape changes of an irregularly shaped object. In the field of seismic exploration, the seismic resolution is the ability of recognizing two adjacent seismic events as distinct two events and not as one blurred event.

Resolution power can be measured by the minimum separation distance between two seismic events that can be resolved as two distinct features on the seismic section. Obviously the sharper the reflection wavelet, and higher signal-to-noise ratio, the better the resolution power will be. The term (resolution power) is used to imply ability of detecting and bringing to vision a certain seismic event

In seismic work, we are concerned with two types of resolutions of seismic reflection events:

vertical resolution and horizontal resolution (explained here-below).

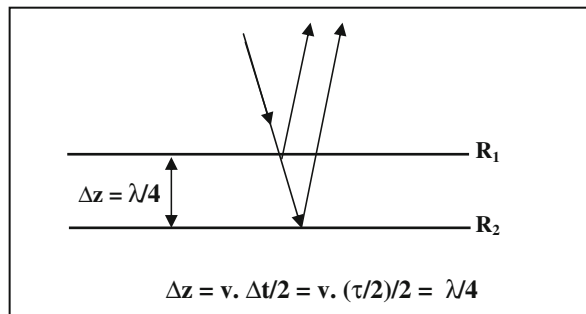
#### 8.6.1 Vertical Resolution of Seismic Signals

Vertical resolution of seismic reflection events, is defined as the minimum vertical distance between two interfaces that give two distinct reflection events on a seismic section. It is basically governed by the wavelength of the seismic signal. The shorter the wavelength (i.e. the higher the frequency) the greater the vertical resolution.

In addition to the frequency factor, depth and reflector spacing have significant effects on the resolution. The vertical resolution is governed by the ratio of the depth separation-distance of the reflectors ( $\Delta z$ ) to the wavelength ( $\lambda$ ) of the incident seismic signal. The lowest limit (resolution limit) of this ratio; ( $\Delta z / \lambda$ ) is found to be (1/4) (Sheriff and Geldart 1995, p. 174). This means that the reflector separation must be more than quarter of the wavelength ( $\Delta z > \lambda/4$ ). This also means that the image separation (events separation measured on a seismic stack section) should be more than half a period ( $\Delta t > \tau/2$ ) in order to be distinctly resolved (Fig. 8.21).

Adoption of the ( $\lambda/4$ ) criterion for the resolution limit, implies that the two events reflected from two neighboring interfaces are separated by a half cycle, which means that depth separation ( $\Delta z$ ) between two neighboring interfaces greater than ( $\lambda/4$ ) will lead to minimum destructive

**Fig. 8.21** The seismic vertical resolution. Minimum reflector separation ( $\Delta z$ ) is equal to ( $\lambda/4$ )



interference between the reflected waves from the two interfaces, causing resolution deterioration.

(i) **Factors Affecting Resolution**

In general the higher the frequency content of the seismic trace the better is the resolution power. Well logs (wireline logs) have greater resolution power than seismic traces since well logs are generated by high frequency sources. These logs can resolve beds on centimeter-meter scale while seismic reflection records cannot resolve so-much detailed variations. Reflection survey data can resolve reflectors at depth-separation of about 10 m at its best. The main factors affecting resolution are reflector spacing, reflector depth, and reflection signal frequency. Closely spaced reflectors cause interferences of reflected waves which lead to loss of resolution. The resolution-power is generally decreasing with depth for the following reasons:

- Earth filter which is cutting high frequencies, that is cutting short wavelengths. Thus for depth of 800 m, say, velocity of 1000 m/s, and frequency of 100 Hz, the wavelength will be 10 m and the resolution becomes only 2.5 m. However, when depth is 3000 m, velocity of 4000 m/s and frequency of 25 Hz, the wavelength will be 160 m and the resolution becomes 40 m. In general resolution gets less (poorer resolution) with increasing depth due to the effect of the earth high-cut filter.
- Increase of velocity due to compaction and decrease of frequency due to the

earth high-cut filter with depth, both are leading to increase of the wavelength and hence decreases the resolution power.

- Application of high-cut filters (as application of the anti-aliasing filter), which lead to attenuation of the high frequencies of the signal and hence result in lowering the resolution power.

(ii) **The problem of Thin Beds**

A special case, related to the subject of resolution which brought appreciable attention by geophysicists, is the problem of resolving thin beds. Two reflectors spaced by less than quarter of a wavelength, have reflection responses depending on the layering model. A layer is regarded as a thin layer when its thickness is less than a quarter of the dominant wavelength (Sheriff 2002, p. 353).

Consider a thin bed of thickness of ( $\lambda/4$ ) and of velocity ( $V_2$ ), sandwiched between two layers of velocities ( $V_1$  and  $V_3$ ) where ( $V_1 = V_3 < V_2$ ), the wave reflected from its top and that from its base will interfere constructively producing a high-amplitude reflection, forming what is normally referred to as the thin-bed effect or tuning effect. If, on the other hand, the thin-bed of velocity ( $V_2$ ) found between two layers of velocities ( $V_1$  and  $V_3$ ) where ( $V_1 < V_2 < V_3$ ), destructive interference will result (Sheriff and Geldart 1995, p. 174). These two models are shown in Fig. 8.22.

Vertical resolution is always improved with higher seismic frequencies. But, due to the earth filtering effect, frequencies get lower with increase of reflector depth.

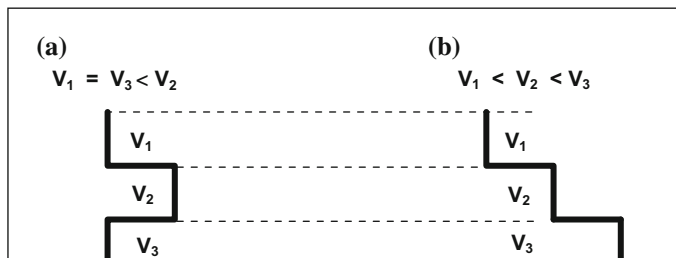


**Fig. 8.22** Two models of a thin bed, having interval velocity ( $V_2$ ). Model A ( $V_1 = V_3 < V_2$ ) and model B ( $V_1 < V_2 < V_3$ )

**Table 8.4** Estimates of the minimum depth interval resolved, corresponding to three values of sampling period

Sampling period (ms)	Highest frequency (Hz)	Wavelength ( $\lambda$ ) (m)	Min. depth-Interval ( $\Delta z = \lambda/4$ ) (m)
1	500	5	1.25
2	250	10	2.50
4	125	20	5.00

Consequently, vertical resolution gets poorer with increasing depth.

Decrease of frequency (that is increase of wavelength) is leading to decrease of the ratio ( $\Delta z/\lambda$ ) below the limiting value of (1/4). For example, an incident wave of (velocity = 1200 m/s, frequency = 40 Hz, wavelength = 30 m), the minimum depth interval between two reflectors to be resolved will be 7.5 m and for a second case of (velocity = 3000 m/s, frequency = 10 Hz, wavelength = 300 m), the minimum depth interval between two reflectors to be resolved will be 75 m.

(iii) **Role of the Sampling Period in Vertical Resolution**

Use of a sampling period ( $\Delta t$ ) which gives a Nyquist frequency ( $1/2 \cdot \Delta t$ ) higher than the cut-off frequency of the highest frequency component of the seismic signal, will avoid aliasing effect. Examples of minimum depth interval ( $\Delta z$ ) for a layer having velocity of 2500 m/s is presented in Table 8.4.

This table shows that the resolution is reasonably good even if the sampling period is as large as 4-ms value. This is adequate for the shallow layers where the velocity is normally less than 2500 m/s. and frequency is less than 125 Hz.

### 8.6.2 Horizontal Resolution of Seismic Signals

Horizontal resolution concerns the ability of recognizing two neighboring reflecting points (on a horizontal reflector) as two distinct points and not one point. The minimum separation distance for two horizontally-adjacent features, is used as measure for the horizontal resolution. Alongside with other methods, the first Fresnel zone is often

taken as a measure of horizontal resolution power on un-migrated seismic data (Sheriff and Geldart 1995, p.177). The radius of the first Fresnel zone is found to be function of frequency, velocity, and travel-time of the seismic reflection wave.

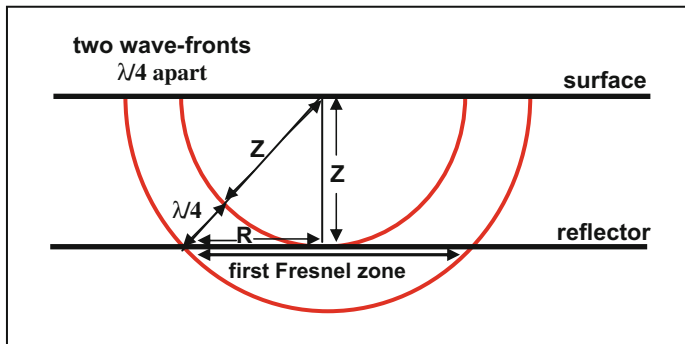
### 8.6.3 Fresnel Zone Formula

The Fresnel Zone concept was originally developed in connection with the physics of Light. According to this concept, a beam of light, incident on a reflector will illuminate a limited area of its surface, and reflection will take place from the area of that surface and not from a point. In the same way an incident seismic wave-front would be reflected from a surface-area of the reflector. Thus, the incident seismic energy is reflected from a defined area of the reflector surface, rather than from a point (Sherrif 1977).

Fresnel Zone concept is based on the assumption that all of the reflected energy contained in the positive half of the incident wave-front, is contributing in illuminating of the reflection area, which is circular in shape in case of vertical incidence. The reflected energy comes from the area that is affected by the positive half of the cycle of the incident wave. The incident energy will be reflected from the part of the reflector which is within the half cycle following the reflection onset (Sheriff 1980). The energy reflected from this zone is constructively interfering to make up the reflection event. In terms of wavelengths, this occurs for all of the energy reflected within quarter wavelength of the incident wave (Fig. 8.23).

Lateral resolution is determined by the radius (**R**) of the first Fresnel zone, which is related to the signal's frequency (**f**), reflection time (**T**) and propagation velocity (**v**) by an expression derived by (Sheriff and Geldart 1995, pp. 152–155):

**Fig. 8.23** Fresnel zone for a spherical wave. Two wave-fronts separated by quarter wavelength ( $\lambda/4$ ).  $R$ , Fresnel-zone radius



$R = v(T/4f)^{1/2}$  for incident spherical wave

and

$R = v(T/2f)^{1/2}$  for incident plane wave

These functions show clearly that the radius of the first Fresnel zone ( $R$ ) is function of the propagation velocity, reflection time, and frequency. The variation is direct with velocity ( $v$ ) and square root of reflection time ( $T$ ), and inverse with square root of frequency. The functions also show that the area of the zone is inversely proportional to frequency ( $f$ ). Thus, Fresnel Zone is larger for low frequency components than for high frequencies.

It is important to note that Fresnel Zone radius cannot be used as a measure for horizontal resolution on migrated seismic sections. This is

understandable since migration has the effect of collapsing Fresnel Zones. For this reason, use of Fresnel Zones in the study of horizontal resolution, is applicable only on unmigrated data.

### 8.7 The Common Numbering Systems

To express a sequence of entities, a certain counting system is used in which special symbols have been adopted. These symbols differ with different languages. The familiar system we are normally using is the decimal numbering system, in which we use ten different symbols (**0, 1, 2, 3, 4, 5, 6, 7, 8, 9**). To continue numbering beyond the number (**9**), certain combinations of these symbols are used. Examples of numbering systems are presented in Table 8.5.

**Table 8.5** Numbering systems. The decimal and binary are the most commonly used numbering systems

0, 1, 2, 3, 4, 5, 6, 7, 8, 9	Radix = 10 (decimal system)
0, 1, 2, 3, 4, 5, 6, 7, 8	Radix = 9
0, 1, 2, 3, 4, 5, 6, 7	Radix = 8 (octal system)
0, 1, 2, 3, 4, 5, 6	Radix = 7
0, 1, 2, 3, 4, 5	Radix = 6
0, 1, 2, 3, 4	Radix = 5
0, 1, 2, 3	Radix = 4
0, 1, 2	Radix = 3
0, 1	Radix = 2 (binary system)
0, 1, 2, 3, 4, 5, 6, 7, 8, 9, A	Radix = 11
0, 1, 2, 3, 4, 5, 6, 7, 8, 9, A, B	Radix = 12
...	...
...	...
0, 1, 2, 3, 4, 5, 6, 7, 8, 9, A, B, C, D, E, F	Radix = 16 (hexa-decimal system)

This table shows that it is always possible to devise a new numbering system, but the most suitable for us is the decimal system and most suitable for computers (computations and storage) is the binary system.

Decimal system	...	$10^5$	$10^4$	$10^3$	$10^2$	$10^1$	$10^0$
Binary system	...	$2^5$	$2^4$	$2^3$	$2^2$	$2^1$	$2^0$
Octal system	...	$8^5$	$8^4$	$8^3$	$8^2$	$8^1$	$8^0$
Hexa-decimal system	...	$16^5$	$16^4$	$16^3$	$16^2$	$16^1$	$16^0$

### 8.7.1 Numbering System Concept

In any numbering system, a number is represented by a suitable sequence of digits, where each digit has its own form, position, and value. Usually, the digits are written from right to left, where the least-value digit is written at the right end and the greatest-value at the left end. These are called the **(least-significant digit)** and **(most-significant digit)** respectively. Number of symbols used in the decimal system (called, **Radix**) is **(10)**. Other numbering systems based on the same rules used in the decimal system, but with different radix-values, can be devised. The number, in any numbering system can be represented as a mathematical sequence, represented as follows:

### 8.7.2 Applications of the Concept

The most important application of the numbering system concept is done in system-to-system conversion. The conversion process may be divided into the following functions:

- Conversion to decimal,
- Conversion to binary,
- Conversion to octal, and
- Conversion to hexadecimal.

These functions shall be presented with examples to clarify the procedure in each case.

$$[ \text{Number} ] = \dots + \dots + E R^4 + D R^3 + C R^2 + B R^1 + A R^0$$

where **R** is the radix, and the letters (**A, B, C, ...**) are the digits of the number.

The following table shows the concept applied to the four most commonly applied numbering systems:

#### 8.7.2.1 Conversion to Decimal System

Conversion is done by applying the mathematical sequence that defines the numbering system concerned. Examples of the conversion process are given in the following examples:



In these examples, we found:

$$[47]_D = [101111]_B = [57]_{Oct}$$

and

$$[0.593]_D = [0.10010]_B = [0.4574]_{Oct}$$

### 8.7.2.3 Conversion from Binary to Octal and to Hexa-Decimal

The octal number is separated into 3-digit groups starting from the point preceding the fraction part of the number. Each group is substituted by the corresponding octal number. In conversion to hexa-decimal number, the same procedure is followed except that the group is now made up of 4 digits instead of 3 digits. Again each group is substituted by the corresponding hexa-decimal number.

equivalences for octal conversion	equivalences for Hexa-Decimal conversion	
<b>0 (=000)</b>	<b>0 (=0000)</b>	<b>8 (=1000)</b>
<b>1 (=001)</b>	<b>1 (=0001)</b>	<b>9 (=1001)</b>
<b>2 (=010)</b>	<b>2 (=0010)</b>	<b>A (=1010)</b>
<b>3 (=011)</b>	<b>3 (=0011)</b>	<b>B (=1011)</b>
<b>4 (=100)</b>	<b>4 (=0100)</b>	<b>C (=0100)</b>
<b>5 (=101)</b>	<b>5 (=0101)</b>	<b>D (=1101)</b>
<b>6 (=110)</b>	<b>6 (=0110)</b>	<b>E (=1110)</b>
<b>7 (=111)</b>	<b>7 (=0111)</b>	<b>F (=1111)</b>

**Examples:**

$$[001\ 001\ 010\ 001 . 100\ 101]_B = [1121.45]_O$$

$$[0010\ 0101\ 0001 . 1001\ 0100]_B = [251.94]_{HD}$$

It is to be noted here that there is yet another less-common numbering system called the binary-coded decimal (BCD) numbering system. In this system, each of the decimal digits is substituted by the corresponding group of the binary digits. Each of these groups consists of 4 binary digits, as in the following example:

$$[635]_D = (6) \quad (3) \quad (5)$$

$$[635]_D = [0110 \quad 0011 \quad 1001]_{BCD}$$

### 8.7.2.4 Addition and Subtraction of Binary Numbers

The same approach used in addition and subtraction of numbers in the decimal system, is applied in case of the other numbering systems. The rule of (Carry) of the multiples of 10 is applied. For the Binary numbers, the rules to be remembered are the following:

subtracted (subtrahend) into its complement by changing the zeros to ones and the ones to zeros and adding the digit (1) to the resulting number (the Two's Complement number). Subtraction is replaced by addition process. This is the procedure normally followed by the digital computers.

<u>for addition</u>	<u>for subtraction</u>
$0 + 0 = 0$	$0 - 0 = 0$
$1 + 0 = 1$	$1 - 0 = 1$
$0 + 1 = 1$	$1 - 1 = 0$
$1 + 1 = 10$	$10 - 1 = 1$

#### Examples for Addition:

<u>decimal</u>	<u>octal</u>	<u>binary</u>
5	5	0101
+7	+7	+ 0111
+13	+15	+1101
<hr/>	<hr/>	<hr/>
[ 25 ] <sub>D</sub>	[ 231 ] <sub>O</sub>	[ 11001 ] <sub>B</sub>

#### Examples for subtraction:

<u>decimal</u>	<u>octal</u>	<u>binary</u>
25	31	11001
- 12	- 14	- 1100
<hr/>	<hr/>	<hr/>
[13 ] <sub>D</sub>	[15 ] <sub>O</sub>	[1101 ] <sub>B</sub>

There is another method to do the subtraction process, and that is by use of what is called (Two's Complement method). The subtraction process starts with converting the number to be

To clarify the process let us take the example of subtraction of the number [+53]<sub>D</sub> from the number [+67]<sub>D</sub>, assuming that the subtraction process is done by an 8-bit computer. This is done as follows:

$[67]_D = [01000011]_B$   
 $[53]_D = [00110101]_B$

**Two's Complement of  $[00110101]_B$**   
 $= [11001010]_B + 1 = [11001011]_B$

**Subtraction becomes addition of the two numbers, thus:**  
 $[67]_D = 01000011$   
 $[53]_D = 11001011 +$

**By summing we get  $[14]_D = [100001110]_B$**

For an 8-bit computer, the digit (1) appearing after the 8th digit will be outside the computer binary-word limit and so will be neglected and the result will be the 8-digit word (1110) which is  $[14]_D$ .

the decimal numbering (1, 2, 3, ...). Note that after the digit (9) in the decimal system comes (10) and after the digit (F) in the hexa-decimal system comes (10), and after the digit (7) in the octal system comes (10), and after the digit (1) in the binary system comes (10). This means that, after the complete set of digits of each system comes (10), then counting continues. The following table shows this method applied for the hexa-decimal, decimal, octal, and binary systems.

### 8.7.3 Counting in the Different Numbering Systems

Here is a table of different numbering systems (hexa-decimal, decimal, octal, and binary). Each column contains the numbering corresponding to

<u>Hexadecimal</u>	<u>Decimal</u>	<u>Octal</u>	<u>Binary</u>
0 10 20 30 .	0 10 20 30 .	0 10 20 30 .	0 10 100 110 .
1 11 21 31 .	1 11 21 31 .	1 11 21 31 .	1 11 101 111 .
2 12 22 32 .	2 12 22 32 .	2 12 22 32 .	
3 13 23 33	3 13 23 33	3 13 23 33	U U
4 14 24 34	4 14 24 34	4 14 24 34	
5 15 25 35	5 15 25 35	5 15 25 35	
6 16 26 36	6 16 26 36	6 16 26 36	
7 17 27 37	7 17 27 37	7 17 27 37	
8 18 28 38	8 18 28 38		
9 19 29 39	9 19 29 39		
A 1A 2A 3A	U U	U U	
B 1B 2B 3B			
C 1C 2C 3C			
D 1D 2D 3D			
E 1E 2E 3E			
F 1F 2F 3F			
U U			

From mid 1950s till mid 1960s a jump in the seismic data processing took place. Within this interval, the analogue magnetic-tape recording and processing, followed by the introduction of digital technique, were introduced. A third and equally important factor that boosted the seismic data processing is the adoption of concepts borrowed from the communication theory which considered the seismic wavelet as a travelling signal similar to the electromagnetic signal.

The input data to the processing system consists mainly of the digital seismic traces, recorded by the field recording system. The fundamental principle on which processing is based upon, is that the seismic trace is considered to be as a digital signal of value (amplitude) which is function of the reflection travel time. In order to extract the useful information the seismic signal (seismic reflection wavelet), a number of mathematical and statistical processes, are applied. These processes are considered to be the tools employed to do the required analyses.

## 9.1 The Seismic Processing Tools

The raw seismic data acquired in the field, which form the input to the processing system, are normally digitally recorded traces on special magnetic tapes. The reflection wavelets received by a surface-positioned detection-system (the geophone group) are digitally recorded as function of recording time forming the seismic trace.

In order to extract the useful message (geological information) from these recorded data, these seismic traces are subjected to a set of analysis procedures, using certain processing tools. These tools are numerical analysis techniques applied on the input seismic traces. The most common tools applied in seismic data processing are:

- Fourier Analysis
- Correlation functions computations
- Convolution (frequency filtering)
- Deconvolution (inverse frequency filtering)
- Frequency- and velocity filtering
- Equalization (trace scaling)
- Sample Editing (time-shifting, sign-changing, sample zeroing)

These processes form the basic processing tools in the hand of the geophysicist, ready to be used in processing of seismic reflection data.

### 9.1.1 The Sine Function

The building brick of any physically realizable function is the sine function. According to Fourier theorem, a time- or distance-function, is made up of a sum of infinite number of sine-functions. Due to its important role in processing in general, and in Fourier analysis in special, an introductory treatment of the sine function shall be given here-below, preceding the discussions of the processing tools listed above.

One way to generate a sine function is by using a geometric approach. Let us consider a unit circle

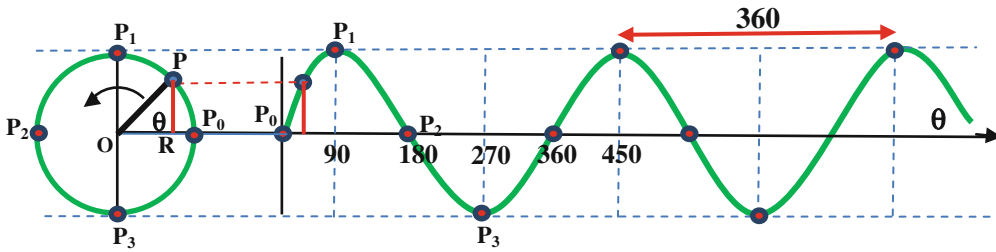


**Fig. 9.1** Generation of the sine function ( $\sin \theta$ )

of radius equal to unity, in which the radius is rotating with constant rotation speed about the circle centre. At a given time, the radius (OP in Fig. 9.1) makes an angle ( $\theta$ ) with the x-axis, and its tip, point (P) has its projection on the x-axis represented by point (R). By definition, the sine function ( $\sin \theta$ ) has a value given by the length (PR). Now, as the radius rotates about the centre point (O) the length, PR (=  $\sin \theta$ ) varies with the angle ( $\theta$ ). By drawing the value of the PR-length as function of ( $\theta$ ), we obtain the curve for the sine function ( $\sin \theta$ ), as it is shown in Fig. 9.1.

relation between the two unit systems; degrees and radians:

$$360^\circ = 2\pi \text{ rad}$$

Given ( $\pi = 3.1415927$ ), the relation between the two systems is that  $1 \text{ rad} = 57.2958^\circ$ , or  $1^\circ = 0.017453 \text{ rad}$ . The argument of sine functions ( $\theta$ , in this example) is normally quoted in radians.

### 9.1.2 The Degrees-Radians Relationship

Referring to Fig. 9.1, the point (P) is rotating at constant speed and the generated curve is made up of repeated cycles corresponding to the repeated rotation cycles of the point P around the circle circumference. The generated ( $\sin \theta$  curve) repeats regularly every  $360^\circ$ . The complete angle swept by the rotating arm is from ( $\theta = 0$ ) when P is at location ( $P_0$ ) to ( $\theta = 360$ ) when P is back at location ( $P_0$ ) passing through all of the points ( $P_0, P_1, P_2$  and  $P_3$ ).

It should be noted here that angles can be expressed in radians rather than in degree-units. An angle ( $\theta$ ) in radians is defined as the ratio between the subtending arc divided by the radius of the circle in which the angle is central. When the arc length is equal to the radius, the angle value is 1 rad. Since circumference of a circle is equal to  $2\pi$  times its radius, the value of the total central angle is  $2\pi$ . This leads to the important

### 9.1.3 Parameters of the Sine Function

The general form of the sine function is that it is function of angle ( $\theta$ ). Other common forms of this function are: function of time  $s(t)$  and function of distance  $s(x)$ , thus:

$$s(\theta) = a \sin(\theta + \phi)$$

or,

$$s(t) = a \sin(2\pi f_t t + t_p), \quad f_t = 1/\tau$$

or,

$$s(x) = a \sin(2\pi f_x x + x_p), \quad f_x = 1/\lambda$$

where, ( $a$ ) is amplitude, ( $\phi$ ) is phase angle, ( $f_t$ ) is temporal frequency, ( $f_x$ ) is spatial frequency, ( $\tau$ ) is period, ( $\lambda$ ) is wavelength, ( $t_p$ ) is phase shift in time units, and ( $x_p$ ) is phase shift in distance units.

The maximum value of the sine function is equal to the length of the rotating arm applied for

generating the sine function considered above. A sine function, represented by a sine curve (sometimes called sinusoid) is completely defined by three parameters: amplitude (**a**), frequency (**f<sub>t</sub>** or **f<sub>x</sub>**) and phase (**Ø**, **t<sub>p</sub>**, or **x<sub>p</sub>**). The amplitude is of positive value (+**a**) represents a peak and negative value (-**a**) represents a trough of the given sinusoid.

The most common form of the sine function is the form **a sin(2πft + t<sub>p</sub>)** quoted as function of time (**t**). The frequency, (**f**) is expressed in cycles per second. The sine function is of infinite length extending along the time axis in both of the negative and positive directions. Part of a sine function and its three characteristic parameters are shown in Fig. 9.2.

### 9.1.4 The Frequency Concept

Any periodic motion, as the rotation-arm model shown in Fig. 9.1, is specified by two periodicity parameters: the frequency and the period of the motion. Frequency is defined to be the number of revolutions (cycles) made in one second. The length of the time interval (normally measured in seconds or milliseconds) for one cycle, is called the period. The relation between frequency (**f**) and period (**τ**) is:

$$f = 1/\tau$$

For the rotation arm, shown in Fig. 9.1, the period (**τ**) is the time interval during which the

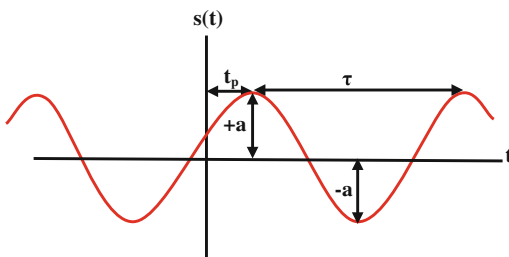


**Fig. 9.2** Part of a sine function, a  $\sin(2\pi ft + t_p)$ , and its characteristic parameters amplitude (*a*), period ( $\tau = 1/f$ ), and phase shift (*t<sub>p</sub>*)

arm sweeps a complete central angle (**360°**), which is (**2π**) when expressed in radian units. When frequency is expressed in terms of rate of change of the angle (**dØ/dt**), measured in radians per second, it is usually called, radian frequency. Thus, for constant rate, we can write:

$$\omega = \theta/t = 2\pi/\tau = 2\pi f$$

where, (**ω**) is the radian frequency (rad/s) and (**f**) is the cyclic frequency (cycle/s).

The frequency (**f**) is normally referred to as cyclic frequency, measured in cycles per second, to differentiate it from the radian or angular frequency (**ω**) which is measured in radian per second.

### Frequency Units

The unit normally used in measuring frequency is the Hertz (Hz), where 1 Hz is 1 cycle/s. Another closely related measurement-unit applied in measurement of frequencies is the Octave. Instead of quoting the frequency in its absolute units (Hertz), it is quoted in frequency ratios measured in Octave-units. It is defined as the number of times (**n**) with which a frequency (**f<sub>2</sub>**) value gets doubled over a reference frequency (**f<sub>1</sub>**). A frequency ratio (**f<sub>2</sub>/f<sub>1</sub>**) is one Octave if (**f<sub>2</sub>/f<sub>1</sub> = 2**). In general, the number of octaves (**n**) is related to the ratio (**f<sub>n</sub>/f<sub>1</sub>**) by:

$$f_n/f_1 = 2^n$$

$$n = (1/\log 2) \cdot \log(f_n/f_1)$$

**(n) is number of Octaves**

Frequency ratio	Value in octave-units	Frequency examples
2 <sup>1</sup> : 1	1	(10–20) Hz = 1 octave
2 <sup>2</sup> : 1	2	(10–40) Hz = 2 octaves
2 <sup>3</sup> : 1	3	(10–80) Hz = 3 octaves
2 <sup>1/2</sup> : 1	1/2	(10–14.1) Hz = 1/2 octave
2 <sup>1/3</sup> : 1	1/3	(10–12.8) Hz = 1/3 octave

**Examples:**

It is common practice that the slope of frequency spectrum is measured in decibel-per-octave units. Thus, for example, an amplitude spectrum defined by four corner frequencies ( $f_1$ ,  $f_2$ ,  $f_3$ ,  $f_4$ ), the slopes of the spectrum between ( $f_1$  and  $f_2$ ) and between ( $f_3$  and  $f_4$ ) are normally quoted in decibel per octave, where  $f_2/f_1 = f_4/f_3 = 2$ . A frequency spectrum of this form is given in Fig. 9.3.

The frequency bandwidth of such a filter-form is considered to be the frequency range between the two points located at  $-6$  db level on the filter amplitude spectrum as shown in Fig. 9.3.

### 9.1.5 The Phase Concept

The phase expresses the position of the cycle of a sinusoid in relation to the time zero. The convention followed by geophysicists is that the phase shift of a sinusoid is considered as the interval between the time zero and the nearest peak of that sinusoid. As stated above, the argument of the sine function is either angle ( $\theta$ ), a  $\sin(\theta + \theta)$ , or time ( $t$ ), a  $\sin(\omega t + t_p)$ . The terms ( $\theta$ ) and ( $t_p$ ) are representing the phase parameter.

Phase is measured in degrees when the argument of the sine function is angle or in time units when the argument is time. It is always possible to convert phase values from degrees to time units and vice versa using the fact that one period-length is equal to ( $360^\circ$ ), or to ( $2\pi$  radians). Thus if the phase angle is ( $90^\circ$ ) then the time-equivalent is quarter of the period and so on. Since, by definition, phase is represented by

the time interval between time zero and the nearest peak, the value of the phase must be confined within the range  $(-\tau/2)$  and  $(+\tau/2)$ , that is between  $(-180^\circ)$  and  $(+180^\circ)$ .

When the peak falls exactly on time zero, the phase is zero. If, however, the peak falls later in time than time zero, the phase is called a “lag” phase and the phase angle, in this case, is given a negative sign. If, on the other hand, the peak falls before time zero, the phase is described as “lead” phase and the phase angle is given a positive sign. When a trough coincides with the time zero, we get a case where the peaks become at equal distances from the time zero, and the phase can be called either  $(-180^\circ)$  or  $(+180^\circ)$ . These definitions are explained in Fig. 9.4.

Phase expresses the relative position of a sine wave with respect to the time of origin that is position relative to time zero. The value of phase may be expressed in fractions of the period or in time units (usually in seconds, or milliseconds), considering that one complete period ( $\tau$ ) is equivalent to  $(2\pi)$  or  $(360^\circ)$ . Common examples of phase measurements are shown in Fig. 9.5.

### 9.1.6 Temporal and Spatial Frequencies

Frequency ( $f_t$ ) is the number of cycles per second when the argument of the sine function is time,  $s(t)$ . In the  $x$ -domain, where the argument of the sine function is distance ( $x$ ), the frequency ( $f_x$ ) is expressed in cycles per meter. The frequencies ( $f_t$ ) and ( $f_x$ ) are termed temporal and spatial frequencies respectively. The period ( $\tau$ ), is equal to the time interval separating two neighboring

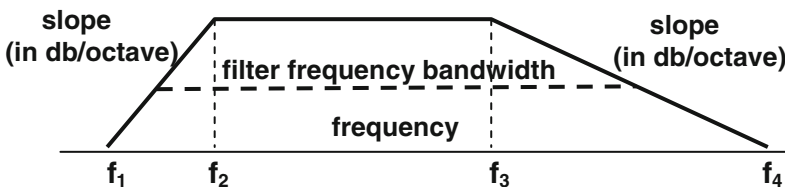


**Fig. 9.3** Slopes of a four-corner spectrum quoted in decibel (db) per octave units, where  $f_2/f_1 = f_4/f_3 = 2$

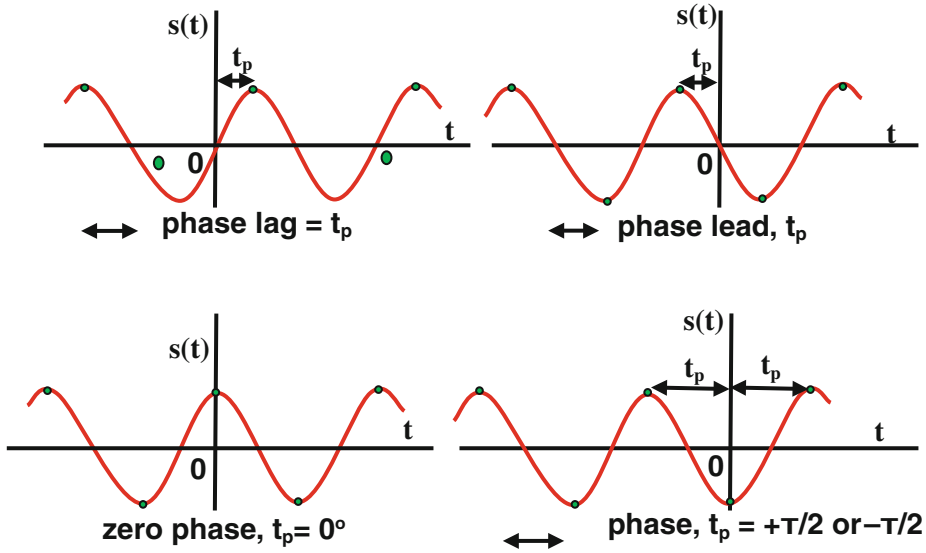
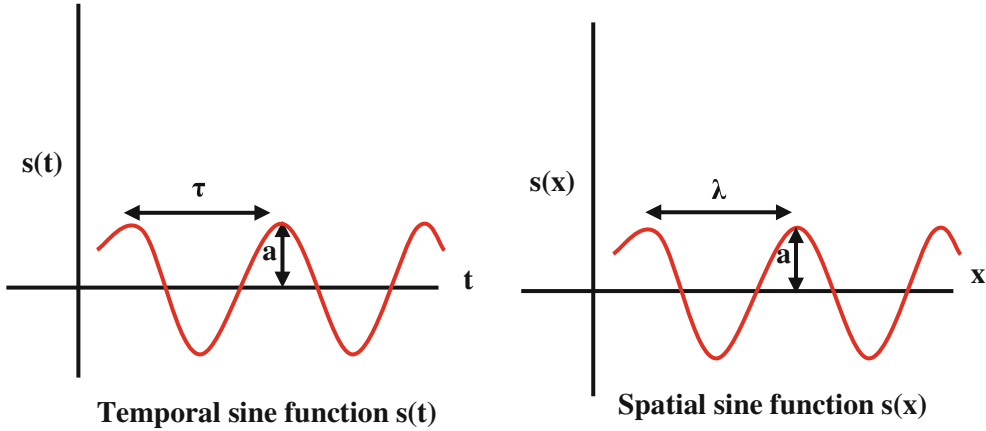


Fig. 9.4 Phase terminology

Fig. 9.5 Common examples of phase-shift, with their corresponding terminologies

sine waves with different phase shifts	phase	degrees	period
	Phase lag	- 90°	+ $\tau/4$
	Zero phase	0°	0°
	Phase lead	+ 90°	- $\tau/4$
	Out-of phase	+ 180° - 180°	+ $\tau/2$ - $\tau/2$



**Fig. 9.6** Definition of the period ( $\tau$ ) and wavelength ( $\lambda$ ) of a sine function in the two domains,  $s(t)$  and  $s(x)$

peaks, in a time-domain sine function. Likewise, the distance separating two peaks in x-domain sine function represents the wavelength ( $\lambda$ ) as shown in Fig. 9.6.

In radians units, we have the temporal relation ( $\omega = 2\pi f_t = 2\pi/\tau$ ) and the corresponding spatial relation ( $k = 2\pi f_x = 2\pi/\lambda$ ). Another important relation is the one connecting the temporal parameters with the spatial parameters, which is:

$$v = \lambda/\tau$$

It should be noted that when frequency is quoted as ( $f$ ) without the subscript ( $t$ ), it is normally meant to be the temporal frequency ( $f_t$ ).

### 9.1.7 Propagating Sine Wave

The rotating arm model (shown above), helped in generating a one dimensional sine function that depends on one variable which is angle ( $\theta$ ) or time ( $t$ ). The time-dependent sine function describes the case of stationary (non-propagating) periodic motion. However, we may have a two-dimensional sine function  $s(x, t)$  describing the case of a propagating sinusoidal wave. In its

simplest form, this type of function has the form (Richardson 1953, p. 38):

$$s(x, t) = a \sin 2\pi(t/\tau - x/\lambda)$$

Using the relationships ( $\omega = 2\pi f_t = 2\pi/\tau$ ) and ( $k = 2\pi f_x = 2\pi/\lambda$ ), the function can be written as:

$$s(x, t) = a \sin(\omega t - kx)$$

where  $k$  is constant known as the wave number,  $v$  is propagation velocity, and  $\omega$  is the radian frequency measured in radians per second.

It is important to note that the wave propagation velocity ( $v$ ) is connected with both of the temporal frequency ( $f_t$ ) and wavelength ( $\lambda$ ) by the simple relationship:

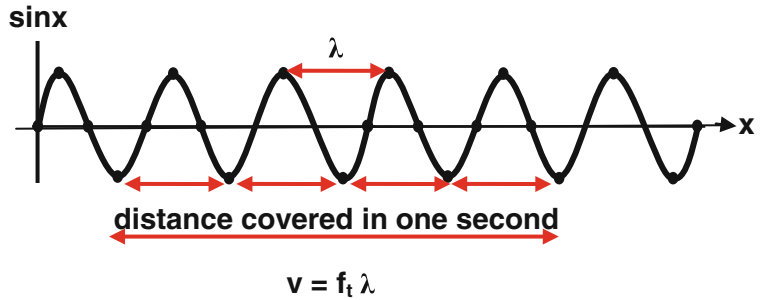
$$v = f_t \lambda$$

or,

$$v = \omega/k$$

Using a simple pictorial method, the velocity formula ( $v = f_t \lambda$ ) can be derived. Referring to Fig. 9.7, the number of cycles ( $f_t$ ) of a

**Fig. 9.7** Derivation of the relation connecting propagation velocity ( $v$ ) with frequency ( $f_t$ ) and wavelength ( $\lambda$ )



propagating sine wave measured in 1 s is multiplied by the cycle length (wavelength,  $\lambda$ ) gives the total distance covered in that 1 s, which is the propagation velocity ( $v$ ). Thus ( $v = f_t \lambda$ ).

(iv) The integral of  $f(t)dt$  over a complete period is convergent.

It so happened that almost all geophysical phenomena, including the seismic signal, obey Dirichlet conditions and hence can be analyzed by Fourier Theorem.

## 9.2 Fourier Analysis and Concept of Spectra

In 1807, Joseph Fourier (1768–1830) presented his theorem (now identified by his name) which states that any function such as  $f(t)$ , satisfying certain restrictions can be expressed as a sum of an infinite number of sine waves. In 1809 Dirichlet formulated the mathematical restrictions (normally referred to as Dirichlet conditions) under which the theorem is mathematically valid. The restrictions are:

### 9.2.1 Fourier Series

According to Fourier Theorem, any periodic function,  $f(t)$  of period ( $\tau$ ), satisfying Dirichlet conditions, can be represented by the sum of sinusoidal functions of frequencies which are multiples of the fundamental frequency of that function. Mathematically, the periodic function  $f(t)$  is expressed by the following infinite series (called Fourier series):

$$f(t) = a_0 + \sum_{n=1}^{\infty} (a_n \cos n\omega t + b_n \sin n\omega t)$$

- (i) The function is periodic,  $f(t) = f(t + \tau)$ , where ( $\tau$ ) is the period.
- (ii) The function is sectionally continuous, with finite number of discontinuities.
- (iii) The function is possessing finite number of maxima and minima.

where ( $\omega$ ), is the fundamental frequency (angular frequency, in radians). That is:

$$\omega = 2\pi f = 2\pi/\tau$$

The constants ( $a_0$ ,  $a_n$ , and  $b_n$ ) which are called (Fourier coefficients) can be determined by the finite integrals:

$$\mathbf{a}_0 = \frac{1}{\tau} \int_{-\tau/2}^{\tau/2} f(t) dt$$

$$\mathbf{a}_n = \frac{2}{\tau} \int_{-\tau/2}^{\tau/2} f(t) \cos n\omega t dt$$

$$\mathbf{b}_n = \frac{2}{\tau} \int_{-\tau/2}^{\tau/2} f(t) \sin n\omega t dt$$

These three expressions are derived by multiplying both sides of the Fourier series in turn by (1), ( $\cos n\omega t$ ), and ( $\sin n\omega t$ ), and integrating with respect to ( $t$ ) over the period length ( $\tau$ ). The derivation is based on use of the orthogonality properties of the sine and cosine functions, which are (for  $m$  and  $n$  being integers):

$$\int_{-\tau/2}^{\tau/2} \sin mt \sin nt dt = \int_{-\tau/2}^{\tau/2} \cos mt \cos nt dt = \tau/2 \text{ for } m=n, \text{ and } (=0, \text{ for } m \neq n)$$

and,

$$\int_{-\tau/2}^{\tau/2} \sin mt \cos nt dt = 0, \text{ for all } m \text{ and } n$$

The frequencies ( $\omega_n$ ) that are multiples of the fundamental frequency ( $\omega$ ), are called harmonic

of frequencies ( $\omega_n$ ) and amplitudes ( $\mathbf{a}_n$  and  $\mathbf{b}_n$ ). The term ( $\mathbf{a}_0$ ) represents the DC level of the function  $f(t)$ .

### Odd and Even Functions

For an odd function  $f_o(t)$  in which  $f_o(-t) = -f_o(t)$

the coefficients ( $\mathbf{a}_n$ ) become all equal to zero, since in this case:

$$\begin{aligned} \mathbf{a}_n &= \frac{1}{\tau} \int_{-\tau}^{\tau} f_o(t) \cos n\omega t dt = \frac{1}{\tau} \int_{-\tau}^0 f_o(t) \cos n\omega t dt + \frac{1}{\tau} \int_0^{\tau} f_o(t) \cos n\omega t dt \\ &= -\frac{1}{\tau} \int_0^{\tau} f_o(t) \cos n\omega t dt + \frac{1}{\tau} \int_0^{\tau} f_o(t) \cos n\omega t dt \\ &= 0 \end{aligned}$$

frequencies or just harmonics. Thus a periodic function  $f(t)$  is made up of the sum of an infinite number of harmonics (sine and cosine functions)

Similarly, it can be shown that, for an even function  $f_e(t)$  in which  $f_e(-t) = f_e(t)$ , the coefficients ( $\mathbf{b}_n$ ) become equal to zero for all ( $n$ ).

Thus, when the function  $f(t)$  is odd, the Fourier series will consist of sine terms only and when it is an even function, the series will consist of cosine terms only.

### 9.2.2 Gibbs' Phenomenon

As we have stated above, a periodic signal (period,  $\tau$ ), satisfying other Dirichlet conditions, can be expressed as a sum of sinusoidal components of frequencies;  $n/\tau$ , ( $n = 0, 1, 2, 3, \dots$ ). The zero-frequency component ( $n = 0$ ) represents the DC term. This implies that if we have a signal,  $f(t)$  defined over the time interval ( $t = 0$  to  $t = T$ ), then, according to Fourier Theorem, the function within this interval can be expressed as the sum of the frequency components ( $n/T$ ) where ( $n = 0, 1, 2, 3, \dots, \infty$ ).

Fourier Theorem states that the signal  $f(t)$  will be recovered exactly from the Fourier series only when an infinite number of terms are included in the summation, that is when the integer ( $n$ ) runs from ( $n = 1$ ) to ( $n = \infty$ ). In practice, only a finite number ( $n = N$ , say) of terms is used in the summation. As a result of this truncation of the series (i.e. when  $n$  is finite number), distortion shall occur in the recovered (synthesized) signal. In this case, the sum will shoot beyond the value of  $f(t)$  in the neighborhood of the discontinuities found in  $f(t)$ . The overshoot oscillates about the function value with decreasing amplitude as we move away from the discontinuity. Increasing the number of terms leads to a better

approximation for the continuous parts of the function. This kind of distortions (synthesized-function overshooting- and oscillation-behavior) is normally referred to as Gibbs' Phenomenon (Fig. 9.8).

Application of the Fourier series analysis of periodic functions is found in many standard texts on the subject, see for example (Alsadi 1980, p. 111).

### 9.2.3 Fourier Transform

As it is presented above, Fourier series is restricted to periodic functions, but theory can be extended to cover non-periodic functions. Functions of finite length are called transient functions. With special integrals, it is possible to transform a transient function  $f(t)$  to another form in which it becomes function of frequency  $F(\omega)$ , with no loss of information. The process of converting  $f(t)$  into  $F(\omega)$  is called (Fourier transform) and the reverse process,  $F(\omega)$  into  $f(t)$ , is called (inverse Fourier transform).

The transient function can be considered as a periodic function of infinitely long period. The process of transforming a transient function from its time domain  $f(t)$  to the frequency domain function  $F(\omega)$  and vice versa, are done through a set of integral equations called (Fourier Integral equations) which are more commonly known as Fourier Transform equations. The two equations (Transform and Inverse Fourier transform equations) are B ath (1974, pp. 33–37):

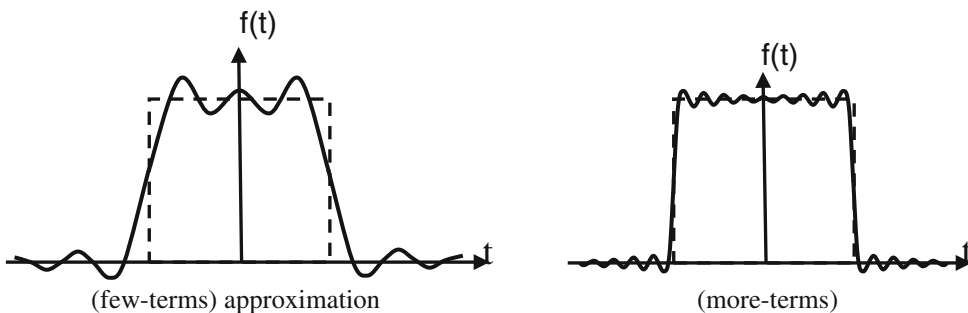


Fig. 9.8 Gibbs' Phenomenon computed for a rectangular pulse for few- and more-terms truncation of Fourier series

$$F(\omega) = \int_{-\infty}^{\infty} f(t) e^{-i\omega t} dt \quad (\text{Fourier Transform})$$

$$f(t) = \frac{1}{2\pi} \int_{-\infty}^{\infty} F(\omega) e^{i\omega t} d\omega \quad (\text{Fourier Inverse Transform})$$

In general, the function  $F(\omega)$  is complex, consisting of a real part  $\mathbf{a}(\omega)$  and imaginary part  $\mathbf{b}(\omega)$ . Thus,  $F(\omega)$  can be expressed as:

The two functions,  $\mathbf{a}(\omega)$  and  $\mathbf{b}(\omega)$ , known respectively as cosine and sine transforms, are defined as:

similar to Light spectrum in which the Light frequency-components appear when analyzed as it passes through a transparent prism. In the mathematical sense,  $F(\omega)$  is complex function consisting of the modulus;  $|F(\omega)|$  called (amplitude spectrum) and the argument  $\Theta(\omega)$ , called

$$F(\omega) = \mathbf{a}(\omega) - i\mathbf{b}(\omega),$$

or.

$$F(\omega) = A(\omega) e^{i\Theta(\omega)}$$

where,

$$A(\omega) = [\mathbf{a}^2(\omega) + \mathbf{b}^2(\omega)]^{1/2}$$

$$\Theta(\omega) = \tan^{-1} [-\mathbf{b}(\omega) / \mathbf{a}(\omega)]$$

$$\mathbf{a}(\omega) = \int_{-\infty}^{\infty} f(t) \cos \omega t dt$$

and,

$$\mathbf{b}(\omega) = \int_{-\infty}^{\infty} f(t) \sin \omega t dt$$

(phase spectrum). The square of the amplitude spectrum is the Fourier power spectrum.

Fourier spectrum can be presented in one of the two forms:  $F(\omega) = \mathbf{a}(\omega) - i\mathbf{b}(\omega)$  and  $F(\omega) = |F(\omega)| e^{i\Theta(\omega)}$ , where,

$$|F(\omega)| = \sqrt{[\mathbf{a}(\omega)]^2 + [\mathbf{b}(\omega)]^2}$$

$$\Theta(\omega) = \tan^{-1} [(-\mathbf{b}(\omega)) / \mathbf{a}(\omega)]$$

### 9.3 Concept of the Frequency Spectrum

The function  $F(\omega)$  expresses the variation of amplitude of the frequency components as function of frequency ( $\omega$ ). This is, in a way,

By using Fourier integral transform, it is possible to transform a function (such as a seismic signal) from its original time-domain function  $f(t)$  to the frequency-domain function  $F(\omega)$ , with no loss of information. In this process the original time domain signal is analyzed into the frequency components (sine functions) constituting that signal. The produced frequency-domain plot

represents the Fourier spectrum of the analyzed function.

### 9.3.1 The Line Spectrum

Based on the nature of the input signal (periodic or non periodic), the computed spectrum is obtained as discrete points or as continuous curve. Frequency analysis of a periodic function involves determination of the Fourier series coefficients of the input function. In this case the output frequency-domain function is plotted as discrete lines along the frequency axis forming what is commonly referred to as the (line spectrum).

The line spectrum  $S_1(\omega)$  of a sine function  $s_1(t) = a \sin\omega_1 t$ , is represented by one line of height proportional to the amplitude ( $a$ ) of the sine function, located at frequency ( $\omega_1$ ). For another sine function,  $s_2(t) = a \sin\omega_2 t$  of frequency ( $\omega_2$ ), will, likewise, be of one line placed at frequency ( $\omega_2$ ). Further, the sum of the two sine functions  $s_1(t)$  and  $s_2(t)$  will have a line spectrum made up of two lines placed at ( $\omega_1$ ) and ( $\omega_2$ ). The principle is shown in Fig. 9.9.

### 9.3.2 The Continuous Spectrum

Analysis of a non-periodic signal, by the Fourier transform, gives continuous amplitude- and

phase-spectra. Through another form of integration (Inverse Fourier transform), it is possible to recover the original time-domain function from the transformed frequency-domain function. For complete recovery, this process requires both of the amplitude spectrum and phase spectrum. The concept of frequency spectra (amplitude- and phase-spectra) computed by Fourier transform equations are illustrated pictorially in Fig. 9.10.

In summary, it can be stated that Fourier series analysis of periodic functions yields line spectra and Fourier transform analysis of non-periodic functions yields continuous spectra.

### 9.3.3 The Fourier Power Spectrum

The total energy ( $E$ ) of a real function  $f(t)$ , such as a seismic signal, is generally taken to be proportional to the integral of the square of its amplitude. That is:

$$E = \int_{-\infty}^{\infty} \{f(t)\}^2 dt$$

It can be shown (Båth 1974, p. 82) that this expression is related to the power spectrum as follows:

**Fig. 9.9** Line spectra of two sine functions,  $s_1(t)$  and  $s_2(t)$  and of their sum  $s_1(t) + s_2(t)$

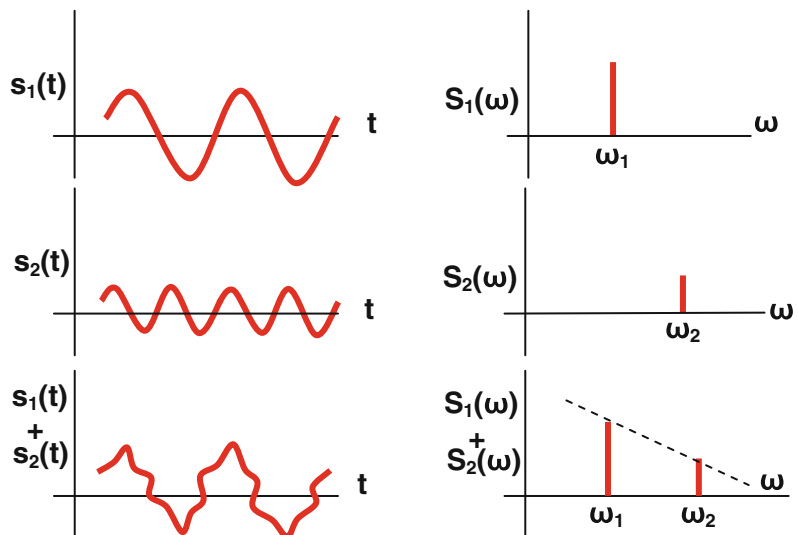
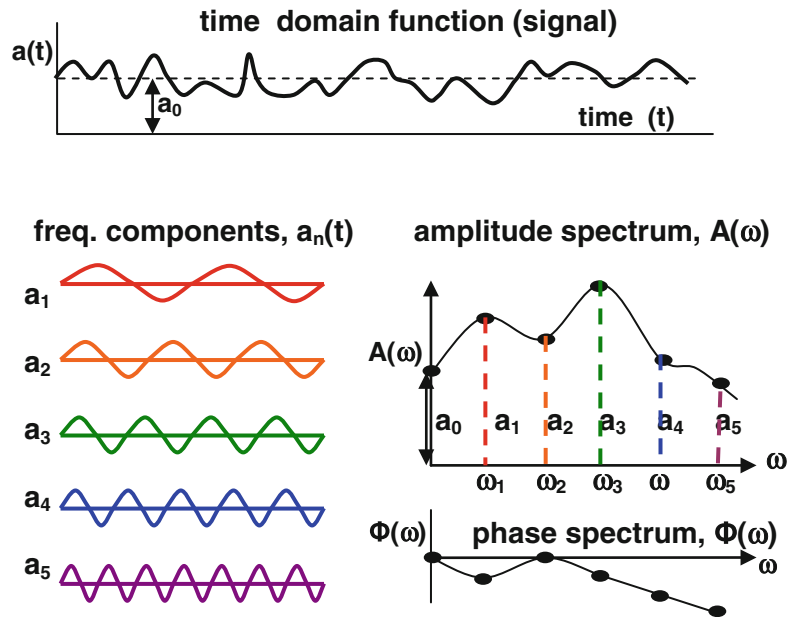


**Fig. 9.10** Pictorial representation of spectrum analysis. The signal (at top of figure) is Fourier-transformed into its frequency components shown as amplitude and phase spectra



$$\int_{-\infty}^{\infty} \{f(t)\}^2 dt = \frac{1}{2\pi} \int_{-\infty}^{\infty} |F(\omega)|^2 d\omega$$

(frequency-domain) function. In fact, any realizable function  $f(t)$  has its own frequency-domain counterpart,  $F(\omega)$ . The two functions  $f(t)$  and  $F(\omega)$  are normally called (Fourier pair), when  $f(t)$  is Fourier-transformable into  $F(\omega)$ , that is,



The real quantity  $|F(\omega)|^2$  is normally considered to be the (power spectrum) or energy spectrum of the function  $f(t)$ . It is important to note here, that the power spectrum is square of the amplitude spectrum.

### 9.3.4 The Two-Domain Concept

With the application of the Fourier transform, it is possible to transform a function from a function of time  $f(t)$ , to a function of frequency  $F(\omega)$  with no loss of information. This implies that a given function can be expressed either as function of time  $f(t)$ , called (time-domain function) or as function of frequency  $F(\omega)$ , which is called

The main advantage of the two-domain concept is that computation is much simplified when working in the frequency domain. The concept is very much like logarithms and anti-logarithms domains. Thus multiplication of numbers becomes simple addition in the logarithm domain. The outstanding example in time series analysis is convolution and deconvolution computations. Convolution and deconvolution processes in the time domain become simple multiplication and division of the corresponding functions in the frequency domain.

To take advantage of this property, some processes in data processing are done by, first Fourier-transforming the signal (such as a seismic trace) from time domain to the frequency

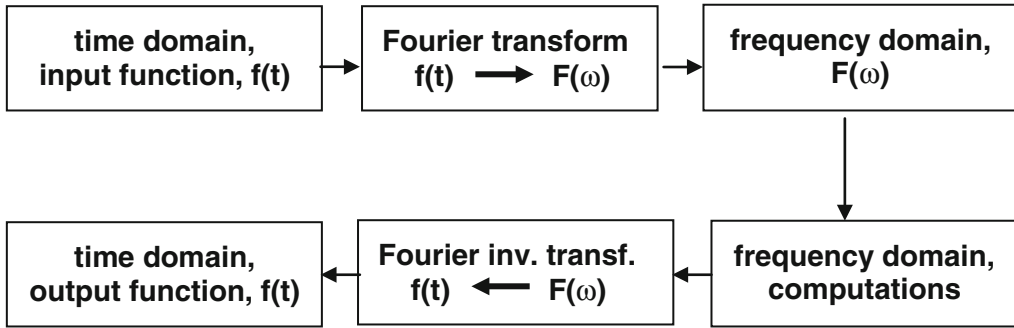


Fig. 9.11 Block diagram showing the principle of domain-to-domain transformation

domain, doing the computation in this domain (which is much faster than in the time-domain) and the result is inverse-transformed to the original time-domain. This is explained as follows (Fig. 9.11).

$$P(\omega) = \int_{-a}^a p(t)e^{-i\omega t} dt = \int_{-a}^a e^{-i\omega t} dt = (2 \sin a\omega)/\omega$$

Hence,

$$P(\omega) = (2 \sin a\omega)/\omega = (2a \operatorname{sinc}(a\omega/\pi))$$

### 9.3.5 Spectrum of the Rectangular Pulse

As an example of application of the Fourier integral, let us determine the frequency spectrum of a rectangular pulse,  $p(t)$  of width  $(2a)$ , and height  $(1)$ . The function is defined as Fig. 9.12:

$$p(t) = 1, \quad -a < t < a \\ = 0, \quad \text{elsewhere}$$

By direct application of the Fourier Transform,  $F(\omega) = \int_{-\infty}^{\infty} f(t)e^{-i\omega t} dt$ , we get:

The resulting spectrum function,  $P(\omega)$  of the transient function,  $p(t)$ , which is a rectangular pulse, is found to be of the form  $(\sin \pi x)/\pi x$  where  $x = a\omega/\pi$ . The value of this function is zero whenever  $(\sin x = 0)$ . This occurs at  $(a\omega = n\pi)$ . At the origin, however, where  $x = 0$ , the function value is equal to  $(2a)$ . With the increase of  $(\omega)$ , the spectrum function  $P(\omega)$  oscillates about the  $(\omega$ -axis) with decreasing amplitude. The Fourier pair,  $p(t) \leftrightarrow P(\omega)$ , is sketched in Fig. 9.12.

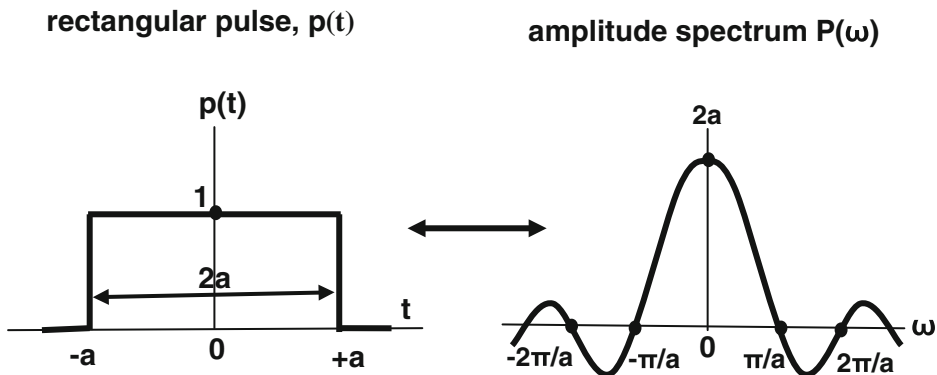


Fig. 9.12 The window pair of the rectangular-pulse, box-car time function,  $p_a(t)$  and its spectrum, sinc-type function,  $P(\omega) = (2\sin a\omega)/\omega$

In the geophysical literature, this function is known as the (**sinc**) function. The function (**sinc x**) is defined as (**sincx**)/x or (**sincπx**)/πx (Sheriff 2002, p. 320). Fourier transform **P(ω)** of the rectangular function (normally called box-car function, **p(t)**) is the sinc function, **2a sinc(aω/π)**.

### 9.3.6 Spectrum of the Spike Pulse

Mathematical analysis proved that there is an inverse relationship between the width of the time-domain function (as a seismic pulse) and its frequency domain amplitude spectrum. Thus, as the pulse gets narrower, the corresponding frequency-domain spectrum becomes wider, and vice versa. This behavior can be readily seen in case of the rectangular pulse-spectrum Fourier pair. The main lobe of its spectrum extends from ( $\omega = -\pi/a$ ) to ( $\omega = +\pi/a$ ). This clearly indicates that the spectrum has inverse relation to the original pulse width (**2a**). In fact, this is one of the important properties that hold for all Fourier pairs of pulse-shaped functions.

According to this principle (called the reciprocity property) it is readily seen that as the

pulse rectangle gets narrower, the corresponding amplitude spectrum gets wider, and in the limiting state, the pulse becomes spike-function (impulse function) with infinitely wide spectrum (Fig. 9.13).

Another important conclusion can be drawn from this behavior, and that is the spike time function contains infinite number of equal-amplitude frequency components. For this reason the spectrum of a spike signal is often described as being white spectrum.

### 9.3.7 The Dirac-Delta Function

The zero-width pulse (impulse) is called (Dirac delta function) and given the symbol  $\delta(t)$ . This special function is defined as being a compressed rectangular pulse defined to be of width, approaching zero and having a unit area (Báth 1974, p. 52). It is considered as being even function and hence it has a real spectrum function which is constant at the value of unity for all frequencies. This means that the Delta function can be synthesized by superposing an infinite number of sine functions which are in phase at

**Fig. 9.13** The reciprocal relation between the width of the time-domain pulse and that of its amplitude spectrum

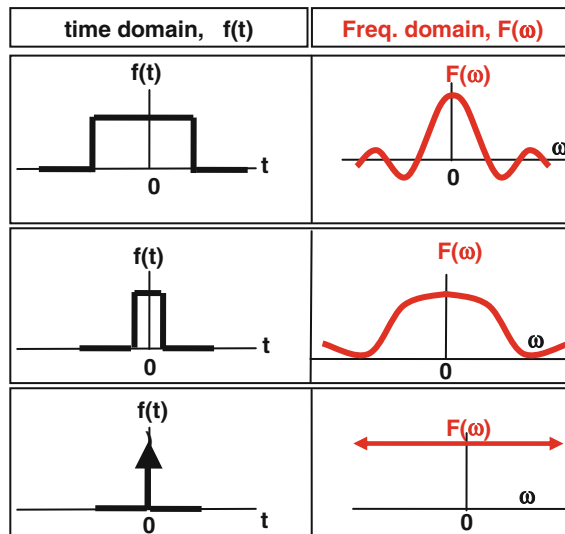
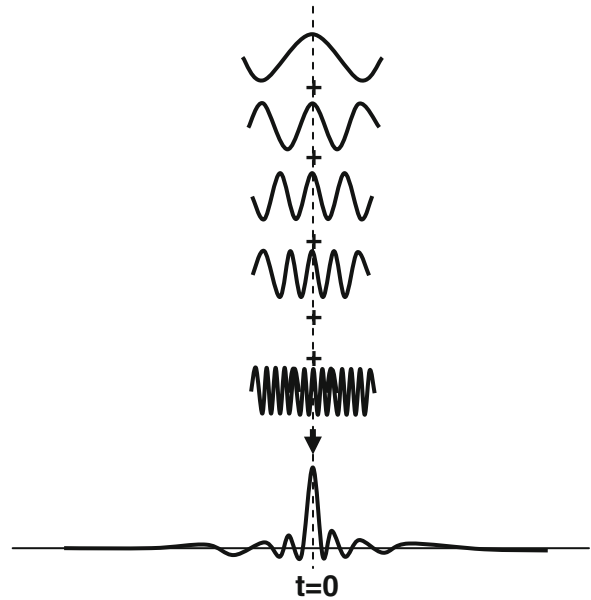


**Fig. 9.14** Synthesis of an impulse function from summing sine functions of equal amplitude and in phase at the origin time,  $t = 0$



one point (at  $t = 0$ ) where the components will add up constructively, and destructively elsewhere as shown in Fig. 9.14.

Dirac delta function,  $\delta(t)$  is not a proper mathematical function. It is usually considered as a mathematical concept which possesses its own mathematical properties. It is defined as:

$$\delta(t) = 0 \quad \text{for } t \neq 0 \quad \text{and} \quad \int_{-\infty}^{\infty} \delta(t) dt = 1$$

The delta function is even,  $\delta(t) = \delta(-t)$ , and it forms the Fourier pair ( $\delta(t) \leftrightarrow 1$ ). Further, we have another important property which states that its convolution with a function leaves the convolved function unchanged, that is:  $\delta(t) * f(t) = f(t)$ .

### 9.3.8 Frequency Limits of Fourier Spectra

Spectra of observed signals are characterized by two main features. The signal prepared for the analysis, is of finite length and it is in digital form. Both of these features impose limits on the frequency limits over which the spectrum is computed.

The signal length ( $T$ , say) defines the lowest, or fundamental frequency ( $f_L = 1/T$ ) in the spectrum. Also, it defines the frequency increment,  $\Delta f (= 1/T)$  of the spectrum computation. The digitization interval, or sampling period ( $\Delta t$ ), on the other hand, sets the upper frequency limit of the spectrum. In fact, the upper limit is the Nyquist frequency ( $f_N$ ) which is equal to  $(1/2\Delta t)$ . With consideration of these limits, spectrum of an observed signal, of finite length ( $T$ ) and digitized at ( $\Delta t$ ) interval, is usually computed for the frequencies:

$$1/T, \quad 2/T, \quad 3/T, \quad \dots, \quad 1/2\Delta t$$

Thus, a digital signal made up of  $(N + 1)$  samples, will be of length ( $T$ ) given by ( $T = N\Delta t$ ). By substituting  $(T/N)$  for ( $\Delta t$ ), computation frequencies will be:

$$1/T, \quad 2/T, \quad 3/T, \quad \dots, \quad N/2T$$

That is at frequencies,  $n f_L$ , where  $n = (1, 2, 3, \dots, N/2)$ .

From this result, we can draw an important conclusion which states that the number of significant frequency-values taken in computing a frequency spectrum of a digital signal, is half the number of the samples of that signal.

Finally, it should be emphasized that the length ( $T$ ), controls the (resolution power) of the computed spectrum, since the frequency interval  $\Delta f$  ( $= 1/T$ ) is inversely proportional to the length ( $T$ ).

### 9.4 The Phase Spectrum

From the previous paragraph, we learned that the frequency spectrum  $F(\omega)$ , of any real time function is generally a complex function, consisting of the modulus;  $|F(\omega)|$  called (amplitude spectrum) and the argument  $\theta(\omega)$ , called (phase spectrum). The importance of the phase characteristics of a seismic signal is that it has direct influence on the signal shape. Signal amplitude, on the other hand has a direct effect on the signal energy. The phase of a frequency component is measured by the time shift of a peak of a cycle with respect to time zero, considered to be the start time. Thus, the start time is the time relative to which all phases of the frequency components are referred to. In general, the phase value may be negative, zero or positive.

Seismic signals, like seismic reflection wavelets, are all of the type of signals which are existing only in the positive side of the origin time. Such functions (called one-sided functions) consist of the sum of frequency components of different amplitudes and different phase shifts.

These are expressed in the frequency domain by the amplitude- and phase-spectra as shown in Fig. 9.15.

In Fig. 9.15, signal-1 has negative time-phase (positive phase-angle), while signal-2 is of zero-phase. The rest of frequency components are of negative phase angles. These amplitude and phase characteristics are shown in the corresponding frequency domain spectra.

#### 9.4.1 The Zero-Phase Spectrum

If all the frequency components are of zero phase (symmetrical about time zero), their sum will give a zero-phase wavelet, symmetrical about zero time. The phase spectrum, in this case, is a straight line drawn along the frequency axis at zero phase-value. Amplitude and the phase spectrum for this case are shown in Fig. 9.16.

Note that the amplitude spectra in the two Figs. 9.15 and 9.16 are the same, but their respective time domain signal-shapes are different. This difference in shape is due only to their different phase spectra. Another useful note is that the recorded seismic reflection wavelet is one-sided signal. It cannot be zero-phase since, by definition, it has no energy before time zero as one-sided signal demands. However, conversion into zero-phase wavelet can be done by

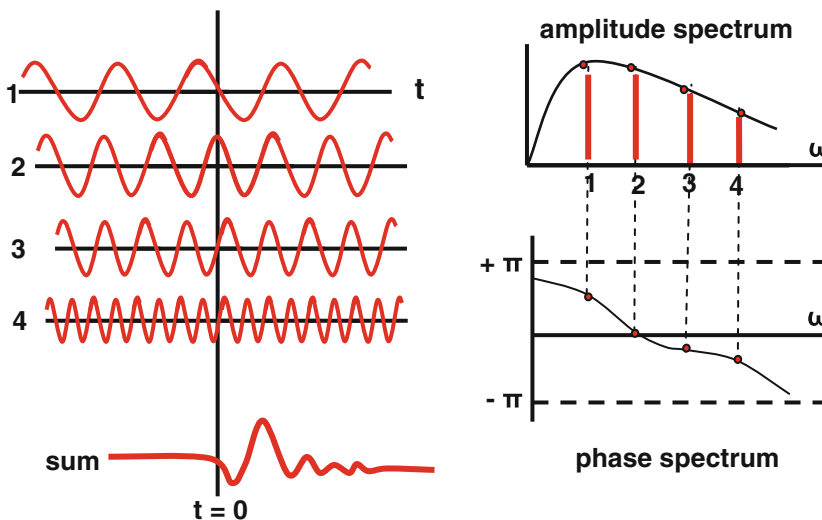
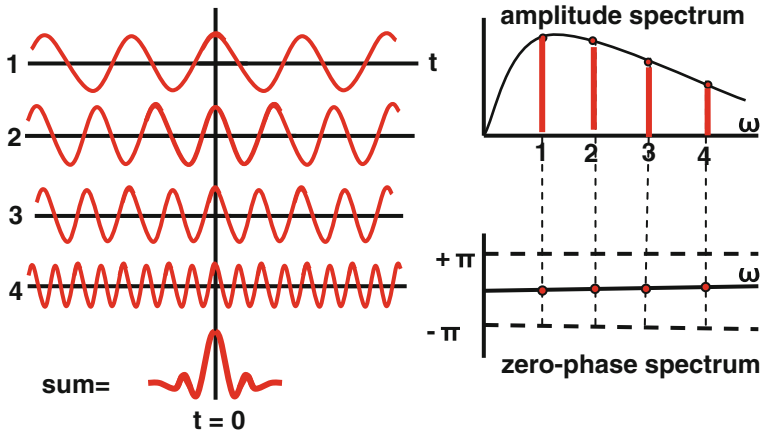


Fig. 9.15 Set of frequency components (sine functions) of a one-sided signal, expressed in the frequency domain by amplitude- and phase spectra



**Fig. 9.16** Set of frequency components (sine functions) of a zero-phase signal, with its amplitude and phase spectra

application of special computer programs. This can be done in processing stage to convert the one-sided wavelet to a zero-phase wavelet of symmetrical shape. This is normally asked for by interpreters for more clear definition of reflection events and easier to follow in the process of interpretation especially for structural purposes.

frequency. In this case, each frequency component will be shifted by the same time shift (Sheriff and Geldart 1995, p. 533). The sum, in this case, will be like the zero phase spectrum (symmetrical wavelet), but the symmetry will be about a time later than zero-time. The phase spectrum will be a straight line inclined to the frequency axis (Fig. 9.17).

**9.4.2 The Linear-Phase Spectrum**

**9.4.3 The Constant-Phase Spectrum**

A closely associated case is the linear phase spectrum, in which the phase is linear function of

The constant phase spectrum is a special case of linear phase spectrum. The shift is not function of

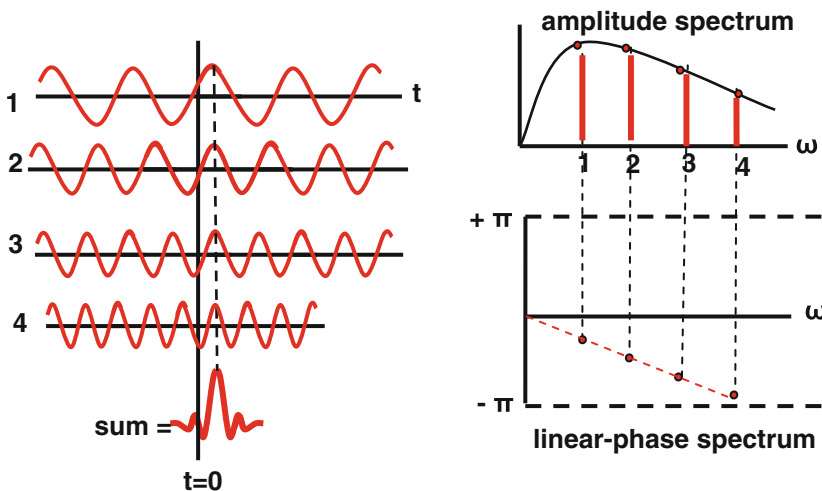


**Fig. 9.17** Set of frequency components (sine functions) of a linear-phase signal, with amplitude and phase spectra

frequency but having a constant value. Thus when the phase value is constant at zero-value, we get a zero-phase spectrum as shown in Fig. 9.16. If the constant shift is a non-zero value, the phase spectrum is also a straight line, but it is parallel to the frequency axis. For example if the constant phase shift is at later-than the time zero by quarter a period ( $\tau/4$ , say), which is equivalent to  $(-\pi/2)$ , the phase spectrum will be a straight line located at  $(\pi/2)$  below the frequency axis. In this case, the frequency components will all have the constant phase of  $(-\pi/2)$  and their sum will give an inverted-symmetry wavelet that has its main peak immediately following the time zero (Fig. 9.18).

If the phases of the frequency components are all equal to  $(+\pi/2)$  instead of  $(-\pi/2)$ , the phase spectrum will be a straight line at  $(\pi/2)$  above the frequency axis. In this case, all the components will have troughs immediately following the time zero, and the wavelet resulting from summing the components will, likewise, have a trough following time zero.

The last interesting constant-phase case is a wavelet having all its component frequencies of equal phases, at the constant phase of  $(-\pi)$ , which is the same as  $(+\pi)$ . The constant-phase

spectrum in this case is straight line parallel to the frequency axis and located at  $(\pi)$  below (or above) the frequency axis. The  $(-\pi)$  or  $(+\pi)$  phase of a component implies that it has a trough at time zero. The wavelet resulting from summing such components will be symmetrical and will have a trough at time zero as shown in Fig. 9.19.

### 9.5 Spectra of Observational Data

As far as Fourier analysis is concerned, an observational function differs from an analytic function in two main aspects. The observed function is not infinite and not continuous as an analytic function would be. Thus, a signal, (normally, time function), inputted to the transformation process, is finite in length and digital in form. Observational functions, which are input for spectral analysis, are usually not continuous and not infinite in length as Fourier Transform integral demands. For this reason, observational spectra suffer from the two types of distortion which are resulting from signal-truncation and signal-digitization. These effects shall be discussed as follows:

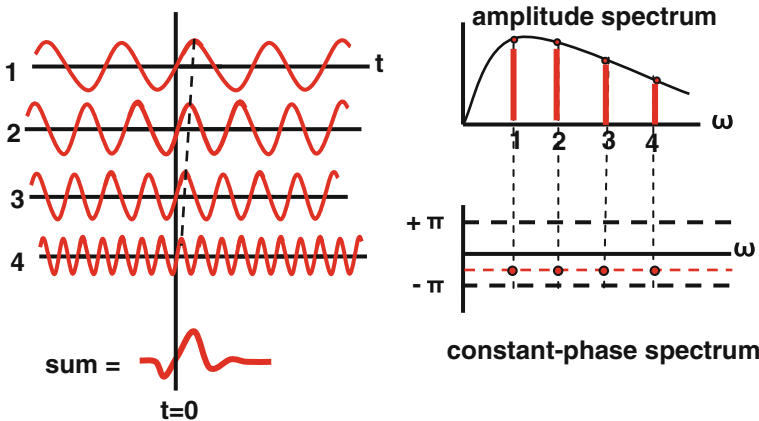


**Fig. 9.18** Set of frequency components (sine functions) of a constant-phase (at phase =  $-\pi/2$ ), with amplitude and phase spectra

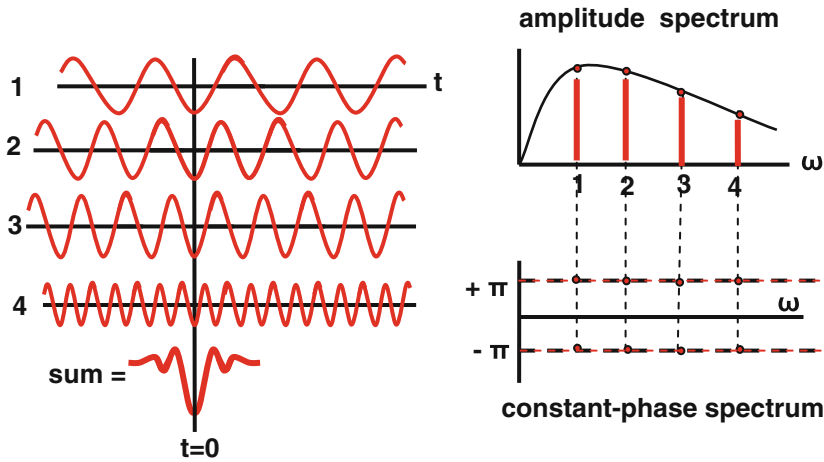


**Fig. 9.19** Set of frequency components (sine functions) of a constant-phase (at phase =  $-\pi$ , or at phase =  $+\pi$ ), with amplitude and phase spectra

### 9.5.1 Truncation Effect and Windowing

Normally, a signal of finite length is effectively equivalent to multiplying of infinitely long signal  $f(t)$  by a rectangular function of finite-length ( $T$ , say) and of constant value (usually equal to unity). This function which is sometimes called box-car function, or box-car time window,  $w(t)$ , is defined by:

$$w(t) = 1 \quad -T/2 < t < T/2$$

$$= 0 \quad \text{elsewhere}$$

infinity to plus infinity. Being computed for signals of finite lengths, spectra of truncated signals are always suffering from distortion which gets more severe the shorter the truncation length.

One of the important properties of Fourier Transform (the convolution Theorem) states that, multiplication of two functions in the time domain becomes convolution in the frequency domain, and convolution in the time domain becomes multiplication in the frequency domain. That is:

$$f_1(t) \cdot f_2(t) \longleftrightarrow F_1(\omega) * F_2(\omega)$$

The truncated function,  $f_{tr}(t)$  is given by  $f_{tr}(t) = f(t) \cdot w(t)$ . This process will isolate (truncate) the length ( $T$ ) desired for the analysis. Truncation, which is an unavoidable process, violates Dirichlet conditions which demands that Fourier Integral must be computed from minus

Truncating of a signal is effectively done by multiplying the infinitely long signal by a box-car function of value (1) over the needed part of the signal, that is  $(f(t) \cdot w(t))$ . By applying the convolution theorem, the Fourier spectrum  $F_{tr}(\omega)$  of the truncated function  $f_{tr}(t)$  is therefore, given by  $F(\omega) * W(\omega)$ , that is:

$$F_{tr}(\omega) = F(\omega) * W(\omega)$$

where  $F(\omega)$  and  $W(\omega)$  are the Fourier transforms of  $f(t)$  and  $w(t)$  respectively.

Since  $W(\omega) = (2/\omega) \sin(\omega T/2)$ , we can write:

$$F_{tr}(\omega) = F(\omega) * (2/\omega) \sin(\omega T/2),$$

This shows that signal truncation incurs a smoothing effect due to convolution of the true spectrum  $F(\omega)$  with the spectrum of the window function,  $W(\omega)$ . In addition of the smoothing effect side lobes are also created. So, the spectrum of a truncated signal is distorted, and the nature of distortion is the smoothing effect and development of side lobes as shown by Fig. 9.20.

Since an infinitely long rectangular pulse has a spectrum approaching an impulse function, it

can be seen (top case in Fig. 9.20) that an un-truncated signal is equivalent to a truncated signal using an infinitely long truncation rectangular function (window). Such a window has an impulse-form spectrum. Theory shows that convolution of an impulse with a function leaves that function unchanged (see Sect. 9.3.7, above).

### 9.5.2 The Rectangular Window (Box-Car)

In order to get the least possible spectrum distortion, the time interval of the window function must be as long and smooth (free of sharp corners) as it can be (Båth 1974, pp. 155–171). Many types of window functions have been developed for application in this field (8 window types were presented by Sheriff 2002, p. 397).

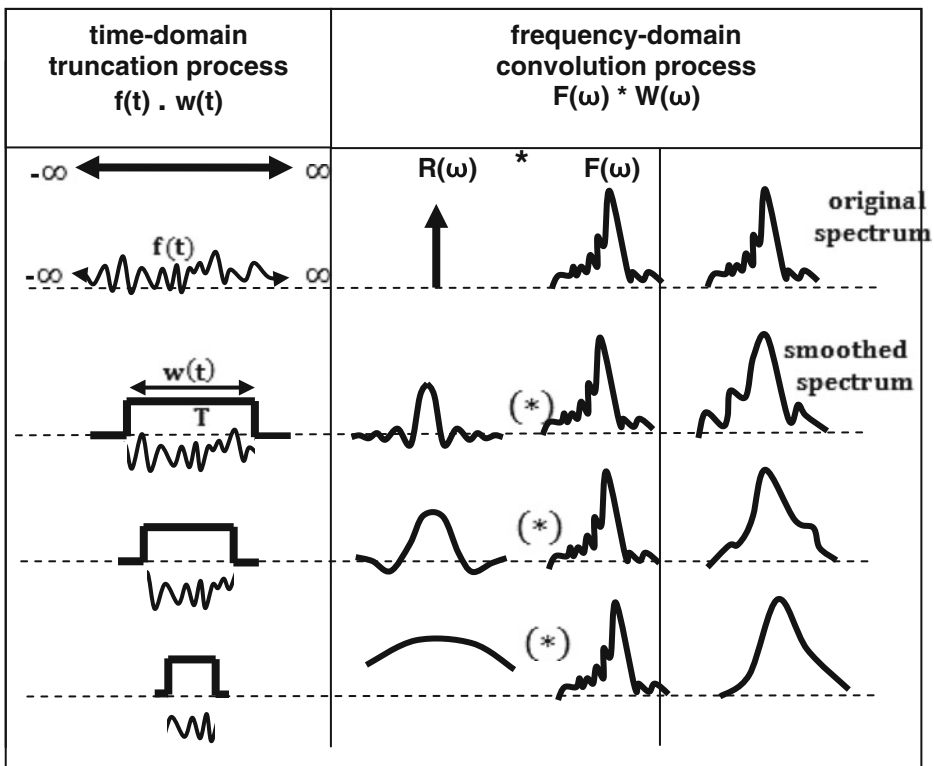


**Fig. 9.20** Effect of varying the truncation window width ( $T$ ) on smoothing of the spectrum  $F(\omega)$  of the truncated signal  $f(t)$ . Smoothing is more severe with shorter length,  $T$

A window designer usually aims at defining a window function that has the least time-domain distortion and at the same time incurs least smoothing effect in the frequency domain. Two types of windows will be presented here:

A window function  $w(t)$ , is in the shape of a rectangular pulse of width  $(2T)$  and height  $(1)$ . It is defined as:

$$w(t) = 1 \quad |t| \leq T$$

$$= 0 \quad |t| > T$$

The spectrum of this window, given by Papoulis (1962, p. 20) is:  $W(\omega) = 2 (\sin \omega T) / \omega = 2T \text{sinc}(\omega T / \pi)$ .

This window is ideal in the time domain as it isolates the function exactly as it is, with no any modification. In the frequency domain, however, it causes relatively high spectrum distortion (smoothing) because of the sharp corners which cause large side lobes. The spectrum window is a sinc-type function in which the width of its central lobe is inversely proportional to the width of the time-domain window.

### 9.5.3 Triangular Window (Bartlett)

This window, commonly known by the name (Bartlett Window), is more often applied window in seismic data processing. It is of a triangular shape, defined as:

$$w(t) = 1 - t/T \quad |t| \leq T$$

$$= 0 \quad |t| > T$$

The spectrum window  $W(\omega)$ , is square of the spectrum of the rectangular function. It is given by Papoulis (1962, p. 21):  $W(\omega) = (4/T) [\sin(\omega T/2) / \omega]^2 = T \text{sinc}^2(\omega T/2\pi)$ .

Bartlett window has a tapering effect on the truncated signal, introducing a change of a linear-scaling type. In the frequency domain, however, it causes relatively less spectrum distortion (less smoothing) because of the sharp impulsive shape of its spectrum. As it is indicated by its formula, Bartlett window (in the frequency domain) has no negative values as the other spectrum windows.

The two windows and their respective spectra are sketched in Fig. 9.21.

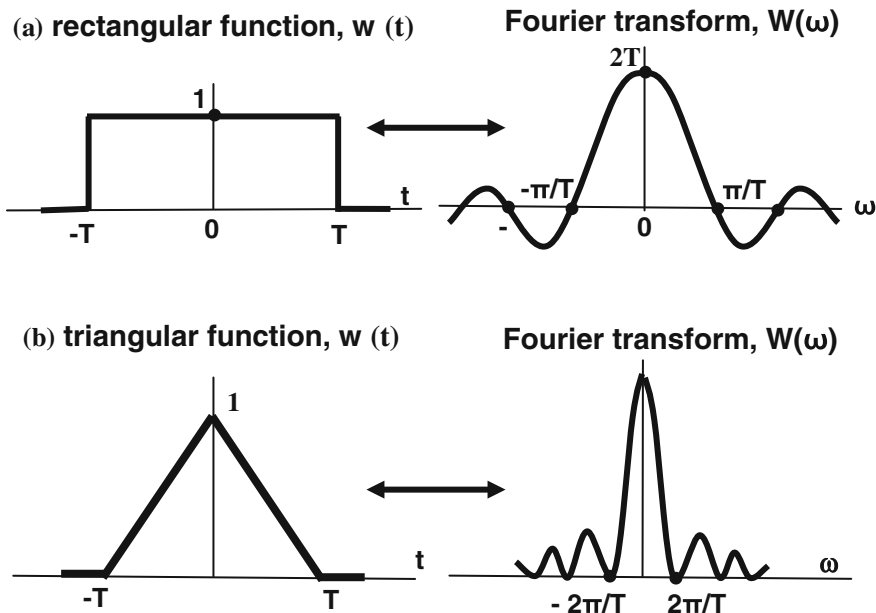


**Fig. 9.21** The two time windows in common use in seismic data processing and their spectra. **a** The rectangular time-function, or Box-car window and **b** the triangular time-function, or Bartlett window

### 9.6 Correlation Functions

#### 9.6.1 Cross Correlation Function, $C_{12}(\tau)$

Given two functions;  $f_1(t)$  and  $f_2(t)$ , the cross-correlation function  $C_{12}(\tau)$  is defined as:

$$C_{12}(\tau) = \int_{-\infty}^{\infty} f_1(\tau) \cdot f_2(t + \tau) dt$$

and, in digital summation over (i), it is:

$$C_{12}(j) = \sum f_1(i) \cdot f_2(i + j)$$

$$C_{12}(\tau) = f_1(\tau) \boxtimes f_2(\tau)$$

where, ( $\boxtimes$ ) represents correlation process, ( $\tau$ ) is called the time lag.

In practice, it is a shift, multiply, and sum process (Fig. 9.22).

#### 9.6.2 Autocorrelation Function $C_{11}(\tau)$

Given a function;  $f_1(t)$ , the autocorrelation function  $C_{11}(\tau)$  is defined as:

for analogue functions:  $C_{11}(\tau) = \int f_1(\tau) \cdot f_1(t + \tau) dt$

for digital functions:  $C_{11}(j) = \sum f_1(i) \cdot f_1(i + j)$

in symbolic form:  $C_{11}(\tau) = f_1(\tau) \boxtimes f_1(\tau)$

This definition can be represented in the following symbolical way:

where, ( $\boxtimes$ ) represents correlation process, ( $\tau$ ) is called the time lag.

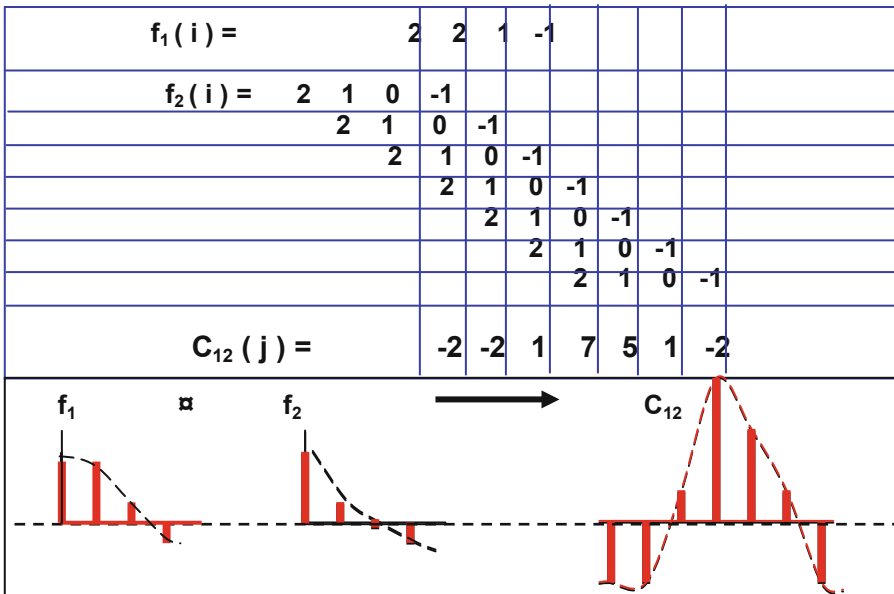
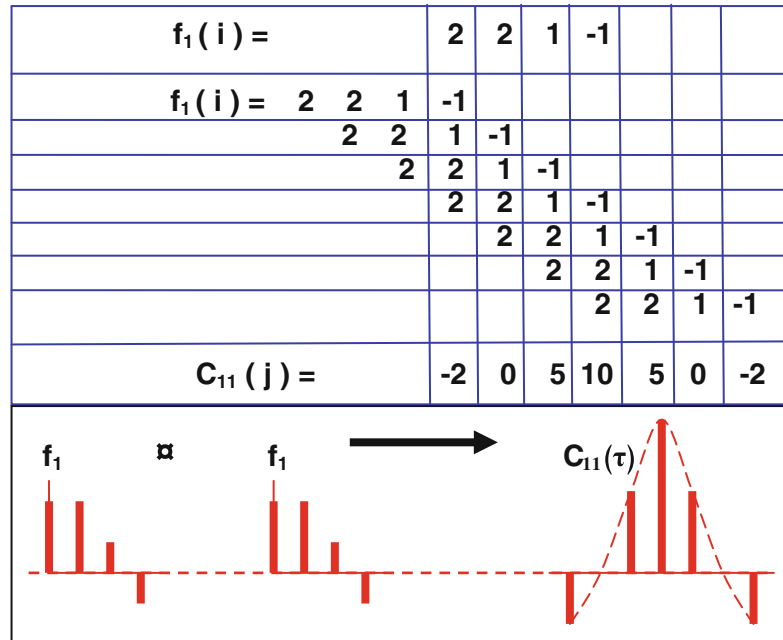


Fig. 9.22 Cross-correlation of the two functions ( $f_1$ ) and ( $f_2$ )

**Fig. 9.23** Autocorrelation of the function ( $f_i$ )



In practice, it is a shift, multiply, and sum process as it is done in computing the cross-correlation function (Fig. 9.23).

The function  $C_{11}(\tau)$  is even function,  $C_{11}(\tau) = C_{11}(-\tau)$ , that is, symmetrical about the point ( $\tau = 0$ ).

maxima at a period equal to the periodicity of the hidden periodic signal if it is existing in the original function. Most intensive use of the autocorrelation functions is in computing power spectra and in the deconvolution computations.

### 9.6.3 Properties and Applications of Correlation Functions

The cross-correlation function serves as a tool to indicate the degree of similarity between the correlated functions. Its peak grows large when the original functions are similar and decreases otherwise. It approaches zero in case of random data as in case of random noise. Thus it can detect signals embedded in random noise. Typical application in seismic exploration is in sweep correlation with seismic traces obtained from Vibroseis sources, and in computing the residual static corrections.

The autocorrelation function can be used in detecting hidden periodicities. In this case the autocorrelation function will show repeated

### 9.6.4 Correlation Functions in the Frequency Domain

Correlation process, which is a shift-multiply-and sum process, becomes a simple multiplication process in the frequency domain, where the amplitude spectra of the involved functions are multiplied and their respective phases subtracted, as shown in the following table.

Time-domain	Frequency-domain
$f_1(t)$	$F_1(\omega)$
$f_2(t)$	$F_2(\omega)$
$c_{12}(t) = f_1(t) \times f_2(t)$	$C_{12}(\omega) = F_1(\omega) \cdot F_2(\omega)$ $\Phi_{12}(\omega) = \Phi_1(\omega) - \Phi_2(\omega)$
$c_{11}(t) = f_1(t) \times f_1(t)$	$C_{11}(\omega) = \{F_1(\omega)\}^2$ $\Phi_{11}(\omega) = 0$

It is useful to note here that the autocorrelation function in the time domain is transformed into power spectrum in the frequency domain. It is also important to note that the phase spectrum,  $\Phi_{11}(\omega)$ , is equal to zero. This provides an alternative method which allows computing power spectra from the autocorrelation function instead of squaring the amplitude spectrum.

### 9.7 Convolution

Like correlation functions, Convolution is a mathematical process taking place between two functions to output a new function the convolution output. Convolution of the two functions;  $f(t)$  and  $h(t)$  is defined by the integral:

$$y(t) = f(t) * h(t) = \int_{-\infty}^{\infty} f(\tau) \cdot h(t - \tau) d\tau$$

and, in digital summation over (j), it is:

$$y_j = f_i * h_i = \sum f_i \cdot h_{j-i}$$

The star symbol (\*) represents convolution computation

Computation of the convolution process is done in the same way as in the correlation process (described above) except for the need to reverse one of the two functions involved in the process. Here is an example to clarify the process of convolving  $f_i$  with  $h_i$  where  $f_i = \{ 2 \ 1 \ 3 \ 0 \ -1 \}$  and  $h_i = \{ 3 \ 1 \ 2 \}$ . The convolution process starts with reversing one of the two functions and then continues with shifting, multiplication, and summing processes, shown as follows:

$f(i) =$			2	1	3	0	-1		
$h(i) =$	2	1	3						
		2	1	3					
			2	1	3				
				2	1	3			
					2	1	3		
						2	1	3	
							2	1	3
$y(i) =$			6	5	14	5	3	-1	-2

There are several other methods to compute convolution. These methods involve use of: special tables, special matrix, and by z-transform. Methods of computation and mathematical properties of the convolution process are summarized in Alsadi (1980, p. 88–90).

The process involved in convolution (shift-multiply-and-sum process) is shown graphically in Fig. 9.24, in which the function  $f(t)$  is convolved with the function  $h(t)$ .

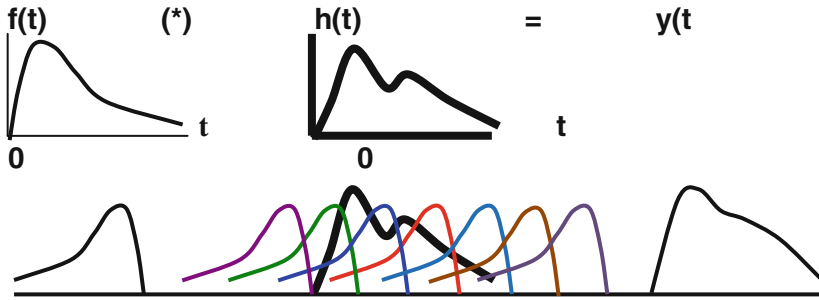


**Fig. 9.24** Convolution of the functions  $f(t)$  and  $h(t)$

In this example,  $h(t)$  is kept stationary while the function  $f(t)$  after being reversed, moved along the time-axis, with the multiplication and summation processes. The output is a new function,  $y(t)$ .

In the frequency domain, the convolution between two time functions becomes multiplication between their respective amplitude spectra and addition of the two phase spectra.

$$C_{11}(t) = f_1(t) * f_1(-t)$$

These results gave another form of definition of the cross-correlation and autocorrelation functions in terms of convolution processes.

Convolution is the time-domain mathematical computation that takes place in the process of frequency-filtering of signals.

time -domain	frequency -domain
$f(t)$	$F(\omega)$
$h(t)$	$H(\omega)$
$y(t)$	$Y(\omega)$
$y(t) = f(t) * h(t)$	$Y(\omega) = F(\omega) \cdot H(\omega)$ $\Phi_y(\omega) = \Phi_F(\omega) + \Phi_H(\omega)$

By comparing the convolution definition with that of the cross-correlation of the two functions  $f_1(t)$  and  $f_2(t)$ , it can be shown that:

$$C_{12}(t) = f_1(t) * f_2(-t)$$

and

### 9.8 Deconvolution

As its name implies, deconvolution is a mathematical process which counteracts a previously done convolution process. It is a mathematical

process that can result in computing one of two convolved functions, given the convolution output together with one of the two input functions. Thus, for a convolution process  $\mathbf{f}(\mathbf{t}) * \mathbf{h}(\mathbf{t}) = \mathbf{y}(\mathbf{t})$ , deconvolution is the process of finding the function  $\mathbf{f}(\mathbf{t})$ , say, given the output function  $\mathbf{y}(\mathbf{t})$  and the second input function  $\mathbf{h}(\mathbf{t})$ , that is:

$$\mathbf{y}(\mathbf{t}) = \mathbf{f}(\mathbf{t}) * \mathbf{h}(\mathbf{t})$$

Deconvolution is the process of finding a function,  $\mathbf{g}(\mathbf{t})$ , called deconvolution operator which, by convolution with the output function  $\mathbf{y}(\mathbf{t})$ , will recover the original input function  $\mathbf{f}(\mathbf{t})$ , that is:

$$\mathbf{f}(\mathbf{t}) = \mathbf{y}(\mathbf{t}) * \mathbf{g}(\mathbf{t})$$

By substitution in the last equation, we get:

$$\mathbf{f}(\mathbf{t}) = \mathbf{f}(\mathbf{t}) * \mathbf{h}(\mathbf{t}) * \mathbf{g}(\mathbf{t})$$

In mathematics, there is a special function, the Dirac delta function  $\delta(\mathbf{t})$ , which has the property of outputting the same function when it is convolved with any input function (Bracewell 1965, p. 75), that is:

$$\mathbf{f}(\mathbf{t}) * \delta(\mathbf{t}) = \mathbf{f}(\mathbf{t})$$

Applying this property, we get:

$$\mathbf{h}(\mathbf{t}) * \mathbf{g}(\mathbf{t}) = \delta(\mathbf{t})$$

which expresses the type of relation existing between the convolution operator,  $\mathbf{h}(\mathbf{t})$  and deconvolution operator,  $\mathbf{g}(\mathbf{t})$ .

In seismic reflection surveying, the source function is represented by the function  $\mathbf{f}(\mathbf{t})$  and the seismic recorded trace that is created from the passage of the source wavelet through the earth material is  $\mathbf{y}(\mathbf{t})$ . Thus, to undo the convolution process and determine  $\mathbf{f}(\mathbf{t})$  from the known seismic trace  $\mathbf{y}(\mathbf{t})$ , the equation  $\mathbf{f}(\mathbf{t}) = \mathbf{y}(\mathbf{t}) * \mathbf{g}(\mathbf{t})$  is worked out if  $\mathbf{g}(\mathbf{t})$  is known. Because, in general, the filter response of the earth  $\mathbf{h}(\mathbf{t})$  is unknown, deconvolution operator  $\mathbf{g}(\mathbf{t})$  cannot be determined using a deterministic method. For

this reason a special statistical method is employed.

In the frequency domain, convolution between two time functions, become multiplication of their respective spectra, and using the Fourier pair  $\delta(\mathbf{t}) \leftrightarrow 1$ , we get:

$$\begin{aligned} \mathbf{H}(\omega) \cdot \mathbf{G}(\omega) &= 1 \\ \mathbf{G}(\omega) &= 1/\mathbf{H}(\omega) \end{aligned}$$

Thus, in frequency domain, the relation between convolution operator  $\mathbf{h}(\mathbf{t})$  and deconvolution-operator  $\mathbf{g}(\mathbf{t})$ , becomes simple arithmetic multiplication process.

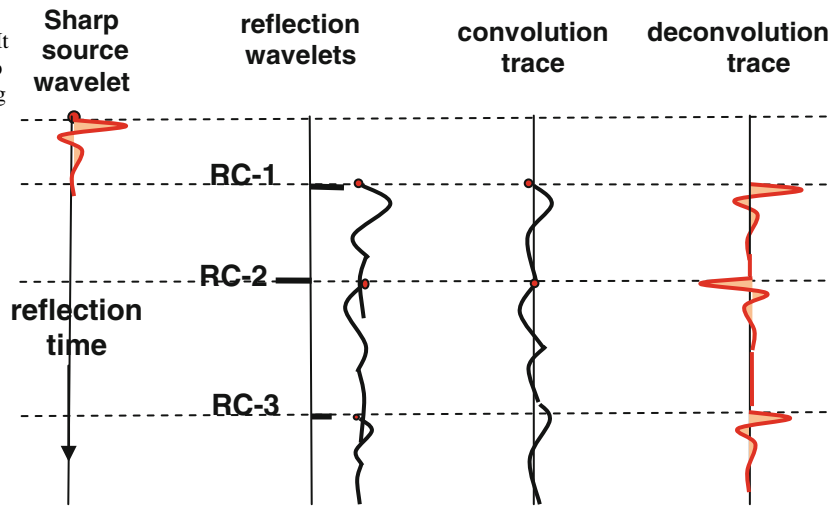
### 9.8.1 Deconvolution Main Objectives

As far as the reflection wavelet is concerned, there are two main types of distortion-sources; loss of high frequency-components, mainly due to the earth high-cut filter and generation of multi-reflections, as reverberations and ghosts. The net effect of these two types of distortion is changing the source function into an extended, low-frequency, low-energy wavelet. In certain shooting conditions we may have other types of wavelet distortion like reverberations, ghosts in land shooting, or ringing and bubble-oscillation effects in marine shooting. In general, seismic trace (created by convolution processes) is made up of a series of overlapping filtered wavelets. As a result, the recorded reflection wavelet will suffer from loss of resolution (due to earth filtering action) and shape distortion (due to overlapping of repeated reflections).

Deconvolution is the process which restores the original pulse-shaped source function that is retrieval of the lost high frequencies, and removal of the repeated reflection wavelets (dereverberation and deghosting). The total environment of the trace distortions and role of deconvolution in wavelet-restoration is shown schematically in Fig. 9.25.

This figure summarizes the two types of distortion (shape distortion and overlapping of

**Fig. 9.25** The deconvolution objectives. It recovers the original sharp source wavelet by undoing the convolution (earth high-cut filtering) and removing multi-reflection events as reverberations



repeated reflections), which take place during the seismic reflection journey. These changes are produced by convolution processes. Deconvolution is, therefore, the process that can unravel these convolution processes and recover the undistorted seismic trace. After deconvolution, the recorded reflection wavelets become well separated spike-shaped wavelets and free of reverberations.

### 9.8.2 Spiking (Whitening) Deconvolution

Based on the type of wavelet-distortion resulting from convolution processes affecting the source wavelet during its travel, there are two most commonly used types of deconvolution. These are the spiking deconvolution and the gapped deconvolution (explained as follows).

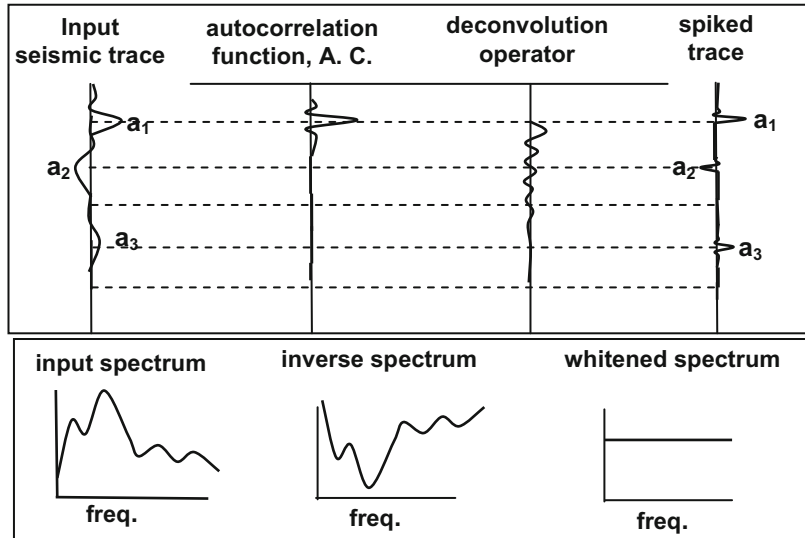
In the time-domain, this type of deconvolution is described, as spiking deconvolution, because it produces compressed spike-like reflection wavelets. In the frequency domain, it is whitening because its output spectrum is flat (white spectrum) over wide frequency range of the data. Spiking deconvolution counteracts the high-cut filtering effect (convolution process) that the source wavelet experiences due to inelastic attenuation.

Derivation of the spiking deconvolution operator is based on a statistical approach. It depends on a principle called Least-Square Wiener's Optimality (Robinson and Treitel 1967). The operator wavelet (inverse filter) is derived from the autocorrelation function of the input trace. By convolving the derived operator with the input trace, the spiking deconvolution is obtained.

Referring to Fig. 9.26, consider an input seismic-trace record containing primary reflections ( $a_1, a_2, a_3$ ). From the autocorrelation function the deconvolution operator is derived and, on application (convolving it with the input trace), will output all the reflection events collapsed into spike-shaped wavelets. Application of this type of operator (spiking deconvolution operator), will output the spiky primary reflections.

In the frequency domain (lower part of Fig. 9.26), the whitening deconvolution operator is designed such that at each frequency, the value of the operator spectrum is the inverse of the value of the trace spectrum, at that frequency. In other words, the product of the two spectrum-values (input spectrum and its inverse) at each frequency is equal to unity. This mathematical process produces a frequency-spectrum of constant value along the frequency axis, i.e. producing white spectrum output.

**Fig. 9.26** Whitening (Spiking) deconvolution of a seismic trace in the time- and frequency domains



A closely related type of deconvolution, is the so-called (signature deconvolution) or (signature). This is derived by a statistical method. The procedure is computing the average spectrum of the shot-gather traces, then, from the inverse of this average, the time-domain deconvolution-operator is derived and convolved with the shot traces. This approach gives better estimate of the source wavelet, because of the averaging process.

### 9.8.3 Gapped Deconvolution

As we have mentioned before, the main distortions that occur to the seismic trace is signal deformation (inelastic attenuation effect) and wavelet repetition (reverberation). Whitening deconvolution restores the wavelet original shape, but the reverberation is removed by the other non-whitening type of deconvolution, known as (Gapped or Predictive Deconvolution).

Reverberation reflections appearing on a seismic trace are exhibited on the autocorrelation function as side-lobes separated by an interval equal to the reverberation period. The deconvolution operator is derived from the autocorrelation function of the trace just as in the case of

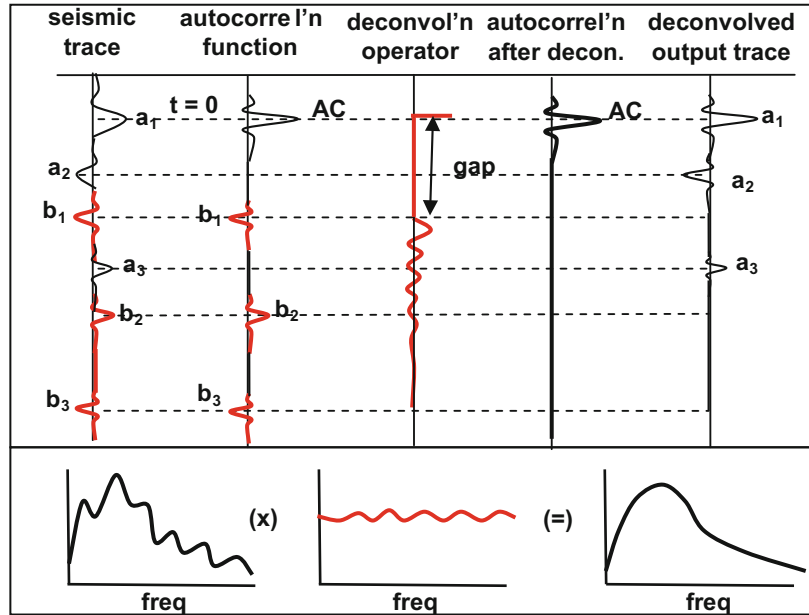
whitening deconvolution. The derived operator, in this case, consists of an isolated spike at its first point followed by a series of zero sample-values (the gap) and then the operator series of samples.

Referring to Fig. 9.27, consider an input seismic-trace record containing primary reflections ( $a_1, a_2, a_3$ ) and reverberation reflections ( $b_1, b_2, b_3$ ). From the autocorrelation function the deconvolution operator is computed and then applied (convolved with) to produce the output trace with the reverberations removed.

With this form of deconvolution, the operator (called Prediction Error operator or Prediction Error filter) will effectively predict the reverberation onsets on the seismic trace and subtract them leaving only the unpredictable events of random distribution which are the primary reflections and random noise.

In the frequency domain reverberations, which are appearing on the input trace, cause corresponding undulations to its amplitude spectrum. The aim of the gapped deconvolution is to remove reverberation events. This is achieved through removing these spectrum-undulations by smoothing of the input spectrum. The deconvolution operator in this case (filter having a gap-length equal to the

**Fig. 9.27** Gapped deconvolution (de-reverberation) of a seismic trace in the two domains. In the frequency domain deconvolution is done by smoothing of the trace-spectrum



reverberation period) does not whiten the wavelet spectrum (unless the gap is very short). It smoothes the spectrum by removing the ripples caused by the reverberation. This is shown at the bottom of Fig. 9.27.

Spiking deconvolution is considered as a special case of the gapped deconvolution in which the gap-length is only one sample-period. Because the noise existing within the spectrum width was not spectrum-equalized (i.e. not whitened), the output trace is not as noisy as the spiking deconvolution.

### 9.8.4 Noise Behaviour Under Deconvolution

#### (i) Case of Whitening Deconvolution

A normal seismic trace contains coherent events such as primary reflections, multi-reflections, coherent and random noise. The general characteristics of random noise (also called white noise) is that it has a white spectrum, which implies that all its frequency components are of equal amplitude. In the case of whitening

deconvolution, the operator in the frequency domain, is the inverse of the total spectrum of the data which includes both of the signal and noise. Ideally, the spiking deconvolution output is a spike-shaped reflection signals in the time domain and flat spectrum (white spectrum) in the frequency domain (Fig. 9.28).

Considering the frequency-domain deconvolution, noise gets amplified at the spectrum parts where the S/N ratio is low. The noise amplitude is thus, amplified in the frequencies outside the signal main frequency-band. It is usually observed that seismic data, outputted from whitening deconvolution, contain increased noise level.

In order to avoid the phenomenon of noise development, there are two alternative options. The first option is to remove noise before derivation of the operator as by using the shaped deconvolution, in which the autocorrelation function is filtered with a band-reject filter before being used in the derivation of the operator. In this way, the whitening process is confined to that part of the spectrum where the signal-to-noise ratio is high, and hence less noisy

output trace will be obtained. This type of deconvolution is called shaped (or band-limited) deconvolution.

The second option of avoiding noise development is application of a band-pass filter to the deconvolved data. This option is the more often followed in normal processing-work.

### (ii) Case of Gapped Deconvolution

The process of smoothing out the ripples caused by the reverberations in the amplitude spectrum would theoretically have no effect on the S/N ratio (Fig. 9.28). The signal-to-noise characteristics of the input spectrum remained unchanged under gapped deconvolution. In general, gapped-deconvolution output appears to be less noisy than the data outputted from whitening deconvolution.

The role of the gap-length in gapped deconvolution is that the shorter the gap, the more whitening effect occurs but with more development of whitened random noise. The opposite effect happens when the gap-length increases. Thus, with increased gap length, noise level is reduced but whitening effect is decreased, leading to deterioration of resolution of the reflection wavelets. In view of this discussion, it appears that a compromise is needed to be made between resolution and the noise level resulting from whitening deconvolution. This can be controlled by the choice of the optimum gap-length of the applied gapped deconvolution.

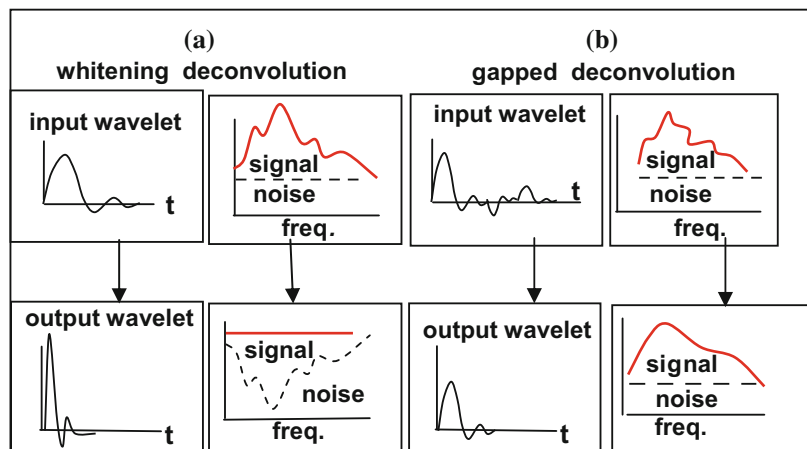
A closely related issue is the often needed practice of adding a small percentage of white noise to the input amplitude spectrum before computing of the spiking deconvolution operator. In the frequency domain, the operator is derived from multiplication of the input spectrum by its inverse. This is equivalent to dividing spectrum by itself for each frequency component. If a frequency component happened to be of near-zero amplitude, instability problem occurs. Thus, to avoid division by near-zero value, a constant value is usually added to the input amplitude spectrum. In the time domain, this is equivalent to adding a constant to the autocorrelation function at zero-lag. The addition process is usually done by multiplying the zero-lag autocorrelation value by a chosen scaling constant. Typical values of this factor is within a small range of 1.01–1.05.

## 9.9 Frequency Filtering

### 9.9.1 Definition of the Filtering Process

Coloured glass objects are filters which pass certain components of the spectrum of white light on basis of wavelength. Likewise, seismic detectors (as geophones) are filters which pass components of a seismic signal on basis of frequency. Another type of filtering is velocity

**Fig. 9.28** **a** Whitening deconvolution. **b** Gapped deconvolution in the time- and frequency domains



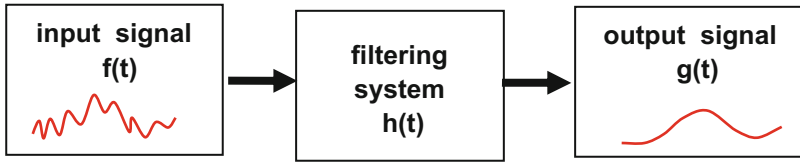


**Fig. 9.29** Definition of filtering process. It is an input-output system

filtering, which does the separation of components on the basis of propagation phase velocity.

The frequency-filtering is a sorting process that separates frequency components on basis of frequency. These filters may be natural or artificial. A propagating signal in nature (electrical, electromagnetic, or seismic) suffers from the filtering effect. The earth, for example, acts as a filter that passes the low-frequency components of the propagating seismic wave. Artificial frequency filtering, by analogue or by digital instruments, can be made to separate selected frequency components of the signal.

Frequency filtering is a convolution process that can be done by mathematical computation. It is considered to be an input-output system from which a filtered function,  $g(t)$ , is obtained from an input function,  $f(t)$  as shown in Fig. 9.29.

The frequency-filtering of seismic signals is a process that allows certain frequency components of the input signal to pass and masking or weakening rest of components. In this way, frequency filtering can be viewed as frequency-

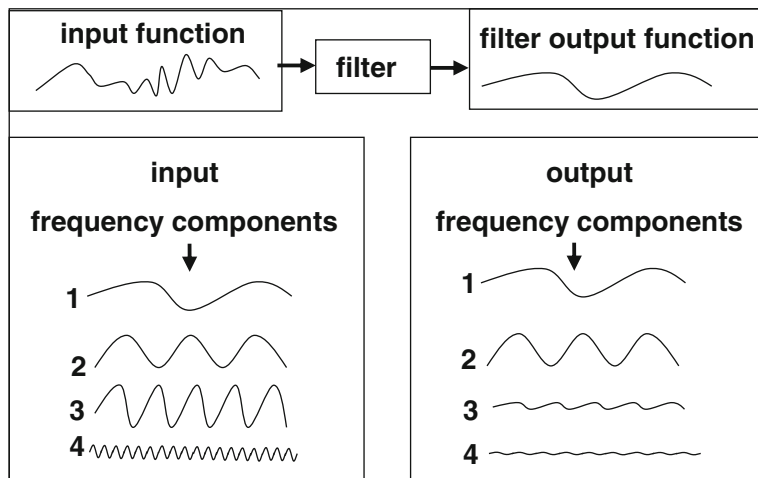
dependant scaling process. The principle of filtering of a seismic signal is shown in Fig. 9.30.

The filtering system may be of analogue mode, as in the earth filtering of seismic signals, or digital mode as is done in digital recording and processing of the digitally recorded signals.

### 9.9.2 Role and Objectives of Filtering in Seismic Exploration

Frequency filtering plays an important role in the field of seismic exploration. To start with, the source wavelet experiences low-pass filtering by the earth during its source-to-receiver propagation. In normal seismic exploration, it is noticed that the recorded reflection wavelets, and due to earth filtering, gets lower in frequency content with increase of reflector depth. At about 4 km-depth, the amplitude of a 40 Hz reflection-wavelet is one-third, of that of the 20 Hz, while that for a 100 Hz wavelet is about

**Fig. 9.30** Principles of the frequency filtering, attenuation of certain frequency components from the input function



one fortieth (McQuillan et al. 1984, p. 38). For this reason, seismic resolution deteriorates with increasing reflector-depth.

Seismic detectors impose filtering effects on the received seismic energy (signals and noises), causing changes of form and severity decided by their own response characteristics.

The recording system is normally equipped with a high-cut type of filter (the anti-alias filter) to cut out those frequencies higher than the Nyquist frequency to avoid aliasing. All these filters are of analogue type applied to the seismic wavelet before being converted to the digital mode. One property which is common to all analogue filters is that they all have non-zero phase spectra. This implies that each frequency component of the signal which is inputted to an analogue filter shall experience its own time-delay. As a consequence of this phenomenon, all analogue filters are expected to incur waveform distortions of the filtered seismic signal. The role of frequency filtering in the seismic reflection exploration is shown (Fig. 9.31).

Recording systems are usually equipped with special analogue filters to be applied to seismic data before being converted to digital mode. The two main reject analogue filters are the anti-alias filter and the Notch filter. The anti-alias filter is of high-cut type of filter that can remove those frequencies which are higher than the Nyquist frequency. This filter is normally put in operation

in order to avoid the occurrence of aliasing in the digitized data.

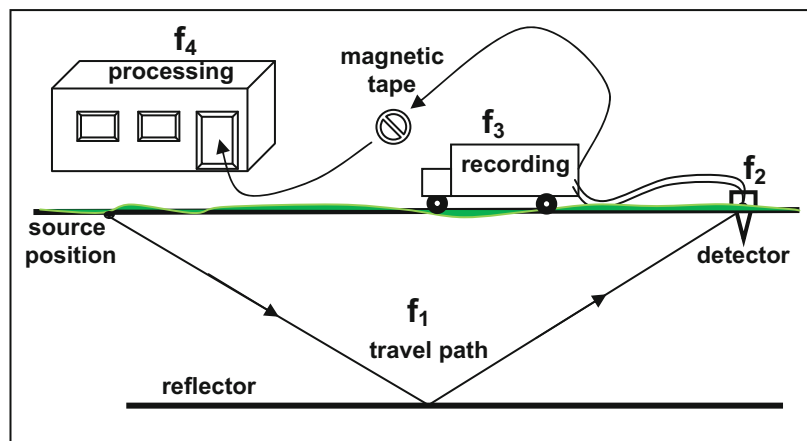
The Notch filter is another reject-filter which can reject a defined narrow band of frequencies. Recording systems normally include an analogue Notch filter for the special purpose of removing electrically-induced mono-frequency interfering signals as those emitted by high-tension power lines. Typically, the power-line frequency is 50 Hz, in certain countries and 60 Hz in others.

Both of these filters (anti-alias filter and Notch filter) are also applicable in digital mode. Thus, in processing, a digital anti-alias filter is applied when re-sampling of the data is done. Likewise, a digital notch filter may be applied to the digital data if a mono-frequency noise is detected.

### 9.9.3 Concept of the Linear System

A linear filtering system is defined as that system whose output is linearly dependent on its input. Linearity is also called superposition principle. Thus, for a linear system, the relation between input function  $f(t)$  and output,  $g(t)$  is that, for inputs  $[c_1 f_1(t) + c_2 f_2(t)]$  we get an output  $[c_1 g_1(t) + c_2 g_2(t)]$ . The linearity property allows flexibility of positioning of the filtering process in the seismic processing sequence. Thus, in principle, the net effect is the same whether the

**Fig. 9.31** Role of frequency filtering in the seismic exploration activities. The filters: ( $f_1$ ) is the earth filter, ( $f_2$ ) the detector filter, ( $f_3$ ) the recorder filter, ( $f_4$ ) the digital processing filter



filtering is done on seismic traces before being stacked or on the stacked trace after stacking (Fig. 9.32).

There is another closely related concept, which is, in fact another property of filtering systems. This is the time-invariance property. A system is time invariant (stationary) when its response is independent of time. In other words, for a certain input  $f(t - t_s)$  we get an output  $g(t - t_s)$  for any time shift ( $t_s$ ). The two properties, linearity and being stationary, are independent of each other.

It is important to note that all frequency filters, including natural analogue filters and the artificially-applied digital filters, applied in data processing, are of linear, time invariant systems.

### 9.9.4 The Filter Impulse Response

Filters differ in their filtering capabilities. Theoretically, the filtering capability of a filtering system ranges from the extreme case where it is passing the input signal with no change (all-pass filtering) to all-cut or no-pass case. The filtering

capability is function of the physical properties of the filtering device, if it is analogue. It is function of the parameters of the designed filtering function if it is digital. The efficiency of a filter in filtering action is expressed by the filter response characteristics for the particular filtering system.

One of the more common ways to determine the filter response is done by inputting an impulse function. The output of the filtering system from inputting an impulse function is considered as measure for the filtering capability of that system. This is a logical decision, because the impulse function contains the infinite frequency range. In fact the spectrum of the impulse is real and infinite in extent, and thus the output gives an ideal expression for the system filtering efficiency. The impulse response of a filtering system (Fig. 9.33) is the output of the system for an impulse-function input.

The impulse response function of a linear system is proportional to the amplitude of the input impulse function. When the input impulse is delayed with respect to the origin time, the response function is delayed by the same amount. Furthermore, the response function is

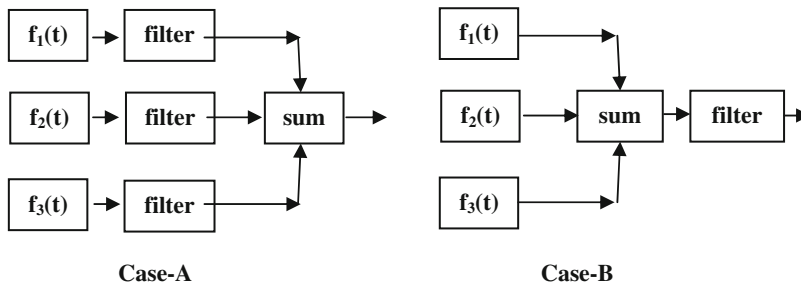


**Fig. 9.32** Superposition principles of linear systems. Summing of filtered signals (*case-A*) is equivalent to filtering of their sum (*case-B*)

**Fig. 9.33** Impulse response of a linear system

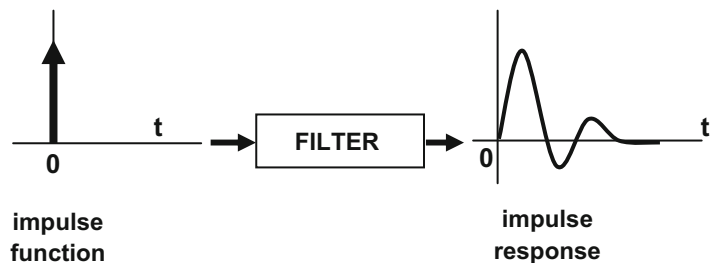
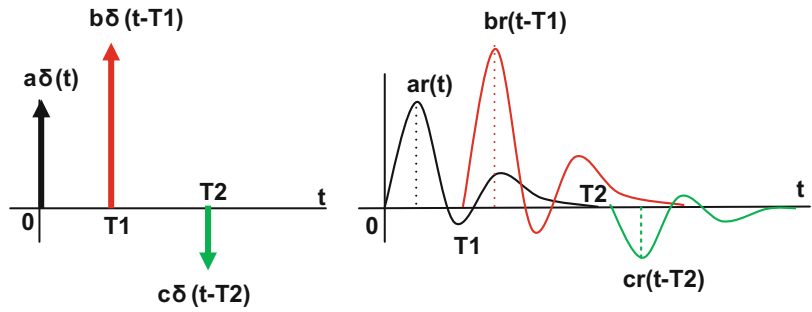


**Fig. 9.34** Impulse response functions,  $r(t)$  of three differently scaled and shifted impulse functions  $\delta(t)$



scaled by the input impulse amplitude. Referring to Fig. 9.34, we have three impulses; first impulse is at time zero, second impulse at time  $T1$ , and third impulse has negative value (inverted polarity) and located at time  $T2$ . The response functions are scaled and shifted accordingly, as seen in Fig. 9.34.

**9.9.5 Mechanism of the Filtering Process**

The linearity property of filtering systems implies that an input to a filtering system made up of sum of a number of functions, will give an output which is the sum of outputs produced if the functions were individually inputted. Thus, if the input to a linear system is a series of impulse functions, then the output will be the sum of the corresponding impulse-response functions. The output will be the sum of the impulse responses where each response function is scaled by the amplitude of its impulse function, and shifted by the impulse time-shift. This can be mathematically represented as follows:

Suppose the input to a linear system is made up of the series of impulses,  $a_0\delta(t)$ ,  $a_1\delta(t - \Delta t)$ ,  $a_2\delta(t - \Delta t)$ , ...,  $a_M\delta(t - M\Delta t)$ . Each of these impulses will make the filter to output the impulse response function scaled (weighted) by the impulse amplitude and shifted by the impulse time-shift. The output of the system due to the input series of impulses will be the algebraic sum of the overlapping impulse response functions (Fig. 9.35). That is:

$$\text{Filter output} = a_0r(t) + a_1r(t - \Delta t) + a_2r(t - 2\Delta t) + \dots + a_Mr(t - M\Delta t)$$

This process which involves shifting, multiplication and summing is a convolution process.

**9.9.6 Filtering in the Two Domains**

In time domain, filtering is convolution process that takes place between the input function and the impulse response function of the filtering system. Symbolically, the output function  $g(t)$ , of a filter for an input  $f(t)$ , is expressed as:

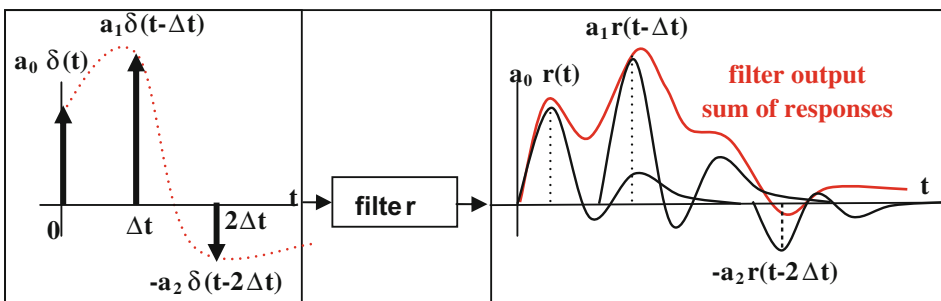
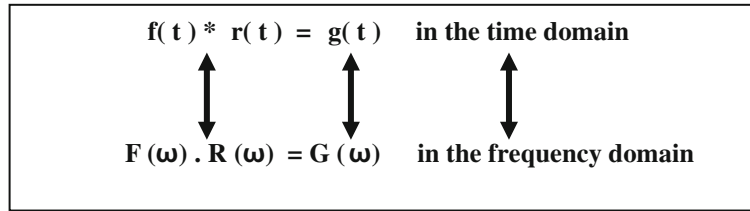


**Fig. 9.35** Three-sample input function to a linear filtering system. The output is the sum of weighted and shifted impulse response functions of the filter

$$g(t) = r(t) * f(t)$$

simple multiplication in the frequency domain. The relationship is as follows:



where  $r(t)$  is the impulse response function of the filter.

The impulse response of several filters connected in tandem is equal to the convolution of their impulse responses. Thus, the impulse response of the three filters  $R_1(t)$ ,  $R_2(t)$ , and  $R_3(t)$ , connected in tandem, is  $R_1(t) * R_2(t) * R_3(t)$ , since we consider the output from the first filter as input to the second filter and the output of these two filter as input to the third filter. Further, we may note that, according to the convolution properties, the output is the same regardless of the order of the filters in the sequence.

In conclusion, an input function can be approximated by a series of uniformly spaced impulses, each of which has the amplitude equal to the value of the function at the time-location of the impulse. The impulse amplitude will act as the scaling factor (weight factor) to the impulse response function of the filter. The filter output will be the algebraic sum of all the weighted and shifted impulse response functions. An analogue function can be considered as a digital function for which the sampling period is zero. This means that filtering mechanism we have just described is applicable to the analogue function as well.

In the frequency domain, filtering becomes multiplication of the amplitude spectrum of the input function with the transfer function of the filter, and addition of the corresponding phase spectra. We recall from the convolution theorem that convolution in the time domain, becomes

where the function  $R(\omega)$ , usually referred to as the (Transfer Function, or system function), is the Fourier transform of the filter impulse-response function,  $r(t)$ . It is, in general, complex quantity made up of real part  $|R(\omega)|$ , called the amplitude characteristics of the filter and imaginary part  $\theta(\omega)$ , the phase characteristics. That is:

$$R(\omega) = |R(\omega)|e^{i\theta(\omega)}$$

### 9.9.7 Types of Filters

Depending on the applied basis of classification, there are several ways used in filter classification. Since the response function is the principal parameter that defines the filter, the main classification scheme is dependent on the response characteristics of the filter. Based on the response characteristics, filters are classified into the three main types: low-pass, high-pass, and band-pass filters. The low-pass filter passes the range  $(0 - \omega_c)$ , the high-pass filter passes all frequencies above a defined lower limit  $(\omega_c)$ , and the band pass filter passes a defined frequency range  $(\omega_1 - \omega_2)$ . The frequency response functions of these filters are sketched in Fig. 9.36.

### 9.9.8 Application of the Band-Pass Filter

In order to decide on the type of filter to use in filtering of a certain time function (such as a seismic

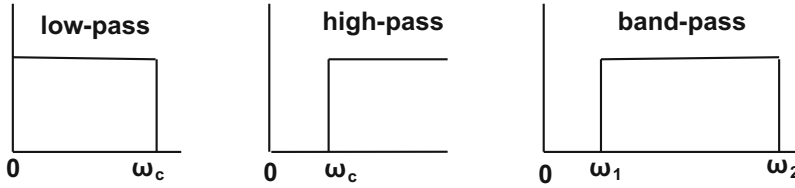
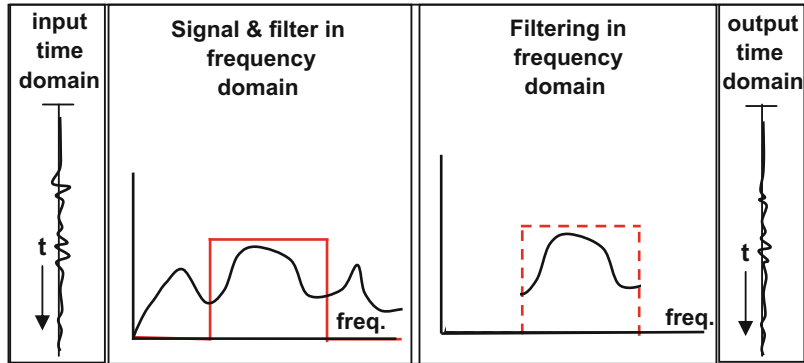


**Fig. 9.36** Types of filters. Transfer functions of low-pass, high-pass, and band-pass filters

**Fig. 9.37** Band-pass filtering by multiplying the box-shaped transfer function of the filter with the amplitude spectrum of input function and Fourier inverse transforming the result



shot record), the time function is first Fourier transformed into frequency domain function, producing its frequency spectrum. The input to the filter is the time-domain function prepared in digital mode. Measures should have been taken to avoid the occurrence of aliasing prior to the sampling (or re-sampling) process. Since digital filters separate components on the basis of frequency, signal and noise frequency-spectra must be computed and their frequency bands are determined.

A band-pass filter is defined so that it will pass the signal, and filter out the noise. The ideal case is that the transfer function is a rectangular-pulse (box-car) type of function which has the constant value of unity over the frequency-band to be passed and zero outside that band. In the frequency domain, filtering is effected by multiplying the transfer function of the filter with the amplitude spectrum of the input function. At the same time the phase of the filter shall be added to that of the input frequency components causing time shifting (and certain amount of shape-distortion) to the filtered wavelet. To avoid phase changing of the input frequency-components, zero-phase-filter is normally designed.

The filtering output is the result of multiplying the filter-amplitude spectrum by signal spectrum,

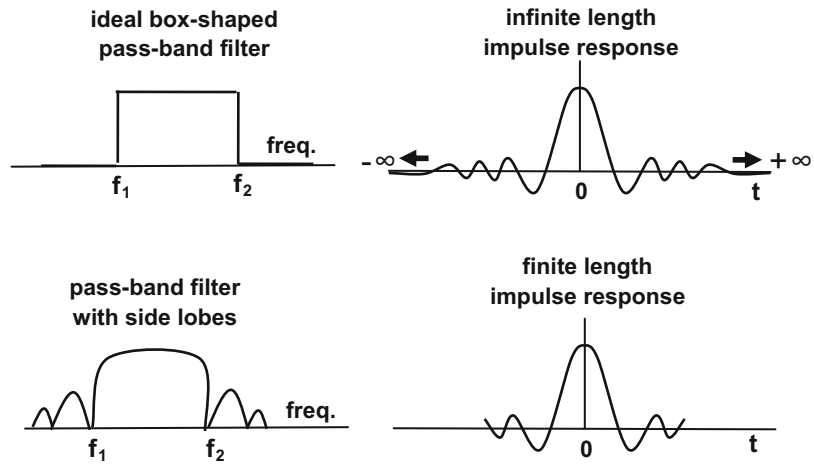
and then converted by Fourier inverse-transform to time domain (Fig. 9.37).

### 9.9.9 Filter Shape (Side-Lobes Problem)

In practice, filter design is usually made in the frequency domain, since in this way, the frequency spectrum becomes easier to visualize and easier for doing the design manipulation. The band-pass filter, which is the most commonly applied filter in seismic data processing, has the shape of rectangular pulse in its ideal form. It passes a defined frequency band and cuts out all other frequencies present in the signal under the filtering process. In the frequency domain, filtering is done by multiplying the box-shaped transfer function with the amplitude spectrum of the input signal function. This is equivalent to convolution of the filter impulse response with the input signal function in the time domain.

Theory of the filtering in the time domain (convolution), demands that the impulse response must be of infinite extent, which is not the case in practice. In other words, the impulse

**Fig. 9.38** Development of side lobes because of truncating of the impulse response to a finite length



response function is always truncated to a finite length. This would result in distortion of the ideal box-shape transfer function. The nature of distortion is expressed in development of side lobes which, effectively, results in adding extra band-pass extensions to the originally defined box-type transfer function (Fig. 9.38).

Effectively, truncation of the infinitely-long impulse response function becomes convolution operation between the spectrum of the impulse response and the spectrum of the truncation box-car type function. As a result of truncation, development of the side lobes and smoothing effect are obtained. Both of these distortions get less severe with longer truncation window. For more details of this phenomenon see for example (Báth 1974, pp. 95–97).

The filtering process will be multiplication of the transfer function that has the side lobes with the input spectrum. The result of this process is passing additional parts of the input spectrum which are present outside the required band ( $f_1 - f_2$ ) as well as the ( $f_1 - f_2$ ) frequency range. Passing additional unwanted parts of the input spectrum (called spectral leakage) is an unavoidable phenomenon that occurs merely because of truncation of the impulse response. The ideal filter, designed to pass only a defined part within ( $f_1 - f_2$ ) range, cannot avoid passing other parts outside this range because of the side lobes (Fig. 9.39).

### 9.9.10 Effect of the Filter Length

Side lobes development depends on two main factors: the truncation-length of the filter response function and the slopes of the derived transfer function. In general, it is found that as the length of the filter response function is increased, the side-lobes amplitude decreases and side lobes number is increased (Fig. 9.40).

It is also found that amplitude of the side lobes gets larger when the truncation point is located at a high-part of the response function, and gets smaller when the truncation point is nearer to a zero-crossing. In order to minimize these effects, filter length is increased and truncation point is positioned at a point where the response value is close to zero value.

### 9.9.11 Effect of the Filter Spectrum Shape

Another important effect on the side lobes is the effect of the shape of the filter transfer function. The more gently sloping filter margins the less the side lobes amplitude will be. In practice the, filter is made of a trapezoidal- rather than of rectangular-shape, where the filter margins are sloping lines rather than vertical lines. The filter is defined by four frequency points, called corner frequencies ( $f_1, f_2, f_3, f_4$ ) (Fig. 9.41).

**Fig. 9.39** Effect of side lobes in passing unwanted parts of the input function because of truncation of the impulse response to a finite length

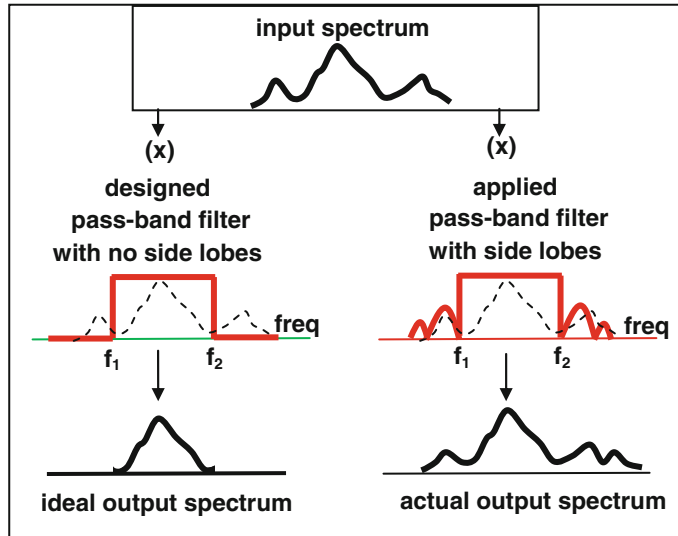
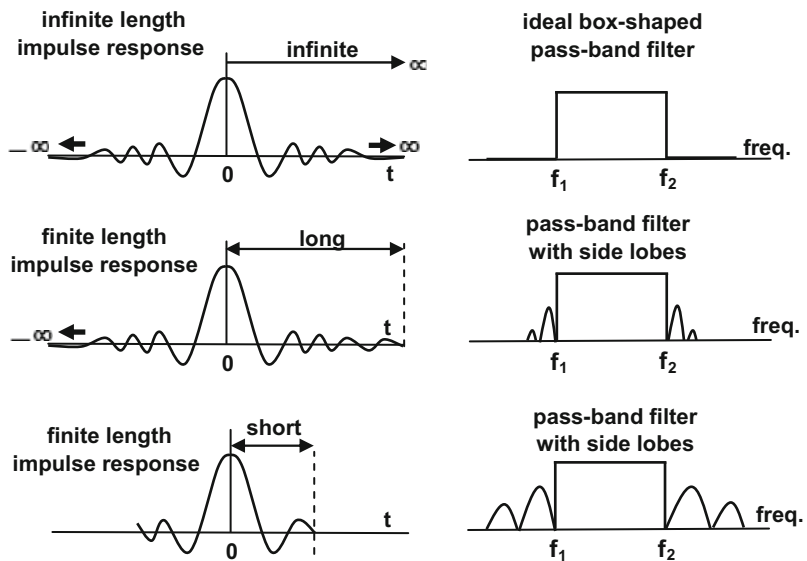


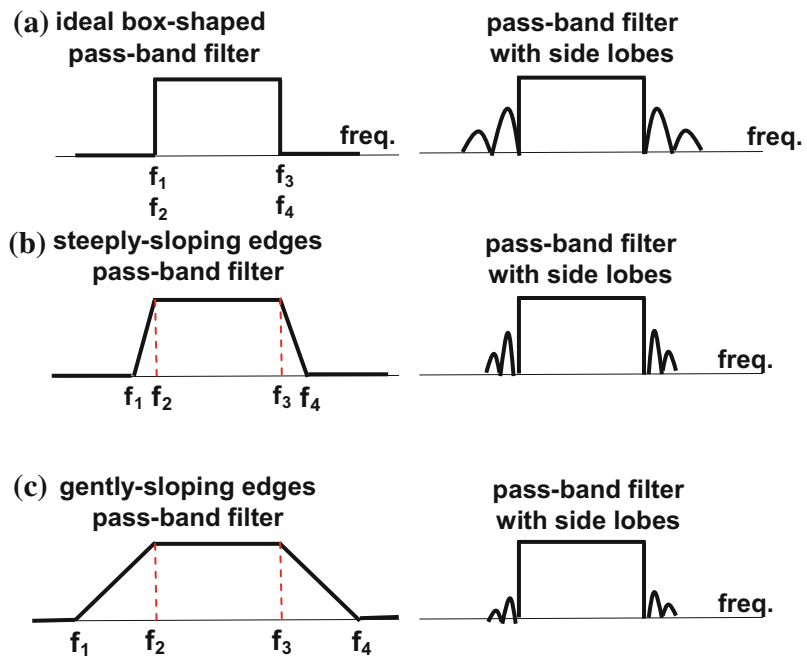
**Fig. 9.40** Effect of filter length (time length truncated from the filter impulse response function) on amplitude and number of side lobes



The frequency separations,  $(f_1 - f_2)$  and  $(f_3 - f_4)$ , are used as measures for the slopes of the filter edges. The effect of the filter shape on the side lobes is shown in Fig. 9.41. In this figure, three cases are shown. In the first case (case-A) the ideal box-shaped filter is of vertical edges, which can be considered as being formed

of four corner frequencies, where  $(f_2)$  is at zero-separation from  $(f_1)$  and  $(f_4)$  is at zero-separation from  $(f_3)$ . The following two cases (cases B and C) are with different non-zero separations. Comparing case B with case C, it is seen that the larger the separation (the more gentle slopes) the smaller the side lobes.

**Fig. 9.41** Effect of filter shape. Amplitude of developed side lobes gets less with increase of the separation between the corner frequency pairs ( $f_1 - f_2$ ) and ( $f_3 - f_4$ )



**9.9.12 Minimization of the Truncation Effect**

Because of truncation of the filter response function, the computed filter amplitude spectrum will develop side lobes which, on application, bring about distortion effects. Some measures are available, however, to lessen side lobes effects. Thus to minimize truncation effect, a process (time-domain windowing) is applied to the truncated impulse response function. In seismic data processing work, the window type commonly used is the Bartlett window. This window is a triangular time-function of amplitude, equal to unity at time zero. The windowing process is done by multiplying (in the time domain) the impulse response function by the Bartlett window of length equal to the required length of the applied impulse response (Fig. 9.42).

Bartlett windowing smoothes out and reduces the side lobes appearing in the amplitude spectrum of the truncated impulse response. This is due to the convolution process that takes place

between the transfer function of the truncated impulse response and the frequency-domain Bartlett window. For this reason the process is usually referred to as Bartlett smoothing. It is to be noted that some authors call Bartlett windowing as Bartlett smoothing because it smoothes out the truncated impulse response which brings the truncation points to zero-level with the result of much-reduced side lobes.

**9.9.13 Filter Normalization**

When different filters (filters with different bandwidths) are applied at different times to a seismic trace, the filter outputs will show different amplitude levels depending on the bandwidth value. In principle, larger bandwidth filters give filtered data of large amplitude level compared with the output of the data filtered with shorter bandwidth. In order to avoid this situation and get equalized amplitude level for the data outputted from filters of different bandwidths, filter normalization is often carried out. This is done

**Fig. 9.42** Bartlett windowing has the effect of smoothing the filter transfer function and removing or much reducing the side lobes

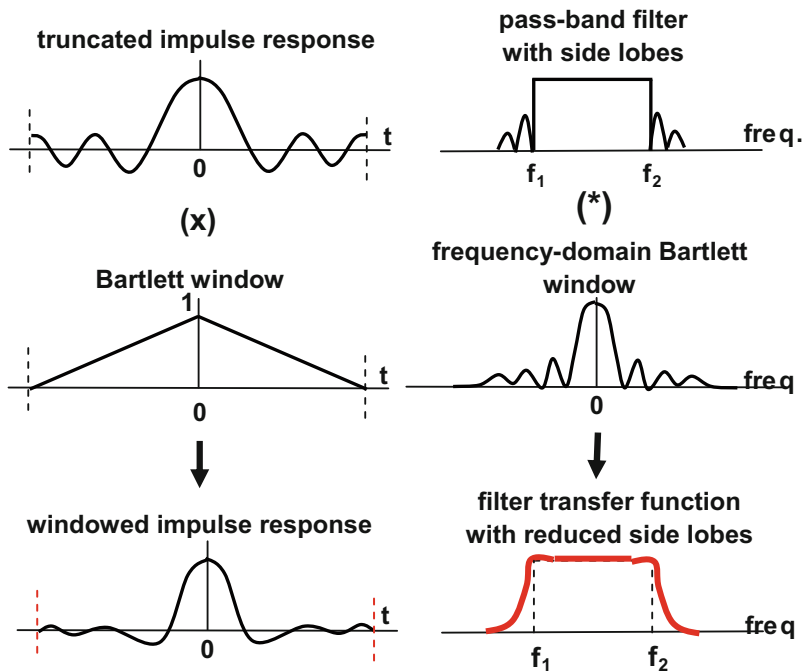
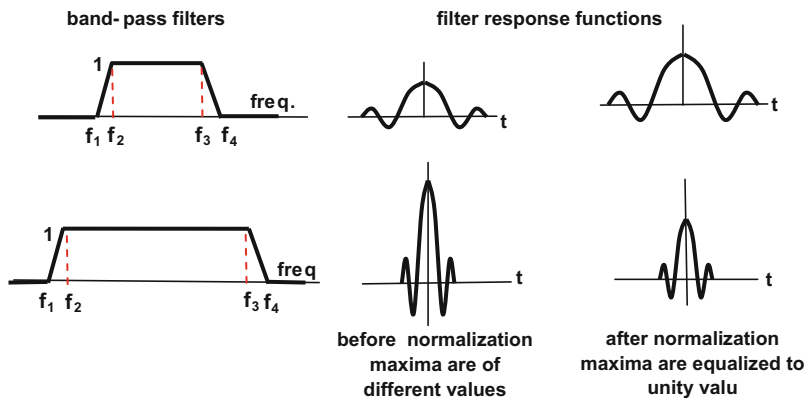


**Fig. 9.43** Filter normalization process



by dividing each sample-value of the response function by the maximum value of the response function. With this type of scaling, each response curve is normalized with respect to its maximum value, whereby the maximum value becomes unity for all filters regardless of their bandwidths (Fig. 9.43).

Filter normalization is essential procedure if data is prepared for amplitude preservation, as in case of stratigraphic interpretation based on

amplitude characteristics. Normalization is not necessary if the filtered data gets time-variant equalization.

### 9.9.14 Time-Variant Filtering

The seismic trace consists of a sequence of reflection events recorded at different times depending on the reflector depths. Spectra of

these events differ according to their arrival times. In general, high frequency components are dominant at the shallow parts of the trace. Lower frequencies are more dominant with increasing record time. For this reason different filters are needed to filter the different parts of the trace. The normal practice is to apply filters of bandwidths that vary with the time of the reflection arrivals. This process is called time-variant filtering (TVF).

In practical applications, a number of filters are designed to be applied at a sequence of time-points (called knee times) specified along the given seismic trace (stacked or un-stacked trace). The input trace is filtered separately with each of the specified filters, and each of these output traces is scaled with an amplitude scaling function such that the scalar has a value of unity at the relevant knee time and linearly decreases to zero-value at the two adjacent time knees (except for the first and last scalars). For the first scalar, the scalar value keeps at the value of unity for times from the first knee time to the beginning of trace. Similarly, for the last scalar (from the last

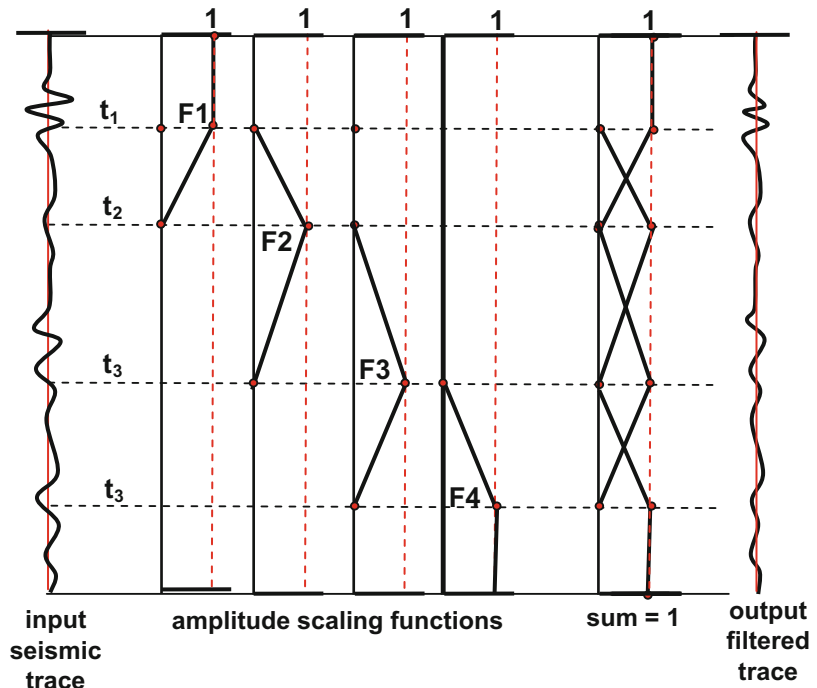
knee time to the end of the trace), the scalar is kept at unity-value. The final output is the sum of all of these separately filtered and scaled traces.

The sum of the scalar values at any time of the trace is equal to unity and the applied band-pass filter, by this method, is made to vary smoothly with trace-time. Effectively, the seismic trace is subdivided into a number of overlapping segments (time gates) which secure smooth and continuously changing filtering down the whole trace. The technique is shown in Fig. 9.44.

### 9.9.15 The Filter Tests

Filter tests (or filter analysis processing) is a series of processing tests aiming at determination of the optimum time-variant filter which gives the best possible signal-to-noise ratio of reflection events. Filter test is carried out by passing a defined part of a seismic section (50–100 traces, say) through a series of trial band-pass filters. This is commonly conducted in two stages. First, the chosen section is passed through band widths

**Fig. 9.44** Principles of the time-variant filtering (TVF). Four filters ( $F_1, F_2, F_3,$  and  $F_4$ ) are applied in filtering of an input trace, at knee times ( $t_1, t_2, t_3, t_4$ ) using four scaling functions. Scalars sum and the output filtered trace are also shown



in which the high-cut frequency is kept fixed while the low-cut frequency is varied. A typical filter test involves using the trial frequency bands: (6–45, 8–45, 10–45, 12–45, 14–45) Hz.

The outputted sections are then interpreted and the optimum filter is determined. In the second stage, this process is repeated with the trial bandwidths that have their low-cut frequency is fixed at the value determined in the first stage and the high-cut frequency is varied. Supposing that the optimum bandwidth determined from the first stage is (12–45) Hz, the trial filters for the second stage will be something like (12–25, 12–30, 12–35, 12–40, 12–45, 12–50) Hz.

In both of these two stages, choosing the optimum filter is based on certain criteria examined for the reflection wavelet and reflection horizon appearing in the chosen section. These are mainly the reflection energy (wavelet amplitude), continuity, resolution, and noise level. As a guide that can help in the determination, is that it is expected that high frequencies are present in the shallow parts of the section, while lower frequencies are more dominant in the deeper reflection horizons. Another tool used in giving more quantitative assessment of frequencies is by computing Fourier amplitude spectra. This can be done for time-gates selected by the processing geophysicist at the zones of interest.

### 9.9.16 Phase Removing Filtering

Analogue filters have non-zero phase spectra, and hence different frequency components are time-shifted by different amounts, giving distorted wavelet shapes. This is expected to happen since, under filtering the phase of the filter is added to that of the data. In cases where different analogue filters have been applied, it becomes desirable to remove the phase shifts (which may be variable), and get a zero-phase output data.

The process of removing phase from a set of data, involves getting the impulse response of the analogue filter, reversing it in time, and re-filtering that set of data. The principle, on which this process depends upon, is that

reversing the impulse response in time causes the phase to reverse in the algebraic sign, while keeping the amplitude spectrum unchanged.

## 9.10 Frequency-Wave Number (FK) Filtering

Fourier transform is applied to transform a time-domain function  $\mathbf{f}(\mathbf{t})$  into frequency domain  $\mathbf{F}(\boldsymbol{\omega})$ . In just the same way a distance-domain function  $\mathbf{f}(\mathbf{x})$  can be transformed into spatial frequency-domain or wave-number domain,  $\mathbf{F}(\mathbf{k})$ . In the geophysical literature, **F-K** filtering comes under different names, such as dip filtering, fan filtering, pie-slice filtering, and velocity filtering. The more commonly known term is (**F-K** filtering) which expresses the role of the two-dimensional Fourier transform of two-dimensional  $\mathbf{t-x}$  functions such as seismic records and seismic stack sections.

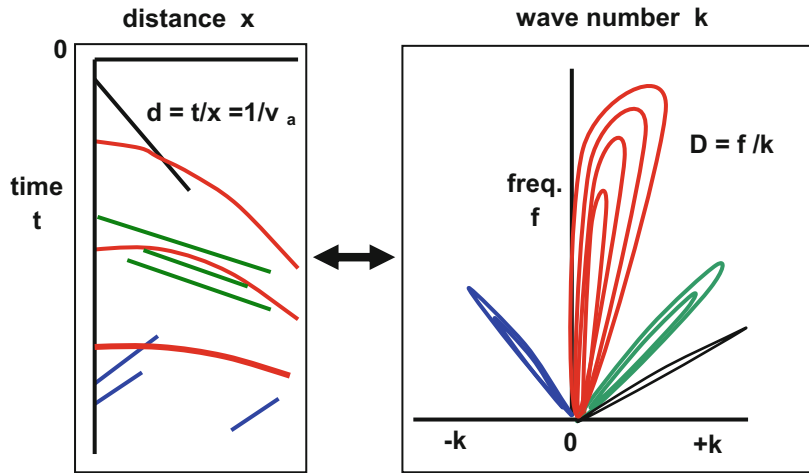
### 9.10.1 The $\mathbf{t-x}$ and **F-K** Domains

In case of two-dimensional functions, Fourier transforms are similarly applicable, using the two-dimensional Fourier Transform. A seismic record (or seismic section) is effectively a two-dimensional function. It is a function of both time and distance  $\mathbf{f}(\mathbf{t}, \mathbf{x})$  and can be Fourier-transformed into the combined frequency (**F**) and wave-number (**K**).

A normal shot record shows, in general, the seismic events which are mainly the direct arrivals, refraction arrivals, and reflection arrivals in addition to coherent noise (events with apparent velocities) like ground roll and sound waves. Reflection (and diffraction) events are curved and the rest of events are all linear events of dips governed by their propagation velocities (Fig. 9.45).

On the **F-K** plane (Fig. 9.45), the linear  $\mathbf{t-x}$  events are mapped as linear **F-K** events with their appropriate **F-K** slopes which are in inverse relationship to the  $\mathbf{t-x}$  dips. The events of the back-scatter noise (dipping opposite to the rest of linear events), is mapped on the negative side of

**Fig. 9.45** Sketch of a seismic shot record showing common seismic events: refraction (*black*), reflection (*red*), coherent noise (*green*), and back scatter coherent noise (*blue*). These events are mapped on the corresponding F-K domain



the **K**-axis. Due to their curved shapes, reflection events (showing relatively wide “dip” range) are mapped to their appropriate positions on the **F-K** plane.

The main features of the F-K transform are the following (Fig. 9.45):

- (i) A linear event of dip (**d**) in the **t-x** domain will map as a linear event in the **FK** map passing through the origin and having a slope (**D**) equal to (**1/d**). The **FK**-filter, which discriminates seismic events on basis of dip, is called dip filter, and because of the velocity-dip relationship ( $v_a = 1/d$ ), it is also called velocity filter.
- (ii) All linear parallel events (events with the same dip) in the **t-x** domain, regardless of

increasing (or decreasing) dip values, which transform into the **F-K** plane as a range of dipping lines covering the dip-range of the curved **t-x** event. An event with dip approaching zero-value would be transformed on to a vertical line along the **F**-axis on the **F-K** plane.

### 9.10.2 Application of the F-K Filtering

An **FK** filter can be designed such that it can pass part of the **FK** amplitude spectrum and reject the rest of the transformed energy. In this way, the transfer function of the **FK** filter, **R(F, K)**, can be defined as follows:

$$R(F, K) = 1, \text{ for the dip range } (D_1 > F/K > D_2) \\ = 0, \text{ elsewhere}$$

their positions in the **t-x** plane, will transform to the one-dip line through the origin on the **F-K** plane. Different dips (**d**) in the **t-x** plane, transform into the corresponding dips (**D**) in the **F-K** plane.

- (iii) A curved event in the **t-x** plane transforms into a wedge-shaped zone in the **F-K** plane. A curved event is considered as a series of short linear segments with

Such a filter can be made to pass, or cut out, all **FK** energy found within the two straight lines of slopes (**D**<sub>1</sub> and **D**<sub>2</sub>) as shown in Fig. 9.46. Usually it is made to act as a reject-filter.

In practice, **FK** filtering is carried out through a sequence of steps. First, the seismic data is transformed into **FK** domain by application of Fourier two-dimensional transform. On the produced **FK** plane, the noise energy is defined by

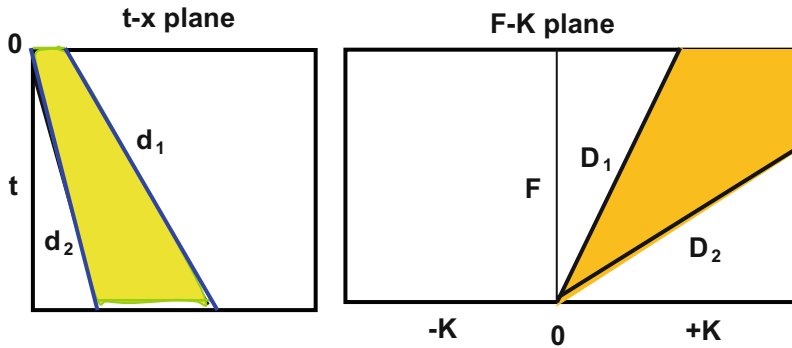


**Fig. 9.46** Method of defining the FK filter. It will pass (or reject) FK energy bounded by the two lines of slopes  $D_1$  and  $D_2$  in the  $FK$  plane. Symbols ( $d$  and  $D$ ) are the dips of the event in  $t$ - $x$  plane and  $F$ - $K$  plane respectively

drawing a polygon containing the unwanted parts (reject zones) of the **FK** spectrum. The filtering process is done by setting to zero all amplitude values in the defined reject zones. By inverse Fourier transform, the **t-x** domain, with the noise removed, of the filtered data is recovered.

**FK** filtering is normally done by application of special computer programs as part of the seismic data processing software-package. Plot of the **FK** domain (the two-dimensional spectrum), is normally presented as contour-values of the **FK** amplitude spectrum or using color-coded plot. Actual examples of the **FK** filtering are shown in Fig. 9.47.

## 9.11 Seismic Trace Equalization

In an equalization process of a seismic trace, the trace amplitudes are so adjusted that their average is constant over a window of a defined length, sliding down the trace. In this process the mean of trace amplitudes, (e.g. RMS amplitudes) over a sliding window, are equalized. With this process, abnormal variations in amplitude level are minimized. Weak reflection events are relatively boosted while abnormally high amplitudes are reduced. The net effect of equalization is to produce more homogeneous amplitude level within the one trace and for all traces of a given data set. In principle, amplitude equalization can conceal amplitude variations caused by

stratigraphic changes. For this reason, severe equalization is not recommended especially when the data processing is directed towards stratigraphic interpretation.

### 9.11.1 The Need for Trace Equalization

Sometimes, seismic traces show abnormal variation in the energy level (amplitude values) taking place in certain parts of the one trace. The whole trace, or group of traces in a given data set (shot record or stack section), may show abnormally low (or abnormally high) energy level compared with the rest of traces in that set. Factors which can lead to unbalanced energy level, may originate in the field because of inadequate detection and recording conditions or at a certain stage in the processing sequence.

Factors affecting amplitude value can be divided into two groups:

#### (i) Time-invariant factors:

These are factors which are of constant value (not changing with time) affecting the energy level of the whole seismic trace. Typical examples of this type of factors are: the effect due to the trace-offset, source and receiver detection conditions, or due to channel recording conditions. This can occur in processing as in case of variable fold applied in CMP stacking.

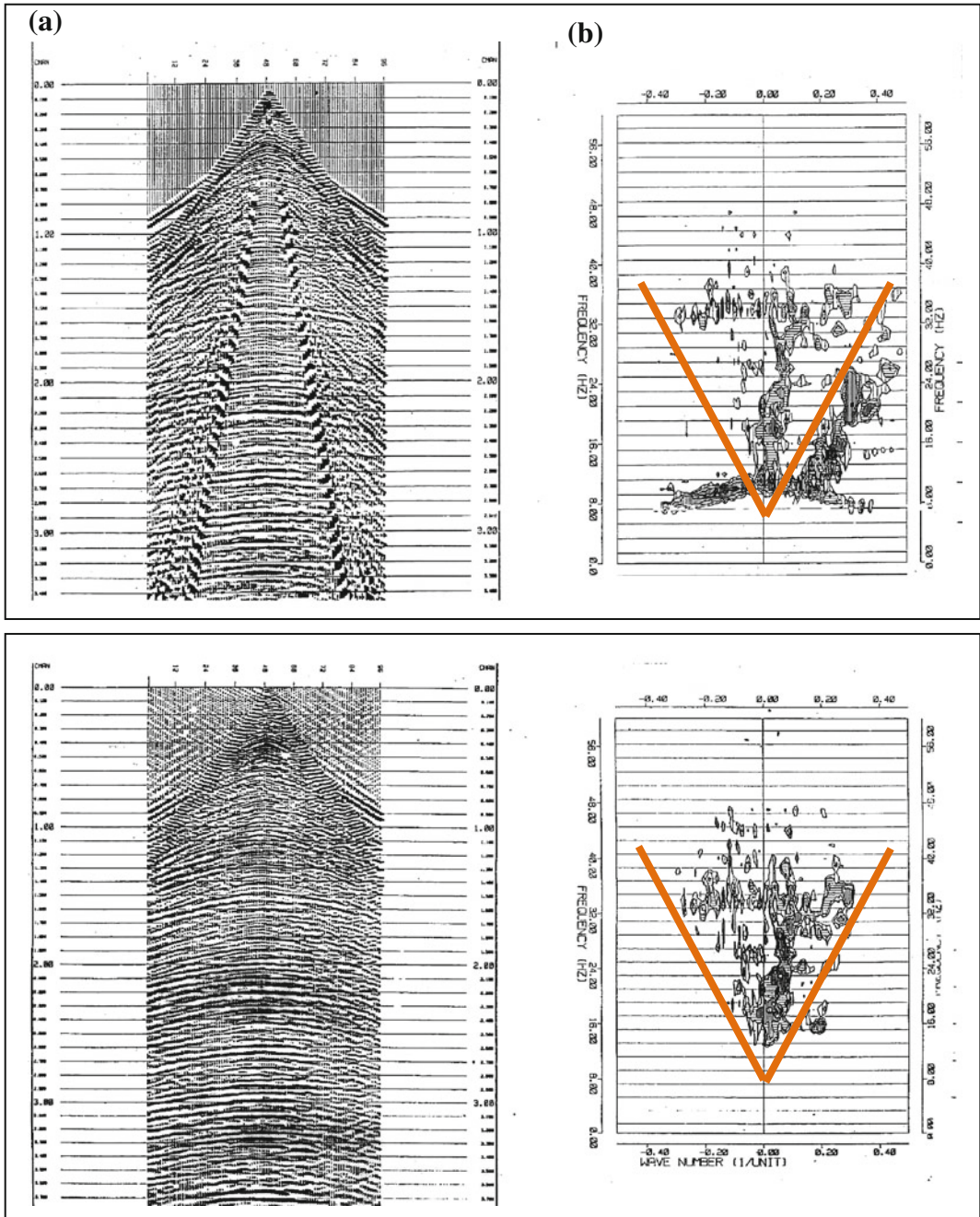


**Fig. 9.47** Actual examples of FK filtering. **a** t-x domain, shot records before and after FK filtering. **b** FK domain, the corresponding FK spectra

(ii) **Time-variant factors:**

These are factors affecting certain parts of the trace at different times, as the effects of, noise bursts that may occur to the trace during detection or

recording, time-variant processes as in time-variant filtering or time-variant deconvolution.

It should be noted that amplitude changes due to geometrical spreading and inelastic attenuation

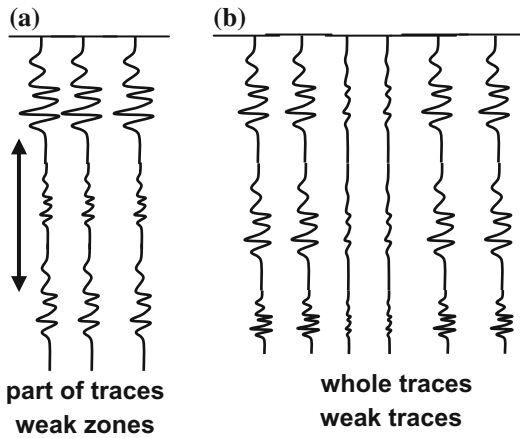


**Fig. 9.48** Cases of abnormal energy levels requiring equalization processing. **a** Part of the trace is abnormally weak (weak zones), **b** Group of traces in a data set showing low energy level

are systematic (uniform) type of changes and they are compensated by their relevant processing procedures. These changes are not included in the data-equalization treatment.

Common cases of abnormal seismic energy (trace amplitudes) are shown in Fig. 9.48.

In view of these two groups of amplitude-changing factors, two types of trace equalization are in common processing applications, these are: time-invariant and time variant equalization.

### 9.11.2 Time-Invariant Equalization

Time-invariant equalization is a scaling process whereby the scaling factor is kept constant for the whole seismic trace, or for the whole of group of traces, in a shot record or in a stack section regardless of time of application. This type of equalization is normally applied in cases where traces are weak due to weak energy-sources or due to source and receiver poor coupling conditions (Fig. 9.48).

One common method used in time-invariant equalization, is done by scaling of each trace of the data-set, using a scaling factor which is constant for the whole trace length and its value is inversely proportional to the square root of the average power of that trace. Thus, one form

(RMS amplitudes) scaling factor (SF) is derived from the amplitudes ( $a_n$ ) of the trace by applying a formula of the form:

$$\text{SF} = \text{constant}/(\mathbf{p})^{1/2}$$

where,  $\mathbf{P} = (1/N)\sum (a_n)^2$ ,  $n = 1, 2, 3, \dots, N$ .

The average power ( $\mathbf{P}$ ) is computed from the square root of the sum of the amplitude squared,  $\sum(a_n)^2$ , divided by the total number ( $N$ ) of trace samples ( $a_n$ ).

### 9.11.3 Time-Variant Equalization

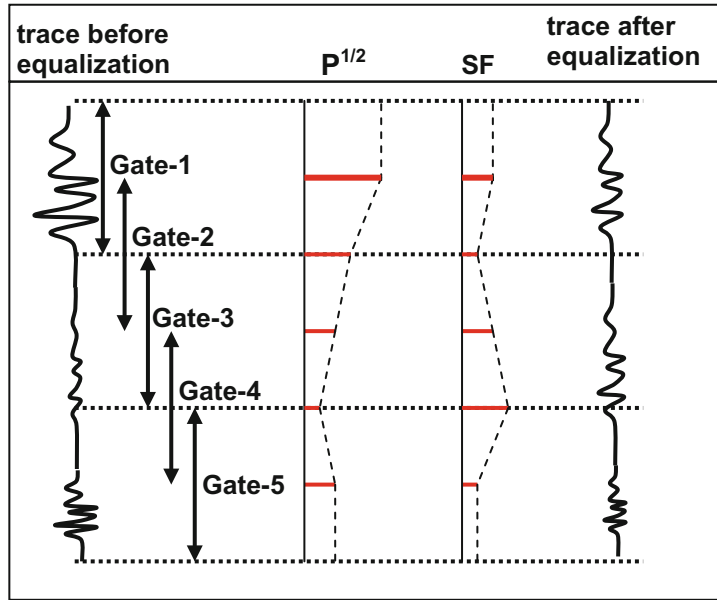
Time-variant equalization or time-variant scaling (TVS) is, in principle, the same as time invariant equalization except that several scaling factors are used per trace instead of one scalar used in the time-invariant scaling.

One form of time-variant equalization is carried out by dividing the input trace into a number of time-gates which may be of different lengths. As we have done in the invariant equalization computation, the scaling factor, which is inversely proportional to the average power, is calculated per each gate. The scaling factor of each gate is applied at the center of the gate, and linear interpolation of the factors is performed between gate centers. Gates may be designed to be overlapping with user-specified overlap-percentages. The process is multiplying each sample value of the trace by the corresponding scaling value. Time-variant equalization is shown schematically in Fig. 9.49.

The scaling factor ( $\mathbf{SF}$ ) is in inverse relationship with the square root of the average power ( $\mathbf{p}^{1/2}$ ) of the gate.

This type of trace scaling is called (Unity Scaling), and there is another type of time-variant scaling called (Square Root Scaling) which uses ( $\mathbf{p}^{1/4}$ ) instead of ( $\mathbf{p}^{1/2}$ ). This means that scaling factor in unity scaling is proportional to amplitude, whereas the scaling factor in the square-root scaling is proportional to the square root of amplitude. The Square Root Scaling preserves amplitude variation more than Unity Scaling.

**Fig. 9.49** Time-variant scaling (TVS) using equal gates with 50 % overlapping



For structural interpretation the attention is on the continuity of the reflection horizon and, therefore, amplitude preservation is not that important. Traces are equalized to help in picking and following up the reflection horizon. In stratigraphic interpretation where amplitude preservation is needed, equalization which can remove relative differences in amplitude levels is not applied, or its implementation is done with large-gate equalization.

### 9.12 Trace-Samples Manipulations

In the course of processing we may need to move samples of the digital seismic trace from place to place (time-shifting), or to change the algebraic

signs of certain samples of a trace which is also called (polarity reversing). In certain cases in the processing work, there may be needs to set to zero of the values of some selected samples.

Such practices are implemented in processes such as static correction, normal move-out (NMO) correction, trace editing, trace muting, and in re-formatting of the seismic data before being recorded on a certain storage medium. These activities are considered to be important and, sometimes, mandatory operations normally followed in processing of seismic reflection data. For these reasons sample manipulations are considered as important tools used in the seismic data processing.

With the introduction of the digital recording in the mid 1960s, a fundamental change in processing of the seismic data began. Application of the Information Theory to seismic exploration was made possible by the Geophysical Analysis Group (GAG), 10 years before, coupled with the great advances in the computer industry, laid down the basis of the modern seismic data processing.

The Information Theory has been developed during the Second World War to enhance S/N ratio of the radar signal. The outcome of the GAG research activities is that new effective mathematical analyses were introduced to be applied on the seismic-wavelet. Under these analyses, the seismic wavelet is treated as a propagating signal, like that generated, transmitted, and received electromagnetic signal.

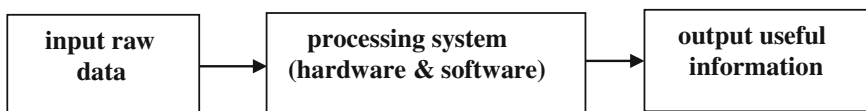
With the application of the principles of Information theory (in electrical and electromagnetic

fields), seismic signal processing was developed into the now-known highly effective structural and stratigraphic exploration tool.

---

## 10.1 General Overview

Seismic data processing is a sequence of mathematical and statistical processes carried out on the acquired raw seismic data in order to extract more readily interpretable data conveying useful geological information. A processing activity can be represented as an input-output system in which the seismic recorded data, as the input, and the final stack data as the output. The processing system involved in this operation is made up of two main parts; the processing computer system (the hardware) and the computer operation and application programs (the software). This is summarized as follows:



The processing operation normally includes a group of steps (processing tools) which are mathematical and statistical manipulations aiming at clarifying the seismic reflection signal and other required objectives.

To achieve these three main objectives, the input data provided by the field crew, is subjected to a series of processes, called the processing sequence. In more details, the main processes carried out by a processing system, can be summarized as follows:

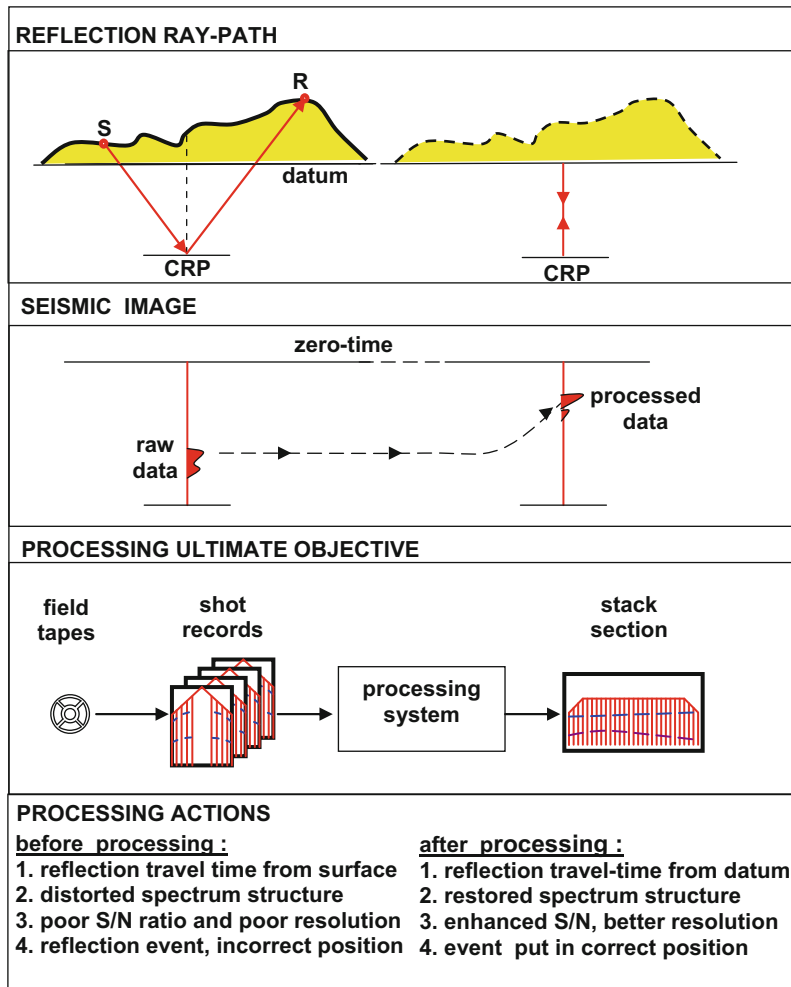
### 10.1.1 Main Processing Objectives

Main objectives of the data processing, is to achieve corrected form of the seismic reflection signal through:

- Enhancement of signal-to-noise ratio.
- Correction of the reflection travel-time to a defined datum plane.
- Correction of shape and position of the reflector seismic image

1. Reformatting of the recorded data
2. Removal of noises and interferences
3. True amplitude recovery
4. True spectrum recovery
5. Equalization of the seismic traces
6. Correction of the travel time of shot traces to a defined datum level (static correction)
7. Correction of the travel time of shot-traces to the zero-offset positions (NMO correction)
8. CDP-gather sorting and trace-stacking

**Fig. 10.1** Summary of seismic data processing and objectives



9. Correction of shape and position of reflector images (seismic migration)
10. Display and storage of the final seismic stack-data

Starting with the raw seismic shot-records (the basic input-element), a series of processing steps are performed to produce the ultimate aim, the stack section, which is the corrected seismic image of the geological reflectors in the surveyed area.

The ultimate objectives of the processing of the seismic reflection data are explained in (Fig. 10.1).

The ultimate end product of processing is a seismic reflection signal, of correct frequency spectrum, enhanced S/N ratio, and its arrival time is corrected so that it becomes the vertical reflection travel time, measured with respect to a defined datum level.

### 10.1.2 Role of Processing in Seismic Exploration

Seismic records of a series of shot points together with other relevant technical data are sent by the seismic field crew to the processing centre to get processed. The end product is the seismic stack sections which represent depth images of sub-surface geological sections. This expresses the importance of the processing work which is occupying a central position between the data acquisition and the data interpretation (Fig. 10.2).

Based on the concepts, borrowed from the Information Theory, processing software were developed and applied to produce correct and clear seismic signals and consequently giving clear and high-resolution images of the subsurface geological structures.

### 10.1.3 Main Processing Activities

To achieve the objectives that are required from processing of seismic reflection data, the raw field data are passed through a sequence of steps (the processing sequence) using certain processing-controls (the processing parameters) for each step of the sequence. The standard processing sequence normally followed in processing of the field data, involves a sequence of activities starting with preconditioning of the field data, carrying out certain measures to enhance the S/N ratio, correcting arrival times and ending with the stacked data to be handled to the interpreter. These activities are summarized as follows:

#### (i) Data Preconditioning

In this step, all corrupted data found within the raw data are removed or corrected by a process called (data editing). Recovery of the original signal amplitude and original signal waveform are carried out in this stage also. **Frequency filtering**, inverse filtering (deconvolution) and other such-like processes are applied in the preconditioning work to get a data-set free of corrupted data. Preconditioned data are then inputted for the following processes.

#### (ii) Travel-Time Corrections

There are two main corrections to be carried out to reflection travel-time. These are the static and the dynamic normal move-out (NMO) corrections. In the static correction, the effect of surface topography on the reflection travel-time is removed; whereas, the NMO correction removes the effect of the receiver offset (receiver distance from the source point). The outcome of these two processes are making the reflection travel-time of each reflection event as it would be if both of the source and receiver were occupying a common position at a point located on a fixed datum level.



**Fig. 10.2** Elements of seismic exploration: Data acquisition, processing, and interpretation. Processing occupies a central position between field acquisition and interpretation stages

### (iii) **Signal Enhancement**

The most effective process in signal enhancement is what is called the common depth point (CDP) stacking. In this process several seismic traces generated from the same reflection point (i.e. same CDP trace-gather) are algebraically summed-up. The result of this sum is a new trace (the stack-trace) is representing the mean of the traces in the CDP-gather. In this process, reflection signals on the individual traces are summed constructively producing stronger (larger amplitude) reflection signal. The seismic noise, being of random nature, is destructively summed, and hence gets reduced.

Application of digital filters is another option for reducing noises and other unwanted interferences and enhancing the reflection signal. There are several types of filters. The most commonly applied type is the frequency filter which discriminates seismic events on the basis of frequency. Another well known filter is the velocity filter (also called frequency-wave number (Fk) filter which discriminates events on the basis of their apparent velocity. Frequency filters and velocity filters are powerful tools in seismic signal enhancement.

### (iv) **Structural Amendment**

In certain cases, where there are structural complexities (folds and faults) in the subsurface geological structure, the seismic image of the corresponding seismic stack section will have structural distortions of magnitude depending on the degree of the structural complexities. This type of distortion occurs because of shifting of the location of the reflection point due to dipping of the reflectors. Another type of distortion results from the diffraction phenomenon which is associated with terminating reflectors like faults and pinch-outs. Restoration of seismic sections affected by such distortions is made by a special process (the seismic migration).

### (v) **Data Storage and Display**

For quality control purposes, paper displays (or on-screen displays), after each processing step is normally produced. The final product, which consists of stack sections of seismic lines (or stack data-volume, in case of 3D surveying) is recorded on a certain storage medium. This is an

important processing step in which the final processing product is recorded on a permanent storage medium (usually on magnetic tapes) ready to be delivered to the interpretation geophysicist who will load it in his interpretation system.

In addition to the conventional seismic stack sections, other types of sections may be produced according to special requests from the interpreter. Examples of such data are seismic-attribute sections in which parameters other than amplitudes (such as frequency, phase or propagation velocity) are displayed in the form of seismic sections (seismic attribute sections). Such sections are additional tools helping in the interpretation process, especially in stratigraphic interpretation.

## 10.1.4 The Processing Sequence

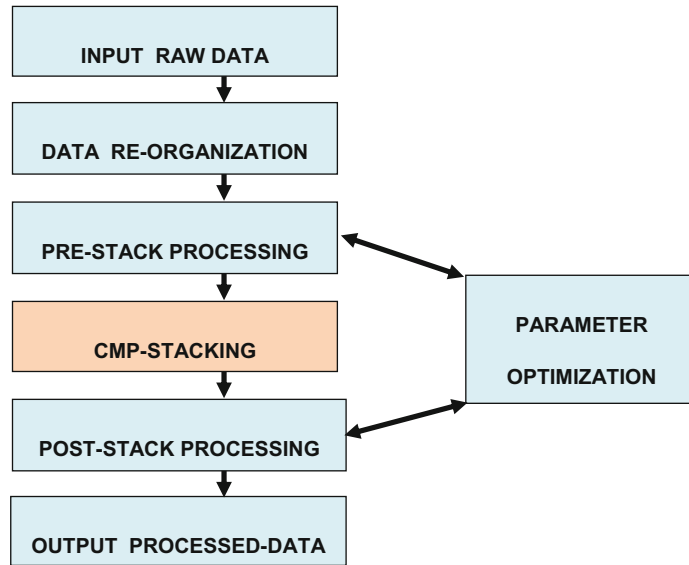
In order to get a seismic section made up of traces containing reflection wavelets which are corrected with respect to shape and corrected with respect to travel-time, a set of processing-steps is normally performed. These steps are taken in sequence, where some are mandatory (compulsory) and others are optional, decided by the processing geophysicist according to need.

There is no fixed sequence for the processing steps. Details of seismic data processing differ with different processing centers, and may vary from data-set to data-set in the same center. However, there is a kind of a standard form for the basic processing steps normally followed in all processing activities.

To simplify discussions, processing activities are divided into four stages of processing. These are: data re-organization, pre-stack processing, parameter optimization, and post-stack processing (Fig. 10.3).

The raw data provided by the field crew, which form the input data to processing, consist of two sets of data: the seismic shot records (normally recorded on magnetic tapes) and the supporting "statistics" data (normally recorded on CDs or magnetic tapes). The shooting statistics include the observer report in which complete descriptions and notes on the recorded shots are documented. The report also includes the

**Fig. 10.3** The main stages of data processing used in seismic reflection exploration



shooting geometry and, often, the field statics computed with respect to a defined datum level.

The input to the processing system comprises basically of seismic traces sorted into shot-gather records. Each seismic trace contains a series of seismic events representing the reflection wavelets recorded at their respective arrival times. In this state (raw-data state), the reflection wavelets are generally weak and distorted seismic signals. The travel-times of the arriving reflection-wavelets need to be corrected to be relative to a constant-elevation datum level. Corrections and data rectification are done in the processing centre, using specialized computer software.

The input data are subjected to a sequence of processing steps which can be grouped into four major stages. These are:

Stage-1.

Data re-organization

- Data reformatting and loading
- Demultiplexing
- Sweep removal from Vibroseis data
- Vertical stacking

- Geometry data and field statics storing
- Trace header assignment

Stage-2.

Pre-stack Processing

- Data re-sampling
- Trace editing
- Static correction
- Noise attenuation
- Spherical divergence correction
- Deconvolution
- Equalization
- CMP sorting
- Residual static correction
- Pre-stack migration
- NMO correction
- Muting

Stage-3.

Parameter optimization

- Velocity analysis
- Residual static analysis
- Deconvolution analysis
- Filter analysis
- Equalization analysis

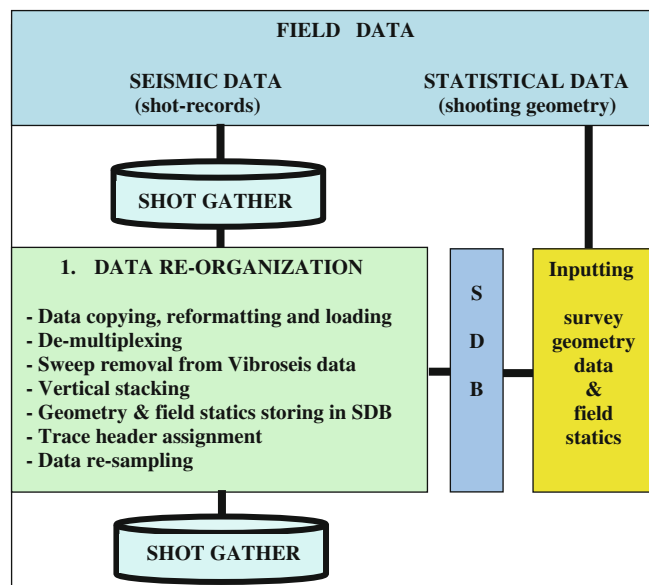
- Mute ramp analysis
- Stage-4.  
Stack and Post-stack Processing
- CMP stacking
  - Post-stack deconvolution
  - Frequency filtering
  - Equalization
  - Final stack-sections outputting

These sequential steps are usually presented in a flow-chart form (called the processing flow chart) are discussed in more detail, in the following sections.

## 10.2 Data Re-organization

In this phase of data processing, the seismic data received by the processing centre, is subjected to some re-organization processes, together with certain preparations done prior to the signal enhancing processing. These operations, which are collectively referred to as data re-organization, consist of the following processes (Fig. 10.4):

**Fig. 10.4** Main steps which are taken in data re-organization stage. Input is the field shot-gather records and output is re-organized shot-gather records. *SDB* denotes the seismic data base included in the processing system



### 10.2.1 Seismic Data Copying, Reformatting, and Loading

Before starting with any processing step, a copy of the field tapes is made. The original tapes are stored in a safe place, while the copy-tapes are used in the processing. This is necessary procedure for safety purposes.

The copy-tapes are reformatted into a format that complies with the particular processing software employed in the processing centre. After being reformatted, the data is loaded to the system, ready to be used in the subsequent processing steps.

### 10.2.2 Data De-multiplexing

This is a compulsory step to be taken if the field seismic data is in multiplexed form. In case the data is in multiplexed form, the trace-samples are sorted in sample-sequential mode. Demultiplexing is a process whereby the samples are re-sorted into

trace-sequential mode. The demultiplexed data is a series of traces each of which consists of its own sequence of samples. To further clarify the concept, suppose we have four-trace record, where,

Trace-A is made-up of the samples  $\mathbf{a}_0, \mathbf{a}_1, \mathbf{a}_2, \mathbf{a}_3, \dots, \mathbf{a}_N$ ,

Trace-B is made-up of the samples  $\mathbf{b}_0, \mathbf{b}_1, \mathbf{b}_2, \mathbf{b}_3, \dots, \mathbf{b}_N$ ,

Trace-C is made-up of the samples  $\mathbf{c}_0, \mathbf{c}_1, \mathbf{c}_2, \mathbf{c}_3, \dots, \mathbf{c}_N$ ,

Trace-D is made-up of the samples  $\mathbf{d}_0, \mathbf{d}_1, \mathbf{d}_2, \mathbf{d}_3, \dots, \mathbf{d}_N$ ,

When samples are organized in groups sequenced in the order of sample number, (sample sequential mode), it is said that the data is in multiplexed form, and when the samples are organized in the sequence of traces (trace sequential mode), the data is said to be in demultiplexed form. Thus, re-arrangement of the sample values in the order of sample number ( $\mathbf{a}_0, \mathbf{b}_0, \mathbf{c}_0, \mathbf{d}_0, \mathbf{a}_1, \mathbf{b}_1, \mathbf{c}_1, \mathbf{d}_1, \mathbf{a}_2, \mathbf{b}_2, \mathbf{c}_2, \mathbf{d}_2, \dots, \mathbf{a}_N, \mathbf{b}_N, \mathbf{c}_N, \mathbf{d}_N$ ) gives the multiplexed mode of data storage and when the arrangement is in the order of trace number ( $\mathbf{a}_0, \mathbf{a}_1, \mathbf{a}_2, \dots, \mathbf{a}_N, \mathbf{b}_0, \mathbf{b}_1, \mathbf{b}_2, \dots, \mathbf{b}_N, \mathbf{c}_0, \mathbf{c}_1, \mathbf{c}_2, \dots, \mathbf{c}_N, \mathbf{d}_0, \mathbf{d}_1, \mathbf{d}_2, \dots, \mathbf{d}_N$ ), the demultiplexed mode of storage is obtained.

The necessity of demultiplexing comes from the fact that computer programs deal with seismic traces in the form of time-series of sample values, sequenced per each trace (trace-sequential mode (demultiplexed mode)).

### 10.2.3 Sweep Removal

According to the convolutional model of the seismic trace, the recorded trace,  $\mathbf{y}(\mathbf{t})$ , in case of Vibroseis shooting, is given by:

$$\mathbf{y}(\mathbf{t}) = \mathbf{s}(\mathbf{t}) * \mathbf{r}(\mathbf{t}) + \mathbf{n}(\mathbf{t})$$

where,  $\mathbf{s}(\mathbf{t})$ ,  $\mathbf{r}(\mathbf{t})$ , and  $\mathbf{n}(\mathbf{t})$  are the source function (Vibroseis sweep), the reflectivity function, and seismic-noise function respectively.

As we have learnt from the convolution section, that cross-correlation  $\mathbf{C}_{12}(\mathbf{t})$  of a function  $\mathbf{f}_1(\mathbf{t})$ , with a second function  $\mathbf{f}_2(\mathbf{t})$  is the same as

convolution of the first function,  $\mathbf{f}_1(\mathbf{t})$  with the reversed second function,  $\mathbf{f}_2(\mathbf{t})$ , that is:

$$\mathbf{C}_{12}(\mathbf{t}) = \mathbf{f}_1(\mathbf{t}) * \mathbf{f}_2(-\mathbf{t})$$

and

$$\mathbf{C}_{11}(\mathbf{t}) = \mathbf{f}_1(\mathbf{t}) * \mathbf{f}_1(-\mathbf{t}).$$

By applying this property on the equation of the trace convolutional model,  $\mathbf{y}_c(\mathbf{t})$ , we get:

$$\mathbf{y}_c(\mathbf{t}) = [\mathbf{s}(\mathbf{t}) * \mathbf{h}(\mathbf{t}) + \mathbf{n}(\mathbf{t})] * \mathbf{s}(-\mathbf{t})$$

hence,

$$\mathbf{y}_c(\mathbf{t}) = \mathbf{a}(\mathbf{t}) * \mathbf{h}(\mathbf{t}) + \mathbf{n}(\mathbf{t}) * \mathbf{s}(-\mathbf{t})$$

where,  $\mathbf{s}(\mathbf{t}) * \mathbf{s}(-\mathbf{t})$  is the autocorrelation  $\mathbf{a}(\mathbf{t})$  of the sweep function.

Thus, in order to extract the impulsive-like record of the reflections in their actual reflection-times, the recorded traces are cross-correlated with the applied sweep, which is equivalent to convolution with the reversed sweep. This process can be done in the field by the Vibroseis recording system, or later by the processing software (Fig. 10.5).

In this process, it has been shown that cross-correlation of the Vibroseis seismogram with the sweep function resulted in convolution

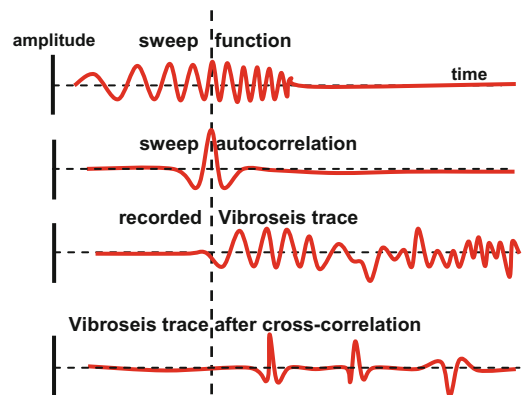


**Fig. 10.5** Sketch of sweep function, sweep autocorrelation, recorded Vibroseis trace, and Vibroseis trace after cross-correlation

of the reflectivity function with the autocorrelation function of the sweep. Further more, the addition of the  $n(t)] * s(-t)$  will produce filtering effect to the noise (Lavergne 1989, p. 59).

### 10.2.4 Vertical Stacking

Generally speaking, trace stacking involves algebraic summing of the sample values (from traces) having common recording-time. Usually, the sum is divided by the number of involved traces, to get the mean value instead of the absolute sum. An example of stacking three traces is shown in Fig. 10.6.

Vertical stacking, involves summing corresponding traces from several shot-records, executed in the same location. This is done normally with weak surface-sources (such as weight dropping and Vibroseis) to get enhanced reflection signals. Vertical stacking is applied without doing any time-corrections to the traces before being summed together (Fig. 10.7).

Vertical stacking is normally done in the field where the recording system is equipped with the appropriate software to perform the process. However, it can be done in the processing centre when the need arises.

### 10.2.5 Geometry Data and Field Statics Loading

Survey-geometry data give all information pertinent to the geometrical layout of all survey points (source- and receiver-points) used in the seismic survey. Essential elements of the surface layout are the following:

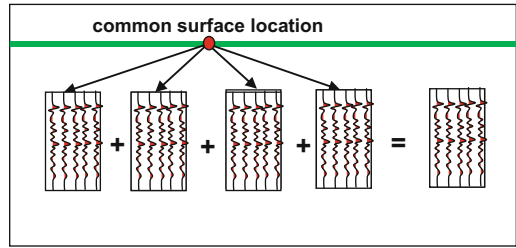


**Fig. 10.7** Principle of vertical stacking. Four shot records having one common surface location are vertically stacked to produce one shot record

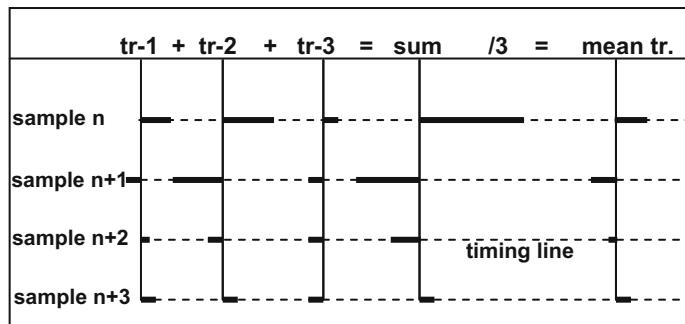
- (i) Spread parameters (Total live seismic channels, trace offset, and receiver spacing)
- (ii) Coordinates (x, y, z) of each source and receiver points
- (iii) Shot identification number, shot spacing, shot coordinates
- (iv) Receiver sequence number, receiver spacing, receiver coordinates
- (v) Geometrical shape of the seismic line

With these shooting statistics, which describe the surface positions of survey elements, the corresponding subsurface data are determined. This is achieved by running a special module of the processing package (the Geometry Module). The subsurface elements worked out in this processing step are:

- (i) CMP sequence numbers, coordinates, and CMP-spacing,
- (ii) CMP gather-traces, and number of traces in each gather (fold of coverage)

Seismic crews usually provided the geometry data in a file called SPS-file (Shell Processing Support) which is written in a special SEG standard format. The SPS-file is normally stored

**Fig. 10.6** The principle of trace stacking. Three traces are stacked to produce the sum trace, and dividing by 3, the mean trace



on CD or on magnetic tape. For QC purposes, a special plot (called the coverage diagram) can be produced to display the distribution of the surface and subsurface geometry-data.

### 10.2.6 Trace Header Assignment

The seismic trace is considered as a record of seismic amplitude variation with reflection time, in addition to various types of noise. In short, it is amplitude time-function. In order to be able to direct the processing system to a particular trace, each trace is provided with identification information called the (Trace Header). Among other things, trace header of a particular trace will specify to what shot-point or to what CMP a particular trace belongs.

The trace header consists of two parts, the header name and the header value. For example, a trace belonging to shot number (17), recorded by channel (123), whose offset is (2450 m), and included in the gather of CMP having x-coordinate (1273.54 m), will have the following headers:

Header name	Header value
SHOT	17
CHAN	123
OFFSET	2450
CMP-X	1273.54

The field trace has only a limited number of header names. These headers contain information concerning the shot record that it belongs to, like shot ID, channel number, trace sequence-number, flags for first and last-trace positions, and few others. It does not include any information on distances, coordinates or subsurface information. These distance-related information, are added to the trace, as headers, only after running the geometry module. This is done in an important processing step called (header assignment). These are distance-related and subsurface information (offset, coordinates, CMP coordinates,) which are added to the trace as new headers. Some headers are automatically added by the system, after certain processing steps, as

for example, the header (fold) is created after CMP-stacking step.

### 10.2.7 Data Re-sampling

In its digital form, the trace consists of a series of regularly-spaced sample-values. Normally, the field trace is sampled at 2 ms sampling period and re-sampled into 4 ms sampling period, before being input to processing. In order to avoid possibility of aliasing, a digital anti-alias filter is applied to the data prior to the re-sampling process. The type of the anti-alias filter is high-cut filter that removes frequency components higher than the Nyquist frequency. Since Nyquist frequency ( $f_N$ ) is tied up to the sampling frequency ( $f_s$ ), by the relationship ( $f_N = f_s/2$ ), there will be no need to specify the anti-alias filter. The software is designed to identify the filter system-function, once the sampling period (or the sampling frequency) is specified by the user.

## 10.3 Pre-stack Processing

The output from the re-organization stage is still in shot-gather domain, where the data is in de-multiplexed (trace-sequential) form. These shot-records are used as input to the following stage of processing, the pre-stack processing stage which includes a sequence of steps; the pre-processing steps, as shown in (Fig. 10.8):

### 10.3.1 Trace Editing

Together with the observer report, all shot records are inspected for data quality. There may be some shots which are very weak, or, for some reasons, corrupted to the extent of being useless to include in the processing. Weak traces or traces which are abnormally noisy are, likewise, omitted from processing or just zeroed altogether. Traces with reversed polarity, if any, are rectified.

The process of trace editing is normally done by direct visual inspection of all of the input shot

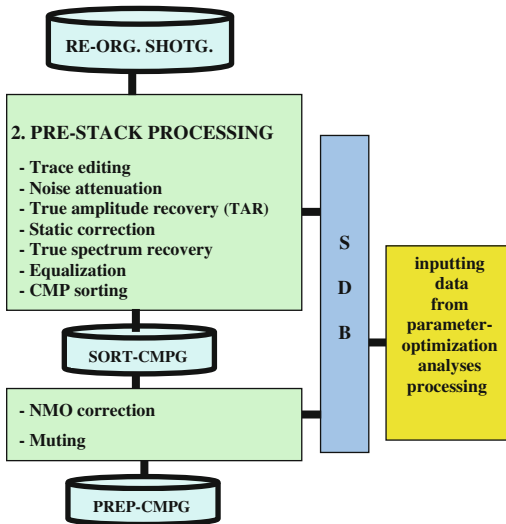


**Fig. 10.8** Main steps, taken in pre-stack processing stage. Input is the re-organized shot-gathers (SHOTG) and output is pre-processed common mid-point gathers (PREP-CMPG). *SDB* denotes the seismic data base included in the processing system

records which are normally displayed on the screen.

### 10.3.2 Noise Attenuation

There are several types of noise that may be found recorded with the reflection signal. Measures to attenuate noise and lessen its effect on the signal resolution are taken in processing as well as those measures taken during the acquisition activities. The objective of noise attenuation at this stage of processing is to attenuate, as much as possible, the two types of noise which are the coherent and the incoherent (random) noise.

The coherent noise which is commonly observed in field shot records is the low-frequency, high energy surface waves, known as the (ground roll). This type of noise (coherent noise) can be removed by the application of a low-cut frequency filter or by the application of FK filter.

The technique often applied to remove coherent noise is done by FK filtering. The process starts with computing the 2D Fourier

spectrum of the input shot records, and then the part of the spectrum corresponding to the noise is identified and removed (spectrum-edited) in the spectrum-domain. By Fourier inverse transform of the edited spectrum, the original time-domain data can be recovered with the noise removed. An actual FK filtering example is presented in Fig. 10.9.

Alternatively, trial and error approach may be used to find the appropriate low-cut (LC) filter that can, on application, remove the coherent noise. Example of attenuation of coherent noise by low-cut filtering is presented in Fig. 10.10.

The other type of noise (the random noise), is normally of broader frequency-band and lower energy. It is more difficult to attenuate than the coherent noise, because of the overlap between its spectrum and that of reflection signals. Because of its random nature, this type of noise is very effectively attenuated in the stacking processes (vertical stacking and CMP stacking). Another option is to apply a suitable band-pass (or band-cut) frequency filter.

### 10.3.3 True Amplitude Recovery

As a matter of fact, the reflection wavelet suffers from time-variant attenuation effects during its source-to-receiver journey. These are mainly the geometrical spreading (spherical divergence) and inelastic attenuations. In addition to that the amplitude is scaled in the recording system by an appropriate gain, making the amplitude value within the system recording dynamic range. This means that the reflection amplitudes appearing in the field shot-records do not express the true reflection coefficients, but modified by these additional attenuation factors.

True amplitude Recovery (TAR) is a processing step which aims at adjustment of the recorded wavelet amplitude and recovery of the true amplitude that represents the reflection coefficient. This is achieved by corrections for these factors, namely, removal of the imposed gain and compensation for the geometrical spreading and inelastic attenuation effects.

**Fig. 10.9** An actual case of application of an FK-filter. **a** Shot record, **b** shot 2D Fourier spectrum, **c** shot spectrum with the noise spectrum removed, **d** recovered shot record with coherent-noise removed

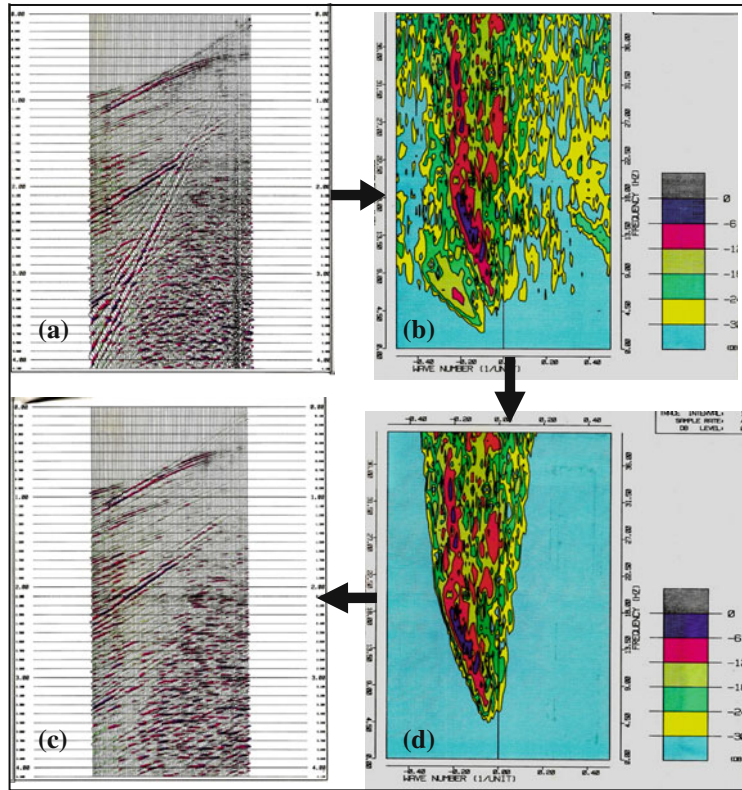
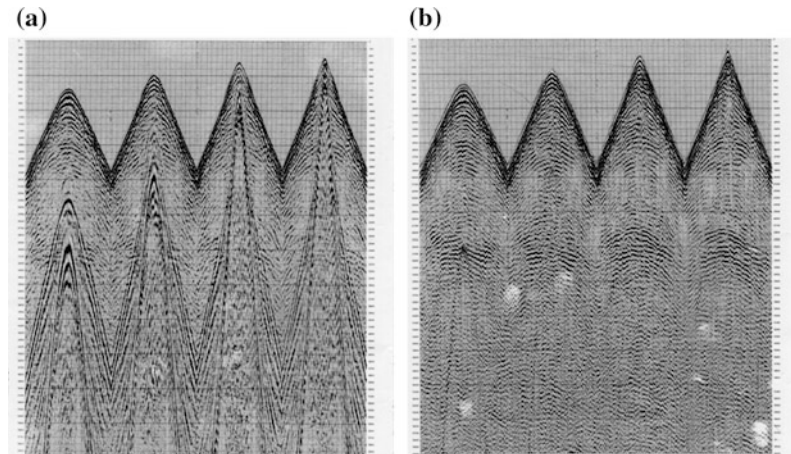


**Fig. 10.10** Ground roll attenuation by use of a low-cut (LC) filter. **a** Shot record, input from a 3D survey with prominent coherent nose, **b** out-put shot record with the noise removed by LC filter



**(i) Gain Recovery**

The gain-value applied during recording to each sample of the seismic trace is recorded alongside that sample. As a first step in TAR, the software is directed to remove the effect of the

recorder-applied gain from the sample value, recovering the true amplitude as detected by the geophone group. The gain-correction factor  $F_G$  due to the applied time-variant gain  $G(t)$  may be represented by:

$$\mathbf{F}_G = 1/G(\mathbf{t}).$$

### (ii) Geometrical Spreading

This is amplitude attenuation caused as a result of spreading of the wave front as it travels away from the source region. Since the attenuation is inversely proportional to travelled distance, the correction factor ( $\mathbf{F}_{GS}$ ) is of the form:

$$\mathbf{F}_{GS} = \mathbf{v}(\mathbf{t}) \cdot \mathbf{t}$$

where  $\mathbf{v}(\mathbf{t})$  is the velocity time-function for the reflection travel-path medium.

According to (Newman 1973), the more appropriate geometrical spreading correction-factor for a layered medium is ( $\mathbf{v}^2(\mathbf{t}) \cdot \mathbf{t}$ ) instead of ( $\mathbf{v}(\mathbf{t}) \cdot \mathbf{t}$ ) that was derived for homogeneous media.

### (iii) Inelastic Attenuation

Inelastic attenuation takes place because of energy-absorption due to dissipation of seismic energy into heat due to friction. Studies has shown that this is a frequency-dependant effect and given by the exponential function,  $\exp(-\alpha \mathbf{x})$  where ( $\alpha$ ) is the attenuation factor which varies linearly with frequency, and ( $\mathbf{x}$ ) is the travelled distance (Sheriff 2002, p. 2). The travelled distance ( $\mathbf{x}$ ) can be substituted for, by  $\mathbf{v}(\mathbf{t}) \cdot \mathbf{t}$ .

The correction factor for inelastic attenuation ( $\mathbf{F}_{IA}$ ) is of the form:

$$\mathbf{F}_{IA} = \mathbf{e}^{+\mathbf{av}(\mathbf{t}) \cdot \mathbf{t}}$$

Inelastic attenuation is the third and last step in the TAR correction. The three steps can be combined in one compact correction factor ( $\mathbf{F}_{TAR} = \mathbf{F}_G \cdot \mathbf{F}_{GS} \cdot \mathbf{F}_{IA}$ ), hence:

$$\mathbf{F}_{TAR} = \left[ \mathbf{v}(\mathbf{t}) \mathbf{t} \cdot \mathbf{e}^{+\mathbf{av}(\mathbf{t}) \cdot \mathbf{t}} \right] / G(\mathbf{t}).$$

As this formula shows, there are two parameters that need to be inputted; the attenuation factor ( $\alpha$ ) and the velocity function  $\mathbf{v}(\mathbf{t}) \cdot \mathbf{t}$ . The first step is applying the gain recovery, then the geometrical spreading using a velocity function  $\mathbf{v}(\mathbf{t})$ , which is representative of the area. For the

third TAR-correction, the parameter ( $\alpha$ ) is estimated from the slope (expressed in db) of the decay-line of a trace after being corrected for gain and geometrical spreading.

With TAR correction, the reflection amplitudes are preserved which means that reflection amplitudes express the true relative changes of reflection coefficients along the reflector.

At present, amplitude adjustments are done as regards to geometrical spreading and gain removal with no special processing as regards to inelastic attenuation. This is because of the application of the spiking deconvolution which restores the high frequencies lost by the earth high-cut filtering effect. A common amplitude adjustment processing is what is called the surface-consistent amplitude compensation (SCAC). This is a gain-correction process for each shot-record to correct for cross-coupling at both of the shot and receiver ends. The compensation is computed to remove amplitude changes due to the trace shot-to-receiver offset.

## 10.3.4 Field Static Correction

Static correction is a travel-time correction which reduces the reflection travel-time to what it would be, if both the source and receiver were located on a defined horizontal datum-level. It is essentially a time bulk-shift made to each trace, making reflection travel-time to be measured from the fixed datum plane. Each sample of the trace is shifted in time by an amount which is constant to all samples of the trace, hence the name **static correction** as opposed to another correction, the (**dynamic correction**), in which the shift varies with the sample-time. The dynamic correction is usually referred to as NMO correction.

The principle of static correction is shown in (Fig. 10.11). Here the static correction is virtually placing of the source and receiver on the defined datum plane and the correction is the same time shift (static) for all of the reflection events.

The datum plane is chosen to be slightly below the base of the weathering zone. It can be

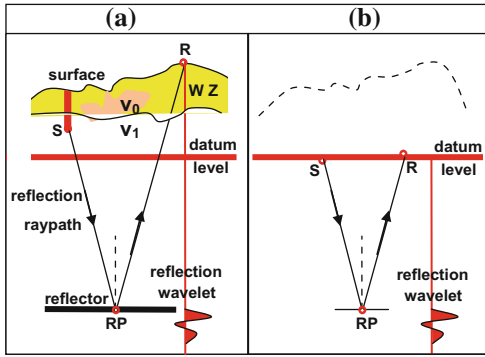


**Fig. 10.11** Principle of static correction. **a** Ray-path, and **b** seismic image of the seismic trace, before and after static correction. Effect of the weathering zone (W.Z.) is indicated

the sea mean level or any horizontal plane defined at a suitable elevation. With the datum plane defined, the time shift (static correction) can be easily calculated from knowledge of thickness and propagation velocity of the weathering zone, which can be determined in the field by up-hole surveying or by especially designed refraction surveys.

Static correction (called the total field statics) consists of two parts; the shot static ( $\Delta t_S$ ) and the receiver static ( $\Delta t_R$ ). In application, the total static ( $\Delta t$ ) will shift a trace by the sum of these two static corrections, that is:  $\Delta t = \Delta t_S + \Delta t_R$ . The principle is explained in Fig. 10.12.

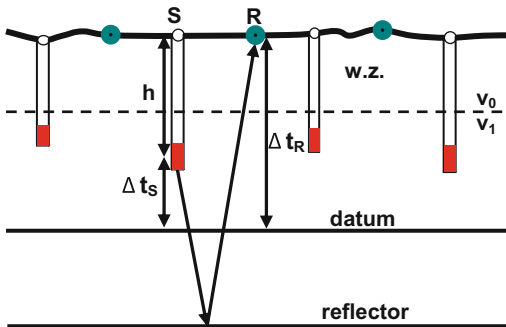


**Fig. 10.12** Definition of shot static ( $\Delta t_S$ ) and receiver static ( $\Delta t_R$ ) in dynamite shooting where the source is dynamite charge placed at the bottom of the shot-hole,  $h$

To compute shot static ( $\Delta t_S$ ), the surface layer (weathering zone, w.z.) parameters are required. These are the surface elevation ( $e$ ), weathering zone thickness ( $z$ ), weathering zone velocity ( $v_0$ ), sub-weathering zone velocity ( $v_1$ ) in addition to the shot-hole depth ( $h$ ). Depending on the relative position of the base of weathering zone relative to the datum level, static computation cases can be grouped under three main groups. These are presented in Fig. 10.13.

In marine surveying, there is a problem in computing static correction, similar to that of the effect of too-low topography (case of surface being lower than datum level) in land surveys. Here we have the sea base of the sea (sea floor), is of varying depth and the relatively low-velocity water layer. With no static correction application, the image of a deep reflector will be distorted. For example, the reflection image of a horizontal plane reflector, will not appear as horizontal reflection horizon, but distorted. This is because the reflection travel-times will be larger in the deep parts of the sea than those recorded in the shallow parts, as shown in Fig. 10.14.

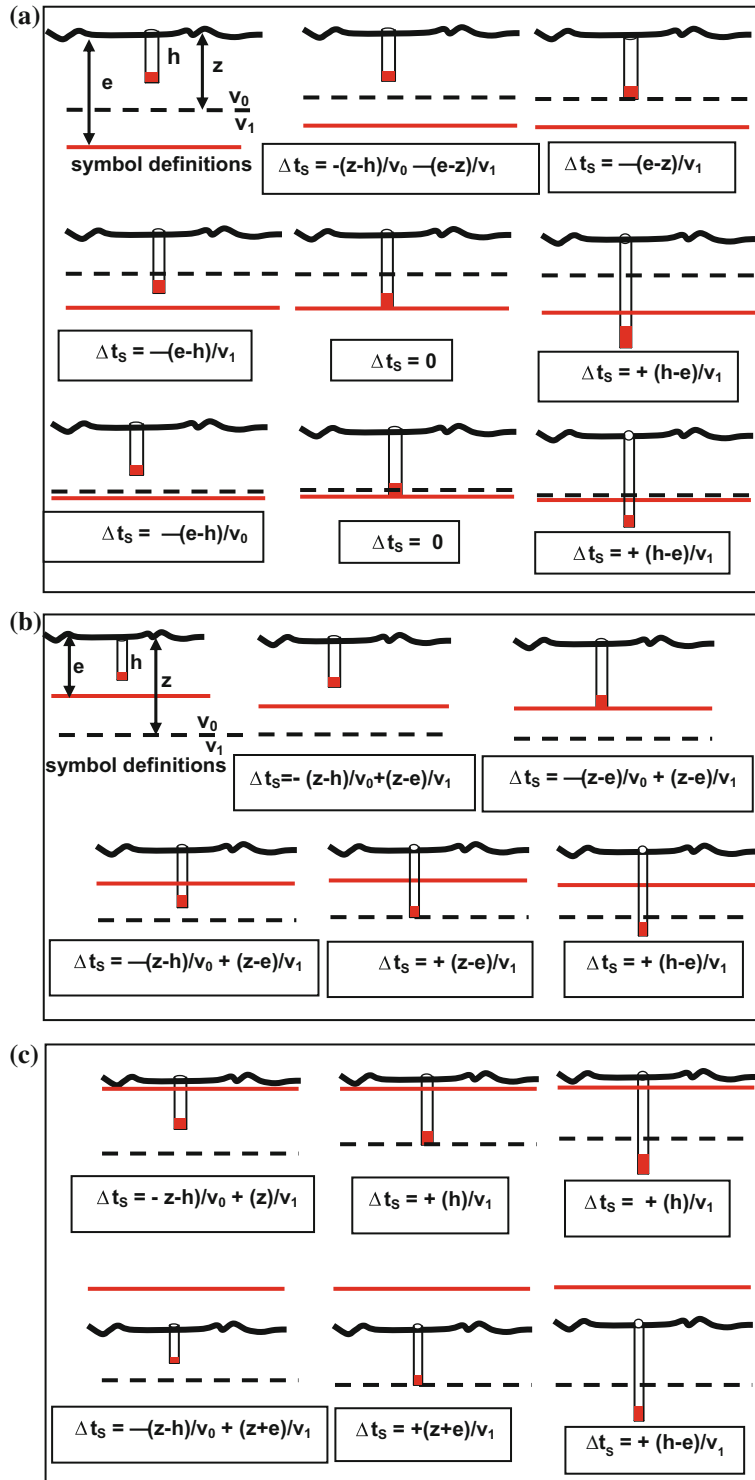
Given the water velocity ( $V_w$ ), rock velocity ( $V_R$ ), and sea depth ( $d_w$ ), the static correction ( $\Delta t_m$ ), for a survey point (source or receiver) placed at the sea surface, is made to compensate for the water-layer effect. The correction ( $\Delta t_m$ ), called (replacement static correction), is given by:

$$\Delta t_m = -(d_w/V_w) + (d_w/V_R)$$

The principle, applied here, is the same as that used in computing static correction for the case when the datum plane is above the ground surface (Fig. 10.13c).

For the second part of the static correction for land surveying, the receiver correction ( $\Delta t_R$ ), can be determined using the same principles followed in determining ( $\Delta t_S$ ). However, in practice, a more accurate method depending on the value of the vertical time ( $t_v$ ), is used. For those receivers which are located at positions coinciding with shot-point locations, the receiver correction ( $\Delta t_R$ ) is computed from:

**Fig. 10.13** A Static correction ( $\Delta t_s$ ) computation **a** Datum plane is below or on base of weathering zone; **b** Datum plane is within the weathering zone; **c** Datum plane is on, or above, ground surface



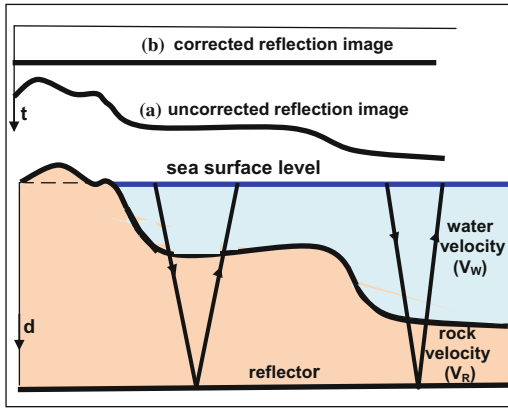


**Fig. 10.14** Static correction ( $\Delta t_m$ ) computation in marine surveying. (a) uncorrected seismic reflection event of a horizontal reflector. (b) reflection event with static correction

$$\Delta t_R = \Delta t_S - t_v$$

where ( $t_v$ ) is the time required for a direct wave travelling from the source charge, covering the vertical distance to the surface. Arrival time (read from the up-hole break) of this wave is recorded by a geophone-group placed near the shot location for this purpose. The sign of ( $\Delta t_S$ ) in this formula must be taken into consideration and ( $t_v$ ) is always positive. For other receivers, whose locations do not coincide with shot-positions, the receiver static is found by linear interpolation. The total static correction is the sum of the source and receiver statics for the particular trace.

Another very often applied method to compute statics is what is called (refraction statics). This is based on determination of refraction arrivals of

waves refracted from the base of the low-velocity weathering zone. With special software, refraction arrivals (refraction first breaks) are automatically picked and used in statics computation. It is faster, but it is not as accurate as the conventional method described above.

### 10.3.5 Application of Deconvolution

There are two basic types of deconvolution, in common application in seismic data processing: Spiking (or Whitening) deconvolution which results in equalizing of amplitudes of frequency components (spectrum whitening) and Gapped (or Predictive) deconvolution which is attenuating multiples from shallow reflectors, as in removing ghosts, and reverberations.

#### (i) Removal of Earth Filtering Effect by Spiking Deconvolution

In dynamite shooting the source function is in the form of an impulse (spike form) which travels through the earth to the reflector and back to the receiver where it is detected and then recorded. On detection, the reflection wavelet is no more that sharp, impulsive form, but in the form of broad, low energy, and low frequency wavelet. Loss of the high-frequency components is brought about as a result of the earth high-cut filtering effect. These wavelet-changes are due to changes of both of amplitude and phase spectra that the earth high-cut filter imposes. In processing, this earth filtering effect is reversed, and the original impulsive source-function is restored by applying spiking (whitening) deconvolution (Fig. 10.15).

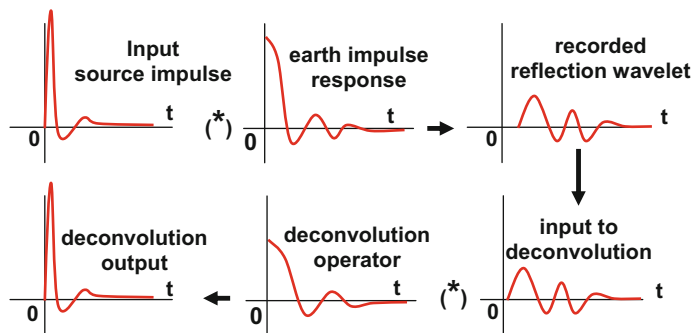


**Fig. 10.15** Effect of earth filtering is convolution of the input source impulse with the earth response function. The original source impulse is restored by spiking (whitening) deconvolution

The term (spiking) refers to the action made by the spiking deconvolution, which is the retrieval of the spike-shape (impulsive form) of the source function. In the frequency domain, the spike-shaped function becomes broad and flat spectrum (making all frequency components of same amplitude). Amplitude spectrum of this form is described as white spectrum, hence the term (whitening deconvolution).

### (ii) The Spiking Deconvolution Operator

The mathematical derivation of the deconvolution filter (called the deconvolution operator) is based on Wiener least-squares optimality principle, in which, an operator (shaping filter), is computed from an input function and then, convolved with that function and shape it into another desired output. Spiking deconvolution can be considered as a special case of a shaping filter where the desired shape is a spike. This process begins with computing the autocorrelation function (ACF) of the gate defined for the process. From the ACF, a deconvolution operator is derived which, on convolution with the input gate, will give the desired output of spike-shaped reflection wavelet. For the random distribution of reflection events (an assumption required by the underlying theory), the ACF is approaching a spike at zero-lag and zero at all other lags (Fig. 10.16a).

It is easier to visualize the process in the frequency domain (Fig. 10.16b), where the amplitude spectrum of the deconvolution operator is an

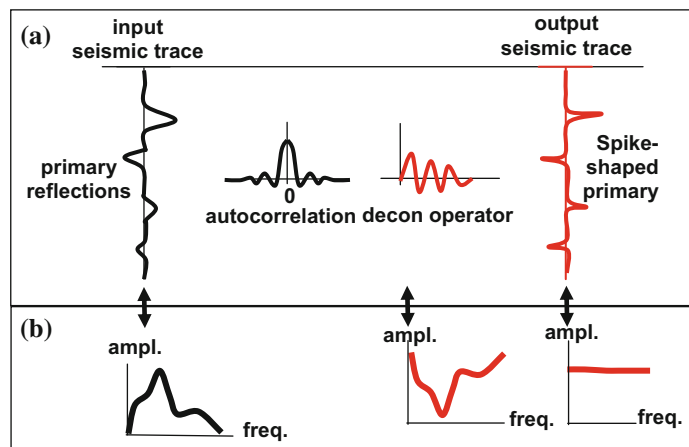
inverse of the amplitude spectrum of the wavelet to be deconvolved. Since deconvolution, in the frequency domain, is a division-process (or multiplication by the inverse of operator spectrum), the output becomes nearly flat (constant value) over wide frequency bandwidth. This is called whitening deconvolution. Whitening deconvolution has the side effect of strengthening noise that happens to be within the spectrum frequency-range of the signal. Boosting of random noise is a common observation on seismic sections which have been undergone whitening deconvolution.

### (iii) The Time-variant Deconvolution (TVD)

Usually, spiking deconvolution is applied in time-variant manner (time-variant deconvolution, TVD). The trace is divided into gates (normally with 50 % overlapping), and an operator is derived from the autocorrelation for each gate, then these gates are scaled and summed to produce the final deconvolved trace. The process is repeated for each of the input traces (Fig. 10.17). The technique is the same as that used in time-variant filtering (TVF).

A closely related type of deconvolution is called (signature deconvolution) or (designature). The procedure is to use the average spectrum of the shot-gather traces then from the inverse of the calculated average the deconvolution operator is derived and convolved with the individual traces of that shot. This approach gives better estimate of the source wavelet, because of the averaging process.

**Fig. 10.16** Design of spiking (whitening) deconvolution operator from the autocorrelation function. **a** Time-domain and **b** frequency domain



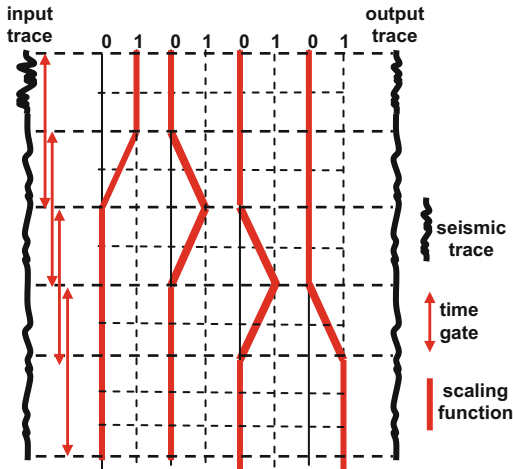


**Fig. 10.17** Method of applying the time-variant deconvolution, using 50 % overlapping gates

Spiking deconvolution results in compressing of the reflection wavelets, leading to reduction in the possibility of wavelets-overlapping, which may take place especially with thinly-layered geological sections. The application of deconvolution is, therefore, helping in avoiding the overlapping effect and hence increasing the resolution power of reflection events.

**(iv) Removal of Reverberations by Gapped Deconvolution**

The two major factors bringing about wavelet distortion are earth filtering and reverberations. Spiking deconvolution handles the distortion due to earth filtering and the gapped deconvolution is applied to remove reverberations which are mainly occurring in marine seismic data.

The water layer is bounded by the water free-surface which is of reflection coefficient equal to  $(-1, \text{approximately})$  for an upward travelling seismic wave, and by the sea-floor surface which is usually of a relatively large reflection coefficient. In marine shooting, multiple reflections occur within the water layer. A detector at the water surface will receive the primary reflection from a deep reflector followed by a series of multiple arrivals named reverberations (Fig. 10.18). Though not so common, reverberation may also occur in the low-velocity surface layer in land survey-data.

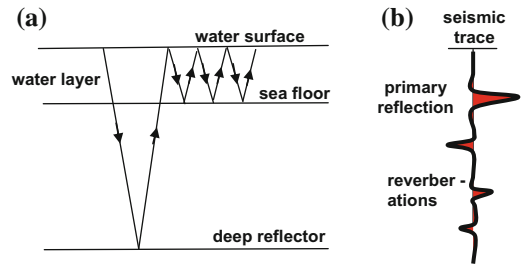


**Fig. 10.18** Development of reverberations within the surface water layer. **a** Ray-path geometry of primary and reverberation reflections. **b** Seismic images of the primary and reverberation reflections

Removing reverberations (de-reverberation) is accomplished by applying the gapped deconvolution which is also called predictive deconvolution because it can predict the arrival times of the repeated arrival of the event to be removed. In marine shooting, reverberation arrival-times are equal to the two-way time of the passage of the signal through the water layer. The operator of the predictive-deconvolution is derived from the autocorrelation function of the selected time-gate, just as in the case of whitening deconvolution. It is useful to note that the autocorrelation of a trace having reverberation-events will possess side-lobes separated by an interval equal to the reverberation period.

**(v) The Predictive (Gapped) Deconvolution Operator**

The difference between the predictive deconvolution operator and the spiking operator is that the prediction operator consists of an isolated spike at its first point followed by a series of zero sample-values (the gap), followed by the operator values. In this sense, spiking deconvolution is considered as a special case of the gapped deconvolution in which the gap-length is only one sample-period.

The predictive deconvolution operator (called Prediction Error operator or Prediction Error filter) will effectively predict the reverberation onsets on the seismic trace and subtract them leaving only the unpredictable events which consist of the primary reflections with random noise. Gapped deconvolution, in the time- and frequency-domain is shown in Fig. 10.19.

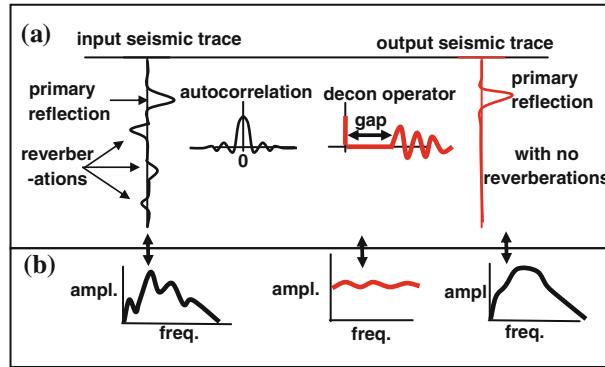


**Fig. 10.19** Design of gapped (predictive) deconvolution operator for removing reverberations. **a** time-domain and **b** frequency domain

In the frequency domain, the gapped deconvolution operator acts as a smoothing operator that smoothes out the ripples that appear in the spectrum due to presence of reverberations in the input data. Since the noise existing within the spectrum width was not whitened, the output trace is not as noisy as the spiking deconvolution.

**(vi) The Deconvolution Parameters**

Deconvolution depends on a number of interrelated parameters which are normally determined by special processing tests designed for this purpose. These are:

- Gate length, and number of gates per trace are decided upon, depending on the variation of the reflection wavelet-characteristics in the trace. Normally, two to three gates of 2–3 s length each are applied. Operator length is, as a rule of thumb, taken to be about 10 % of the gate length.
- Operator gap of the applied predictive deconvolution should be slightly larger than the reverberation period to be able to efficiently remove reverberations. In spiking deconvolution, usually a small operator gap (8–16) ms is used. With this small-gap operator, fairly spiked reflection-events with less spiky noise will be obtained.
- Pre-whitening noise, to help in computation stability. For this purpose a small amount of white noise, typically 1–2 %, of the zero-lag of the autocorrelation is added. In effect it is giving the amplitude spectrum a dc level in order to avoid dividing by near-zero value in deconvolution-computations.

**10.3.6 Trace Equalization**

Trace equalization is normally included in the processing to get a reasonably balanced form of the trace. Processing software provide several alternative options of the way to equalize the trace. One way to equalize the trace is by applying an AGC-type of scaling. This is carried out by defining a gate-length (of about 500 ms length) which slides down the trace at one sample-interval at a time. In the first position, at the top of the trace, the mid sample of the gate is multiplied with a factor proportional to the inverse of the average power of all the sample-values found within the defined gate. This multiplication process is repeated in the second gate-position, and so on until the whole trace is completely covered (Fig. 10.20).

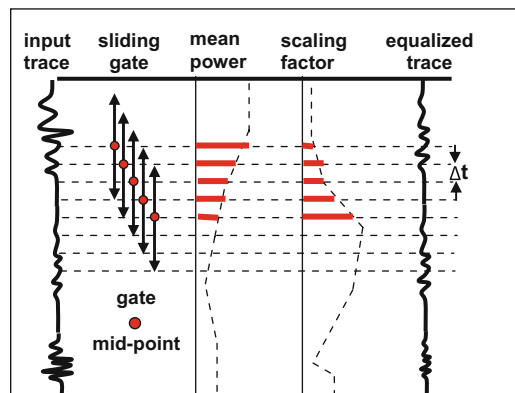


**Fig. 10.20** Time-variant AGC-scaling (TVS) using equal gates with 50 % overlap,  $\Delta t$  is the sampling period

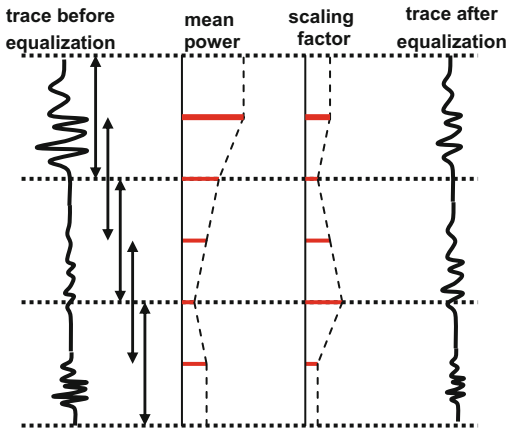


**Fig. 10.21** Equalization, time-variant scaling (TVS) using equal gates with 50 % overlaps

The drawback of AGC scaling is that it does not preserve relative amplitude variation, and the shorter the adopted gate the more amplitude smoothing will be. For this reason it should not be applied in data prepared for stratigraphic interpretation.

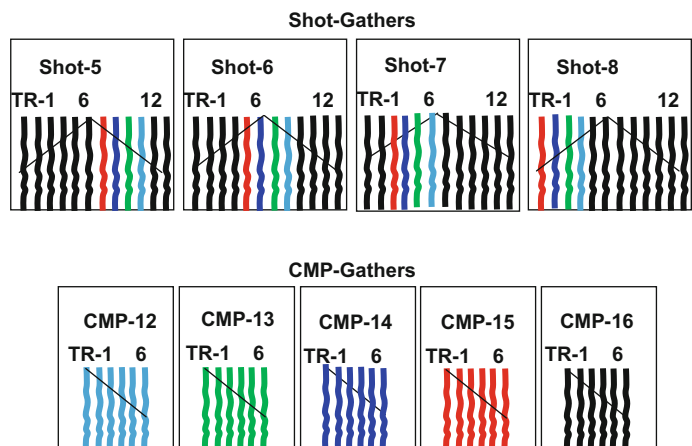
The more common time-variant equalization (or time-variant scaling, TVS) methods are those depending on the use of overlapping gates of different-lengths. The scaling factor (proportional to the inverse of the mean power) of each gate is applied at the center of the gate, and linear interpolation of the factors is performed between gate centers. Often, gates are designed to be of equal lengths, overlapping with user-specified overlap-percentages, normally at 50 % overlap (Fig. 10.21).

### 10.3.7 CMP-Sorting

The field seismic data received by the processing centre consists of a series of shot records recorded on a magnetic tape in the sequence of shooting implemented in the field. In other words the received seismic traces are grouped in shot-gathers which are subjected to the re-organization and pre-processing steps. Since in the following processing phase, the CMP-traces are going to be stacked, the traces which are sorted in shot-gathers are re-sorted into CMP-gathers in which the traces are normally arranged in sequence of increasing offset. In fact the CMP-record looks like an end-on type of shooting spread. The number of traces per certain CMP-gather is equal to the fold of coverage for that CMP. The process is just regrouping of the traces such that all traces belonging to a CMP are grouped together under that particular CMP. The process is shown pictorially in Fig. 10.22.

The sorting shown in Fig. 10.22 is taken from an example seismic-line in which a 12-channel spread with move-up steps of 2 receiver points. There are 12-traces in each shot-gather, and the nominal fold is 6, implying that the full-fold CMP-gather is made up of 6 traces. In this figure we are using the gathers for the CMP-12, CMP-13, CMP-14, and CMP-15. The traces involved come from 6 different shots which are: shot-3, shot-4, shot-5, shot-6, shot-7, and shot-8. In Fig. 10.22 only four shot-gathers (shot-5 to shot-8) and five CMP-gathers are shown.

**Fig. 10.22** Sorting of *shot-gather* traces into *CMP-gather* traces, applied on shot and CMP example-records. Shot and CMP numbers are hypothetical



### 10.3.8 NMO Correction

Reflection travel time ( $T_x$ ) of seismic signal reflected from a horizontal reflector and received at a point on surface at distance ( $x$ ) from the source location is given by:

$$T_x = \left[ \left( \frac{x}{v} \right)^2 + (T_0)^2 \right]^{1/2}$$

Normal moveout (NMO) is defined to be the difference ( $\Delta T$ ) between the slant reflection time ( $T_x$ ) and the vertical reflection time ( $T_0$ ) for the same CMP (Fig. 10.23), that is:

$$\Delta T = T_x - T_0$$

That is,

$$\Delta T = \left[ \left( \frac{x}{v} \right)^2 + (T_0)^2 \right]^{1/2} - T_0$$

where ( $v$ ) is propagation velocity assumed to be constant for the medium.

For a sufficiently small offset-to-depth ratio ( $x/vT_0 \ll 1$ ), normal move out ( $\Delta T$ ) can be approximated by expanding the square root in the ( $\Delta T$ ) formula with the Binomial Theorem to give:

$$\Delta T = x^2 / 2T_0v^2$$

With this approximation, the formula was transformed from the exact hyperbolic function

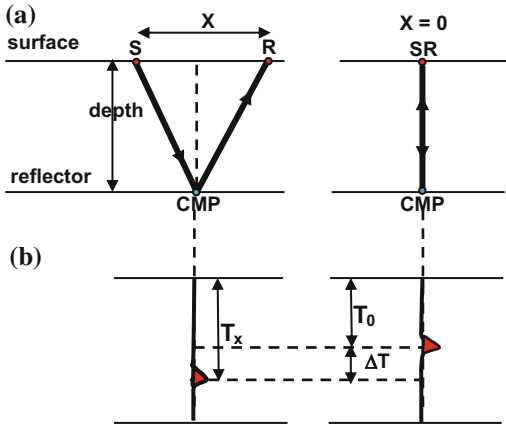


**Fig. 10.23** Definition of the Normal Move-Out (NMO,  $\Delta t$ ), **a** reflection ray-path, and **b** reflection image

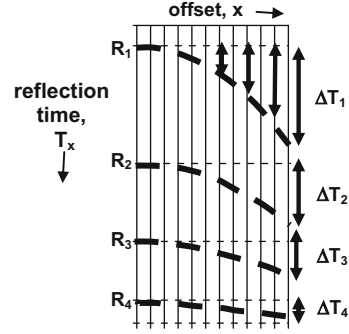


**Fig. 10.24** Variation of the NMO parameter ( $\Delta T$ ) as shown in a seismic record. ( $\Delta T$ ) increases with trace offset and decreases with depth of reflector

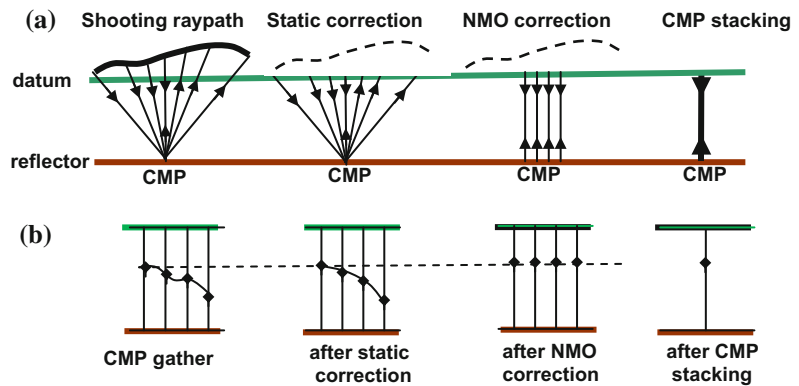
to the approximate parabolic form which can express, more clearly, the mathematical relationships of the NMO parameters ( $x$ ,  $T_0$ , and  $v$ ). It is shown that ( $\Delta T$ ) is directly proportional to square of offset ( $x$ ) and inversely proportional to vertical time ( $T_0$ ) and inversely proportional to square of velocity ( $v$ ). On a seismic reflection record, ( $\Delta T$ ) is clearly seen to increase as the trace-offset increases and decreases with increasing reflector's depth for the same offset (Fig. 10.24).

#### NMO Application

In processing of reflection data, seismic traces, before being stacked, must be NMO-corrected. This involves removing the extra time in the reflection travel-time from the reflection slant time. Arrival reflection times in each gather will be corrected to what it would be if the trace offset is zero. With this correction, the common-reflector events in the gather traces (from a given horizontal reflector) will all have the same arrival-times. Thus, when the gather traces are NMO-corrected, will, on stacking, give boosted reflection amplitude. NMO correction, involves calculating ( $\Delta T$ ) accurately for each sample of the trace and then the sample is shifted up the trace by the calculated  $\Delta T$ -value.

Unlike static correction where the correction is constant (static) for all the trace samples, NMO correction varies with the sample time and that is why it is also called dynamic correction. Static correction is, effectively, placing both of the source and receiver on a common horizontal

**Fig. 10.25** Concepts of static and NMO corrections. **a** Ray-path of CMP reflections, **b** seismic image of seismic traces of a CMP gather, after static correction, NMO correction and CMP stacking



plane, the adopted datum plane. Likewise, NMO correction, effectively, places the source and receiver on a common position on the datum plane. With the static and NMO corrections, reflection events from a horizontal reflector (on a CMP-gather), will be aligned on the same timing line, giving enhanced reflection amplitude on stacking of the CMP trace-gather. These concepts are shown in (Fig. 10.25).

**Role of Velocity in NMO Correction**

To compute the NMO correction ( $\Delta T$ ), we need to have the offset ( $x$ ) and ( $T_0$ ) which are known parameters. What is left to be determined is the correct velocity ( $v$ ) which is usually not readily available. The usual way to determine velocity is through special velocity analysis processing.

In the derivation of the  $\Delta T$  expression, velocity is assumed to be constant for the medium. In this case the ray-path is straight line. The more realistic model for the subsurface geology is a layered medium with velocity increasing with the layer depth. This model would give a curved ray-path instead of straight path as it would be in case the medium is homogeneous having one constant velocity.

An effective velocity for a multi-layer medium is an average velocity or RMS velocity. It has been shown (Dix 1955) that, use of the RMS velocity (instead of the average velocity) for the multi-layer medium will lead to a ray-path which is closer to the actual curved ray-path and give optimum NMO correction. Processing geophysicists are used to call the velocity which is

used in NMO correction as (stacking velocity). This is because the velocity, when it is optimum, gives an accurate  $\Delta T$ -correction, and hence, best stack response. Since RMS-velocity is the nearest to stacking velocity, RMS-velocity is often used as an alternative terminology for the stacking velocity.

**NMO Residual**

The difference between the correct  $\Delta T$  and the erroneous  $\Delta T$  is called NMO-residual (or residual NMO), and may be given the symbol ( $\Delta\Delta T$ ) or  $\Delta^2 T$ , defined as:

$$\Delta^2 T = \Delta T_e - \Delta T$$

where  $\Delta T$  corresponds to the correct velocity ( $v$ ) and  $\Delta T_e$  corresponds to the applied (erroneous) velocity ( $v_e$ ).

Using the approximate  $\Delta T$ -formula, we can write:

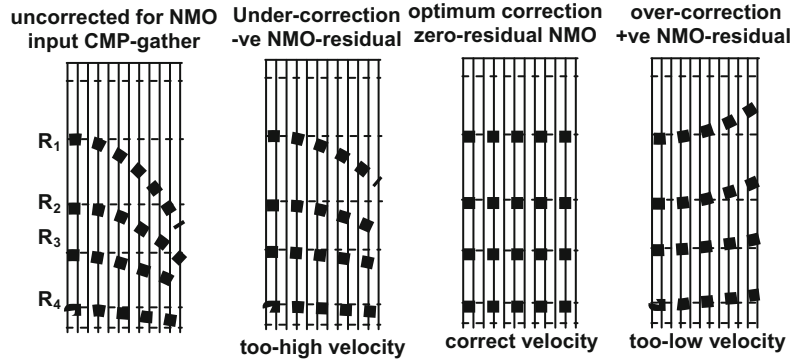
$$\Delta^2 T = (x^2/2T) \cdot \left[ (1/v_e)^2 - (1/v)^2 \right]$$

This formula shows that we get positive NMO-residual ( $\Delta^2 T$ ) called over-correction when ( $v_e < v$ ), or negative (under-correction) when ( $v_e > v$ ). This is explained pictorially in Fig. 10.26.

**NMO-DMO Correction**

So far, discussion was concerned with horizontal multi-layer model where NMO is computed using RMS velocity which can be derived from the interval velocities of the different layers by

**Fig. 10.26** Schematic representation of the effect of the applied stacking velocity on the residual-NMO



applying Dix formula. In case of complex geological structures and dipping reflectors, there is no simple formula for the NMO correction. In case of a dipping reflector, the increase in reflection time for a given reflector is function of dip as well as for offset. Change in reflection travel-time due to dip is called dip move-out (DMO). This means that in case of dipping reflectors, we need to correct for the dip move-out (DMO) as well as for NMO.

When the reflector is dipping, there cannot be a common reflection point (CRP) nor common depth point (CDP). In fact, for the commonly used shooting method, reflection points get dispersed over the reflection plane. They move up-dip with increasing offset (Fig. 10.27).

In Fig. 10.27, the four reflection ray-paths, having one common point (the CMP), will each produce a seismic trace. These traces contain reflection events which are reflected from the dispersed reflection points (RP, RP<sub>1</sub>, RP<sub>2</sub>, RP<sub>3</sub>.) and not from one point as in the case of

horizontal reflector. For this type of source-receiver set-up, there is one point that is common to all of these ray-paths, which is the source-receiver midpoint (the CMP). The subsurface position of the CMP is considered to be the reflection point (RP) for the reflection ray-path perpendicular to the dipping reflector. The group of traces which belong to the same CMP is referred to as the (CMP-Gather).

The CMP concept is more general than that of the CDP. In fact the CDP is a special case of CMP which is applicable when the dip is zero. Thus, when the reflector is horizontal (dip is zero) all the points CRP, CDP, and CMP will all coincide with each other.

In processing, DMO correction effectively moves the reflection point of each trace in the CMP-gather to the point which is the projection of the CMP on to the dipping reflector that is to point CRP in Fig. 10.28.

It is important to note that, with this type of source-receiver layout (equal offset step-ups), we

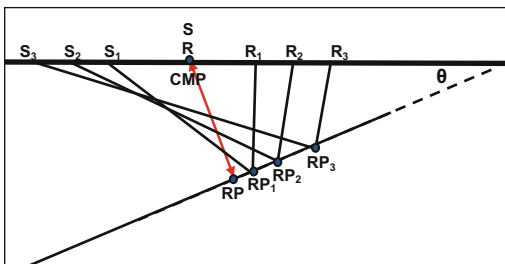


**Fig. 10.27** Definition of the common midpoint (CMP) in case of dipping reflector. Its subsurface position is the reflection point (RP) of reflection path is perpendicular to the dipping reflector

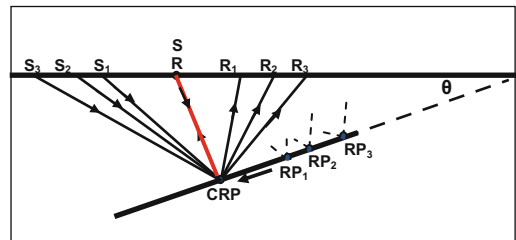


**Fig. 10.28** Principle of DMO correction, moving the reflection points of the CMP gather-traces to coincide with the CRP which is the projection of the CMP onto the dipping reflector

cannot have a common reflection point (CRP). However, in processing (as in DMO, and in pre-stack migration), reflection arrivals of a CMP-gather traces, from a dipping reflector, are corrected such that the end result will be corresponding to rays being reflected from a common reflection point (CRP) which is the projection of the CMP onto the dipping reflector. This is, effectively, moving back of the RPs to one common point, the CRP (Fig. 10.28).

DMO is effectively removing, the dispersal of the RPs of non-zero offset ray-paths, where both of the reflection-point location and reflection arrival time are changed. This implies that DMO has the action of migration and that is why it is sometimes called (pre-stack partial migration). In recent years, full pre-stack migration is carried out instead of DMO, especially in cases of complex geological structures which involve severely dipping strata.

### 10.3.9 Trace Muting

Ideally, the traces, corrected for NMO, should be freed from non-reflection signals before being input to the following processing step; the CMP stacking. Normally, the early parts of a seismic trace contain large amplitude arrivals of the direct and refracted waves. Another important factor that makes the early parts of the trace undesired is the effect of NMO correction on the early arriving non reflection events. It introduces abnormal amplitude stretching of these early arrivals. Also, during seismic recording, a noise burst (noise with abnormally high amplitude) may be also recorded. A typical example of noise burst is that caused by cable jerk in marine shooting, or by sudden mechanical agitation in land shooting. Such events could be recorded at any time during sensing or during recording.

In processing, these abnormal events are removed by a process called (muting) which is carried out simply by zeroing the undesired parts of the trace. The muting process is done by multiplying the trace by a scaling function which is of zero-value over the parts to be muted and unity over the rest of the trace. The change from

zero to unity is usually made gradually and not abruptly. Thus, in order to avoid creating spikes or sudden breaks in the trace at the extremities of the mute-zone the scaling function takes the ramp shape. To secure gradual change, a ramp-type of function is used in muting rather than a step-type of function. The time of the ramp part of the scaling function is called (ramp length). Trace muting is sometimes called ramping because of the use of ramp scaling function. The concept is shown in Fig. 10.29.

The muted zone can be at the beginning of the trace, at end of the trace, or located within the trace. These are called on-muting, off-muting, and surgical muting, respectively (Fig. 10.30).

With the muting step, the pre-processing stage is completed. The corrections made in this stage, consist of two types of corrections: signal form restoration and signal reflection time correction. The first group of corrections is directed to enhancing the reflection signal by spectrum restoration, amplitude corrections, and noises removal. The second group of the pre-processing steps is directed towards correction of the reflection travel-time (to vertical time measured from a defined datum plane) by static and NMO corrections. Input to this stage of processing is the field shot-records and the output is the same shot records but corrected and re-sorted into CMP trace gathers.

As an example for the main processes done in pre-processing, a centre-spread shot (48 channels) was subjected to the following

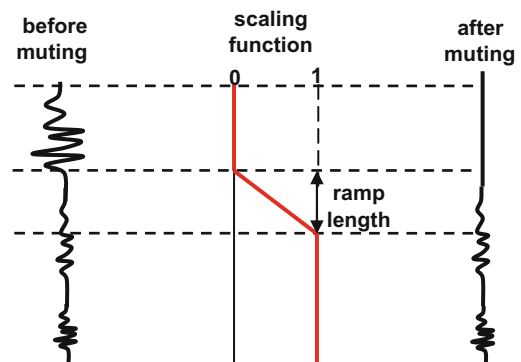


**Fig. 10.29** Concept of trace muting, using mute ramp-function

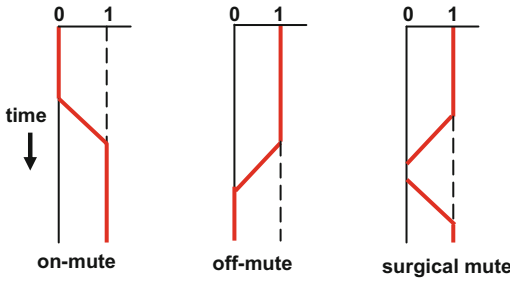


**Fig. 10.30** Types of mute-functions; on-mute, off-mute, and surgical mute

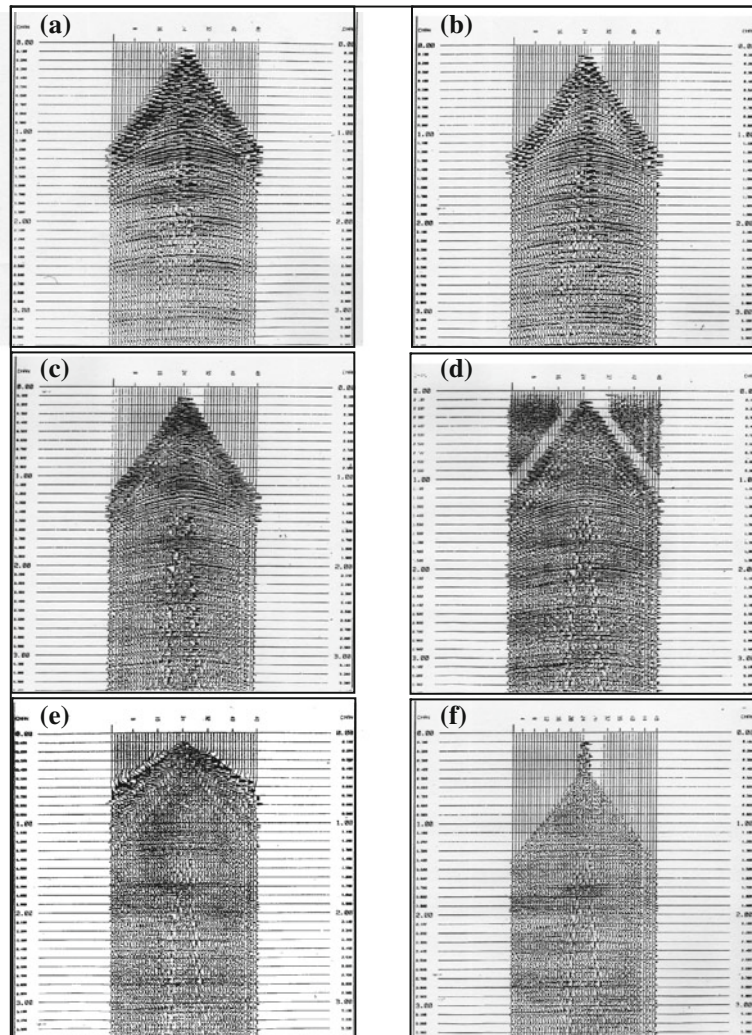
pre-processing steps (trace edit, geometrical spreading correction, whitening deconvolution, NMO correction, and muting of the first arrivals).

Output of these processes are shown in the following Fig. 10.31.

### 10.4 Stack and Post-stack Processing

The output from the previous pre-processing stage is in the form of CMP-gather records, with traces corrected with respect to static, NMO, and other signal enhancing processing. This will be the input to the final set of processing steps which are directed to further signal enhancement and position-restoration of reflection events. The principal processing steps following the stacking

**Fig. 10.31** Seismic shot-record (48-channel, centre-spread) subjected to the pre-processing steps: **a** raw-field shot record, **b** editing of 2 traces with geometrical spreading correction, **c** whitening deconvolution, **d** time-varient equalization, **e** NMO correction, **f** muting of first arrivals



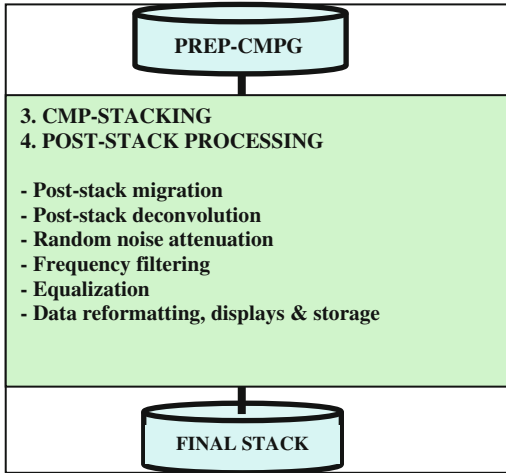


**Fig. 10.32** Main steps normally taken in stack and post-stack processing stage

process are collectively referred to as post-stack processing, or just, post-processing. The main steps included in the pos-processing stage, are summarized in Fig. 10.32.

### 10.4.1 CMP Stacking of Seismic Traces

Stacking of a group of seismic traces is a process by which seismic traces are summed up together to form one output trace, called the stack trace. The process involves finding the algebraic sum of the values of trace-samples which have a common recording time. The output is normally divided by the number of traces entering in the summation to get the arithmetic mean of the traces. In seismic data processing, there are three

main types of stacking. These are: CMP stacking, vertical stacking, and horizontal stacking.

### 10.4.2 CMP Stacking

The process of CMP-stacking, introduced by (Maine 1962), is summing the trace-gather of a CMP. This is done after both static and NMO corrections are applied to the gather-traces in order to bring reflection events in phase. The stack trace is normally subjected to a certain scaling process as finding the arithmetic mean of the summed traces with or without weighting. Thus, each CMP-gather will, after stacking, give one stack trace showing enhanced reflection wavelet with marked (S/N) enhancement of the reflection events (Fig. 10.33).

The CMP-stack can be considered as a process that has its own characteristic response which is mainly dependent on the velocity (stacking velocity) used in the NMO correction. The stacking-response curve has a maximum value corresponding to the optimum stacking velocity. The response falls from the maximum value when velocity deviates from the optimum. Too-low velocity (positive NMO residual) and too-high velocity (negative NMO residual), make the stacking response to fall from its maximum value (Fig. 10.34).

The main advantage of the CMP stack is enhancing the seismic reflection signal. This is because reflection events are summed in phase resulting in constructive interference whereas the background noise, being of random nature, is destructively interfering with each other resulting

**Fig. 10.33** Stacking of CMP gather, 6 traces, after NMO-correction. S/N enhancement in stack trace is clearly shown

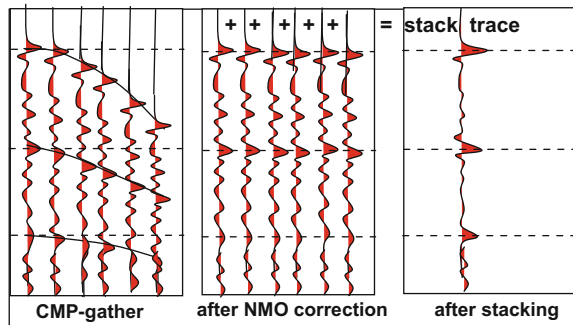
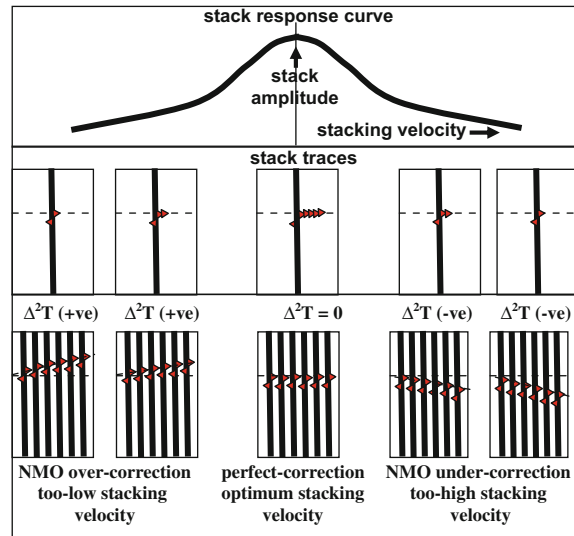


**Fig. 10.34** Schematic representation of stack response curve. It is function of the stacking velocity. The *curve* shows maximum at the optimum stacking velocity



with noise-attenuation. The increase in S/N ratio due to CMP stacking is estimated to be of the order of square root of the number of the traces in the CMP-gather (that is square root of the fold of coverage).

Another important advantage of the CMP stack is attenuating multiple reflections. The attenuation is done on the basis that a multiple would have a greater NMO than a primary reflection that occurs at the same arrival time. As velocity is generally increasing with depth, a multiple is recognized from its apparent abnormally-low stacking velocity. Seismic events such as multiple reflections and diffraction arrivals (when appearing on a CMP-gather) show larger NMO value than the primary reflection at the same time. Thus, when NMO-correction, with optimum stacking velocity, will align the primary arrivals but leave the non-primary arrivals with large NMO residual. On stacking, primary reflection will add up constructively while multiples and other non primary reflections will be attenuated because of the residual NMO.

### 10.4.3 Vertical Stacking

Vertical stacking, involves summing corresponding traces from several shot-point records which are executed in the same location. This is

done normally with weak surface-sources (such as weight dropping and Vibroseis sources) to get enhanced reflection signals. Vertical stacking is applied without doing any time-corrections to the traces before being summed together.

### 10.4.4 Horizontal Stacking

The term (horizontal stacking) is used to refer to stacking of a number of traces belonging to the same shot-point, or to the same CMP. This type of stacking is rarely applied in normal processing activities. However, it is applied in certain cases of too-weak reflection signals recorded amid a highly noisy background. Although horizontal stacking results in losing reflection character, it will help in improving reflection strength and reduce noise level. The computation applied in horizontal stacking involves a running-average type of procedure. The method can be explained as follows:

Referring to Fig. 10.35, we have a shot record made up of 6 traces (TR<sub>1</sub>–TR<sub>6</sub>). Using three-trace averaging, the first three traces (TR<sub>1</sub>, TR<sub>2</sub>, TR<sub>3</sub>), NMO-like correction is applied to the traces with respect to the first trace (TR<sub>1</sub>) in this group, and then, stacked to produce the stack trace (STR<sub>2</sub>) which will replace the group mid-trace (TR<sub>2</sub>) in the original record. The

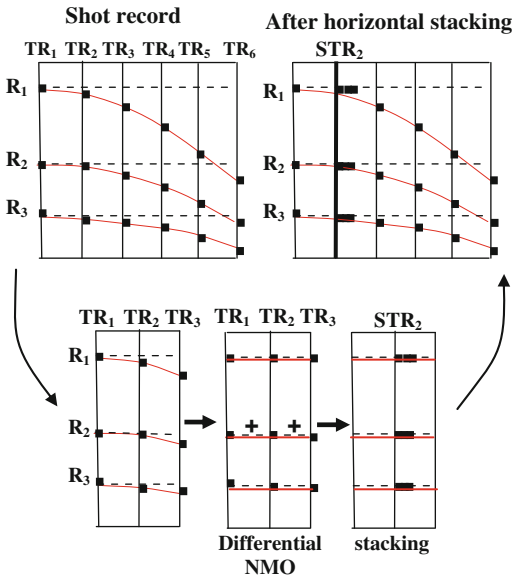


**Fig. 10.35** Concept of horizontal stacking. The first 3 traces ( $TR_1, TR_2, TR_3$ ) are subjected to differential NMO and stacked to produce stack trace ( $STR_2$ ) replacing the group mid-trace ( $TR_2$ ) in the original record

process is repeated with the second three-trace group ( $TR_2, TR_3, TR_4$ ) to produce ( $STR_3$ ) replacing ( $TR_3$ ) in the original record. This process is repeated until the whole record is completed. In this example we chose the group to consist of three traces. The number of traces taken in the group is optional, but, usually not too-large number.

The important point in this process is the application of NMO-like correction to the traces prior to stacking. This correction (called differential NMO) is done with respect to the first trace (trace of the smallest offset) in the group.

### 10.4.5 Diversity Stacking

Before summing the traces in a CMP gather, the individual traces are weighted in such a way as to either attenuate or exclude undesired noisy traces. A stacking process in which the gather traces are inversely weighted in respect to their individual mean power over certain parts of the trace is called (diversity stack). This is applied in the

usual CMP stack as well as in vertical stack, to attenuate noise bursts and abnormally-high amplitude arrivals (such as ground roll), and to prevent them from appearing in the stacked trace. The term is also applied to stacking in which amplitudes which are exceeding some specified threshold are completely excluded instead of being given the appropriate weights (Sheriff 1973, p. 60).

### 10.4.6 The Stack Section

The stack trace is obtained from summing of all NMO-corrected traces in the CMP-gather, a process which is repeated for all the CMP-gathers after being CMP sorted. From displaying these stack traces in the order of CMP sequence-number, the stack section is obtained.

A stack section represents a subsurface seismic image of the subsurface geological structure. Normally, the stack section is provided with top-label showing the CMP sequence numbers, elevation, and static correction drawn as function of distance along the seismic line. Another important label (normally drawn below the section) is the fold of coverage drawn as function of the CMP sequence number.

A seismic stack section can be looked upon as a two dimensional function representing the variation of amplitude with respect to both of the distance ( $x$ ), measured along the seismic line, and two-way vertical time ( $t$ ), that is  $f(x,t)$ . A typical stack section is shown in Fig. 10.36.

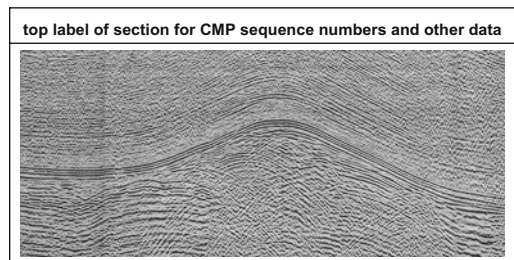


**Fig. 10.36** A conventional seismic stack section

### 10.5 Seismic Migration

Reflection seismology was developed in the 1920s and by 1930s it evolved into a common exploration tool. Various methods of transforming the seismic reflection section (the end product of the any seismic reflection survey) for revealing the true subsurface structure were investigated in the 1940s. These methods were labeled with the term (Migration). This is because the process involves moving, or migrating, the reflection events appearing on a seismic section to their true position in depth. Using techniques based on wave-fronts curves and diffraction patterns were given by Hagedoorn in 1954. Since then the migration techniques have developed through many phases. It started with manual (graphical) computation in the pre-computer times then it developed into a sophisticated computer-based computation, as it is done at present (Robinson 1983).

Seismic migration can be implemented either before CMP stacking (Pre-stack migration, PRSTM) or after the stacking process (Post-stack migration, POSTM).

#### 10.5.1 Distortions in the Stack Section

The seismic stack section represents the undistorted seismic image of the subsurface geological structure only when it is made up of continuous horizontal reflecting interfaces. When we have folded formations (dipping reflectors) and faulted beds (terminated reflectors), the stack section becomes a distorted image of the subsurface geology. Migration is the process that can restore the undistorted image of the subsurface geological section.

There are two cases in which distortions can occur in the seismic stack section. These are: distortions due to dipping reflectors and distortions due to terminating reflectors.

##### (i) Distortions due to Reflector Dipping

With dipping reflectors, shifting of the reflection event (horizontally and vertically) from its true position occurs. Alongside with the event-position shifting, there will be decrease of

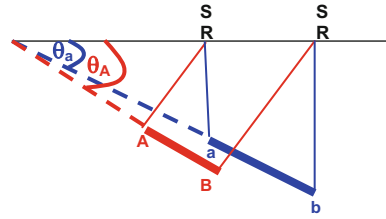


**Fig. 10.37** Distortions in case of a dipping reflector ( $AB$  of dip angle  $\theta_A$ ). Its position is shifted to ( $ab$  of dip angle  $\theta_a$ ), where  $ab > AB$  and  $\theta_a < \theta_A$

the dip-angle and lengthening of the reflection event (Fig. 10.37).

Stack sections of folded strata in the form of anticlines and synclines are distorted in such a way that the anticline flanks are exhibited with smaller dips while those of synclines are with greater dips. In such cases of geological structures, distortions take the form of widening of anticlines' crests and narrowing of synclines' bottoms.

Another case of distortions associated with folding is presence of a too-tight syncline (curvature width  $\ll$  depth). We have, in this case, a reflector having dips in opposite directions allowing zero-offset receivers to receive more than one reflection events coming from different reflection points. The resulting seismic image shows what is called a (buried focus or bow-tie event) which is a reflection image having a shape, far from the real structure, showing very misleading stack-section feature. The bow-tie event usually consists of three branches which can be shown to be the case from considering reflection ray-paths for zero-offset receivers,

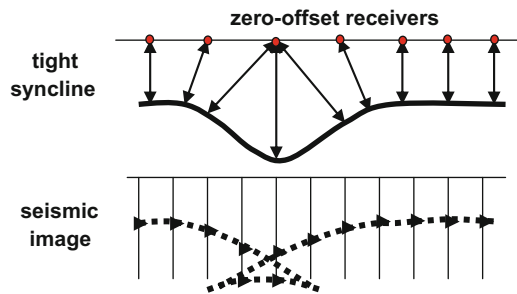


**Fig. 10.38** Distortions (bow-tie events) due to reflection arrivals from too-tight syncline. Multi-reflection arrivals were created by the syncline reflector

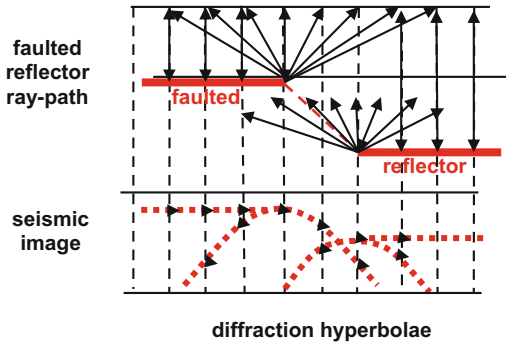


**Fig. 10.39** Distortions (hyperbolic events) due to diffraction arrivals created by a faulted reflector. Two diffraction points were created by the fault

remembering that a stack section is effectively made up of zero-offset traces (Fig. 10.38).

(ii) **Distortions due to Reflector Termination**

A terminating reflector (as a faulted reflector) can lead to creation of wave diffraction. On the stack section the diffraction arrivals appear in the form of hyperbolic events which are interfering with reflection events and obscuring fault zones. Diffraction hyperbolae caused by the reflector termination are shown in Fig. 10.39.

To sum up, the stack seismic section of folded and faulted reflectors is distorted image. Types of distortions for such structural features are summarized in Fig. 10.40.

The stack-section can be considered as a forward transformation-process which transforms a given sub-surface geological structure into the

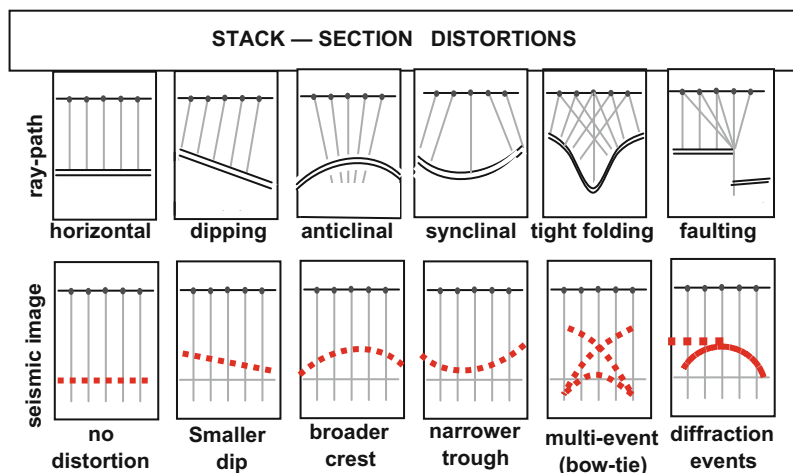
corresponding seismic image. In cases of folded and/or faulted geological formations, the resulting seismic image of the corresponding reflection events are expressed by distorted seismic images. Seismic migration is the inverse-process which transforms the seismic reflection image into the undistorted image of the causing geological structure. With the appropriate migration parameters, the dipping reflection events are positioned in their correct positions and their dips are corrected to their true values. Migration would also remove the diffraction arrivals (diffraction hyperbolae) and increase the resolution of the causing structural and stratigraphic features as faults and pinchouts.

By virtue of the modern advances in software development, migration processes often give dramatic improvements in the restoration of the original undistorted images of the seismic stack sections. In particular, migration is normally very effective in removing diffraction arrivals and in increasing fault resolution. This is remarkably displayed in the following illustration (Fig. 10.41).

**10.5.2 Problem Statement**

A stack seismic section is made up of stack traces which are effectively zero-offset traces. Each reflection event on such a seismic section is mapped (plotted) directly below the surface

**Fig. 10.40** Summary of the distortions occurring in the seismic stack section of folded and faulted geological reflectors



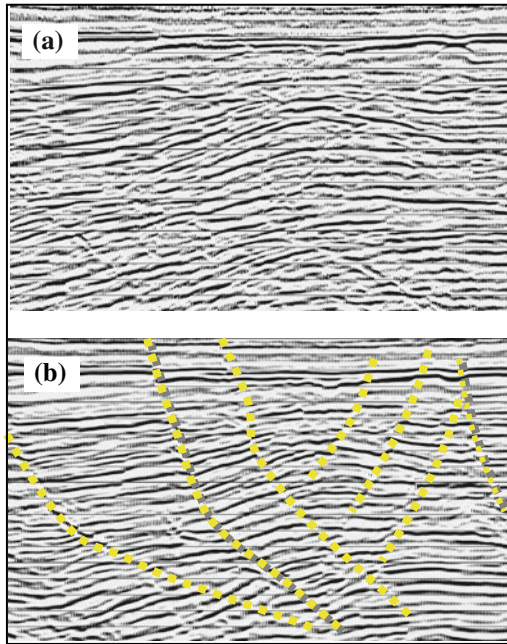


**Fig. 10.41** Migration effect in collapsing diffraction arrivals and enhancing fault resolution. **a** Un-migrated stack section, **b** the same section after being migrated

position of its CMP. In actual fact, the reflection point is located vertically below the CMP only if the reflector is horizontal. When there is a component dip along the seismic line, the actual reflection point is displaced in the up-dip direction. In other words, the stack section shows erroneous reflection positions in the presence of

dip. The result of this process is a distorted geometrical shape of the dipping reflection images. Another problem is presence of diffraction points (as those created by reflector faulting) would lead to diffraction arrivals which are fictitious structural events interfering with the reflection events. Seismic migration is a restoration process which restores reflection positions to their correct surface locations at the correct vertical reflection time, and removes diffraction arrivals.

The surface represented by a reflection image appearing on an un-migrated stack section is called the (record surface), and the actual geological surface causing that reflection image is called the (reflector surface). These two surfaces coincide only if they are flat and horizontal (Robinson and Trietel 1980, p. 375). A reflection surface representing a dipping reflector on a stack section is always placed in the wrong position. Thus, a reflection event appearing on a stack trace, and hence a reflection segment, is misplaced whenever the causing reflector is dipping (Fig. 10.42).

Referring to Fig. 10.42, it is shown that a reflection event on a dipping reflector is recorded at point (M) at record time ( $T_M$ ), but displayed at point (S) at record time ( $T_S$ ) (Fig. 10.42a). The true reflection position of point (M) of a trace recorded at the source-receiver common position ( $P_S$ ) is observed on the stack trace plotted

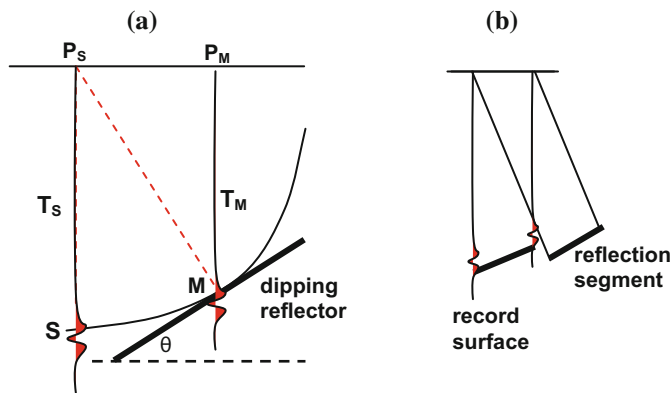


**Fig. 10.42** Nature of distortion in unmigrated stack sections in case of dipping reflector, **a** reflection event shifting from its true position at M to false position at S,

**b** reflection segment distortion includes position shifting and changes in both of its dimensions and dip-angle

vertically below position ( $P_S$ ) at the same reflection time. That is travel time ( $P_S-M$ ) is equal to travel time ( $P_S-S$ ). In this way the event is placed in the wrong position as it has been shifted both horizontally and vertically from its true position.

For the same reason, a dipping reflection segment (Fig. 10.42b), will occupy a wrongly-placed position relative to its true position. In addition to its wrong placement, the reflection segment will experience changes in its dimensions and in its dip-angle. Migration process is the process that can remove all these distortions from the stack section and bring about the required restorations to recover the true reflection surface.

### 10.5.3 Geometry of the Distortions

The geometry of the ray-path of a reflection from dipping interfaces, shows that not only its position is misplaced but its dip and segment-length are changed (Fig. 10.43).

Referring to this Fig. 10.43, the ray-path geometry, of distortions brought about due to the vertical plotting of the stack trace would lead to the following mathematical relationships (velocity,  $v$  is assumed to be constant):

$$\begin{aligned} \sin \theta_m &= \tan \theta_s, (\theta_m > \theta_s) \\ \Delta x_m &= (vT_s/2) \sin \theta_m = (vT_m/2) \tan \theta_m \\ \Delta T_m &= T_s - T_s \cos \theta_m \\ T_m &= T_s \cos \theta_m \end{aligned}$$

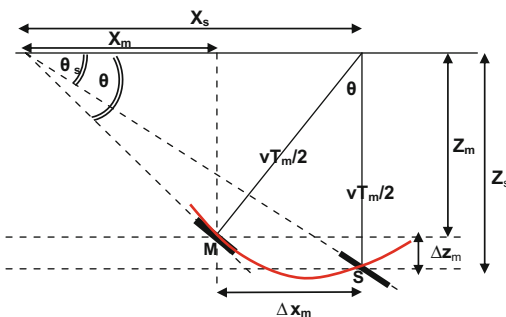


**Fig. 10.43** Geometry of the distortions in stack section of dipping reflection segments

where, ( $X_s, Z_s, T_s, \theta_s$ ) refer to the stacked section geometry before migration, and ( $X_m, Z_m, T_m, \theta_m$ ) refer to the stacked section geometry after migration. The terms ( $\Delta x_m, \Delta T_m$ ) represent the restoration shifts realized in the migration process.

These relations tell that migration results in the following restorations:

- (i) Segment length decreased ( $M < S$ )
- (ii) Segment dip increased ( $\theta_m > \theta_s$ )
- (iii) Shifting the segment horizontally and vertically by ( $\Delta x_m$ ) and ( $\Delta T_m$ ) respectively in up-dip direction ( $S$  moved to  $M$ ). Both shifts are functions of the reflector dip as well as of its depth (reflection time and velocity of the medium).

### 10.5.4 Relationship of Post-migration Dip to Pre-migration Dip

Considering the equation ( $\sin \theta_m = \tan \theta_s$ ), called the migrator's equation (Sheriff and Geldart 1995, p. 326), which shows that the actual reflector dip ( $\theta_m$ ) is always greater than the dip of the reflector image ( $\theta_s$ ) on the zero-offset section (the stack section). The fact that the maximum value of ( $\sin \theta_m$ ) is unity means that maximum value of ( $\tan \theta_s$ ) in this case is unity, which means that ( $\theta_s$ ) maximum value, expected to appear on a zero-offset section, is  $45^\circ$ .

The dip measured on a zero-offset time-section (unmigrated section) is expressed by  $\tan \theta_s$ , where:

$$\tan \theta_s = \Delta T_s v / 2 \Delta x_s = \sin \theta_m$$

hence,

$$\Delta T_s / \Delta x_s = (2/v) \sin \theta_m$$

This means that the maximum possible time slope (dip,  $\Delta T_s / \Delta x_s$ ) expected to be found on a zero-offset time section, is  $(2/v)$ , where ( $v$ ) is the minimum stacking velocity in the section. Migrated section will always show dipping reflectors at greater dip angle ( $\theta_m$ ) than the corresponding dip-angle ( $\theta_s$ ) in the un-migrated section.

### 10.5.5 Types of Migration Techniques

The history of migration principles started with the history of the exploration seismic method (Robinson 1983b, p. 95). In 1921, J.C. Karcher established reflecting interfaces by manually-drawn envelopes to the circular arcs centered at the surface observation points. This processing step (applied by Karcher in 1921) is historically considered to be the first migration process that was applied for seismic reflection data. In the 1950s a step forward in the development of migration computations was taken by Hagedoorn who introduced a graphical method based on drawing the wavefront-maximum convexity curves (Hagedoorn 1954).

With the introduction of the digital processing systems (including special computer programs) in the mid 1960s, migration lengthy computations were made practical. During the 1970s–1980s interval, three main methods dominated the migration computation processing. These are; Diffraction stack (Kirchhoff Stack), Finite-Difference, and FK migration. In recent years, the modern the Reverse Time Migration (RTM) was introduced.

Development trend of migration techniques seems to be towards building more sophisticated algorithms for computing pre-stack depth migration, based on wave equation modeling.

Here, a short definition notes is given to the common methods used in seismic migration,

starting with the early manual and semi-manual methods for historical interest.

#### (i) Dip-Bar Migration Method

This method is historically the earliest migration technique (after Karcher primitive migration) applied to migrate dipping reflection events. Prior to computer time, seismic migration was performed by this graphical method called (Dip-Bar Method).

This method is based on calculating the real dip-angle ( $\theta$ ) from the equation:

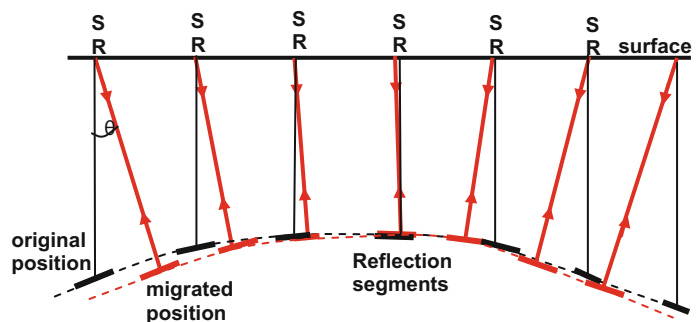
$$\sin \theta = \Delta t \cdot v / 2 \Delta x$$

where  $\Delta t$  is the difference in reflection times observed at adjacent zero-offset traces,  $\Delta x$  apart, assuming constant average velocity,  $v$  (Dobrin 1960, p. 136).

Once the velocity ( $v$ ) is known or assumed, the true dip angle ( $\theta$ ) can be calculated and each reflector segment is shifted up-dip by the determined dip-value ( $\theta$ ) to the new migrated position. This process is repeated with all of the reflector segments producing the final migrated section (Fig. 10.44).

It should be noted that the dip measured on a stack section is the true geological dip if the profile is in the dip direction, that is, the line is perpendicular to strike. If, however, the line is at azimuth ( $\alpha$ ) with the true-dip direction, then migration requires adjustment of the migration velocity. For a single dipping reflector with uniform overburden velocity ( $v$ ), the correct

**Fig. 10.44** Principle of the dip-bar migration method. Segments are shifted from their original positions to the migrated positions



migration velocity is  $(v/\cos \alpha)$ , (McQuillin et al. 1984, p. 93). Of course, this method is now obsolete.

(ii) **Wave-front Common Tangent Method**

This is the manual method which was applied by Karcher in 1921 to migrate his single-fold section, drawn on paper (paper-section processing). For each zero-offset reflection event, a wave front (circular arc for constant-velocity assumption) is drawn passing through the event to be migrated. Position of the reflector is then sketched so that it is tangent to each of these circular arcs. The resulting tangent line marks the migrated position of the section.

The principle underlying this method, shown in Fig. 10.45, is that the ray-path from a source-receiver (S, R) common position (zero-offset receiver) is normal to the dipping reflector, and hence the reflector surface is tangent to the incident wave-fronts. For constant velocity medium, the wave-fronts will have the shape of circular arcs as shown in the following figure Fig. 10.45.

(iii) **Wave-front Stacking Method**

In a stack section which is made up of zero-offset traces, a reflection event has known reflection-time but unknown reflection-point position. From the velocity field, the wave front can be constructed. It is the locus of equal two-way reflection times,  $T_s$ , in Fig. 10.46. For constant velocity, the wave front is in the shape of a semi-circle centered on the source-receiver

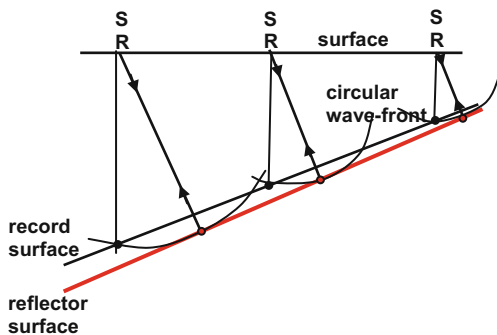


**Fig. 10.45** Principle of wave-front common tangent migration. Geometry of the ray-paths transmitted from source-receiver (S, R) common positions and reflected from a dipping reflector

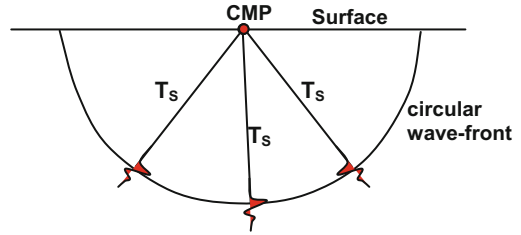


**Fig. 10.46** Construction of a circular wave-front

common point (CMP). The position of the reflection event, which is a point on the wave-front, is unknown. It can be anywhere on that circular wave-front (Fig. 10.46).

The wave-front is constructed by duplicating the trace many times and applying to it, an NMO-like corrections using the assumed velocity field (Fig. 10.47).

For a given reflection event this process is repeated for all points on that event-segment. By summing of all the produced wave-front arcs, that is by (wave-front stacking process), this process will result in migrating the section, since sample values (amplitude values) sum constructively at true position and destructively elsewhere. Alternatively, this is done by drawing the common tangent (common envelope) to the wave-fronts.

(iv) **Wavefront-Maximum Convexity Method**

This method is based on drawing wave fronts and diffraction curves known as curves of maximum convexity. This approach was introduced by Hagedoorn (1954). The method was originally applied in computing migration graphically, but later on, it was adapted to be done by computers.

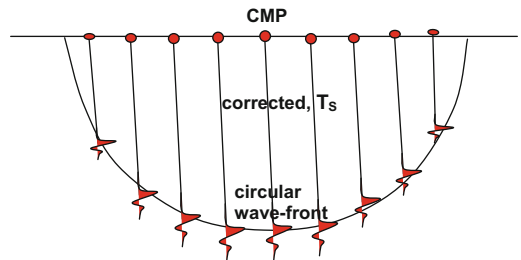


**Fig. 10.47** Duplicating (with NMO-like correction) of an input stack-trace to create the wave-front for the particular reflection event

Two facts are employed in the process of migration. First, the diffraction point is located at the apex of maximum convexity curve (the diffraction curve), and secondly, the wave front (semi-circle for constant velocity) of a reflection event intersects the maximum convexity curve at two points. The first point (unmigrated-position point), marks the point at which the reflection segment is tangent to the diffraction curve. The second point (the migrated-position point), is the diffraction point (the curve apex). The migration process is done by drawing appropriate maximum convexity and wave-fronts curves and moving of reflection events to the apex of the appropriate diffraction curve (maximum convexity curve).

To explain the method, the steps needed to carry out the migration can be presented in the form of a manual procedure. Based on the velocity field of the section, a wave-front curve and a diffraction curve (maximum convexity curve) are constructed. The diffraction curve is slid laterally until a part of it becomes tangent to the unmigrated segment at point  $P_S$  (Fig. 10.48a). The wave-front curve is placed with its central axis passing through the reflection point to be migrated. The position of the migrated point is located at the apex of the diffraction curve (Fig. 10.48b). The true after-migration position of the segment will be the segment which is passing through the point ( $P_M$ ) and tangent to the wave-front, having its central axis through point ( $P_S$ ).

This process results in migrating the segment at point ( $P_S$ ) into its reflector surface segment passing through the apex of the diffraction curve, point ( $P_M$ ).

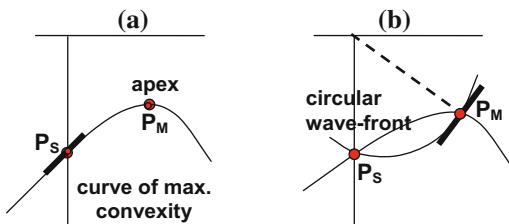


**Fig. 10.48** Principle of migration by maximum convexity curve method: **a** record surface of reflection segment, and curve of maximum convexity, and **b** wave-front intersecting the maximum convexity curve

Like the wave front graphical method, this method is now obsolete.

#### (v) **Diffraction Stack (Kirchhoff) Method**

Diffraction stack migration is based on the assumption that a reflector is made up of closely spaced diffraction points each of which produces a diffraction-arrivals event (hyperbolic curve for constant velocity) as seen by surface receivers. The true position of the diffraction point is located at the apex of that hyperbolic curve. All diffraction arrivals from the point-diffraction source will fall on that hyperbola. For a continuous reflector (reflector with no termination points), the reflector's unmigrated image, is considered to be formed from the superposition of the diffraction hyperbolae. The reflection event appears as a result of constructive interference at those diffraction points is considered to be making up the reflection surface (Fig. 10.49).

If, however, the reflector is terminating, the termination point, acting as a diffraction point, will create a diffraction hyperbola that appears superposed on the stack section. This hyperbola can be collapsed to the hyperbola-apex, which is located at the diffraction-point. One of the migration methods used in collapsing diffraction arrivals is based on diffraction-stack (also called Kirchhoff-stack) migration.

Based on this approach, migration of a point in a record section is achieved by summing all data values (sample values) falling along the diffraction-hyperbola that is centered at that point. Result of summation along the hyperbola is assigned to the apex of that hyperbola. By considering the record section to be the outcome of superposition of all the hyperbolae generated by the diffraction points, each point on the section is replaced by the sum of amplitudes falling at the intersections of the established hyperbola (centered at that point) with the seismic traces in that section. When the summed amplitude-values belong to the diffraction arrival they will be in phase and constructive interference will result. If, on the other hand, the values are not diffraction arrivals, a destructive interference will result in cancellation, leaving only the diffraction amplitudes to be summed and placed at the apex of the hyperbola.

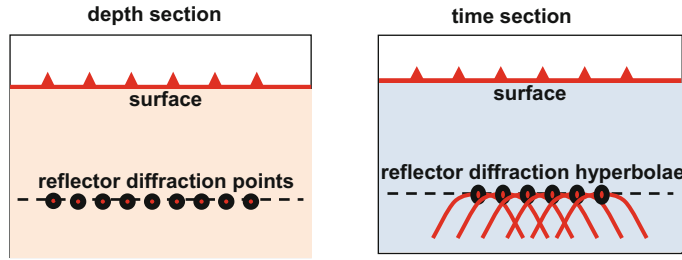


**Fig. 10.49** Diffraction stack migration is based on considering the reflector is made-up of closely spaced diffraction points, each of which generates a diffraction hyperbola

To further clarify the method, the diffraction hyperbola (for the given velocity field) is drawn on the section, then sum (stack) all the trace-amplitudes (sample values) found at the points of intersection of the hyperbola with the traces of the section. The summation result is plotted at the apex of the hyperbola. The process is repeated for every sample of that trace. By repeating this process for all possible apexes and for all traces in the given section, the whole section will be migrated. The method is schematically presented in Fig. 10.50.

Diffraction stack (Kirchhoff) migration incorporates scaling and other processes before summation in order to reconstruct the amplitude and phase of the migrated traces properly. This migration method can be performed as time migration (using RMS velocities) or as depth migration (using interval velocities).

(vi) **Finite Difference Method**

This method is based on the principle of the downward continuation principles of the wave field observed at the surface level of the seismic section (Claerbout 1976). Migration computation is carried out by solving the wave-equation based on finite-difference approximation. At the time when this method was introduced (mid 1970s), it was called the Wave-Equation Migration. Later, Lerner and Hatton (1976) showed that both of the diffraction stack migration and the wave equation migration were in fact based on the same model, but with different computation approaches. Diffraction stack method solves the wave equation by integration and the “wave equation” migration method by finite difference computations. Hence the term (wave equation migration) was replaced by the term (finite-difference migration), leaving the term (wave equation

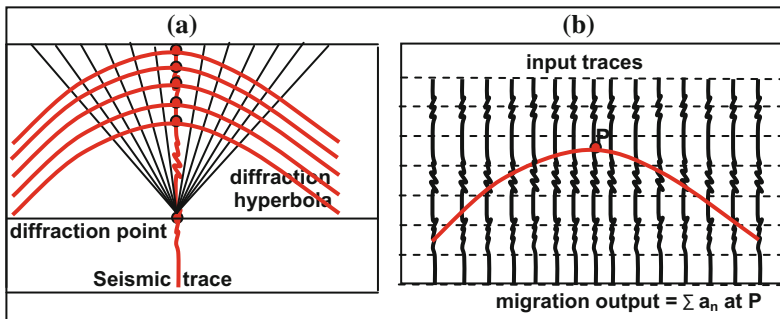


**Fig. 10.50** Principle of diffraction-stack migration. **a** The seismic trace is the result of summations done for all the hyperbolic arrivals. **b** Diffraction stack migration is

by placing at the apex (P) the sum of amplitudes found at intersection points of the hyperbola with the traces in the section

migration) to be applied for all methods which are based on wave-equation solution. Likewise, the term (diffraction stack) was also replaced by the term (Kirchhoff migration) since it has been shown later in 1970s, that diffraction stack is an expression of the Kirchhoff integral solution of the wave equation (Robinson 1983b, p. 99).

The Finite Difference method is based on a reflector model called (exploding-reflector model). According to this model, the reflector is made up of closely spaced diffraction points, and the record section is created from rays which are normal to the reflector surface and received by the zero-offset receivers. The exploding-reflector travel times must be doubled (or using half of the medium velocity) in order to get a record section having the same ray-path geometry as that obtained with the normal stack sections (zero-offset traces).

The record section (the input to migration process) represents the seismic amplitude as function of distance ( $x$ ) and time ( $t$ ) recorded at surface plane (depth = 0), that is  $f(x, t, z = 0)$ . Given the velocity field and, with the aid of wave-motion equation, the function  $f(x, t, z = \Delta z)$  is reconstructed at depth of ( $\Delta z$ ) below the surface. In the next step, the output of the previous step  $f(x, t, z = \Delta z)$  is inputted to the following step to work out the wave field (seismic amplitude) at depth ( $2\Delta z$ ). For an  $N$ -reflector section, the downward computation is repeated

until depth ( $z$ ) of the  $N$ th reflector (at  $z = N\Delta z$ , say) is reached.

To clarify the concept let us consider the effect on a record section containing diffraction arrivals created by a point diffractor. The input section shows the hyperbolic diffraction event. By use of wave equation computations, the section is simulated at a lower level, at depth ( $z = \Delta z$ ). At this level, the process results in showing how the section looks when the zero-offset receivers were placed at this depth. With progressive downward shifting of the receivers, the diffraction hyperbola diminishes as the computation level approaches the true location of the diffraction point-source. When the receivers were at the level of the diffraction point, the diffraction hyperbola would have been completely collapsed. At this stage, the section, down to that level ( $z = N\Delta z$ ), is completely migrated. The process is schematically shown in Fig. 10.51.

According to this model, migration becomes a process which is reversing the wave propagation, which constructs the reflector states that existed at time ( $t = 0$ ) from the input time section which is the zero-offset traces recorded at time ( $t = \text{total reflection travel time}$ ).

#### (vii) Frequency-Wave Number (FK) Migration

This method of migration (sometimes called Stolt Migration) was developed in 1978 by Stolt (1978). The technique is based on

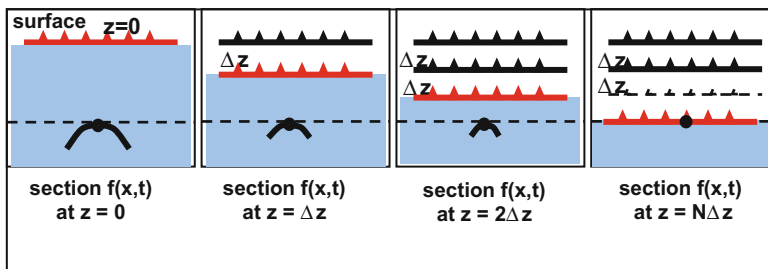


**Fig. 10.51** Principle of the downward continuation method. By successive downward shifting of the zero-offset receivers, the hyperbola shrinks and completely collapsed at the true position of the diffraction source

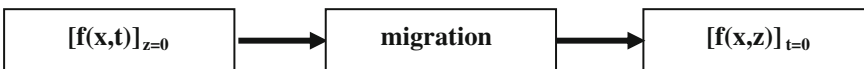
two-dimensional Fourier transform of the stack section, which is essentially a two dimensional function of time and distance domain,  $f(\mathbf{t}, \mathbf{x})$ , into **FK** domain. Migration is carried out in the **FK** domain and then apply the 2D Fourier inverse transform to transform the data back into the original time-distance,  $f(\mathbf{t}, \mathbf{x})$  domain. The technique was extended to cover variable velocity by (Gazdag 1978).

(viii) **Hybrid Migration Method**

The method is based on frequency-space finite difference migration. This method (called Omega-x migration) can handle both steep dips and lateral-velocity variation (Sheriff and Geldart 1995, p. 334).

**10.5.6 Time Versus Depth Migration**

Effectively, migration is an inversion process transforming seismic data from time domain (seismic time image) to depth domain (seismic depth image). The input to migration is the seismic record which can be non-zero offset (pre-stack, CMP-gathers) or zero-offset traces (stacked CMP-gathers). The amplitude in the input set of traces, can be considered as a two-dimensional function of distance ( $\mathbf{x}$ ) and time ( $\mathbf{t}$ ) as seen by receivers on the adopted datum plane, that is at zero-depth level ( $\mathbf{z} = 0$ ). After migration, the time image is transformed into the corresponding true image position and true geometrical shape. Migration can be considered as re-mapping of the seismic amplitude as function of distance ( $\mathbf{x}$ ) and depth ( $\mathbf{z}$ ). The migration output is the true geological depth-picture seen at the start time ( $\mathbf{t} = 0$ ). This is summarized as:



Whether it is pre-stack or post-stack-migration, output can be plotted as time section  $f(\mathbf{x},\mathbf{t})$  or depth section  $f(\mathbf{x},\mathbf{z})$ . It is matter of scaling

only, where the depth ( $\mathbf{z}$ ) is equal time ( $\mathbf{t}$ ) multiplied by the velocity scaling-factor ( $\mathbf{v}/2$ ), that is ( $\mathbf{z} = \mathbf{t}\mathbf{v}/2$ ). The crucial parameter in differentiating between time-migration and depth-migration is velocity. Time-migration assumes velocity to change only in vertical direction, whereas depth migration assumes velocity variation in both vertical and horizontal directions (Sheriff 2002, p. 84 and p. 359). These two cases are explained as follows.

(i) **Case-1 Velocity varies vertically only**

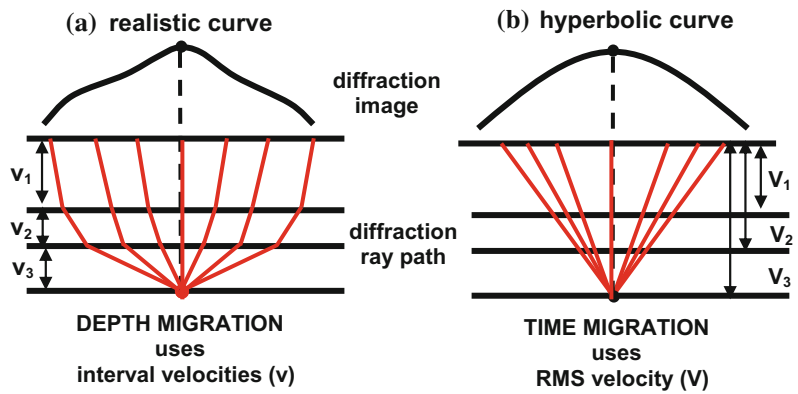
This is the case of a geological section made up of horizontal layers with interval velocities increasing with depth. Geometry of the true-diffraction ray-paths, in this case, shows that the diffraction curve is generated in accordance with Snell's law which governs refractions at interfaces. The resulting diffraction curve for the layered medium (Fig. 10.52a) is not that smooth hyperbolic curve produced by a constant-velocity (RMS velocity) medium (Fig. 10.52b). In both cases, the curve apex (the diffraction point) and the emergence point of the vertical diffraction ray, fall on the vertical line passing through the diffraction point.

Depth migration computes curve-shape exactly, taken into consideration the propagation ray as it refracts according to Snell's law, whether the reflection interfaces are horizontal or inclined. Time migration on the other hand, approximates the curve by an idealized hyperbolic curve by using a constant value for the velocity. The value normally-used is the RMS velocity derived (by Dix-formula) from the interval velocities of the horizontal layers.

Time migration uses RMS velocity which is not exact velocity, but approximation of the velocity field. In depth migration, which uses

realistic interval-velocity field, leads to more accurate positioning of the diffracting point and hence better image focusing.

**Fig. 10.52** Difference between depth- and time migration, case of vertical velocity variation. Depth migration uses individual interval velocities, whereas time migration uses RMS velocity for the whole section



(ii) **Case-2 Velocity varies vertically and horizontally**

By ray tracing method, it is possible to determine the position of the diffracting point accurately, if the diffracted ray is followed as it refracts at interfaces according to Snell’s law. It is observed that the apex of a diffraction curve is located on the diffraction ray that approaches the surface plane at right angles. This is considered as the basic concept upon which migration process is considered to be depth migration. Essentially, the process is depth migration when it observes horizontal changes in velocity (allowing for the ray bending at interfaces) even if interfaces are not horizontal (Sheriff and Geldart 1995, p. 333).

Referring to Fig. 10.53a, the apex of the diffraction curve coincides with the emergence point of the vertical diffraction ray. The apex point is shifted laterally with respect to the diffraction point (Fig. 10.53b). Depth migration positions diffraction point correctly whereas time migration is incomplete (diffused shape) and placed at wrong position, as it is shifted with respect to the true position of the diffraction point. Thus, depth migration results in accurate imaging and accurate positioning, whereas time migration results in wrong positioning and incomplete imaging (Fig. 10.53c).

The usual options decided upon in choosing of migration type are post-stack or pre-stack time (or depth) migration. The normal trend now is in the direction of using pre-stack time migration. Pre-stack depth migration proved superior in

terms of fault resolution and in enhancing of the S/N ratio (Lorentz and Bradley 2012).

**10.5.7 Migration Parameters**

Migration restoration efficiency is dependent on quality of the input seismic data, degree of complexity of the subsurface geology, the

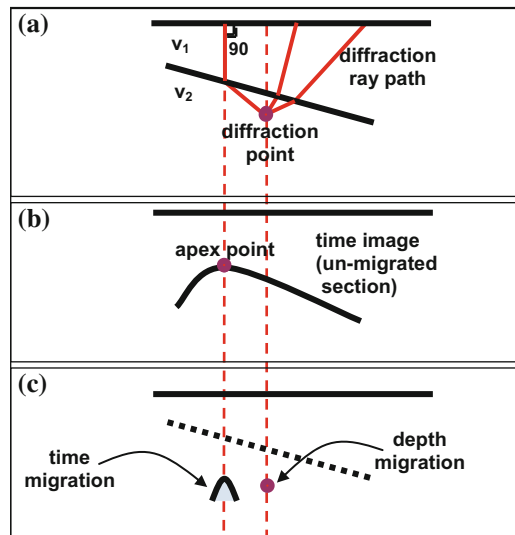


**Fig. 10.53** Difference between depth- and time migration, case of velocity variation in both horizontal and vertical directions. **a** Diffraction ray-path, **b** Diffraction curve (record surface) having shifted apex, **c** Migration output showing focused and properly placed diffraction point by depth migration compared with incomplete imaging by time migration

appropriate migration software, and the appropriate migration parameters which secure full migration efficiency in positioning of the reflection events and removing of the diffraction arrivals. The main migration parameters which the processing geophysicist must optimize are the following:

- Migration Aperture
- Reflector Dip
- Velocity-field
- Target Depth
- Trace Spacing
- Layer Thickness
- Data quality

#### (i) Migration Aperture

The migration aperture is defined to be the lateral displacement of a reflection event moved when a section is properly migrated. In Kirchhoff method it is expressed by the number of traces (included in the one hyperbola) taken in the summation process.

In case of dipping reflectors, the aperture width ( $\Delta x_m$ ) is given by:

$$\Delta x_m = (vT_s/2) \sin \theta_m$$

This formula shows that the aperture width ( $\Delta x_m$ ), is directly proportional to the three factors: velocity ( $v$ ), dip ( $\theta_m$ ), and reflection time ( $T_s$ ). This implies that the aperture is larger with deeper and steeper reflectors. Usually, the aperture is calculated such that it corresponds to the steepest dipping event that is required to be fully migrated.

For practical reasons, it is not always possible to use the full aperture width. There are cases in which an incomplete (i.e. truncated) aperture is used. Thus, for example, migration is incomplete near the edges of migrated seismic sections. This adverse edge-effect is inherent in migration implementations whether we have 2D- or 3D-data. Due to aperture truncation that occurs at the boundaries of sections, incomplete migration will result near section boundaries.

#### (ii) The Reflector Dip

Referring to the equations expressing the geometry of migrating dipping events, the position correction is expressed by the two parameters:

the up-dip shifting ( $\Delta x_m$ ) and the upward shifting ( $\Delta T_m$ ), where:

$$\Delta x_m = (vT_s/2) \sin \theta_m$$

and

$$\Delta T_m = T_s - T_s \cos \theta_m$$

These equations show that migration is shifting (by  $\Delta x_m$  and  $\Delta T_m$ ) of the reflection event to its correct position. The apparent dip (dip component in the direction of the seismic line) shall change to the higher value ( $\theta_m$ ) after migration.

#### (iii) The Velocity Field

As it is with dip, inaccurate velocity leads to incomplete migration process. Since the width of the migration aperture is function of velocity (and dip) it is expected that we get under, or over, migration depending on whether the inputted velocity-values are too low or too high respectively. Because of the direct relationship between the aperture and the velocity, incorrect velocity will lead to improper aperture. For optimum migration, the velocity field should be as close as possible to the real geological.

The effect on images of synclines and anticlines is that, too-slow velocity causes under-migration, leading to too-narrow syncline-images and leading to too-wide anticline images, whereas too-fast velocity causes over-migration, leading to too-wide synclines and too-narrow anticlines. In practice, however, the applied velocity-functions are smoothed and scaled before they are inputted in the migration process. In case of diffraction arrivals, too-slow velocity causes under migration, with which the diffraction hyperbola is only partially collapsed, and too-fast velocity causes over-migration where artifacts (called migration smiles) are created.

#### (iv) Target Depth

From the ray-path geometry of dipping reflector appearing in a stack section, it is evident that the migration time ( $T_m$ ), required to move a segment of a diffraction hyperbola to its apex, is function of the segment record-time ( $T_s$ ), velocity ( $v$ ), and its true dip ( $\theta_m$ ). The equation connecting these variables is ( $T_m = T_s \cos \theta_m$ ).

In diffraction stack migration, amplitude data, falling on the diffraction hyperbola are summed and placed at the apex. This means that data from deeper parts (deeper than the apex) of the section are required in order to have full migration. Thus, in order to shift (migrate) a reflection segment up dip to migration time ( $T_m$ ), there is need to have data from time ( $T_s = T_m + \text{extra time } \Delta T_m$ ). For example, for a segment dipping by 45-degrees, there is need to include data from a recording time equal to ( $T_m / \cos 45 = 1.41 T_m$ ). As a rule of thumb, we need to include an extra time of about 50 % of the targeted migration-time in order to have fully migrated section.

#### (v) Trace Spacing

For increase of resolution, and to avoid aliasing in the spatial sampling, the stack-trace spacing ( $\Delta x$ ) should be small compared with the shortest wavelength of the reflected event. The spacing ( $\Delta x$ ) is related to velocity ( $v$ ), dip ( $\theta$ ), and frequency ( $f$ ) as expressed in the equation:

$$\Delta x = v / (4f \sin \theta)$$

Guided by this formula, a remedy can be suggested for the possibility of occurrence of spatial aliasing. If it is not possible to use a small-enough trace spacing, then high frequencies (and/or the too-steep events), should be filtered out prior to migration processing. This is not a desirable remedy since this would limit structural resolution in both vertical and horizontal directions. Also, filtering out of steep events is not desirable as they may remove some of the target events themselves.

A more practical and commonly used procedure is the application of (trace interpolation) processing. Based on the dip field of the data set, the interpolation algorithm would work out interpolated traces from the given stack traces prior to migration. With this method a new trace is created between each two adjacent traces. The new trace is an average of the two adjacent traces concerned. The final result is a new seismic section of traces spaced at half the spacing of the input section. This new section is then inputted to migration. In case of steep dips and high

frequencies, trace-interpolation is strongly recommended; otherwise, dip and frequency-filtering must be applied.

#### (vi) Layer Thickness

The downward continuation technique followed in migration (as in the finite-difference method) is carried out by discrete depth intervals. Selection of the depth step (slab-thickness) depends on several factors such as velocity, dip, and data frequency-content.

Too-large thickness-interval (layer thickness) causes under-migration, kinks in reflector continuity, and noise dispersion. Under-migration, these distortions are increases with increasing dips. It is recommended, therefore, to use smaller thickness-intervals in the presence of steep dips. Layer thickness adopted in migration of a seismic stack section is normally taken in the range (20–30) ms (Sheriff and Geldart 1995, p. 333).

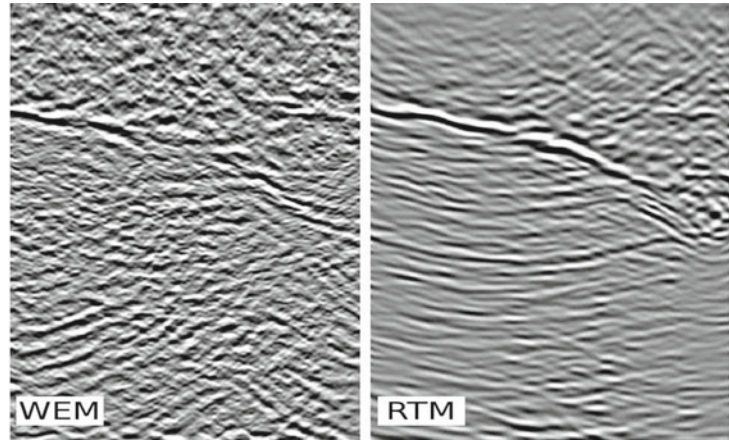
#### (vii) Data Quality

Enhancement of the signal-to-noise ratio (S/N), of the input data, and removal of abnormal non-reflection events, improve migration efficiency. In the presence of severe ambient noise, smearing effect develops on the migrated sections. In addition to that, spikes and bursts of amplitudes in the input stack section may spread out into non-collapsed remnant hyperbolic artifacts. These features, commonly known as “smiles”, can be avoided by removing all abnormal amplitude-bursts in the data prior to migration. Signal enhancement and noise suppression can significantly improve migration output and avoid abnormal features.

### 10.5.8 Migration Techniques in Future

The most up-to-date technique applied in seismic migration, publicized at present, is called the (Reverse-Time Migration, RTM) method. The concept, on which this method is based on, was introduced in the early 1980s. It involves very lengthy computations and that is why only nowadays, with the increased computer speed, that it started to be applied, though on very

**Fig. 10.54** Increase of resolution and S/N ratio of Reverse-Time Migration (RTM) compared with conventional wave-equation migration (WEM) (Araya et al. 2009)



limited scope of application. For comparison of the RTM migration with the conventional wave-equation migration, migrated sections are shown in Fig. 10.54.

The main features of the reverse time migration technique can be summarized by the following points:

- It is a pre-stack reverse-time, depth migration, based on wave equation solution.
- It is based on reverse-time, forward modeling, of wave field of the shot-gathers.
- It requires much more computational power and it is estimated that its cost is about 10-times that of the conventional wave-equation migration.
- It has no dip limitation and thus it is used in migration of data from areas having structural and velocity complexities, giving accurate positioning and signal clear focusing.

## 10.6 Application of Filtering and Equalization

A good practice is to provide the interpreter with two final migrated sections: one data-set with, and one without the application of the filtering and without equalization. Since interpretation software is usually equipped with filtering and equalization modules, the interpreter can use the option that suits his purpose best. This will give the interpreter the freedom for preparing the data for other specialized processing that suits specific

interpretation purposes. Examples of such processing are attributes and impedance inversion computations.

### 10.6.1 Frequency Filtering

In general, a seismic trace shows reflection wavelets of frequency spectra that vary with the depth of the reflector. The frequency tends to decrease as the reflection travel-time increases. It is therefore, expected that the signal-noise interaction varies with reflection time. This phenomenon is the basis for the application of a time-variant filtering (TVF). If the area is large and showing complex geology, there may be need for a distance-variant filtering as well. However, spatial variation of the filter is rarely applied.

Specification of the frequency band-pass filter is normally found through a special filter-test processing. With the aid of Fourier-spectrum analysis, the frequency changes with reflection-time can be investigated. Based on the spectrum analysis and the filter test, a time variant filtering system is designed and applied to the stacked and migrated data-set.

### 10.6.2 Equalization

In order to preserve reflection amplitude characters, the time-variant scaling is applied with relatively long gates (2–3 s). This is taken in

consideration when the data is prepared for stratigraphic interpretation. For structural interpretation, however, shorter gates may be used. As in the case of filtering, equalization parameters are normally determined by special processing tests.

There are few more optional steps which can be applied in addition to the basic steps done in the post-processing stage. Examples of these options are processes directed towards random-noise attenuation and enhancement of the continuity of the reflection horizons. Processing software, usually contain modules (under the names like coherency filtering and trace mixing) which can be used to attenuate random noise and improve continuity of reflection horizons. In normal practice these processes are applied with extra care as these bring about smearing effects and loss of identity characteristics of reflection events.

### 10.6.3 Data Storage and Display

The end result, which is migrated, filtered, and equalized stack section, is passed to the interpreter, stored on magnetic tapes, in standard recording format (usually in trace-sequential format) that is compatible with the technical specifications of the particular computer system used by the interpreter.

Together with the tapes, the interpreter is provided with paper displays of the delivered stack sections. The common scales of the displayed sections are 25 traces per cm. for the horizontal scale and 10 cm. per second, for the vertical scale. The section is also provided with top label and side label which contain statistical data pertinent to the particular seismic line. Usually the top label includes information on surface elevation, static correction and fold of coverage. The side label contains information on the field and the optimum parameters used in processing.

## 10.7 Parameter Optimization

The processing sequence, normally followed to process a set of seismic reflection data, consists of a sequence of procedures with special

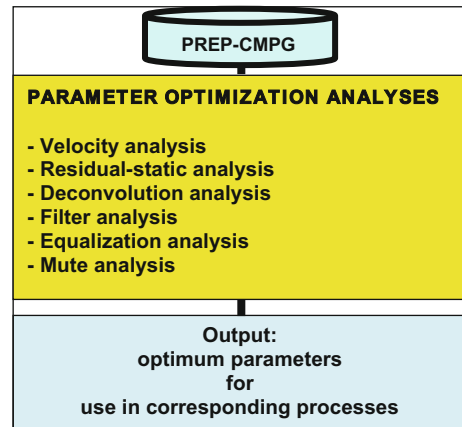


**Fig. 10.55** Main processing steps normally done in parameter optimization analyses

processing parameters. The efficiency of a certain process is mainly controlled by the parameter applied. Thus, for example, a frequency-filtering process depends on the band-width parameter adopted. Other parameters for the filtering process are, the operator-length, operator-truncation window, gate-length, TVF time-knees, and so on. The important thing here is that the applied parameters must be optimum, producing the best results in terms of reflection-signal clarity, and accuracy of the reflection-event geometry.

The techniques followed in the determination of processing parameters are based on the trial-and-error approach. A sample section made up of a series of traces is passed through a certain processing-step (filtering for example) repeated several times and at each time a different trial processing-parameter is used. By comparative study of the different outputs, the optimum parameter (which gives the best processing objective) is determined.

The main processing tests (parameter optimization analyses), normally performed, are shown in Fig. 10.55

### 10.7.1 Velocity Analysis

Velocity parameter is of prime importance in seismic processing. Its role is in enhancement of the reflection signal of the seismic stack data. An

optimum velocity value, used for the NMO correction, gives best stacking response in terms of signal-to-noise ratio. For this reason it is called stacking velocity. May be it is more appropriate to be called “NMO-correction velocity”, since its direct application is in the NMO correction which precedes the stacking process.

To derive the optimum stacking-velocity function (velocity as function of reflection time), a data-set made-up of a group of CMP traces is chosen at a location on the seismic line where the analysis is to be done. The chosen data-set (15–25) CMP gathers are taken from the Pre-processing CMP-sorted traces which are preconditioned data with static correction applied to them. The CMP-gather traces are NMO-corrected using several trial velocity functions and then CMP-stacked. Zero NMO-residuals and maximum stacking response are attained when the applied velocity is optimum.

The range of velocity values applied cover a range of a defined low velocity to a high velocity value, corresponding to the expected velocity range of the area. A typical velocity range at the shallow part of the record is (1–2) km/s, and at the deep part is (3–6) km/s. This process (called velocity analysis) is repeated at several locations (called control points) on the one seismic line.

Velocity analysis software-versions, usually output the results in form of mini-stacks arranged in the order of the applied velocity functions, together with a kind of contour map of “stack-amplitude” as function of velocity and record time. This type of display is normally referred to as (velocity-spectrum display). By visual inspection, the velocity spectrum is interpreted by marking (on the screen-displays) the optimum stacking velocity as function of record time. Usually, the CMP-gather (of the central CMP of the chosen CMP group), is displayed to show the extent of NMO residuals resulting from application of the different velocity-functions. Output of the velocity analysis includes; the velocity spectrum (normally, colour-coded power map), centre CMP-gather traces, and the mini-stacks corresponding to the applied trial stacking velocity functions. A typical display of the velocity analysis is given in Fig. 10.56.

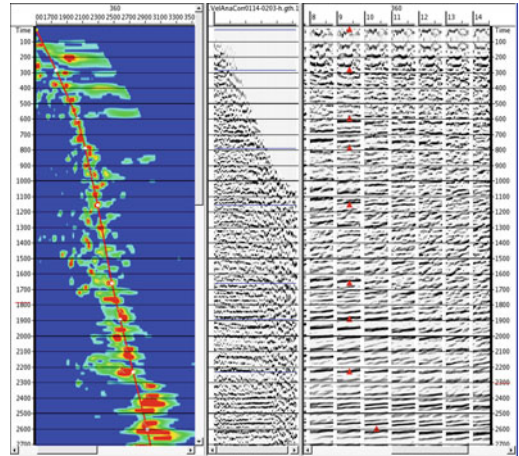


**Fig. 10.56** Typical velocity analysis output: Interpreted colour-coded power display (velocity “spectrum”), NMO-corrected gather traces of the central CMP, and a panel of mini-stacks corresponding to 7 trial velocity functions

Maximum wavelet power means that, with the applied stacking velocity, perfect NMO correction is achieved (zero-residual NMO correction) and that any other different velocity applied in the NMO correction would lower the amplitude of the stack wavelet. Often, processing geophysicists refer to the stacking velocity as RMS velocity, as it is nearest in value to the stacking velocity.

### 10.7.2 Residual-Static Analysis

Due to unpredicted variation of the velocity and thickness of the surface layer (the weathering zone or low-velocity layer, as it is sometimes called), small but significant errors are introduced in the computed field-static corrections. These errors are called (residual statics). Plotting the values of residual statics along the seismic line may show two components of variations; the slow and gradual variations, (the long-wave statics), and the fast and random variations (the short-wave statics). In the course of the residual statics analysis, another type of errors (called NMO residuals) may be identified. This type of errors is identified by its offset-dependent variations. It is created as a result of application of inaccurate NMO-corrections.

From inspection of the available stack section, one can observe the need for the correction. Presence of residual statics is expressed as unaligned and poor-continuity reflection events.

Computation of the short-wave residual statics is based on use of statistical principles. The corrections are assumed to be time-invariant and surface-consistent. The surface-consistency concept (one correction value for all traces occupying one surface-location) is honored in the computation process. The input to this process is the CMP gathers provided by the last step (the CMP-sorting step) in the pre-processing stage. The input gather traces should possess header values for the numbers and location-coordinates of the input shots and receiver points).

Referring to Fig. 10.57, the applied computation processes can be summarized by the following steps:

- (i) The CMP-gather traces, for each CMP, are corrected for the field-statics and for the

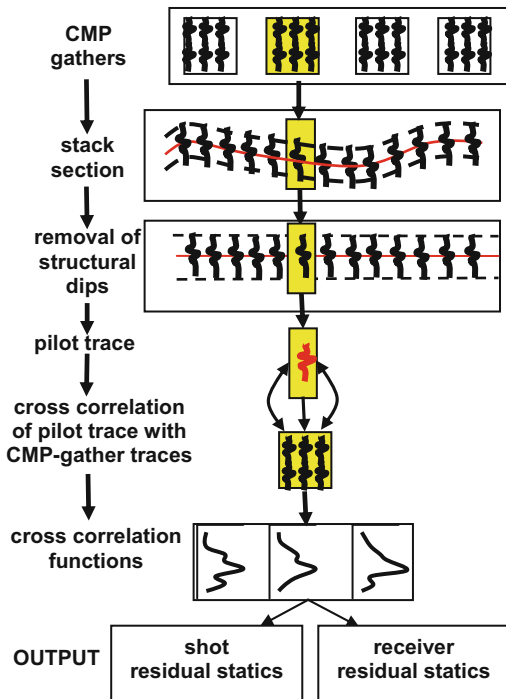


**Fig. 10.57** Principle of residual statics analysis. Computation is based on cross-correlation of the pilot trace with each of the input CMP-traces

NMO then a preliminary stack section is produced.

- (ii) The time difference due to dip is eliminated defining gates enclosing the reflection event. With this process (removing of dip effect and correcting for datum statics and NMO), the reflection time differences remaining on events in the selected gates are due to residual statics which are computed by the following statistical technique.
- (iii) A model trace (also called the pilot trace), from the traces of each CMP-gather traces, is computed. The model trace is computed by stacking (summing) all traces in the gather except the one to be corrected. It is important to note here that the CMP traces have no common-shot, and no common-receiver locations. This situation supports the statistically-random nature of the existing residual statics. The pilot trace is considered to have error-free static correction, since the sum of the random residuals is approaching zero-value.
- (iv) The residual-static value for each trace of the CMP-gather, contributing to the pilot trace, is then found by cross-correlating the gate-part of the trace with the pilot trace. Measurement of the correlation lag-time of the peak of the cross-correlation function, gives the residual-static value for that trace. This process is repeated with all of the CMP-gathers of the seismic line under analysis.
- (v) The last step in the residual statics computations is determination of the residual statics for the source and receiver points separately. This is achieved by working out the arithmetic mean of the residuals for the common-source, and for the common-receiver respectively.

The cross-correlation functions are normally displayed for inspection and editing when required.

Adjustment of the field statics is then made by adding algebraically the residual value to the field static value of the particular trace. As a common practice, several iterations (normally 2–

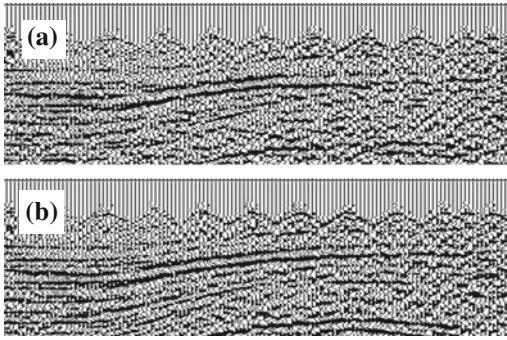


**Fig. 10.58** Seismic stack section, subjected to residual static correction. **a** Stack section before residual static correction, **b** same section with residual static correction applied

3 times) of residual analyses are applied to get more refined and accurate residuals. The first residual analysis is applied, followed by velocity re-analysis, then a second residual analysis is carried out and the new values are applied, followed by a second velocity analysis. After the twice or three-times iterations of the analysis-duet (residual static analysis and velocity analysis), a final and more accurate total statics and optimum stacking-velocity functions are determined. From each iteration, a residual static file of the final residual statics, is stored in the system data-base ready for application when requested. On application, residual statics usually give marked improvement in both continuity and strength of the reflection events. An actual case of residual static application is shown in Fig. 10.58.

Here, in Fig. 10.58, marked improvement in continuity and strength of the reflection horizons is clearly seen.

### 10.7.3 Deconvolution Analysis

The deconvolution process depends on a number of interrelated parameters which are normally determined by special test processing (deconvolution analysis). The main deconvolution parameters, which need to be determined in these analyses, are: type of deconvolution, gate-length, number of gates per trace, operator length, and

operator gap. Gate length and number of gates per trace depend on the variation of the reflection wavelet-characteristics in the trace. Normally 2 or 3 gates, each of which is of length of (2–3) s are applied. Operator length is, as a rule of thumb, taken to be about 10 % of the gate length. Operator gap of the applied predictive deconvolution should be slightly larger than the reverberation period.

For whitening deconvolution, a small gap of about (8–16) ms is normally applied. Pre-whitening noise of about 0.5 % of the zero-lag value of the autocorrelation function is added to help in securing computation stability.

The procedure, followed in determination of the deconvolution parameters, is based on the trial-and error approach, normally followed in parameter optimization processing. For pre-stack deconvolution, the data-set consists of CMP gather traces for the assigned data set. From inspection of the brute-stack, the objective of the deconvolution, and hence the deconvolution adequate type are decided. The most important parameters to be tested are directed towards determination of the gate-length and the operator length. Since the operator length is defined to be about 10 % of the gate length, determination of the optimum gate-length is sufficient to do in this test. The same data-set is deconvolved using different gate-lengths and the produced panel of stack sections of the deconvolved CMP traces, are compared for the degree of wavelet whitening and reverberation removal. As an aid for evaluation of the parameter performances, the autocorrelation functions of the deconvolved traces are computed and displayed for study. Ideally, the optimum parameter will produce a sharp autocorrelation function with near zero-level side-lobes.

### 10.7.4 Filter Analysis

Filter tests (or filter analysis processing) is a series of processing tests aiming at determination of the optimum time-variant filter which gives the best possible signal-to-noise ratio of reflection events. Filter test is carried out by passing a defined part

of a seismic Section (50–100 traces, say) through a series of trial band-pass filters. This is commonly conducted in two stages. First, the chosen section is passed through band widths in which the high-cut frequency is kept fixed while the low-cut frequency is varied. For example, the trial bands are (6–45, 8–45, 10–45, 12–45, 14–45) Hz. The outputted sections are then interpreted and the optimum filter is determined. In the second stage, this process is repeated with the trial bandwidths have their low-cut frequency is fixed at the value determined in the first stage and the high-cut frequency is varied. Supposing that the optimum bandwidth determined from the first stage is (12–45) Hz, the trial filters for the second stage will be something like (12–25, 12–30, 12–35, 12–40, 12–45, 12–50) Hz.

In both of these two stages, choosing the optimum filter is based on certain criteria examined for the reflection wavelet and reflection horizon appearing in the chosen section. These are mainly the reflection energy (wavelet amplitude), continuity, resolution, and noise level. As a guiding tool that can be used in giving more quantitative assessment of frequencies, is by computing Fourier amplitude spectra. In aiding of the filter-test interpretation, it is useful to remember that the natural trend of frequency changes is the decrease of frequency content as depth increases.

### 10.7.5 Equalization Analysis

Equalization analysis aims at determination of the optimum equalization-parameters which are mainly: the type of scaling function, time-gate

length, and gate time-shifting along the trace. In practice, no intensive effort is spent on finding optimum equalization parameters. The type of scaling and time-variance scheme, are fairly known, if the purpose of the processing is planned for structural or for stratigraphic type of interpretation. As a general rule, the equalization should not be so severe that amplitude characters are removed. Moderate scaling effect is preferred to give a balanced section and at the same time keeping the amplitude-characters for the individual reflection events are preserved.

### 10.7.6 Mute Analysis

Out of the three types of muting (on-mute, off-mute, and surgical mute), the on-mute is the most usually applied mute. The other two types are rarely applied. The on-mute is applied to cut-out the first arrivals and the early refractions which are highly affected by the NMO correction. This is necessary as these events are stretched by NMO to an extent that they can, on stacking, obscure the shallow reflection events if any.

Two main parameters concern the muting ramp function. These are the ramp start-time (onset-time) and the ramp length. By the same usual trial-and-error method, A data-set (NMO-corrected CMP-gather traces) of part of the seismic line, is subjected to ramp functions of different onset times. A panel output (stack sections) is produced for the applied different ramp-lengths. From comparative study of these stack sections, the optimum mute parameters (mute onset time and ramp length) are determined.

The principal techniques used in seismic exploration are based on reflection or refraction of P-waves generated artificially from seismic energy sources. These techniques are mainly directed towards exploring petroleum deposits at depths reaching thousands of meters below surface. The same types of waves, with certain modifications, are also applicable in exploring shallower geological and archaeological features.

In support to the usual seismic tools (reflection and refraction P-waves), there are other less commonly applied techniques used in the seismic exploration. These techniques are all depending on generating, recording and processing of seismic waves. The groups of methods (called here extra or specialized exploration tools) are basically seismic exploration tools, but differ in the source function of generated waves and in the source–receiver layout geometry. These supporting exploration tools, referred to here as (extra exploration tools) shall be briefly presented in this chapter.

---

## 11.1 Seismic Exploration with S-waves

An S-wave moving in an arbitrary direction, the particle motion can be resolved into horizontal and vertical components, called the SV and SH waves. In certain cases, when the particle motion of an S-wave is confined to one plane, it is known as plane-polarized wave, as SV- or SH-wave.

Like P-wave, the S-wave gets reflected and refracted at interfaces, and hence can also be used as an exploration tool. Unlike SV-waves, SH-waves incident on interfaces do not cause wave conversion. For this reason, SH-waves are more commonly used in S-wave exploration than SV-wave. Both of the energy source and detectors are designed in such a way as to generate and detect the SH-components.

The limitation in the use of S-wave is that it does not propagate through liquid media.

### 11.1.1 Shear-Waves Generation

To generate an S-wave, we need an energy source that can create horizontal vibration creating a seismic wave that penetrates the earth in nearly vertical direction. The energy-source is so designed that it will generate stronger SH-waves than SV-waves. The SV-wave may generate P-wave when hitting an interface at an oblique incidence, whereas SH does not. For this reason SH-wave is more commonly used in S-wave surveying.

There are several types of S-wave energy sources, all of which have the common feature which is creating horizontal particle-vibration for the nearly vertically advancing S-wave. In the field of engineering geophysics, a hammer is blowing horizontally a metal plate which is vertically planted in the earth. For larger energy-penetration, horizontal vibration systems have

been especially designed to create SV or SH waves. For SH waves the vibration direction of the source-plate is made to create vibrations confined to the horizontal plane and perpendicular to propagation direction.

The coupling mechanism is secured by special metal plates provided with spikes driven into the earth during vibration. Signal enhancement can be effected by vertical stacking of repeated source-activations.

### 11.1.2 Role of the Shear-Wave Velocity in Interpretation

Shear waves, can serve as an effective exploration tool when both S-waves and P-wave surveying data ( $V_S/V_P$  ratio) is available for the same area. S-waves amplitude is considered as an effective indicator for studying fracture developments, in particular. For example, abnormally-low amplitudes indicate presence of rock-fracturing, and so on.

Shear-wave velocity ( $V_S$ ) is related to the shear modulus ( $\mu$ ) by  $V_S = (\mu/\rho)^{1/2}$ . From the elastic moduli inter-relationships it can be shown that the ratio of S-wave velocity ( $V_S$ ) to the P-wave velocity ( $V_P$ ) is given by:

$$V_S/V_P = [(1 - 2\sigma)/(2 - 2\sigma)]^{1/2}$$

This relation shows that ( $V_S/V_P$ ) ratio is function of Poisson's ratio ( $\sigma$ ) only. Thus, it is possible to calculate Poisson's ratio ( $\sigma$ ), from the relationship:

$$\sigma = (1 - 2R^2)/(2 - 2R^2),$$

where ( $R = V_S/V_P$ )

This is an important relationship, since it is possible to relate the velocity ratio ( $V_S/V_P$ ) to the elastic constants of the medium, which means that it furnishes an effective tool for stratigraphic exploration.

A survey, in which both P-waves and S-waves are generated and recorded, will provide information to give indications as to stratigraphic

changes as porosity, fracturing developments, sedimentary facies, and fluid contents. All of these geological features can produce changes in the elastic constants of the medium. Stratigraphic interpretation of the measured P- and S-wave velocities, may be done by plotting the calculated Poisson's ratio ( $\sigma$ ) against the ( $V_S/V_P$ ) ratio, and investigate abnormal behavior (if existing) of the resulting curve.

In comparison with P-waves, S-waves tend to be of narrow-band and low-frequency spectrum. Further, we have S-wave reflection events are of different timing due to differences in velocity of the two waves. Another feature an interpreter needs to be aware of, is that static correction (applied in S-waves processing) is liable to change with time of surveying, due to unpredicted movement of the near-surface water table.

## 11.2 Vertical Seismic Profiling (VSP)

Like well velocity surveying, Vertical Seismic Profiling (VSP) is done by lowering a detector into a bore-hole, and taking readings at much closer point-locations (typically at 25 m spacing). This technique was introduced into seismic exploration during the 1970s (Galperin 1973; Wuenschel 1976; Hardage 1983). The main differences between VSP and well-velocity shooting, is in the detector spacing and in recoding duration-time. Conventional well-velocity survey is concerned with measuring the travel-time of the source-to-detector direct wave. In the case of VSP shooting, recording time is extended to time which is long enough to be able to record arrivals of wave energy reflected from deep interfaces.

### 11.2.1 Field Set-up and Types of VSP

Basically the field set-up is the same as the check-shot recording system. A seismic energy is generated at a surface point which is detected by a detection system placed at different depths down a bore-hole. There are two types of VSP field set-ups; these are the (zero-offset VSP), where a single source is placed at a short distance

from the well-head, and the (offset-VSP) where the source is placed at long distance (of about one-to-two kilometers) from the well-head. The zero-offset VSP, which is the more commonly applied type, can help in identifying and removing multiple reflections, whereas the offset-VSP can help in obtaining information about structural and stratigraphic features existing in the areas around the well-location. Such information can be used in studying faults, facies changes, and fracturing systems.

### 11.2.2 The VSP Field Operation

VSP energy sources (like weight dropping or vibrator) are the same as those employed in normal seismic reflection surveying. The more common source is the air-gun submerged in a water or mud-filled pit. The recording process is repeated at regular depth intervals. At each detector stop-location (normally at 25 m spacing), a recording is made and a seismic trace is produced. The source location can be close to the well head (zero-offset VSP) or at long offset, (long-offset VSP). At each depth-stop the source function is repeated several times and vertically stacked to enhance the reflection signal and attenuate random noise.

A geophone-detection system, with specially designed clamping devices, is lowered down the well to a defined depth and a recording is made.

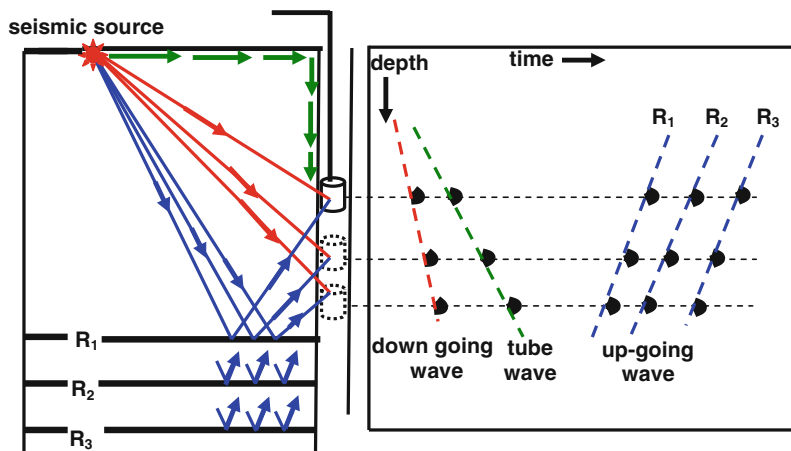
Recording is usually started with the detector placed at the bottom of the well, and repeated at each stop-location upwards. To cut on noise level, vertical stacking of several records made for each recording-stop. For verification of the constancy of the source waveform, a monitor detector is located near the source for recording the source wavelet. An important type of coherent noise occurring in VSP recording is the tube-waves. These waves are much reduced by the more efficient detector coupling and can be completely removed in the processing stage. The survey can be done in cased (and in uncased) wells, with the detector, well-coupled to the well-wall.

### 11.2.3 The VSP Seismic Record

In addition to recording of the first arrivals, which is the main concern in well velocity surveying, VSP recording is extended to allow recording reflected waves as well as the directly arriving waves. The recorded seismic traces contain the first arrivals (direct down-going wave), primary reflection arrivals (up-going waves), and multiple reflections and various types of seismic noises (Fig. 11.1).

Use of VSP data is equivalent to that obtained from both of the check-shot (well velocity-survey) data and the continuous sonic-logging data. From travel-time of the first arrivals (direct wave arrivals), velocity functions are derived,

**Fig. 11.1** VSP ray-path of direct (down-going) and reflection (up-going) waves, and their corresponding arrivals record



and from the (up-going wave arrivals), VSP section (matching normal seismic section) is obtained. The VSP section can be obtained for deep reflectors which include those reflectors which are deeper than those reached by drilling.

At each detector stop-location, a recording is obtained of a seismic trace which, in general, contains seismic-wave arrivals of direct waves (down-going wave), tube-waves, primary reflected waves (up-going wave), and multiple-reflection waves. Sketch of the ray-paths and corresponding seismic traces are shown in Fig. 11.2.

A typical real-data, VSP record is shown in Fig. 11.3.

### 11.2.4 The VSP Data Processing

Processing of VSP raw-data includes the following basic steps:

- Data editing
- Vertical stacking of common stop-location
- Removing of the coherent noise (tube-waves)
- Estimation and subtracting of down-going waves

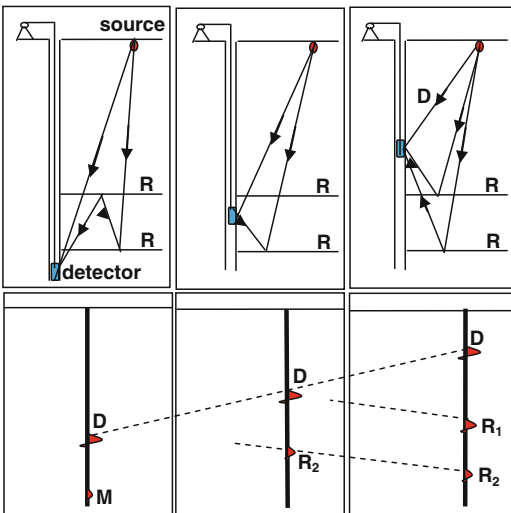


**Fig. 11.2** Sketch showing VSP ray-paths and corresponding seismic traces of down-going and up-going waves and corresponding records for two-reflector model. D-direct, R-primary, M-multiple

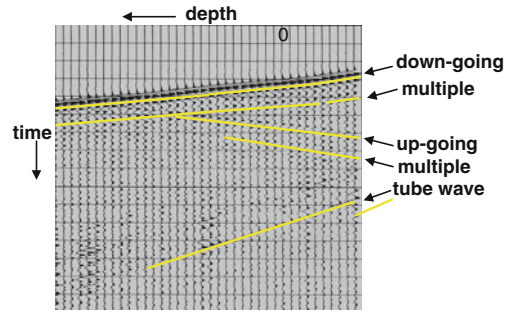


**Fig. 11.3** VSP record showing down-going and up-going waves and their multiples. Tube waves appear in the lower half of the record

- Removing of multiples of down- and up-going waves by predictive deconvolution
- Filtering of random noise

The key step in processing of VSP data is to align horizontally the wave-arrivals of an event (down-going or up-going waves) by trace-shifting process. By applying an upward shift (time-shift which is equal to the first-arrival times), the down-going waves are separated. Similarly, by applying an upward shift to the up-going waves, they (the up-going waves) are separated.

By arranging the so-processed seismic traces in depth-wise sequence, a seismic VSP-section is obtained. Each seismic trace of a VSP section contains two main sets of wave arrivals; down-going waves (direct and multiples arrival) and up-going waves (reflections and multiples). Consequently, the VSP section will show the two corresponding sets of seismic events having opposite dip-directions (Fig. 11.4).

Separation of events, are done by imposing time shifts to the traces equal to the arrival times of the first arrivals. The direct waves and their multiples (if they are present) increase in arrival-times with depth, while the primary reflections and their multiples, decrease in arrival-times with depth (Fig. 11.4a). The first step in the separation process is upward time-shifting of the traces by the respective first-arrival times of the down-going events. This process would result in horizontal alignment of the down-going arrivals and their multiples (Fig. 11.4b). Also, the up-going wave events become more steeply dipping. In (Fig. 11.4c), the

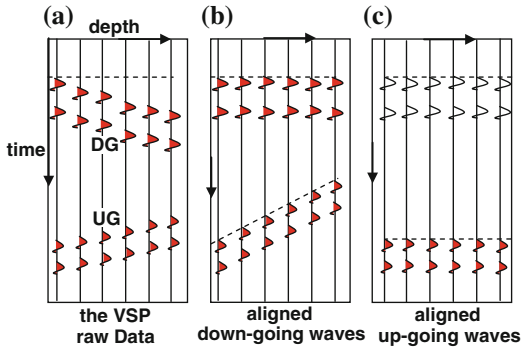


**Fig. 11.4** Sketch showing VSP record, **a** raw-data showing the two sets of events (down-going and up-going waves and their multiples), **b** the down-going arrivals are aligned after the traces being up-shifted, and **c** record with the down-going waves subtracted leaving the up-going arrivals aligned after traces were down-shifted

same shifts have been applied to the original traces, but in opposite direction, bringing about horizontal alignment to the up-going events. With this process, primary reflection events are placed at time equal to that shown by a normal seismic reflection section passing through that VSP-surveyed well. Multiples are removed by applying predictive deconvolution.

The main application of the VSP record is in calibration of seismic stack sections, in the same way as it is done with application of synthetic seismograms. Since the reflection wavelets are preserved, VSP-data provide useful information on acoustic impedances and other petrophysical properties of geological formations not reached by the drill hole. These are the advantages of the near-vertical (or short-offset) VSP recording. For the long-offset VSP, there are other additional advantages like furnishing lateral subsurface coverage, and the development of converted shear waves which give shear wave information.

### 11.3 Seismic Tomography

The term tomography has a Greek origin meaning cross section drawing. In general, tomography denotes determination of a certain physical property of an object from measurements made

on rays passing through that object. The X-ray tomography is a technique applied in medical examination and in certain other fields of application. The computer assisted tomography (termed CAT-scan) technique uses X-rays that have penetrated a body along many ray-paths in many directions. In medical examination, tomography is used to explain the loss in intensity of the X-rays because of the absorptive properties of different parts of the body (Sheriff and Geldart 1995, p. 492).

Seismic tomography is a type of inverse modeling (inversion process) carried out for the purpose of determining a subsurface geological model based on travel-time measurements. Usually the changes found in the measured travel times are interpreted in terms of velocity changes. Other geophysical parameters, such as the attenuation factor, may be investigated by amplitude modeling.

#### 11.3.1 The Forward and Inverse Modeling Concepts

A common geophysical phenomenon is that a geological anomaly produces a corresponding anomaly in one of the natural geophysical fields. An anomalous high-density body, for example, creates a corresponding high-gravity anomaly in the Earth gravity field. The change produced by a geological anomaly to the geophysical field, may be referred to as the (geophysical response) of the causing geological feature.

Modeling processes are usually divided into two types. These are the (direct modeling) and the (inverse modeling). The direct modeling, also called forward modeling, is based on assuming the geological anomaly (model shape and physical properties), and followed by computing its geophysical response. The inverse modeling, on the other hand is computing a model that can give a geophysical response which is closest to that observed. The two types of modeling process are explained in Fig. 11.5.

Geophysical exploration is invariably based on measuring geophysical fields (natural as gravity

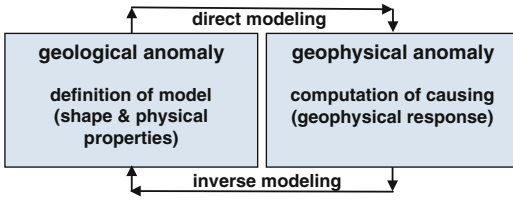


**Fig. 11.5** Definition of the direct and inverse modeling processes

field or artificial as seismic wave-field) and interpreting the observed values. Thus the interpretation process is normally based on the inverse modeling process. The usual seismic data interpretation is a typical example of inverse modeling. Direct modeling is applied more often in interpretation of gravity and magnetic data where models are assumed and their anomalies are calculated and compared with those observed. The differences are minimized by altering the model specifications and re-computing the corresponding geophysical response. With several iterations of this process, the final accepted model is then determined.

**11.3.2 Types of Seismic Tomography**

There are two types of seismic tomography; reflection tomography which deals with reflection travel-time measurements, and transmission tomography which deals with source-to-receiver ray-paths along which the seismic rays are transmitted with no reflection occurring in the travel-paths (Sheriff 2002, p. 361). The more commonly applied technique is the transmission, borehole-to-borehole (also called cross-hole) method. In this method, a set of source points are distributed down a borehole and a set of receivers located in a second borehole, as shown in Fig. 11.6.

Another form of the seismic tomography is the surface-to-borehole technique. In this method the source points are located on the surface and the receiver points are distributed down the borehole, as shown in Fig. 11.7.

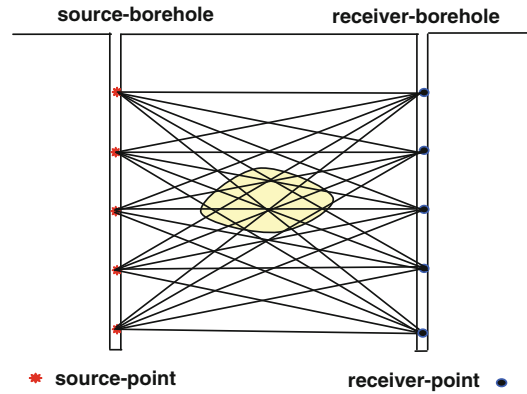


**Fig. 11.6** Seismic tomography, by borehole-to-borehole transmission. All involved wave ray-paths, traversing an anomalous body, are shown

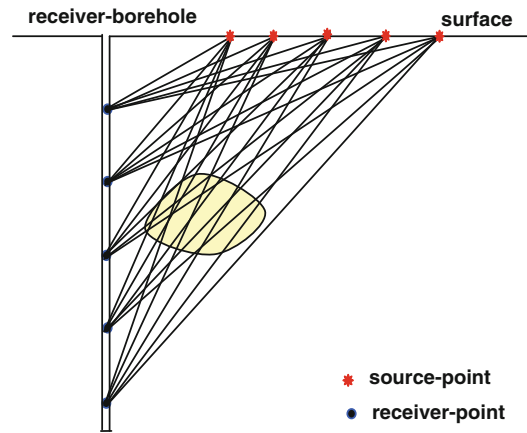


**Fig. 11.7** Seismic tomography, by surface-to-borehole transmission. All the involved ray-paths traversing an anomalous body are shown

**11.3.3 Interpretation of Tomography Data**

Tomography data interpretation is carried out by iterative, forward modeling process. The interpretation process is started by computing the travel times assuming a velocity model for the medium between the two boreholes. By comparing the computed travel-times for the model with those actually measured, the model is re-adjusted and the comparison is repeated. An iteration approach is followed in this process in

which the process is repeated several times until observed and computed travel-times become closest to the measured travel-times. At this point the produced velocity distribution is considered to be the realistic velocity-distribution in the studied area. Computations involved in tomography interpretation are usually carried out with specially-designed tomography-algorithm.

Detailed reviews of the seismic tomography technique are presented in some geophysical literature as in Gadallah and Fisher (2009) and Sheriff and Geldart (1995).

### 11.4 4D (Time-Lapse) Surveying

The term 4D surveying denotes a 3D survey repeated over the same area at specified time-interval. For this reason it is also called time-lapse surveying. The produced data volume is a three dimensional function of seismic amplitude value, expressed as function of (x, y, and z). The 4D survey gives repeated 3D data volumes at a sequence of time-intervals. The concept can be envisaged pictorially as presented in Fig. 11.8.

Time-lapse measurements refer to geophysical measurements repeated after a certain time interval (time-lapse) in order to study changes in certain rock properties which may have occurred during that interval. A typical time-lapse operation is repeating 3D seismic surveying over an oil-field to monitor changes which may take place in some of reservoir parameters. All of these changes in reservoir parameters, or some of them, may take place as a result of accumulating production or due to fluid injections.

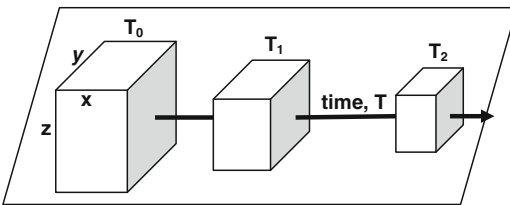


**Fig. 11.8** Sketch-representation of the 4D concept. The 3D survey at time  $T_0$  is repeated at later times,  $T_1$  and  $T_2$

In order to accurately measure the changes, data acquisition and data processing are kept the same in all of the executed surveys. Geophones are usually cemented at the bottom of shallow boreholes, in order to fix the receiver coupling for the repeated surveys. Seismic sections from the first survey (base survey), can be subtracted from those made at later times, to give (difference-sections) to clearly display the changes (Sheriff and Geldart 1995, p. 499).

The more commonly studied features of a reservoir by means of time-lapse surveying are behavior of the gas cap, gas-water contacts, and oil-water contacts. These investigations are based on interpreting the changes observed on the reflection-wavelet shape and on reflection events geometry. Interpretation of the time-lapse data can also give useful information on reservoir parameters, such as pressure of pore-fluid, type of pore-fluid, and temperature changes.

### 11.5 Multi-component (3C and 4C) Recording

In normal seismic reflection surveys, the P-wave is recorded by geophones designed to record only the vertical component of the arriving seismic wave. In fact, the arriving seismic wave includes other components of particle vibrations. The arriving wave, at a certain point, on the surface (or on the sea-floor), can be fully measured by recording its three mutually perpendicular components. This can be accomplished by using three orthogonal detectors, where each detector is designed to measure one component, hence the name three component (3C) method. The set of the orthogonal 3C system is often placed at the observation point in such a way that it will measure the three components, the vertical, the East-West, and the North-South components (Keary et al. 2002, p. 76).

The main advantage of the 3C technique is that it can detect S-waves as well as P-wave, separately at the same time. Since, with P-wave inclined incidence, wave-conversion occurs, it is

always expected that an S-wave is arriving at detectors as well as the reflected P-wave. In the processing stage the recorded waves are separately processed. Studies of fracturing and porosity are typical applications of the 3C surveying method.

Another closely related detection system, called (4C) recording system, in which another detector which is a hydrophone-type, is added to the 3C system. The 4C recording seismometer is used in marine environment using ocean bottom seismometers consisting of three orthogonal geophones and a hydrophone (Sherrif 2002, p. 147).

---

## 11.6 Passive Seismic Surveying

Seismic exploration techniques which involve measurements of the Earth seismic field without using artificially created energy sources are termed (passive seismic techniques). Typical example of application of this technique is measuring microseisms and the natural seismic noises. Passive seismic is sometimes called (low-frequency seismology) because it is based on detection of low-frequency seismic waves. Usually the survey is done using 3C detection systems which are setup to record data over long listening times (several hours to several days).

In petroleum seismic exploration, passive seismic is applied in studying fluid behavior in oil-reservoirs. Fluid movements due to injection or due to production may cause changes in the micro-seismicity pattern. Recently, sophisticated detection-systems have been applied in the field data acquisition. The detection system is usually coupled to the earth firmly and made to record the micro-seismic events for long recording-time (several hours per one reading).

---

## 11.7 Tau-P Transform

The Tau-P Transform is a processing tool, which helps in filtering coherent events that are interfering with the reflection signals. Concept and

way of application of this tool is briefly presented, as follows:

A record of a shot-gather (or CMP-gather) is considered as 2D function,  $f(\mathbf{x}, t)$ , which expresses the variation of seismic amplitude in the  $\mathbf{x}$ - $t$  domain. The main events observed in an  $\mathbf{x}$ - $t$  record can be surface waves or body waves which, in general, include direct, refracted, reflected, and diffracted waves. Some of these events appear as linear arrivals (as surface waves, direct, and refracted waves) and other events (as reflections and diffractions) take the form of hyperbolic curves.

Seismic data (shot gather, or CMP gather) can be transformed into another domain without loss of information. By Fourier transform, it is possible to transform the  $f(\mathbf{x}, t)$  into the corresponding spectrum-domain (the FK domain) in which the seismic amplitude is expressed as function of frequency and wave-number. Another transform, Radon transform (also called slant stack), re-maps the  $f(\mathbf{x}, t)$  function of the seismic amplitude from the  $(\mathbf{x}$ - $t)$  domain into the  $(\boldsymbol{\tau}$ - $\mathbf{p})$  domain, where  $(\boldsymbol{\tau})$  is intercept time of the event at  $(\mathbf{x} = \mathbf{0})$ , and  $(\mathbf{p})$  is the apparent dip of the event  $(d\mathbf{t}/d\mathbf{x})$ , measured as the slope of the event in its  $(\mathbf{x}$ - $t)$  domain. This measured dip represents the reciprocal of the apparent velocity (termed, slowness). On the  $(\boldsymbol{\tau}$ - $\mathbf{p})$  domain, linear events in the  $(\mathbf{x}$ - $t)$  domain, transform into points, and the hyperbolic events into ellipses (Sheriff 2002, p. 348).

A slant stack is obtained by applying a linear move-out (LMO) process followed by summing the amplitudes over the offset axis. This process is accomplished by applying a time shift, to each trace, proportional to its distance from a defined reference point, then stacking the so-shifted traces. Radon transform is sometimes called (slant stack) for the similarity of the end results in these two processes.

One important application is removing coherent noise and refractions. Such events can be zeroed in the  $(\boldsymbol{\tau}$ - $\mathbf{p})$  domain, then, by inverse  $\boldsymbol{\tau}$ - $\mathbf{p}$  transformation, the noise-free record can be recovered. Special algorithms can be used in  $(\boldsymbol{\tau}$ - $\mathbf{p})$  transform implementation.

## 11.8 Amplitude Variation with Offset (AVO)

The term AVO (Amplitude variation with offset), or AVA (Amplitude variation with angle of incidence) is used to express variation of reflection amplitude as function of offset (or function of angle of incidence). The amplitude variation with offset (AVO) is found to be dependent on Poisson's ratio as well as on impedance contrast across the reflection interface. AVO has the same information contained in a combined P- and S-waves data.

Reflection coefficient variation with angle of incidence is (as expressed by Zoeppritz equations) showing irregular variation with increasing angle of incidence (or with increasing offset). Depending on the geological environment (distribution of the acoustic impedance on both sides of the interface) the reflection coefficient can vary from large-negative to large-positive values. This behavior can therefore be used as an indicator to predict lithological changes or type of fluid deposits.

For AVO analysis, the reflection amplitude (measured from shot records) must be true amplitude, unmodified by application of processing steps of types which indorse amplitude changes such as severe filtering or equalization. Since AVO analyses are made on gather traces (non-stacked traces) noise effect is large and, therefore, certain data-preconditioning processing is needed to remove the incurred distortions. The types of processing that must be avoided in order to secure amplitude preservation is excluding of all processing types which bring about mixing, averaging, time-variant scaling and severe filtering. Amplitude variation due to varying conditions near the source- and receiver-points must be corrected for.

AVO is considered to be one of the effective tools used in direct hydrocarbon detection exploration. It can be used to explore reservoir and subsurface geological conditions, since it can give indications on lithological changes, reservoir

conditions, and presence of high-pressure gas zones. Another significant application of the concept is determination of boundary outlines and areal extensions of hydrocarbon reservoirs. Improved accuracy in interpretation is achieved when supported with additional geological and geophysical information.

Detailed coverage of AVO is found in Sheriff and Geldart (1995, pp. 78–81), and in Gadalla and Fisher (2009, pp. 183–195).

---

## 11.9 Seismic Attributes

In the field of the seismic stratigraphy, the term (Seismic Attribute) is used for calling one of the parameters of the seismic reflection wavelet. The attribute in this sense is a measured or computed value of a seismic parameter of a (or, related to) the reflection wavelet. Typical seismic attributes are wavelet amplitude, frequency, and phase. Many other attributes have been developed since early 1980s, when the basic attributes were put to application as stratigraphic exploration tools. More than 50 attributes have been devised so far, as quoted in the geophysical literature.

Being dependant on the wavelet parameters, seismic attributes carry useful information on certain physical properties of the medium traverse by the reflection wavelet. An attribute can help in clearer identification of stratigraphic features, patterns, and oil-reservoir characteristics. The seismic attribute is more sensitive to one of the wavelet parameters than the qualitative examination of the wavelet overall changes. Because of this property (direct link with the wavelet parameters), seismic attributes lend themselves as active indicators for stratigraphic changes and to direct hydrocarbon detection.

A normal seismic trace is considered as a time function of the parameter (amplitude). After being converted into the attribute-domain, we get an attribute trace which is a function of the attribute value that varies with the reflection time. By converting all of the seismic traces of a stack

section, a seismic attribute-section (or attribute volume, in case of 3D data) is obtained.

Any of the wavelet attributes can be plotted as a function of the reflection time producing the corresponding seismic-attribute trace. When all of the traces of a seismic section are transformed into the

attribute domain, we get an attribute section. Attribute sections (like frequency sections, or velocity sections), are common tools applied by interpreters in their seismo-stratigraphic interpretation. More information on this important exploration tool is given in Chap. 13.

Seismic interpretation is the third and last stage in the seismic exploration project. In the two preceding stages (data acquisition and processing), reflected waves were first generated then processed to give the stacked seismic sections (or data volumes) in a form ready for the concluding exploration stage which is the data interpretation. This involves transition of these seismic data into the corresponding geological information.

Success of this process (geological interpretation of seismic data) depends largely on the coordination between the geophysical and geological knowledge. Those techniques which were applied in pre-computer times were dependent on manual and semi-manual procedures with emphasis on establishment of the structural changes of the subsurface reflectors. In recent years, with the advances witnessed by computers and specialized software, the interpretation process became faster and more efficient in exploring the geological structural as well as stratigraphic features.

---

## 12.1 Scope and Objectives

Seismic interpretation is basically an inverse problem solution. Given the seismic data, in the form of seismic stack sections, interpretation procedure is carried out to extract the corresponding subsurface geological picture. To aid in the interpretation process, additional geological and geophysical data are made available to the interpreter to use. These data include the velocity

field, sonic logs, and density logs which are normally obtained from well logging and VSP surveys.

The interpretation process aims at extraction of geological information from the seismic stack data. The scope of interpretation is now extended to include exploring stratigraphic changes and direct hydrocarbon detection. In addition to isochrones and structural depth maps, modern interpretation activities include modeling (direct and inverse modeling) and computing of seismic attributes.

---

## 12.2 The Seismic Interpretation Tools

The geological nature of an area can be divided into two main types of geological changes: the structural and the stratigraphic changes. The seismic stack section (or 3D stack-data volume) is a picture (seismic image) that carries information about the geological features (structural and stratigraphic) with their mineral and fluid contents. On this basis, it is possible to divide the seismic interpretation techniques into two main approaches (interpretation tools). These are: the travel-time tool and the waveform tool, each of which is aided by the seismic wave propagation velocity (Fig. 12.1), are defined as follows:

- (i) The travel-time tool:  
Reflection travel-time computations lead to determination of the variation of the reflector

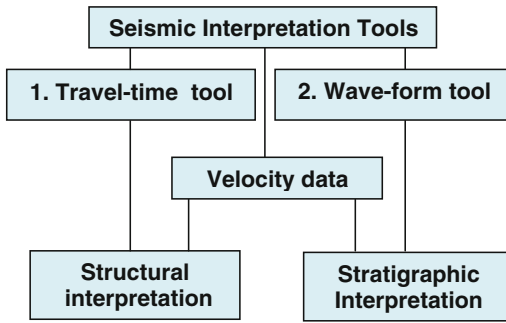


**Fig. 12.1** The two interpretation-tools: the travel time tool for structural interpretation and the waveform tool for stratigraphic interpretation

depth along the seismic line. This means that this approach (travel-time analysis) would serve as a structural interpretation tool. In particular, the structural features: folding and faulting are mapped with this tool.

(ii) The wave-form tool:

The spectrum structure of the reflection wavelet is function of the physical properties of the rock medium through which the seismic reflection wave has traveled. The wavelet energy level (expressed by the wavelet amplitude) is related to the reflection coefficient which, in turn related to the contrasts in the acoustic impedance across interfaces. The other wavelet parameters (frequency and phase characteristics) are influenced by the rocks physical properties as lithology, porosity, and fluid contents. In other words, the wave-form changes serve as an effective stratigraphic interpretation tool.

## 12.3 The Seismic Structural Interpretation

This approach represents the conventional way of interpreting seismic reflection data that has been followed by most interpreters since the establishment of the seismic reflection method in the 1930s. Essentially, this involves measuring the two-way vertical time at the CMPs of the stack section (migrated stack section), and plotting the values, relative to a defined datum level,

along the seismic line. For each reflector of the studied area, the three-dimensional structural picture is established. The end result is presented in the form of a time (or depth) contour-map.

The interpreter usually produces a time-map (called time structural map, or isochron map) which can be converted into depth structural map using the appropriate velocity field of the area. Due to the velocity vertical and lateral variations, the two contour maps (the time- and the depth-maps) are expected to show some dissimilarity. In addition to geometrical shape of reflectors, another set of maps showing changes of formation thicknesses are calculated. Reflection time-intervals between two adjacent reflectors are computed and converted into thicknesses using the corresponding interval velocity. The resulting maps (called isopach maps) are used in the studies of sedimentary environments, in sediment-source zones, and other geologic changes.

### 12.3.1 Structural Interpretation Sequence

In a procedure similar to that normally followed in the seismic data processing, interpretation is carried out by a sequence of steps, the interpretation sequence. The standard sequence involves four main steps: reflection identification, the isochron map, the velocity map, and depth map computations. The standard sequence normally followed in seismic structural interpretation is presented in Fig. 12.2.

(i) **Reflection Identification and Picking**

This is the initial stage in any seismic interpretation project. Reflection horizons are chosen based on their continuity and amplitude strength (high signal-to-noise ratio). To attach stratigraphic definitions to seismic reflection events, a synthetic seismogram from a near-by well, is computed. Sometimes it is found that there is some difference in time between the synthetic seismogram and the seismic section. This is due to the differences in the way the two types of data were recorded and processed. This phenomenon (called phase difference) is taken into consideration when doing the stratigraphic calibration.

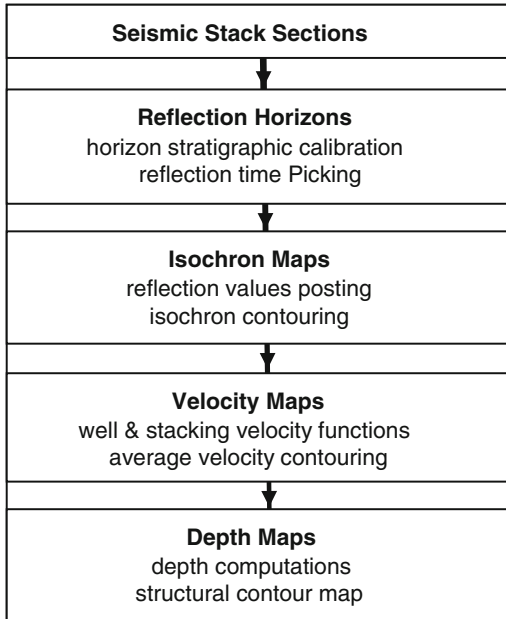


**Fig. 12.2** Standard sequence normally followed in seismic structural interpretation

Reflection times of the reflection horizon are read (manually or electronically) by a process called (reflection picking). The process is carried out for the same horizon in all of the sections in the area. Care is needed to be taken when the reflectors are affected by faults. A common difficulty, met with, is the mistie-phenomenon. In the process of tying horizons picked at intersecting sections, reflection times may not coincide. This problem, which may be due to anisotropy or other causes, needs special treatment to make the horizons at the intersections, to tie perfectly at intersections.

#### (ii) The Isochron Map

The picked reflection values are posted onto the seismic lines at regular intervals, and then a contour map is drawn to produce the isochron map which expresses the structural behavior of the reflector. Another set of contour maps are also drawn for the iso-time intervals (time-interval between two adjacent reflectors). The produced time-interval contour maps correspond to the depth interval (or isopach) contour map. Interval changes may indicate true thickness changes or velocity changes, which both can give significant geologic information.

#### (iii) The Velocity Map

There are two main sources for the velocity data for the surveyed area. The velocity functions obtained from well velocity surveys, or VSP surveys, and the stacking velocity functions used in the NMO-correction that was applied in the processing stage. Well velocity survey provides more accurate velocities, but available only at the limited number of well locations. The normal procedure is to compute a smoothed contour map of the average velocity functions (derived from the stacking velocity) and get it calibrated with the well velocity functions.

#### (iv) The Depth Map

Based on the smoothed average velocity map and the isochron map (corrected for misties), the depth contour map is computed. At each CMP of the area, a depth value ( $z = vt/2$ ) is computed from the velocity value ( $v$ ) and the reflection two-way vertical time ( $t$ ) which is known at that point. Sometimes the interval velocity is used instead of the average velocity. In this case, thicknesses are computed and total depth of each reflector is found by summing thicknesses.

The resulting map represents the structural contour map, with the fault-lines clearly marked on. The contour lines are drawn at uniform intervals which are normally chosen to be within (20–40) m.

In practice, another faster approach is applied. This is accomplished by use of the time-depth relationship which is derived directly from the well velocity survey or from the VSP data obtained from a nearby well. An actual example of such a time-depth curve is given here-below Fig. 12.3.

Use of the time-depth curve for depth conversion is valid provided that no appreciable velocity changes occurring in the area. The approach is suitable to be applied in small areas which are geologically simple and with no severe velocity changes.

In addition to the structural map another type of depth-domain maps can be made. These are the (isopach maps) in which contour values are representing formation thicknesses rather than the reflector depths. Isopach maps are very helpful especially in drawing some useful stratigraphic information.

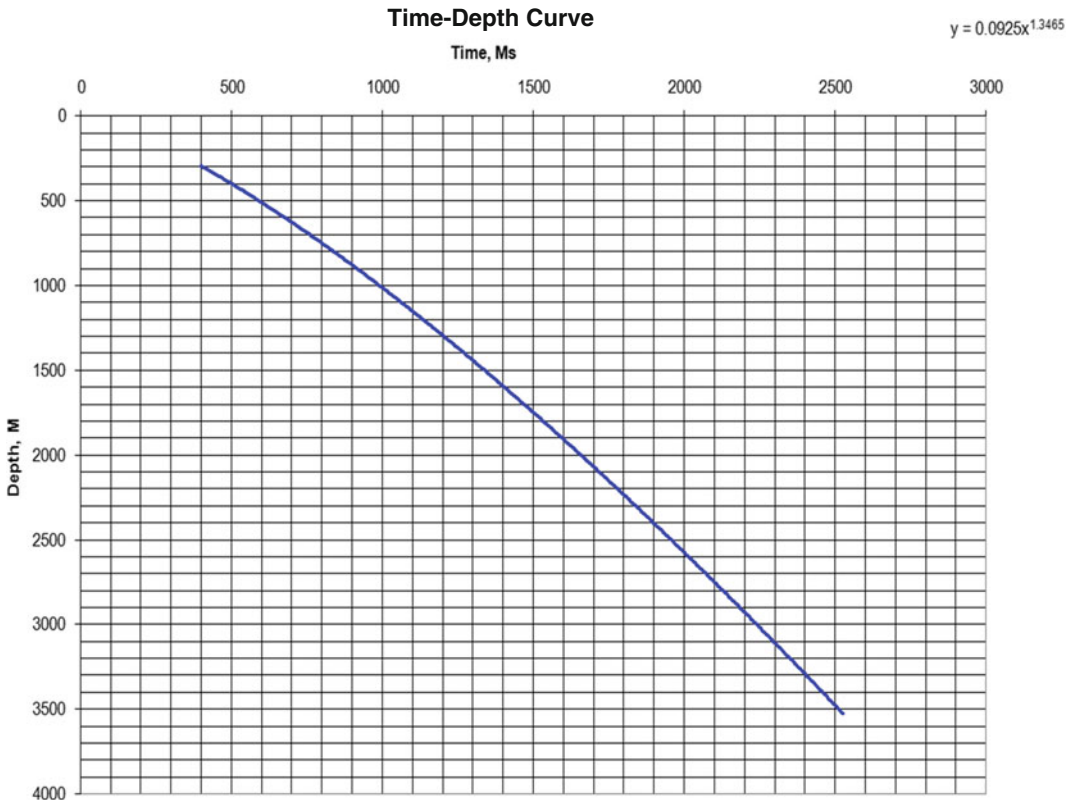


**Fig. 12.3** An actual time-depth curve used in the depth conversion process

### 12.3.2 The Seismic Structural Features

The simplest structural form of a reflection event appearing in a seismic stack section is the horizontal reflection horizon that has no geometrical deformations. In real world, reflection events are often affected by structural distortions of different types and different forms. The most common types of distortions of reflection horizons are folding and faulting features.

#### (i) The Seismic Image of Folding

Fold images shown by seismic sections vary according to the geological nature of the area. Reflection horizons can be simple linear horizontal or dipping events. The horizons may be affected by folding of various degrees of intensities (Fig. 12.4).

Most common folding features which may be observed in seismic sections are anticlines,

synclines, and monoclines. Focusing effects appearing with anticlines and bow-tie events appearing with tight synclines are possible distortive features which may be observed in seismic stack sections. Seismic migration is applied to remove these interferences.

#### (ii) The Seismic Image of Faulting

A fault feature appears on a seismic section as a break in the reflection event with some shift in the vertical (and/or horizontal) of the two faulted parts. Identification of faults on seismic sections, are not always easy to do. Data quality, resolution, and fault specifications (such as fault throw, fault type, and break sharpness) are factors controlling the success of fault identification. Typical seismic images of faulted reflectors are presented in Fig. 12.5.

Fault identification is often an easy issue when the throw is relatively large and the wavelet of the reflection horizon is well resolved.

**Fig. 12.4** Examples of seismic stack sections showing **a** practically horizontal and **b** folded horizons

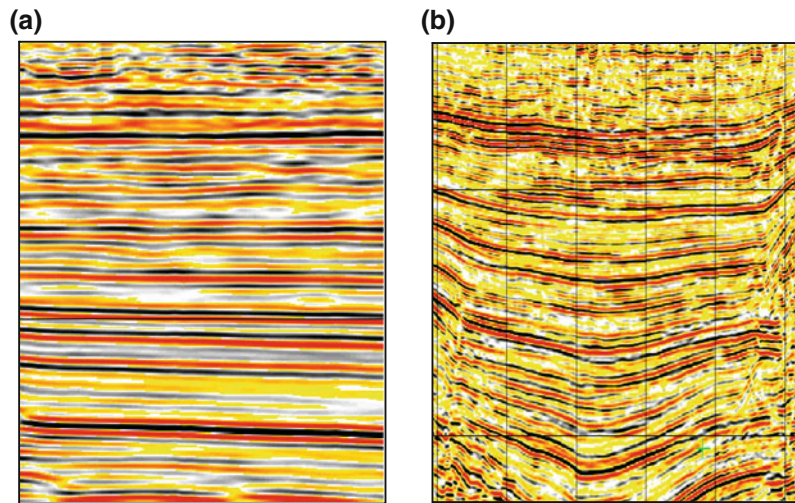
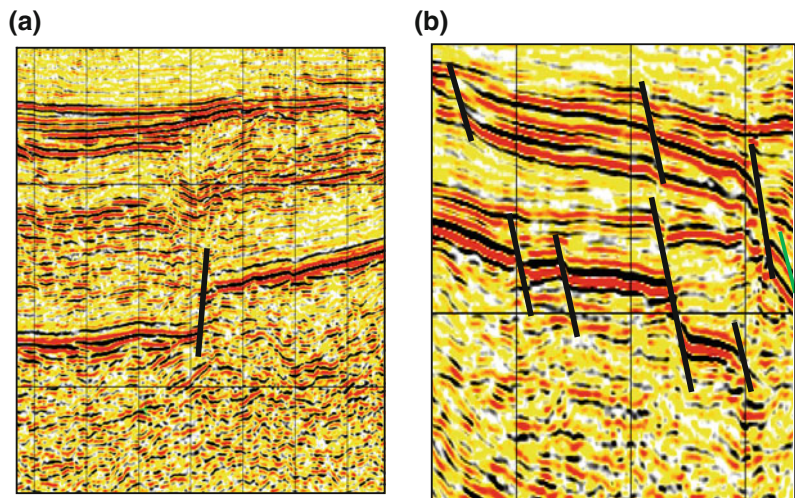


**Fig. 12.5** Examples of seismic stack sections showing faulted reflection horizons.

**a** Section showing one normal fault and  
**b** Section showing several normal faults



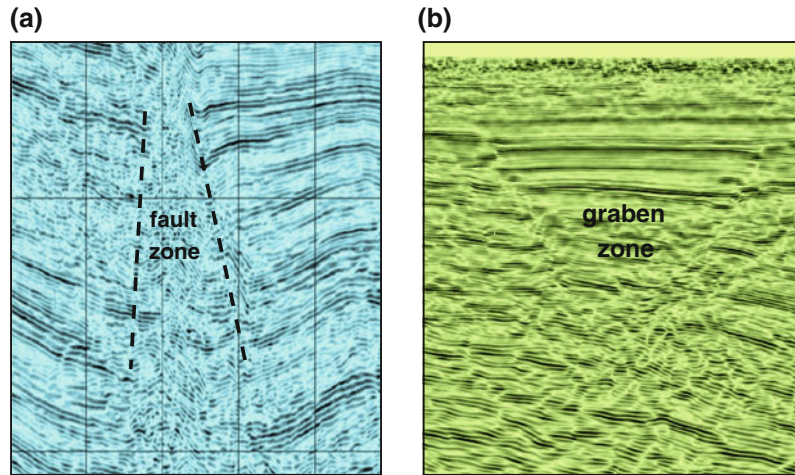
However, sometimes diagnosis of faults is not that easy. Difficulty in identification of faults is mainly because of small fault throw and poor break-sharpness. Very often the fault feature is not a clear-cut break of the reflection horizon, but it is exhibited as a limited non-reflection zone. The appearance of a fault zone, rather than a sharp fault plane, may be due to presence of fractured and crushed rocks in that part of the reflector that is affected by faulting.

In cases where the faults are not clear, interpreters usually seek help by other side features. Reflection wavelet characteristics used in the picking process across the fault zone. If this was

not decisive, the interpreter can investigate the continuity of the horizon between intersecting seismic lines. Existence of a fault may lead to creation of a mistie-phenomenon if the fault was not indorsed in the interpretation of that horizon. Another indication of faulting is finding a sudden change in reflector dip. Care should be taken in this case as the sudden change in dip may be due to intensive folding and not due to faulting.

Under certain geological conditions, the fault zone suffers from some local deformations (as layer dragging or sagging) in addition to rock fracturing. These fault side-effects may lead to reflection-wavelet weakening, or complete

**Fig. 12.6** Examples of seismic stack sections showing. **a** Deformation in the fault zone, and **b** Double-fault (graben) zone



disappearance of reflection wavelets in the vicinity of the fault zone. Typical seismic images of deformations due to faulted reflectors are presented in Fig. 12.6.

In unmigrated sections, terminating reflectors exhibit diffraction events due to arrivals of diffracted waves from reflector termination points. The apex of the hyperbolic diffraction curve is located directly over the diffraction source which is the faulted end of the affected reflector. This means that diffraction arrivals can serve as a handy tool for fault identification especially when the fault break occurs over a clean-cut plane and not across a zone of crushed-rocks.

## 12.4 The Seismic Stratigraphic Interpretation

As it is mentioned above, this approach is depending on interpreting the changes of the reflection waveform rather than the reflection travel-time. In practice, it is found that waveform changes caused by stratigraphic changes are easily obscured with noises. Usually, marine seismic data give better resolved stratigraphic changes than land seismic survey data. Extraction of stratigraphic information from seismic data depends on a set of principles and techniques forming a branch of applied science called (seismic stratigraphy).

The main objective of stratigraphic interpretation is determination of the types of stratigraphic

features appearing on seismic sections. Typical examples of such features are: facies changes, sand lenses, reefs, and unconformities.

### 12.4.1 Role of the Seismic Wavelet in Stratigraphic Interpretation

The seismic reflection wavelet is the net result of the interaction that occurred between the source signal and the stratified earth medium that the source pulse experienced during its reflection travel-journey from the source to the receiver. In addition to the loss in energy brought out as a result of the reflection and transmission coefficients, the physical properties of the traversed geological formations, contribute to the modifications of the wavelet waveform (spectrum structure). Each physical property of the travel path has its own signature on the travelling seismic wavelet. These changes imposed by the different properties of mineral and fluid contents (water, oil, or gas) can be considered as messages waiting for unraveling and understanding their geological implications.

In stratigraphic interpretation it is helpful to recall that the seismic trace is formed from a convolution process between the source wavelet and the series of reflection coefficients of the formations met with by the travelling wavelet. Further we note that there is a direct relation

between the acoustic impedances of these formations and the wavelet amplitude and polarity.

To sum up, wavelet energy content and frequency content (including wavelet polarity) are all parameters carrying messages on the stratigraphic changes of the subsurface geological formations. The same principle is applied in the more specialized technique in exploring the type of hydrocarbon, the method commonly referred to as direct hydrocarbon detection, DHD.

### 12.4.2 Basic Stratigraphic Concepts

Stratigraphy (geology of sedimentary rocks), is a branch of geology which deals with the study of the rock-layers including, origin, lithology, composition, chronologic succession, and correlation. Seismic stratigraphy is concerned with the study of sedimentary formations (stratigraphic changes) based on seismic data. The basic concept underlying the seismic stratigraphic analyses is that a sedimentary sequence is expressed in terms of corresponding seismic reflection events (seismic sequence).

In studying a stratigraphic phenomenon, two closely related aspects need to be considered, geological and geophysical aspects. The geological aspect is that a sedimentary section was formed as a result of precipitation under continental and marine environments. The layering geometry and rock composition of the large sedimentary basins are largely controlled by the sea-level changes. The other aspect is of geophysical nature in which the seismic reflection-events (representing the stratigraphic features appearing on seismic sections), have geometric forms and wavelet characters which are directly related to the causing geological (stratigraphic) features. With these two aspects in mind, seismic interpretation is implemented.

A summary of the basic definitions and concepts of seismic stratigraphy is given as follows:

#### (i) Seismic Stratigraphy and the Depositional Sequence

Seismic stratigraphy, that includes sequence analyses and reflection events configuration patterns, are based mainly on development mechanism of

sedimentary basins which are largely controlled by sea-level changes. One or more contemporaneous depositional systems (fluvial, delta, continental shelf or slope) compromise the principal elements of basin fill. These deposition systems constitute the seismic depositional sequences. Diagnosis and delineation of the fundamental basin-fill sedimentary units from seismic sections is referred to as seismic sequence analysis. In essence, seismic stratigraphy principal concepts are developed to describe precipitation processes and environments involved in creation of the sedimentary basins.

Due to sea-level changes, the coastline changes position accordingly. The coast line may advance land-ward (sea transgression) or retreat sea-ward (sea regression). With the sea-rise, for example, sedimentation area advances land-ward making a depositional pattern called (Coastal Onlap) and the vertical component of the sedimentation zone is called (Coastal Aggradation). In general, a sedimentary system made up of several sedimentary layers, which were contemporaneously-deposited under the same deposition-environment and bounded by unconformity subsurface, is called a (depositional sequence).

A depositional sequence (time-stratigraphic unit) is therefore defined as a set (package) of sedimentary layers deposited contemporaneously as components of the same depositional system created under the same depositional environments. The unit-package (sequence) is usually bounded by an unconformity surface at both its top and its bottom.

#### (ii) *The Seismic Sequence*

This is the expression of a depositional sequence as a seismic image appearing on a seismic section. It is a group or package of seismic reflection events which are bounded by unconformity surfaces at both of its top and base.

#### (iii) *The Seismic Facies*

This is a genetically related set of seismic reflection events appearing on a seismic section, corresponding to a given set of sedimentary rock-types (lithofacies). A (seismic facies unit) possesses its own distinctive seismic characteristics which are expressing its sedimentary properties and depositional environments.

#### (iv) The Seismo-Stratigraphic Analysis

Seismo-stratigraphic analysis is the interpretation-process to extract stratigraphic features from seismic data. It involves two levels of analysis: seismic-sequence analysis followed by seismic-facies analysis that deals with the seismic lithofacies within each seismic sequence. Two main criteria are used in seismo-stratigraphic interpretation: the reflection configuration patterns and the seismic waveform variation.

### 12.4.3 Reflection Configuration Patterns

Reflection configurations representing seismic facies found within a seismic sequence can appear in the form of simple or complex patterns. Simple parallel reflection events are generally representing shallow-water shelf deposits, while complex, sigmoidal-shaped events are representing down-slope depositional environments, as those deposits taking place at shelf edges.

Seismic studies proved that there is a relation connecting the geological depositional package and the configuration pattern of the corresponding seismic image. A seismic event representing a facies unit, for instance, can assume a simple or complex pattern, according to the sedimentary process that created that unit. Analyses of these patterns for seismo-stratigraphic interpretation are usually done on two levels; seismic sequence analysis and seismic facies analysis. The main seismo-stratigraphic patterns are briefly presented as follows (Mitchum and Vail 1977; Sheriff 1980)

#### (i) Parallel Reflection Patterns

Examples of simple configurations are parallel or divergent alignments corresponding to the sedimentation patterns which can be horizontal planes or, as in most cases, they can be inclined in down-dip direction, indicating gradual basin subsidence (or faulting) that occurred during deposition. These can also indicate material drape that was taking place contemporaneous with deposition.

In a sedimentary basin, parallel alignments assume different attitudes with respect to

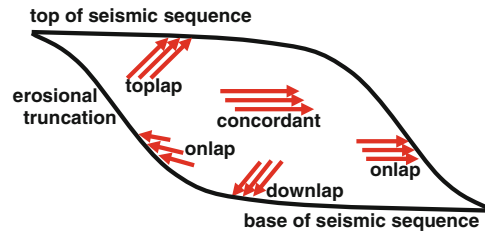


**Fig. 12.7** Sketch of simple configuration (parallel alignments) patterns of seismic facies in a seismic sequence

pre-sedimentation surfaces, or with respect unconformity surfaces. In this respect, seismic facies may be found terminating against top (toplap), or against the base (baselap) of a seismic sequence unit (Fig. 12.7).

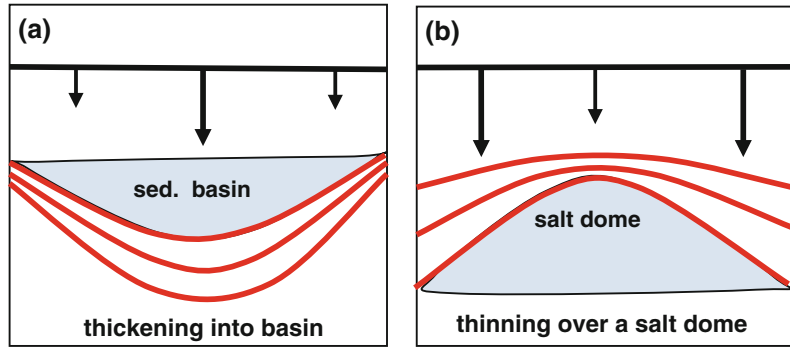
In describing these events (Fig. 12.7), the following terminologies are in common use (Sheriff 1980):

- Toplap reflections are terminating at the upper surface of the seismic sequence unit. It is also called offlap. It indicates deposition near wave-base, that is, high energy deposits (Sheriff 1980, p. 90).
- Downlap reflection-events are dipping downward and ending at the sequence lower surface, indicating seaward end of the sequence unit.
- Erosional Truncation reflections are terminating along an unconformity surface due to post-depositional erosion.
- Onlap reflections are horizontal (or pointing upward) and ending at the surfaces of a sequence unit. The onlap may be further labeled as costal (coastal onlap) to indicate that it is landward progressive deposit. These reflections are usually representing strata filling a negative relief feature as channel fill, trough fill, basin fill (Sheriff 1980, p. 205).
- Concordant reflections are reflection events which are parallel (usually horizontal) to sequence boundaries.

#### (ii) Unparallel Reflection Patterns

Reflection events in this case are not parallel to each other, but taking the form of converging or diverging events. Such patterns of seismic events normally indicate changes in formation thickness

**Fig. 12.8** Convergent and divergent reflection patterns. **a** Thickening into basins, and **b** Thinning over salt dome



which occur as a result of either structural activities, as in case of growth of salt bodies, or because of stratigraphic activities as in case of sediment influx into ocean depressions. In these cases, thickness shall experience changes which are expressed into the corresponding convergence or divergence in the corresponding seismic reflection events.

Typical cases of such events are the convergent reflection events observed over salt domes, where the layers are thinning over the salt body. In contrast to this case is divergence of reflection events which usually represent thickening of basinal formations, normally seen dipping in the direction of a basin centre (Fig. 12.8).

Sometimes these two types of configurations are called inward convergence (for convergence) and outward convergence (for divergence).

### (iii) Sedimentary Basins Configuration Patterns

With sufficient sediment influx, the rate of subsidence is greater at the centre of the basin, leading to thickening into-basin patterns. Thus, thickening of a formation into a basin indicates both subsidence and abundance of sediments fed into that basin. A thick, reflection-free, image in the deep part of the basin indicates rapid deposition and rapid subsidence.

Thinning of prograding seismic sequence into basin may be due to greater compaction at the basin deeper parts, indicating compactable type of lithology (as clay and sand deposits, for example). Thinning due to scarce sediments can be used as guide for determination of the sediment-source location. Further, thinning over

uplift is indicative of growth structures. A possible cause of growth may be shale-doming or salt diapirism. In such cases the uplift-structure is subsiding at a slower rate than the region surrounding the uplift. This means that the uplift-structure is growing up in relation to the surrounding area resulting in thinning of the overlying formations.

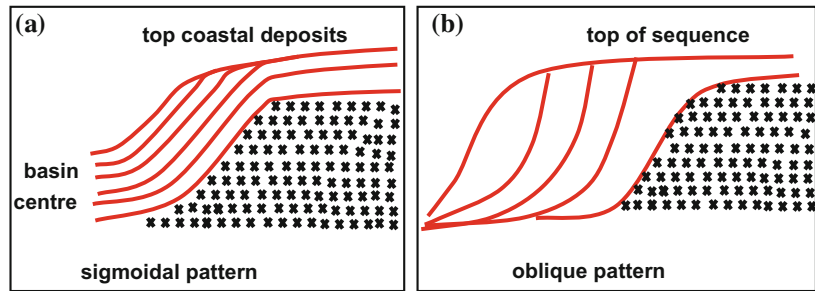
Concerning interpretation of reflection configuration patterns of the thickening and thinning phenomena, it is useful to note that, in seismic sections, the convergence and divergence phenomena may result because of velocity changes and not due to real thickness changes. This must be taken into consideration before giving final conclusion as regards thickness-change interpretation.

### (iv) Reflection Complex Configurations

Complex patterns indicate prograding deposits formed by two building components: out-building and up-building of sediments. The phenomenon occurs over continental shelves and slopes and also in association with deltaic-environments deposition. These patterns (known as progradation deposits) are subdivided into sigmoidal and oblique configuration patterns (Fig. 12.9).

Sigmoidal reflection patterns are gentle S-shaped events with the top of the pattern being parallel to the upper boundary of the sequence unit. It corresponds to sedimentary growth created by out-building with significant up-building processes. This is accomplished through smooth transition from top coastal formation towards basin centre. The process is accompanied with thinning due to increased compaction and general decrease of the deposited material. Sigmoidal

**Fig. 12.9** Complex reflection patterns. **a** Sigmoidal configuration pattern and **b** Oblique configuration pattern



patterns are indicative of deep-water fine material deposited in quiet, low-energy deposition environments.

The Oblique reflection pattern, show toplap or angularity with the upper boundary of the sequence unit. Sedimentary growth, in this case, is mainly outbuilding. This indicates deposition near the wave-base, in high-energy environment with good sorting, giving coarse grain, and delta-platform type of sediments.

Seismic configuration patterns within a sequence-unit may exhibit irregular and unorganized patterns, normally referred to as hummocky, shingled, contorted, irregular, chaotic, or reflection-free zone. Such unorganized reflection events are taken to be representing turbulent depositional environments.

#### 12.4.4 Seismo-Stratigraphic Features

Reflection configurations can serve as indicators for the deposition environment and on the historical development of the sedimentary deposition process. Thus, for example, parallel horizons indicate deep water deposition that has taken place on stable basement. Rising and falling of the basement surface in relation to the coastal area give rise to changes in thickness according to influx rate of deposition as well as on the direction of the sea-level movement. Deltaic fans, sand bars, channel infill, denudation, sediments compaction, and other stratigraphic processes, all leave their individual signatures on their corresponding seismic images. In short, geological stratigraphic features appearing on a particular geological section have their own

seismic images (seismo-stratigraphic features) on the corresponding seismic section.

The following discussion shall be concerning the principal stratigraphic features which are observable on seismic sections, with emphasis on those features having significance as regards oil stratigraphic traps.

##### (i) Sand Lenses

These are buried stream channels or buried lakes, filled with sand and covered with impervious deposits as shale or clay. Because of the contrast in acoustic impedance the surface of the high-porosity sand-body becomes an interface of reflection coefficient of value and algebraic sign depending on the extent of contrast in physical properties between the lens material and the surrounding host medium.

Typically, sand lenses (especially gas-filled lenses) exhibit abnormally high-amplitude reflections. The reflection event, caused by the upper surface of such a gas-saturated sand lens, is commonly known as a bright spot (Fig. 12.10).

Other related phenomena are the (flat spots) representing gas-oil contact surface, and (dim spot) representing interfaces separating two media having abnormally small impedance contrast. Because of the relatively low velocity of the sand lens, a reversal in polarity of the wave reflected from the upper surface of the lens. It is also noticed that there is increase in travel-time of waves reflected from deep reflectors, which are traversing the sand body. This is expected to happen because of low velocity of the sand lens.

##### (ii) Reef Bodies

A reef body is made up of skeletal remains normally deposited on shoals surrounded by deep

**Fig. 12.10** Seismic section showing high-amplitude reflection event, possibly, it is a bright-spot feature

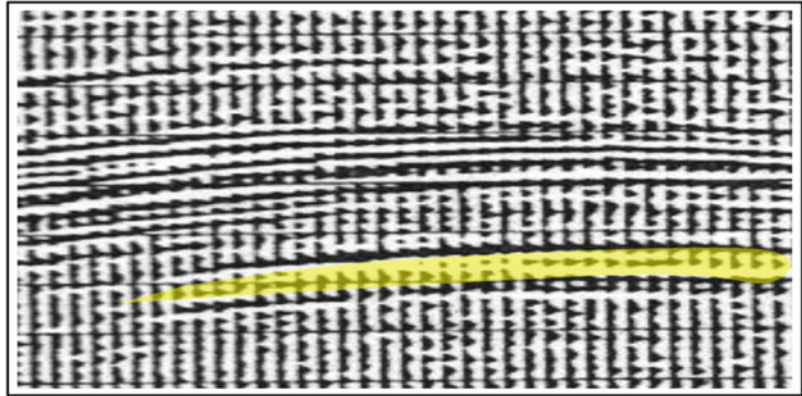
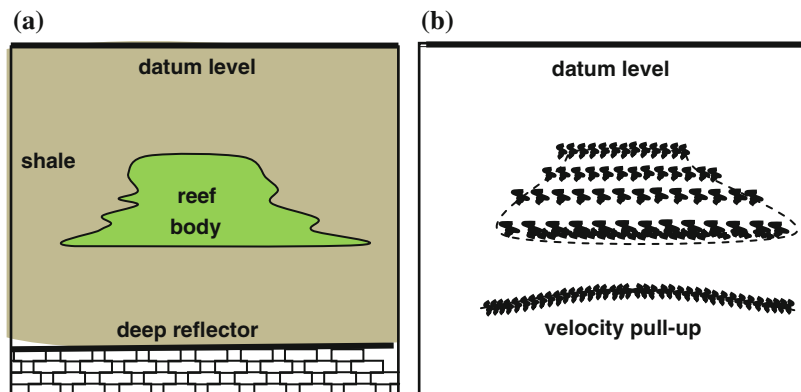


**Fig. 12.11** Sketch representation of a reef body amid shale host medium (a), and the corresponding seismic image (b) showing the velocity pull-up phenomenon



water as shelf surfaces and shelf margins. Favorable environment for the growth of coral reef is calm, clear, and warm water. Reef deposits, made up of porous limestone rocks, are normally found within consolidated mudstone or shale

The seismic event representing the reflection from the upper surface of the reef body differs from that of the sand lens in two ways: first reef boundaries are usually rugged surfaces which result in creating diffractions and wave scattering and weak and unclear coherent reflections. In this case, identification of reefs is achieved with the help of the reflection events produced by those overlying formations which are draping across the reef top. The second difference between reef and sand lens seismic events is that the velocity of the reef material is higher than that of the host medium. This property makes the reef body to act as a converging lens for the waves penetrating the reef. As a result of the converging effect a false or

apparent seismic anomaly may be created for the waves reflected from reflectors below the reef body. For the same high-velocity property, reflection events, from deep reflectors (reflectors below the reef-body), passing through the reef, may cause up-curving of those events, creating what is called a (velocity pull-up) phenomenon (Fig. 12.11).

Other additional indicators helping in diagnosis of reef seismic events are the appearance of diffraction events and the abnormally weak reflection events coming from reflectors found below the reef body. The diffraction events are created from the jagged and terminating nature of the reef surface. The weakening effect is attributed to the absorption and filtering effects of the reef rock-matter.

### (iii) Salt Domes

Within the zone occupied by the salt-body no reflection events are seen. This reflection-free zone

**Fig. 12.12** Sketch showing: **a** salt dome within a shale medium and some reflectors, and **b** the corresponding seismic image

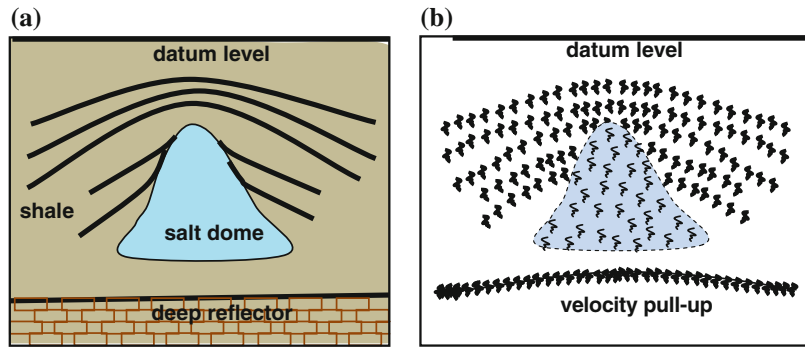
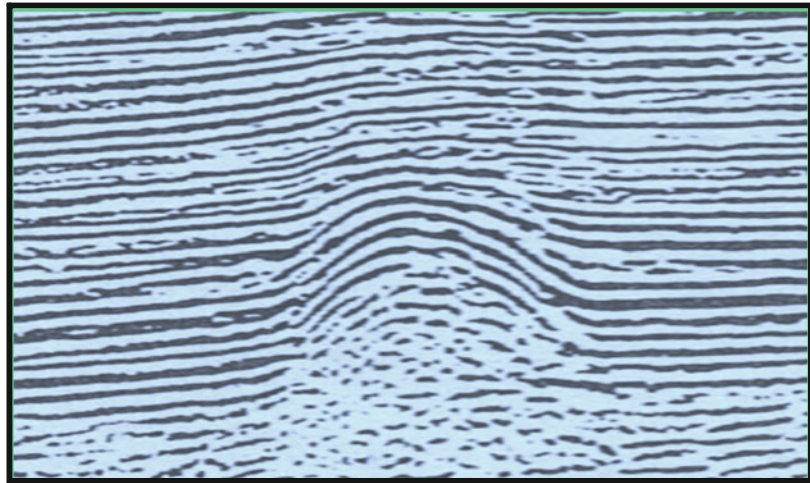


**Fig. 12.13** Example of an actual seismic image of a salt dome piercing and folding of overlying formations



is a common feature that serves as a characteristic property aiding in salt dome identification. Another characteristic feature is the thinning of the up-pushed formations which are overlying the salt dome. Diffraction arrivals may develop from the termination points of the reflectors that are pierced by the growing salt material. As it is the case with reef bodies, salt domes affect the seismic images of the deep reflectors in which the reflection ray-paths pass through the salt deposits. Since the salt velocity is higher than that of the surrounding medium, a false structural feature (the pull-up phenomenon) is generated.

Most prominent features used in identifying a salt dome is the termination of reflection images at the salt dome surfaces, and absence of reflection events within the salt body. In other words, the region defining the salt dome becomes reflection-free zone (Fig. 12.12).

By virtue of the vertical and horizontal pushing forces resulting from the growing salt body, folding and faulting of the overlying sedimentary cover take place. The formations, pierced by the migrating salt, will appear as reflection events terminating against the boundaries of the salt body. Also, because of the differential pressure effect, it is expected to see thinning of those parts of the formation found above the salt dome. An actual seismic image of a salt dome is shown in Fig. 12.13.

#### (iv) **Unconformity**

The unconformity feature is of fundamental importance in the seismo-stratigraphic studies as it acts as the basis of defining seismic sequences. The unconformity surface is marking a deposition-break geological episode. It is representing a period of non-deposition or a period of

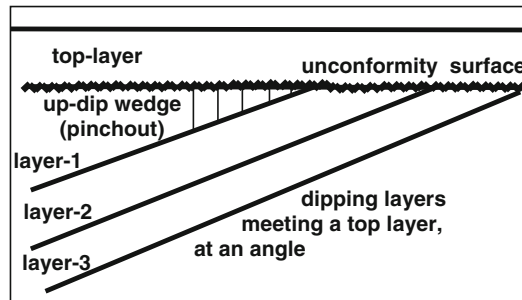
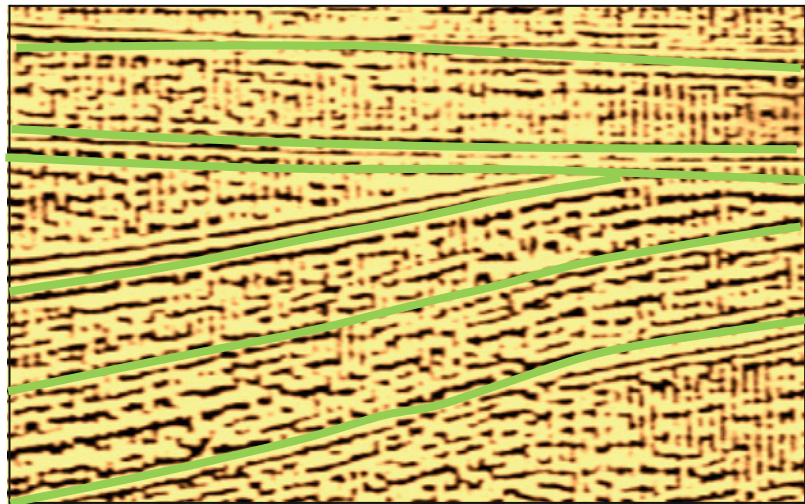


**Fig. 12.14** Sketch representation of the angular unconformity showing the angular relation between dipping layers and a overlying horizontal layer, with pinch-out feature

**Fig. 12.15** Typical Seismic image of an angular unconformity, showing a clear pinch-out feature



erosion, followed by resumption of deposition. When the unconformity plane is at an angle with the overlying sediments, it shows clearly on seismic sections exhibiting an up-dip wedge (pinch-out zone) against the overlying layers. Because of the angular relation between the two sets of formations involved in the unconformity, this feature is normally called angular unconformity (Fig. 12.14).

On seismic sections, the angular unconformity is readily recognizable from the angular relation and pinch-out phenomena. A typical seismic image of the unconformity is shown in Fig. 12.15.

The unconformity surface usually acts as a normal reflector, but it is not expected to be of constant wavelet amplitude because of the variation of the reflection coefficient as the surface crosses different formations. For the same reason,

the reflection wavelet characteristics may vary along the reflection event representing the unconformity surface.

In cases where the unconformity surface is irregular or rugged, diffraction and scattering of the incident waves, may occur, leading to quality deterioration of the unconformity-generated reflection horizon. The effect may be so severe that it will be difficult to delineate the unconformity extensions.

The most common example of this case is the basement surface which is considered as an unconformity feature. Due to the jagged or undulation nature of the basement surface, diffraction events may be generated. The basement surface unconformity (better called disconformities rather than unconformity) is readily recognizable on the seismic section, as an

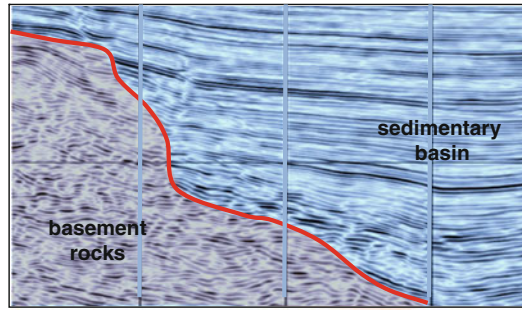
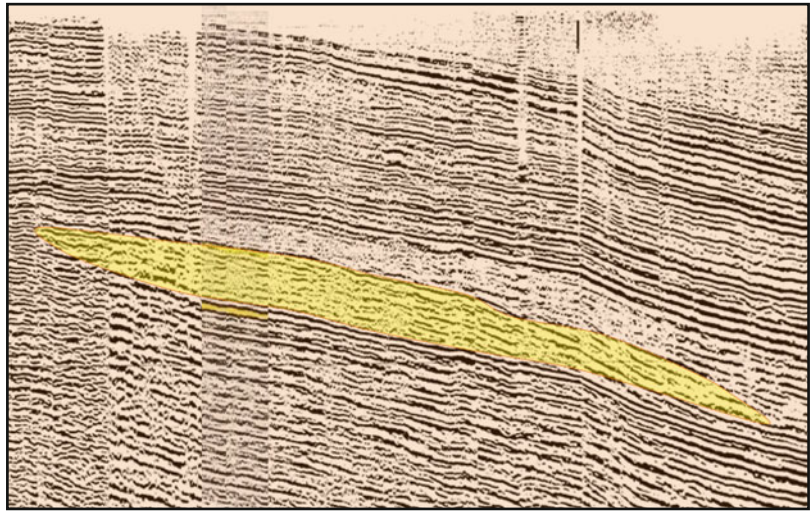


**Fig. 12.16** Seismic image of a sedimentary basin having reflection events terminating against an irregular basement surface (discontinuity)

**Fig. 12.17** Seismic image of a stratigraphic anomaly, representing facies changes occurring over a shelf area



irregular geometrical shape surface at which reflection events of sedimentary formations, terminate. Below the basement surface, coherent reflection events disappear (Fig. 12.16).

#### (v) **Facies Changes**

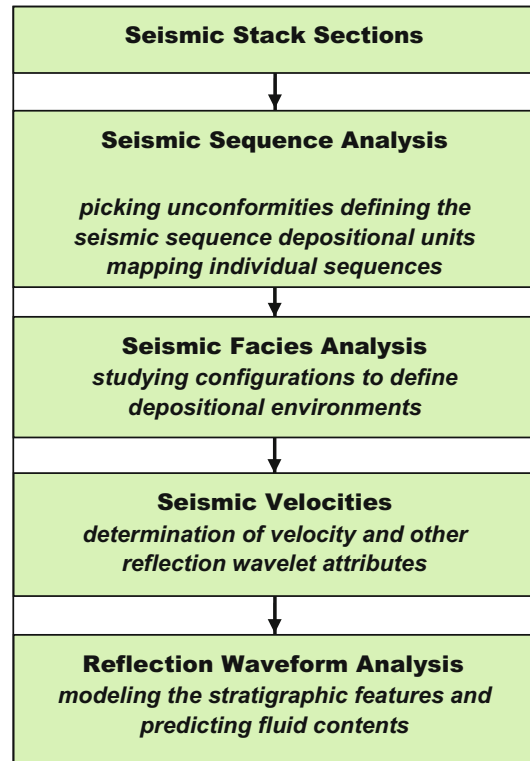
Within a basin, sedimentary facies which are of coarse-grained deposits are found near basin margins, while more fine (silt or shale) sediments are found near basin centre. Usually, marked changes in rock lithology are found in the areas where deltaic deposition environments prevail.

On seismic stack sections, the stratigraphic facies changes give corresponding anomalous seismic events. More often such events indicate

seismic facies units associated with the deltaic deposits (Fig. 12.17).

As regard deep marine conditions, two types of mechanism are suggested on submarine erosion and deposition. A submarine channel may be created as a result of river erosion or by turbidity currents. River action may lead to formation of sediment fans on the continental shelves, whereas turbidity currents can give rise to deep submarine channels which are filled with relatively high density sediments. On seismic sections, turbidites are expected to be expressed by locally-defined chaotic reflections. The other major group of marine deposits includes the whole range of carbonate rocks. These are the chemical deposits

**Fig. 12.18** Standard sequence normally followed in seismic stratigraphic interpretation (modified after Sheriff 1980, p. 22)



(from aqueous solutions) and the organic deposits (from parts of living organisms). Typical isolated bodies of carbonate nature are the reef deposits.

#### 12.4.5 Stratigraphic Interpretation Sequence

Three main types of analyses are normally applied in seismic stratigraphic interpretation. These are:

- i. Identification of the major seismic sequences.
- ii. Delineation of seismic facies found within the seismic sequences.
- iii. Computations of waveform parameters.

The seismic sequence analyses would establish the major depositional units (stratigraphic sequences), while seismic facies analyses are directed towards determination of lithofacies and depositional environments.

As in structural interpretation procedure, stratigraphic interpretation is carried out through a sequence of steps; the stratigraphic interpretation sequence (Fig. 12.18).

The input to the interpretation process is the stack section which has been subjected to a sequence of processing of the type that preserve the waveform unreformed. The stratigraphic interpretation starts with the identification of the major seismic sequences by marking the bounding unconformity surfaces of the seismic sequences. From the event configuration patterns, the stratigraphic units and sedimentary environments are determined. In the following steps, wavelet attributes, velocity and acoustic impedance inversion are done. The whole interpretation work is concluded by determination of the subsurface stratigraphic model including lithological changes, deposition environments, and hydrocarbon contents.

The main parameters commonly applied in the interpretation process are grouped in the following table (Vail et al. 1977).

Seismic reflection parameter	Geological interpretation
Reflection configuration	Bedding patterns Depositional processes Erosion Palaeogeography Fluid contacts
Reflection continuity	Bedding continuity Depositional processes
Reflection amplitude	Velocity-density contrast Bed spacing Fluid content
Reflection frequency	Bed thickness Fluid content
Areal association of seismic facies units	Depositional environment Sediment source Geologic setting
Interval velocity	Estimation of lithology Estimation of porosity Fluid content

In the 1980s, these parameters were grouped under one general term; the (seismic attributes) which were developed extensively as stratigraphic interpretation tools (Chen and Sidney 1997; Barnes 2001).

## 12.5 Direct Hydrocarbon Detection and Seismic Attributes

In the same way as the stratigraphic changes affect the reflection wavelet, presence of hydrocarbon deposits causes waveform changes. Interpretation tools and procedures employed in hydrocarbon detection are commonly referred to as (direct hydrocarbon detection). All known hydrocarbon indication-tools (hydrocarbon indicators) are related to waveform parameters, as amplitude, frequency, phase, and propagation

velocity. These indicators and their exploration potentialities are briefly reviewed in this section.

### 12.5.1 Hydrocarbon Indicators

Geophysical studies proved that presence of hydrocarbon matters in the pores of a sedimentary formation leads to lowering of both of the seismic velocity and bulk density of those formations (Sheriff 1980, p. 186). This means that we get a corresponding change in the reflection coefficient (and hence in reflection amplitude) of the interface separating the hydrocarbon-bearing rocks and the surrounding medium. The direct dependence of these parameters on fluid contents of rock formations, make them active indicators in hydrocarbon detection.

These indicators are explained as follows.

#### (i) Amplitude

Amplitude of the reflection wavelet is an expression of the wavelet energy-level which is controlled by the overall physical properties of the subsurface geology. In particular, types and quantities of fluid content (water, oil, and gas). A common observation is that presence of hydrocarbon gas in a rock formation results in lowering of the seismic velocity. As a result of this phenomenon we get increase of the reflection coefficient, and hence large amplitudes over the gas-reservoir. Normally, the reflection-event representing the top boundary of the gas-saturated formation exhibits polarity reversal. This abnormal seismic feature was recognized in the early 1970s and was given the name (Bright Spot).

In presence of gas, it is found that amplitude of the reflected wavelet changes with offset. The study tool that expresses this phenomenon is known in the geophysical literature by the term (amplitude versus offset, AVO). In general, for low impedance contrast, as in the case of gas reservoir, AVO shows, in general, increase of reflection amplitude with the receiver-offset. Amplitudes of reflections from top of gas reservoir (negative reflection), or from its base (positive reflection), will both show increase with offset, causing an AVO anomaly over the reservoir (Sheriff and Geldart 1995).

In order to keep amplitude changes restricted to the stratigraphic nature of the medium and to its hydrocarbon contents, amplitude-preservation processing must be applied.

(ii) **Frequency**

An abnormal lowering of frequencies of the reflection events from reflectors beneath the hydrocarbon reservoirs is brought about by the strong filtering effects of the hydrocarbon-bearing formations. For this reason (filtering effect), a low-amplitude shadow is produced by a hydrocarbon reservoir.

Frequency, as an important attribute of the reflection wavelet, is another active indication tool for presence of hydrocarbon deposits.

(iii) **Phase**

The attribute (phase) is generally useful in the study of reflector termination and polarity reversals. In this way, phase is considered as an effective indicator of faults, pinch-outs, and angular unconformities.

(iv) **Velocity and Acoustic Impedance**

In the mid 1970s, geophysical researches were directed towards employing the interval velocity and acoustic impedance in stratigraphic exploration and in direct hydrocarbon detection. Examples of these pioneering publications are; Sheriff (1975), Taner and Sheriff (1977), Dobrin (1977), Nestvold (1987). In this regards, the procedure is built on computing interval velocity sections (or acoustic impedance sections) derived from the normal stack sections. This process is an inverse modeling which is normally referred to as (inversion process).

Two main changes take place from hydrocarbon presence in a reservoir formation; increase in the reflection coefficients (with possible polarity reversal), and increase in the travel-time (time-delay) of the reflection wavelet passing through that formation. Due to the time-delay effect, it is expected to see an abnormal sagging of the reflection events from reflectors found below the hydrocarbon reservoirs.

The typical role of the parameter (velocity) is the velocity lowering-effect resulting from presence of hydrocarbon (gas, in particular) in a porous

formation. In addition to that the velocity factor can be used in exploring lithological variations and pressure conditions since velocity is function of the rock physical properties (elasticity and density). One of the common usages of the velocity is detection of reservoir gas-pressure conditions. Normally, overpressure reduces velocity.

## 12.5.2 Seismic Attributes

In the geophysical literature, the term (attribute) is used to mean a property or a parameter attributed to a certain seismic element. It serves as a specific character related to a geophysical element. For example, it is said that the fold of coverage is a CDP attribute, and the azimuth (or, offset) is bin attribute, because fold and azimuth are parameters of the CDP and bin respectively.

Being dependant on the wavelet parameters, seismic attributes carry useful information on certain physical properties of the medium traverse by the reflection wavelet. An attribute can help in clearer identification of stratigraphic features, patterns, and oil-reservoir characteristics. The seismic attribute is more sensitive to one of the wavelet parameters than the qualitative examination of the wavelet overall changes. Because of this property (direct link with the wavelet parameters), seismic attributes lend themselves as active indicators for stratigraphic changes and for direct hydrocarbon detection.

(i) **Seismic Attribute Definition**

In the field of the seismic stratigraphy, the term (Seismic Attribute) is used for calling one of the parameters of the seismic reflection wavelet. The attribute in this sense is a measured or computed value of a seismic parameter of a (or, related to) the reflection wavelet. Typical seismic attributes are wavelet amplitude, frequency, and phase. Many other attributes have been developed since early 1980s, when the basic attributes were put to application as stratigraphic exploration tools. Tens of attributes have been devised so far, as quoted in the geophysical literature.

(ii) **Seismic Attribute Section**

A normal seismic trace is considered as a time function of the parameter (amplitude). After

being converted into the attribute-domain, we get an attribute trace which is a function of the attribute value that varies with the reflection time. Any of the wavelet attributes (amplitude, frequency, or phase) can be plotted as a function of the reflection time producing the corresponding seismic-attribute trace.

By converting all of the seismic traces of a stack section into the attribute domain, a seismic attribute-section (or attribute volume, in case of 3D data) is obtained. Attribute sections, (like frequency sections, or velocity sections), are common tools applied by interpreters in their seismo-stratigraphic interpretation.

### (iii) Types of Seismic Attributes

Seismic attributes constitute an open set of values of any physical, mathematical, or statistical measurable quantity related to seismic reflection wavelets. Typical attributes are the wavelet-parameters (amplitude, frequency, and phase). Other parameters, like direct amplitude measurements, gradients, arithmetic-mean, RMS-mean, median, cross-correlation, and parameters computed from frequency-spectra, are included in the family of seismic attributes. Sometimes, velocity and velocity-dependent tools (as acoustic impedance), is considered as seismic attribute on the basis that it is a parameter related to the reflection wavelet.

All these attributes are derived from stacked data, but there is an attribute derived from pre-stack data (from gather traces), and that is the (amplitude-versus offset, AVO) which is found to be an effective tool in exploring gas-saturated formations.

Within two decades, after the concept of attributes was introduced in 1979 (Taner et al. 1979), hundreds of attributes were defined (Chen and Sidney 1997; Barnes 2001). Thus, in addition to the basic attributes (instantaneous amplitude, frequency, and phase), published in 1979, other attributes were devised. Examples of these are: polarity, interval velocity, absorption coefficient, the quality factor (Q factor), acoustic impedance, amplitude-versus-offset (AVO), and many more.

Classification and historical development of seismic attributes were published by many

authors as Taner et al. (1994), Chen and Sydney (1997), Taner (2001), Liner (2004), Chopra and Marfurt (2005), and Brown (2011). These classification schemes differ in the basis applied for the classification process. Based on the computational approach applied in the derivation of the attribute, the seismic attributes can be divided into two main groups (Taner 2001). These are the instantaneous attributes and the wavelet attributes. The first group consists of the instantaneous amplitude, frequency, and phase, while the second group includes wavelet parameters which are sensitive to physical properties and geometrical shapes of the reflection interfaces.

### The Instantaneous Attributes

The three basic instantaneous attributes are usually derived from the seismic stack trace, using the time-domain Hilbert Transform (Taner et al. 1979). The instantaneous amplitude is related to the energy level of the reflection wavelets and hence it can give information on the lithology and porosity changes. The instantaneous frequency is more sensitive to changes in the inelastic absorption property of the rock medium and in studying sedimentary facies. The third and last attribute in this group, is the instantaneous phase which is considered to be very active tool in showing reflection-termination phenomena as they appear with faults, unconformities, and pinch-outs.

### The Wavelet Attributes

These attributes are determined by frequency-domain computations (using Fourier Transform) of the seismic reflection wavelet. According to (Taner 2001), these attributes are subdivided into two sub-groups: the physical attributes and the geometrical attributes. The Physical Attributes are sensitive to the physical properties of the rock medium as lithology, porosity, acoustic impedance, and fluid contents. They also act as indicators for the changes in the inelastic absorption, propagation velocity, acoustic impedance, and AVO parameters (gradient and intercept of the AVO plot). The Geometrical Attributes are sensitive to variation of the geometrical shapes of the reflection interfaces. This means that these

attributes are suitable for exploring structural changes as folding, faulting, and geological dip.

In order to get better statistical support in the seismic attribute interpretation, several attributes can be used in the interpretation process. One way of the use of several attributes is computing a new attribute from combination of several other attributes. As an example on using multi-attribute approach is the use of three wavelet-attributes (Krehbiel 1999). In this study a (trivariate attribute) was derived from wavelet amplitude, amplitude derivative, and autocorrelation.

**Spectral Attributes**

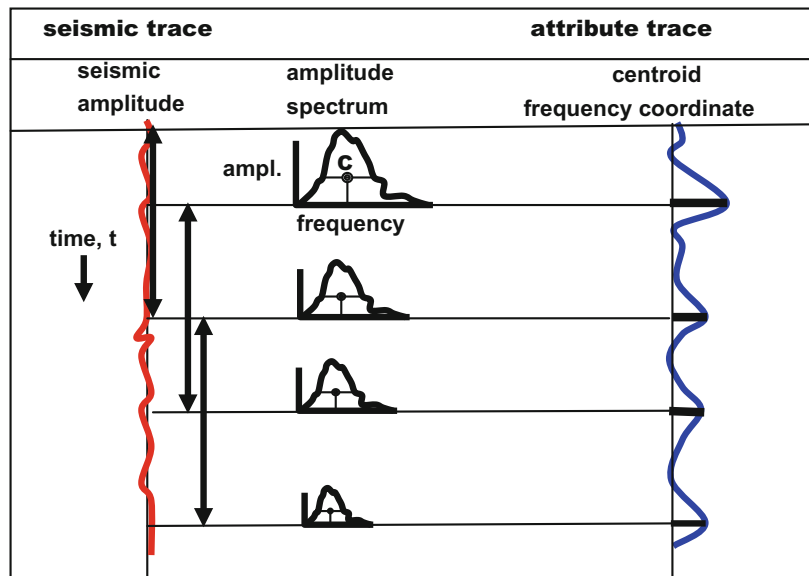
The basic concept underlying attribute derivation based on Fourier-spectra is not new. Spectral attributes were introduced in early 1970s (Båth 1974, pp. 203–218). In a study based on earthquake P-waves spectra, several spectral attributes (called then, spectrum parameters), were introduced to explore properties of the Earth Upper mantle (Al-Sadi 1973). In later years, spectral attributes were made use of in the field of seismic reflection exploration. During the 1990s, more emphasis was directed to application of attributes based on Fourier spectral analysis of the seismic reflection wavelet (Barnes 1993a; Trappe and Hellmich 1998; Addy 1998; Partyka

et al. 1999). The spectral attribute is derived directly from the amplitude spectrum (or from the power spectrum) of the seismic wavelet. Any parameter of the spectrum function can be computed to be a seismic attribute. Examples of these parameters are: the spectrum peak (maximum value), spectrum gradient, area under the spectrum-curve, spectrum width, and spectrum centroid.

One of the spectral attributes (the Spectrum Centroid) was introduced by (Al-Sadi 1973), and was later applied to seismic reflection wavelet (Barnes 1993b, p. 420). This attribute is considered to be one of the most efficient seismic attributes, because each of the Centroid coordinates is function of the distribution manner of the frequency components of the analyzed wavelet. Computation of this attribute is done by a sliding window with length and shift-step which are decided upon by the processing geophysicist. The principle of deriving of the spectrum-centroid coordinates, is shown in Fig. 12.19.

In 1995, the Spectrum-Centroid attribute section was computed for a seismic stack section (Fig. 12.20). In this figure both of the attribute sections (instantaneous amplitude, and Spectrum-Centroid sections) are presented for comparison purposes.

**Fig. 12.19** Sketch showing the definition of the attribute trace. Spectral attribute (spectrum centroid, C) is presented as function of reflection time



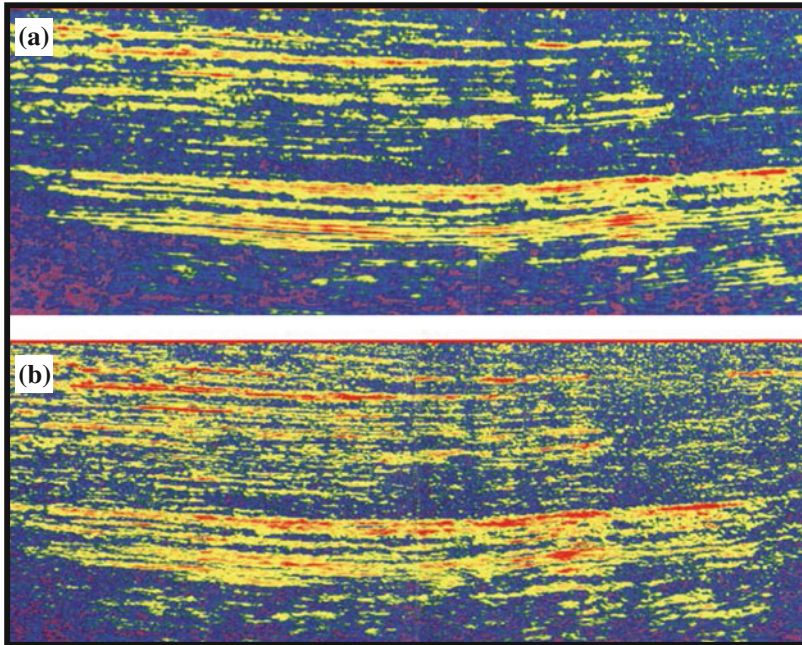


**Fig. 12.20** Seismic-Attribute colour-coded sections. **a** Spectrum centroid section and **b** Conventional instantaneous amplitude section (Alsadi 1998)

In this Fig. 12.20, the section of the Centroid attribute represents variation of one of the centroid coordinates (the amplitude coordinate).

From comparison of the two attribute-sections, it can be noticed that the Centroid Attribute section is showing better resolution.

## References

- Acheson, C. H., 1963, Time depth and velocity depth relations in Western Canada. *Geophysics*, vol. 28.
- Addy S.K., 1998, Neural Network Classification Method Helps Seismic Interval, Interpretation, Oil & Gas Journal, No. 38, pp 47–59.
- Al-Chalabi, M., 1979, Velocity determination from seismic reflection data: In *Developments in Geophysical Exploration methods*, Vol. 1, Fitch, ed., pp 1–68, Amsterdam: Elsevier.
- Al-Sadi, H. N., 1973, Dependence of the P-wave amplitude spectrum on focal depth. *Pure and Applied Geophysics*, vol. 104, p 439–452.
- Al-Sadi, H. N., 1980, Seismic Exploration, Technique and Processing. Birkhäuser Verlag, Basel, 215p.
- Al-Sadi, H. N., 1992, 3D surveying of inaccessible areas, presented to the Iraqi tenth geological conference (in Arabic Language), 17p.
- Al-Sadi, H. N., 1994, Use of the loop spread in seismic surveying of a rugged mountain, presented to the twelfth Iraqi geological conference (in Arabic Language), 12p.
- Al-Sadi, H. N., 1998, New Seismic Attributes for Stratigraphic Exploration, presented to the thirteenth Iraqi geological conference, (in Arabic Language), 9p.
- Al-Sadi, H. N., and Baban, N., 2014, Introduction to Gravity Exploration Method. 203p, Sulaymaniyah University, Kurdistan Region, Iraq, Sulaymaniyah.
- Araya-Polo, M. et al., 2009, 3D Seismic Imaging through Reverse-Time Migration on Homogeneous and Heterogeneous Multi-Core Processors, *Scientific Programming*, vol. 17 no. 1–2, pp. 185–198. IOS, Press publications.
- Aud, B. W., 1974, Abnormal pressure zones can be predicted by seismic data. *World Oil*, Aug-74, pp. 37–39.
- Barnes, A., 1993a, When the Concepts of Spectral Frequency and Instantaneous Frequency Converge, *Leading Edge*, Oct-1993, P.1020–1023.
- Barnes, A., 1993b, Instantaneous spectral bandwidth and dominant frequency with applications to seismic reflection data, *Geophysics*, vol. 58, P.119–428.
- Barnes, A., 2001, Seismic attributes in your facies: *CSEG Recorder*, 26, Sept., pp. 41–47.
- Båth, M., 1971, Average crustal structure of Sweden., *Pur. Appl. Geophys.*, vol. 88, p. 75–91.
- Båth, M., 1973, *Introduction to Seismology*. BirkhäuserVerlag, Basel, 395p.
- Båth, M., 1974, *Spectral Analysis in Geophysics*. 563p., Elsevier Scientific Publishing Company, Amsterdam.
- Båth, M., 1979, *Introduction to Seismology*, BirkhauserVerlag, 428p, Basel, Switzerland.
- Birch, F., 1966, Compressibility, Elastic Constants, in *Handbook of Physical Constants*, by S. P. Clark, Geological Society of America, *Memoir* 97, p. 97–173.
- Bracewell, R., 1965, *The Fourier Transform and its Applications*. McGraw Hill Book Company, 381p. New York.
- Brown, A. R., 2011, Interpretation of three dimensional seismic data, 7th. edition, *AAPG Memoir* 42 (9), 646p.
- Bullen, K. E., 1965, *An Introduction to the Theory of Seismology*, The University Press, 381p, Cambridge, England.
- Chen, Q. and Sidney, S., 1997, Seismic attribute technology for reservoir forecasting and monitoring: *The Leading Edge*, 16, no. 05, 445,447–448, 450,453–456.
- Chopra, S., and Marfurt. K.J., 2005, Seismic attributes-a historical perspective, *Geophysics*. Vol 70(3) p.3SO–28SO.
- Claerbout, J. F., 1976, *Fundamentals of Geophysical Data Processing*, McGraw-Hill, New York, 274p.
- Deregowsky, S. M. 1986, What is DMO?, *First Break*, vol. 4, No. 7, P. 6–24.
- Dix, C., 1955, Seismic Velocities from Surface Measurements. *Geophysics*, vol. 20, p. 68–86.
- Dobrin, M. B., 1960, *Introduction to Geophysical Prospecting*. McGraw Hill Book Company, 446p. New York.
- Dobrin, M. B., and Savit, C. H., 1988, *Introduction to Geophysical Prospecting*. McGraw Hill Book Company, New York, 867p.
- Dobrin, M., 1977, Seismic Exploration for Stratigraphic Traps, *AAPG Memoir*, P329–352.
- Evenden, B. S., and Stone, D. R., 1971, *Instrument Performance and Testing*. in *Seismic Prospecting Instruments*, 195p, GebruderBorntraeger, Berlin, Germany.

- Ewing, M., Jardetzky, W., and Press, F., 1957, *Elastic Waves in Layered Media*, McGraw-Hill, 380p., New York.
- Faust, L. Y., 1951, Seismic Velocity as a Function of Depth and Geologic Time, *Geophysics*, vol. 16, pp. 192–206.
- Gadalla, M. R. and Fisher, R., 2009, *Exploration Geophysics*, Springer-Verlag, Berlin, 262p.
- Galperin, E. I., 1973, Vertical seismic profiling, SEG, Tulsa, Oklahoma, USA.
- Gardner, D. H., 1938, Measurement of relative ground motion in reflection recording. *Geophysics*, vol. 3, pp. 40–45.
- Gardner, G. H., Gardner, L. W., and Gregory, A. R. 1974, Formation velocity and density-the diagnostic basics for stratigraphic traps, *Geophysics*, 39, 770–780.
- Gardner, L. W., 1939, An areal plan of mapping subsurface structure by refraction shooting. *Geophysics*, vol. 4, pp. 247–259.
- Gassman, F., 1951 Elastic waves through a packing of spheres. *Geophysics*, vol. 16, p. 673–685.
- Gazdag, J., 1978, Wave equation migration by phase shift, *Geophysics*, vol. 43, p.1342–1351.
- Grant, F. S., and West, G. F., 1965, *Interpretation Theory in Applied Geophysics*. McGraw-Hill, 584 p., New York.
- Green, C. H. 1938, Velocity determination by means of reflection profiles. *Geophysics*, vol. 3, p: 295–305.
- Gregory, A. R., 1977, Aspects of rock physics from laboratory and log data that are important to seismic interpretation, AAPG memoir 26, p. 15–46.
- Gurvich, I., 1972, *Seismic Prospecting* (translated from Russian by Jean Agrell). 463p., Mir publications., Moscow.
- Hagedoorn, J. G., 1954, A process of seismic reflection interpretation. *Geophysical Prospecting*, vol. 2, p. 85–127.
- Hardage, B. A., 1983, *Vertical Seismic Profiling*. Handbook of Geophysical Exploration. Geophysical Press, London.
- Kanasewich, E. R., 1973, *Time Sequence Analysis in Geophysics*. 352p., The University of Alberta Press, Edmonton.
- Kaufman, H., 1953, Velocity functions in seismic prospecting. *Geophysics*, vol. 18, pp. 289–297.
- Kearey, P., Brooks, M., and Hill, I., 2002, *An Introduction to Geophysical Exploration*, Blackwell Science Ltd., Oxford, 262p.
- Krehbiel, S. C., 1999, *Trivariate Attribute Displays*, Leading Edge, Nov.-1999, pp. 1248–1257.
- Kulhanek, O., 1976, *Introduction to Digital Filtering in Geophysics*. Elsevier, Amsterdam, 169 p.
- Larner, K. and Hatton, L., 1976, Wave equation migration. Two approaches. 8<sup>th</sup> Annual Offshore Technology Conference, Houston, Texas.
- Lavergne, M., 1989, *Seismic Methods*, 172 p., Editions Technip, Paris.
- Levin, F. K., 1971, Apparent velocity from dipping interface reflections, *Geophysics*, vol. 36, p.510–516.
- Liner, C. L., 2004, *Elements of 3D Seismology*, PennWell, Tulsa, Oklahoma, 526p.
- Lombardi, L. V., 1955, Notes on the Use of Multiple Geophones, *Geophysics*, vol. 20, p.
- Lorentz, M. and Bradley, R., An Introduction to Migration, on the link: <http://www.geol.lsu.edu/jlorenzo/ReflectSeisml97/rcbradley/WWW/rcbradley1.html> retrieved on 10 December 2012.
- Louden, L. R., Mathews, W. R., McClendon, R. T., Rehm, W. A., Aud, B. W., 1971, Ultra deep drilling guided by seismic data: Part 2. *World Oil*, 171, June, pp. 97–105.
- Maton, A., Hopkins, J, Johnson, S., LaHart, D., Warner, M., Wright, J., 1995, *Exploring Physical Science*, Prentice Hall, 818p, Englewood Cliffs New Jersey, USA.
- Mayne, W. H., 1962, Common reflection point horizontal stacking techniques, *Geophysics*, vol. 27, p.927–938.
- Mayne, W. H., 1967, Practical considerations in the use of common reflection point technique, *Geophysics*, vol. 32, p.225–229.
- McQuillin, R., Bacon, M., Barclay, W., 1984, *An Introduction to Seismic Interpretation*. Graham & Trotman, 287p., London.
- Mitchum, R. M. & Vail, P. R., 1977, *Seismic Stratigraphy Interpretation Procedure*, AAPG Memoir 26, p. 135–144.
- Nafe, J. E. and Drake, C. L. 1963, *Physical properties of marine sediments*, The Sea, Interscience, New York, 794–815.
- Nestvold, E. O., 1987, The use of 3D seismic in exploration, appraisal and field development, Proc. 12th World Petroleum Congress, Houston, 1987, 2, 125–132, Wiley, Chichester.
- Nettleton, L. L., 1940, *Geophysical Prospecting for Oil*, McGraw Hill Book Company, 440 p., New York.
- Newman, P., 1973, Divergence effects in a layered earth, *Geophysics*, vol. 38, p.481–488.
- Papaulis, A., 1962, *The Fourier Integral and its Applications*. 318p., McGraw-Hill New York.
- Parasnis, D. S., 1971, *Physical Property Guide for rocks and minerals*. Geoph. Mem. 4/71, (ABEM.) Stockholm, Sweden.
- Parr, J. O., Jr., and Mayne, W. H., 1955 A New Method of Pattern Shooting, *Geophysics*, vol. 20, p. 539–565.
- Partyka, G, et al., 1999, Interpretational, Applications of Spectral Decomposition in Reservoir Characterization. Leading Edge, March-1999, P.353.
- Pennebaker, E. S., 1968, Seismic data indicate depth magnitude of abnormal pressures. *World Oil*, June 68, pp. 73–78.
- Pickett, G. R., 1969, Principles for Application of Borehole Measurements in Petroleum Engineering, *Log Anal.*, May-June, p. 22–33.
- Poulter, T. C., 1950, The Poulter seismic method of geophysical exploration, *Geophysics*, vol. 15, p.181–207.
- Reynolds, E. B., 1970, Predicting overpressured zones with seismic data. *World Oil*, Oct- 70, pp. 78–82.

- Richardson, E. G., 1953, *Sound*, Edward Arnold & Co., 352p, London, England.
- Richter, C. F., 1958, *Elementary Seismology*, Freeman and Company Inc., 768p.
- Robinson, E. A., 1954, Predictive deconvolution of time series with applications to seismic exploration. Cambridge, MIT, Geophysical Analysis Report no. 7, (reprinted in *Geophysics*, v32, (pp. 418–484, 1967).
- Robinson, E. A., 1967, *Statistical Communication and Detection with Special Reference to Digital Data Processing of Radar and Seismic Signals*. Hafner, New York, USA. 362p.
- Robinson, E. A., 1983a, *Seismic Velocity Analysis and the Convolutional Model*. IHRDC, Boston, USA. 290p.
- Robinson, E. A., 1983b, *Migration of Geophysical Data*. IHRDC, Boston, USA., 208p.
- Robinson, E. A., and Treitel, S., 1967, Principles of Digital Wiener Filtering. *Geophys. Prospect.*, vol. 15, p. 311–333.
- Robinson, E. A., and Treitel, S., 1980, *Geophysical signal analysis*, Prentice Hall Inc., Englewood Cliffs, N. J., 466p.
- Sharma, P., 1976, *Geophysical Methods in Geology*. Elsevier, Amsterdam.
- Sheriff, R. E., 1980, *Seismic Stratigraphy*. IHRDC, 227p., Boston, USA.
- Sheriff, R. E., 1969, Addendum to Glossary of Terms used in Geophysical Exploration *Geophysics*, vol. 34, p. 255–270.
- Sheriff, R. E., 1973, *Encyclopedic Dictionary of Exploration Geophysics*, Society of Exploration Geophysicists (SEG), Tulsa, Oklahoma, USA.
- Sheriff, R. E., 1975, Factors affecting amplitudes. *Geophysical Prospecting*, Vol. 23, P.125–138.
- Sheriff, R. E., 1977 Limitations on resolution of seismic reflections and geologic detail derivable from them. In *seismic Stratigraphy-Applications to Hydrocarbon Exploration*, AAPG, Memoir 26, pp. 3–14.
- Sheriff, R. E., 2002, *Encyclopedic Dictionary of Exploration Geophysics*, Society of Exploration Geophysicists (SEG), Tulsa, Oklahoma, USA.
- Sheriff, R. E., and Geldart, L. P., 1995, *Exploration Seismology*. Cambridge University Press., 592p., UK.
- Stolt, R. H., 1978, Migration by Fourier transform, *Geophysics*, vol. 43, p.23–48.
- Taner, M. T., 2001, Seismic attributes: CSEG, Recorder, 26, 48–56.
- Taner, M. T., and Sheriff, R. E., 1977, Application of amplitude, frequency and other attributes to stratigraphic and hydrocarbon determination. AAPG Memoir 26. P301–328.
- Taner, M. T., J. S. Schuelke, R. O'Doherty, and E. Baysal, 1994, Seismic attributes revisited: 64th Annual International Meeting, SEG, Expanded Abstracts, 1104–1106.
- Taner, M. T., Koehler, F., and Sheriff, R. E., 1979, Complex seismic trace analysis. *Geophysics*, vol. 44, P1041–1063.
- Telford, W. M., Geldart, L. P., Sheriff, R. F., 1990, *Applied Geophysics*. Cambridge University Press., Cambridge, 770p.
- Trappe, H. and Hellmich, C., 1998 A real Prediction of Porosity thickness from 3D seismic Data by means of neural Networks, EAGE, 59th. Cong. And Exhibition Extended Abstracts.
- Vail, P. R., Mitchum, R. M., and Thompson, S., 1977, Seismic Stratigraphy and global changes of sea level, Application to hydrocarbon exploration, Payton, C., E., ed., AAPG Mem. 26, Tulsa, Oklahoma, 516p.
- Walton, G. C. 1972, Three Dimensional Seismic Method. *Geophysics*, vol. 37, No. 3, p. 417.
- West, S. S., 1950, Dependence of seismic wave velocity upon depth and lithology. *Geophysics*, vol. 15, pp. 653–662.
- Wuenschel, P. C., 1976, The vertical array in reflection seismology, *Geophysics*, vol. 41, p.219–232.
- Wyllie, M. R. J., A. R. Gregory, and G. H. F. Gardner, 1958, An Experimental Investigation of Factors Affecting Elastic Wave Velocities in Porous Media, *Geophysics*, vol. 23, pp. 459–493.

---

# Index

## 0–9

1D seismic function, 140  
2D seismic function, 140, 166  
2D seismic line, 141  
2D seismic surveying limitations, 141  
3C recording system, 297  
3D data displays, 166  
3D data processing, 144  
3D data volume, 143, 297, 300  
3D field data acquisition, 153  
3D seismic function, 139, 166, 297  
3D seismic reflection surveying, 139, 153  
3D spread geometry, 149  
3D survey cost elements, 147  
3D survey design, 160  
3D survey preplaning, 146  
3D surveying definition, 148  
3D surveying of inaccessible areas, 144  
4C recording system, 298  
4D surveying, 297

## A

Absorption coefficient, 48, 318  
Acoustic logging, 16  
Air-gun, 65, 118, 293  
Aliasing, 162, 163, 181–185  
Aliasing effect remedy, 184, 186, 189  
Aliasing frequency, 122, 183, 185  
Aliasing in the frequency domain, 185  
Amplitude, 35, 38, 39, 48, 67, 68, 71, 89, 295, 298, 299, 302, 316, 318, 319  
Amplitude of reflection wavelet, 299, 302, 307, 313, 317, 319  
Amplitude of sine function, 197, 198, 200, 210  
Amplitude spectrum, 40, 185, 200, 206–208, 210, 220, 224, 226, 231, 232, 235, 238–240, 260, 262, 319  
Amplitude variation with angle, 46, 299  
Amplitude variation with offset, 46, 299

Analogue recording system, 121, 122, 124  
Angle of incidence, 45, 46, 73, 93, 299  
Angle of reflection, 46  
Angle of refraction, 92, 95  
Angular frequency, 199, 203  
Angular unconformity, 313, 317  
Angular unconformity seismic image, 313  
Anti-alias filter, 122  
Apparent velocity, 39, 63, 64, 248, 298  
Aquapulse, 118  
Aquaseis, 118  
Array response concept, 127  
Array response curve, 129  
Array response function, 129  
Audio-frequency magnetic surveying, 9  
Autocorrelation function, 218–221, 223–226, 252, 260, 261, 289  
AVA, 46, 299  
Average velocity, 17, 59, 60, 63–65, 303  
AVO, 46, 299  
Azimuth, 19, 149, 150, 156, 160, 162, 276, 317

## B

Band-pass filter, 226, 231, 232, 237, 285, 289  
Bartlett window, 217, 235  
Baselap reflections, 308  
Bin, 150, 151, 159, 162, 163, 317  
Bin attributes, 150, 162, 317  
Bin dimensions, 160, 162–164  
Bin size, 147, 150, 162  
Binary numbering system, 194  
Binning, 150  
Body waves, 36, 37–39, 51, 63, 127, 128, 133, 298  
Borehole compensated (bhc) sonic log, 17, 19, 66  
Bow-tie event, 272, 304  
Bright spot seismic image, 310  
Bulk modulus, 30–32  
Buried focus event, 272

**C**

CDP concept, 80  
 CDP trace gather, 110  
 Centre spread, 106  
 Checkerboard spread, 159  
 CMP concept, 62, 79, 81, 266  
 CMP-gather, 67, 81, 263, 266–271, 281, 287–289, 298  
 CMP sorting, 249, 263, 288  
 CMP stacking, 240, 250, 254, 267, 269, 270, 272, 302  
 Coastal aggradation, 307  
 Coastal onlap, 307, 308  
 Coherent noise, 39, 40, 127, 131, 238, 254, 293, 294, 298  
 Coherent noise attenuation, 127  
 Concept of spectra, 203  
 Concept of the linear system, 228  
 Concordant reflections, 308  
 Constant-phase spectrum, 213, 214  
 Continuous spectrum, 207  
 Continuous velocity logging, 65, 66  
 Continuous velocity survey, 64  
 Convergent reflection patterns, 309  
 Convolution, 117, 174, 176, 197, 208, 211, 215, 216, 220–223, 227, 230–232, 251, 260, 306  
 Convolutional model, 174, 175, 251  
 Convolution in frequency domain, 208, 215, 221  
 Corner frequencies, 200, 233–235  
 Correlation functions, 197, 218–220  
 Correlation functions in frequency domain, 219  
 Cosine transform, 206  
 Critical refraction, 95  
 Cross correlation function, 218  
 Cross-line, 150, 151, 162, 163, 166  
 CRP-Concept, 79  
 Cubical dilatation, 28, 31, 33, 37  
 Cyclic frequency, 199

**D**

Data box, 151, 164, 166  
 Data display, 166  
 Data playback, 126  
 Data preconditioning, 247  
 Data re-organization, 166, 248–250  
 Data storage, 3, 248, 251, 286  
 Data storage and display, 248, 286  
 Data volume, 105, 140, 151, 152, 161, 166  
 DB unit, 49, 129  
 Decibel, 49, 200  
 Decimal numbering system, 190  
 Deconvolution, 197, 208, 221–226, 247, 256, 259–262, 264, 268, 289  
 Deconvolution, analysis, 249, 289  
 Deconvolution in frequency domain, 208, 222  
 Deconvolution objectives, 223  
 Deconvolution parameters, 262, 289  
 Delay-time concept, 98  
 Demultiplexing, 249–251  
 Depth map, 301–303

De-reverberation, 261

Diffraction from terminating reflectors, 83, 306  
 Diffraction hyperbola, 83–86, 164, 273, 278, 280, 281, 283, 284  
 Diffraction seismic image, 83  
 Diffraction-stack migration, 279  
 Diffraction travel-time function, 84  
 Digital function, 176, 178–181, 185, 231  
 Digital function functional representation, 180  
 Digital function graphical representation, 181  
 Digital function tabular representation, 180  
 Digital function time-series representation, 180  
 Digital function z-transform representation, 180  
 Digital recording system, 122, 125  
 Digital seismic trace, 176, 197, 243  
 Dim spot seismic image, 310  
 Dinoseis, 115, 119  
 Dip-bar migration, 276  
 Dip move-out (DMO), 76, 79, 81, 161, 266, 267  
 Dip move-out (DMO) correction, 161, 266  
 Dirac-delta function, 210  
 Direct hydrocarbon detection, 3, 299, 301, 307, 316, 317  
 Distortions in stack section, 275  
 Divergent reflection patterns, 309  
 Diversity stacking, 273  
 DMO correction, 161, 265, 266  
 Downlap reflections, 308  
 Drill-hole casing, 11  
 Dynamic correction, 256, 264  
 Dynamic range, 121, 124, 125, 254  
 Dynamite, 18, 23, 40, 65, 102, 107, 113, 114, 117, 118, 128, 135, 137, 259  
 Dynamite cords exploding, 116

**E**

Elasticity, 1, 23, 28, 53, 54, 57, 317  
 Elastic moduli, 30, 32, 292  
 Electrical arc, 118  
 Electrical induction logging, 13  
 Electrical logging, 12, 15  
 Electrical resistivity logging, 12  
 Electrical resistivity surveying, 7  
 Electromagnetic surveying, 8  
 End-on spread, 106, 107, 131  
 Equalization, 197, 236, 240, 242, 243, 249, 262, 263, 285, 289, 299  
 Equalization analysis, 249, 289  
 Equipotential surveying, 8  
 Exploding-reflector model, 86, 87, 280  
 Exploration seismology history, 3

**F**

Facies changes seismic image, 314  
 Faust formula, 56  
 Feathering effect, 154  
 Field static correction, 256

Filter analysis, 237, 249, 289  
 Filter impulse response, 229, 232  
 Filter normalization, 235, 236  
 Filter spectrum shape, 233  
 Filter tests, 237, 289  
 Filtering in the two domains, 230  
 Finite difference migration, 281  
 FK filtering, 239–241, 254  
 FK migration, 276  
 Flat spot seismic image, 310  
 Fold of coverage, 108–112, 145–147, 150, 155, 160, 162, 163, 252, 263, 270, 271, 286, 317  
 Folding frequency, 182, 184  
 Forward modeling, 104, 285, 295, 296  
 Fourier analysis, 197, 203, 214, 319  
 Fourier coefficients, 203  
 Fourier integral, 205, 206, 209, 215  
 Fourier inverse transform, 254, 281  
 Fourier pair, 208–211, 222  
 Fourier power spectrum, 206, 207  
 Fourier series, 203–205, 207  
 Fourier spectrum, 206, 215, 254, 319  
 Fourier transform, 170, 171, 185, 205, 207–209, 214, 215, 231, 238, 240, 281, 298, 318  
 Frequency concept, 199  
 Frequency domain function, 205, 232  
 Frequency filtering, 114, 173, 197, 226–228, 247, 250, 285  
 Frequency limits of fourier spectra, 211  
 Frequency of sine function, 199  
 Frequency spectrum, 171, 185, 200, 206, 209, 211, 232, 247, 292  
 Frequency units, 199  
 Frequency-wave number (FK) filtering, 238, 239, 240, 254  
 Frequency-wave number (FK) migration, 276, 280  
 Fresnel zone formula, 189  
 Fundamental frequency, 203, 204, 211

**G**

Gain recovery, 255, 256  
 Gamma-ray rock-density logging, 15  
 Gapped deconvolution, 223–226, 261  
 Gas-Gun, 118  
 Geoflex, 116, 119  
 Geograph, 114, 119  
 Geometrical spreading, 41, 47–49, 69, 173, 174, 241, 254, 256, 257, 270  
 Geometrical spreading correction, 268  
 Geophone, 39, 106, 107, 119, 121, 122, 125, 127, 129, 131, 133–135, 159, 161, 178, 226, 297, 298  
 Geophysical exploration project, 3  
 Geophysical logging, 10, 11  
 Ghost reflection, 75  
 Gibbs' phenomenon, 205  
 Gravity method, 4  
 Ground roll, 39, 127, 133, 238, 254, 271  
 Group velocity, 50, 51, 63, 64

**H**

Head wave, 95, 96, 99, 106  
 Hertz, 171, 172, 179, 183, 187, 199  
 Hexa-decimal numbering system, 195  
 High-pass filter, 231  
 Hooke's law, 29, 30, 33  
 Horizontal resolution, 187, 189, 190  
 Horizontal stacking, 269, 270  
 Huygens' principle, 42, 82, 86  
 Hybrid migration, 281  
 Hydrophone, 18, 119, 120, 298

**I**

Impulse function, 210, 216, 229, 230  
 Incoherent noise, 39, 40, 127, 172  
 Induced polarization surveying, 7  
 Inelastic attenuation, 47–49, 170, 223, 224, 241, 254, 256  
 Inlines, 150, 151  
 Instantaneous amplitude attribute, 318  
 Instantaneous frequency attribute, 318  
 Instantaneous phase attribute, 318  
 Instantaneous velocity, 58, 59  
 Interface, 42–47, 53, 68, 71, 73–75, 79, 84–86, 89–93, 95, 96, 98, 105, 113, 133, 173, 176, 187, 272, 276, 281, 282, 291, 299, 302, 310, 316, 318  
 Interval velocity, 17, 59–61, 64, 65, 302, 303, 316–318  
 Inverse dispersion, 51  
 Inverse modeling, 103, 295, 296, 317  
 Isochron map, 143, 302, 303  
 Isopach contour map, 302, 303

**K**

Kirchhoff migration, 280

**L**

Lamé's elastic coefficients, 31  
 Land 3D spread, 153, 155  
 Linear-phase spectrum, 213  
 Line spectrum, 207  
 Listening time, 117, 298  
 Logarithmic decrement, 49  
 Log Interpretation, 19  
 Longitudinal waves, 37  
 Loop shooting, 159  
 Love waves, 2, 38, 39  
 Low-frequency seismology, 298  
 Low-pass filter, 231  
 Low velocity layer (LVL) characterization, 135, 136  
 L-spread, 155

**M**

Magnetic method, 6, 9  
 Magnetic tape recording, 2, 125, 136  
 Magneto-telluric currents surveying, 9  
 Marine 3D spread, 153

- Marine data acquisition, 120  
 Marine seismic sources, 118  
 Maximum delay wavelet, 178  
 Maxipulse, 118, 119  
 Migration aperture, 161, 164, 283  
 Migration fringe, 160, 161, 164  
 Migration parameters, 273, 282  
 Migration techniques, 272, 276, 284  
 Minimum delay wavelet, 178  
 Multi-component recording, 297  
 Multiple reflections, 39, 75, 134, 155, 270, 293  
 Multiple reflections types, 293  
 Multiplexing unit, 122  
 Mute analysis, 289  
 Muting, 243, 249, 267, 289
- N**
- Natural gamma-ray logging, 15  
 Neutron gamma-ray logging, 15, 16  
 NMO correction, 62, 67, 246, 247, 249, 256, 264–267, 269, 287, 289  
 NMO-DMO correction, 165  
 NMO in case of a dipping reflector, 78  
 NMO in case of a horizontal reflector, 76  
 NMO in case of multiple horizontal reflectors, 78  
 NMO residual, 265, 269, 270, 287  
 Noise attenuation, 127, 249, 254, 286  
 Noise test, 131, 133  
 Normal dispersion, 50, 58  
 Normal move-out (NMO), 76, 84, 85, 243, 247  
 Numbering system concept, 191  
 Nyquist frequency, 122, 163, 182–187, 211, 228, 253
- O**
- Oblique reflection pattern, 310  
 Octal numbering system, 191, 195  
 Octave, 199, 200  
 Oil-well drilling, 10  
 One-sided function, 212  
 Onlap reflections, 308
- P**
- Parallel reflection patterns, 308  
 Parameter optimization, 166, 248, 249, 286, 289  
 Passive seismic surveying, 298  
 Period of sine function, 198, 199  
 Periodic function, 35, 203–205, 207  
 Phase concept, 200  
 Phase of sine function, 198, 199  
 Phase removing filtering, 238  
 Phase spectrum, 171, 206, 207, 212–214, 220  
 Phase velocity, 50, 51, 63, 227  
 Piezoelectric substance, 120  
 Pinchout seismic image, 86  
 Plane waves, 35  
 Planet Earth, 2, 4, 6, 8, 9, 20, 36, 43, 46, 53, 58, 59, 74, 89, 103, 105, 114, 116, 119, 134, 170, 173–175, 177, 188, 222, 227, 259, 261, 291, 295, 298, 306, 319  
 Point-diffractor, 82  
 Poisson's ratio, 30, 32, 36, 46, 53, 292, 299  
 Post-stack migration, 88, 272  
 Post-stack processing, 166, 248, 250, 268  
 Power spectrum, 206–208, 220, 319  
 Prediction error operator, 224, 261  
 Predictive deconvolution, 224, 261, 262, 289, 294, 295  
 Pre-stack migration, 81, 161, 249, 267, 272  
 Pre-stack processing, 166, 248, 249, 253  
 Processing objectives, 246  
 Processing of seismic reflection data, 86, 197, 243, 247  
 Processing sequence, 18, 166, 228, 240, 246, 247, 248, 286  
 Progradation deposits, 309  
 Propagating sine wave, 202, 203  
 P-waves, 17, 44, 45, 53, 66, 73, 113, 291, 292, 319
- Q**
- Quality factor (Q), 48, 318
- R**
- Radioactivity logging, 14, 15  
 Radioactivity method, 4, 9  
 Radon transform, 298  
 Ramp function, 289  
 Ramp length, 267, 289  
 Random noise, 40, 127, 219, 224, 225, 254, 261, 286, 293, 294  
 Random noise attenuation, 127, 269  
 Ray, 9, 12, 14, 15, 18, 41, 42, 61, 75, 79, 81, 86, 92, 107, 139, 141, 149, 267, 280, 281, 284, 295, 296  
 Rayleigh waves, 38, 39, 53  
 Reciprocity principle, 210  
 Rectangular (box-car) window, 216  
 Red noise, 40  
 Reef seismic image, 312  
 Reflection coefficient at inclined incidence, 72  
 Reflection coefficient at normal incidence, 73  
 Reflection complex configurations, 309  
 Reflection configuration patterns, 308, 309  
 Reflection from dipping reflectors, 74  
 Reflection from horizontal reflectors, 75  
 Reflection from multiple reflectors, 75  
 Reflection identification, 19, 302  
 Reflection interface, 46, 71, 81, 86, 281, 299, 318  
 Reflection picking, 303  
 Refraction from a faulted refractor, 100  
 Refraction in a medium of linear velocity variation, 99  
 Refraction in a multi-layer medium, 99  
 Refraction profiling, 101  
 Refraction surveys, 101, 102, 257  
 Refraction travel-time curve, 100

- Refraction travel-time function, 96, 98, 99  
 Replacement static correction, 257  
 Residual static analysis, 249, 289  
 Resolution cell, 151, 163  
 Reverberations, 222–224, 226, 259, 261, 262  
 Reverse time migration (RTM) main features, 287  
 Ricker wavelet, 177  
 Root mean square (RMS) velocity, 59, 61  
 Rotary drilling, 10
- S**
- Salt domes seismic image, 2, 102  
 Sampling period, 125, 151, 160, 163, 164, 176, 179, 181, 182, 185, 186, 189, 211, 231, 253  
 Sampling process, 163, 178, 179, 181–183, 185, 186, 253  
 Sampling theorem, 181, 182  
 Sand lenses seismic image, 310  
 Sedimentary basins configuration patterns, 309  
 Seis-loop spread, 155  
 Seismic attributes, 248, 299, 301, 316–319  
 Seismic data filtering, 239, 240  
 Seismic data recording, 121, 125  
 Seismic data volume, 140, 151, 159  
 Seismic detectors, 119, 226, 228  
 Seismic energy sources, 1, 113, 118, 291  
 Seismic facies, 307, 308, 315, 316  
 Seismic facies analysis, 308  
 Seismic fan shooting, 101, 102  
 Seismic field crew, 136, 247  
 Seismic image of faulting, 304  
 Seismic image of folding, 304  
 Seismic interpretation tools, 301  
 Seismic method, 4, 139, 141, 276  
 Seismic migration, 69, 86, 247, 248, 272, 273, 276, 284, 304  
 Seismic noise, 39, 40, 106, 126, 132, 248, 293, 298  
 Seismic noise characterization, 126  
 Seismic processing tools, 197  
 Seismic profiling technique, 107  
 Seismic reflection data acquisition, 113  
 Seismic reflection signal, 39, 169–171, 246, 247, 269  
 Seismic reflection surveying, 64, 80, 105, 222, 293  
 Seismic sequence, 307–309, 312, 315  
 Seismic sequence analysis, 307, 308  
 Seismic signal, 39, 47, 113, 116, 121, 122, 169, 170, 172, 173, 187, 189, 206, 212, 227, 245, 249, 264  
 Seismic signal parameters, 170  
 Seismic signal spectrum, 170  
 Seismic stratigraphic interpretation, 306, 315  
 Seismic structural features, 304  
 Seismic structural interpretation, 302  
 Seismic tomography, 101, 103  
 Seismic tomography data interpretation, 296  
 Seismic tomography types, 296  
 Seismic trace, 18, 19, 49, 80, 81, 106, 111, 124, 140, 162, 173–175, 177, 178, 188, 197, 208, 222–224, 229, 237, 240, 246, 248, 251, 255, 263, 266, 269, 285, 293, 294, 299, 317, 318  
 Seismic trace equalization, 240  
 Seismic transmission tomography, 91, 103  
 Seismic velocity, 53, 57, 59, 64, 68, 69, 103, 163, 316  
 Seismic velocity inversion, 68  
 Seismic wave diffraction, 81  
 Seismic wavelet, 4, 169, 170, 173, 177, 197, 245, 306, 319  
 Seismic wave propagation, 301  
 Seismic wave reflection, 71  
 Seismic wave refraction, 92, 100  
 Seismic waves, 1, 2, 4, 23, 40, 48, 53, 58, 59, 64, 71, 82, 86, 103, 116, 119, 134, 150, 291, 298  
 Seismic wave transmission, 89, 91  
 Seismo-stratigraphic analysis, 308  
 Seismo-stratigraphic features, 310  
 Seis-square spread, 155  
 Self Potential (SP) surveying, 8  
 Shear modulus, 30, 31, 292  
 Shear-waves generation, 291  
 Shotpoint, 107, 136  
 Shot record, 39, 67, 71, 107, 126, 131, 134, 231, 238, 240, 242, 248, 253, 254, 263, 267, 270, 299  
 Shot record display, 127  
 Shot salvo, 155  
 SH-waves, 38, 39, 44, 95, 291  
 Side lobes problem, 235  
 Sigmoidal reflection patterns, 309  
 Signal enhancement, 3, 131, 248, 268, 284, 292  
 Signal length, 170, 211  
 Signal resolution, 39, 134, 187, 254  
 Signal strength, 134, 170  
 Sinc function, 210  
 Sine function, 171, 197–200, 202, 206, 210  
 Sine function parameters, 198  
 Sine transform, 206  
 Slant stack, 298  
 Smiles features, 284  
 Snell's Law, 93–96, 99, 281  
 Sonic logging, 11, 16, 17  
 Sparker, 118  
 Spatial frequencies, 200  
 Specific dissipation, 49  
 Spectral attributes, 319  
 Spectra of observational data, 214  
 Spectrum analysis, 171, 285  
 Spectrum-centroid attribute, 319  
 Spectrum of the rectangular pulse, 209  
 Spectrum of the spike pulse, 210  
 Spherical divergence, 48, 49, 254  
 Spiking deconvolution, 223, 225, 256, 260–262  
 Spontaneous potential (SP) logging, 13  
 Spread configuration, 105, 106  
 Spread template, 155, 160  
 SPS-file, 252  
 Stacking process, 254, 269, 271, 272, 277, 287  
 Stacking response, 269, 287  
 Stacking velocity, 59, 61, 62, 64, 144, 265, 269, 270, 287, 303

- Stack section, 69, 83, 86, 140, 142, 143, 151, 176, 187, 238, 240, 247, 248, 271–278, 280, 281, 284, 286, 289, 295, 300–302, 304, 315, 317, 319
- Stack-section distortion, 273
- Static correction, 219, 243, 246, 247, 249, 256, 257, 261, 271, 287, 288, 292
- Station lines, 150
- Steam-Gun, 118
- Strain, 23, 26–34, 36, 37, 73
- Stratigraphic interpretation sequence, 315
- Streamer, 120, 153, 154
- Stress, 1, 23, 24, 26, 28–30, 32, 33, 73
- Structural interpretation sequence, 302
- Sublines, 150
- Subsurface coverage, 108, 109, 112, 295
- Surface consistent amplitude compensation, 256
- Surface coverage, 108, 111
- Surface waves, 36, 38, 39, 69, 115, 127–129, 131, 254, 298
- SV-waves, 38, 44, 73, 291
- Swath parameters, 160, 161
- Swath shooting, 150, 156, 157
- S-waves, 36–38, 45, 46, 53, 54, 291, 292, 297, 299
- Sweep length, 116
- Sweep removal, 117, 249, 251
- Sweep taper, 158
- Synthetic seismogram, 17, 19, 66, 174–176, 295, 302
- T**
- Tau-P transform, 298
- Telluric currents surveying, 9
- Template parameters, 160, 161
- Temporal frequency, 35, 198, 202
- Thumper, 114
- Time average equation, 54
- Time-depth curve, 303
- Time-invariant equalization, 242
- Time-lapse surveying, 297
- Time slice, 152, 153
- Time-variant deconvolution (TVD), 260
- Time-variant equalization, 236, 242, 263
- Time-variant filtering (TVF), 236, 241, 260, 285
- Time versus depth migration, 281
- Toplap reflections, 308
- Trace editing, 243, 249, 253
- Trace equalization, 240, 262
- Trace header assignment, 249, 253
- Trace interpolation, 284
- Trace muting, 243, 267
- Transient function, 205, 209
- Transmission coefficient at normal incidence, 89
- Transmittance, 89
- Transverse waves, 1, 37
- Travel-time corrections, 69, 247
- Triangular (Bartlett) window, 217
- True amplitude recovery (TAR), 246, 254
- Truncation effect, 215, 235
- T-spread, 155
- Two-domain concept, 208
- Two-way transmission coefficient, 90, 91
- U**
- Unbalanced split spread, 106
- Unconformity seismic image, 313
- Unipulse, 118, 119
- Up-hole surveying, 91, 92, 135, 257
- V**
- Vaporchoc, 118, 119
- Velocity analysis, 62, 64, 67, 78, 265, 287, 289
- Velocity analysis Method, 67
- Velocity by  $T - \Delta T$  Method, 67
- Velocity by  $X^2 - T^2$  method, 66
- Velocity-density relationship, 54
- Velocity-depth relationship, 58
- Velocity-elasticity relationship, 54
- Velocity function, 58–60, 64, 65, 67, 256, 287, 293, 303
- Velocity-geological age relationship, 56
- Velocity map, 302, 303
- Velocity-overburden pressure relationship, 57
- Velocity-porosity relationship, 55
- Velocity pull-up, 311
- Vertical resolution, 187–189
- Vertical seismic profiling (VSP), 18, 19, 91, 119, 292–295, 303
- Vertical stacking, 114, 115, 118, 252, 254, 269, 270, 292–294
- Vibroseis, 3, 116–119, 134, 178, 219, 251, 270
- Voxel, 151, 163, 164
- VSP data processing, 294
- VSP field operation, 293
- VSP seismic record, 293
- W**
- Wasp, 118, 119
- Wave conversion, 43, 44, 46, 47, 73, 95, 170, 291
- Wave dispersion, 49, 63
- Wave-front, 41, 42, 47, 63, 81, 116, 139, 148, 189, 277, 278
- Wave-front common tangent method, 278
- Wavefront-maximum convexity method, 277
- Wave generation, 43
- Wavelength, 15, 35, 39, 49, 50, 63, 127–129, 133, 178, 187, 188, 198, 203, 284
- Wave motion equation, 32–34, 36, 54
- Wave number, 35, 63, 202, 238, 248
- Wave scattering, 82, 311
- Wavelet attributes, 300, 315, 318
- Wavelet concept, 177
- Wavelet delay properties, 178
- Wavelet energy, 178, 302, 307
- Weight dropping, 114, 134, 270, 293
- Well completion, 20
- Well velocity surveying, 16, 17, 64, 91, 92, 292, 293

Whitening deconvolution, [223–226](#), [260](#), [261](#), [289](#)

White noise, [40](#), [225](#), [226](#), [262](#)

White spectrum, [210](#), [223](#), [225](#), [260](#)

Wildcat drilling, [10](#)

Windowing, [215](#), [235](#)

## **X**

X-spread, [155](#)

## **Y**

Young's modulus, [30–32](#)

## **Z**

Zero-phase spectrum, [212](#), [214](#)

Zoeppritz equations, [45](#), [46](#), [73](#), [299](#)